NASA Conference Publication 2309

Combustion Fundamentals Research

Proceedings of a conference held at
NASA Lewis Research Center
Cleveland, Ohio
April 16-18, 1984

NASA

NASA Conference Publication 2309

Combustion Fundamentals Research

Proceedings of a conference
sponsored by NASA Lewis Research Center
and held at NASA Lewis Research Center
Cleveland, Ohio
April 16–18, 1984

NASA
National Aeronautics
and Space Administration

Scientific and Technical
Information Office

1984

FOREWORD

The Lewis Research Center is the National Aeronautics and Space Administration's principal field installation for aerospace propulsion and power generation research and development. Therefore, a substantial part of the Center's activities is devoted to progress in the technology of aircraft propulsion. Results of this work are published as NASA reports and as articles in the technical journals. In addition, an occasional technical conference assists us in communicating more directly with others in the engineering field. Accordingly, this Combustion Fundamentals Research 1984 Conference is held to provide a forum for selected researchers from industry, academe, and the government to review results of recent and current Lewis-sponsored fundamental research in combustion and the fluid mechanic processes which typify the flowfields in the gas-turbine combustor environment. This meeting also provides an opportunity for technical dialogue among the participants.

Combustion fundamental research is being conducted at Lewis Research Center to provide improved analytical models of the complex flow and chemical reaction processes which occur in the combustor of gas turbine engines in order to provide engine manufacturers with more powerful design tools to reduce the development time of new concepts and to increase the durability of these concepts. The objectives are to obtain a better understanding of the various physical processes that occur in the gas turbine combustor and to develop analytical models which can accurately describe these processes. The main thrusts in this program are as follows: (1) combustion computational fluid mechanics - analytically characterize the physical phenomena associated with turbulent reactive flows; (2) model verification experiments - provide benchmark data with well-specified boundary conditions to assess the accuracy of the computational models; (3) fundamental experiments - achieve a more complete understanding of the fundamental processes occurring in reacting flows; and (4) advanced numerics - develop improved numeric techniques which can be applied to highly turbulent, recirculating, reacting flowfields.

The research activities described in this conference represents most of the NASA Lewis-sponsored work in this area. The research is classified under the subject areas of fuel sprays, fluid mixing, radiation-chemistry, and combustion dynamics. Each presentation summarizes the progress and current status of the project. If more detail is desired, discussion with the principal investigator is invited. In most cases, previous publications are listed.

Edward J. Mularz
Conference Chairman

CONTENTS

D1

N84 20526

MEASUREMENTS IN LIQUID FUEL SPRAYS

Norman Chigier
Department of Mechanical Engineering
Carnegie-Mellon University

The goal of our research on the measurement of liquid fuel sprays is to study the effects of atomizer design and to characterize the atomization and vaporization processes in sprays under well controlled conditions. The scope of this study is limited to the events directly preceding combustion in the liquid fuel sprays. Measurement techniques are being used to provide information as a function of space and time on droplet size, shape, number density, position, angle of flight and velocity. Three spray chambers have been designed and constructed for: (i) air-assist liquid fuel "research" sprays; (ii) high pressure and temperature chamber for pulsed diesel fuel sprays; and (iii) coal-water slurry sprays. Recent results utilizing photography, cinematography, and calibration of the Malvern particle sizer are reported. Systems for simultaneous measurement of velocity and particle size distributions using Laser Doppler Anemometry/Interferometry and the application of holography in liquid fuel sprays are being calibrated.

Parker Hannifin has designed an air assist swirl atomizer for use in basic research studies at several universities (Carnegie-Mellon, Purdue, UC/Irvine). This atomizer has been fitted into the basic research spray chamber in which uniform low turbulence intensity air flows vertically downward. The liquid fuel spray is injected downward along with the uniform air flow. Detailed measurements of the distributions of particle size, particle velocity, and gas velocity will be made throughout the sprays under conditions of well controlled initial and boundary conditions.

Design and construction of the high pressure and high temperature swirl chamber has been completed to withstand maximum pressures of 60 atm. and maximum temperatures of 370°C. Two quartz windows, 89mm in diameter, are fitted to the chamber for optical access. An electromagnetically controlled pulsed diesel injector has been operated with the chamber and preliminary photographic studies have been made. The air-assist swirl atomizer will, at a later stage, be installed in this high pressure chamber.

The coal-water slurry spray test facility was operated with a Parker Hannifin counter swirl atomizer to investigate fundamental processes leading to combustion of coal-water slurries. This research is focused on two areas: the vaporization of water and the devolatilization of the coal particles in the spray. Preliminary studies on drop size, shape, and distribution were made using photography, cinematography, and the Malvern particle sizer. High quality images of commercial coal-water (70% to 30% concentration) slurry spray at various atomizing air pressure and slurry feed rate have been made. The magnification of these pictures is 8.4 times lifesize and is about 1 inch distance from the nozzle tip. The spray appeared very dense in the photographs. The smallest particle/droplet size that can be distinguished on the edges of the spray is in the order of 40-50 microns. There is evidence of low-frequency pulsations in the spray in both photographic and high speed cinematographic results.

Samples of diluted coal-water slurry were measured by the Malvern particle

sizer for size distribution. The results showed that the coal particle SMD fell within the size range of 2 microns to 1.5 microns for an obscuration ranging from 0 to 90 percent.

The behavior of the Malvern 2200 particle sizer was investigated by analyzing a non-varying calibration reticle produced by Laser-Electro optics. Some of the important parameters varied during the experiment were: photomask tilt angle, distance between photomask and receiver lens, and receiver lens focal length. All of these variables proved to be very crucial in the determination of size distribution by the Malvern.

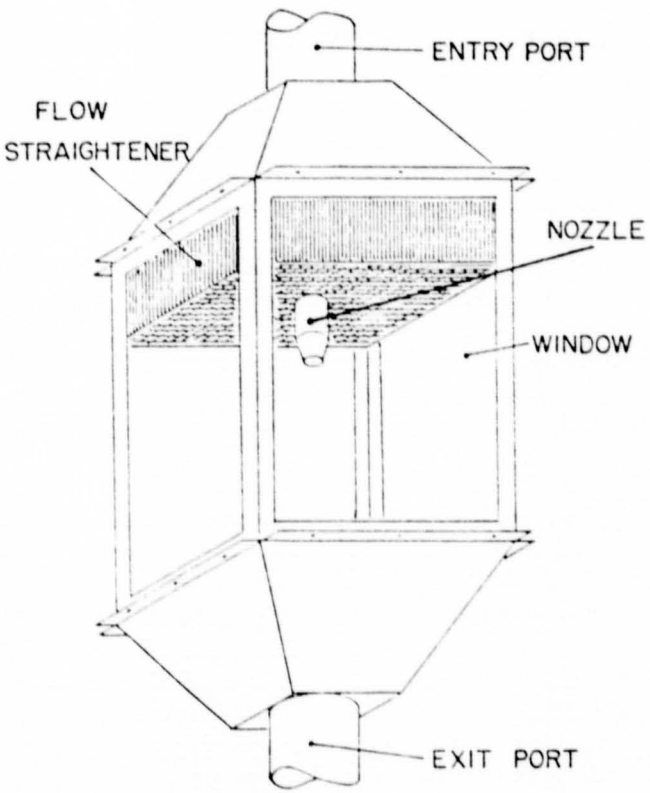

SPRAY CHAMBER

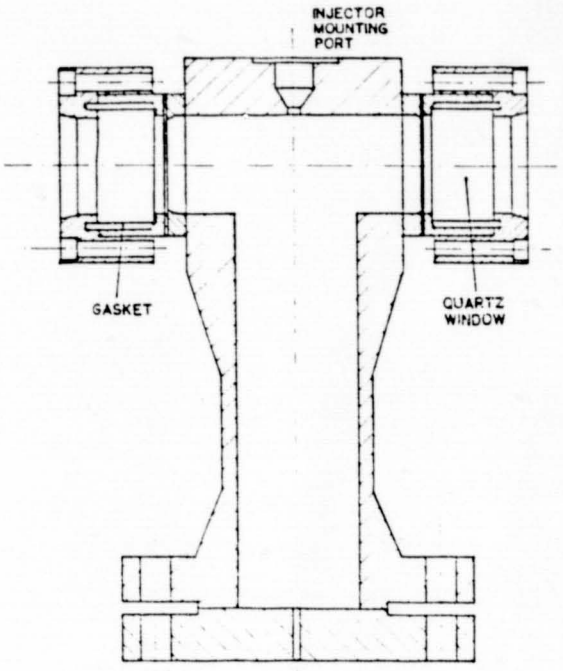

SPRAY CHAMBER

CHAMBER

Max temperature	370°C
Max pressure	60 atm
Diameter	120 mm
Height	460 mm
no of window ports	2
Diameter	89 mm

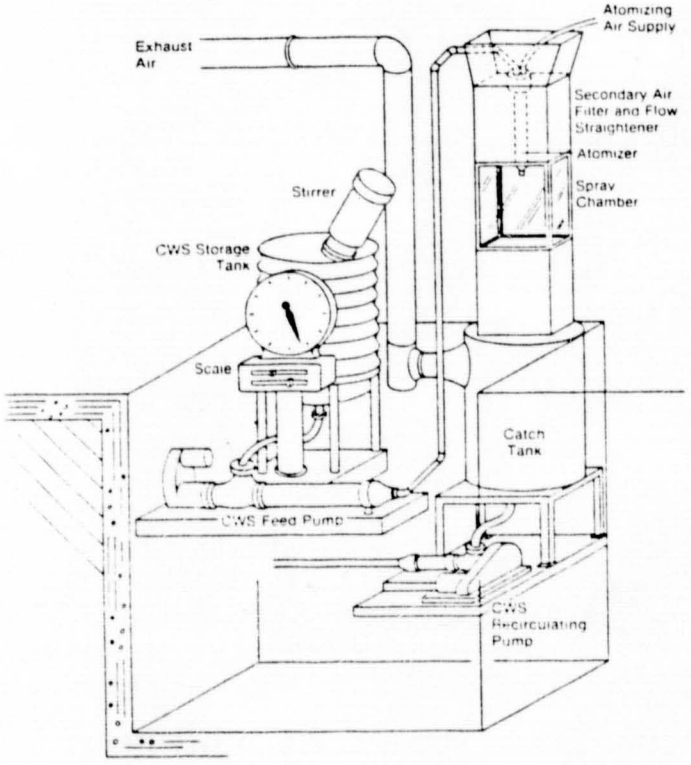

Three-Dimensional View of the Experimental System to Study Coal-Water Slurry Sprays

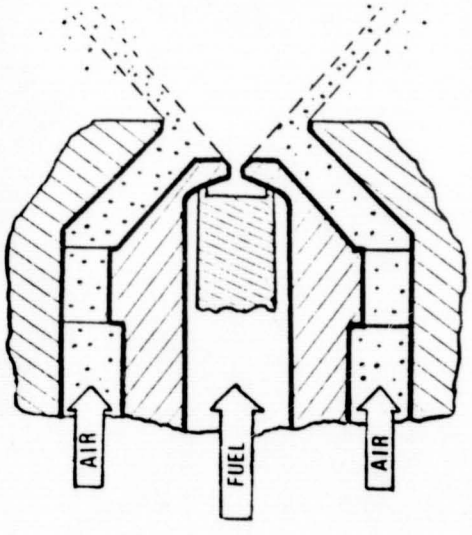

Air Assisted Atomizer

Fuel: 50% Ethylene Glycol, 50% Water by volume.

Fuel pressure: 20 psi, Nozzle: 60 degree solid cone.

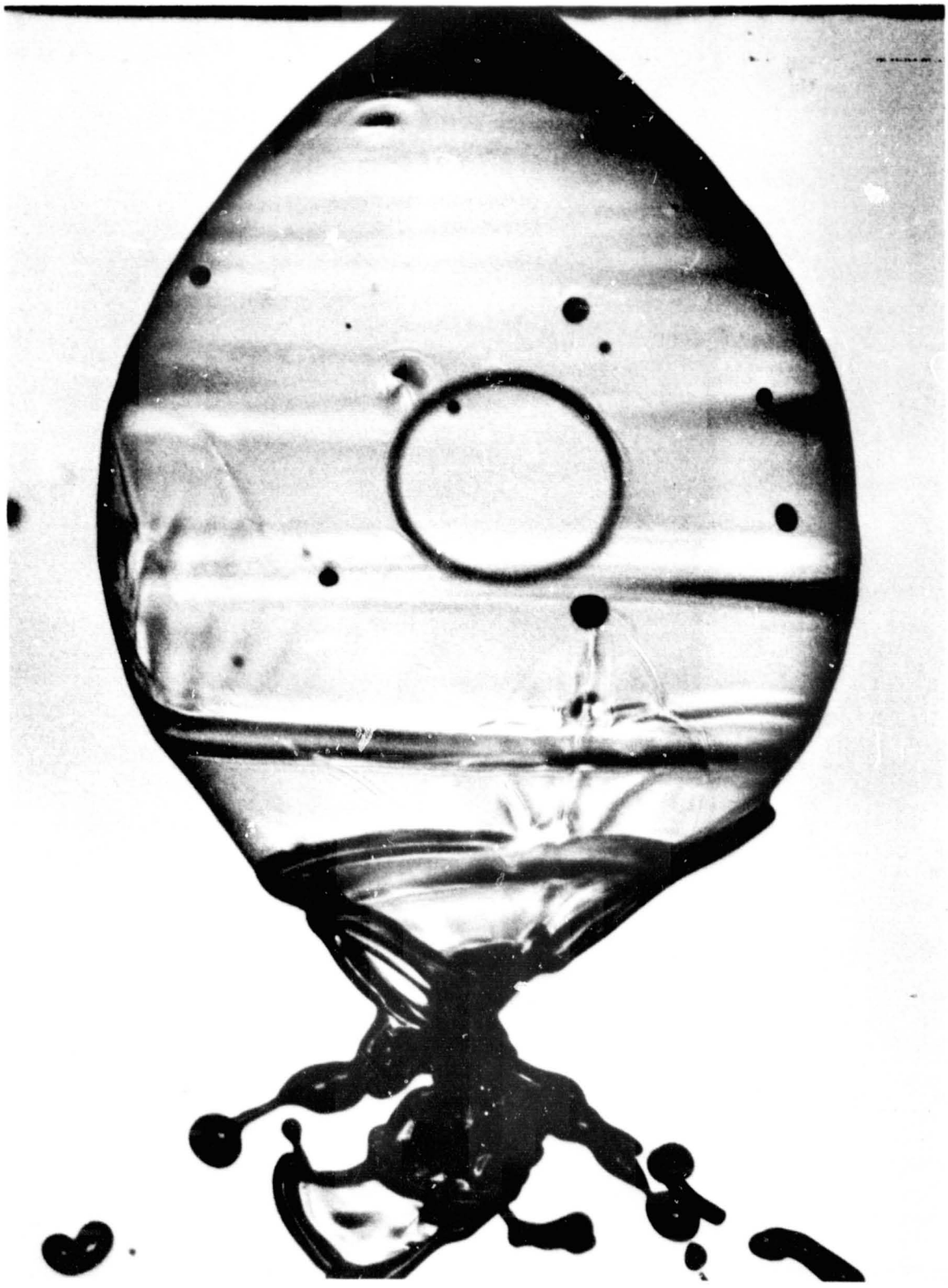

Fuel: 50% Ethylene Glycol, 50% Water by volume.

Fuel pressure: 21 psi, Nozzle: 60 degree solid cone.

Fuel: 50% Ethylene Glycol, 50% Water by volume.

Fuel pressure: 40 psi, Nozzle: 45 degree solid cone.

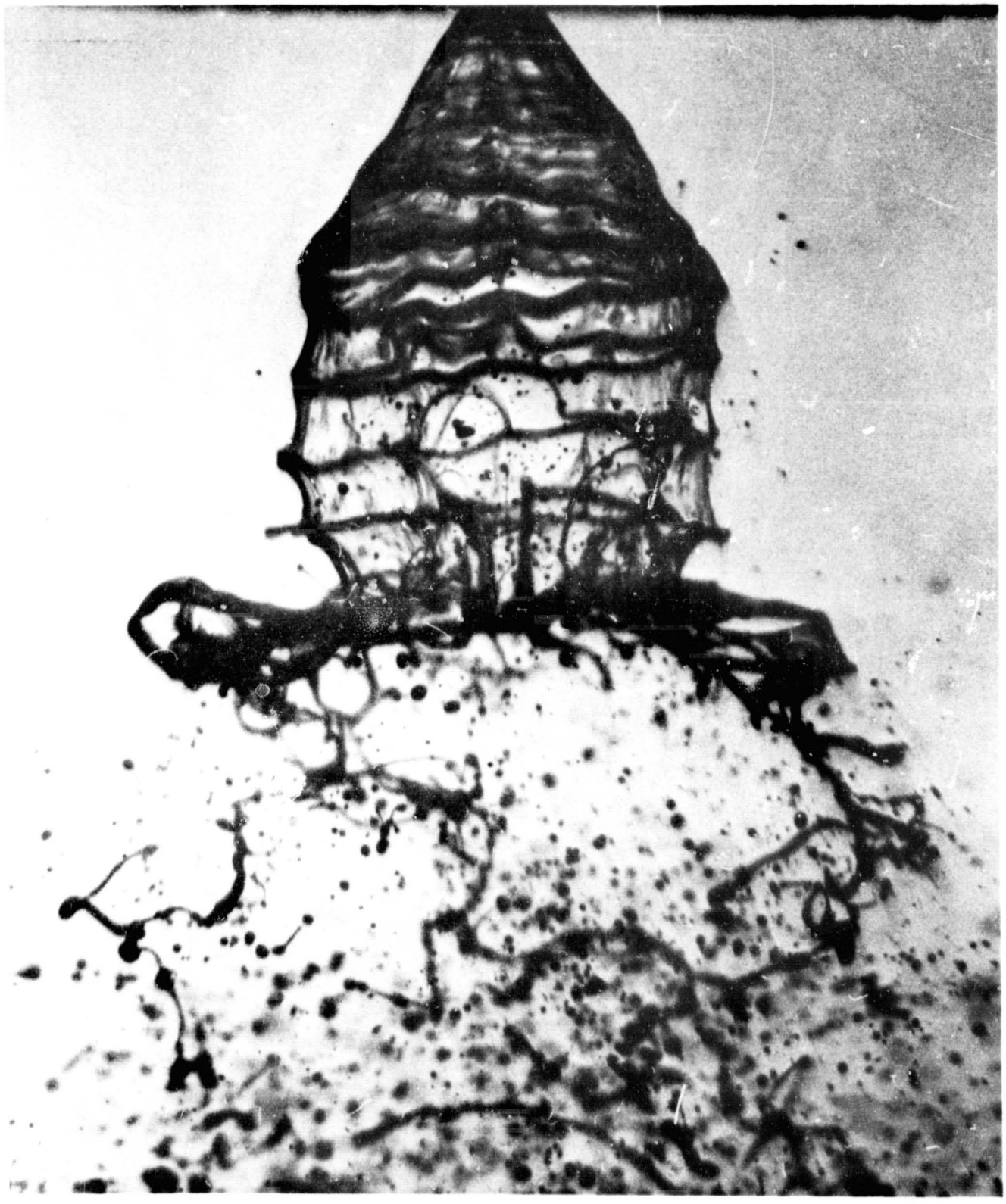

Fuel: 50% Ethylene Glycol, 50% Water by volume.

Fuel pressure: 70 psi, Nozzle: 45 degree hollow cone.

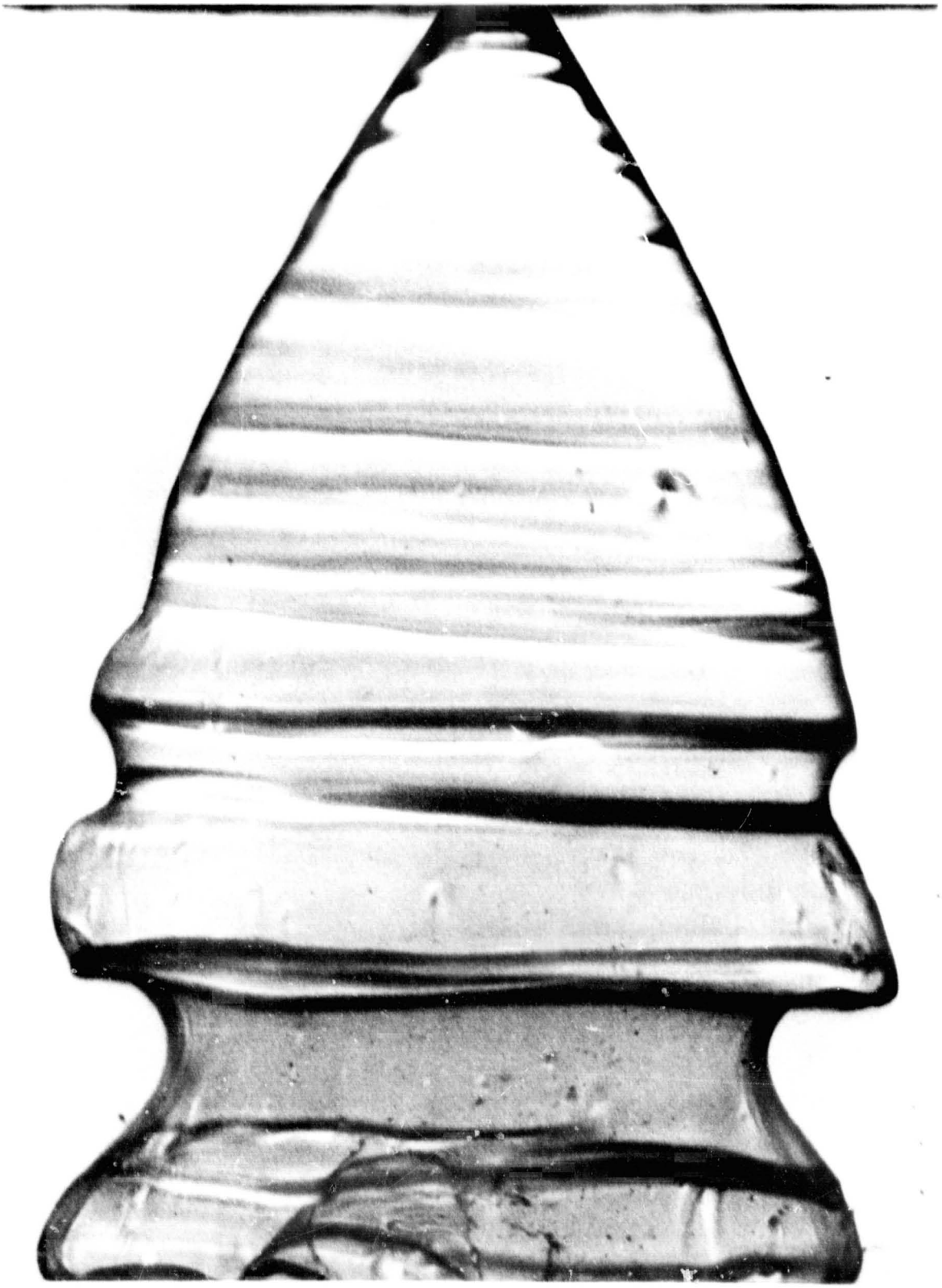

Fuel: 50% Ethylene Glycol, 50% Water by volume.

Fuel pressure: 80 psi, Nozzle: 45 degree solid cone.

Slurry: 210 lb/hr, 22 psi; Air: 44 psi

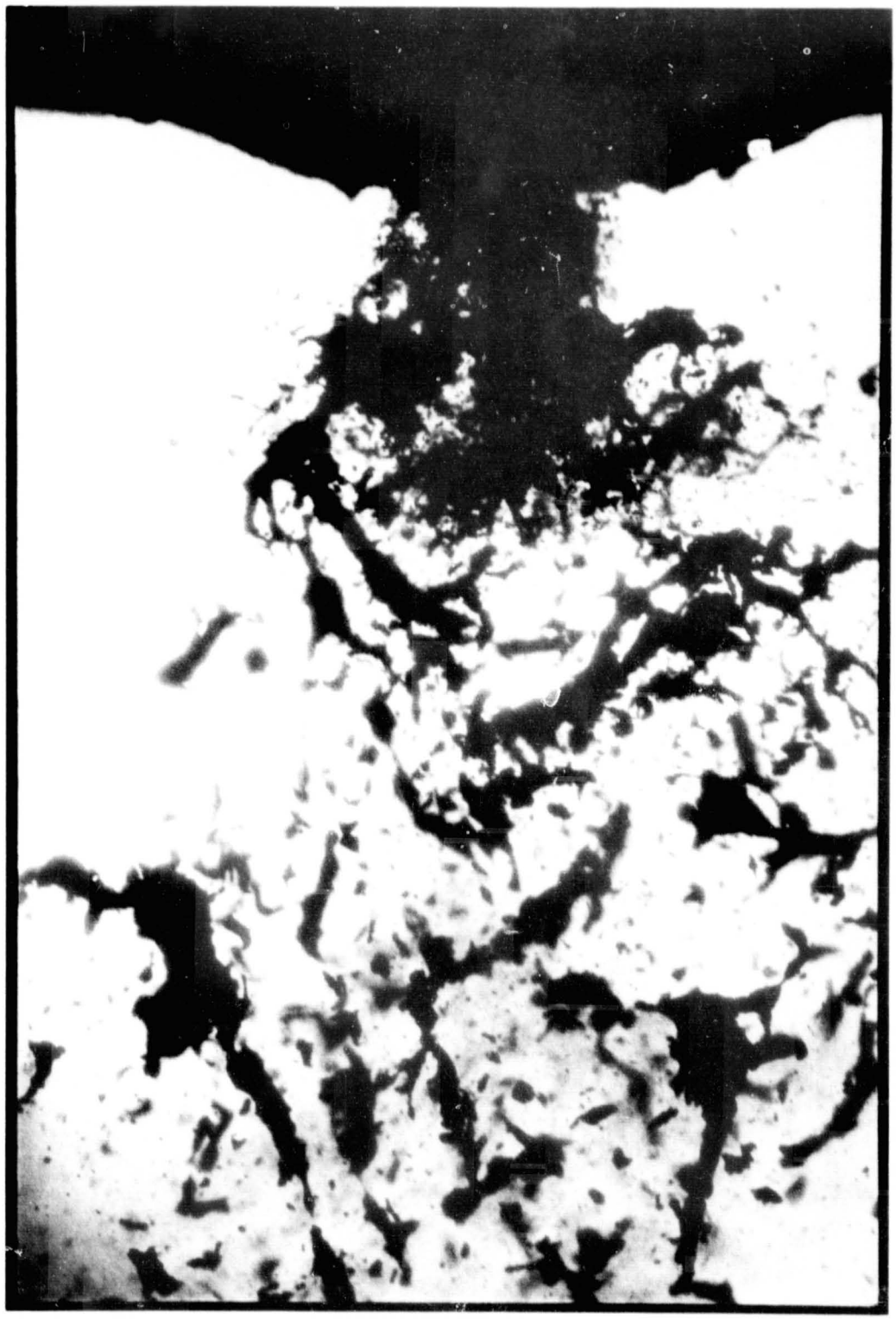

Slurry: 360 lb/hr, 42 psi; Air: 73 psi

Slurry: 360 lb/hr, 50 psi; Air: 132 psi

Slurry: 500 lb/hr, 48 psi; Air: 45 psi

Slurry: 500 lb/hr, 72 psi; Air: 162 psi

Variation of SMD with the distance between the calibration mask and receiver lens.

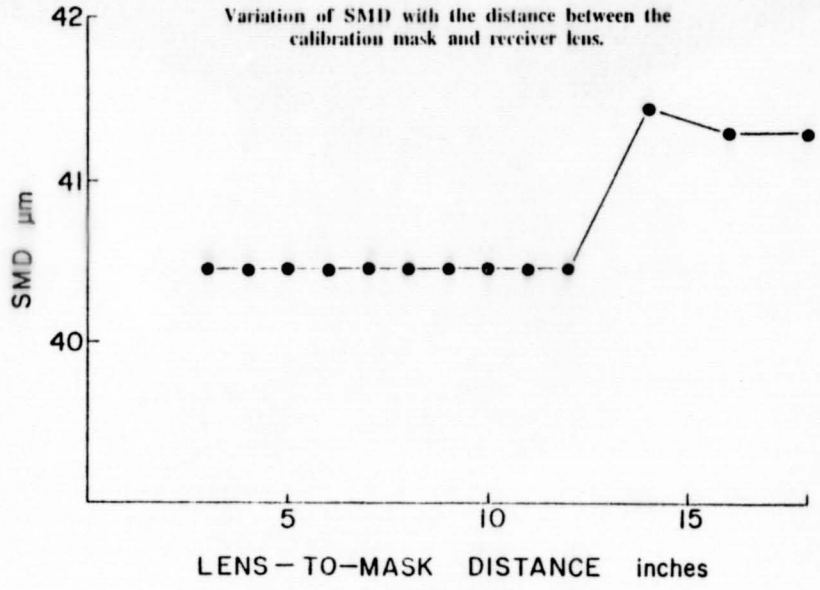

Variation of SMD with calibration mask tilt angle.

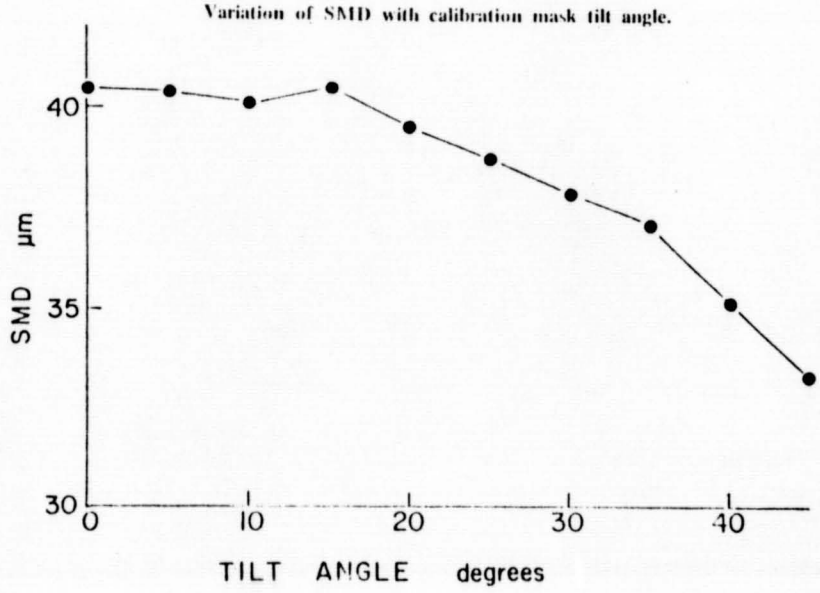

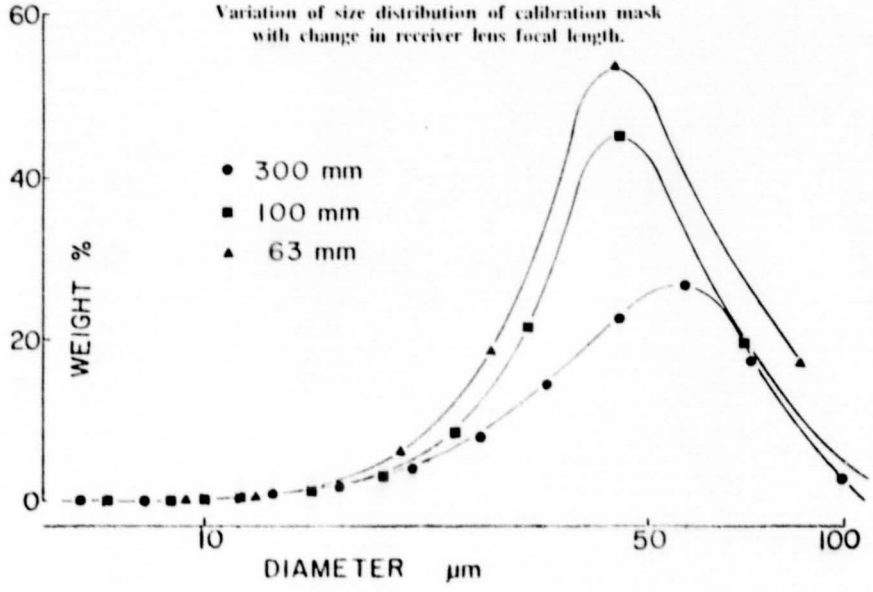

FUEL SPRAY DIAGNOSTICS

Maria A. Bosque
NASA Lewis Research Center

To understand the combustion process of liquid reactants, it is necessary to obtain information about the distribution and atomization of the injected liquid phase. Turbulence and relative velocities between the fuel's gas phase and liquid droplets affect the evaporation, burning rate and pollutant formation. This will affect other combustor performance parameters such as combustion efficiency, pollutant emissions and combustion stability. The measurement of size and velocity distribution of the liquid injected into the combustor is of vital necessity. The experimental data will be used by numerical modelers in deriving mathematical relationships that will describe the combustion process.

Several laser measurement methods are being studied to provide the capability to make droplet size and velocity measurements under a variety of spray conditions. The Droplet Sizing Interferometer (DSI) has promised to be a successful technique because of its capability for rapid data acquisition, compilation and analysis. Its main advantage is the ability to obtain size and velocity measurements in air-fuel mixing studies and hot flows.

The existing DSI at NASA Lewis is a two-color, two-component system. Two independent orthogonal measurements of size and velocity components can be made simultaneously. It also uses an off-axis large-angle light scatter detection. The fundamental features of the system are optics, signal processing and data management system. The major component include a transmitter unit, two receiver units, two signal processors, two data management systems, two Bragg cell systems, two printer/plotters, a laser, power supply and color monitor.

The laser diagnostic investigation will consist of various experiment configurations for fuel nozzle characterization tests. Water will be used as a fuel substitute. General probe volume positions will be obtained for mapping the fuel nozzle flow distribution and variations with test conditions. A fuel nozzle/swirler combination will simulate fuel/air mixing characteristics; small particles will be used for seeding the flow field.

Two contracts have been awarded for further development and improvements to the system. These contract efforts promise to extend the size range capability, reduce beam alignment difficulties and reduce the system sensitivity to laser beam quality and differences in the relative intensity of the beams.

REFERENCES

1. Bachalo, W. D.; Hess, O. F.; and Hartwell, C. A.: An Instrument for Spray Droplet Size and Velocity Measurements. J. Eng. Power, Vol. 102, No. 4, Oct. 1980, pp. 798-806.

2. Bachalo, W. D.: Method for Measuring the Size and Velocity of Spheres by Dual-Beam Light-Scatter Interferometry. Applied Optics, Vol. 19, p. 363, Feb. 1980.

3. Mularz, E. J.; Bosque, M. A.; and Humenik, F. M.: Detailed Full Spray Analysis Techniques, NASA TM-83476, 1983.

FUEL SPRAY DIAGNOSTICS PROGRAM

PURPOSE
- CONDUCT FUNDAMENTAL COMBUSTION PROCESS RESEARCH USING DIAGNOSTIC MEASUREMENTS FROM A UNIQUE LASER INTERFEROMETER APPARATUS.

METHOD
- NON-INTRUSIVE MEASUREMENT PROBE FORMED BY COHERENT LASER BEAMS THAT PRODUCE INTERFERENCE FRINGE BANDS.
- DROPLETS/PARTICLES GENERATE LIGHT SCATTER PATTERNS WHICH ARE DETECTED WITH PMT.

YIELD
- FAST REAL TIME DATA ANALYSIS OF FLOW CHARACTERISTICS.

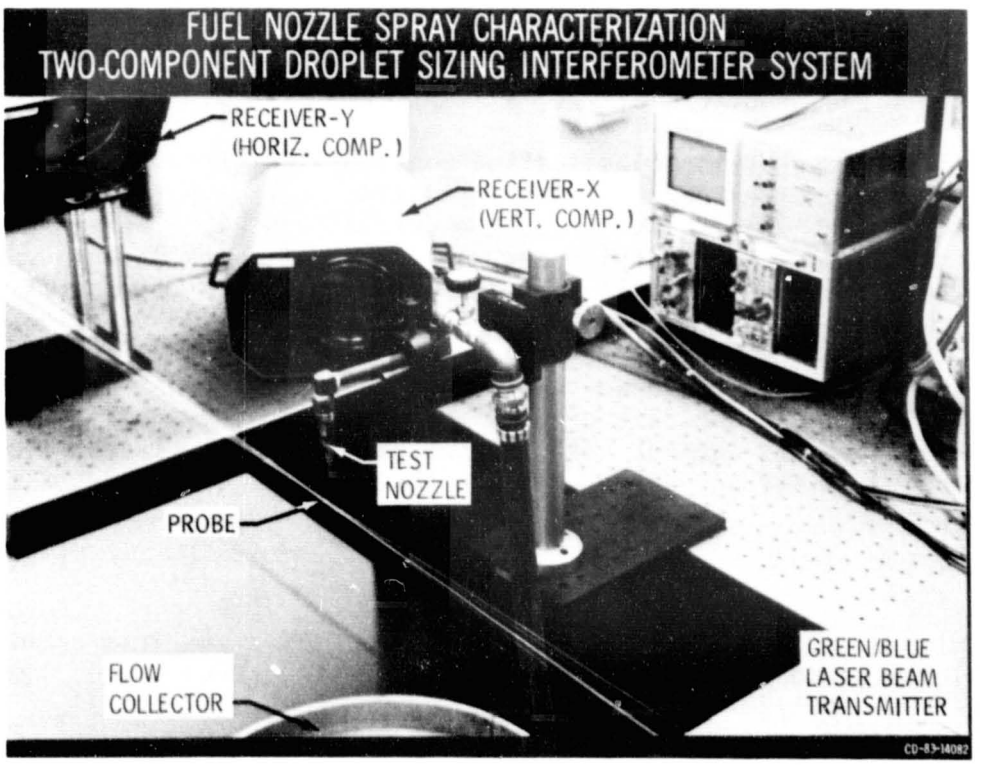

DROPLET SIZING INTERFEROMETER SYSTEM LINE DRAWING (ONE-COMPONENT)

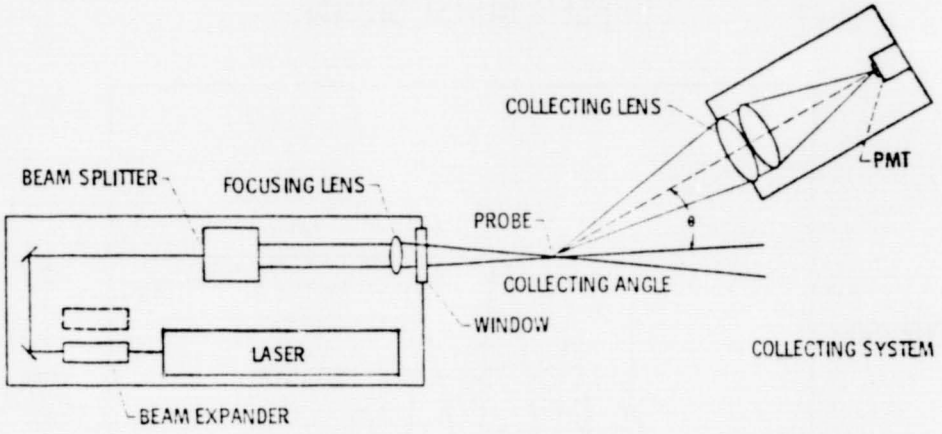

FORMATION OF FRINGES IN PROBE VOLUME OF DS:

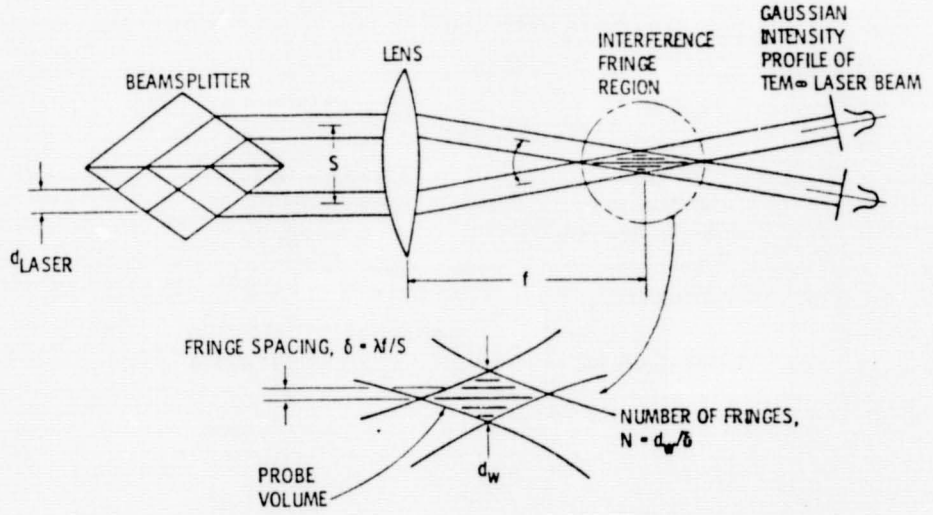

DOPPLER BURST SIGNAL

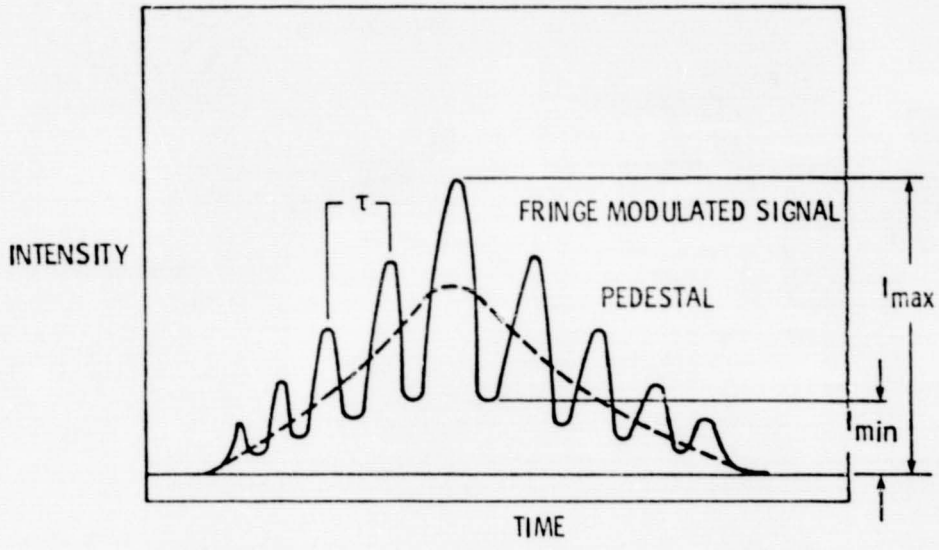

NOZZLE CHARACTERIZATION TEST

Nozzle	Delavan-Hollow Cone (4.00-wda-45)
Position	3.8 inches from nozzle
Airflow rate	400 scfm max.
Water flow rate	135 scfh max.
Pressure	15-60 psig.
Temperature	70 F

(This nozzle has been previously characterized with a Malvern System)

NASA LeRC FUEL SPRAY DIAGNOSTICS PROGRAM

EXPERIMENT DESCRIPTION
•SPRAY CHARACTERIZATION - H_2O - VARIOUS NOZZLE TYPES - PRESSURE DIFFERENTIAL EFFECTS SIZE AND VELOCITY DISTRIBUTION - SEVERAL SAMPLING PLANES •TURBULENCE STUDIES - SEEDED - VARIOUS AIR SWIRLER CONFIGURATIONS - VANE ANGLE EFFECTS - AIRFLOW SPLITS •FUEL-AIR REACTION STUDIES - VARIOUS EQUIVALENCE RATIOS - FUEL PROPERTY EFFECTS - MEASURE TURBULENCE INTENSITY

RESOURCES

- FUEL SPRAY DIAGNOSTICS FACILITY
  (SW-5, ERB , NASA LEWIS)
- DEVELOPMENT AND IMPLEMENTATION OF ADVANCED DIAGNOSTIC TECHNIQUES
  (SPECTRON DEVELOPMENT LABORATORIES,INC.,CALIFORNIA)
- PHASE DETECTION TECHNIQUE STUDY
  (AEROMETRICS,INC. ,CALIFORNIA)
- MEASUREMENT OF SPRAY COMBUSTION PROCESSES
  (UTSI GRANT, TENNESSEE)
- COMBUSTION CHARACTERISTICS IN THE TRANSITION REGION OF LIQUID FLUID SPRAYS
  (DREXEL UNIVERSITY GRANT,PHILADELPHIA)

DEVELOPMENT AND IMPLEMENTATION OF ADVANCED DIAGNOSTIC TECHNIQUES*

Cecil F. Hess
Spectron Development Laboratories, Inc.

The objectives of this work are to establish the performance and limitations of two optical techniques for spray characterization, and to design and build an instrument based on these techniques.

Two techniques have been identified which offer great potential in the measurement of sprays. The first is referred to as "IMAX", and it consists of a nonintrusive pulse height analyzer. The second is referred to as "Visibility/Intensity (V/I)" and it performs a size measurement by examining the visibility and the pedestal intensity of a Doppler burst. The research conducted over this past year indicates that the IMAX technique provides a larger dynamic range and higher accuracy than V/I. It also shows that the two-color IMAX concept provides a higher S/N primarily because of the high efficiency in spectrally separating the two signals.

The two-color IMAX concept is described in Figure 1a. Two small beams of a given wavelength (4880Å) are crossed in the middle of a larger beam of different wavelength (5145Å) thus identifying a region of almost uniform intensity within the large beam. The two small beams will interfere where they cross and a fringe pattern will be formed in the middle of the large beam. Droplets crossing the fringes also cross the middle of the large beam. Since the peak intensity of the large Gaussian beam is known, a unique relationship between droplet size and scattered light is established. The velocity of the droplets is also measured using the classical Doppler approach. Figure 1b shows a schematic representation of the breadboard system used to acquire the reported data.

The size distribution of two kinds of sprays are reported here. The first is produced by a Berglund-Liu droplet generator with dispersion air. Monodisperse, bimodal, and trimodal sprays with an angle of about 10° were thus produced, and the results are shown on Figure 2a. The theoretically predicted sizes are 49 μm, 62 μm, and 70 μm, respectively. Good accuracy and resolution can, therefore, be observed. The second spray was produced by a pressure nozzle. The results are shown on Figure 2b. In order to test the resolution of the system, data were obtained using three different size ranges: 5 to 50 μm; 10 to 100 μm; and 20 to 200 μm. This is one of the most difficult self-consistency tests imposed on any technique, and most available techniques will show a shift in the predicted data. IMAX shows excellent matching of the data.

The Visibility/Intensity Technique is described in Figure 3. This technique makes use not only of the visibility of a Doppler signal but also the peak intensity of the pedestal. Both parameters are available in the signal and their cross-correlation can be used to eliminate faulty signals produced in many practical environments. This technique will especially prevent small

*Contract No. NAS3-23538

particles (high visibility) from appearing as large. Figure 3 shows a Doppler trace where both the visibility and the peak intensity of the pedestal are indicated. There is a relationship between the size of the droplet and the amount of scattered light given by Mie theory. This relationship can be used to eliminate signals with an apparently different size by using the following logic: Droplets that produce a certain visibility are associated with a given size; hence, they should scatter light with a given intensity (characterized by I_p). Two exceptions are contemplated: First, droplet with the correct visibility will scatter different amounts of light due to the Gaussian nature of the probe volume's intensity; second, droplets with an erroneous visibility will not scatter light with an intensity corresponding to their apparent size.

Results for both Visibility/Intensity and visibility only are shown in Figure 4. Figure 4a shows the data of the spray formed of primary droplets and doublets. Figure 4b shows results similar to Figure 4a but obtained with visibility only. Notice how much broader the later distributions are. Figure 4c shows a spray containing primary droplets, doublets and triplets. Figure 4d shows results similar to Figure 4c but obtained with visibility only. Notice that the later distribution is broader and the resolution is not as fine.

Both the accuracy and resolution of these measurements are very good. The theoretically predicted sizes are 53 μm, 66 μm, and 76 μm. The corresponding measured diameters are (52 to 54), (63 to 65), and 73 μm.

Larger errors (about 20%) can be expected when measuring the size at a higher visibility (80%).

Based on the above concepts, an Advanced Droplet Sizing System (ADSS) was developed. Photographs of the optics and electronics are shown in Figure 5. Very exhaustive tests are presently being conducted to establish and ensure the performance of the ADSS.

IMAX CONCEPT
FOR SPRAY CHARACTERIZATION

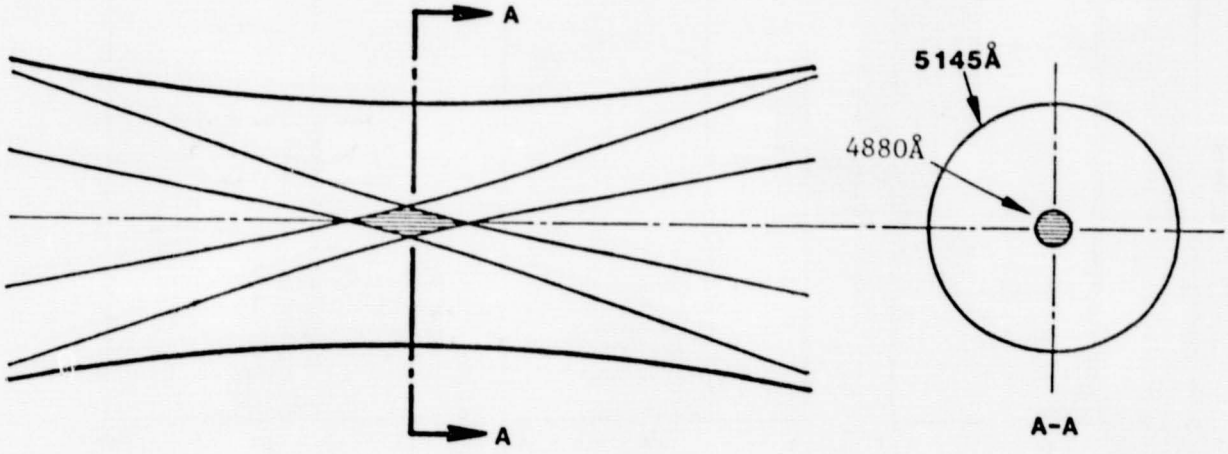

Figure 1a. Probe Volume of Two-Color IMAX Technique

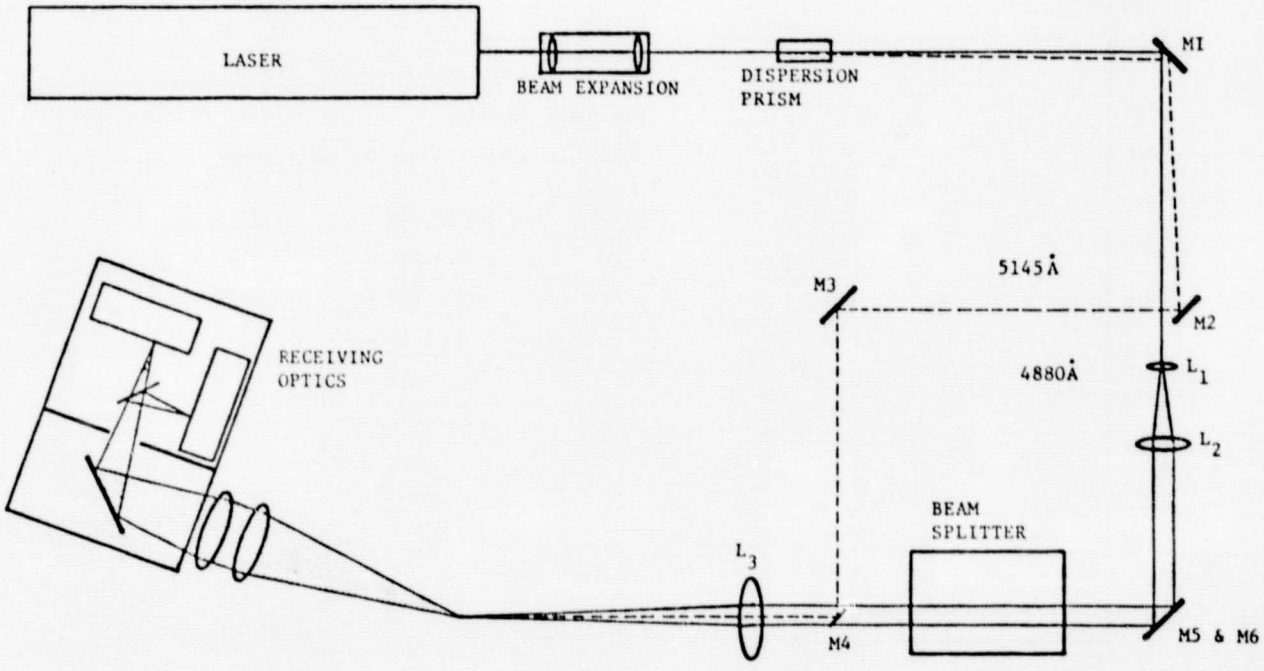

Figure 1b. Schematic IMAX Breadboard System

IMAX DROPLET SIZE MEASUREMENTS

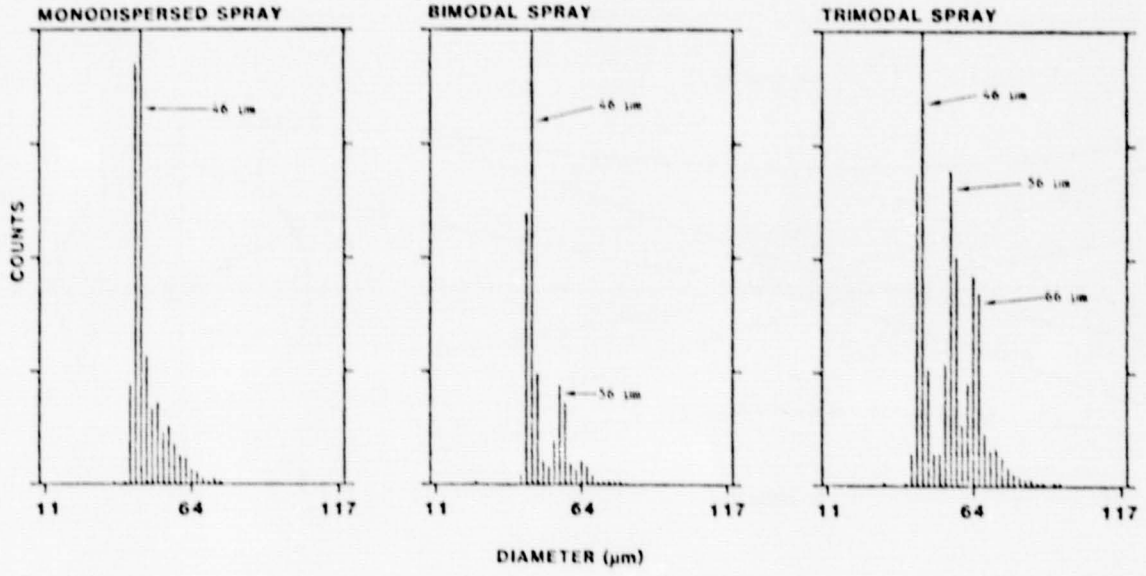

Figure 2a. Size Distribution of Spray Produced by a Berglund-Liu Generator with Dispersion Air

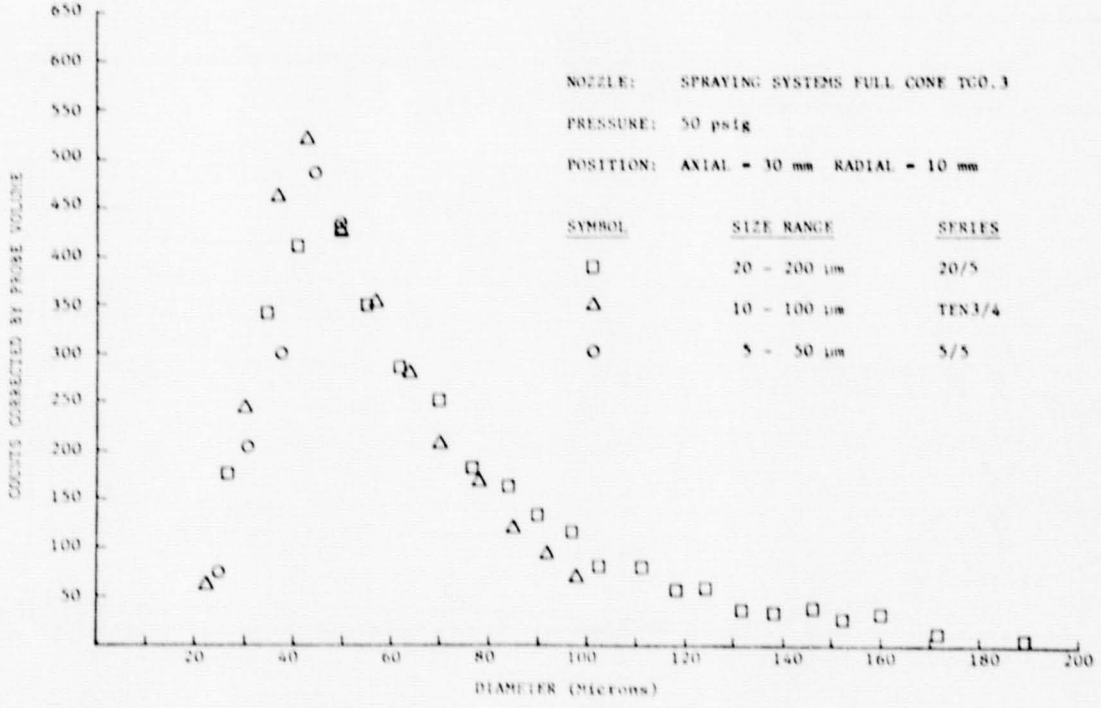

Figure 2b. Size Distribution of Spray Produced by a Pressure Nozzle

THE VISIBILITY/INTENSITY TECHNIQUE

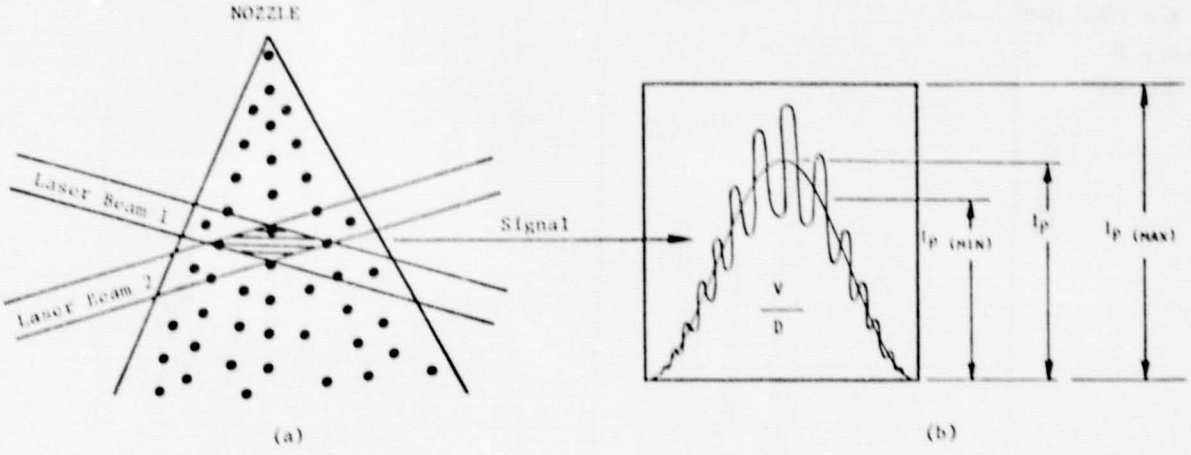

Figure 3.

SIZE DISTRIBUTIONS OF BIMODAL AND TRIMODAL SPRAYS WITH VISIBILITY AND VISIBILITY/INTENSITY

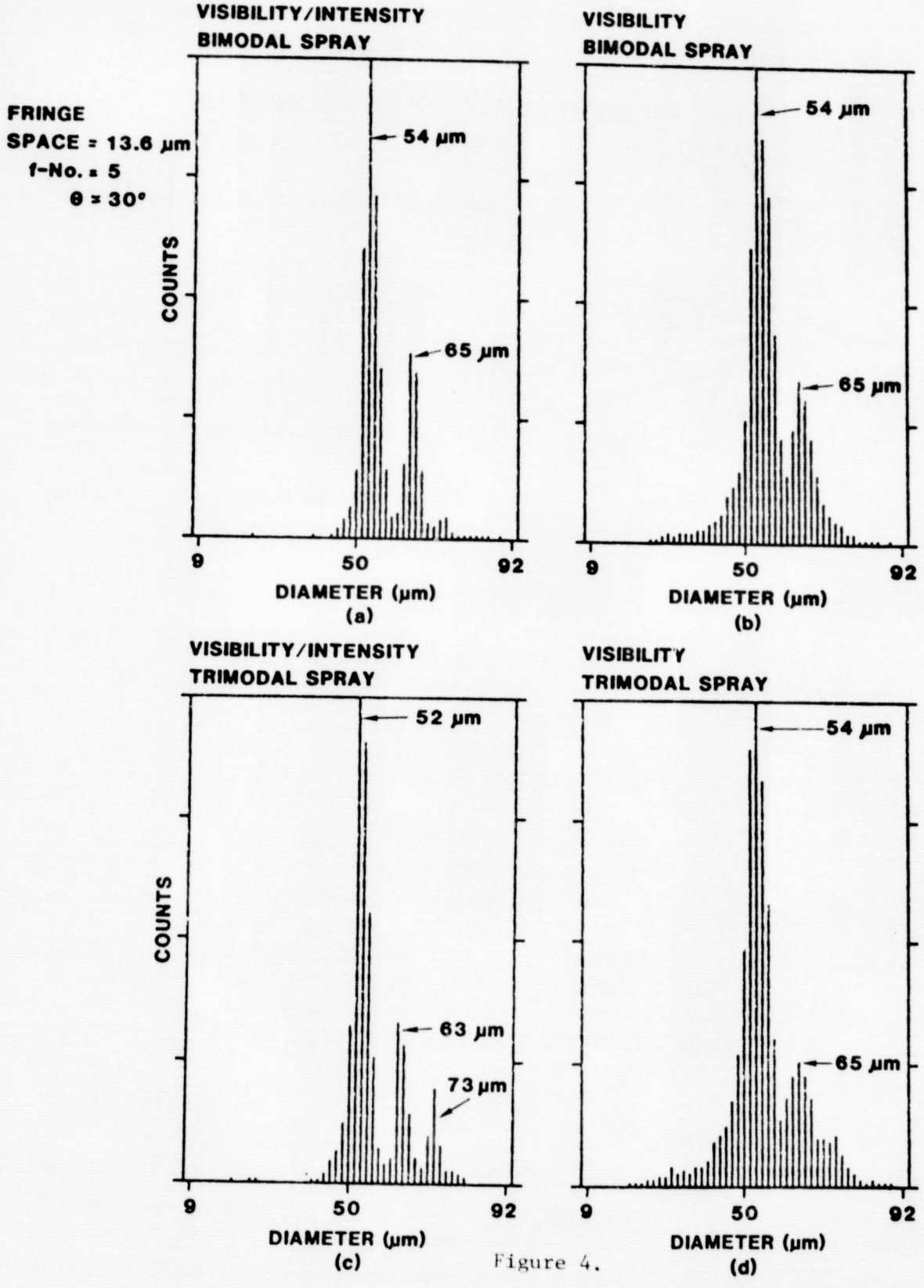

Figure 4.

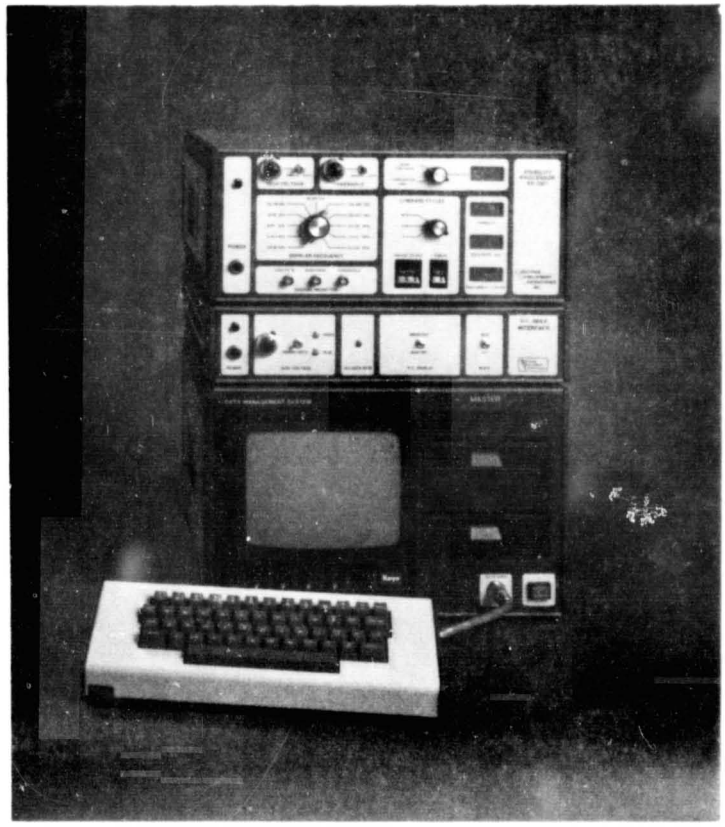

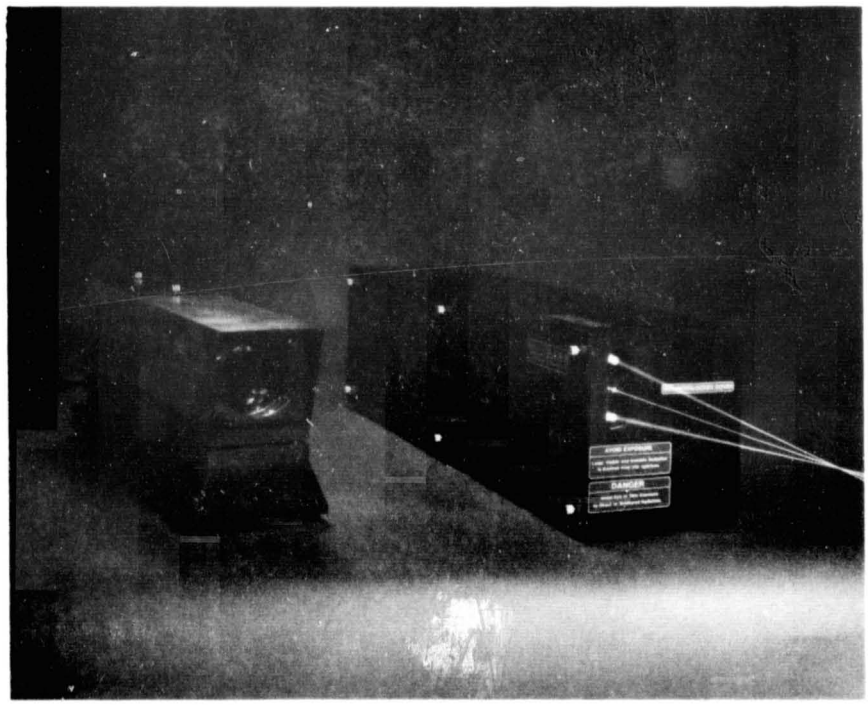

Figure 5. Electronic Components and Optical Heads of the Advanced Droplet Sizing System

D4

ANALYSIS AND TESTING OF A NEW METHOD FOR DROP SIZE AND VELOCITY MEASUREMENTS USING LASER LIGHT SCATTER INTERFEROMETRY

W. D. Bachalo
Aerometrics, Inc.

Research was conducted on a laser light scatter detection method for measuring the size and velocity distributions of spray drops. The work was motivated by the need for accurate fuel spray data in a variety of research and development activities related to combustion applications. Presently, there is considerable interest in obtaining measurements of the fuel drop and air motions within the spray combustor. It is known that the turbulent motions influence the reactions by increasing the oxygen supply to the burning fuel. Thus, the droplet size and velocity distributions are important data to be obtained when characterizing the combustion process. The need for simultaneous size and velocity measurements has been recognized for even general characterizations of sprays. This is especially true when the nozzles are operating in turbulent flow environments or when the nozzles generate drops that are moving at relatively high velocities and subsequently relax to the ambient flow speed in accord with their initial momentum.

The requirement for simultaneous measurements of drop size and velocity has led to the combination of the laser Doppler velocimeter (LDV) with various particle sizing methods[1,2,3]. However, experience has shown that the available methods are adversely affected by the measurement environment. The conditions include high drop number densities, beam attenuation by the surrounding drops and optical access ports, and the presence of small combustion generated particulate. Many of these measurement limitations have been eliminated by deriving a method that performs the measurements independent of the beam intensity.

The method consists of an optical system which is the same as a LDV except that three detectors are located at selected spacings behind the receiver aperture. Drops passing through the intersection of the two beams scatter light which produces an interference fringe pattern. The temporal frequency of the fringe pattern is the Doppler difference frequency which is linearly proportional to the drop velocity while the spatial frequency is linearly related to the drop diameter. The spacing of the fringes is also dependent upon the light wavelength, beam intersection angle, drop refractive index (unless reflected light is measured), and the location of the receiver. Measurement of the spacing of the fringe pattern produced by the scattered light may be achieved by placing pairs of detectors at selected spacings in the fringe pattern or its image. As the fringes move past the detector at the Doppler difference frequency, the detectors produce identical signals but with a phase shift proportional to the fringe spacing. The utilization of three detectors ensures that phase ambiguity does not occur, provides redundant measurements for signal validation and allows an expanded operating range while maintaining good sensitivity.

An experimental effort was conducted to verify the theoretical analysis, evaluate signal phase processing methods, and investigate the effects of signal quality upon the measurements. The optical system was arranged to provide the flexibility

needed in evaluating the parameters that influence the measurements. Only two detectors were used in the present investigations. After investigating several signal processing concepts, a breadboard processor was developed and interfaced to an IBM microcomputer. Simultaneous phase and Doppler period measurements were made and transmitted to the computer to form size and velocity distributions.

Several drop sources were used to establish the test conditions. A Berglund-Liu generator was used to produce monodisperse drop streams. The monodisperse stream could be directed through various parts of the measurement volume. Several spray nozzles were also used including pressure atomizers of moderate flow rates, high volume nozzles that produced large drops and spinning disk atomizers that produced small drops in a narrow distribution.

Initially, tests were performed using the monodisperse drops to verify the theoretical analysis. The results obtained were in complete agreement with the theory for all of the optical parameters tested. The parameters included the laser beam intersection angle, the detector spacing, and light scatter detection angle. Off-axis backscatter was also evaluated. These tests showed that the light scattered internally was measured when the drops were transparent. Dye was used to produce opaque drops which then resulted in the measurement of reflected light. Measurements based on reflected light can be made independent of the drop index of refraction.

Spray interference effects were evaluated by passing the laser beams through the spray and measuring the monodisperse drop stream. This had an insignificant effect on the measurements. The small differences observed were in most part a result of the spray interference with the monodisperse droplet stream. The effect of the attenuation of the individual laser beams was tested by attenuating one of the beams by 90%. Such attenuations can occur, for example, when large drops pass through the beams outside of the measurement volume. As expected, this had no effect on the measurements.

Sprays were measured to assess the performance of the basic system in real environments. In the first case, the spinning disk atomizer was used to generate drops in the small size range. Measurements were obtained at three size range settings and the results compared to determine the consistency of the data. The agreement was good and the mean size agreed with the results obtained with other methods. Direct comparisons were also made of the measurements obtained in a spray generated by a pressure atomizer. The data obtained by Delavan Inc. and our method showed good agreement of both the mean size and the distribution.

In summary, the recognized characteristics of the method are:

- linear relationship between the measured phase angle and drop size
- size range of approximately 100 at a single optical setting
- simultaneous size and velocity measurement
- relative insensitivity to beam or light scatter attenuation
- high spatial resolution
- operation is similar to an LDV

- adaptable to existing LDV systems
- can perform measurements independent of refractive index

An instrument is currently being developed for delivery to NASA Lewis. Development work is continuing on the refinement of the analysis, sample volume characterization, and the mass flow measurement capability. Further evaluations of the method will be made in combustion environments. The development of the technology for performing two-component velocity measurements in two-phase flows is required.

REFERENCES

1. W. M. Farmer, "Measurement of Particle Size, Number Density, and Velocity Using a Laser Interferometer," *Appl. Opt.*, rm Vol. 11, 1972, p. 2603.

2. A. J. Yule, N. A. Chigier, S. Atakan, and A. Ungut, "Particle Size and Velocity Measurement by Laser Anemometry," *AIAA 15th Aerospace Sciences Meeting*, Los Angeles, Paper no. 77-214, 1977.

3. W. D. Bachalo, "Method for Measuring the Size and Velocity of Spheres by Dual-Beam Light-Scatter Interferometry," Appl. Opt., Vol. 19, No. 3, 1980.

DEVELOPMENT GOALS

PRODUCE AN INSTRUMENT TO ACCURATELY MEASURE DROP SIZE AND VELOCITY DISTRIBUTIONS TO ADDRESS THE FOLLOWING:

- SPRAY CHARACTERIZATIONS
- SPRAY CHARACTERIZATIONS IN COMPLEX TURBULENT FLOWS
- TWO-PHASE TURBULENT FLOW MEASUREMENTS
- SPRAY DROP MEASUREMENTS IN COMBUSTION

PHASE/DOPPLER SPRAY ANALYZER

OBJECTIVE: INVESTIGATE THE CHARACTERISTICS OF A NEW METHOD FOR MEASURING THE DROP SIZE AND VELOCITY DISTRIBUTIONS IN SPRAYS

TASKS:

- PRODUCE THEORETICAL DESCRIPTIONS OF THE LIGHT SCATTERED BY SPHERES AT THE INTERSECTION OF TWO LASER BEAMS
- GENERATE THE THEORETICAL RELATIONSHIP BETWEEN THE MEASURED INTERFERENCE FRINGE PATTERN AND THE DROP SIZE
- EXPERIMENTALLY VERIFY THE THEORETICAL ANALYSIS USING MONODISPERSE DROPS
- EVALUATE SIGNAL PROCESSING METHODS
- TEST THE SELECTED PROCESSING METHOD

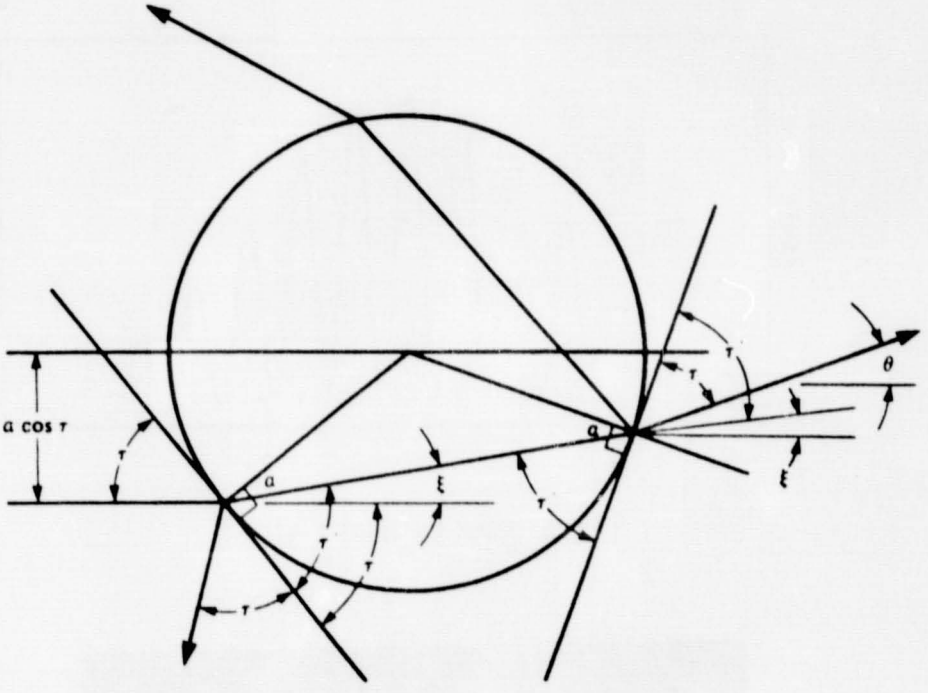

GEOMETRICAL DIAGRAM OF LIGHT RAYS SCATTERED BY A SPHERE.

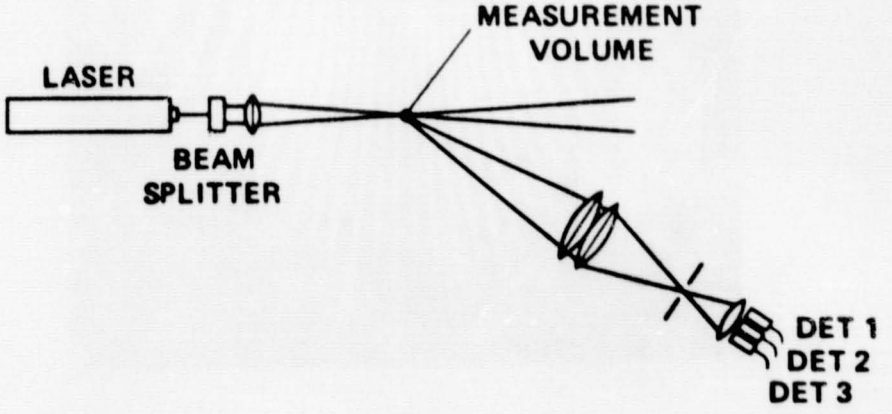

SCHEMATIC OF THE OPTICAL SYSTEM FOR AN LDV AND THE DROPLET SIZING SYSTEM.

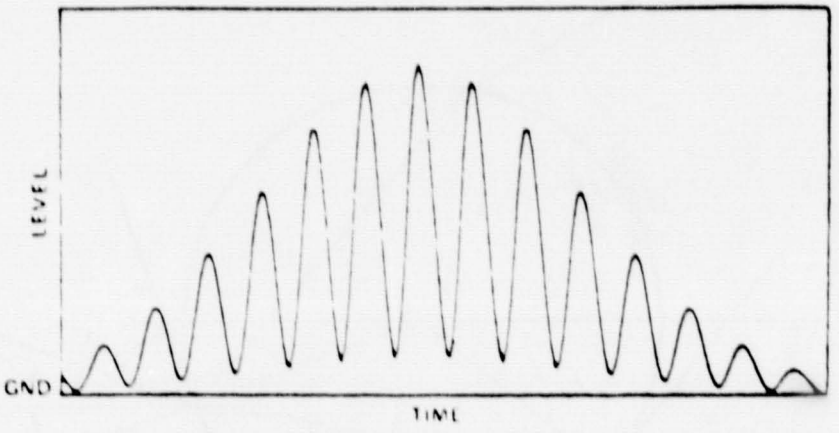

LASER DOPPLER BURST SIGNAL.

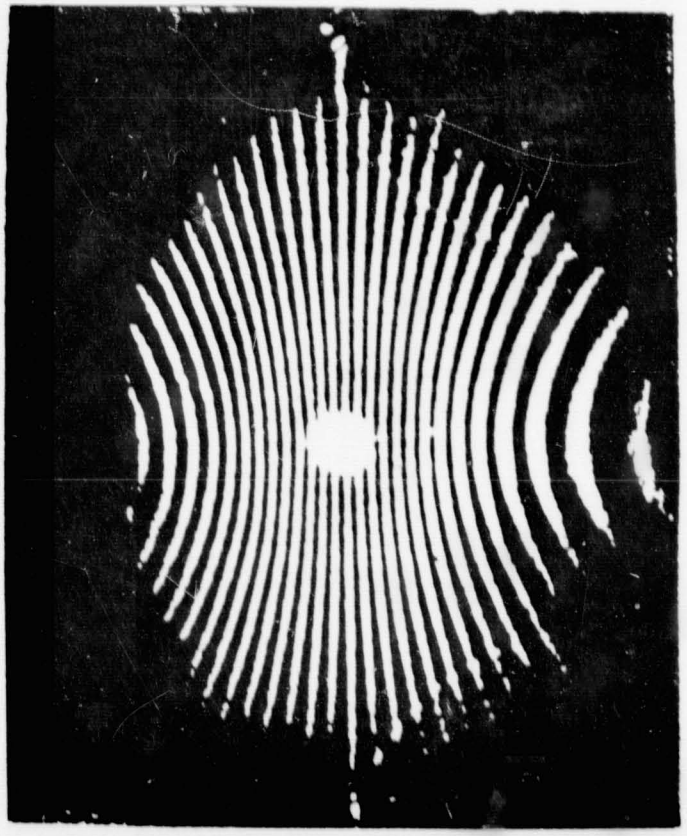

SCATTERED LIGHT INTERFERENCE FRINGE PATTERN PRODUCED BY A DROPLET.

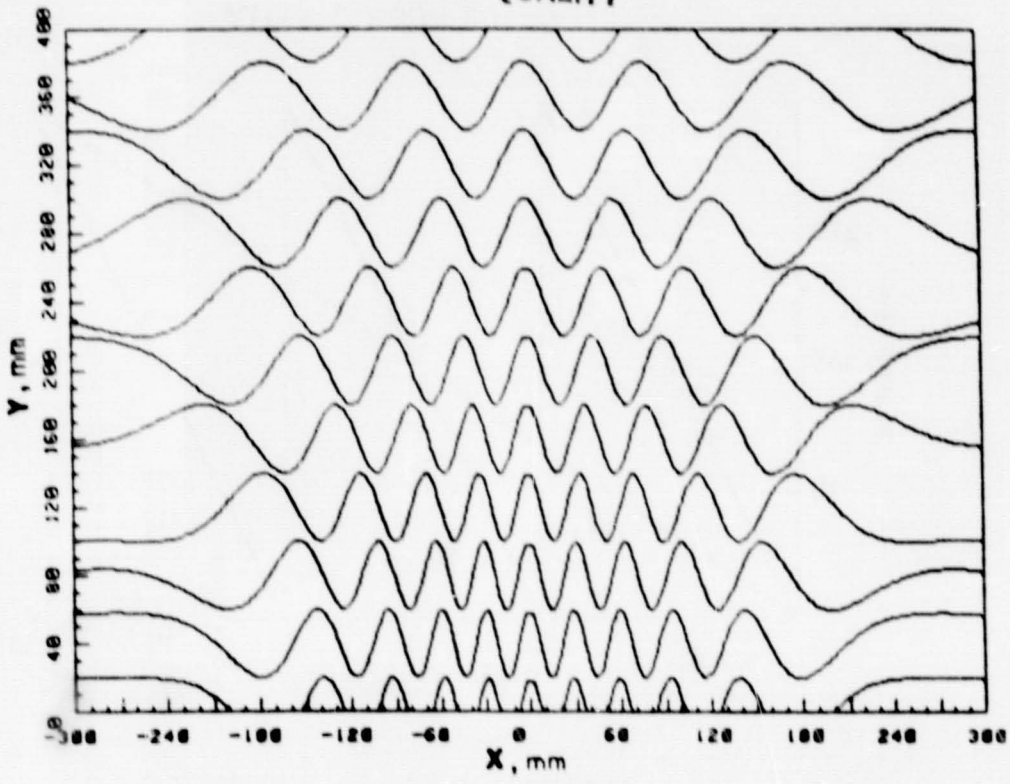

COMPUTED INTERFERENCE FRINGE PATTERN PRODUCED BY A DROPLET.

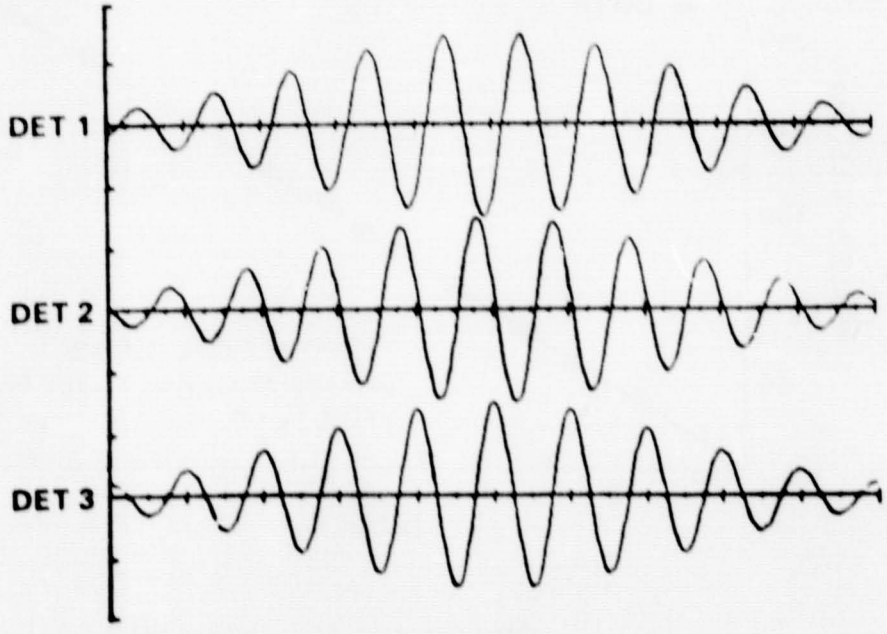

HIGH PASS FILTERED DOPPLER BURST SIGNALS ILLUSTRATING THE PHASE SHIFT BETWEEN DETECTORS.

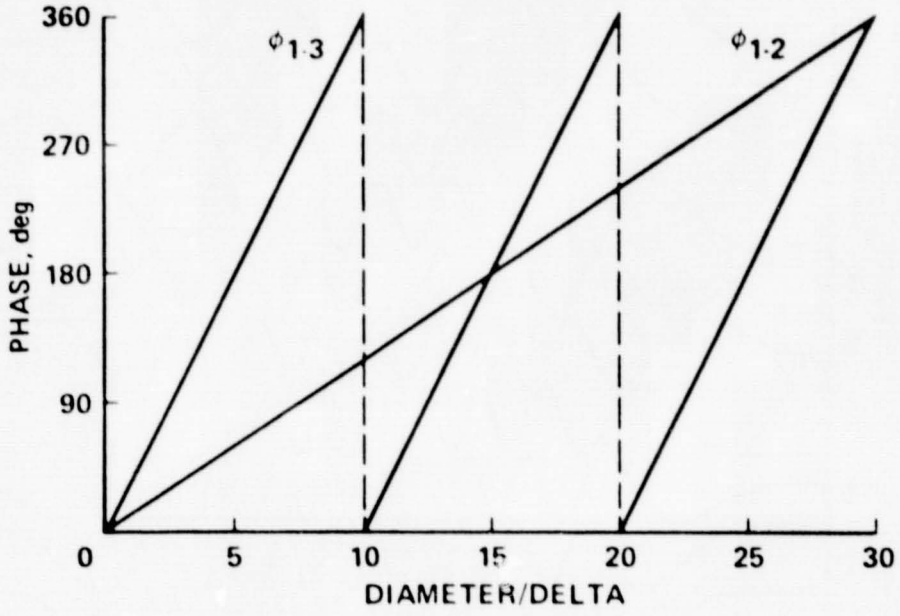

RELATIONSHIP FOR THREE DETECTORS.

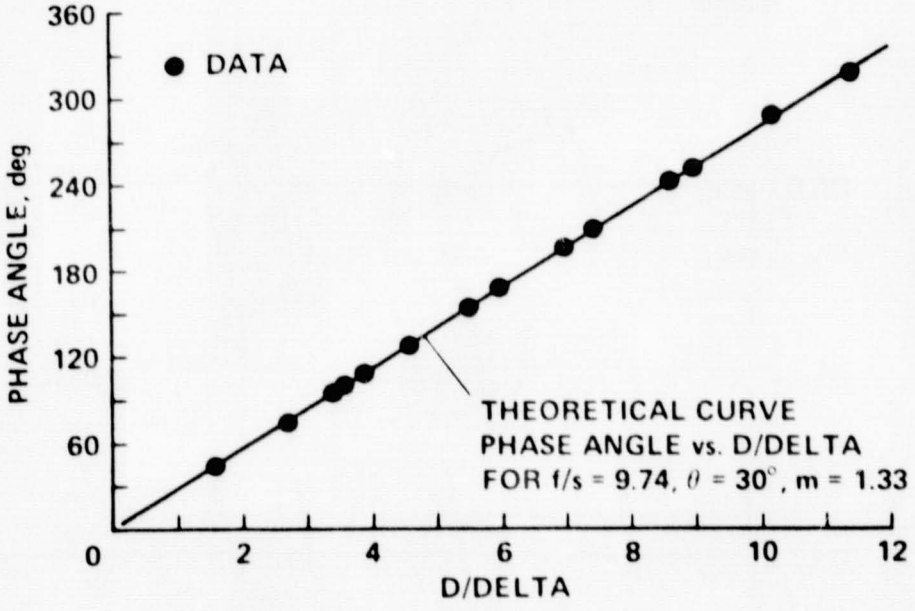

COMPARISONS WITH EXPERIMENT.

THEORETICAL PREDICTION SHOWING THE PHASE VARIATION WITH THE DIMENSIONLESS DROP SIZE.

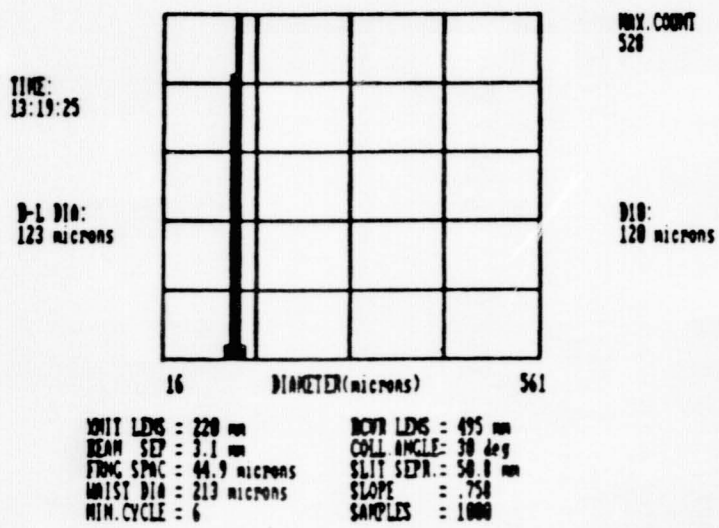

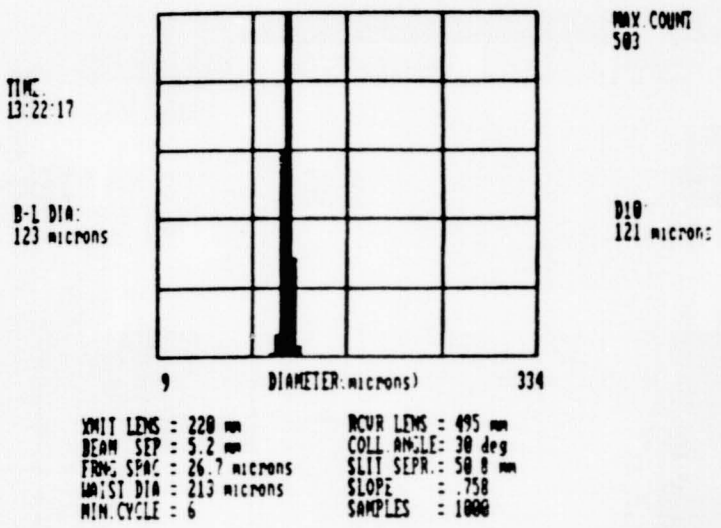

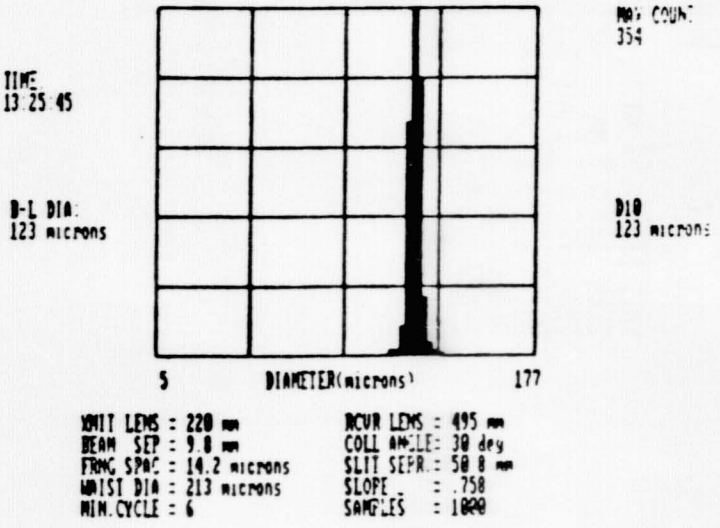

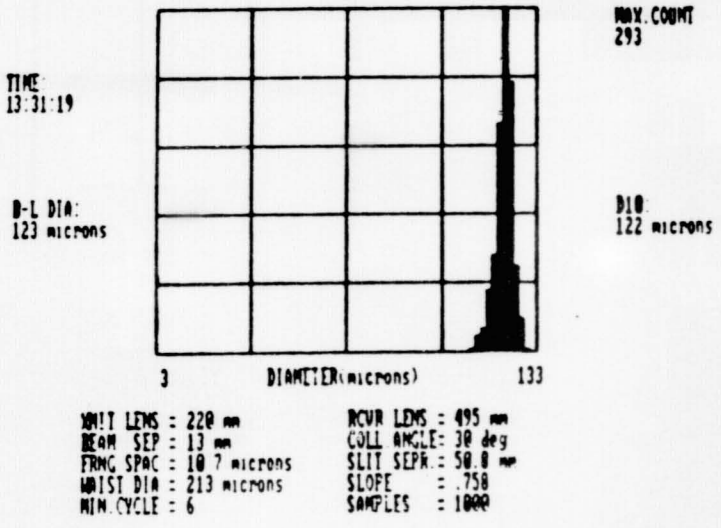

FRINGE SPACING VARIATIONS.

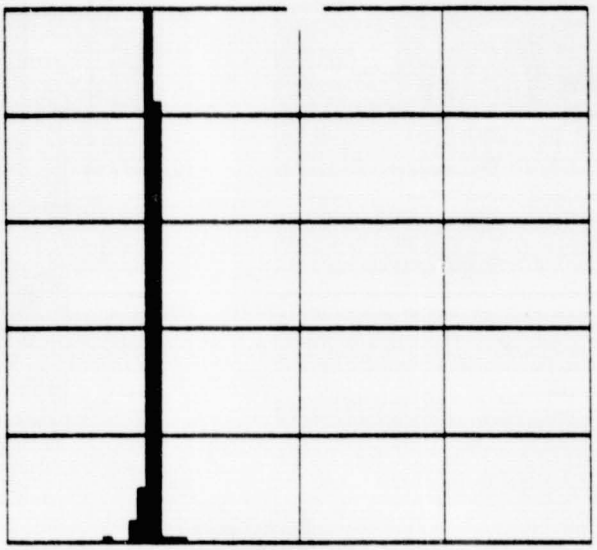

XMIT LENS = 90 mm
BEAM SEP = 8 mm
FRNG SPAC = 7.1 microns
WAIST DIA = 87 microns
MIN.CYCLE = 3

RCVR LENS = 495 mm
COLL.ANGLE= 30 deg
SLIT SEPR.= 50.8 mm
SLOPE = .758
SAMPLES = 1000

1-NEW PARAMETERS 2-REPEAT RUN 3-LIST RESULTS 4-END ? ■

MONODISPERSE DROP SIZE VARIATIONS.

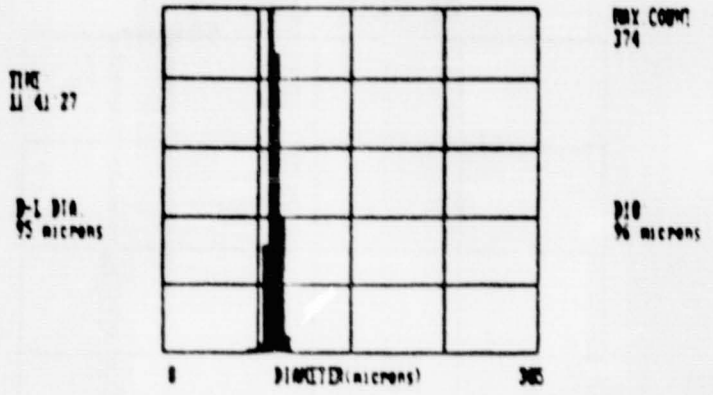

WHIT LENS : 220 mm
BEAM SEP : 11.4 mm
FRNG SPAC : 12.2 microns
MOIST DIA : 213 microns
MIN CYCLE : 6

BCKR LENS : 495 mm
COLL ANGLE : 30 deg
SLIT SEPR : 25.4 mm
SLOPE : .750
SAMPLES : 1000

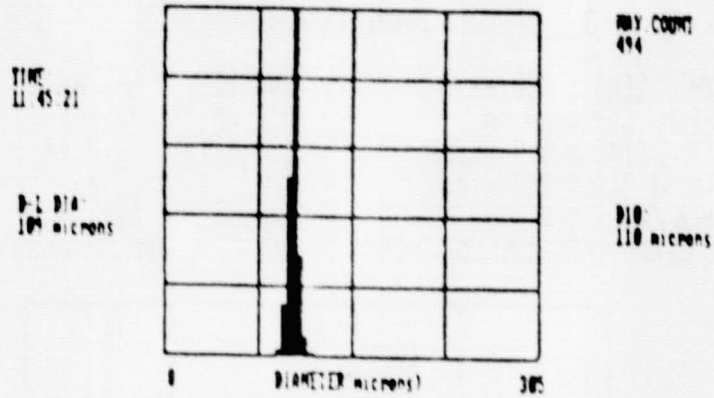

WHIT LENS : 220 mm
BEAM SEP : 11.4 mm
FRNG SPAC : 12.2 microns
MOIST DIA : 213 microns
MIN CYCLE : 6

BCKR LENS : 495 mm
COLL ANGLE : 30 deg
SLIT SEPR : 25.4 mm
SLOPE : .750
SAMPLES : 1000

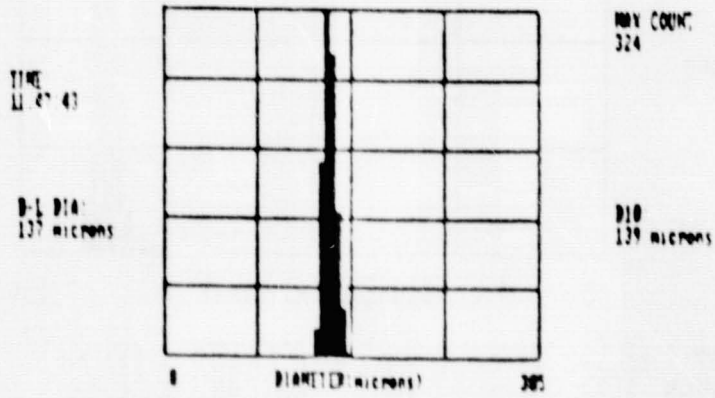

WHIT LENS : 220 mm
BEAM SEP : 11.4 mm
FRNG SPAC : 12.2 microns
MOIST DIA : 212 microns
MIN CYCLE : 6

BCKR LENS : 495 mm
COLL ANGLE : 30 deg
SLIT SEPR : 25.4 mm
SLOPE : .750
SAMPLES : 1000

MONODISPERSE DROP SIZE VARIATIONS.

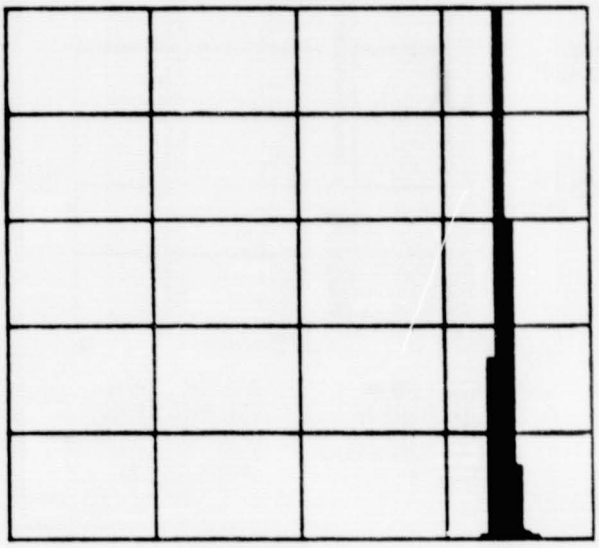

XMIT LENS = 220 mm
BEAM SEP = 14 mm
FRNG SPAC = 9.9 microns
WAIST DIA = 213 microns
MIN.CYCLE = 8
RCVR LENS = 495 mm
COLL ANGLE= 30 deg
SLIT SEPR.= 50.8 mm
SLOPE = .758
SAMPLES = 500

BEAM ATTENUATION TESTS - EQUAL BEAM INTENSITIES.

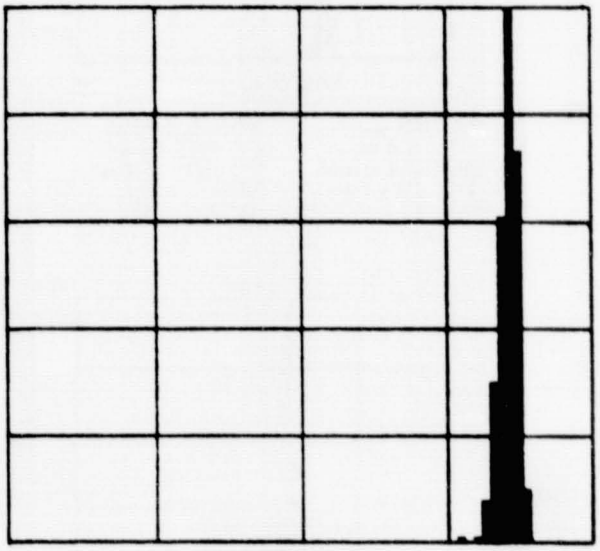

XMIT LENS = 220 mm
BEAM SEP = 14 mm
FRNG SPAC = 9.9 microns
WAIST DIA = 213 microns
MIN.CYCLE = 8
RCVR LENS = 495 mm
COLL.ANGLE= 30 deg
SLIT SEPR.= 50.8 mm
SLOPE = .758
SAMPLES = 500

BEAM ATTENUATION TESTS - ONE BEAM ATTENUATED.

(90:10 RATIO)

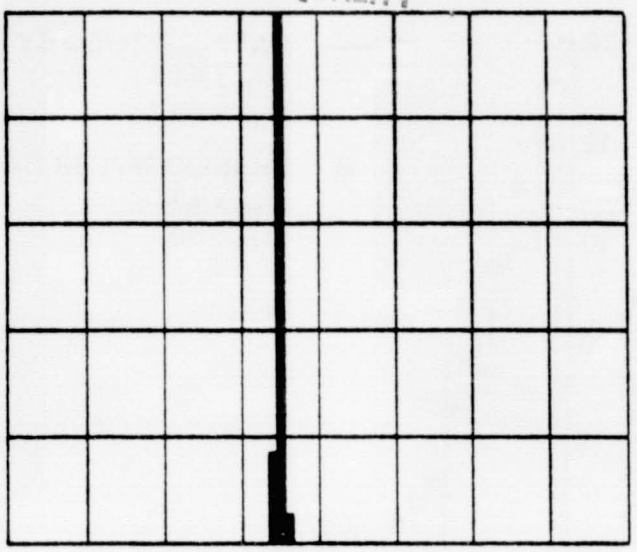

XMIT LENS = 220 mm
BEAM SEP = 18.6 mm
FRNG SPAC = 7.4 microns
WAIST DIA = 213 microns
MIN.CYCLE = 10

RCVR LENS = 495 mm
COLL.ANGLE= 150 deg
SLIT SEPR.= 50.8 mm
MAX. DIA. = 280 microns
SAMPLES = 8237

BACKSCATTER TEST - OPAQUE DROPS.

FIRST SURFACE REFLECTION.

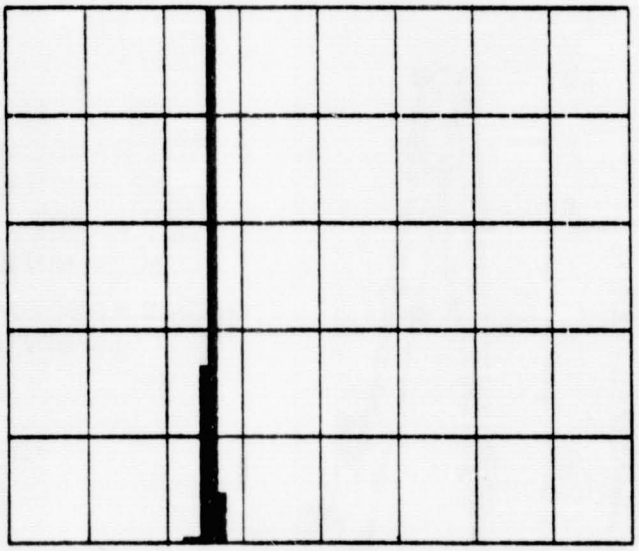

XMIT LENS = 220 mm
BEAM SEP = 5 mm
FRNG SPAC = 27.8 microns
WAIST DIA = 213 microns
MIN.CYCLE = 3

RCVR LENS = 495 mm
COLL.ANGLE= 150 deg
SLIT SEPR.= 50.8 mm
MAX. DIA. = 357 microns
SAMPLES = 1005

BACKSCATTER TEST - TRANSPARENT DROPS,

PREDICTION FOR INTERNAL REFLECTION.

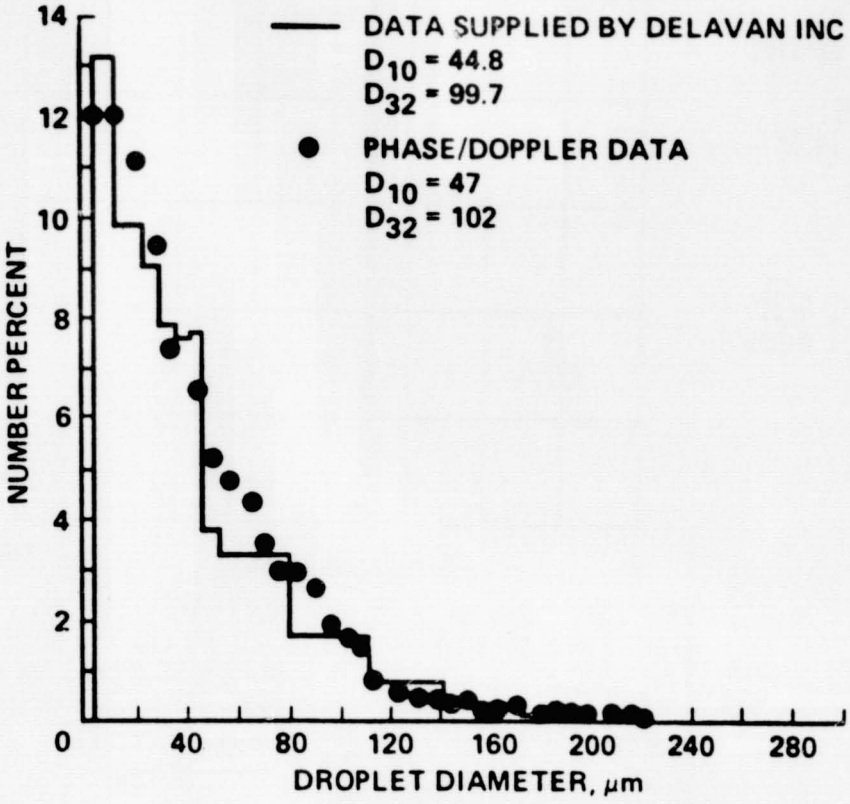

COMPARISON OF DROP SIZE DISTRIBUTIONS MEASURED WITH OTHER MEANS.

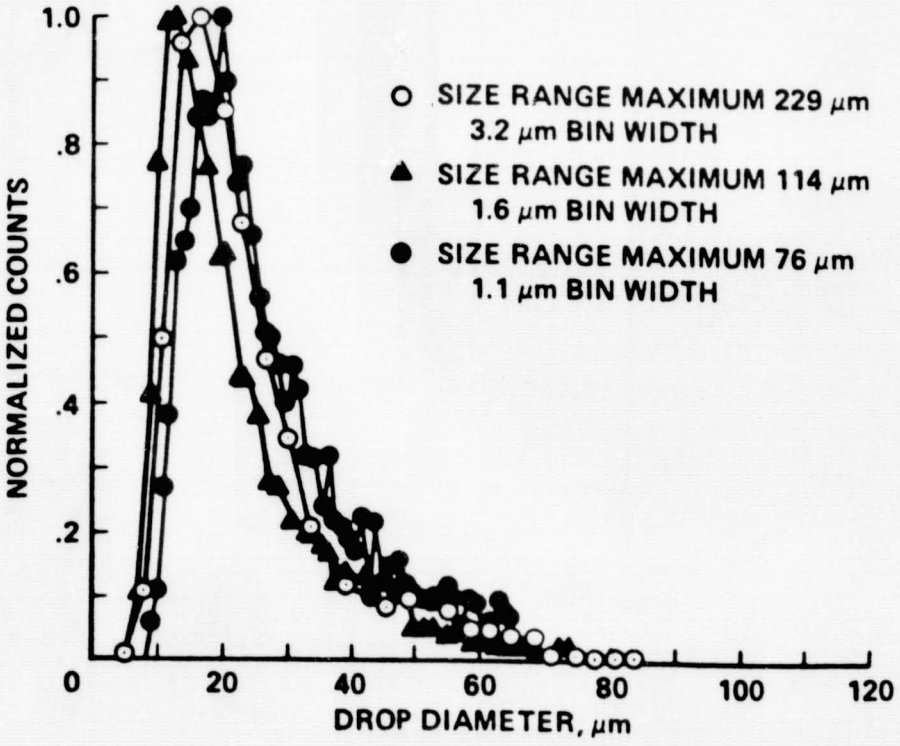

COMPARISONS OF DROP SIZE DISTRIBUTIONS MEASURED AT THREE SIZE RANGE SELECTIONS.

POTENTIAL CHARACTERISTICS OF THE METHOD

- LINEAR RELATIONSHIP BETWEEN THE MEASURED PHASE ANGLE AND DROP SIZE
- SIZE RANGE OF 30 OR GREATER AT A SINGLE OPTICAL SETTING
- OVERALL SIZE RANGE OF 3 TO 2000 MICRONS
- SIMULTANEOUS SIZE AND VELOCITY MEASUREMENTS
- RELATIVE INSENSITIVITY TO BEAM OR LIGHT SCATTER ATTENUATION
- HIGH SPATIAL RESOLUTION
- OPERATION IS SIMILAR TO AN LDV
- ADAPTABLE TO EXISTING LDV SYSTEMS
- CAN DISTINGUISH BETWEEN GAS PHASE AND DROPLETS
- REDUCED SENSITIVITY TO MISALIGNMENT
- CAN PERFORM MEASUREMENTS INDEPENDENT OF REFRACTIVE INDEX

SUMMARY

EVALUATIONS WERE CONDUCTED ON A NEW SPRAY DROP SIZE AND VELOCITY MEASUREMENT METHOD

- THEORETICAL ANALYSES OF THE LIGHT SCATTERING PHENOMENA WERE DEVELOPED
- EXPERIMENTAL TESTING VERIFIED THE ANALYSES
- MEASUREMENTS UNDER SIMULATED SPRAY CONDITIONS WERE CONDUCTED
- COMPARISONS OF SPRAY MEASUREMENTS WITH OTHER METHODS SHOWED GOOD AGREEMENT
- SIGNAL PROCESSING METHODS WERE DEFINED AND TESTED

MEASUREMENT OF SPRAY COMBUSTION PROCESSES*

C. E. Peters, E. F. Arman, J. O. Hornkohl and W. M. Farmer
Applied Physics Research Group
The University of Tennessee Space Institute

The objectives of this planned three-year investigation of spray combustion processes include the following:

(1) Making measurements of noncombusting spray fields to aid in developing adequate computational models of the dynamic interaction between the droplets and the turbulent gas phase.

(2) Making measurements of hydrocarbon-air spray flames to provide benchmark results that can be used in the verification and refinement of numerical models of the entire spray combustion process.

(3) Developing techniques for making laser measurements in typical spray combustion environments, along with techniques for acquiring, processing, displaying, and interpreting the data.

The freejet configuration selected for the experimental study is shown in figure 1. The central droplet-air jet is the exhaust from a plain-jet atomizer of the type investigated by Lorenzetto and Lefebvre (ref. 1). At a nominal air velocity of 100 m/s, the atomizer provides a Sauter mean droplet diameter of 60-80 μm. The diameter of the centerbody is 5.4 cm, the diameter of the atomizer nozzle exit is 1.27 cm, and the diameter of the outer nozzle exit is 45.7 cm. For the combustion experiments, the recirculation zone formed downstream of the centerbody acts as a flameholder.

Conventional pressure, temperature and flowrate instrumentation is used to monitor and control the experimental apparatus. The gas velocity field in the turbulent spray zone is measured with a laser velocimeter (LV) system, which yields two components of the instantaneous velocity vector of a small seed particle in the optical probe volume. A schematic diagram of the UTSI-developed LV system (ref. 2) is shown in figure 2. The relatively large droplets from the atomizer cannot be assumed to be in dynamic equilibrium with the gas phase; consequently, amplitude discrimination is used to eliminate those light-scattering events that result from large particles in the probe volume. (The diameter of the seed particles is only about 2 μm.) Using this LV technique to measure many light-scattering events for a given position of the probe volume, one can determine two components of the mean gas velocity vector as well as the variances and the covariance.

The large-droplet size and number density, along with one component of the velocity, are measured with the Particle Sizing Interferometer (PSI) technique initially proposed by W. M. Farmer (ref. 3). A schematic diagram of the PSI system developed at UTSI is shown in figure 3.

---

*NASA Grant NAG3-370

In the hydrocarbon spray combustion experiments, space and time-resolved measurements of temperature and species number density will be made with either laser-Raman or laser-fluorescence techniques. The equipment required for these measurements is already available at UTSI. These measurements will be made with the collaboration of Prof. J. W. L. Lewis.

The first year of this research program was devoted to preparing the experimental equipment. A pictorial view of the new spray combustion facility is shown in figure 4. This facility was designed, the required components were procured and/or fabricated, and the facility was installed in one of the UTSI laboratories. The outer air flow is drawn from the atmosphere by a fan located in the downleg of the facility; a variable-speed DC fan-drive motor provides well controlled bellmouth exit speeds up to approximately 11 m/s. As shown in figure 4, turning vanes and screens are used to provide a nearly uniform flow at the bellmouth entrance. The atomizer air is supplied by the UTSI low-pressure compressor system, which provides up to 0.2 kg/s of air flow at pressures up to 10 atm. After passing through a pressure regulator, the atomizer air passes through a choked venturi, which is used to provide an accurate measurement of the flow rate. The atomizer liquid (either water or hydrocarbon fuel) is supplied from a nitrogen-pressurized tank located in a heated enclosure outside the laboratory. The pressure drop across a parallel array of capillary tubes is used to determine the liquid flow rate.

Not shown in figure 4 is the optical table on which the various laser measurement systems are mounted. This table, which is located beneath the freejet test section, provides translation in three directions; a total axial travel of approximately 75 cm is available.

At present (February 1984), all subsystems of the spray combustion facility are operational. All the conventional instrumentation systems have been calibrated and the microcomputer software for processing the signals has been developed. The LV system has been installed and aligned, and all other preparations have been made for commencing the water-droplet experiments. We plan to complete the LV and PSI measurements on the water-droplet system in mid-1984. At that time, the hydrocarbon combustion experiments will be initiated.

REFERENCES

1. Lorenzetto, G. E. and Lefebvre, A. H.: Measurements of Drop Size on a Plain-Jet Airblast Atomizer. AIAA Journal, Vol. 15, No. 7, July 1977, pp. 1006-1010.

2. Farmer, W. M. and Hornkohl, J. O.: Two-Component, Self-Aligning Laser Vector Velocimeter. Applied Optics, Vol. 12, No. 11, Nov. 1973, pp. 2636-2640.

3. Farmer, W. M.: Measurement of Particle Size, Number Density and Velocity Using a Laser Interferometer. Applied Optics, Vol. 11, 1972, p. 2603.

SCHEMATIC OF COAXIAL FREEJET FLOWFIELD

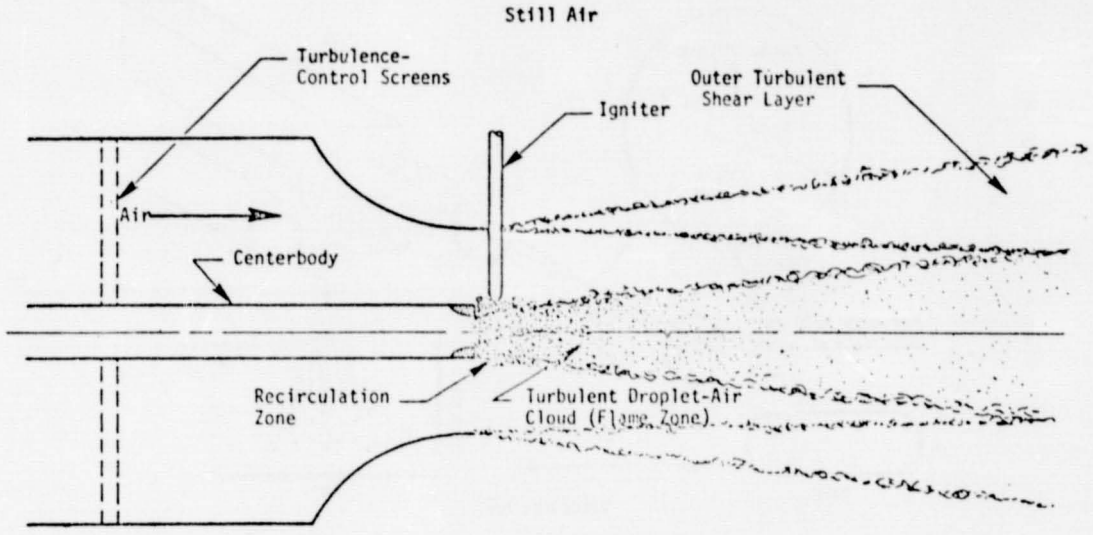

Figure 1.

SCHEMATIC DIAGRAM OF BRAGG-CELL,
FRINGE-TYPE LASER VELOCIMETER OPTICAL SYSTEM

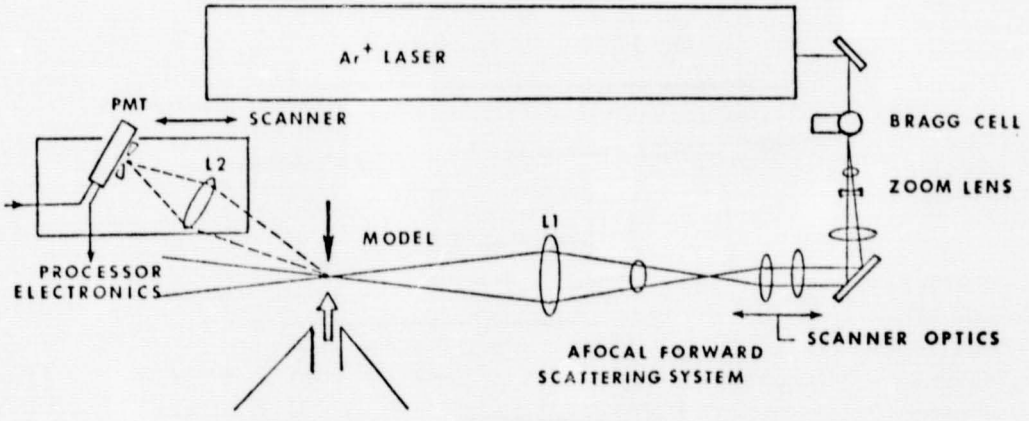

Figure 2.

SCHEMATIC DIAGRAM OF PSI OPTICAL SYSTEM

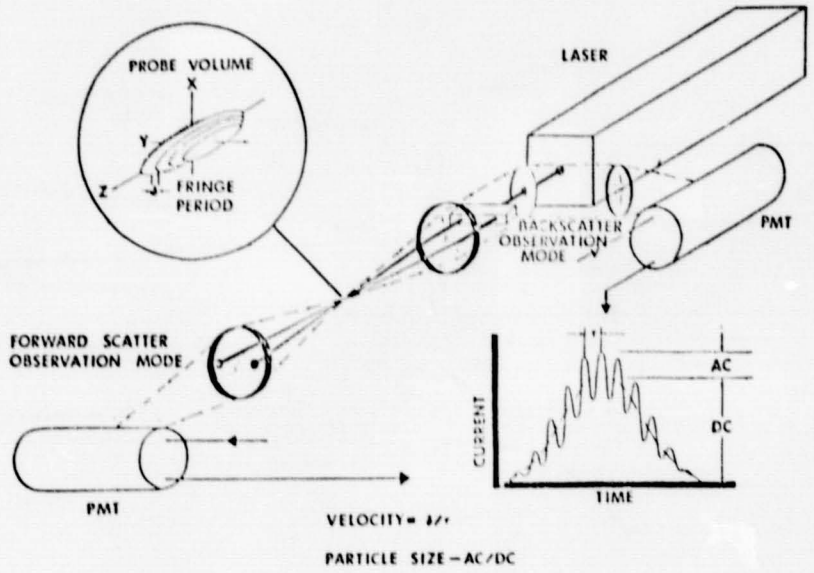

Figure 3.

PICTORIAL VIEW OF THE SPRAY COMBUSTION FACILITY

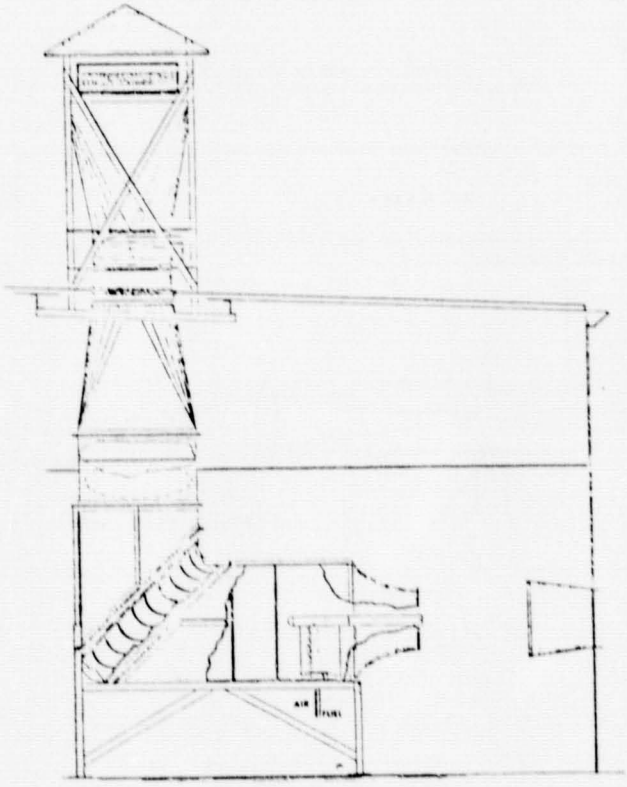

Figure 4.

D6

AUTOMATIC HOLOGRAPHIC DROPLET ANALYSIS FOR LIQUID FUEL SPRAYS*

Alan C. Stanton, Gerald W. Stewart and H. John Caulfield
Center for Chemical and Environmental Physics
Aerodyne Research, Inc.

Substantial attention has been directed toward both modeling and experimental characterization of liquid fuel sprays in order to develop a fundamental understanding of the fluid mechanical and chemical interactions which govern the combustion process in these two-phase flows (ref. 1). Two critical parameters needed to characterize spray combustion are the size and velocity distributions of the fuel spray droplets. Several laser-based optical techniques, including scattered intensity, laser interferometry, and laser velocimetry, have been applied in recent years to measurements in fuel sprays (ref. 2). An alternative approach is holographic analysis of sprays, in which the three dimensional spatial distribution of droplets is recorded in a hologram for subsequent analysis (ref. 3). For such an approach to be practical, however, an automated system for analysis of the holograms is required. The goal of the present research program is to demonstrate an automated approach for droplet hologram analysis and to identify critical requirements for adaptation of this technique to measurements in spray combustion systems.

The basic scheme for automated holographic analysis involves an optical system for reconstruction of the three-dimensional real image of the droplet field, a spatial scanning system to transport a digitizing x-y image sensor through the real image, and processing algorithms for droplet recognition which establish the droplet sizes and positions. The hardware for this system is straightforward. In the present demonstration experiment, we are utilizing the expanded and collimated beam from a 5 mW helium-neon laser for hologram reconstruction, an imaging lens for magnification of the real image field, and a video camera and digitizer providing 512-by-512 pixel resolution with 8-bit digitization. A mechanical stage is used to scan the hologram in three-dimensional space, maintaining constant image magnification. A test droplet hologram provided by Dr. Michael Farmer of the University of Tennessee Space Institute is used for development and testing of the image processing algorithms.

For the case of fuel sprays, where the liquid droplets may be assumed spherical, the image processing problem is simplified in that there is no rotational degree of freedom, and special edge-tracking algorithms for tracing the boundary of complicated shapes are not required. The problem reduces to one of recognizing droplets by comparing pixel intensities against a threshold level which is selected on the basis of the average droplet and background intensities. The droplet location in three dimensional space is then established by finding the position of best focus in the image field. We are studying two approaches for finding the best focus. In the simpler approach, the droplet image areas are

*Work performed under Contract No. NAS3-24094 with G. Neeley of NASA Lewis Research Center as program monitor.

determined at successive image planes by counting the number of pixels above threshold. The plane with the smallest image area is the best focal plane. The second approach, which is expected to be more sensitive, analyzes intensity gradients by examining intensity differences between adjacent pixels at the image boundary. The image plane with the sharpest intensity gradients is chosen as the plane of best focus.

An extension of this technique, which we anticipate will be explored in a future phase of the program, is the determination of droplet velocities and trajectories by the use of multiple exposure holograms (ref. 4). In this approach, a pulsed laser is used to create a hologram by two or more exposures at well-known intervals. The droplet image locations in the reconstructed hologram are determined using the boundary-defining algorithms described above. Finally, statistical pattern recognition techniques would be used to associate droplet image locations at later times with their locations at earlier times.

REFERENCES

1. Chigier, N.: Group Combustion Models and Laser Diagnostic Methods in Sprays: A Review. Combust. and Flame, Vol. 51, No. 2, June 1983, pp. 127-129.

2. Mularz, E.J.; Bosque, M.A.; and Humenik, F.M.: Detailed Fuel Spray Analysis Techniques. NASA TM-83476, 1983.

3. Thompson, B.J.: Holographic Particle Sizing Techniques. J. Phys. E: Sci. Instrum., Vol. 7, 1974, pp. 781-788.

4. Boettner, E.A.; and Thompson, B.J.: Multiple Exposure Holography of Moving Fibrous Particulate Matter in the Respiratory Range. Opt. Eng., Vol. 12, No. 2, March/April, 1973, pp. 56-59.

DROPLET MEASUREMENT TECHNIQUES FOR SPRAY COMBUSTION

GOAL: CHARACTERIZATION OF DROPLET SIZE AND VELOCITY DISTRIBUTIONS IN FUEL SPRAYS

APPROACHES:

- IN-SITU LASER MEASUREMENTS
  - SCATTERED INTENSITY
  - "INTERFEROMETRY"
  - LASER DOPPLER VELOCIMETRY
- HOLOGRAPHY
  - 3-D RECORDING MEDIUM: DROPLET SIZE AND POSITIONS
  - AUTOMATED ANALYSIS SYSTEM REQUIRED FOR TECHNIQUE TO BE PRACTICAL

AUTOMATED DROPLET HOLOGRAM ANALYSIS

1. RECONSTRUCT HOLOGRAM TO OBTAIN REAL IMAGE OF 3-D DROPLET FIELD

2. USE VIDEO CAMERA AND DIGITIZER AND COMPUTER-CONTROLLED MECHANICAL STAGES TO DIGITIZE X-Y IMAGE PLANES ALONG Z DIMENSION

3. USE IMAGE PROCESSING ALGORITHMS FOR DROPLET RECOGNITION AND LOCATION

APPARATUS FOR AUTOMATED ANALYSIS OF DROPLET HOLOGRAMS

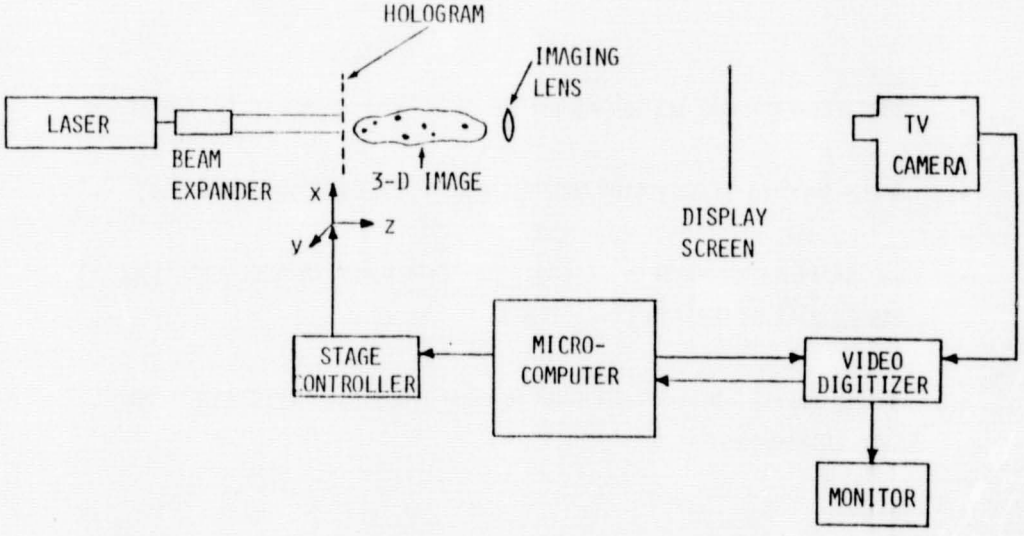

DROPLET BOUNDARY RECOGNITION ALGORITHMS

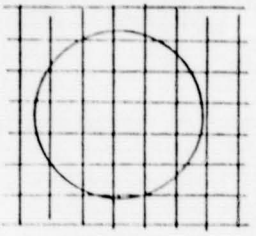

INTENSITY SCANNING

- COMPARE PIXEL INTENSITIES AGAINST THRESHOLD LEVEL FOR DROPLET RECOGNITION
- OBTAIN DROPLET AREAS BY COUNTING NUMBER OF PIXELS ABOVE THRESHOLD
- BEST FOCAL PLANE IS PLANE OF MINIMUM AREA

EDGE GRADIENTS

- DEFINE DROPLET EDGES BY COMPARISON OF INTENSITIES OF ADJACENT PIXELS
- BEST FOCAL PLANE IS PLANE WITH SHARPEST EDGE GRADIENTS

MULTIPLE-EXPOSURE HOLOGRAPHY

- MULTIPLE-EXPOSURE HOLOGRAMS MAP DROPLET DISPLACEMENTS IN 3-D SPACE
- APPLY DROPLET RECOGNITION ALGORITHMS TO FIND DROPLET LOCATIONS
- USE STATISTICAL PATTERN RECOGNITION TECHNIQUES TO ASSOCIATE DROPLET IMAGES AT EARLIER AND LATER TIMES
- OBTAIN DROPLET VELOCITIES FROM MEASURED DISPLACEMENTS AND KNOWN TIME INTERVALS

PREDICTIONS OF SPRAY COMBUSTION INTERACTIONS*

J-S. Shuen, A.S.P. Solomon and G. M. Faeth

The Pennsylvania State University

Measurements were completed in dilute particle-laden jets, nonevaporating sprays and evaporating sprays injected into a still air environment. The flows are stationary, turbulent, axisymmetric and conform to the boundary layer approximations while having well-defined initial and boundary conditions--to facilitate use of the data for evaluation of analysis of the processes. Mean particle (drop) sizes were in the range 2-210 microns over the entire data base. The following measurements were made (as appropriate for the flow): mean and fluctuating phase velocities; mean particle mass flux; particle size; and mean gas-phase Reynolds stress, composition and temperature. Three models of the processes, typical of current practice, were evaluated using both existing and the new data: (1) a locally homogeneous flow (LHF) model, where interphase transport rates are assumed to be infinitely fast; (2) a deterministic separated flow (DSF) model where finite interphase transport rates were considered but effects of turbulence/drop interactions were ignored; and (3) a stochastic separated flow (SSF) model where effects of finite interphase transport rates and turbulent fluctuations were treated using random sampling for turbulence properties in conjunction with random-walk computations for particle (drop) motion. All three models used a k-ε-g model for the continuous phase--which performed well in earlier studies of single-phase jets. The LHF and DSF models did not provide very satisfactory predictions over the present data base. In contrast, the SSF model generally provided good predictions and appears to be an attractive approach for treating nonlinear interphase transport processes in turbulent flows containing particles (drops). Current work is considering measurements and analysis of combusting sprays.

INTRODUCTION

The main objective of this investigation was to complete measurements of the structure of dilute particle-laden jets and sprays in order to support development of analysis of these processes. Test configurations involved injection into still air, yielding stationary, turbulent, axisymmetric flows, having well-defined initial and boundary conditions, which conform to the boundary layer approximations. The complexity of interphase transport was increased systematically, considering particle-laden jets, nonevaporating sprays, evaporating sprays and combusting sprays, in turn. In order to insure that appropriate measurements were made, model development was also

*NASA Grant No. NAG3-190 with R. Tacina of Lewis Research Center serving as NASA Scientific Officer.

undertaken--considering methods typical of current practice. The results of the study have application to the development of rational design methods for aircraft combustion chambers as well as other devices involving spray evaporation and combustion.

The following description of the study is brief. Full details and a complete tabulation of data can be found in papers, reports and theses completed under the study (refs. 1-11). Studies of sprays and particle-laden jets have recently been reviewed by one of us (refs. 12 and 13) and this discussion will not be repeated here. Based on these reviews, and others cited therein, there is general agreement that a most pressing need for gaining a better understanding of spray processes is the creation of a well-defined set of measurements of the structure of these flows--motivating the present investigation.

In the following, experimental and theoretical methods are described first of all. This is followed by a discussion of results already completed for particle-laden jets, nonevaporating sprays and evaporating sprays. The paper concludes with a brief discussion of current work being undertaken in combusting sprays.

EXPERIMENTAL METHODS

Test Apparatus

The same test configuration was used for the particle-laden jets and nonevaporating and evaporating sprays, cf., figure 1. The injector was directed vertically downward within a screened enclosure. The injector and enclosure were traversed, since optical instrumentation was mounted rigidly. An exhaust system was used, to prevent recirculation of fine particles, however, its operation had negligible influence on flow properties at the measuring station.

Test conditions are summarized in tables I and II for the particle-laden jets and the sprays, respectively. In each case, an air jet from the same injector was also tested, in order to establish test procedures by comparison with existing measurements. The particle-laden jets were essentially monodisperse with particle diameters in the range 79-207 microns while the sprays had Sauter mean diameters (SMD) in the range 30-87 microns. In general, measurements were confined to dilute regions of the flow where void fractions exceeded 99%. All the flows were turbulent, with initial jet Reynolds numbers exceeding 10000.

Instrumentation

A single-channel laser-Doppler anemometer (LDA) was used to measure mean and fluctuating velocities of the continuous phase. High concentrations of seeding particles were used to avoid biasing due to flow particles (in the following, "particle" is used to represent "drop" unless the distinction is important). Data densities were high so that measured quantities could be time-averaged. The LDA was also used to obtain mean and fluctuating particle

velocities in the particle-laden jets--after terminating the flow of seeding particles.

Double-flash photography was used to check LDA measurements of particle properties in particle-laden jets and to measure drop size and velocity correlations in the sprays. Drop size distributions obtained in this manner were corrected for depth-of-focus bias. Drop size distributions were also measured by slide impaction--corrected for Reynolds number bias. Finally, a Malvern particle sizer, which operates by Fraunhoffer diffraction of a laser beam, was used to monitor drop size distributions in the nonevaporating sprays, however, this instrument was ineffective in the evaporating sprays due to beam steering by gas-phase density gradients.

Mean particle mass flux and liquid flux in the nonevaporating sprays were measured by isokinetic sampling at the mean gas velocity using a diverging probe. Isokinetic sampling with a heated probe, followed by analysis with a gas chromatograph, was used to measure mean total Freon-11 concentrations in the evaporating sprays. A shielded fine wire (25 micron diameter) thermocouple was used to measure mean gas-phase temperatures in the evaporating sprays. An impact plate was used to measure injector thrust.

Measurements in the particle-laden jets were conducted for $x/d = 1$-50, where x is distance from the injector and d is the injector diameter. Adequate spatial resolution for the sprays could only be achieved for $x/d = 50$ with measurements extending to $x/d = 500$-600, due to the small exit diameter of the injector. For all test conditions, baseline calibration tests were conducted to establish predictions of transport rates to individual particles (drops).

THEORETICAL METHODS

General Description

Three models were considered: (1) a locally homogeneous flow (LHF) model where interphase transport rates are assumed to be infinitely fast; (2) a deterministic separated flow (DSF) model where finite interphase transport rates were considered but effects of turbulence/drop interactions were ignored; and (3) a stochastic separated flow (SSF) model where finite interphase transport rates and interactions between drops and turbulent fluctuations were treated using random sampling for turbulence properties in conjunction with random-walk computations for particle (drop) motion. A k-ε-g model was used to find properties of the continuous phase for all three models, since this approach provided good structure predictions for single-phase jets (ref. 12). The test conditions correspond to steady, turbulent, axisymmetric boundary layer flows having low Mach numbers where effects of viscous dissipation of the mean flow and radiation are small. Other assumptions vary for the LHF, DSF and SSF models and will be treated separately in the following.

LHF Model

The LHF approximation implies that both phases have the same velocity and are in local thermodynamic equilibrium at each point in the flow--which is only

exact for infinitely-small particles. Therefore, the flow corresponds to a single-phase fluid with an unusual equation of state due to the presence of particles. The analysis employed Favre (mass)-averaged governing equations in conjunction with the conserved-scalar formalism of Bilger (ref. 14). This procedure eliminates ad hoc neglect of density velocity correlations and effects of buoyancy in the governing equations for turbulence quantities. The relationship between scalar properties and mixture fraction, needed by this approach, followed past practice in this laboratory (ref. 13). The LHF model does not require detailed information concerning initial drop sizes and velocities; therefore, LHF calculations were begun at the injector exit.

DSF Model

Both separated flow models adopt the features of the LHF model for the gas phase. The dispersed phase was treated by solving Lagrangian equations of motion for the particles and then computing source terms for interphase transport which appear in the governing equations for the gas phase. This involves dividing the particles into a number of groups at the initial condition and then computing their subsequent motion.

Void fractions in the region of computation always exceeded 99%; therefore, the dispersed phase volume, particle collisions and effects of adjacent particles on interphase transport rates could be ignored with little error. Ambient conditions for particles were taken to be local mean gas properties; therefore, effects of turbulent fluctuations on interphase transport, turbulent dispersion and turbulence modulation were ignored--typical of most current spray models (ref. 13). Effects of varying local ambient conditions, however, were considered.

SSF Model

The SSF model treats turbulence/drop interactions by computing drop trajectories as they move away from the injector and encounter a succession of turbulent eddies--using Monte Carlo methods. Properties within each eddy are assumed to be uniform, but to change in a random fashion from one eddy to the next. Trajectory calculations are the same as the DSF model, except that instantaneous eddy properties replace mean gas properties. Eddy properties are found by making a random selection from the probability density functions (PDF) of velocity and mixture fraction. A drop is assumed to interact with an eddy as long as its relative displacement with respect to the eddy is less than a characteristic eddy size and its time of interaction is less than a characteristic eddy lifetime. All these parameters are directly found from the k-ε-g computations.

RESULTS AND DISCUSSION

Particle-Laden Jets

Initial evaluation of the models was undertaken using existing measurements in the literature (refs. 1,2). It was found that the LHF model

was only effective for flows containing tracer-sized particles, that the DSF model was not effective for any flow, and that the SSF model yielded encouraging predictions of flow structure and particle dispersion. The evaluation was not definitive, however, due to uncertainties in initial conditions for existing measurements.

Initial conditions were fully defined for present tests with particle-laden jets--removing earlier limitations. Typical structure measurements and predictions are illustrated in figures 2-6 (u and v are axial and radial velocities, G is particle mass flux and subscripts o and c denote initial and centerline conditions). In figure 2, the agreement between predicted and measured velocities in the gas jet is good--establishing a baseline for the work. The LHF and SSF predictions are nearly identical and are also in good agreement with measurements. Particle velocities, illustrated in figure 3, exhibit more significant effects of the model. The LHF approach underestimates particle velocities since effects of slip are ignored while the SSF model yields good results. Results for centerline particle mass flux, illustrated in figure 4, are similar.

Radial variations of gas and particle properties are illustrated in figures 5 and 6. All gas-phase predictions are similar and are in reasonably good agreement with measurements, however, only the SSF model yields good predictions of mean and fluctuating particle properties. The DSF model underestimates particle spread rates, since effects of turbulent dispersion are ignored while the LHF model overestimates spread rates since slip is ignored.

The flows were too dilute to test predictions of turbulence modulation by the SSF model. Sensitivity studies showed that predictions were most sensitive to initial particle properties.

Nonevaporating Sprays

A portion of the results for nonevaporating sprays is illustrated in figures 7-12. In this case, the LHF predictions are initiated at the injector exit while the separated flow model predictions are initiated at $x/d = 50$, where adequate initial conditions could be measured. Results for mean gas velocities and liquid fluxes along the centerline (figures 7 and 8) are similar: the SSF model yields good predictions while the LHF model overestimates the rate of development of the flow. SMD variation along the axis is illustrated in figure 9. The SMD increases gradually along the axis, due to turbulent drop dispersion. The SSF model correctly predicts this trend while the DSF model yields an opposite trend since turbulent dispersion is ignored.

Radial profiles of mean liquid flux are illustrated in figure 10. Turbulent dispersion of drops causes these flows to extend beyond $r/x = 0.2$, which is the usual boundary for a single-phase jet. The SSF model correctly predicts this trend--which is an encouraging finding--while the other models are unsatisfactory.

Radial profiles of mean drop velocity for the case 1 spray and the SMD of both sprays are illustrated in figures 11 and 12. The correlation between drop

size and velocity is predicted reasonably well by the SSF model--as is the SMD variation.

Turbulence modulation was again not an important factor in these sprays and could not be adequately evaluated. Specification of initial drop properties was found to have the greatest influence or predictions.

Evaporating Sprays

A portion of the findings for evaporating sprays is illustrated in figures 13-16. Tends are qualitatively similar to results for nonevaporating sprays, however, differences between the models are somewhat reduced due to effects of drop evaporation.

Combusting Sprays

Current tests and analysis are extending results to combusting sprays. Initial tests are limited to dilute conditions where the flame is primarily fueled by gas (methane) with a monodisperse stream of drops in coflow with the gas fuel. This system simplifies measurements and the presentation of results and allows greater concentration on the interesting fundamental problem of drop/combusting turbulent flow interactions. Subsequent work will consider flames fully fueled with polydisperse sprays.

CONCLUSIONS

Major conclusions are: (1) the SSF model provides a useful approach for treating turbulence/drop interactions in particle-laden flows and sprays with minimal empiricism and a capability to treat nonlinear effects; (2) the LHF model is a useful simplification for very well-atomized sprays (particle/drop size less than 10 μm) but effects of slip are important for most practical sprays; and (3) the DSF model was not effective for any of the flows examined here, since effects of turbulent particle dispersion and effects of turbulent fluctuations on interphase transport rates are important in most practical sprays.

Specification of initial conditions is the most critical aspect of spray structure predictions. Effects of turbulence modulation were small for present flows, and current SSF model treatment of this phenomenon could not be evaluated decisively. Current work is extending the data base and the model evaluation to dilute combusting sprays.

REFERENCES

1. Shuen, J-S.; Chen, L-D.; and Faeth, G. M.: Evaluation of a Stochastic Model of Particle Dispersion in a Turbulent Round Jet. AIChE J., vol. 29, 1983, pp. 167-170.

2. Shuen, J-S.; Chen, L-D.; and Faeth, G. M.: Predictions of the Structure of Turbulent, Particle-Laden Round Jets. AIAA J., vol. 21, 1983, pp. 1483-1484. Also AIAA Paper No. 83-0066, 1983.

3. Solomon, A.S.P.; Shuen, J-S.; Zhang, Q-F.; and Faeth, G. M.: Measurements and Predictions for Nonevaporating Sprays in a Quiescent Environment. AIAA Paper No. 83-0151, 1983.

4. Shuen, J-S.; Solomon, A.S.P.; Zhang, Q-F.; and Faeth, G. M.: Structure of Particle-Laden Jets: Measurements and Predictions. AIAA Paper No. 84-0038, 1984. Also, to be published.

5. Solomon, A.S.P.; Shuen, J-S.; Zhang, Q-F.; and Faeth, G. M.: Structure of Nonevaporating Sprays: Measurements and Predictions. AIAA Paper No. 84-0125, 1984.

6. Solomon, A.S.P.; Shuen, J-S.; Zhang, Q-F; and Faeth, G. M.: A Theoretical and Experimental Study of Turbulent Nonevaporating Sprays. NASA Report, 1984.

7. Shuen, J-S.; Solomon, A.S.P.; Zhang, Q-F.; and Faeth, G. M.: A Theoretical and Experimental Study of Turbulent Particle-Laden Jets. NASA CR-168293, 1983.

8. Shuen, J-S.; Solomon, A.S.P.; and Faeth, G. M.: The Structure of Particle-Laden Jets and Nonevaporating Sprays. NASA CR-168059, 1982.

9. Solomon, A.S.P.; Shuen, J-S.; Zhang, Q-F.; and Faeth, G. M.: Measurements and Predictions of the Structure of Evaporating Sprays. 22nd National Head Transfer Conference, Niagara Falls, NY, August 1984.

10. Shuen, J-S.: A Theoretical and Experimental Investigation of Dilute Particle-Laden Turbulent Gas Jets. Ph.D. Thesis, The Pennsylvania State University, May 1984.

11. Solomon, A.S.P.: A Theoretical and Experimental Investigation of Turbulent Sprays. Ph.D. Thesis, The Pennsylvania State University, May 1984.

12. Faeth, G. M.: Evaporation and Combustion of Sprays. Prog. Energy Combust. Sci., vol. 9, 1983, pp. 1-76.

13. Faeth, G. M.: Recent Advances in Modeling Particle Transport Properties and Dispersion in Turbulent Flow. Proceedings of ASME-JSME Thermal Engr. Conf., vol. 2, ASME, New York, 1983, pp. 517-534.

14. Bilger, R. W.: Turbulent Jet Diffusion Flames. Prog. Energy Combust. Sci., vol. 1, 1976, pp. 87-109.

TABLE I.-SUMMARY OF PARTICLE-LADEN JET TEST CONDITIONS

Flow	Air Jet	Dilute Particle-Laden Jets			
Case	--	1	2	3	4
SMD (microns)	--	79	119	119	207
Loading Ratio	--	0.20	0.20	0.66	0.66
Injector Exit Conditions:[b]					
Velocity (m/s)					
Air	32.1	26.1	29.9	25.2	25.3
Particle	--	24.1	24.2	21.9	18.5
Particle Mass Flux (kg/m^2s)	--	6.1	6.5	18.9	19.0

[a]Injector exit diameter of 10.9 mm; particle density 2620 kg/m^3.

[b]At flow centerline.

TABLE II.-SUMMARY OF SPRAY TEST CONDITIONS[a]

Flow	Air Jet	Nonevaporating Sprays		Evaporating Sprays	
Case	--	1	2	1	2
Injected Fluid	air	air/oil[b]	air/oil[b]	air/Freon-11	air/Freon-11
Flow Rates, mg/s					
Gas	338	338	216	188	120
Liquid	0	600	1400	1450	1894
Loading Ratio	0	1.8	6.5	7.7	15.8
Jet Momentum, mN	120	137	70	106	60
Initial Velocity, m/s[c]	175	146	43	65	30
Reynolds number[c]	26000	30000	24000	41000	36000
SMD, microns	--	30[d]	87[d]	31[e]	58[e]
Spray Angle, deg.	--	30	33	27	29

[a]Spraying systems air-atomizing injector, 1.2 mm exit diameter.

[b]Vacuum pump oil, Sargent-Welch, Cat. No. 1407K25.

[c]Assuming LHF with air viscosity for Reynolds number.

[d]Measured with Malvern, Model 2200 Particle Sizer @ x/d = 12.6.

[e]Measured by slide impaction at x/d = 50.

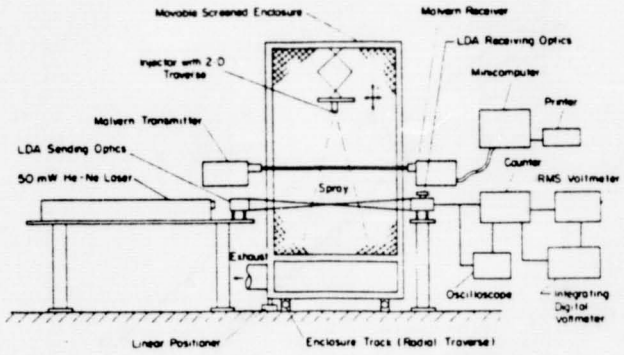

Figure 1.
SKETCH OF THE EXPERIMENTAL APPARATUS

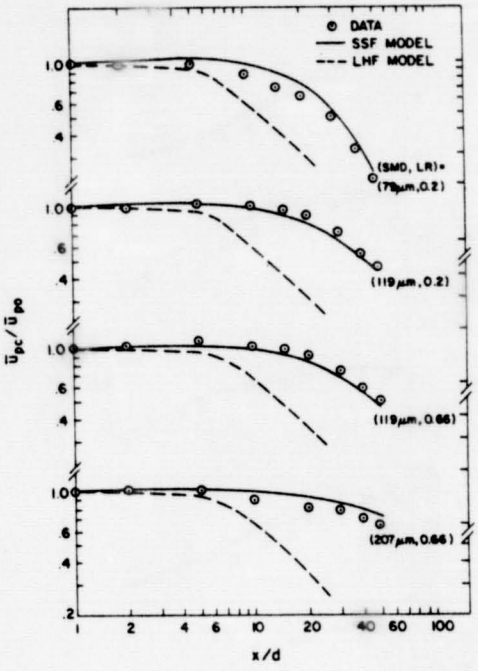

Figure 3.
CENTERLINE MEAN PARTICLE VELOCITY
IN PARTICLE-LADEN JETS

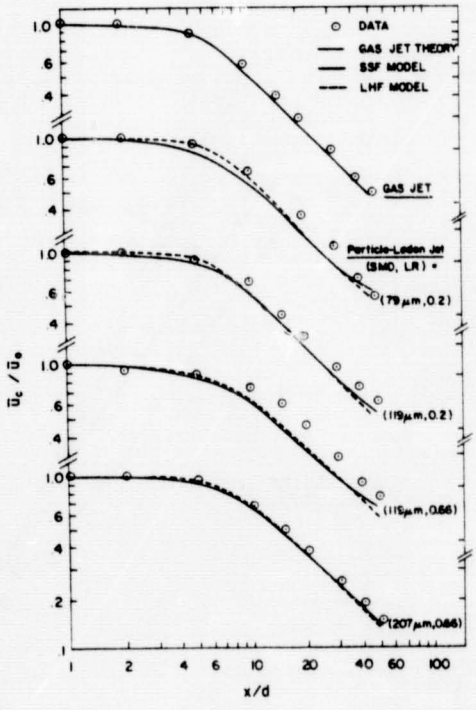

Figure 2.
CENTERLINE MEAN GAS-PHASE VELOCITY
IN PARTICLE-LADEN JETS

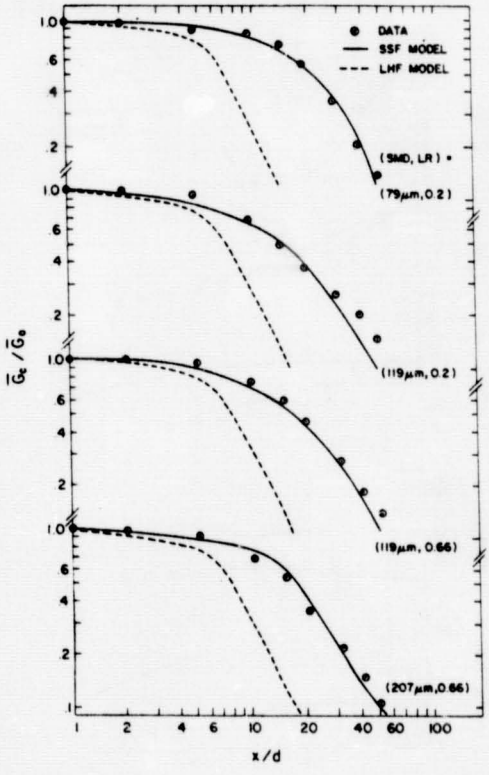

Figure 4.
CENTERLINE MEAN PARTICLE MASS FLUX
IN PARTICLE-LADEN JETS

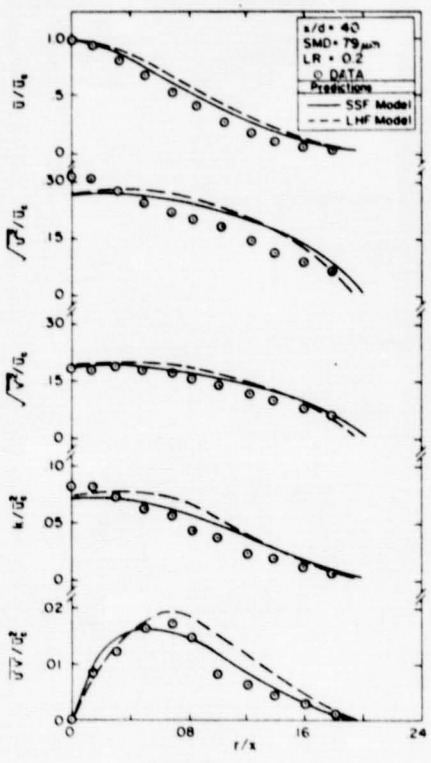

Figure 5.
GAS-PHASE PROPERTIES AT x/d = 40
FOR CASE 1 PARTICLE-LADEN JET

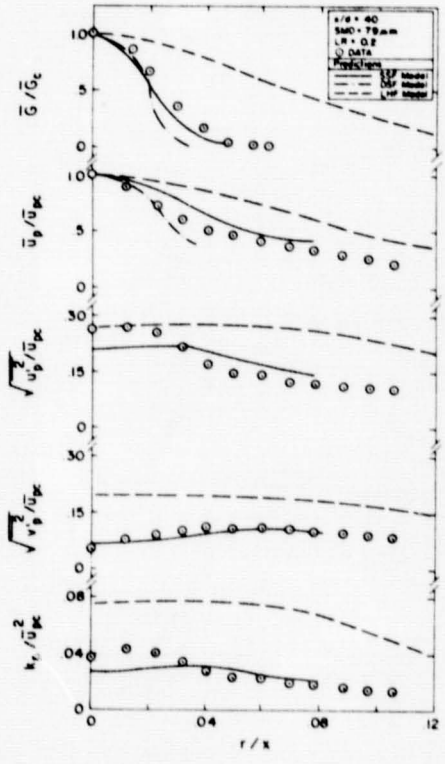

Figure 6
PARTICLE PROPERTIES AT x/d = 40
FOR CASE 1 PARTICLE-LADEN JET

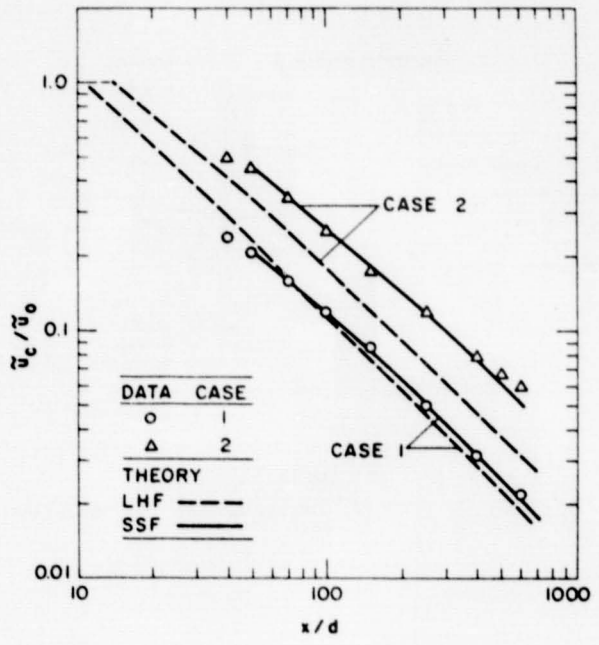

Figure 7
CENTERLINE MEAN GAS-PHASE VELOCITIES
FOR NONEVAPORATING SPRAYS

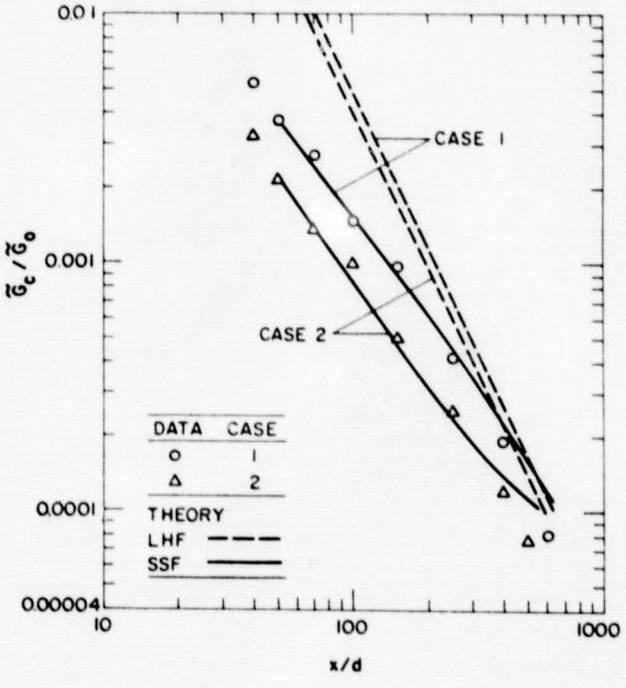

Figure 8
CENTERLINE MEAN LIQUID FLUX
FOR NONEVAPORATING SPRAYS

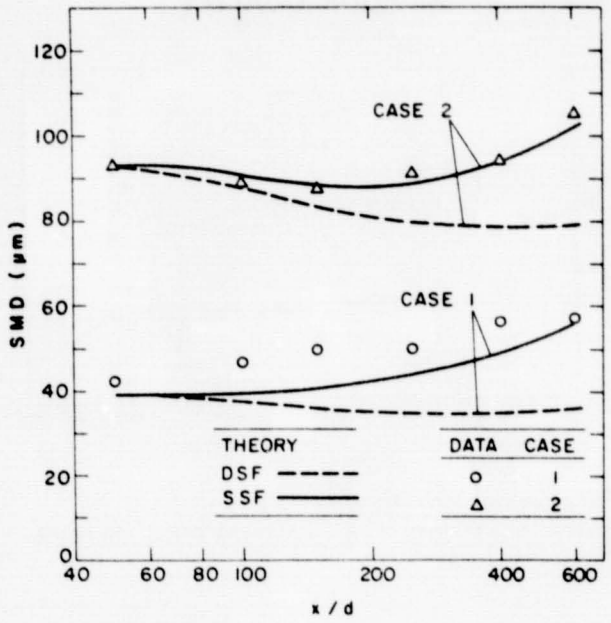

Figure 9
CENTERLINE SMD
FOR NONEVAPORTING SPRAYS

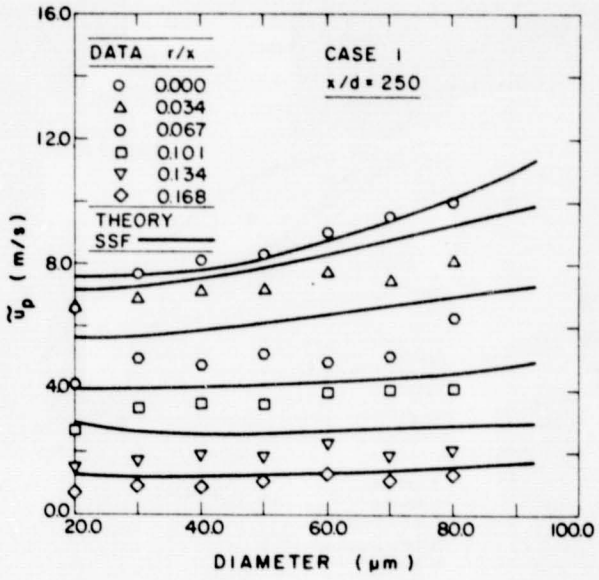

Figure 11
MEAN DROP VELOCITIES AT x/d = 250
FOR CASE 1 NONEVAPORATING SPRAY

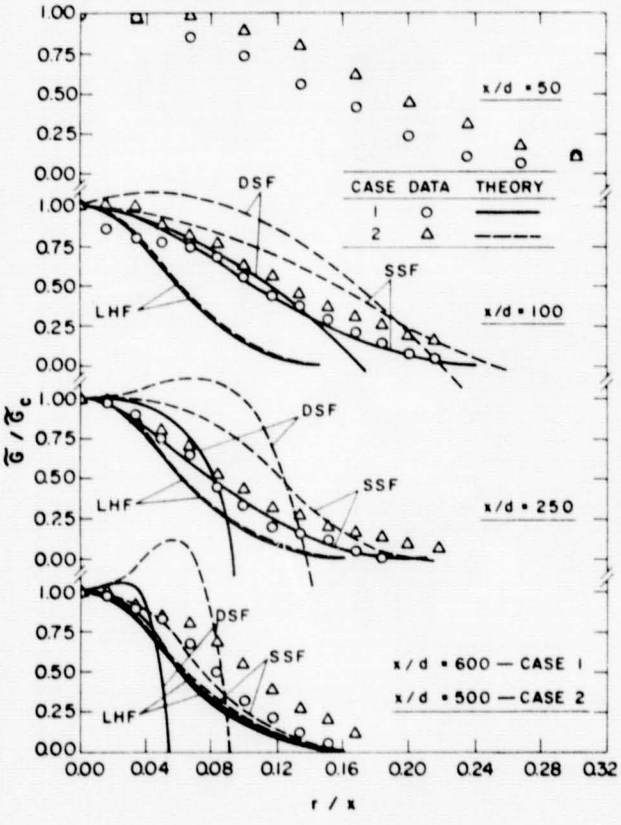

Figure 10
RADIAL PROFILES OF MEAN LIQUID FLUX
IN NONEVAPORATING SPRAYS

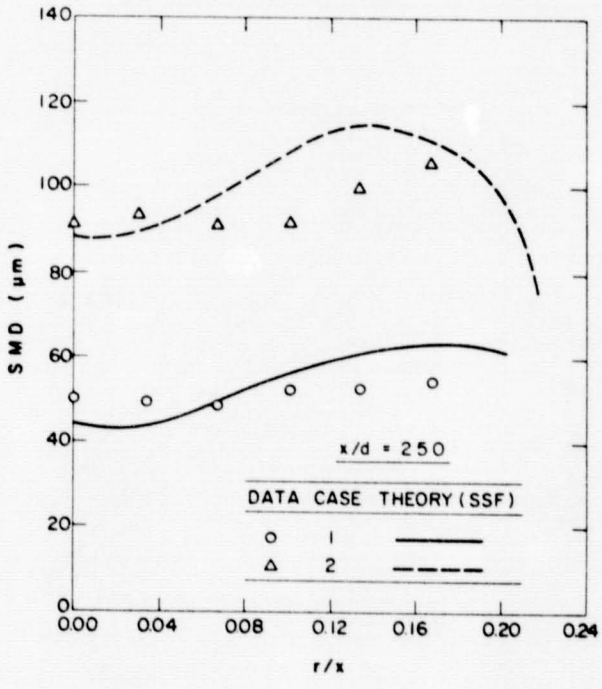

Figure 12
SMD AT x/d = 250
FOR NONEVAPORATING SPRAYS

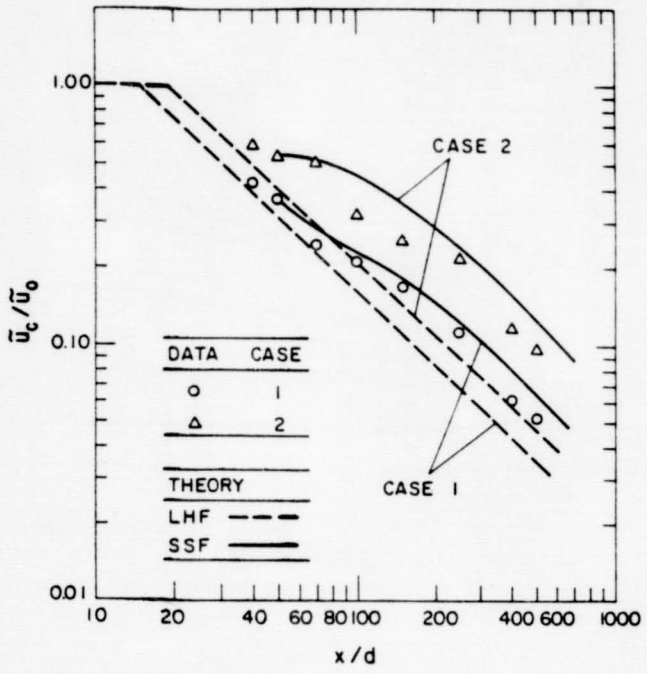

Figure 13
CENTERLINE MEAN GAS VELOCITIES
FOR EVAPORATING SPRAYS

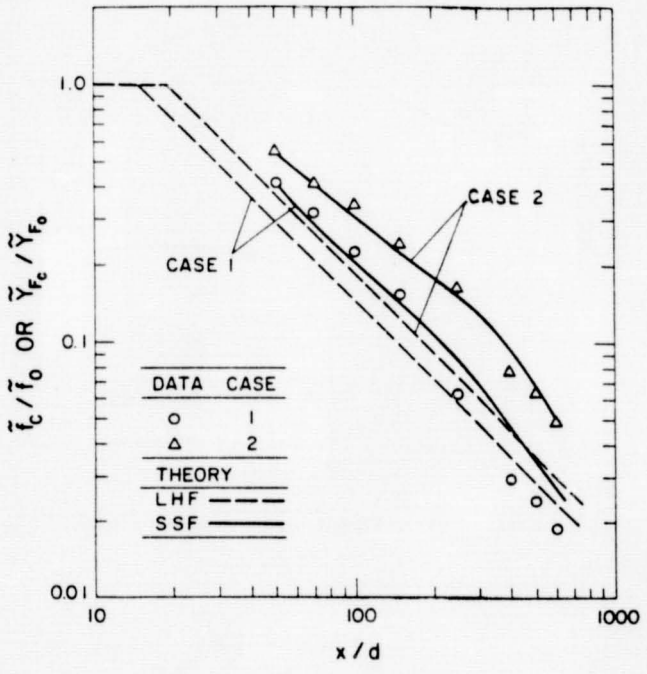

Figure 14
CENTERLINE MEAN FREON-11
CONCENTRATION FOR EVAPORATING SPRAYS

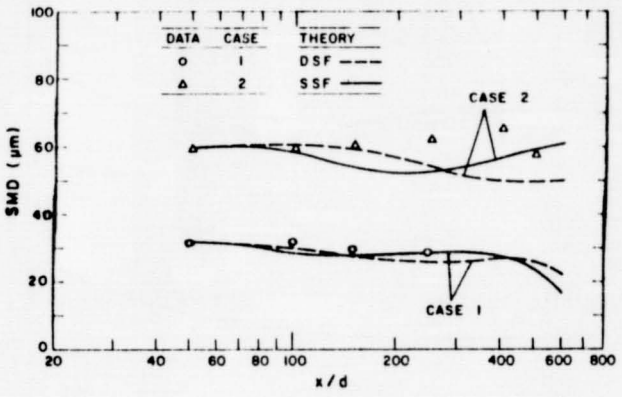

Figure 15
CENTERLINE SMD FOR EVAPORATING SPRAYS

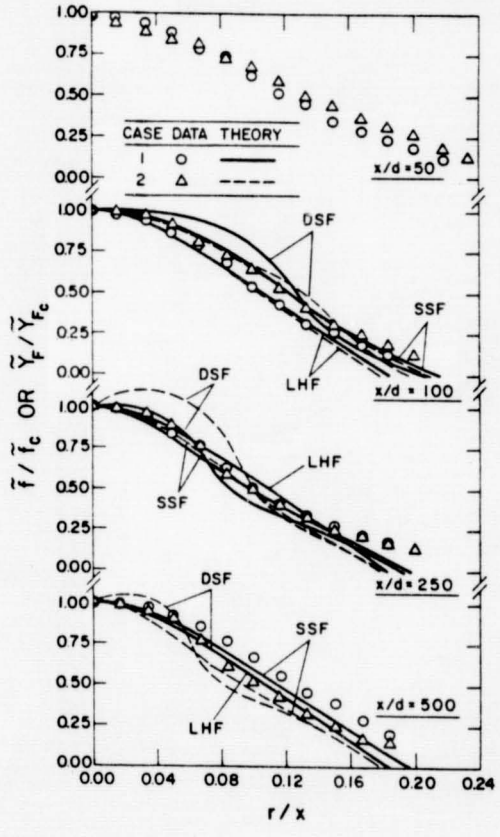

Figure 16
RADIAL PROFILES OF MEAN FREON-11
CONCENTRATION FOR EVAPORATING SPRAYS

EFFECT OF LIQUID DROPLETS ON TURBULENCE STRUCTURE IN A ROUND GASEOUS JET

A.M. Mostafa and S.E. Elghobashi
Mechanical Engineering Department
University of California, Irvine

Accurate prediction of spray combustion is extremely difficult due to the complex physical and chemical phenomena encountered in this two-phase process. The interaction between droplets and the turbulent fluid, turbulence effects on chemical reaction and heat transfer (and hence on droplet vaporization) are just a few examples of the complexity. In order to understand the nature of these interactions, coordinated experimental and theoretical studies need to be performed in a stepwise manner thus isolating the phenomenon to be investigated. A turbulent non-reacting gaseous jet laden with solid particles or evaporating droplets is a flow which allows the study of the interactions between the two-phases.

The recent experiment of Modarress, et al. (1982, 1983), which was performed in parallel with the present work, provided a much needed data to help understand the behavior of two-phase turbulent jets and validate the theoretical models. Elghobashi and Abou-Arab (1983) reviewed existing turbulence models for two-phase flows and indicated that these models are based on ad hoc modifications of single-phase turbulence models. They developed a two-equation turbulence model for incompressible dilute two-phase flows which undergo no phase changes.

In order to validate the proposed model, a turbulent axisymmetric gaseous jet laden with spherical uniform-size solid particles is studied by Elghobashi, et al. (1984). The predictions of the mean flow properties of the two-phases and the turbulence kinetic energy and shear stress of the carrier phase show good agreement with the experimental data.

Mostafa and Elghobashi (1983) extended the proposed model for steady incompressible two-phase flow including phase change. This model is tested for the flow of a turbulent axisymmetric gaseous jet laden with multisize evaporating liquid droplets by Mostafa and Elghobashi (1983). To avoid the problem of density fluctuations of the carrier phase at this stage, only isothermal flow is considered and vaporization is assumed to be due to the vapor concentration gradient. The droplets are classified into finite size-groups. Each group is considered as a continuous phase interpenetrating and interacting with the carrier phase. Predicted results include distributions of the mean velocity, volume fractions of the different phases concentration of the evaporated material in the carrier phase, turbulence intensity and shear stress of the carrier phase, droplet diameter distribution and the jet spreading rate. The results are analyzed based on a qualitative comparison with the corresponding single phase jet flow.

More validation testing of the model is needed via well-defined experiments.

REFERENCES

1- Modarress, D., Wuerer, J., and Elghobashi, S., 1982, "An Experimental Study of a Turbulent Round Two-Phase Jet," AIAA 21st Aerospace Sciences Meeting, Reno, Nevada.

2- Modarress, D., Tan, H., and Elghobashi, S., 1983, "Two-Component LDA Measurement in a Two-Phase Turbulent Jet," AIAA 21st Aerospace Sciences Meeting, Reno, Nevada.

3- Elghobashi, S., and Abou-Arab, T., 1983, "A Two-Equation Turbulence Model for Two-Phase Flows," Phys. Fluids, 26, 931-938.

4- Elghobashi, S., Abou-Arab, T., Rizk, M., and Mostafa, A., 1984, "Prediction of the Particle-Laden Jet with a Two-Equation Turbulence Model", Int. J. Multiphase Flow, in press.

5- Mostafa, A., and Elghobashi, S., 1983, "A Study of the Motion of Vaporizing Droplets in a Turbulent Flow," Ninth International Colloquim on Dynamics of Explosions and Reactive Systems, Poitiers, France.

6- Mostafa, A., and Elghobashi, S., 1983, "Prediction of a Turbulent Round Gaseous Jet Laden with Vaporizing Droplets," Fall Meeting of the Western States Section/The Combustion Institute.

OBJECTIVES

- To predict the flow of a turbulent gaseous jet laden with multisize liquid droplets undergoing vaporization.

- To compare the effects, on the flow field, of vaporizing droplets with those of single phase jet.

ASSUMPTIONS

1. Droplets in a given size-range constitute a dispersed phase - thus for k sizes there will be (k + 1) phases in the flow.

2. Each phase behaves as a continuum (macroscopically).

3. No collisions between droplets (dilute spray).

4. Droplets remain spherical as they decrease in size.

5. Velocity of vapor leaving droplet surface is equal to that of the droplet.

6. Concentration gradient is the only driving force for evaporation.

7. Drag relations of a solid sphere apply to liquid droplets (internal circulation effects on friction drag are counterbalanced by evaporation effects on pressure drag).

THE MEAN MOMENTUM EQ. OF THE CARRIER PHASE

$$\rho_1 \bar{\Phi}_1 U_z U_{z,z} + \rho_1 \bar{\Phi}_1 U_r U_{z,r} = - \bar{\Phi}_1 P_{,z}$$

Convection

$$+ \frac{1}{r}(\bar{\Phi}_1 r \mu_t U_{z,r})_{,r} - \sum_K \bar{\Phi}^K (F^K + \dot{m}^K)(U_z - V_z^K)$$

Diffusion — Momentum Exchange

$$\left\{ + C_{m1}\rho_1 U_{z,r}\left(\frac{\nu_t}{\sigma_\phi}\bar{\Phi}_{1,r}\right) + C_{\phi 5}\frac{1}{r}\left(\frac{k}{\epsilon} r \mu_t U_{z,r}\right)_{,r}\left(\frac{\nu_t}{\sigma_\phi}\bar{\Phi}_{1,r}\right)_{,r} + C_{\phi 5}\frac{k}{\epsilon}\mu_t U_{z,r}\left(\frac{\nu_t}{\sigma_\phi}\bar{\Phi}_{1,r}\right)_{,rr} \right\}$$

New turbulent correlations

THE MEAN CONTINUITY OF THE K th PHASE

$$\rho_2(\bar{\Phi}^K V_z^K)_{,z} + \rho_2(\bar{\Phi}^K V_r^K)_{,r} - \rho_2\left(\frac{\nu_t^K}{\sigma_\phi}\bar{\Phi}^K_{,z}\right)_{,z} - \rho_2\left(\frac{\nu_t^K}{\sigma_\phi}\bar{\Phi}^K_{,r}\right)_{,r}$$

New turbulent correlations

$$= - \dot{m}^K \bar{\Phi}^K$$

mass loss due to evaporation

THEMEAN GLOBAL CONTINUITY

$$\bar{\Phi}_1 + \sum_K \bar{\Phi}^K = 1$$

$C_{m1} = 0.4$ & $C_{\phi 5} = 0.1$

THE MEAN MOMENTUM EQ. OF THE K th PHASE

$$\rho_2 \bar{\Phi}^K V_z^K V^K_{z,z} + \rho_2 \bar{\Phi}^K V_r^K V^K_{z,r} = - \bar{\Phi}^K P_{,z}$$

$$+ \frac{1}{r}\left(\bar{\Phi}^K r \mu_T^K V^K_{z,r}\right)_{,r} + F^K \bar{\Phi}^K (U_z - V_z^K)$$

$$+ C_{m1}\rho_2 V^K_{z,r}\left(\frac{\nu_T^K}{\sigma_\phi}\bar{\Phi}^K_{,r}\right) + C_{\phi 5}\frac{1}{r}\left(\frac{k}{\epsilon} r \mu_T^K V^K_{z,r}\right)_{,r}$$

$$+ C_{\phi 5}\frac{k}{\epsilon}\mu_T^K V^K_{z,r}\left(\frac{\nu_T^K}{\sigma_\phi}\bar{\Phi}^K_{,r}\right)_{,rr} + (\rho_2 - \rho_1) g$$

gravity force

THE CONCENTRATION EQUATION:

$$\rho_1 \bar{\Phi}_1 U_z C_{,z} + \rho_1 \bar{\Phi}_1 U_r C_{,r} = \frac{1}{r}\left(\rho_1 r \bar{\Phi}_1 \frac{\nu_t}{\sigma_C} C_{,r}\right)_{,r}$$

Convection — Diffusion

$$+ \rho_1 C_{,r}\left(\frac{\nu_t}{\sigma_\phi}\bar{\Phi}_{1,r}\right) + \sum_K \bar{\Phi}^K \dot{m}^K (1 - C)$$

Sources

THE TURBULENCE KINETIC ENERGY (K)

$$\rho_1 \Phi_1 U_z K_{,z} + \rho_1 \Phi_1 U_r K_{,r} = \rho_1 \Phi_1 \nu_t U_{z,r}^2$$

Convection — Main Production (P)

$$+ \frac{2}{3}\rho_1 C_{\phi 5}\left(\frac{\nu_t}{C_\mu}\right)\left(\frac{\nu_t}{\sigma_\phi}\Phi_{1,r}\right)_{,r} U_{r,r} - \rho_1 C_{\phi 5}\left(\frac{K}{\epsilon}\right)\nu_t\left(\frac{\nu_t}{\sigma_\phi}\right)\Phi_{1,r} U_{z,r}^2$$

Extra production (P')

$$+ \frac{1}{r}\left(\rho_1 r \Phi_1 \frac{\nu_t}{\sigma_K} K_{,r}\right)_{,r}$$

Diffusion

$$- \rho_1 \Phi_1 \epsilon$$

main Dissipation (ϵ)

$$\left\{ - \sum_k K \Phi^K (F^K + \dot{m}^K)\left(1 - \int \left(\frac{\Lambda_1 - \Lambda_K}{\Lambda_2}\right) F(\omega)\, d\omega\right) + \sum_k (F^K + \dot{m}^K)\left[(U_r - V_r^K)\left(\frac{\nu_t^K}{\sigma_\phi}\Phi_{,r}^K\right) - C_{\phi 5}\left(\frac{\nu_t}{C_\mu}\right)\left(\frac{\nu_t^K}{\sigma_\phi}\Phi_{,r}^K\right)_{,r}\left(1 - \int \left(\frac{\Lambda_1 - \Lambda_K}{\Lambda_2}\right) F(\omega)\, d\omega\right)\right]\right\}$$

Extra Dissipation (ϵ')

THE DISSIPATION RATE OF TURBULENCE ENERGY ($\mathcal{E}$)

$$\rho_1 \Phi_1 U_z \mathcal{E}_{,z} + \rho_1 \Phi_1 U_r \mathcal{E}_{,r} = \frac{1}{r}\left(\rho_1 r \Phi_1 \frac{\nu_t}{\sigma_\epsilon}\mathcal{E}_{,r}\right)_{,r}$$

Convection — Diffusion

$$+ C_{\epsilon 1}\frac{\mathcal{E}}{K}(P + P')$$

Production

$$- \frac{\mathcal{E}}{K}(C_{\epsilon 2}\epsilon + C_{\epsilon 3}\epsilon')$$

Dissipation

TURBULENT DIFFUSIVITY OF LIQUID DROPLETS

$$\nu_\Gamma^K = \frac{\nu_t}{\sigma_\Gamma^K}$$

σ_Γ^K : From Peskin's formula but using other length scales.

INTERFACE PROPERTY TRANSFER

- **MASS TRANSFER:**

$$\dot{m}^K = \frac{12\,\mathcal{D}\,\rho_1}{(d^K)^2}\ln(1+B)\,Sh^K$$

$$B = \frac{C_L - C_\infty}{1 - C_L},$$

$$Sh^K = 2 + 0.55\,Re^{K^{1/2}}\,Sc^{1/3},$$

$Sc = \nu_1 / D$

C_∞ : From it's Conservation eqn.

C_L : From Clausius-Clapeyron expression.

- **MOMENTUM TRANSFER:**

$$F^K = \left(\frac{3}{4d^K}\right)\rho_1 C_D^K \left|\vec{U} - \vec{V}^K\right|$$

$$C_D^K = \frac{24}{R_e^K}\left[1 + 0.1935\,(R_e^K)^{0.635\,W}\right] \quad 20 \le R_e^K \le 200$$

$$\text{or} \quad C_D^K = \frac{24}{R_e^K}\left[1 + 0.135\,(R_e^K)^{0.82 - 0.05\omega}\right] \quad 0 < R_e^K < 20$$

$$\omega = \log_{10} R_e^K$$

THE FLOW CONSIDERD

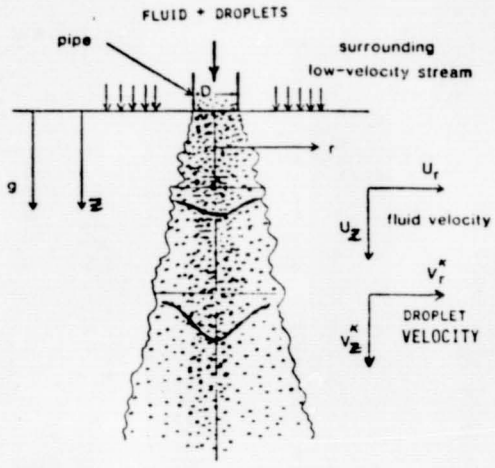

- FLUID : Air
  REYNOLDS NUMBER : 30,000
- DROPLETS : Methanol Alcohol CH_3OH
  DROPLET DIAMETER : 100, 80, 60, 40 & 20 μm with equal mass ratios
  LOADING MASS RATIO : ∞, 1, 0.25 & 0.5
  LIQUID DENSITY : 810 Kg/m^3
  VAPOR DENSITY : $\approx$ 1 Kg/m^3
- FLUID AND DROPLETS EXIST AT UNIFORM AND CONSTANT TEMPERATURE.

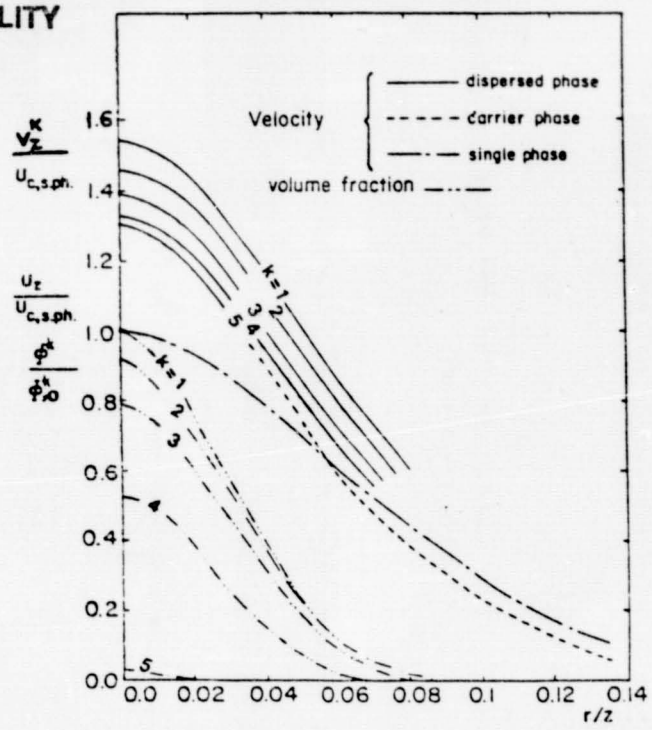

Fig 1 Normalized mean velocities and volume fractions profiles at z/D = 20 and at X_o = 0.5

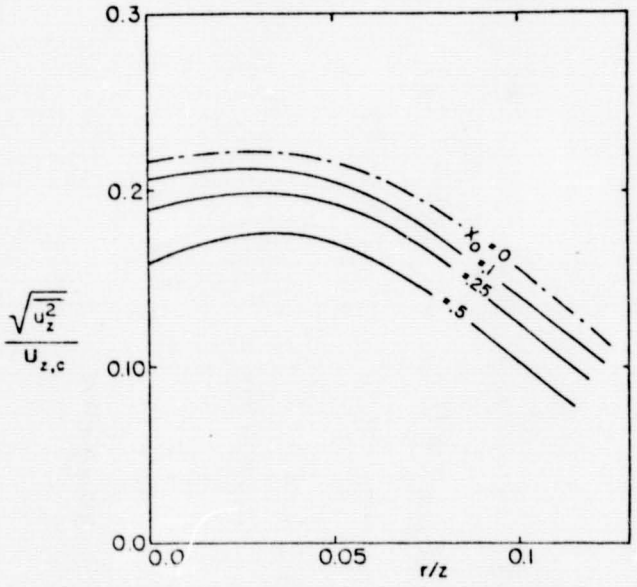

Fig 2 The turbulence intensity distribution under different mass loading ratios at z/D = 20

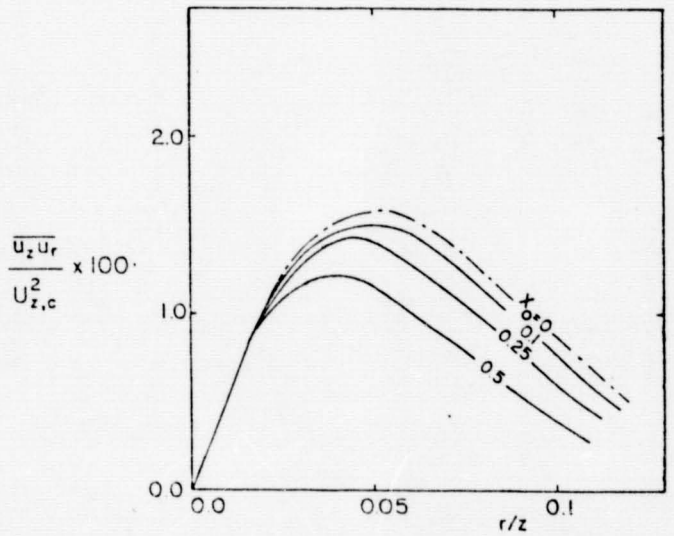

Fig 3 The shear stress distribution under different mass loading ratios at z/D = 20

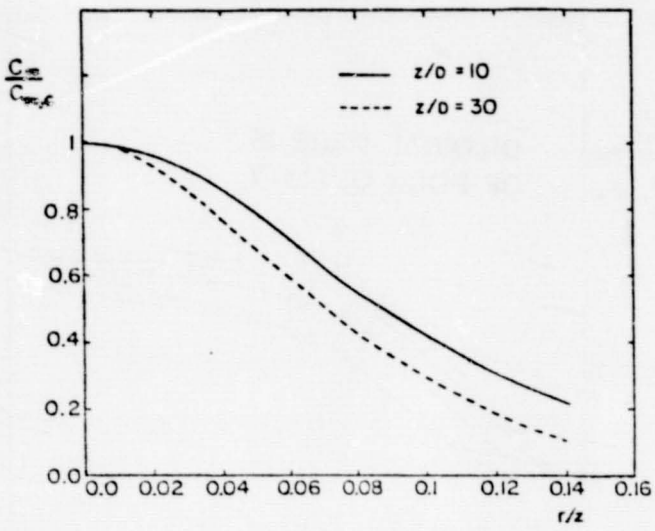

Fig 4 Normalized vapor concentration at different stations and at $X_o = 0.5$

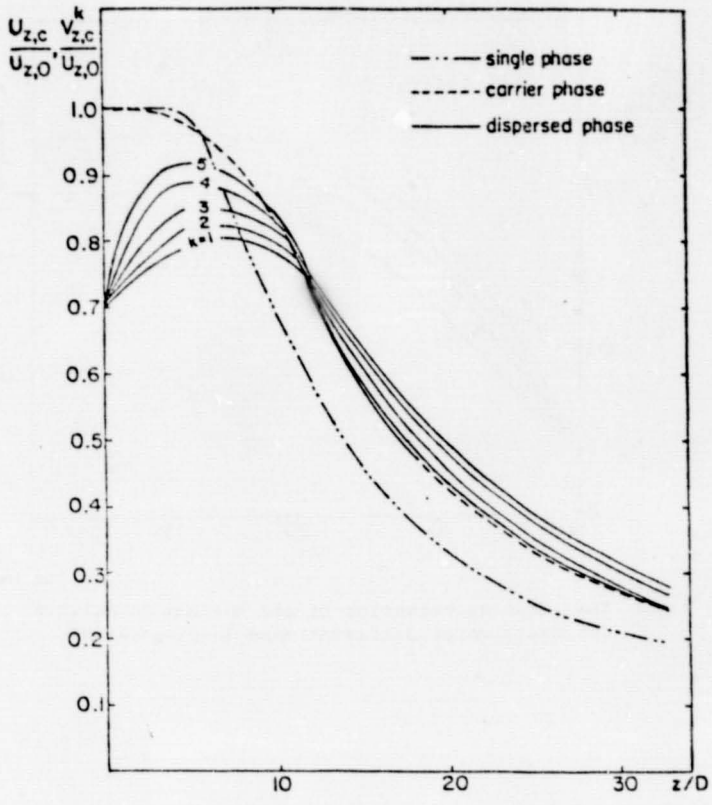

Fig 5 The axial distribution of the mean velocities at $X_o = 0.5$

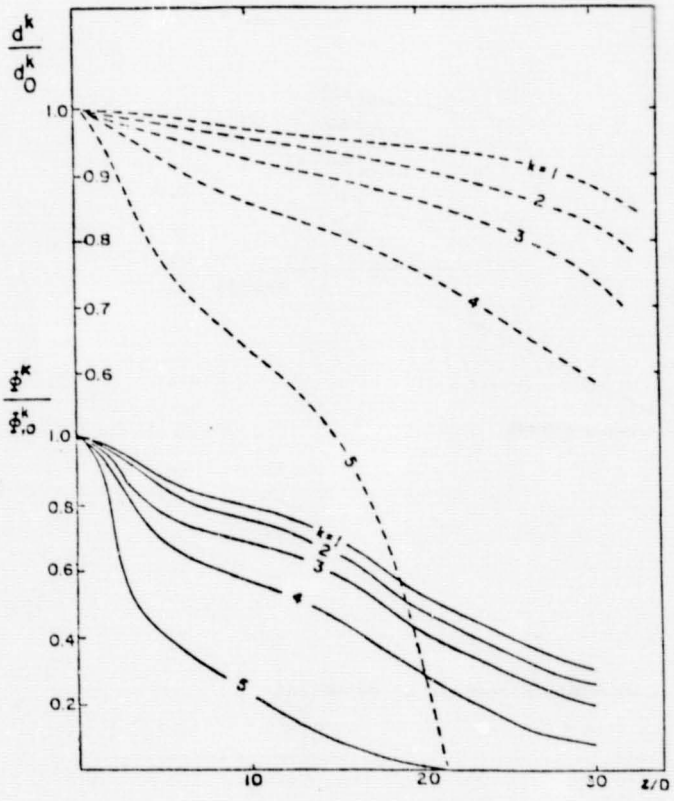

Fig 6 The axial distribution of the volume fractions and the average diameters at $X_o = 0.5$

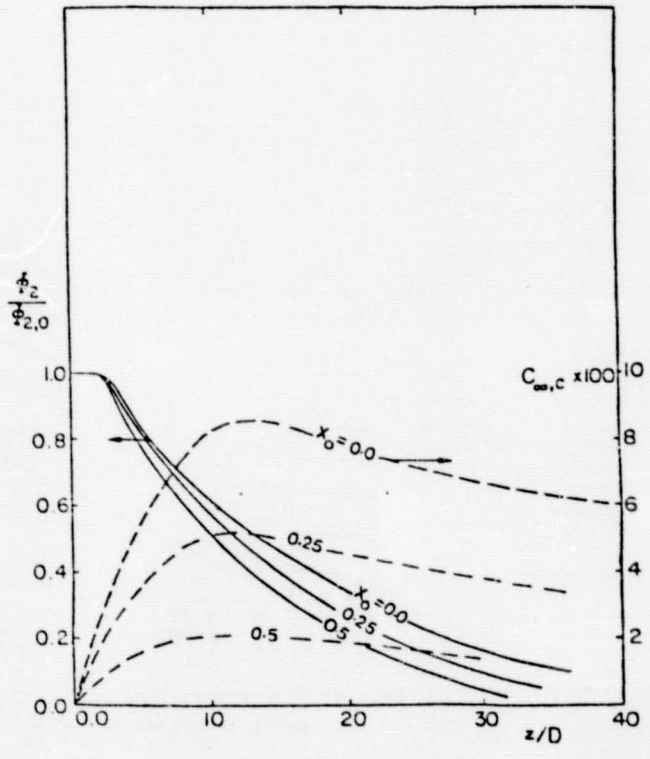

Fig 7 The axial distribution of the droplets volume fraction and vapor concentration

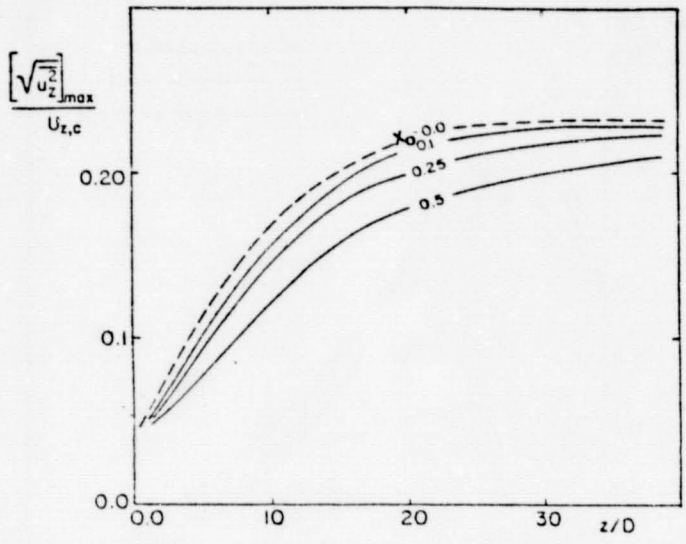

Fig 8 The axial distribution of the maximum turbulence intensity under different mass loading ratios

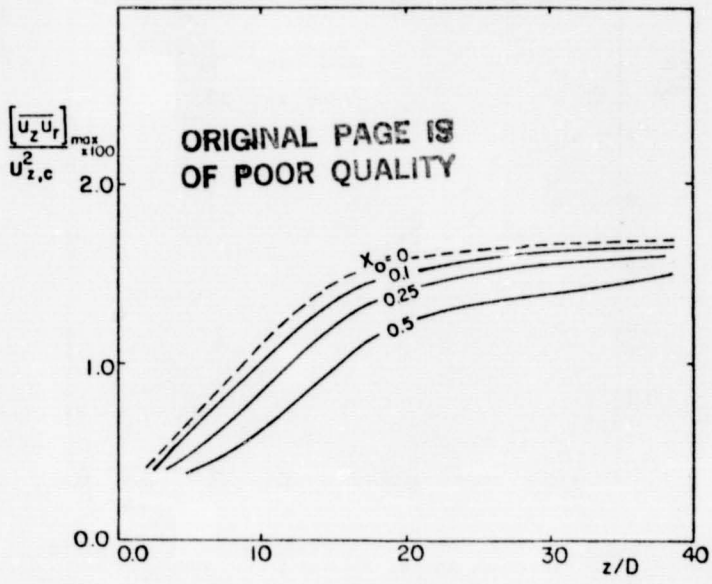

Fig 9 The axial distribution of the maximum shear stress under different mass loading ratios

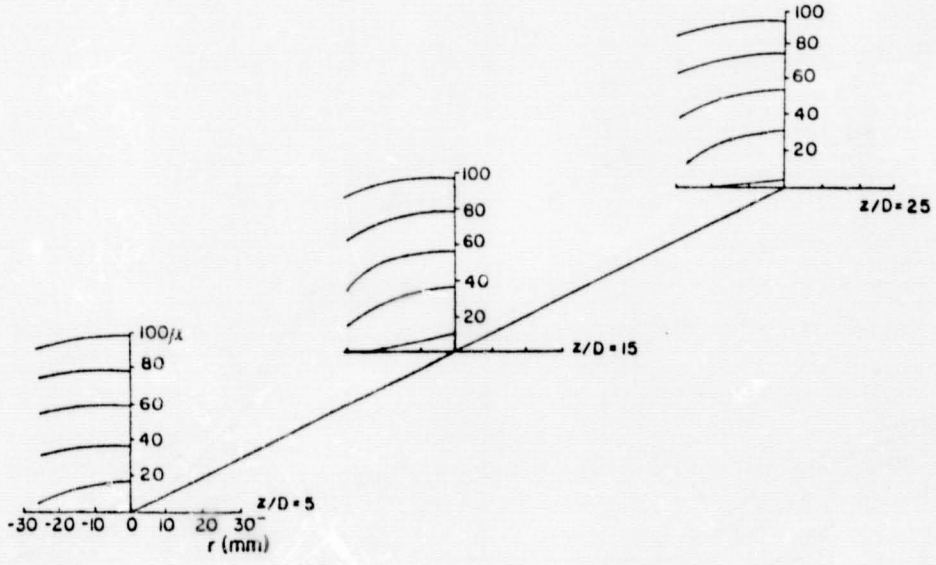

Fig 10 Radial distributions of the local droplets diameters at different axial locations and at X_o = 0.5

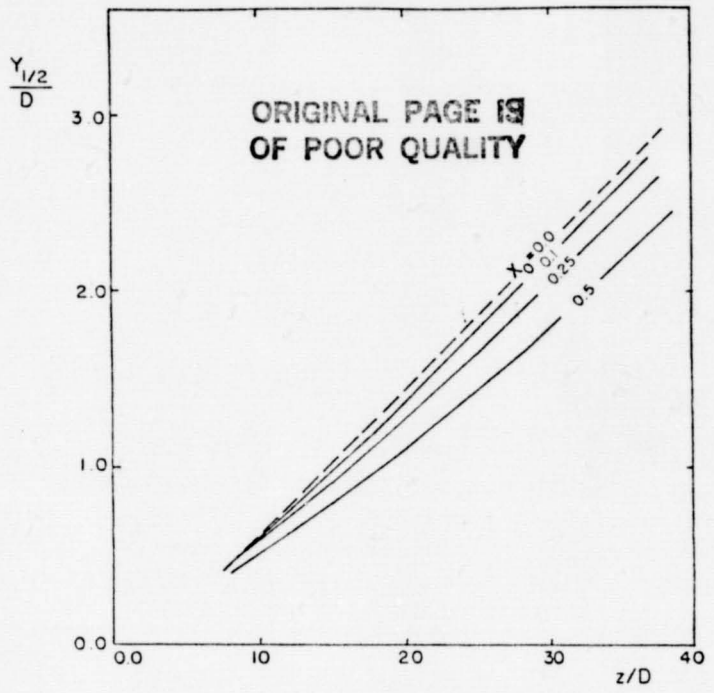

Fig 11 The spreading rate under different mass loading ratios

SUMMARY

- The proposed turbulence model (validated experimentally for solid particles) is applied to predict the turbulent round jet laden with multisize vaporizing droplets.
- Predicted changes in the flow field (mean and turbulent quantities) are significant and should be considered in liquid spray combustion calculations.
- Experiment to validate the proposed model will be performed when funds become available.

COMBUSTION CHARACTERISTICS IN THE TRANSITION REGION OF LIQUID FUEL SPRAYS

Nicholas P. Cernansky, Izak Namer, Robert J. Tidona and Hamid Sarv
Drexel University

There have been a number of studies involving the behavior of fuel sprays in the transition region which encompasses droplets in the 10-80 μm size range. In particular, the effect of droplet size on minimum ignition energy of a spray has been examined. Using swirl atomizers to generate fuel sprays, Ballal and Lefebvre (ref. 1) showed that ignition energies increase with increasing Sauter Mean Diameter (SMD). On the other hand, the experimental work of Chan and Polymeropoulos (ref. 2), in an 8-35 μm monodisperse droplet size range, showed an optimum droplet diameter around 15 μm for which the ignition energy was minimum. However, these systems had limitations induced by droplet size distribution or variations in the flow velocities due to the requirements for monosized droplet formation. Thus, in November 1982, an investigation of the droplet ignition requirement was initiated with the following specific objectives:

1) To map the minimum ignition energies for monodisperse fuel sprays in the transition region as a function of droplet size, number density, equivalence ratio, etc.;

2) To isolate the optimum droplet diameter at which the ignition energy requirement is minimum;

3) To study the effects of changing vaporization environment on the minimum ignition energy;

4) To characterize the ignition requirements of polydisperse fuel sprays in terms of the droplet size distribution; and

5) To determine the effects of droplet size and size distribution on flame speed.

The experimental facility developed for this study consists of a Berglund-Liu Vibrating Orifice Monodisperse Aerosol Generator which produces monosized droplets with diameters having a standard deviation of less than 1% of the mean droplet diameter (ref. 3). Based on the vibrating orifice principle, the droplet size can be calculated from the operating conditions of the instrument (fuel feed rate and vibration frequency). After generation, the droplets are subjected to a flow of dispersion air to prevent coagulation. The air/fuel aerosol passes through a flow reducing section where dilution air is added to achieve the desired stoichiometry. The monodisperse fuel spray then flows through the test section, a square pyrex tube, which houses the ignition electrodes. Both electrodes are mounted on micrometer traversing mechanisms to vary the spark gap. In its current configuration (Fig. 1), the experimental facility is operated with downward flow in order to prevent any accumulation of fuel within the combustor.

An ignition system has been developed to supply a capitance spark with independently variable energy, energy density, and duration. The spark energies are determined by integrating (over time) the product of the voltage and current, recorded by a two-channel digital oscilloscope.

Efforts in the first year have concentrated on the development of the experimental facility and performing exploratory measurements. Preliminary measurements have been made in the 10-74 μm monodisperse droplet size range using n-heptane as fuel. Minimum ignition energies are measured as a function of droplet size, equivalence ratio, and flow velocity. Prior to these measurements, the optimum spark gap and duration corresponding to minimum ignition energies are determined for each operating condition. Further measurements using different fuels including alcohols will be made soon.

REFERENCES

1. Ballal, D.R., and A.H. Lefebvre, "Ignition and Flame Quenching of Flowing Heterogeneous Fuel-Air Mixtures," Combustion and Flame 35, 155, 1979.

2. Chan, K.K., and C.E. Polymeropoulos, "An Experimental Investigation of the Minimum Ignition Energy of Monodisperse Sprays," Paper No. ESSCI 81-21, Eastern States Section, The Combustion Institute Meeting, November, 1981.

3. Berglund, R.N., and B.Y.H. Liu, "Generation of Monodisperse Aerosol Standards," Environmental Science and Technology 7, 2, 147, 1973.

OVERALL OBJECTIVES

Study the effects of droplet size and size distribution on :

- Minimum Ignition Energies
- Flammability Limits
- Flame Speeds

BACKGROUND

- Spray Burning Widespread
  - 30-50% of Total Energy Consumption
- Modes of Spray Combustion
  - Premixed
  - Diffusive
  - Transition
- Transition Region Effects
  - Increased Flame Speeds
  - Reduced NO_x Emissions
  - Broadened Flammability Limits
  - Lower Ignition Requirements

OBJECTIVES OF IGNITION STUDIES

- Map minimum ignition energies for monodisperse fuel sprays in transition region.
- Determine optimum droplet size corresponding to minimum ignition energy.
- Study prevaporization effects on minimum ignition energy.
- Examine size distribution effects in polydisperse sprays on ignition requirements.

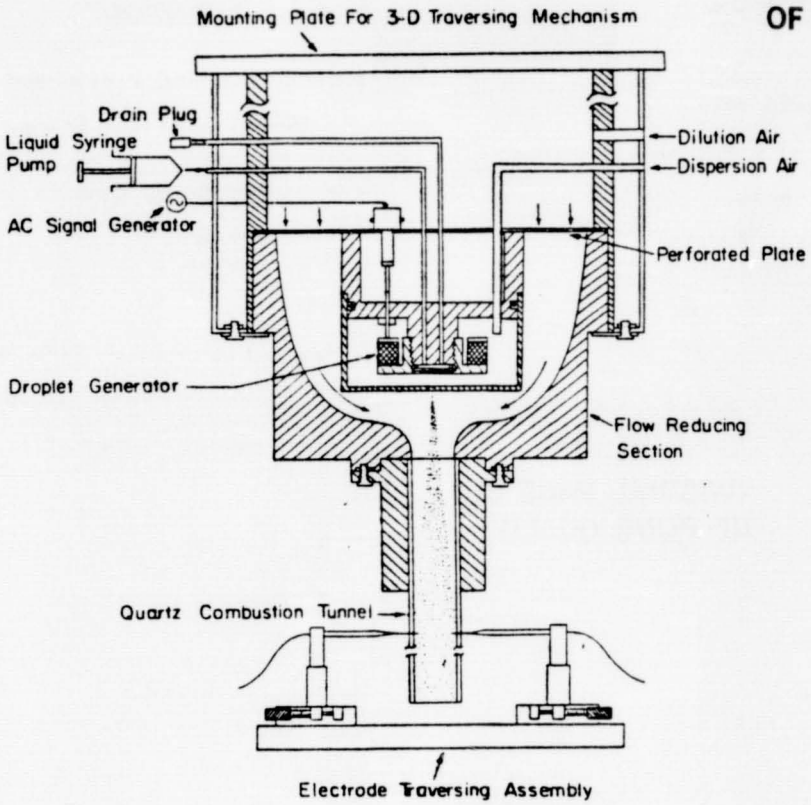

Figure 1. Schematic of the Spray Burner Facility

EXPERIMENTAL VARIABLES

- Droplet Size (10-74 μm)
- Number Density
- Equivalence Ratio
- Extent of Prevaporization
- Flow Velocity
- Fuel Type
- Oxidizer Composition

SUMMARY

- A monodisperse aerosol generator has been modified to study ignition requirements, flammability limits, and flame speeds in the transition region.
- An ignition system has been developed and tested.
- An optical drop sizing system has been designed and fabrication is nearly complete.
- Preliminary measurements of droplet size effects on the minimum ignition energy for n-heptane sprays have been performed.
- Parametric studies of droplet size effects on minimum ignition energies of various fuels including alchohols are in progress.

D16

TURBULENT SWIRLING COMBUSTION*

Holger T. Sommer, Raymond J. Mosula and Ellice Seiden
Department of Mechanical Engineering
Carnegie-Mellon University

EXPERIMENTAL EFFORT

Turbine Combustion Facility

An experimental facility constructed to simulate swirling gas turbine combustion has been subjected to extensive redesign and modification. The program undertaken over the course of the past year consisted essentially of two phases: (1) an assessment of the existing test facility, and (2) a major redesign and reconstruction of those components deemed in need of alteration. As a result of this extensive effort, the test facility at Carnegie-Mellon University has achieved a higher degree of precision and reproducibility. Furthermore, it is believed that those undesirable extraneous effects which plague any fluid mechanics experiment have been substantially reduced. Hence, it is at this time that accurate and reproducible flow measurements can begin.

Measurements and Results

Measurements of the non-reacting turbulent flow produced by two confined, co- and/or counter-swirling jets have been obtained by means of a two-color laser Doppler velocimeter. These results are compared with earlier experiments by Vu and Gouldin (ref. 1), and the numerical predictions of Ramos (refs. 2 and 3). It is shown that under both swirl conditions, a closed recirculation zone is created at the combustor center line. This zone is characterized by the presence of a one-cell toroidal vortex, low tangential velocities, high turbulent intensity, and large dissipation rates of the kinetic energy of turbulence.

THEORETICAL EFFORT

Numerical Modeling of Turbulent Swirling Flows

The major thrust of the theoretical effort has been the adaptation of previously developed computer codes by Lilley (ref. 4) and Ramos (ref. 5) to the above described experiment. Both codes are based on the k-ε turbulence model, while Ramos additionally utilizes a k-ℓ turbulence model.

---

*This project was supported by the NASA Lewis Research Center under contract number NAG3-401.

In his numerical solution, Ramos (ref. 2) includes streamline curvature effects. The streamline curvature effect is being improved and a correction factor for the k-ε model will be developed during the remaining funding period. Because the codes utilize different numerical solution techniques to solve the finite difference equations, comparison between numerical results and measurements will be used to evaluate the quality of both techniques.

Special care will be taken to model the recirculation zone casued by the presence of co- and counter-swirling flows. It will be possible, due to clearly defined experimental boundary and initial conditions, to investigate the influence of turbulence models on complex reacting flows. These conditions have been found to be critical in numerical studies.

REFERENCES

1. Vu, B.T. and Gouldin, F.C.: Flow Measurements in a Model Swirl Flow. AIAA 11th Aerospace Science Meeting, 1980.

2. Ramos, J.I.: A Numerical Study of Turbulent Swirling Flows. Carnegie-Mellon University, Report #CO/81/2, 1981.

3. Ramos, J.I. and Sommer, H.T.: Swirling Flow in a Research Combustor. AIAA 21st Aerospace Science Meeting, Reno, Nevada, 1983.

4. Lilley, D.G. and Rhodes, D.L.: A Computer Code for Swirling Turbulent Axisymmetric Recirculating Flows in Practical Isothermal Combustor Geometries. NASA CR-3442, 1982.

5. Ramos, J.I.: A Numerical Study of Turbulent Confined Swirling Flows. Carnegie-Mellon University, Report #CO/80/4, 1980.

D11

ERROR REDUCTION PROGRAM*
A PROGRESS REPORT

Saadat A. Syed
Engineering Division; Pratt & Whitney Aircraft Group

The combustion chamber of the aircraft gas turbine has to be designed to satisfy the stringent dual engine requirements of reduced fuel consumption and increased durability. Combustor development based on conventional methods to meet these requirements is proving to be increasingly costly and time consuming. A mathematical model of the combustor would be very helpful in reducing cost and time of the design cycle as it would permit most of the work to be done on a computer. Such models are already being used in a limited manner in the industry. More widespread use of these models will be accelerated by the removal of some of the known deficiencies in the present codes. One of these deficiencies is the numerical error, or numerical diffusion, that can be introduced into the calculations under certain conditions. This numerical error is due to the finite differencing scheme, usually upwind or hybrid, used in these codes.

The objective of the Error Reduction Program is to evaluate available finite difference schemes for minimum numerical diffusion, and to incorporate the best available scheme into a three-dimensional combustor performance code.

As a first step toward this end, five schemes (refs. 1 through 5) were selected for initial evaluation. Some of these schemes were combined with bounding schemes to eliminate physically unrealistic undershoots and overshoots. Two basic criteria were used to judge these schemes: they should be conservative, and should produce solutions that exhibit no extraneous maxima or minima (boundedness property). The accuracy of the schemes was evaluated by performing the truncation error analysis, and running one- and two-dimensional test cases and comparing the calculated solutions against the exact solutions. Based on this evaluation, two schemes were selected: QUDS, Quadratic Upstream Differencing Scheme, and BSUDS2, Bounded Skew Upstream Differencing Scheme Two. The first scheme was proposed by Leonard (ref. 1), and the second scheme is the one proposed by Raithby (ref. 2), which is bounded by a new bounding scheme.

The selected two schemes were coded into a two-dimensional computer code, 2D-TEACH, and their accuracy and stability were evaluated by running several test cases (refs. 6 through 8). It was found that BSUDS2 was more stable than QUDS. It was also found that the accuracy of both schemes is dependent on the angle that the streamlines make with the mesh, QUDS being more accurate at smaller angles and BSUDS2 being more accurate at larger angles. However, both schemes, at all angles, were more accurate than the existing hybrid scheme. BSUDS2 was selected to be extended into three dimensions, primarily because it was more stable. This scheme is currently being incorporated into a three- dimensional code, 3D-TEACH.

* This work was conducted under NASA Contract NAS3-23686.

REFERENCES

1. Leonard, B. P., "A Stable and Accurate Convective Modeling Procedure Based on Quadratic Upstream Interpolation", Computer Methods in Applied Mechanics and Engineering, Vol. 19, 1979, pp. 59-98.

2. Raithby, G. D., "Skew-Upstream Differencing Schemes for Problems Involving Fluid Flow", Computer Methods in Applied Mechanics and Engineering, Vol. 9, 1976, pp. 151-162.

3. Agarwal, R. K., "A Third-Order-Accurate Upwind Scheme for Navier-Stokes Solutions at High Reynolds Numbers", AIAA-81-0112, Presented at AIAA 19th Aerospace Sciences Meeting, Jan. 12-15, 1981, St. Louis, Missouri.

4. Rubin, S. G. and Graves, Jr., R. A., "Viscous Flow Solutions with a Cubic Spline Approximation", Computers and Fluids, Vol. 3, 1975, pp. 1-36.

5. Glass, J. and Rodi, W., "A Higher Order Numerical Scheme for Scalar Transport", Computer Methods in Applied Mechanics and Engineering, Vol. 31, 1982, pp. 337-358.

6. Kim, J., Kline, S. J., and Johnston, J. P., "Investigation and Separation of a Turbulent Shear Layer Flow Over a Backward-Facing Step", Report MD-37, Thermosciences Division, Department of Mechanical Engineering, Stanford University, Stanford, California, April 1978.

7. Johnson, B. V. and Bennett, J. C., "Mass and Momentum Turbulent Transport Experiments with Confined Coaxial Jets", NASA CR-165574, November 1981.

8. Johnson, B. V., "Mass and Momentum Turbulent Transport Experiments", NASA Contract NAS3-22771, United Technologies Research Center, Reports R82-915540-15, -16, and -17, 1982.

NEED FOR ERROR REDUCTION

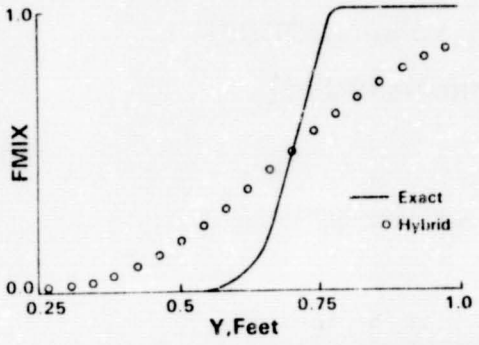

Convection and diffusion of a scalar step in constant property uniform inclined flow. $Pe_x = Pe_y = 60$

OBJECTIVE

To identify and incorporate best available finite difference error reduction scheme into a 3D combustor performance code.

PROGRAM SCHEDULE

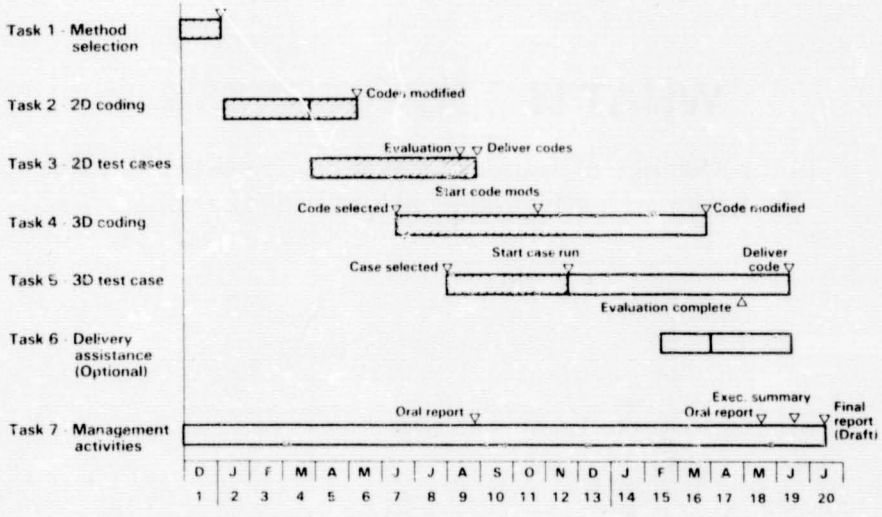

DISCRETIZATION SCHEMES EVALUATED

- Agarwal Differencing Scheme (ADS)
- Quadratic Upwind Differencing Scheme (QUDS)
- Skew Upwind Differencing Scheme (SUDS)
- Spline/Hermetian Schemes
  - Cubic Spline Scheme (CSS)
  - Glass and Rodi Hermetian Scheme (GRHS)
- Flux Blending Schemes
  - Bounded-One
  - Bounded-Two

SCHEMES SELECTED

- QUDS — Quadratic Upwind Differencing Scheme
- BSUDS2 — Bounded Skew Upwind Differencing Scheme Two

WHAT IS BOUNDEDNESS

In the absence of sources the value at node P should be bounded by the values at surrounding nodes.

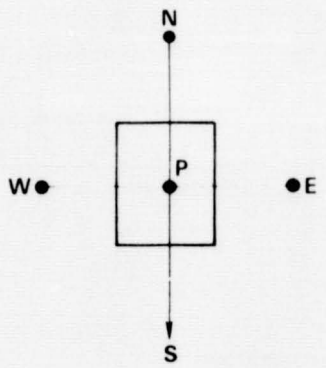

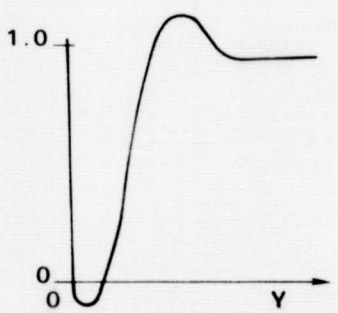

(-2

QUADRATIC UPWIND DIFFERENCING SCHEME (QUDS)

- Finite volume method
- Upwind biased quadratic interpolation for convection terms
- Central differencing for diffusion terms
- Employs extended nine point modecule

$$\phi_w = -\tfrac{1}{8}\phi_{WW} + \tfrac{3}{4}\phi_W + \tfrac{3}{8}\phi_P \text{ ,u > o}$$

$$= -\tfrac{1}{8}\phi_E + \tfrac{3}{4}\phi_P + \tfrac{3}{8}\phi_W \text{,u < o}$$

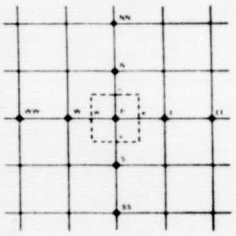

- Scheme is conservative
- Coefficients can become negative
- Solution can become unbounded

BOUNDED SKEW UPWIND DIFFERENCING SHCEME TWO (BSUDS2)

- Finite volume method
- Central differencing for diffusion terms at all Peclet numbers
- Central differencing for convection terms for absolute Peclet numbers less than two
- Blending of upwind and skewed upwind differencing for Peclet numbers greater than two
- Employs compact nine-point molecule
- Scheme is conservative
- Produces bounded solutions

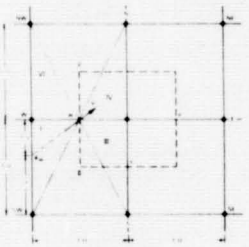

FIRST LAMINAR FLOW TEST CASE

QUDS more accurate over all

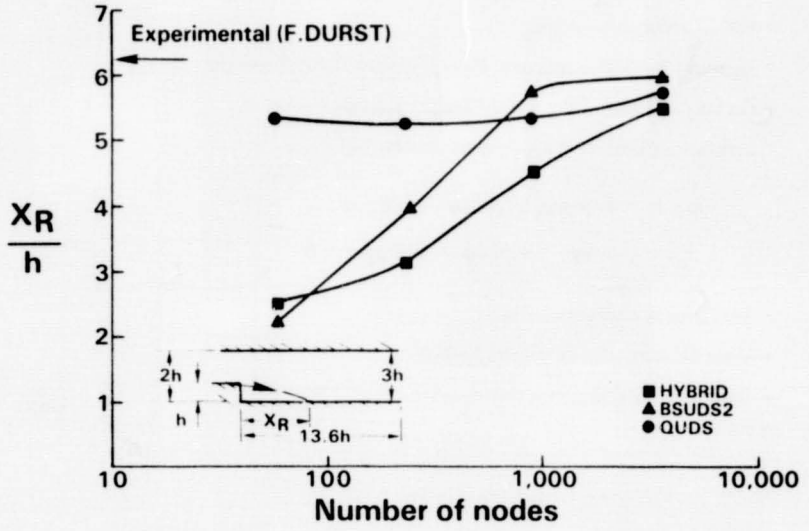

SECOND LAMINAR FLOW TEST CASE

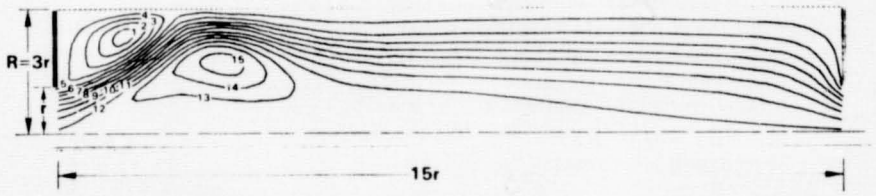

Flow in a sudden expansion with swirl; Re = 450, swirl no. = 0.66, at 45-degree vane angle, contraction ratio = 9.0

STAGNATION STREAMLINES FOR SECOND LAMINAR FLOW TEST CASE ON 40 x 20 MESH

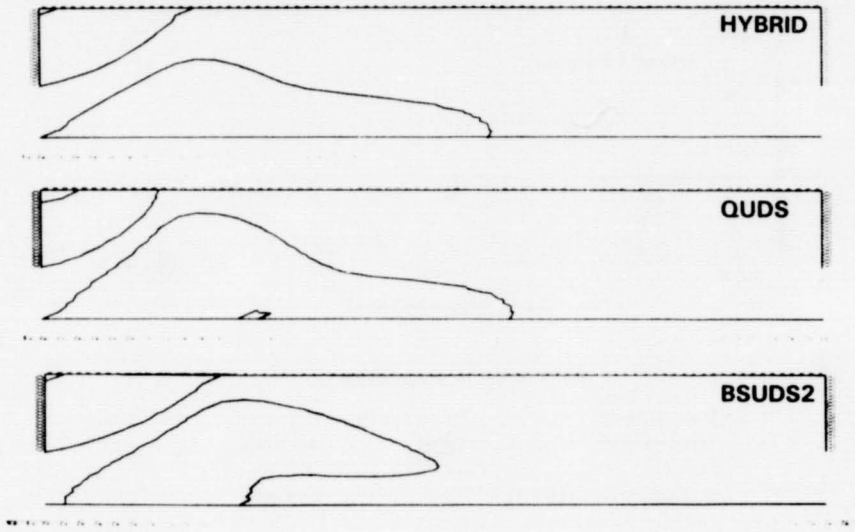

STAGNATION STREAMLINES FOR SECOND LAMINAR FLOW TEST CASE ON 78 x 40 MESH

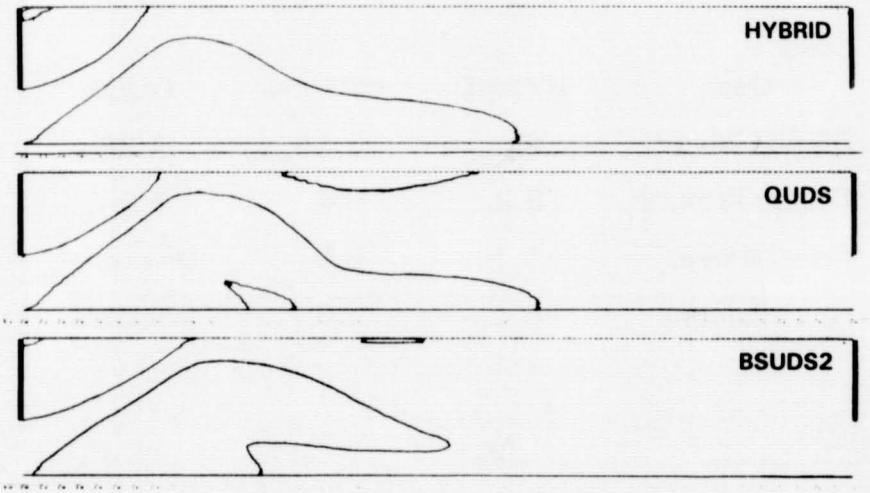

FIRST TURBULENT TEST CASE

Flow over backward facing step

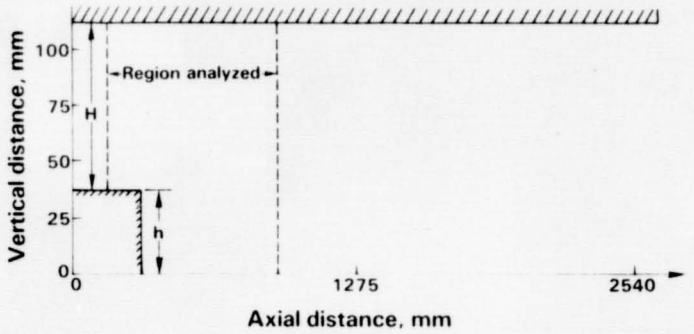

Inlet boundary conditions

Mean velocity	60.11 ft/sec	(18.32 m/s)
Temperature	59°F	(41.2°C)
Pressure	14.7 psia	(101.35 kN/m^2)
Boundary layer thickness	0.33 inch	(8.4 mm)
Turbulence intensity	0.003	

CALCULATED REATTACHMENT POINTS (MEASURED 7 STEP HEIGHTS)

Case	HYBRID	BSUDS2	QUDS
Dumb (15x17)	2.4	2.25	2.28
Coarse (26x29)	5.2	5.4	5.5
Fine (50x56)	5.7	5.9	Unstable
Fine adjusted (74x53)	5.8	5.8	Unstable

SECOND TURBULENT TEST CASE

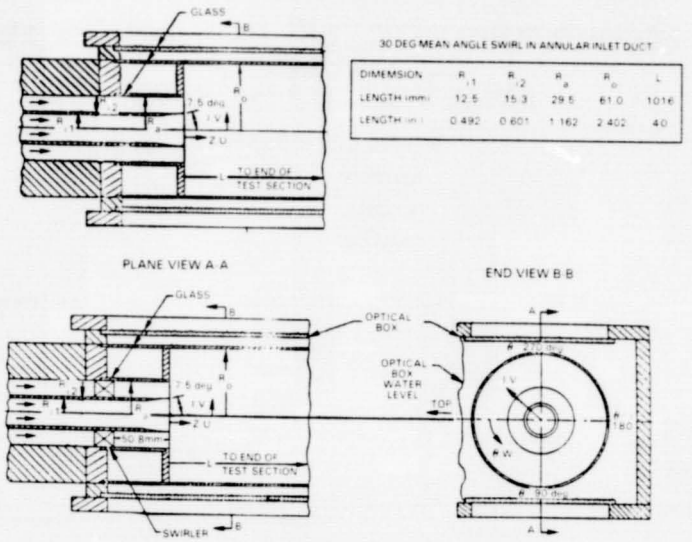

30 DEG MEAN ANGLE SWIRL IN ANNULAR INLET DUCT

DIMENSION	R_{i1}	R_{i2}	R_a	R_o	L
LENGTH (mm)	12.5	15.3	29.5	61.0	1016
LENGTH (in.)	0.492	0.601	1.162	2.402	40

Co-axial jets with and without swirl

SECOND TURBULENT TEST CASE WITH SWIRL

Inlet boundary conditions;

- **Measurements at x = 5mm were used**
- **This plane was considered as inlet plane**

SECOND TURBULENT TEST CASE WITH SWIRL

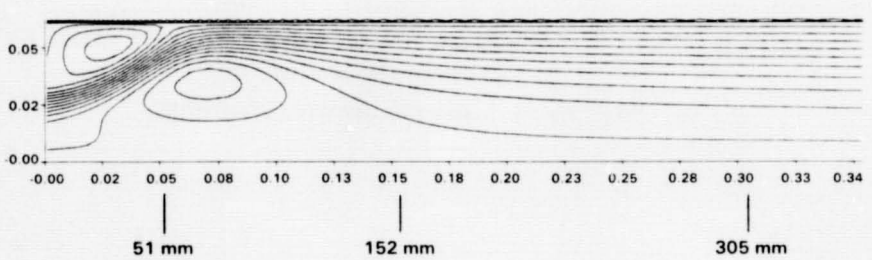

Stations at which comparisons have been made

SECOND TURBULENT TEST CASE WITH SWIRL
COMPARISON OF
AXIAL VELOCITY PROFILES

Coarse grid (40x35)

HYBRID ————

QUDS — — —

BSUDS2 - - - - - - - -

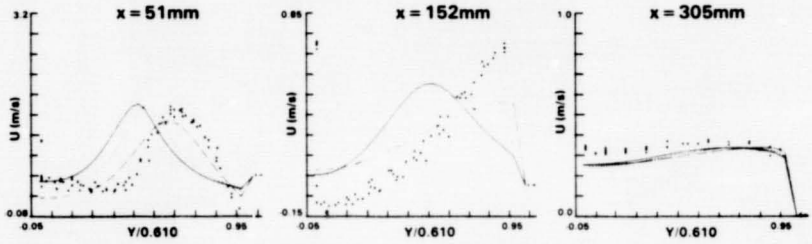

QUDS seems more accurate

No difference in accuracy for fine grid (47x43)

SECOND TURBULENT TEST CASE WITH SWIRL
COMPARISON OF
TANGENTIAL VELOCITY PROFILES

Coarse grid (40x35)

HYBRID ————

QUDS — — —

BSUDS2 - - - - - - - -

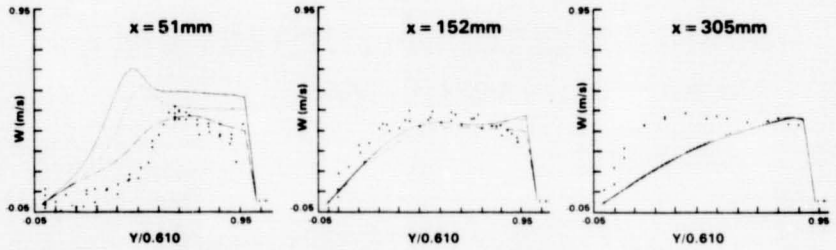

QUDS seems more accurate

No difference in accuracy for fine grid (47x43)

SINGLE CELL CALCULATIONS OF CONVECTION OF NORMAL DISTRIBUTION

$$\phi(x) = \exp(-\tfrac{1}{2}(\eta\Delta^*)^2)$$

$$(\eta = x/\Delta, \Delta^* = \Delta/\sigma)$$

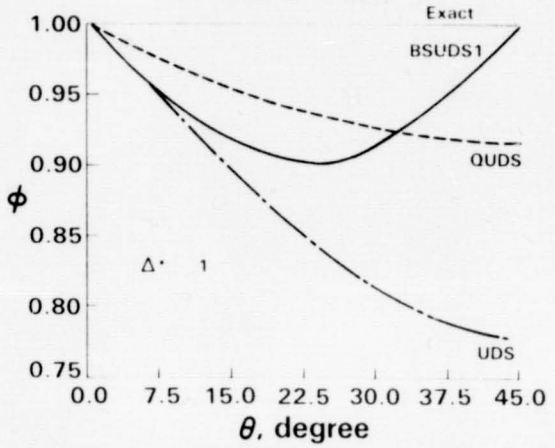

Influence of the flow angle on the error for various difference schemes

OBSERVATIONS

- QUDS unstable — needs a better solver
- No significant differences between HYBRID, QUDS and BSUDS2 for intelligent fine grids (1000-1500 nodes)
- QUDS more accurate than BSUDS2 most of the time
- BSUDS2 more accurate for second laminar test case — very strong streamline curvature
- Flows with swirl more sensitive to difference schemes

N84 20537

D2

APPLICATION OF IMPROVED NUMERICAL SCHEMES

G. M. Neely
NASA Lewis Research Center

There have been a variety of methods used to solve the Navier-Stokes equations. Most schemes which solve the steady state form of these equations employ the SIMPLE (Semi-Implicit Method for Pressure-Linked Equations) method developed by Patankar and Spalding in 1972 (ref.1). Although this scheme has proven to be quite effective, its convergence rate can be improved. This investigation focuses on two approaches which accelerate the solution of the steady state Navier-Stokes equations.

The SIMPLER algorithm (ref. 2), a revised version of SIMPLE, provides a more accurate pressure field for each iteration through the momentum equations, thereby speeding convergence. PISO (Pressure Implicit Split Operator, ref.3) performs a secondary correction of the velocity and pressure fields (after the typical pressure correction) which enhances convergence. Both schemes account for terms neglected in the SIMPLE approach, but do so in slightly different ways.

A series of calculations of two-dimensional driven cavity flow and flow over a step were made to examine the effect of geometry on the performance of these schemes. Computations were carried out on a series of progressively finer grids. The effect of relaxation number on convergence rate was analyzed, using results from SIMPLE as criteria for performance correlation.

Preliminary results indicate the following:
1. The improved schemes promoted convergence by up to sixty percent for the driven cavity and forty percent for flow over a step.
2. For the driven cavity problem, the efficiency of PISO and SIMPLER increased as the number of nodes increased.
3. To ensure faster convergence, higher relaxation numbers must be applied.

References

1. Patankar,S.V. and Spalding, D.B.(1972). A Calculation Procedure for Heat, Mass and Momentum Transfer in Three Dimensional Parabolic Flows, Int. J. Heat Mass Transfer, vol. 15, p.1787.

2. Patankar, S.V. (1979). A Calculation Procedure for Two Dimensional Elliptic Situations, Num. Heat Transfer, vol. 2.

3. Issa, R.I. (1982). Solution of Implicitly Discretised Fluid Flow Equations by Operator-Splitting, Int. Rep. Dept. Mineral Resources Eng., Imperial College, London.

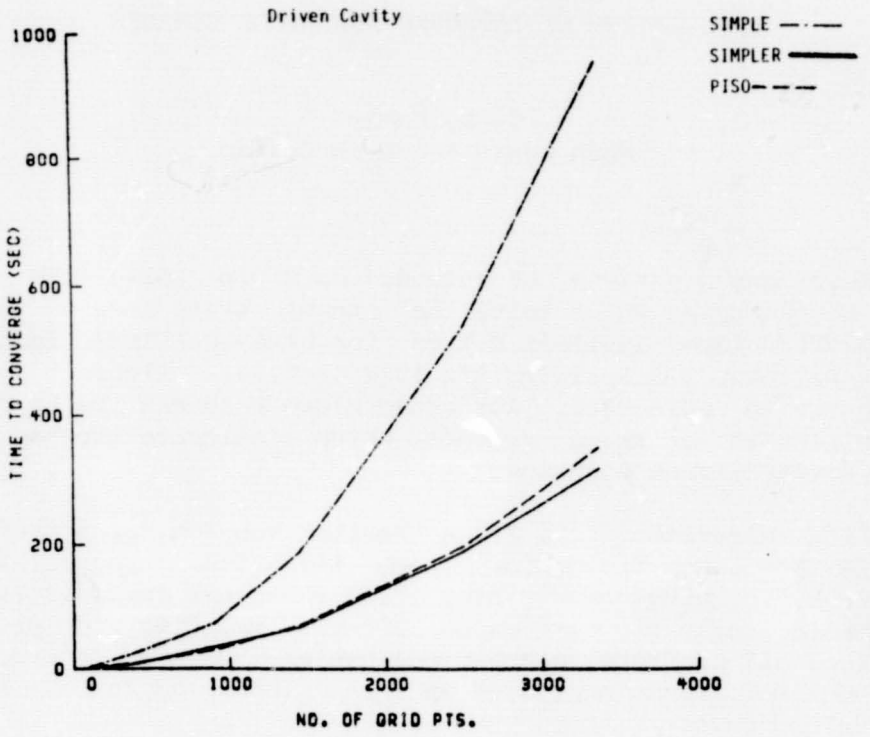

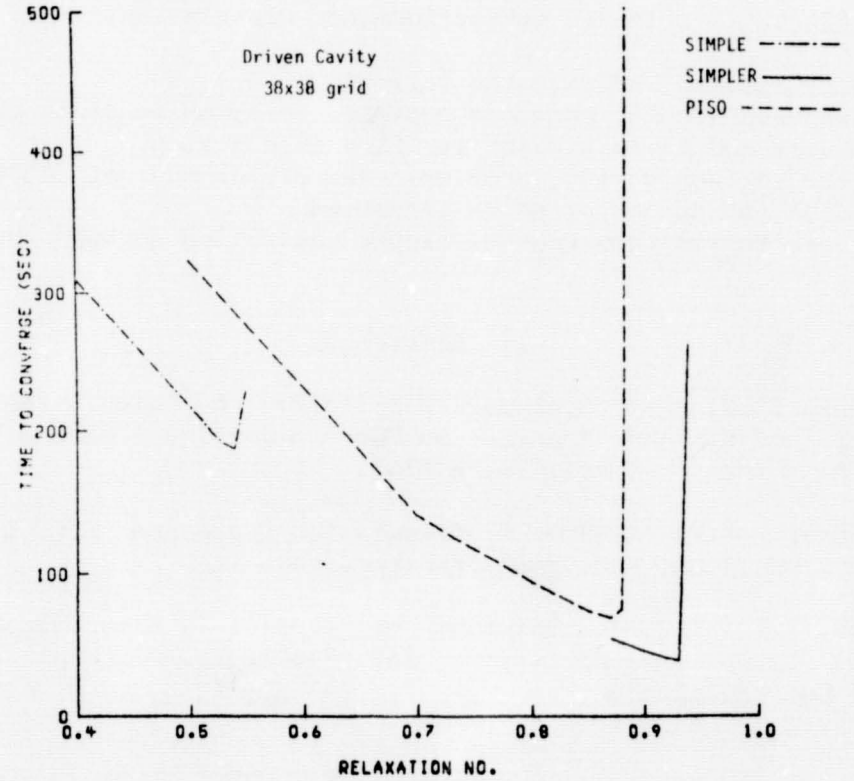

D13

NUMERICAL MODELING OF TURBULENT FLOW

R. W. Claus
NASA Lewis Research Center

Three dimensional combustor calculations are currently stretching the computer hardware capabilities and the computing budgets of gas turbine manufacturers. One of the main reasons for this relates to the large number of complex physical processes occuring in the combustor. Airflow, fuel spray, reaction kinetics, flame radiation, and , not the least of which, turbulence must be modeled and the related differential equations solved. Obtaining accuracte solutions to these modeled equations entails another difficulty. Current combustor codes are, generally, based on the SIMPLE algorithem developed by Patankar and Spaulding, ref. 1. One of the key features of this algorithem is the use of hybrid differencing to approximate the convective terms in the governing equations. In most practical calculations this results in the use of first order accurate upwind differencing for most of the flow field. The overly dissipative solutions obtained using this scheme can mask important flow field features, ref. 2. Ideally, this can be overcome through the use of additional grid points. In three dimensional calculations ,however, this becomes impractical since the computational work involved increases greatly as grid points are added.

Other discussions in this conference will address methods to improve the accuracy of combustor flow field calculations and methods to speed the convergence of the modeled equations. This talk will focus on aspects of merging these two new technologies. The improved accuracy discretization schemes have a negative impact on the speed of convergence of the modeled equations that the improved solution algorithems may not overcome. A description of the causes of this problem and potential solutions will be examined.

REFERENCES

1. Patankar, S.V. and Spaulding, D.B., "A Calculation Procedure for Heat, Mass and Momentum Transfer in Three-Dimensional Parabolic Flows," International Journal of Heat and Mass Transfer, Vol.15, No. 10, Oct. 1972.

2. Claus, R.W.,"Analytical Calculation of a Single Jet in Crossflow and Comparison With Experiment," NASA TM83027, 1983.

ADVANCED NUMERICS FOR MULTI-DIMENSIONAL FLUID FLOW CALCULATIONS

S. P. Vanka
Argonne National Laboratory

In recent years, there has been a growing interest in the development and use of mathematical models for the simulation of fluid flow, heat transfer and combustion processes in engineering equipment (ref. 1). The equations representing the multi-dimensional transport of mass, momenta and species are numerically solved by finite-difference or finite-element techniques. However despite the multitude of differencing schemes and solution algorithms, and the advancement of computing power, the calculation of multi-dimensional flows, especially three-dimensional flows, remains a mammoth task. The following discussion is concerned with the author's recent work on the construction of accurate discretization schemes for the partial derivatives, and the efficient solution of the set of nonlinear algebraic equations resulting after discretization. The present work has been jointly supported by the Ramjet Engine Division of the Wright Patterson Air Force Base, Ohio, and the NASA Lewis Research Center.

FINITE-DIFFERENCING

An efficient finite-difference scheme must represent the differential equations to a high accuracy and must be stable. In spite of the many formally higher order schemes that have been proposed, practical calculations have bee limited to the use of simple first order schemes. The reasons for this are that either the proposed schemes are unstable in general circumstances or they have limited range of formal accuracy. The complexities of the construction of accurate schemes stem from the following flow characteristics.

a) High grid Peclet number

b) Stream lines skewed with grid lines

c) Pressure gradients

d) Nonlinear source terms, also containing derivatives.

In designing any generally useful finite-difference calculation procedure, it is necessary to consider all of the above factors carefully.

The present work of the author is concerned with the integration of several individual ideas into a general purpose algorithm. Two promising schemes that are being considered are the influence scheme approach of Chen et al. (ref. 2) and of Raithby et al. (ref. 3) and the compact differencing approach of Kriess (ref. 4). In the influence scheme approach, the differential operator is analytically integrated

over two (or three) dimensional subdomains after linearizing it with previous iterate values. A profile is assumed for variations along the boundaries. This results in an algebraic linear relation of the form

$$\phi_p = \sum_{i=1}^{8} C_I \phi_I + \sum_{i=1}^{9} D_I Q_I \qquad (1)$$

where ϕ_I are neighbor values and Q_I represent the neighbor source terms. C_I and D_I represent coefficients. The advantages of the above approach are that it fully considers the multi-dimensional effects and is stable at high Peclet numbers.

In a compact differencing scheme the derivatives are represented to a fourth order accuracy but with a tridiagonal structure. The tridiagonal structure is advantageous for the solution of equations and for the treatment of boundary conditions. The compact differencing scheme however has been found in our preliminary work to be unstable (and inaccurate) at the high Peclet numbers of current interest. However the concept can still be used to represent the various other derivatives that occur in the source terms and the pressure gradients. The above two approaches are currently being pursued.

SOLUTION ALGORITHM

The solution of the nonlinear algebraic equations obtained after discretization is a mammoth task. The required computer times are large and convergence is not always assured. Current work in this direction has led to a fully-coupled solution of the nonlinear equations of momentum and continuity. The coupled set of nonlinear equations are solved with a Newton-Raphson method and efficient sparse matrix techniques. The turbulence equations are solved decoupled from the momentum and continuity equations. The equations are also arranged as blocks which are then preordered to reduce the computer storage and time. This algorithm has been extended to reacting flows and successful calculations have been made of isothermal turbulent flows and turbulent confined diffusion flames. The algorithm has been observed to be rapidly convergent and insensitive to variations in grid aspect ratio, flow Reynolds number and the number of finite-difference nodes.

Results of Some Calculations

Several calculations of laminar and turbulent recirculating flows have been made with different finite-difference grids. These have been documented in detail in Vanka (refs. 5, 6 and 7). In all the cases tested, rapid diminution of the residuals in the equations has been observed. Calculations have been made with finite-difference grids up to (80 x 95) size for turbulent flow in a sudden expansion. In the present report two tables are presented which demonstrate generally the observed rates of convergence. The first one is for a turbulent flow in a sudden expansion for the experiments of Craig et al. (ref. 8), with a (80 x 95) grid. The second one shows the rate of convergence for a confined diffusion flame for a configuration studied by Lockwood et al. (ref. 9). The latter calculations employed a (32 x 27) grid.

REFERENCES

1. NASA Phase I Aerothermal Modelling Program, reports NASA CR 168202, NASA CR 168243.

2. Chen, C. J.; and Li, P.: Finite Differential Method in Heat Conduction - Application of Analytic Solution Technique. ASME paper 79-WA-HT-50, 1979.

3. Stubley, G. D.; Raithby, G. D.; Strong, A.B.; and Woolner, K. A.: Simulation of Convection and Diffusion Processes by Standard Finite Difference Schemes and by Influence Schemes. Computer Methods in Applied Mechanics and Engineering, vol. 35, 1982, pp. 153-168.

4. Kriess, H. O.; and Oligar, J.: Comparison of Accurate Methods for the Integration of Hyperbolic Equations. Tellus, vol. 24, 1972, pp. 199-215.

5. Vanka, S. P.; and Leaf, G. K.: Fully-coupled Solution of Pressure-linked Fluid Flow Equations. Argonne National Laboratory Report, ANL-83-73, 1983.

6. Vanka, S. P.: Computations of Turbulent Recirculating Flows with Fully Coupled Solution of Momentum and Continuity Equations. Argonne National Laboratory Report, ANL-83-74, 1983.

7. Vanka, S. P.: Fully Coupled Calculation of Fluid Flows with Limited Use of Computer Storage. Argonne National Laboratory Report, ANL-83-87, 1983.

8. Craig, R. R.; Hahn, E. Y.; Nejad, A. S.; and Schwartzkopf, K. G.: A General Approach for Obtaining Unbiased LDV Data in Highly Turbulent Non-reacting and Reacting Flows. AIAA, 22nd Aerospace Sciences Meeting, Reno, Nevada, 1984.

9. Lockwood, F. C.; El-Mahallawy, F. M.; and Spalding, D. B.: An Experimental and Theoretical Investigation of Turbulent Mixing in a Cylindrical Furnace. Combustion and Flame, vol. 23, 1974, pp. 283-293.

Table 1. Convergence Rate for Craig's Sudden-expansion Flow, 80 x 95 Grid

Iter.	$\delta u/u_{in}$	$\delta v/u_{in}$	$\delta p/u_{in}^2$	δk	$\delta \varepsilon$
1	1.391E-1	2.904E-2	2.766E-1	5.846E-5	8.858E-5
5	2.879E-2	1.059E-2	1.155E-2	4.355E-5	3.344E-5
10	7.300E-2	5.500E-2	1.171E-1	4.584E-5	3.336E-4
15	2.717E-3	3.224E-4	8.086E-4	3.682E-5	5.972E-5
20	1.508E-5	1.360E-5	2.597E-5	4.246E-6	1.970E-6

Table 2. Convergence Rate for Confined Turbulent Diffusion Flame Calculations (Experiments of Lockwood et al.) with 32 x 27 grid

Iter.	$\delta u/u_c$	$\delta v/u_c$	$\delta p/\rho u_c^2$	δk	$\delta \varepsilon$	δf	δg
1	6.51E-1	3.25E-1	7.83E-1	1.75E-2	1.00E+0	2.00E-1	9.90E-2
5	6.75E-1	1.91E-1	5.85E-2	1.91E-4	1.31E-2	2.61E-1	3.32E-2
10	2.60E-2	6.55E-3	5.98E-3	2.67E-5	1.53E-3	1.31E-2	3.67E-3
15	2.48E-3	9.66E-4	3.56E-4	2.73E-6	1.13E-4	2.27E-3	4.66E-4
20	2.54E-4	1.79E-4	2.80E-5	1.39E-5	8.91E-5	2.62E-4	3.85E-5
25	4.34E-5	3.65E-5	1.54E-5	6.05E-7	4.58E-5	2.55E-5	4.95E-6

D15

N84 20540

GRID FLEXIBILITY AND PATCHING TECHNIQUES

T. G. Keith, L. W. Smith, C. N. Yung,
S. H. Barthelson, and K. J. DeWitt

The University of Toledo

The numerical determination of combustor flowfields is of great value to the combustor designer. An a priori knowledge of the flow behavior can speed the combustor design process and reduce the number of experimental test rigs required to arrive at an optimal design. Even 2-D steady incompressible isothermal flow predictions are of use; many codes of this kind are available [1], each employing different techniques to surmount the difficulties arising from the nonlinearity of the governing equations and from typically irregular combustor geometries. We will look at mapping techniques (algebraic and elliptic PDE), and at adaptive grid methods (both multi-grid and grid embedding) as applied to axisymmetric combustors.

ALGEBRAIC GRID GENERATION IN THE STARPIC CODE

The solution of the Turbulent Reynolds Equations for arbitrary geometries can be handled in several ways [1]. One popular technique is to represent a boundary with discrete 90° steps. Atlernatively, the geometry can be mapped into a square solution plane via a variety of available transformations. The simplest transformation is an algebraic one as shown in Figure 2.

On transforming the governing equations, new chain rule terms are introduced, each of which contains a dh/dx term which comes into play only at axial locations where there is a sloping or curved wall segment, thereby mathematically affecting expansion and recirculation in the flow. The complexity of extra terms is offset by the ability of the technique to handle general boundary shapes, as well as the simplification of boundary conditions in the mapped plane. For these reasons algebraic mapping shows great promise. Figures 1 through 6 show the effects of algebraic mapping on the STARPIC code.

ELLIPTIC PDE GRID GENERATION FOR A BIFURCATED COMBUSTOR INLET DIFFUSER

The purpose of a combustor inlet diffuser is to convert kinetic energy to pressure; a reliable prediction method for diffuser flows will lead to the efficacious design of those diffusers. In this work body fitted coordinate transformations are employed in the solution of turbulent flows in a bifurcated combustor inlet diffuser. The work is aimed at comparing the numerical solution for different kinds of transformations with experimental results. Furthermore, different numerical methods will also be employed for comparison. Figures 7 through 12 illustrate this work.

MULTIGRID AND GRID EMBEDDING TECHNIQUE FOR TURBULENT FLOWS IN COMBUSTOR

A multigrid method [2] applied to axisymmetric turbulent flows is useful in speeding convergence of numerical schemes. This method reduces global errors by economical relaxation of errors on coarse meshes instead of by labor intensive relaxation on one fine mesh. The multigrid equations, a summary of the multigrid algorithm, and relationships between coarse and fine meshes for a staggered mesh are depicted in Figures 13 through 17.

Grid embedding [3,4] similar to the multigrid method, uses a fine mesh in steep gradient regions to refine the solution locally, where needed. It eliminates the wasteful process of using a fine grid globally, including in regions where it is not needed. Grid embedding is depicted for a staggered mesh. As indicated in the last figure, this method is still under development. Like the multigrid method, it will steadily be extended to more arbitrary combustor geometries.

REFERENCES

1. Lilley D. G. and D. L. Rhode, "A Computer Code for Swirling Turbulent Axisymmetric Recirculating Flows in Practical Isothermal Combustor Geometries," Grant NAG 3-74, February 1982.

2. Brandt, A., "Multi-Level Adaptive Solutions to Boundary-Value Problems," Mathematics of Computation, Volume 31, No. 138, April 1977, pp. 333-390.

3. Brown, Jeffrey J., "An Embedded-Mesh Potential Flow Analysis," AIAA Journal, Volume 22, No. 2, February 1984, pp. 174-178.

4. McCarthy, D. R. and T. A. Reyhner, "Multigrid Code for Three-Dimensional Transonic Potential Flow About Inlets," AIAA Journal, Volume 10, No. 1, January 1982, pp. 45-50.

1. ALGEBRAIC GRID GENERATION IN THE STARPIC CODE - LARRY SMITH
2. ELLIPTIC PDE GRID GENERATION FOR A BIFURCATED COMBUSTOR INLET DIFFUSER - CHAIN-NAN YUNG
3. MULTIGRID AND GRID EMBEDDING TECHNIQUES FOR TURBULENT FLOWS IN COMBUSTORS - STEVE BARTHELSON

ALGEBRAIC GRID GENERATION AND STARPIC CODE

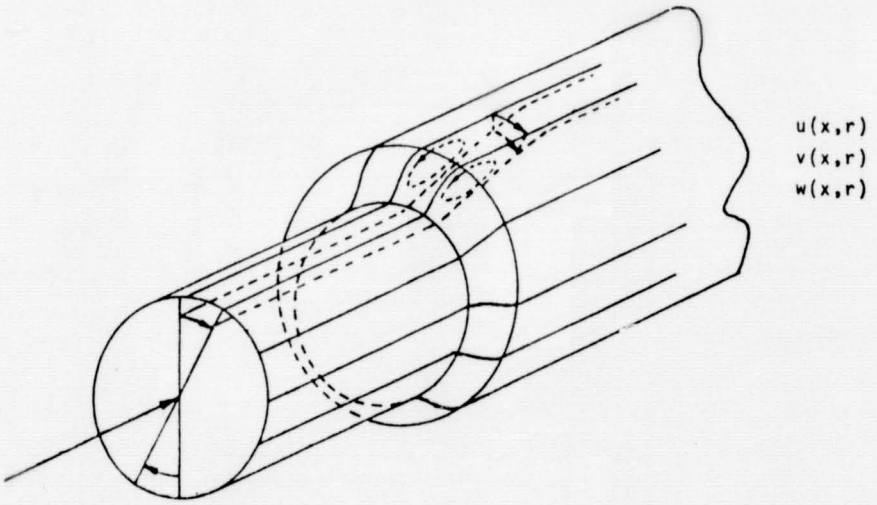

FLOW FIELD AND VARIABLES

GOVERNING EQUATIONS AND MAPPING

TURBULENT REYNOLDS EQUATIONS (IN GENERIC FORM)

$$\frac{1}{r}\left[\frac{\partial}{\partial x}(\rho u r\phi - \Gamma r\frac{\partial}{\partial x}) + \frac{\partial}{\partial r}(\rho v r\phi - \Gamma r\frac{\partial}{\partial r})\right] = S_\phi$$

WHERE ϕ REPRESENTS:

u
v
w
1 (Continuity)
k
ϵ

TRANSFORMATION: $\xi = x$

$\eta = r/h(x)$ where $h(x)$ is any single-valued function.

TRANSFORMATION OF DIFFERENTIAL OPERATORS:

$$\frac{\partial}{\partial x} = \frac{\partial \xi}{\partial x}\frac{\partial}{\partial \xi} + \frac{\partial \eta}{\partial x}\frac{\partial}{\partial \eta} = \boxed{\frac{\partial}{\partial \xi} - \frac{\eta}{h}\frac{dh}{dx}\frac{\partial}{\partial \eta}}$$

$$\frac{\partial}{\partial r} = \frac{\partial \xi}{\partial r}\frac{\partial}{\partial \xi} + \frac{\partial \eta}{\partial r}\frac{\partial}{\partial \eta} = \boxed{\frac{1}{h}\frac{\partial}{\partial \eta}}$$

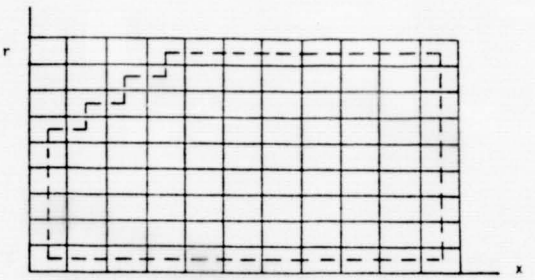

STARPIC PHYSICAL AND SOLUTION PLANE

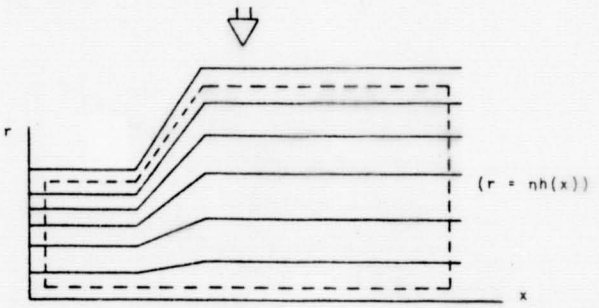

STARMAP PHYSICAL PLANE

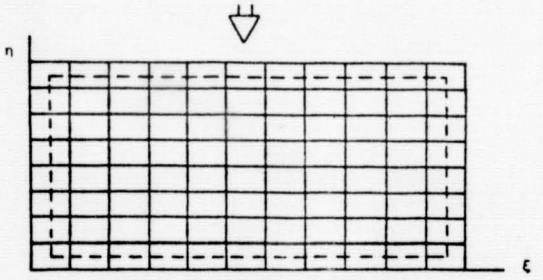

STARMAP TRANSFORMED PLANE

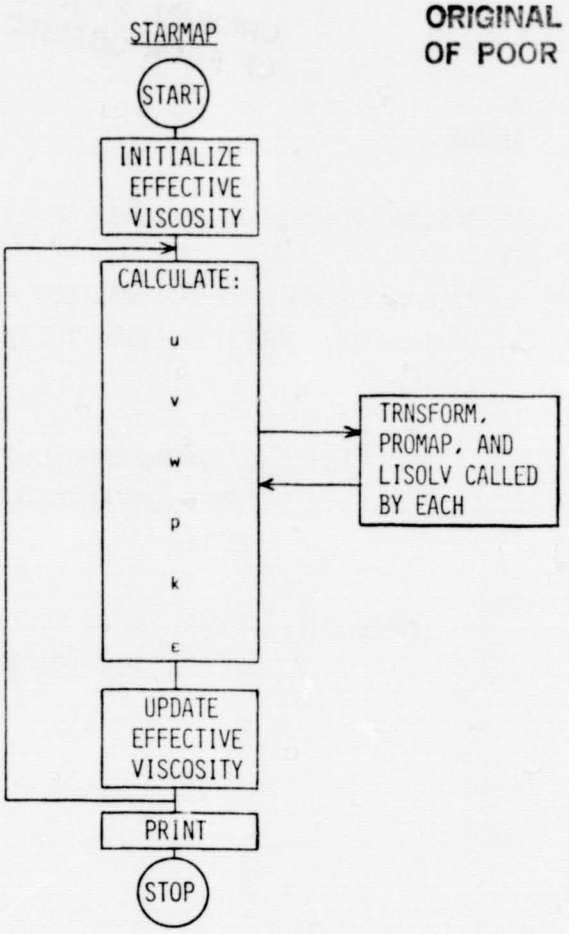

ADAPTED FROM
STARPIC

CONTRASTING STARPIC AND STARMAP

ADVANTAGES OF MAPPING:

ANY SINGLE VALUED FUNCTION VALID FOR $h(x)$.

SOLUTION OCCURS ON A SQUARE MESH IN THE ξ - η PLANE.

BOUNDARY CONDITIONS ARE SIMPLIFIED.

DISADVANTAGES:

ADDITIONAL TERMS ARISE VIA TRANSFORMATION.

HANDLING OF "WALL FUNCTIONS" NOT OBVIOUS.

STATUS

NEARING OPERATION OF COMPLETELY MAPPED CODE.

FOLLOWING FIRST SUCCESSFUL RUN, CODE WILL BE TESTED WITH A VARIETY OF GEOMETRIES IN TWO PHASES:

PHASE (I) VALIDATION OF STARMAP IN DIRECT COMPARISON WITH STARPIC RESULTS;

PHASE (II) GENERALIZATION TO OTHER GEOMETRIES NOT PRESENTLY HANDLED BY STARPIC.

ELLIPTIC PDE GRID GENERATION FOR A

BIFURCATED COMBUSTOR INLET DIFFUSER

FLOWFIELD

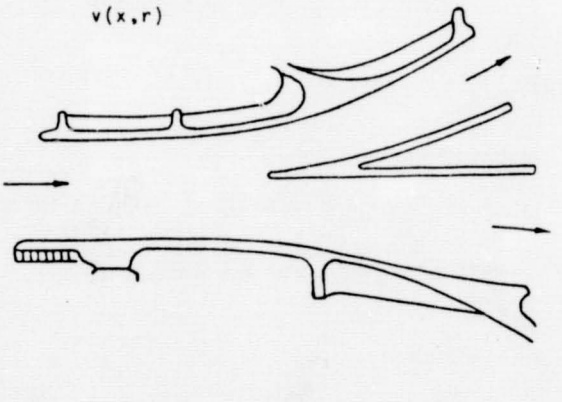

BODY FITTED COORDINATE TRANSFORMATION

$$\frac{\partial^2 x}{\partial \xi^2} + \frac{\partial^2 x}{\partial n^2} = P(\xi, n) \qquad \frac{\partial^2 y}{\partial \xi^2} + \frac{\partial^2 y}{\partial n^2} = Q(\xi, n)$$

WHERE $P = \sigma(\xi_x^2 + \xi_y^2)$ AND $Q = \tau(n_x^2 + n_y^2)$

$$\sigma = -\frac{x_\xi x_{\xi\xi} + y_\xi y_{\xi\xi}}{x_\xi^2 + y_\xi^2} \quad \text{on } n = n_b$$

$$\tau = -\frac{x_n x_{nn} + y_n y_{nn}}{x_n^2 + y_n^2} \quad \text{on } \xi = \xi_a$$

INTERIOR POINTS OF σ AND τ ARE CALCULATED BY LINEAR INTERPOLATION ALONG GRID LINES.

INVERTING YIELDS:

$$\alpha(x_{\xi\xi} + \sigma x_\xi) - 2\beta x_{\xi n} + \gamma(x_{nn} + \tau x_n) = 0$$

$$\alpha(y_{\xi\xi} + \sigma y_\xi) - 2\beta y_{\xi n} + \gamma(y_{nn} + \tau y_n) = 0$$

WHERE

$$\alpha = x_n^2 + y_n^2 \,, \quad \beta = x_\xi x_n + y_\xi y_n \,, \quad \gamma = x_\xi^2 + y_\xi^2$$

TRANSFORMED COORDINATE SYSTEMS

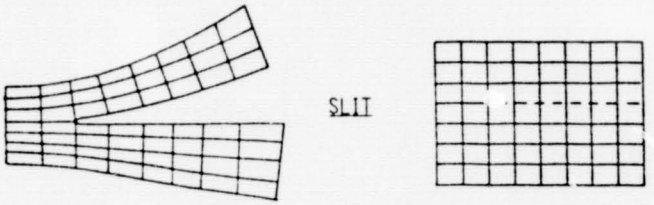

SLIT

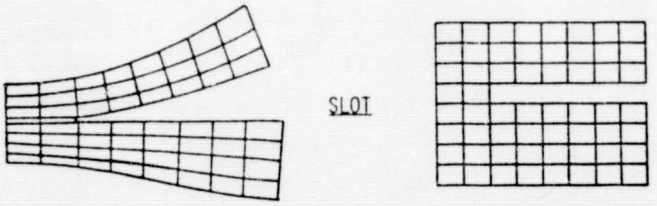

SLOT

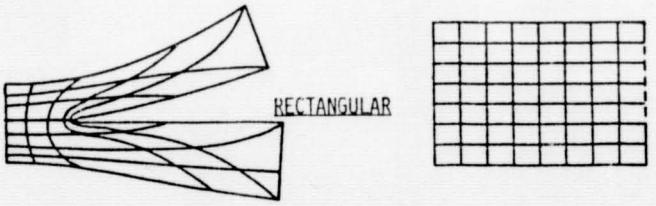

RECTANGULAR

GOVERNING EQUATIONS - COMPUTATIONAL DOMAIN

$$\frac{r_\eta}{J}\frac{\partial G}{\partial \xi} - \frac{r_\xi}{J}\frac{\partial G}{\partial \eta} + \frac{x_\xi}{rJ}\frac{\partial H}{\partial \eta} - \frac{x_\eta}{rJ}\frac{\partial H}{\partial \xi} = S_\phi$$

WHERE $G = \rho u\phi - \frac{\Gamma_\phi}{J}\left(r_\eta \frac{\partial \phi}{\partial \xi} - r_\xi \frac{\partial \phi}{\partial \eta}\right)$

$$H = \rho v r\phi - \frac{r\Gamma\phi}{J}\left(x_\xi \frac{\partial \phi}{\partial \eta} - x_\eta \frac{\partial \phi}{\partial \xi}\right)$$

INTEGRATION OVER A CONTROL VOLUME GIVES

$$\rho r F_1 \phi\Big|_W^E + \rho r F_2 \phi\Big|_S^N - \frac{r\Gamma_\phi}{J}\alpha \frac{\partial \phi}{\partial \xi}\Big|_W^E - \frac{\Gamma_\phi}{J}\gamma \frac{\partial \phi}{\partial \eta}\Big|_S^N$$

$$= S_\phi \text{ (VOLUME)} - \frac{r\Gamma_\phi}{J}\beta \frac{\partial \phi}{\partial \eta}\Big|_W^E - \frac{r\Gamma_\phi}{J}\beta \frac{\partial \phi}{\partial \xi}\Big|_S^N$$

WHERE $F_1 = r_\eta U - x_\eta V$, $F_2 = x_\xi V - r_\xi U$

DISCRETIZED EQUATIONS TAKE THE FORM

$$A_p \phi_p = \sum A_i \phi_i + S_\phi \text{ (VOLUME)} - \frac{r\Gamma_\phi}{J}\beta \frac{\partial \phi}{\partial \eta}\Big|_W^E - \frac{r\Gamma_\phi}{J}\frac{\partial \phi}{\partial \xi}\Big|_S^N$$

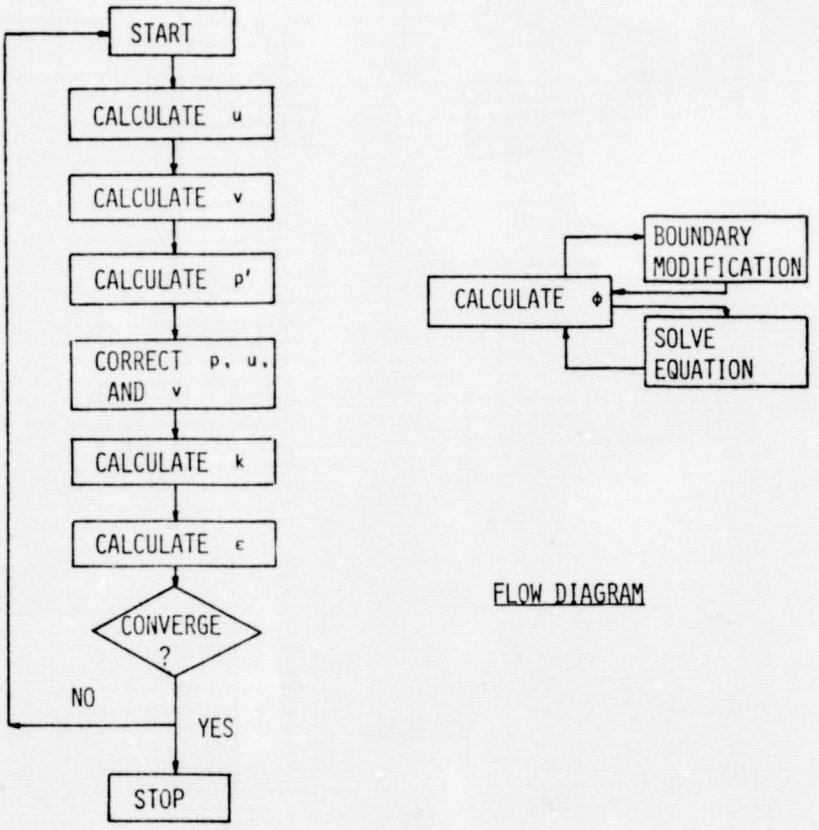

FLOW DIAGRAM

STATUS

TRANSFORMATION OF THE GEOMETRY HAS BEEN ACCOMPLISHED.

TRANSFORMED GOVERNING EQUATIONS HAVE BEEN DISCRETIZED.

COMPUTER CODES TO SOLVE TRANSFORMED EQUATIONS ARE BEING PREPARED.

MULTIGRID ALGORITHM

GRID HIERARCHY

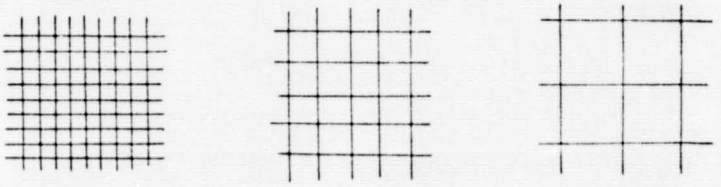

G^K G^{K-1} G^{K-2}

FUNDAMENTAL RELATIONS

LET $D\phi(r,x) - S_\phi(r,x) =$ SET OF TURBULENT REYNOLDS EQUATIONS

IN OPERATOR NOTATION THIS BECOMES

$$L(\phi) = 0$$

FINITE DIFFERENCING ON GRID G^K GIVES

$$L^k(\phi^k) = F^k$$

WHERE F^K IS MADE IDENTICALLY ZERO ONLY ON THE FINEST MESH

CHECK

$$\frac{\left|(\phi^k)_{I+2} - (\phi^k)_{I+1}\right|_{max}}{\left|(\phi^k)_{I+1} - (\phi^k)_{I}\right|_{max}}$$

IF THIS RATIO ~ 0.9, SWITCH TO COARSER GRID. ON GRID G^{K-1}

RELAX THE SET

$$L^{k-1}(\phi^{k-1}) = F^{k-1}$$

WHERE $$F^{k-1} = I_k^{k-1} F^k + \epsilon_k^{k-1}$$

I_k^{k-1} IS THE INJECTION OPERATOR FROM GRID G^{K-1} TO GRID G^K.

ϵ_k^{k-1} IS THE NUMERICAL ERROR AT G^{K-1} RELATIVE TO G^K AND IS ESTIMATED FROM

$$\epsilon_k^{k-1} = L^{k-1}(I_k^{k-1}\phi^k) - I_k^{k-1} L^k(\phi^k)$$

NOTE $$\epsilon_k^{k-1} = f(\phi^k)$$

$$F^{k-1} = g(\epsilon_k^{k-1})$$

THUS, F^{k-1} CHANGES UPON DIFFERENT VISITS TO G^{K-1}.

ONCE ϕ^{k-1} CONVERGES ON G^{K-1}, INTERPOLATION CAN SUPPLY MISSING VALUES IN G^K, I.E.,

$$\phi^k = I_{k-1}^k \phi^{k-1}$$

WHERE I_{k-1}^k IS AN INTERPOLATION OPERATOR FOR G^{K-1} TO G^K.

FOR SMOOTHER RESULTS, A MODIFIED VERSION IS USED

$$\phi_{new}^k = I_{k-1}^k \phi^{k-1} + \phi_{old}^k - I_{k-1}^k I_k^{k-1} \phi_{old}^k$$

$$= \phi_{old}^k + I_{k-1}^k (\phi^{k-1} - I_k^{k-1} \phi_{old}^k)$$

MULTIGRID PROCEDURE

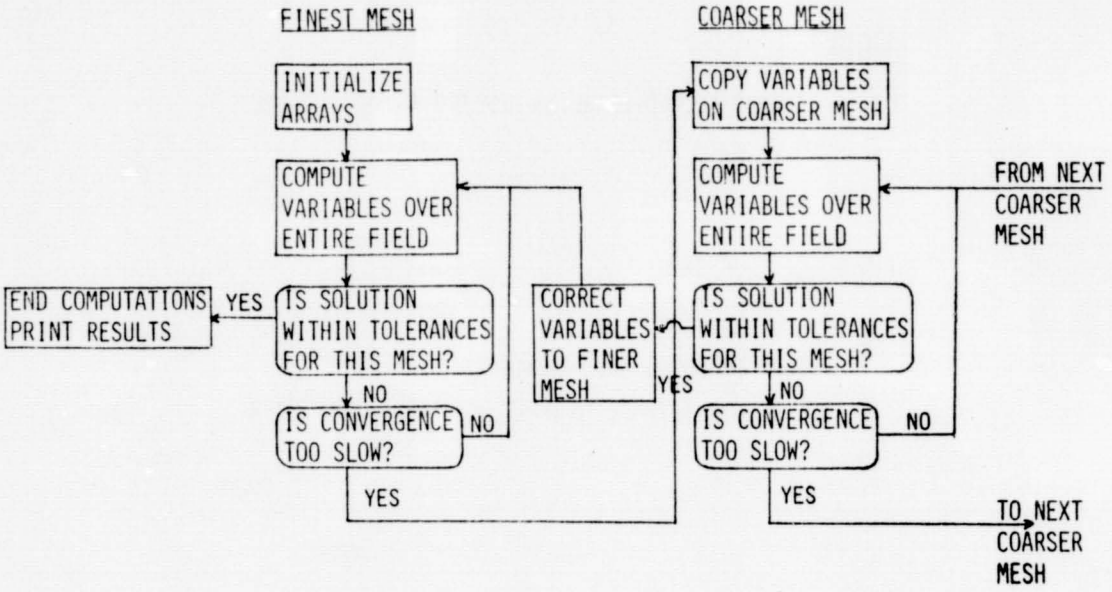

GRID EMBEDDING USING MULTIGRID

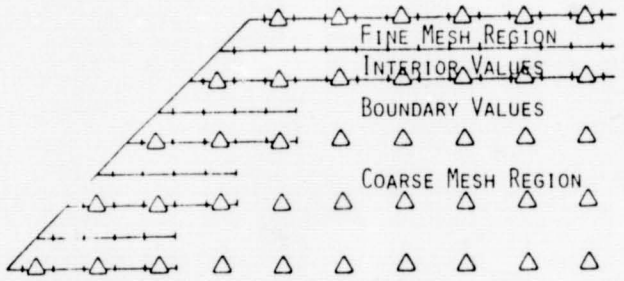

V VELOCITIES ONLY, SHOWN FOR SIMPLICITY

FLOW DOMAIN SUBDIVIDED INTO COARSE MESH REGION AND FINE MESH REGION, WHERE STEEP GRADIENTS REQUIRE MORE RESOLUTION;

△'S ARE FINEST GRID FOR COARSE MESH REGION - IN FINE MESH REGION, FINE GRID IS USED TO REFINE SOLUTION AT △'S;

BOUNDARY VALUES ARE UPDATED FOR EACH COARSE MESH SWEEP BY INTERPOLATION BETWEEN △'S ON BOUNDARY;

$L^k \phi^k = F^k$ IN COARSE MESH REGION, AS BEFORE, AT △'S;

$L^k \phi^k = L^k(I_k^{k+1} \phi^{k+1}) + I_{k+1}^k (F^{k+1} - L^{k+1} \phi^{k+1})$ AT △'S, INTERPOLATING FROM FINE MESH.

STATUS

MULTIGRID METHOD IS BEING APPLIED TO THE STARPIC CODE

FUTURE DEVELOPMENTS

REFINE EXISTING MULTIGRID METHOD
DEVELOP EMBEDDED GRID METHOD
EXTEND BOTH METHODS TO MORE ARBITRARY GEOMETRIES

MASS AND MOMENTUM TRANSPORT EXPERIMENTS WITH SWIRLING FLOW

Bruce V. Johnson and Richard Roback
United Technologies Research Center

An experimental study of mixing downstream of axial and swirling coaxial jets is being conducted to obtain data for the evaluation and improvement of turbulent transport models currently employed in a variety of computational procedures used throughout the propulsion community. The axial coaxial jet study was completed under Phase I and is reported in Ref. 1. The swirling coaxial jet study, which is the subject of this paper, was conducted under Phase II of the contract and is reported in Ref. 2. A TEACH code was acquired, checked out for several test cases, and is reported in Ref. 3. A study to measure length scales and to obtain a limited number of measurements with a blunt trailing edge inlet is being conducted under Phase III of the contract.

Qualitative and quantitative studies were conducted of the flow downstream of swirling coaxial jets discharging into an expanded duct. The ratio of annular jet diameter and duct diameter to the inner jet diameter were approximately 2 and 4, respectively. The inner jet peak axial velocity was approximately one-half the annular jet peak axial velocity and the mean swirl angle in the annular stream was approximately 30 degrees. Results from the studies were related to the five shear regions within the duct: (1) the wake region downstream of the inlet, (2) the shear layer between the jets, (3) the annular recirculation region, (4) the reattachment region, and (5) the centerline recirculation region (Fig. 1).

A flow visualization study was conducted using fluorescence dye as a trace material and high-speed motion pictures to record the dye patterns in selected r-z and r-θ planes. The results of the flow visualization study are summarized with the following observations (Figs. 2 and 3):

1. The high intensity turbulent eddies in the shear layers were not axisymmetric or periodic. The large scale waves and eddies apeared to have a range of wavelengths.

2. Downstream of the centerline recirculation region, the flow initially had large lobes which evolved into a vortex swirl pattern. There was little radial mixing downstream of the recirculation cell.

3. Two major mixing regions were observed: (1) at the interface between the inner jet and the centerline recirculation zone, and (2) at the interface between the inner jet and annular jet streams.

4. Mixing at the interface of the inner stream and the recirculation cell diluted the inner jet concentration and the resulting mixture of fluid from the recirculation cell and the inner jet was entrained by the swirling annular stream.

A detailed map of the velocity, concentration , mass turbulent transport rate and momentum turbulent transport rate distributions within the test section was obtained to provide data for the evaluation and improvement of turbulent transport models. Data sets of velocity component pairs were obtained simultaneously to determine mass turbulent transport rate, concentration and velocity. Probability density

functions (p.d.f.s) of all the forementioned parameters were obtained from the data sets. Mean quantitites (Figs. 4, 6 and 7), second central moments (Fig. 5), correlation coefficients, skewness and kurtosis were calculated to characterize each data set. Following are the principal results from this study:

1. Mixing for swirling flow was completed in one-third the length required for nonswirling flows (Figs. 8 and 9).

2. The principal momentum turbulent transport was in the r-z plane, i.e. $\overline{uv}$, and was attributed to the axial velocity gradients. Peak momentum turbulent transport rates were approximately the same as for the nonswirling flow condition (Fig. 6).

3. The axial mass turbulent transport is gradient rather than countergradient as occurred for nonswirling flow. The peak axial mass transport rates were greater than the peak radial mass transport rates even though the axial concentration gradients were approximately one-seventh the radial gradients (Figs. 4 and 7).

4. The mass turbulent transport process for swirling coaxial flow is very complicated. Mixing appears to occur in several steps of axial and radial mass transport coupled with a large radial mean convective flux. The transport process appears to begin with high concentration fluid from the inner jet mixing with fluid from the centerline recirculation zone. The diluted inner jet fluid is then convected by the negative axial velocities into the large eddy shear region between inner and annular streams.

5. Axial mass turbulent transport correlation coefficients as high as 0.5 were measured. These correlation coefficients were less than the peak mass transport correlation coefficients obtained for nonswirling flow although the axial mass transport rate for swirling flow was greater than that for nonswirling flow.

References

1. Johnson, B. V. and J. C. Bennett: Mass and Momentum Turbulent Transport Experiments with Confined Coaxial Jets, NASA Contractor Report CR-165574 (Interim Summary Report), November 1981.

2. Roback, R. and B. V. Johnson: Mass and Momentum Turbulent Transport Experiments with Confined Swirling Coaxial Jets, NASA Contractor Report CR-168252 (Interim Summary Report), August 1983.

3. Chiappetta, L. M.: User's Manual for a TEACH Computer Program for the Analysis of Turbulent, Swirling Reacting Flow in a Research Combustor. UTRC Report R83-915540-27 prepared under NASA Contract NAS3-22771, September 1983.

FIG. 1

SHEAR REGIONS WITH CONFINED, EXPANDING COAXIAL JETS

a) SWIRLING FLOW

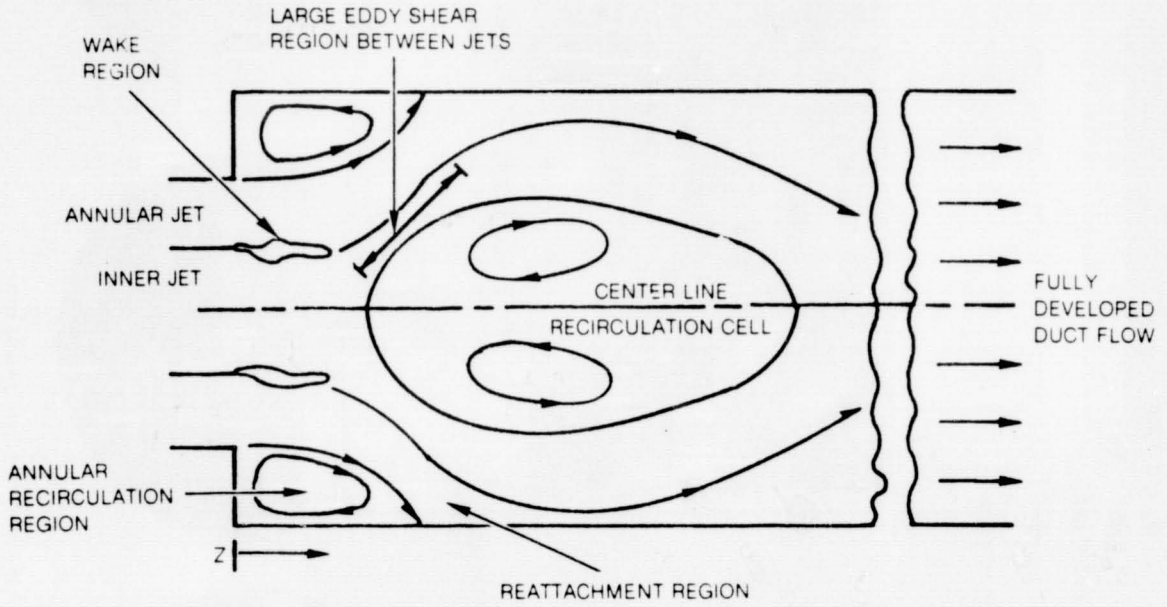

b) NONSWIRLING FLOW

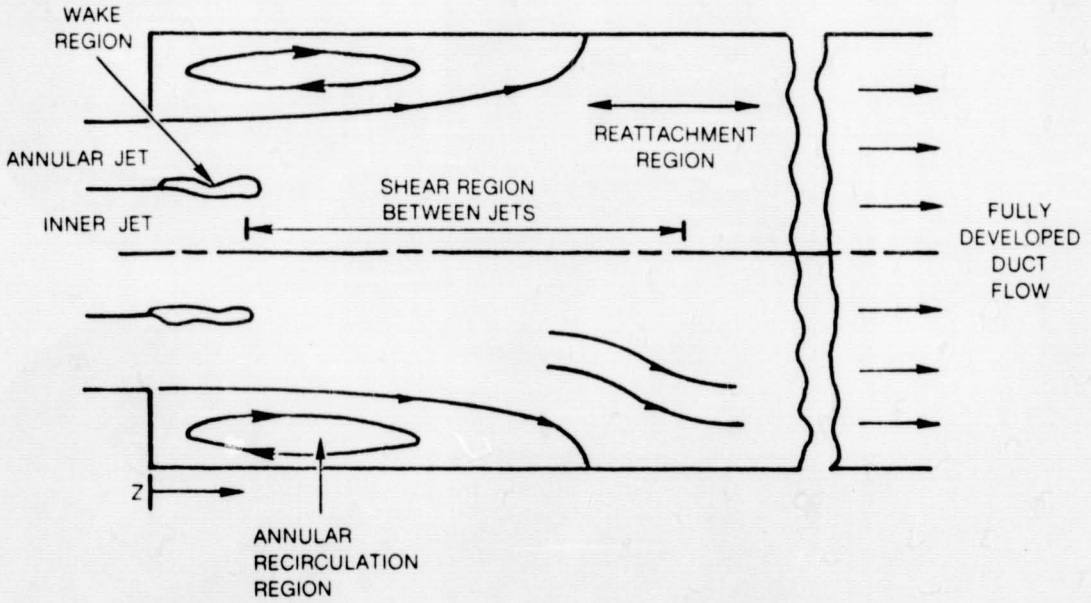

VISUALIZATION OF FLOW

$U_i = 0.52$ m/s $\quad U_a = 1.66$ m/s

$Q_i = 6.2$ gpm $\quad Q_a = 52.8$ gpm

r-z PLANE

$0 < z < 230$ mm

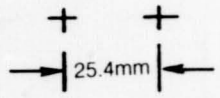

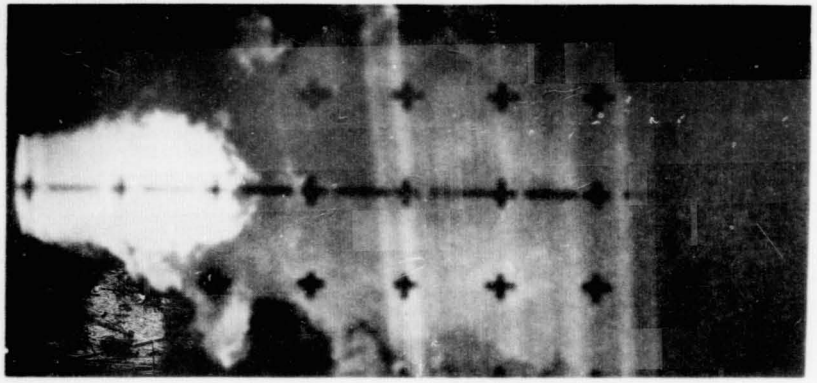

DYE ADDED TO INNER STREAM

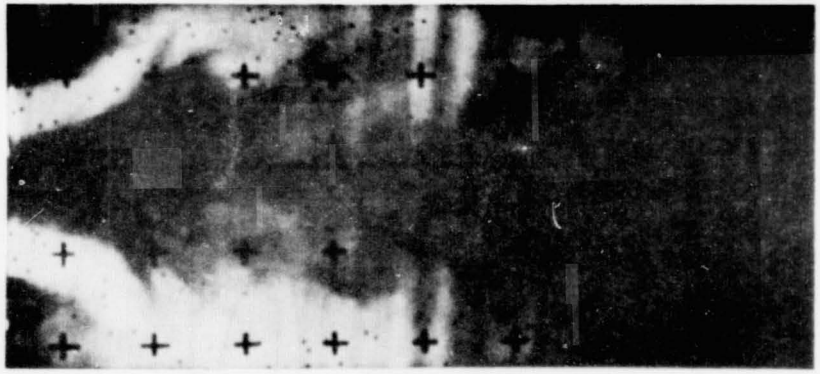

DYE ADDED TO ANNULAR STREAM

r-θ PLANE

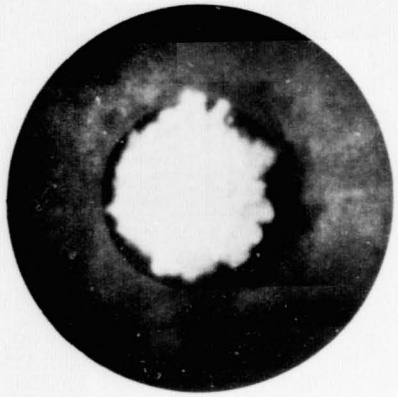

$z = 25$ mm

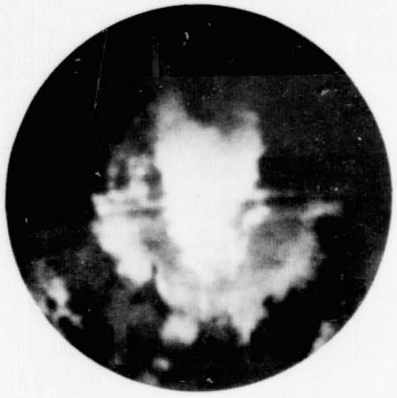

$z = 51$ mm

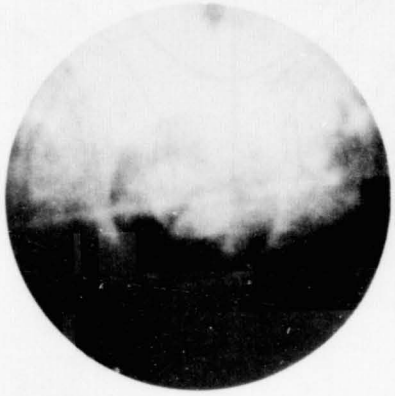

$z = 102$ mm

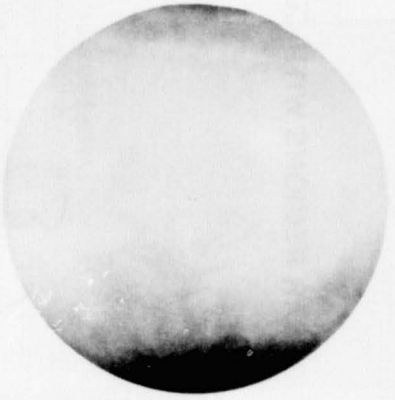

$z = 203$ mm

DYE ADDED TO INNER STREAM

FIG. 2

FIG. 3

VISUALIZATION OF FLOW

$U_i = 0.52$ m/s $U_a = 1.66$ m/s

$Q_i = 6.2$ gpm $Q_a = 52.8$ gpm

DYE ADDED TO ANNULAR STREAM

r-θ PLANE

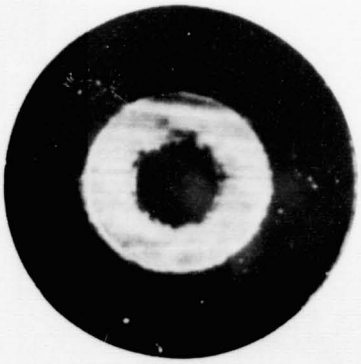

z = 5 mm

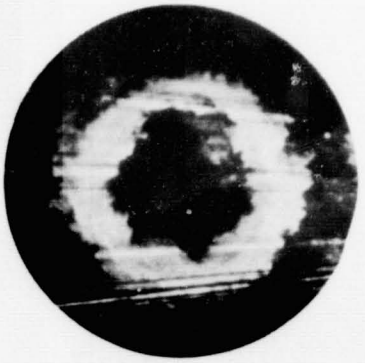

z = 25 mm

z = 38 mm

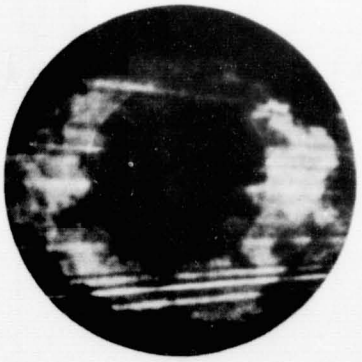

z = 51 mm

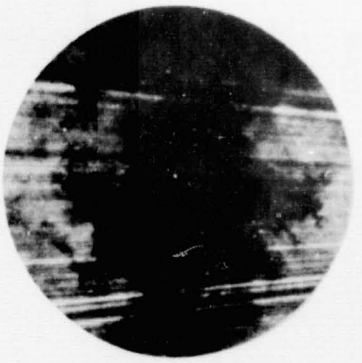

z = 102 mm

z = 152 mm

z = 203 mm

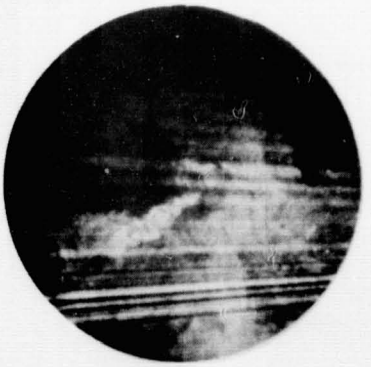

z = 305 mm

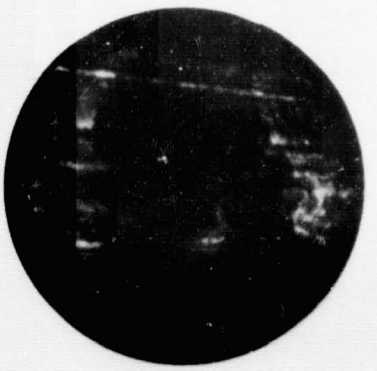

z = 406 mm

FIG. 4

MEAN VELOCITY AND INNER JET CONCENTRATION PROFILES AT z = 25 mm

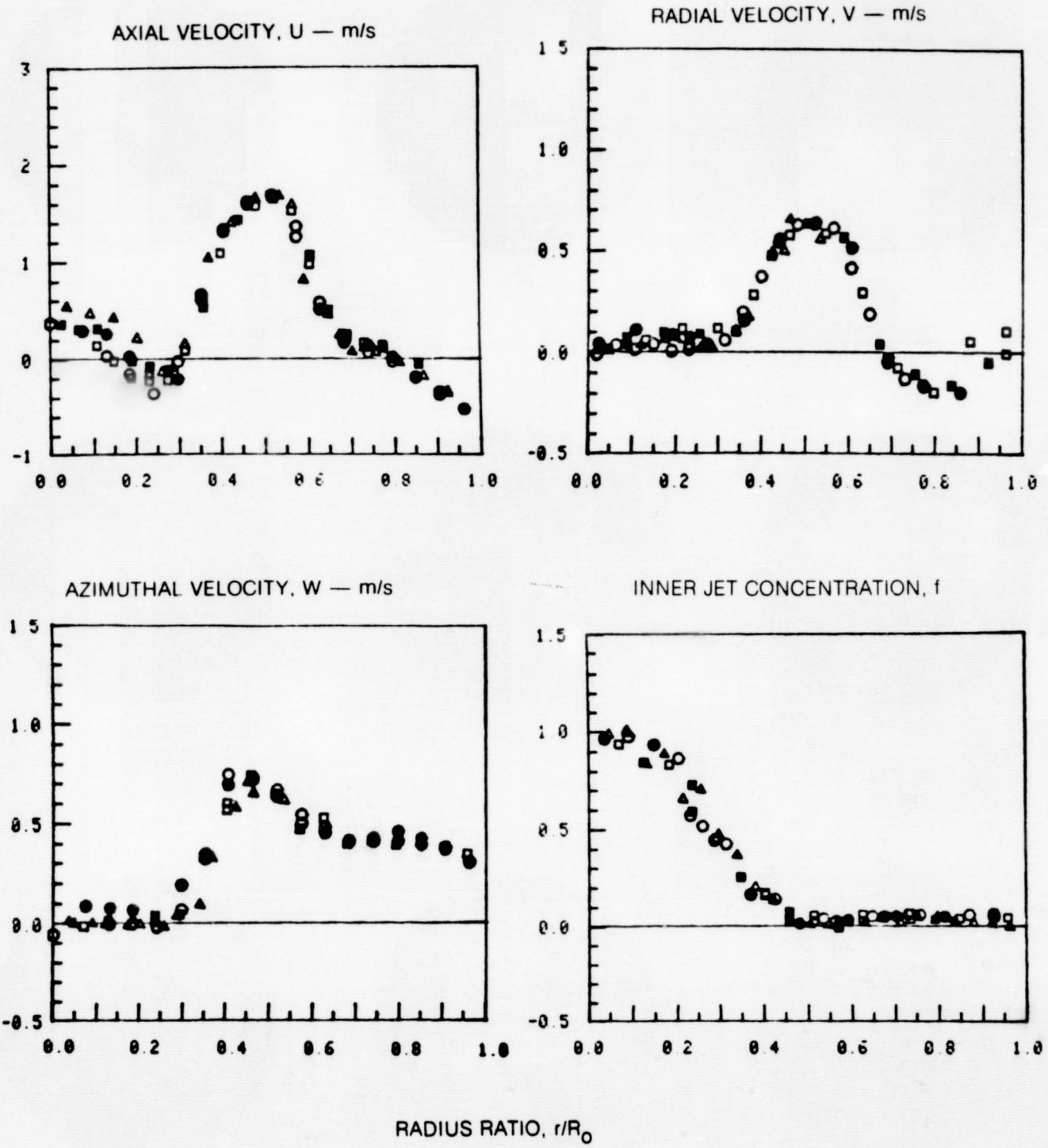

FIG. 5

FLUCTUATING VELOCITY AND INNER JET CONCENTRATION PROFILES AT z = 25 mm

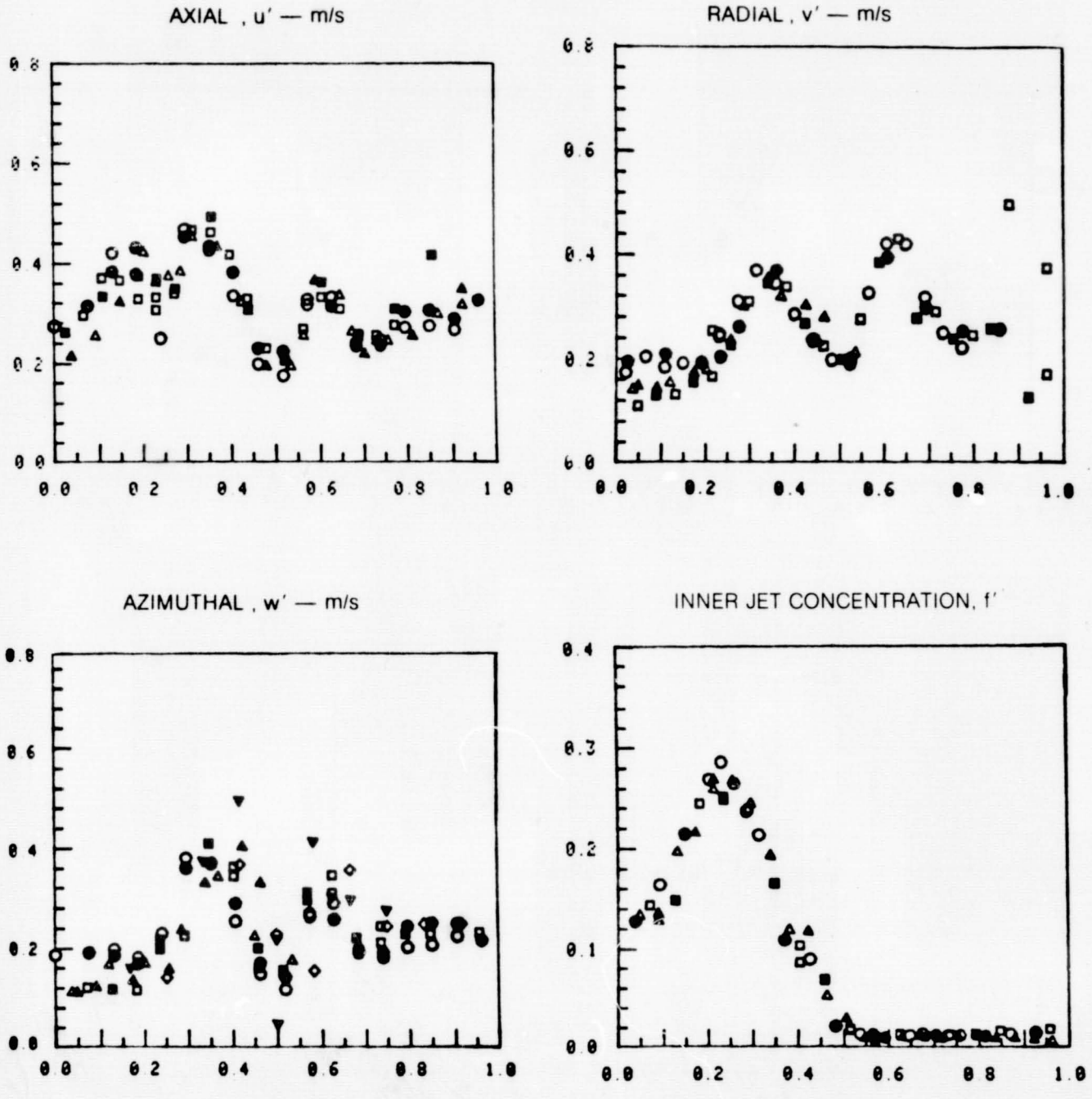

FIG. 6

MOMENTUM TURBULENT TRANSPORT RATE PROFILES AT z = 25 mm

r-z PLANE, $\overline{uv}$ — m^2s^2

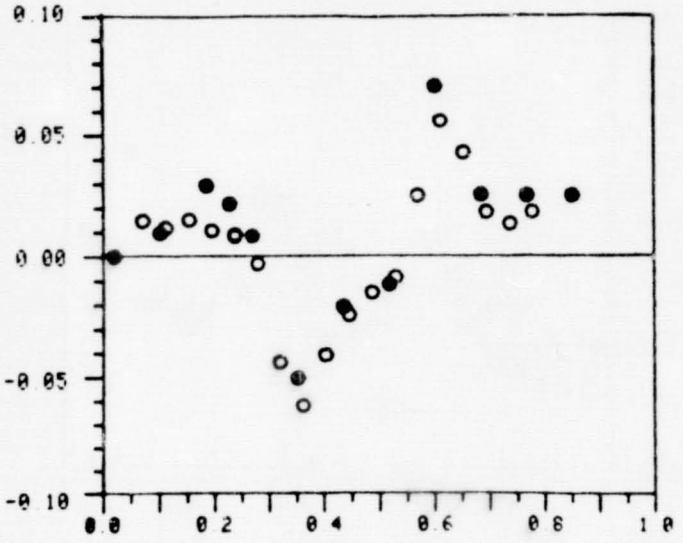

θ-z PLANE, $\overline{uw}$ — m^2/s^2

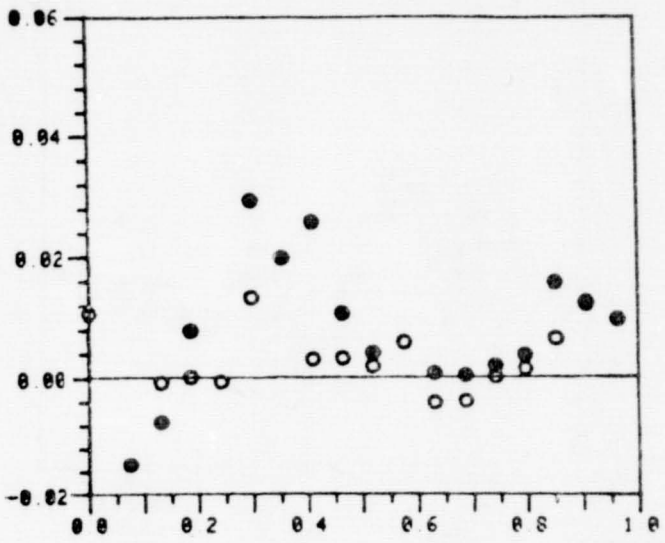

r-θ, PLANE, $\overline{wv}$ — m^2s^2

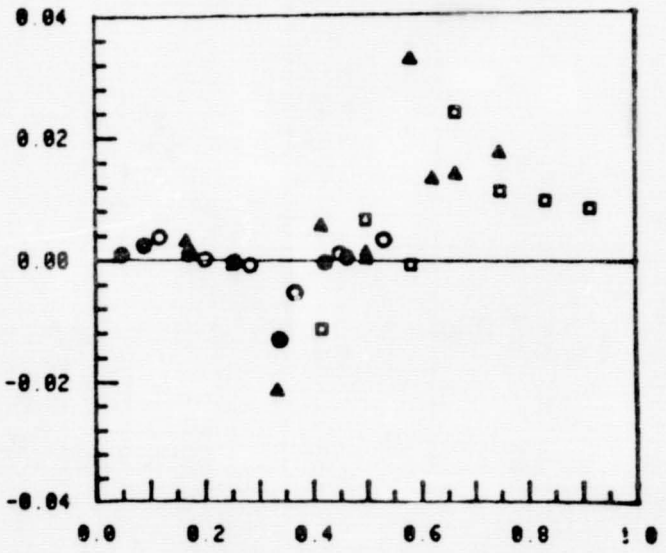

RADIUS RATIO, r/R_o

FIG. 7

MASS TURBULENT TRANSPORT RATE PROFILES AT z = 25 mm

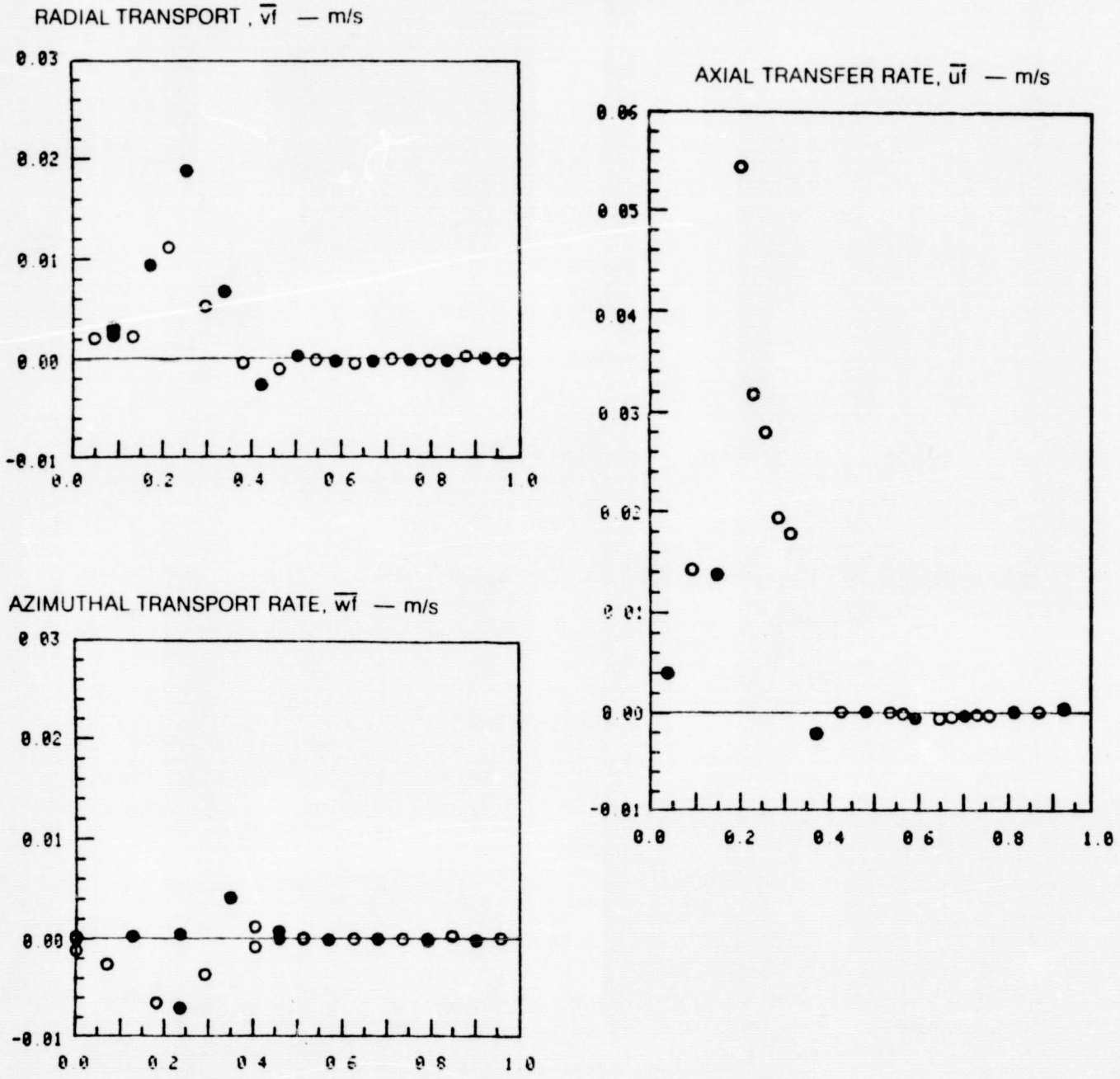

FIG. 8

MEAN AXIAL VELOCITY ALONG TEST SECTION CENTERLINE

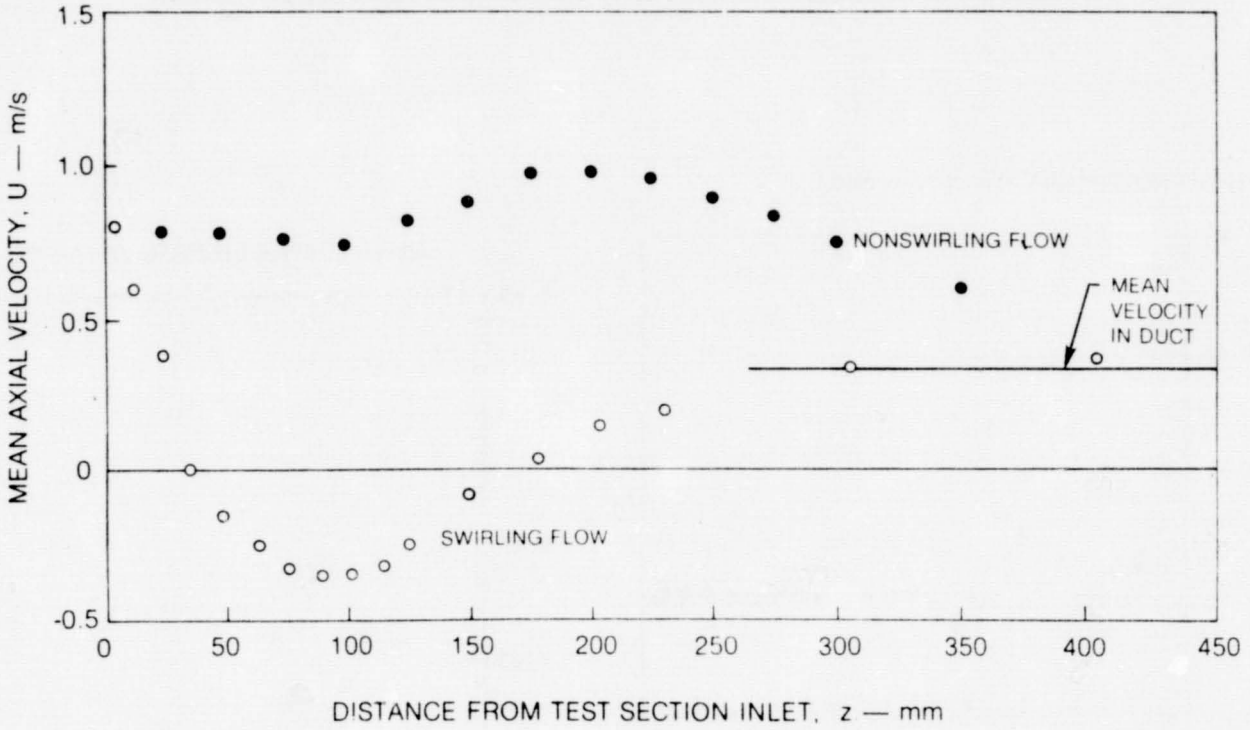

FIG. 9

MEAN INNER JET FLUID CONCENTRATION ALONG TEST SECTION CENTERLINE

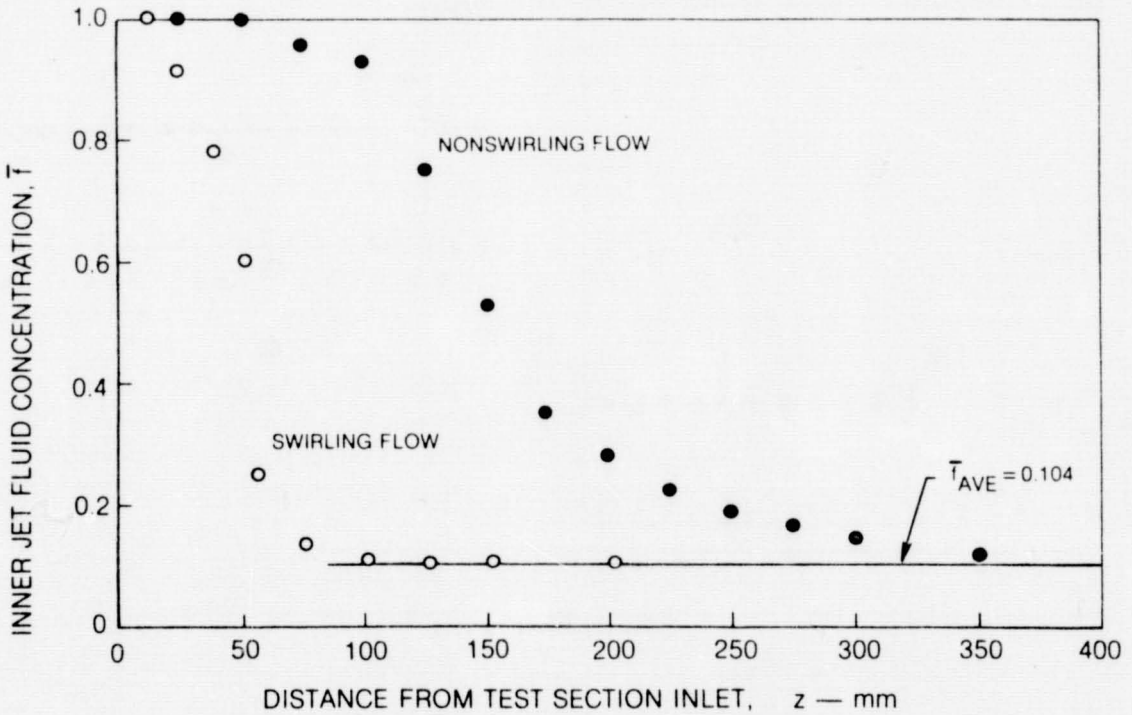

D17

THE INFLUENCE OF LARGE-SCALE MOTION ON TURBULENT TRANSPORT FOR CONFINED COAXIAL JETS*

David C. Brondum and John C. Bennett

Mechanical Engineering Department
University of Connecticut

The existance of large-scale coherent structures in turbulent shear flows has been well documented in the literature (ref.1). The importance of these structures in flow entrainment, momentum transport and mass transport in the shear layer has been suggested by several researchers (ref.2,3). Comparisons between existing models and experimental data for shear flow in confined coaxial jets (ref.4,5) reinforce the necessity of further investigation of the large scale structures. These comparisons show the greatest discrepency between prediction and actual results in the developing flow region where the large scales exist. It was also observed that the momentum transport rate comparisons were very bad. Finally, Schetz (ref.6) has reviewed mixing flows and concluded that large-scale structures were essential aspects of future modeling efforts.

The present analytical effort is a follow-on to a previous contract (ref.7) under which the experimental data was collected. The data consists of all three velocity components as well as concentration data for a turbulent shear flow in a confined coaxial jet with a sudden expansion. The analysis undertaken is similar to that of Blackwelder and Kaplan (ref.8) which was an analysis of a turbulent boundary layer. As they discovered, the bursts within the boundary layer were found to contribute greatly to the momentum transport. As part of the previous contract effort, flow visualization was used extensively and identified large-scale structures within the shear layer. The appearance of these large-scale structures in the mixing layer has led to the search for a burst detector along with detection criteria. Preliminary conditional sampling of the data has been performed and has revealed much information about the transport processes. All analysis to this point has been limited to data acquired at one axial location (102 mm from the origin).

Various conditionally sampled parameters of the data have been plotted and trends observed. Initial efforts were directed toward

* NASA Grant #NAG 3-350

the use of these results in the identification of a suitable burst detector for the flow and also the development of better understanding of the effects on the flow (i.e., mass transport). One such plot is the scatter plot where the velocity fluctuation is plotted as a function of the concentration fluctuation or where fluctuation of one velocity component is plotted against the fluctuation of another velocity component. These types of plots help establish the existance of the large scale in the flow and assist in separating these structures from the general low level turbulence (Fig.1,2). They are also beneficial in determining if the large scale correlation is significant (non-zero, Fig.1 or zero Fig.2).

Other interesting parameters can be established from conditonally sampled data pairs that are contained in the large structure. Based on the scatter plots, the initial choice for a burst detector was large excursions (positive or negative) in concentration fluctuations. The first parameter investigated was the large scale fraction (or ratio of samples with large concentration excursions compared to the total sample size). Plotting this ratio as a function of radius (at a given axial location) yields some trends in the data (Fig.3). The percentage appears to be maximized in the shear layer where the large-scales are known to exist. This adds credibility to the choice of detector of course.

Having established some credibitity for the detector, the efforts were concentrated on the effects of large-scale structure on mass transport. Specifically, the ratio of conditionally-sampled mass transport to overall mass transport was plotted (Fig.4). As with boundary layers, the large-scale structures in shear layers appear to exert considerable influence on mass transport.

Having established procedures for investigating large-scale structures, future efforts will be directed toward several goals: (1) establishing a model of a typical 3-D structure, (2) investigating the regional extent of the influence of large-scale structures, (3) investigating the influence of large-scale structures on counter-gradient transport identified previously (Ref.7), and (4) investigating the recently completed swirl data for similar large-scale effects.

REFERENCES

1. Roshko, A., "Structure of Turbulent Shear Flows: A New Look," AIAA J., Vol. 14, 1976, pp.1349-1357.

2. Winant, C., and Browand, F., "Vortex Pairing: The Mechanism of Turbulent Mixing-Layer Growth at Moderate Reynolds Number", J. Fluid Mech., 63, 1974, pp.237-255.

3. Dimotakis, P. and Brown, G. L., "The Mixing Layer at High Reynolds Number: Large-Structure Dynamics and Entrainment", J. Fluid Mech., 78, part 3, 1976, pp.535-560.

4. Syed, S. A. and Sturgess, G. J., "Velocity and Concentration Characteristics and Their Correlations for Coaxial Jets in a Confined and Sudden Expansion, Part II: Predictions". Proceedings of ASME Symposium on The Fluid Mechanics of Combustion Systems; Boulder, Colorado; March 1981.

5. Habib, M. A. and Whitelaw, J. H., "Velocity Characteristics of a Confined Coaxial Jet. ASME Journal of Fluids Engineering, 101, December 1979.

6. Schetz, J. A., "Injection and Mixing in Turbulent Flow", 68 Progress in Astronautics and Aeronautics, M. Summerfield, Editor, 1980.

7. Johnson, B. V. and Bennett, J. C., "Mass and Momentum Transport Experiments with Confined Coaxial Jets. NASA Contractor Report (CR-165574, November 1981.

8. Blackwelder, R. F. and Kaplan, R. E., "On the Wall Structure of the Turbulent Boundary Layer", J. Fluid Mech, 76, part 1, 1976, pp.89-112.

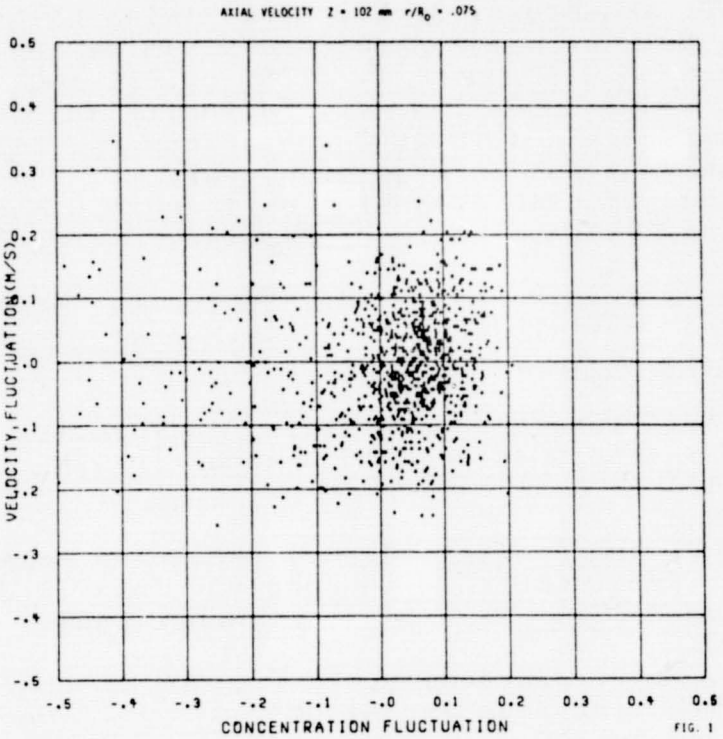

FIG. 1

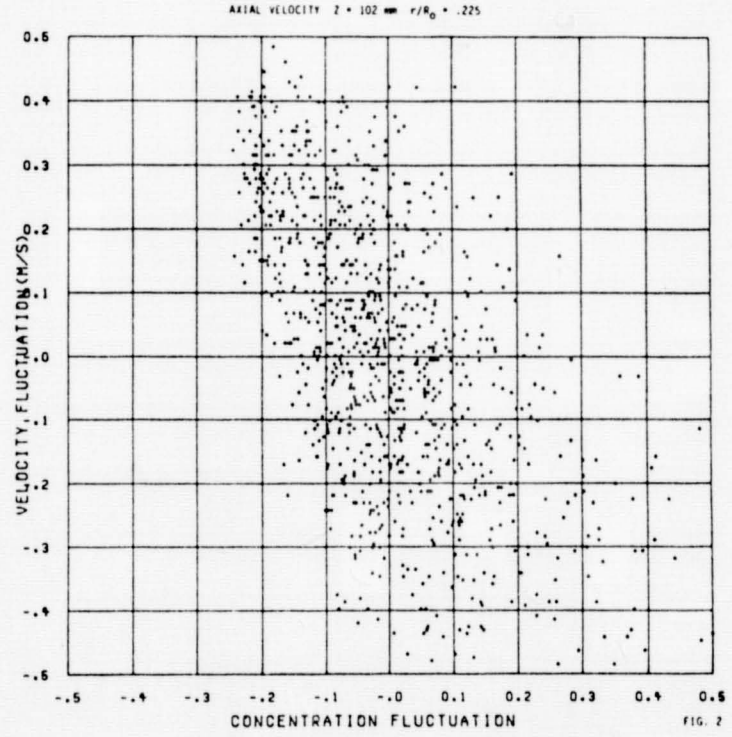

FIG. 2

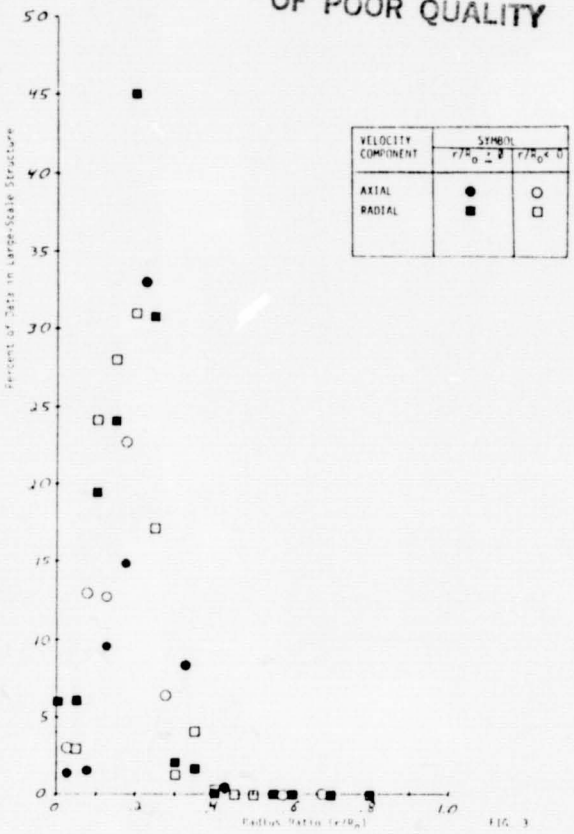

FIG. 3

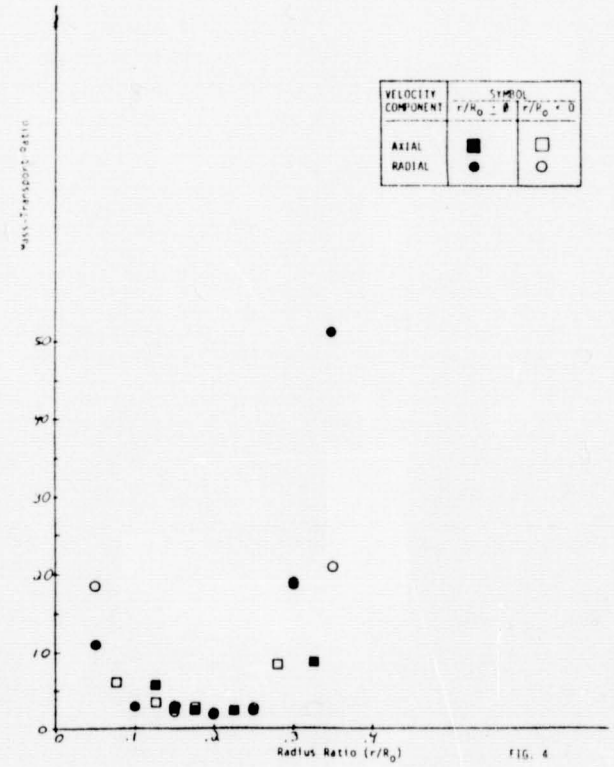

FIG. 4

D18

VELOCITY VISUALIZATION IN GASEOUS FLOWS

R. K. Hanson, B. Hiller, C. Hassa and R. A. Booman
Department of Mechanical Engineering
Stanford University

Techniques yielding simultaneous, multiple-point measurements of velocity in reacting or nonreacting flowfields have the potential to significantly impact basic and applied studies of fluid mechanics. This research program is aimed at investigating several candidate schemes which could provide such measurement capability. The concepts under study have in common the use of a laser source (to illuminate a column, a grid, a plane or a volume in the flow) and the collection of light at right angles (from Mie scattering, fluorescence, phosphorescence or chemiluminescence) using a multi-element solid-state camera (100 x 100 array of photodiodes).

The talk will include an overview and a status report of work in progress with particular emphasis on the method of Doppler-modulated absorption. This technique involves monitoring fluorescence from a plane in the flow which is illuminated with a sheet of light from a tunable, narrow-linewidth laser source. The laser wavelength is set to coincide with an absorption transition of a seeded molecular species, usually iodine, which is Doppler-shifted according to the local velocity of the gas (relative to the direction of the laser beam). The resulting velocity-induced variations in absorption appear directly as variations in the fluorescence intensity, and hence quantitative, simultaneous measurements of fluorescence intensity at a large number of flowfield points can be used to infer the velocity at these points. Separate techniques and results are reported for supersonic and subsonic flows near room temperature.

OUTLINE OF PRESENTATION

- MOTIVATION (NEED FOR MULTIPLE-POINT MEASUREMENTS)
- SUMMARY: TECHNIQUES UNDER INVESTIGATION
  - STREAK RECORDING
    - MIE SCATTERING
    - LASER-INDUCED PHOSPHORESCENCE
  - *LASER MARKING
  - *DOPPLER-MODULATED ABSORPTION/FLUORESCENCE (DMA/F)
    - SUPERSONIC FLOWS
    - SUBSONIC FLOWS
- EXPERIMENTAL RESULTS
- RELATED RESULTS ON SPECIES/TEMPERATURE VISUALIZATION (AFOSR)

STREAK RECORDING

- SEEDED PARTICLES (DROPS) ARE ILLUMINATED BY CW LASER SHEET
- MIE SCATTERING GIVES STREAKS ON FILM (RETICON)
- GRADED INTENSITY BEAM (TRANSVERSE TO SHEET) GIVES POTENTIAL FOR 3-D RECORDING, IF PARTICLES ARE SPHERICAL

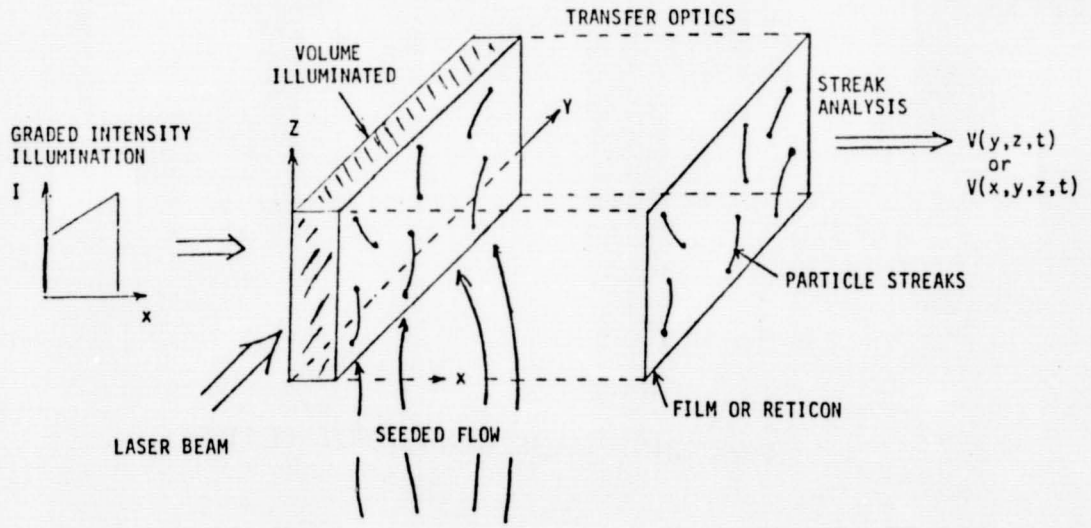

LASER MARKING: CONCEPTS

- A PULSED TUNABLE LASER IS USED TO "MARK" A LINE OR A GRID IN THE FLOWFIELD
- LASER-INDUCED PHOSPHORESCENCE (OR CHEMILUMINESCENCE) PROVIDES LONG-LIVED RADIATION FROM EXCITED FLUID ELEMENTS, OR
- LASER-INDUCED PARTICULATE FORMATION ENABLES TRACKING BY MIE SCATTERING
- MULTIPLE EXPOSURE OF GRID PATTERNS ARE RECORDED ON A SINGLE FRAME OF RETICON CAMERA (OR FILM)
- CANDIDATE MATERIALS: BIACETYL (DROPLET OR VAPOR) FOR PHOSPHORESCENCE
  NO_2/CO FOR CHEMILUMINESCENCE
  SF_6 FOR PARTICLE FORMATION

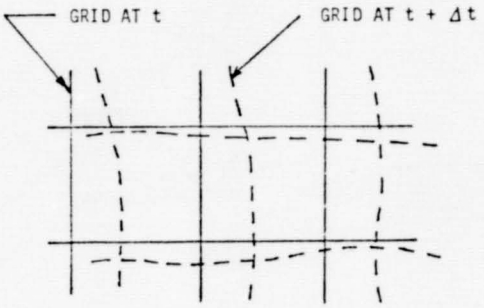

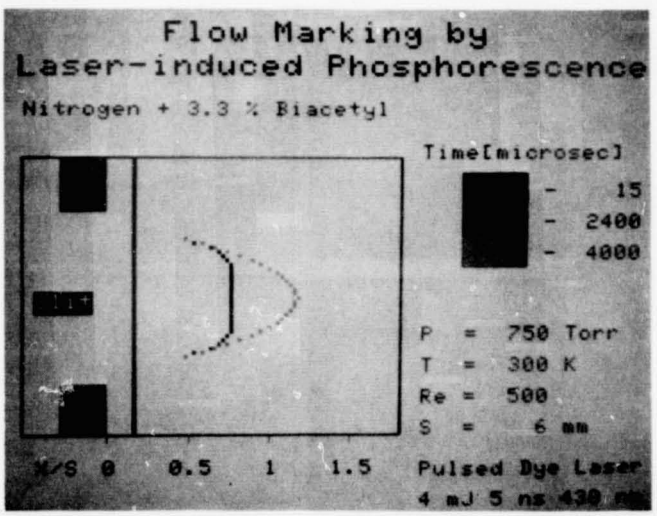

DOPPLER-MODULATED ABSORPTION/FLUORESCENCE (DMA/F)

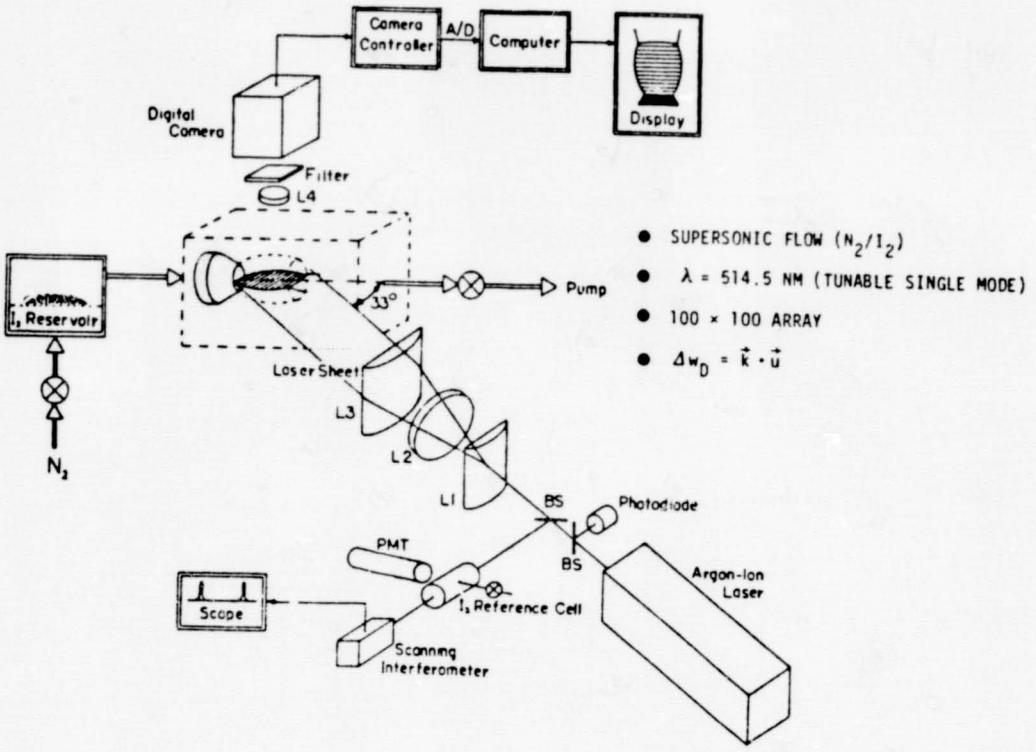

FILM RETICON

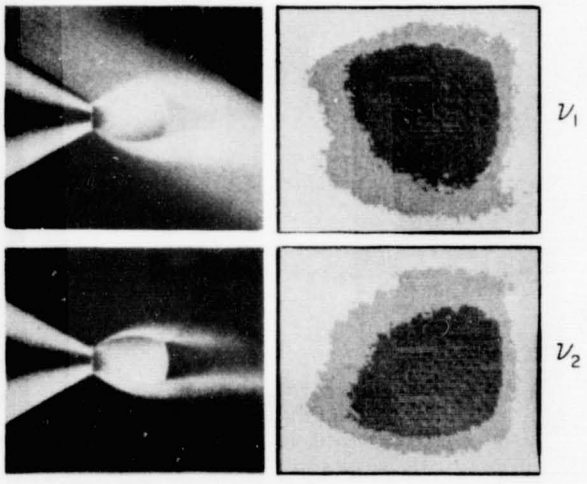

PHOTOGRAPHS AND DIGITAL IMAGES OF FLUORESCENCE DISTRIBUTION AT TWO LASER FREQUENCIES FOR A SUPERSONIC UNDEREXPANDED JET.

DOPPLER-MODULATED ABSORPTION: SUPERSONIC METHOD

Scans of Fluorescence Intensity vs Laser Frequency
for an Off-Axis Pixel

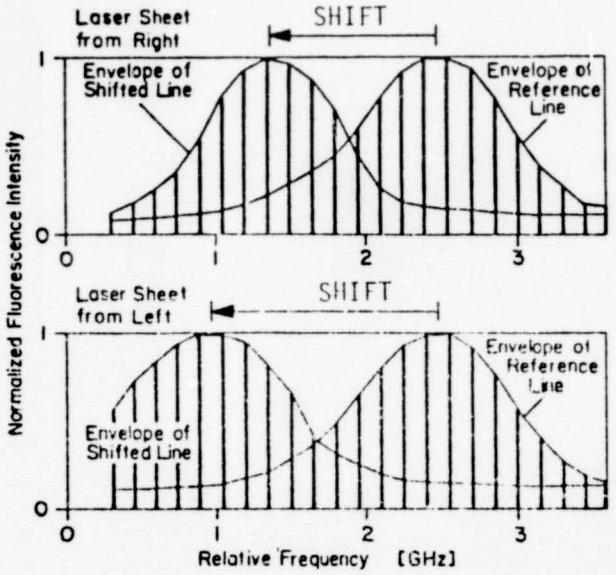

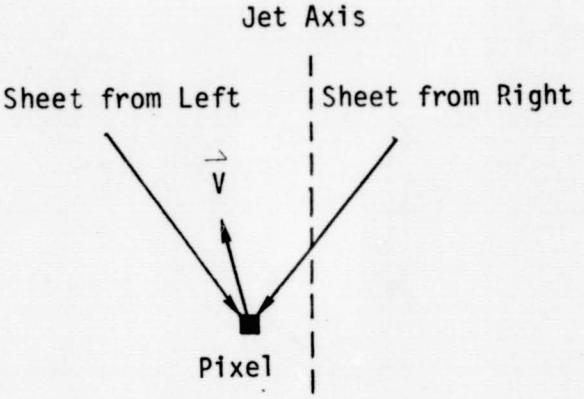

COMPARISON OF MEASURED AND CALCULATED VELOCITY FIELDS IN NEAR FIELD OF UNDEREXPANDED JET

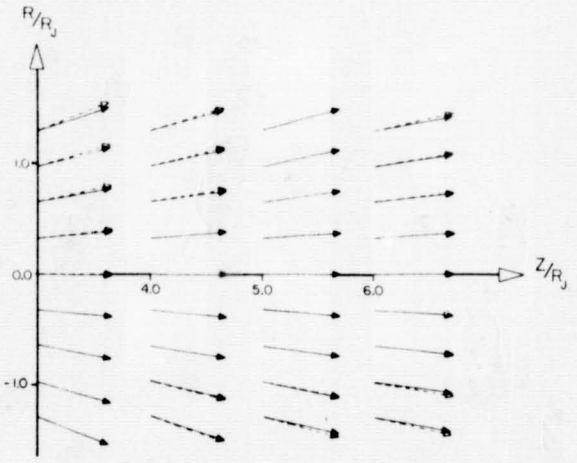

EXTENSION TO SUBSONIC FLOWS

- FIX WAVELENGTH
- MONITOR VARIATION IN INTENSITY BETWEEN FORWARD AND COUNTERPROPAGATING BEAMS TO INFER VELOCITY
- RECORD AT HIGH REPETITION RATE TO DETERMINE U(x,y,t)

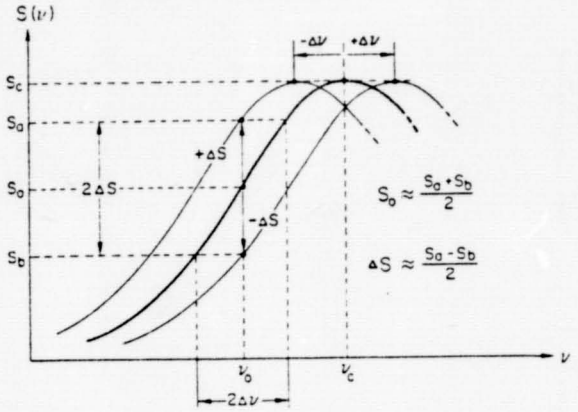

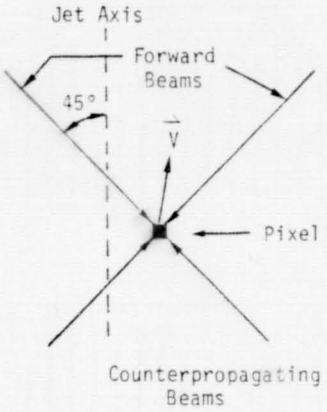

$$u = c(\Delta\nu/\nu_o)$$

$$\Delta\nu = \Delta S/(\partial S/\partial\nu)_{\nu_o}$$

$$= (\Delta S/S_o)\,[g(\nu_o)/(\partial g/\partial\nu)_{\nu_o}]$$

g = lineshape function

VELOCITY VISUALIZATION

SIMULTANEOUS MULTIPLE-POINT VELOCITY MEASUREMENTS BY SENSING DOPPLER-MODULATED LASER ABSORPTION WITH A DETECTOR ARRAY

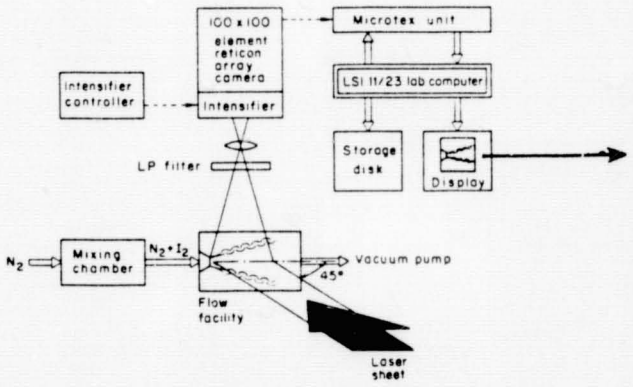

Sketch of detection setup showing the flow field probed by a thin sheet of laser light in the center plane of the jet and the camera imaging the fluorescence distribution perpendicular to the incoming sheet. For clarity, only one of the four sheets is drawn.

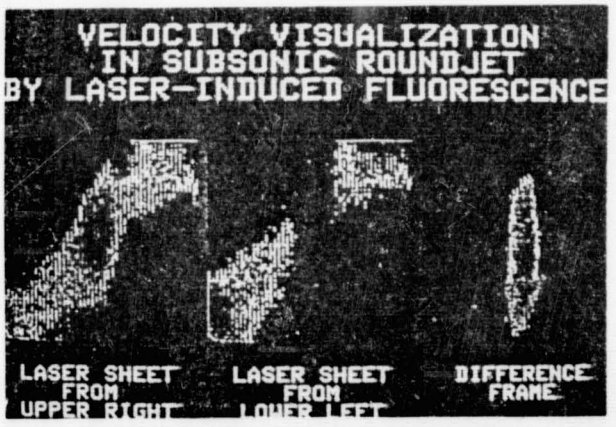

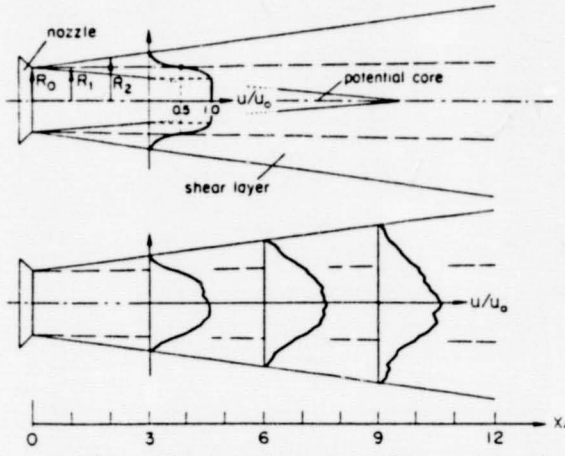

Flow field of a subsonic round jet near nozzle exit. The important features are the potential core in which the center velocity remains constant and the growing annular turbulent shear layer. Three measured velocity profiles are shown.

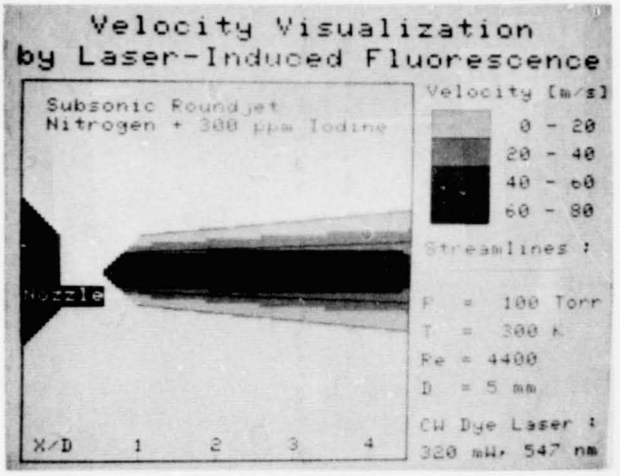

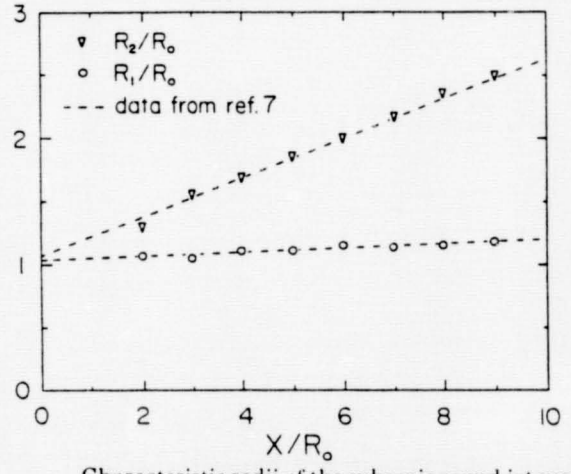

Characteristic radii of the subsonic round jet versus axial position. R_0 is the nozzle radius, R_1 is the radius of the half-velocity point, and R_2 is the radius of the shear-layer edge.

SUMMARY

DOPPLER-MODULATED ABSORPTION/FLUORESCENCE

SIGNIFICANCE:	MULTIPLE-POINT MEASUREMENTS IN UNSEEDED FLOW
STATUS:	FIRST GENERATION EXPERIMENTS COMPLETED SUCCESSFULLY
	SUBSONIC FLOW (FIXED WAVELENGTH)
	SUPERSONIC FLOW (SCANNING CONCEPT)
LIMITATIONS:	LENGTHY RECORDING TIMES
	LIMITED VELOCITY RESOLUTION (1-5 M/SEC)
FUTURE:	IMPROVED TEMPORAL RESOLUTION
	STREAMLINED DATA PROCESSING
	COMBUSTION MEASUREMENTS

D19

N84 20544

INVESTIGATIONS OF FLOWFIELDS FOUND IN TYPICAL COMBUSTOR GEOMETRIES

David G. Lilley
Oklahoma State University

Studies are concerned with experimental and theoretical research on 2-D axisymmetric geometries under low speed, nonreacting, turbulent, swirling flow conditions. The flow enters the test section and proceeds into a larger chamber (the linear expansion ratio D/d = 2, 1.5 and 1) via a sudden or gradual expansion (side-wall angle α = 90 and 45 degrees). A weak or strong nozzle (of area ratio A/a = 2 and 4) may be positioned downstream at x/D = 2 to form a contraction exit to the test section. Inlet swirl vanes are adjustable to a variety of vane angles with values of ϕ = 0, 38, 45, 60 and 70 degrees being emphasized. The objective is to determine the effect of these parameters on isothermal flowfield patterns, time-mean velocities and turbulence quantities, and to establish an improved simulation in the form of a computer prediction code equipped with a suitable turbulence model. The goal of the on-going research is to perform experiments and complementary computations with the idea of doing the necessary type of research that will yield improved calculation capability. This involves performing experiments where time-mean turbulence quantities are measured and taking input conditions and running an existing prediction code for a variety of test cases so as to compare predictions against experiment. Hence the validity of turbulence model modifications can be assessed. If fact, they are also being deduced directly from the measured stresses and velocity gradients.

Three Ph.D. Theses (Rhode, Jackson and Abujelala) and five M.S. Theses (Janjua, Yoon, McKillop, Sander, and Scharrer) have evolved in connection with the investigation over the last three years. New features of the present year's study include the investigation of: a more complex range of swirl strengths; swirler performance; exit nozzle sizes and locations; expansion ratios; and side-wall angles. Their individual and combined effects on the test section flowfield are being observed, measured and characterized. Recent studies on the test facility include:

1. Swirler Performance - with five-hole pitot probe[1] and single-wire hot-wire[2] for time-mean and turbulence characteristics.

2. Gross Flowfield Characterization - flow visualization has been achieved via photography of neutrally-buoyant helium-filled soap bubbles and smoke produced by an injector and smoke wire.[3-5]

3. Time-Mean Flowfield Characterization - with five-hole pitot probe for time-mean velocity field and velocity gradients for a full range of swirl strengths.[3-6]

4. Turbulence Measurements - with single wire[7,8], cross-wire[9] and triple-wire[10] hot-wires, including an assessment of the accuracy and directional sensitivity of the single-wire technique[11], enabling all Reynolds stress components to be deduced.

PRECEDING PAGE BLANK NOT FILMED

5. Turbulence Modeling - limitations and empirical extensions of the k-ε model have been analyzed[12], but relating Reynolds stresses to appropriate time-mean velocity gradients are yielding effective model improvements[13].

6. Computer Predictions - using an advanced computer code[14], tentative predictions[3] have now been supplemented by predictions made using recently-acquired realistic inlet conditions for a complete range of swirl strengths[15], including expansion ratios and downstream nozzle effects[16].

References

1. Sander, G. F., and Lilley, D. G., "The Performance of an Annular Vane Swirler", Paper AIAA-83-1326, Seattle, Wash., June 27-29, 1983.

2. Abujelala, M. T., Jackson, T. W., Ong, L. H., and Lilley, D. G., Studies in Progress, 1984.

3. Rhode, D. L., Lilley, D. G., and McLaughlin, D. K., "On the Prediction of Swirling Flowfields Found in Axisymmetric Combustor Geometries", ASME Journal of Fluids Engineering, Vol. 104, Sept. 1982, pp. 378-384.

4. Rhode, D. L., Lilley, D. G., and McLaughlin, D. K., "Mean Flowfields in Axisymmetric Combustor Geometries with Swirl", AIAA Journal, Vol. 21, No. 4, April 1983, pp. 593-600.

5. Scharrer, G. L., and Lilley, D. G., "Five-Hole Pitot Probe Measurements of Swirl, Confinement and Nozzle Effects on Confined Turbulent Flow", AIAA Paper, Snowmass, CO, June 22-29, 1984.

6. Yoon, H. K., and Lilley, D. G., "Five-Hole Pitot Probe Time-Mean Velocity Measurements in Confined Swirling Flows", Paper AIAA-83-0315, Reno, Nevada, Jan. 10-13, 1983.

7. Janjua, S. I., McLaughlin, D. K., Jackson, T. W., and Lilley, D. G., "Turbulence Measurements in a Confined Jet Using a Six-Orientation Hot-Wire Probe Technique", Paper AIAA-82-1262, Cleveland, OH, June 21-23, 1982, AIAA Journal, 1983 (in press).

8. Jackson, T. W., and Lilley, D. G., "Single-Wire Swirl Flow Turbulence Measurements", Paper AIAA-83-1202, Seattle, Wash., June 27-29, 1983.

9. McKillop, B. E., and Lilley, D. G., "Turbulence Measurements in a Complex Flowfield Using a Crossed Hot-Wire", AIAA Paper, Snowmass, CO, June 27-29, 1984.

10. Janjua, S. I., and McLaughlin, D. K., "Turbulence Measurements in a Swirling Confined Jet Flowfield Using a Triple Hot-Wire Probe", Report DT-8178-02, Dynamics Technology, Inc., Torrance, CA, Nov. 1982.

11. Jackson, T. W., and Lilley, D. G., "Accuracy and Directional Sensitivity of the Single-Wire Technique", Paper AIAA-84-0367, Reno, NV, Jan. 9-12, 1984.

12. Abujelala, M. T., and Lilley, D. G., "Limitations and Empirical Extensions of the k-ε Model as Applied to Turbulent Confined Swirling Flows", Paper AIAA-84-0441, Reno, NV, Jan. 9-12, 1984.

13. Abujelala, M. T., Jackson, T. W., and Lilley, D. G., "Swirl Flow Turbulence Modeling", AIAA Paper, Cincinnati, OH, June 11-13, 1984.

14. Lilley, D. G., and Rhode, D. L., "A Computer Code for Swirling Turbulent Axisymmetric Recirculation Flows in Practical Isothermal Combustor Geometries", NASA CR-3442, Feb. 1982.

15. Abujelala, M. T., and Lilley, D. G., "Confined Swirling Flow Predictions", Paper AIAA-83-0316, Reno, NV, Jan. 10-13, 1983.

16. Abujelala, M. T., and Lilley, D. G., "Swirl, Confinement and Nozzle Effects on Confined Turbulent Flow", AIAA Paper, Cincinnati, OH, June 11-13, 1984.

INVESTIGATIONS OF FLOWFIELDS FOUND IN TYPICAL COMBUSTOR GEOMETRIES

David G. Lilley

Contents

1. Introduction

1.1 The Test Facility

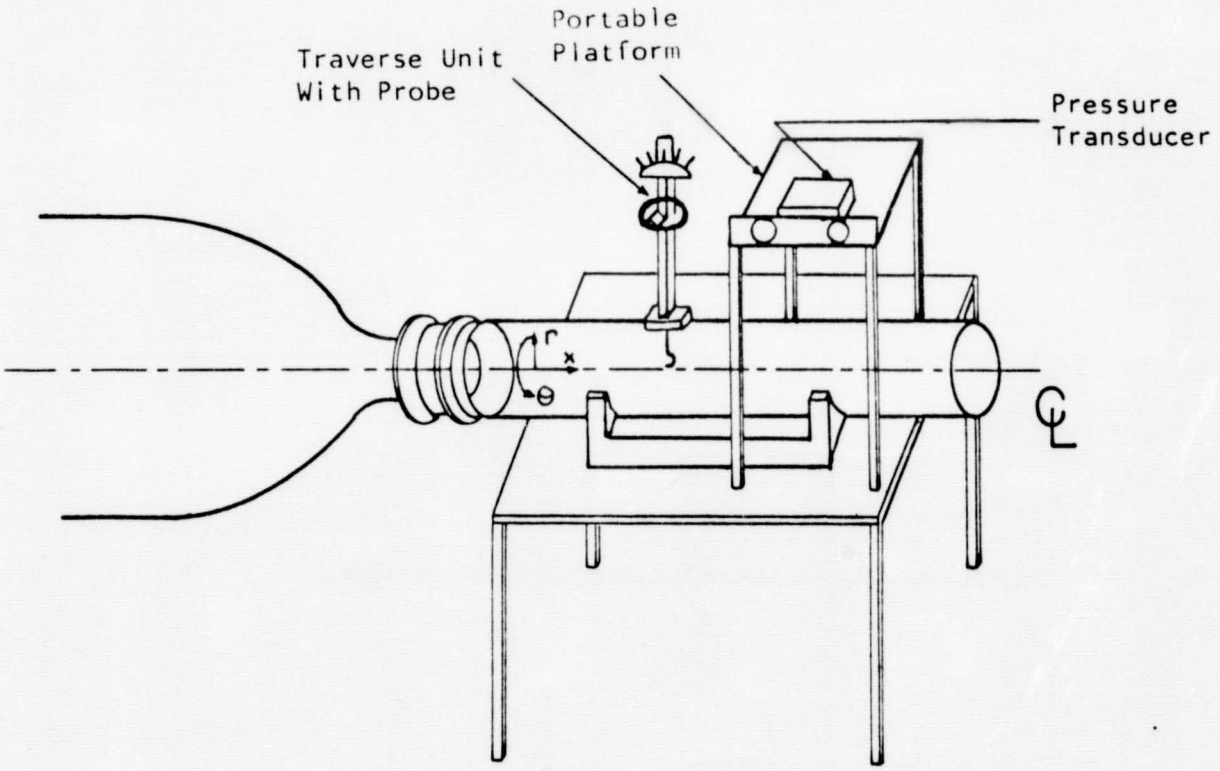

1.2 Research Objectives

1. To determine the effect of:
   * swirl vane angle ϕ
   * side-wall angle α
   * downstream blockage area ratio AR and location L/D

   on:
   * isothermal flowfield patterns
   * time-mean velocities
   * turbulence quantities
2. To establish an improved simulation in the form of:
   * computer prediction code
   * suitable turbulence model

1.3 Research Approach

1. Time-mean flowfield characterization by five-hole pitot probe measurements and by flow visualization.
2. Turbulence measurements by a variety of single- and multi-wire hot-wire probe techniques.
3. Flowfield computations using the computer code developed during the previous year's research program.

2. Progress

2.1 Progress During First Year (1981)

1. Test facility - design and construction, including variable angle swirler and expansion blocks.
2. Experimental techniques - flow visualization, five-hole pitot probe and reduction computer code.
3. Computational code development - advanced version of a primitive-variable solution procedure - STARPIC.
4. Flowfield characterization - emphasis on time-mean flow character, using flow visualization, five-hole pitot probe and tentative predictions.

2.2 Progress During Second Year (1982)

1. Higher swirl strengths - flow visualization and five-hole pitot probe measurements.
2. Swirler effectiveness - exit profiles of u, v, w, and p accurately established.
3. Flowfield predictions - the need for specifying the inlet conditions very precisely.
4. Downstream blockage - effects of area ratio and axial location studied by flow visualization, five-hole pitot probe and corresponding computer predictions.
5. Turbulence measurements - in nonswirling and swirling flow via one-wire, two-wire and three-wire hot-wire methods.

2.3 Progress During Third Year (1983)

1. Smaller expansion ratios - D/d = 1, 1.5 and 2
2. Turbulence measurements - at higher swirl strengths, with and without downstream blockage
3. Turbulence modeling - developments from measured Reynolds stresses and time-mean velocity gradients
4. Flowfield predictions - for corresponding situations

3. Results [ϕ = 45 degrees]

3.1 Swirler Performance

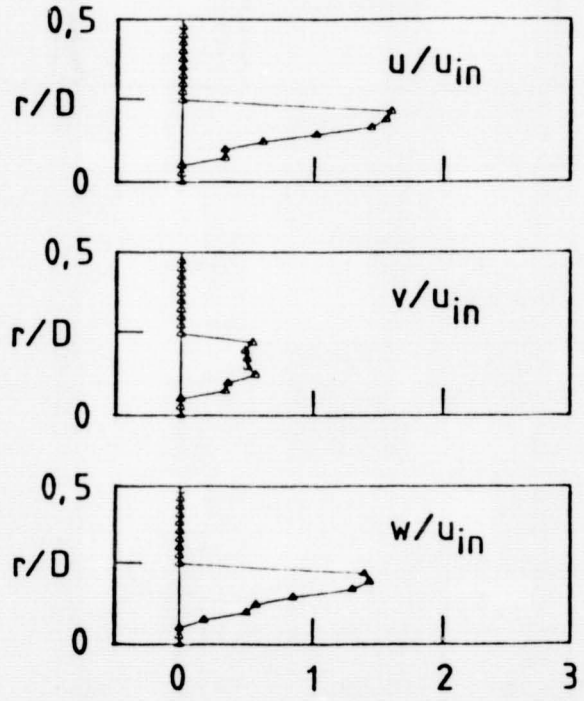

3.2 Time-Mean Velocity Profiles

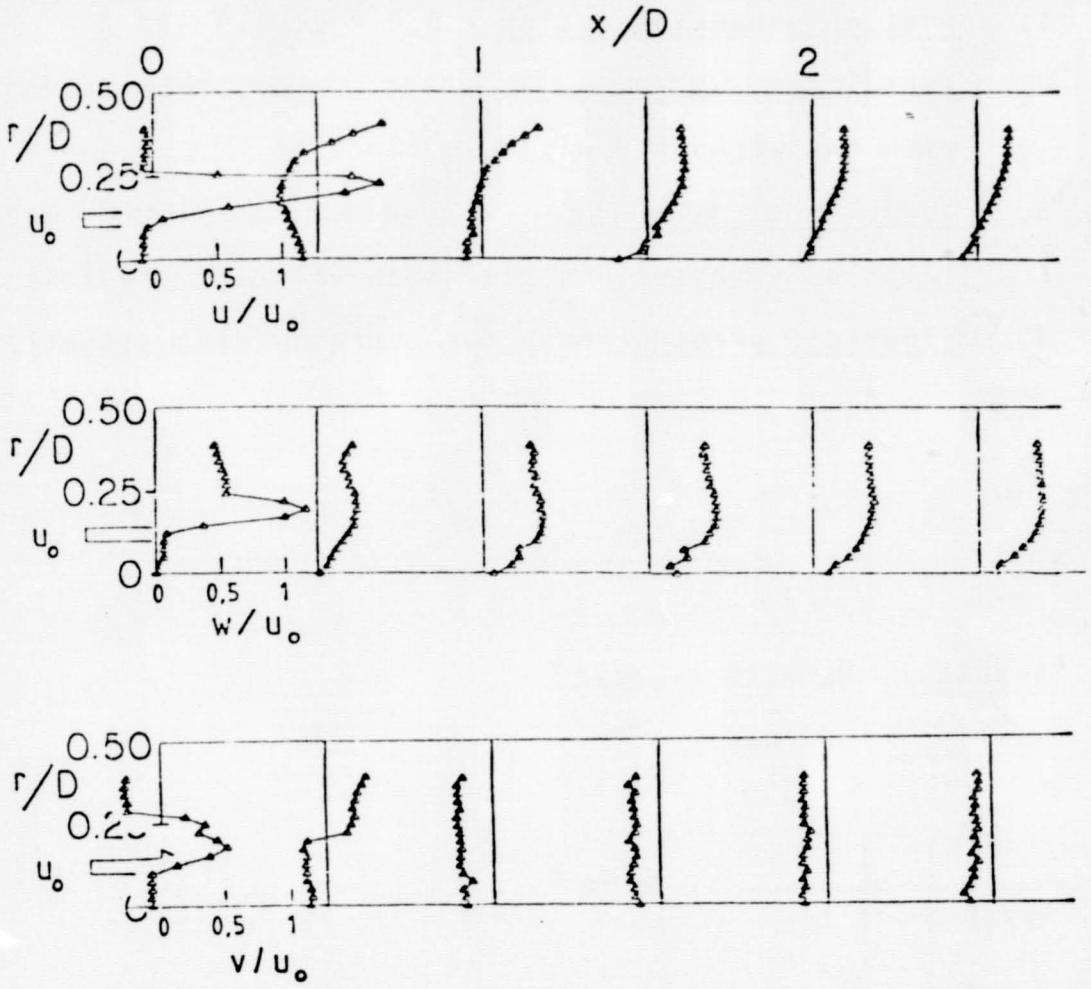

3.3 Turbulent Normal Stress Profiles

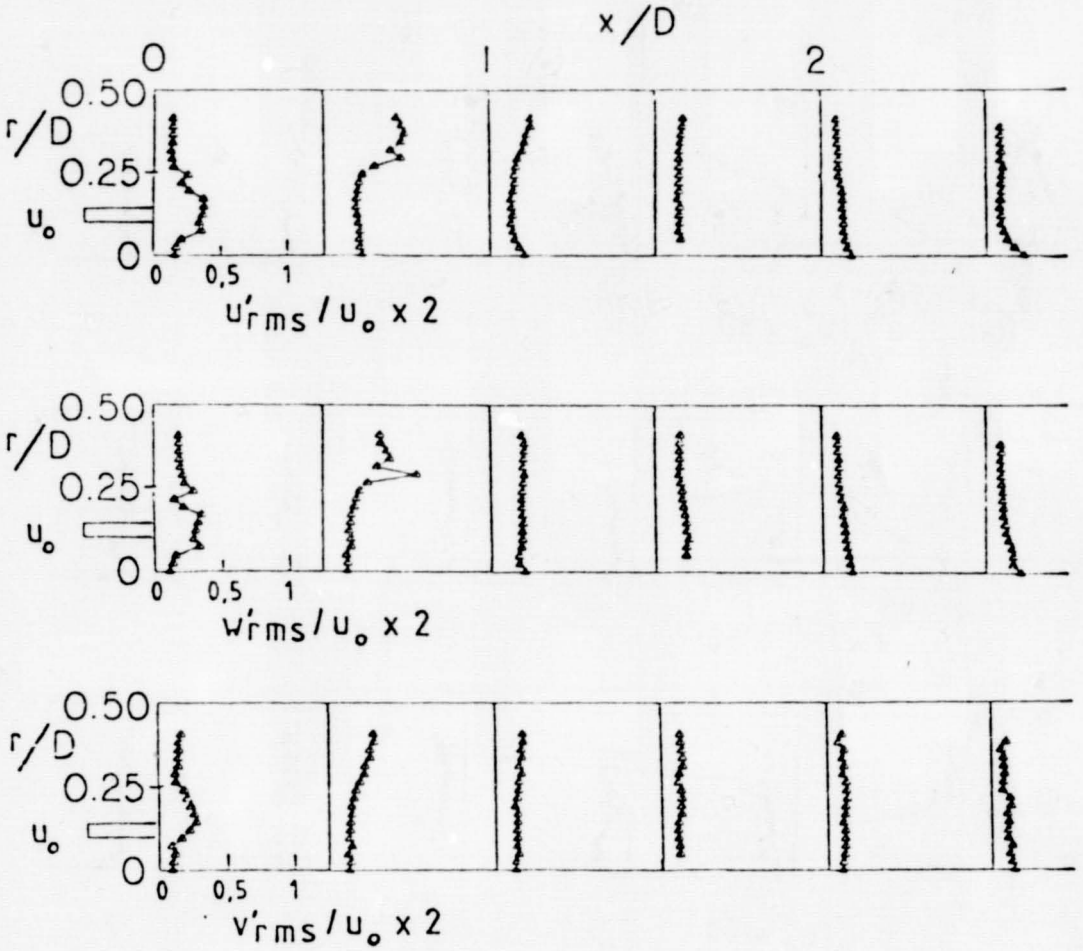

3.4 Turbulent Shear Stress Profiles

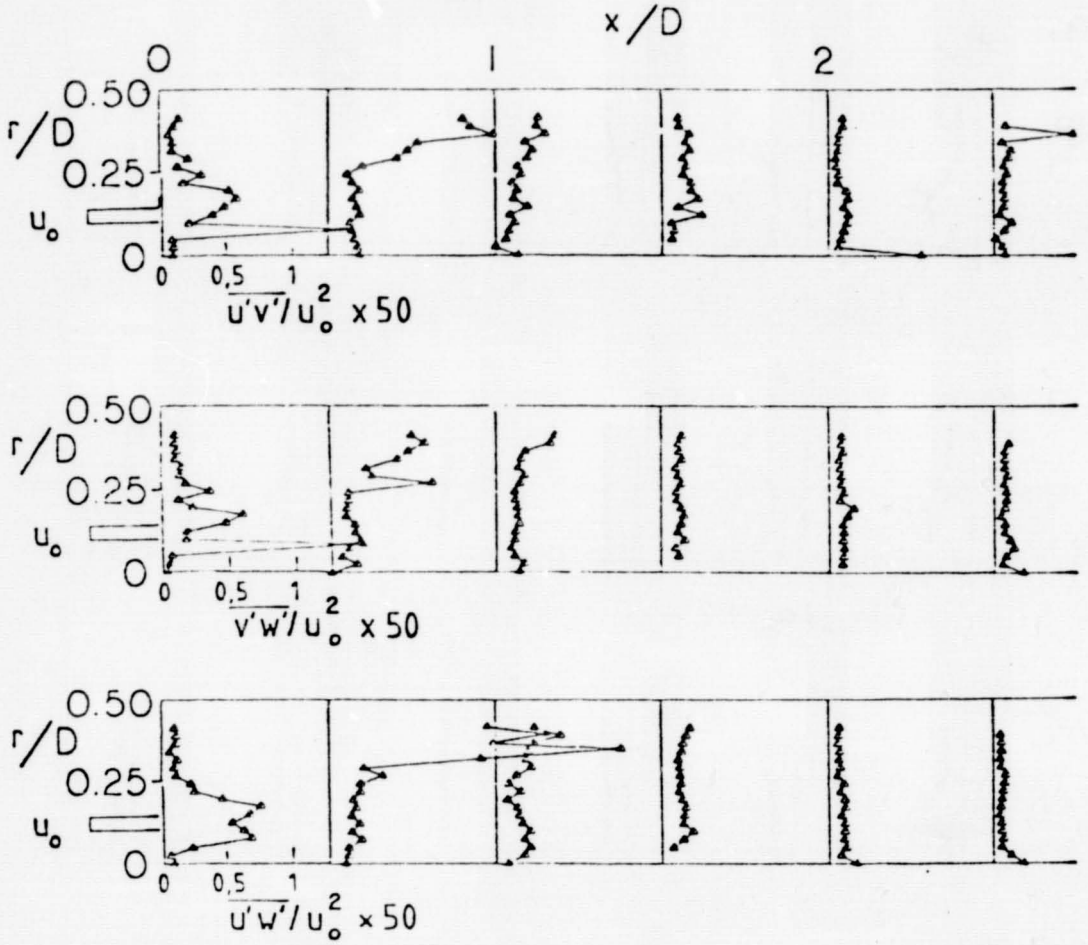

3.5 Predicted Profiles

Using optimum k-ε parameters of Ref. 12

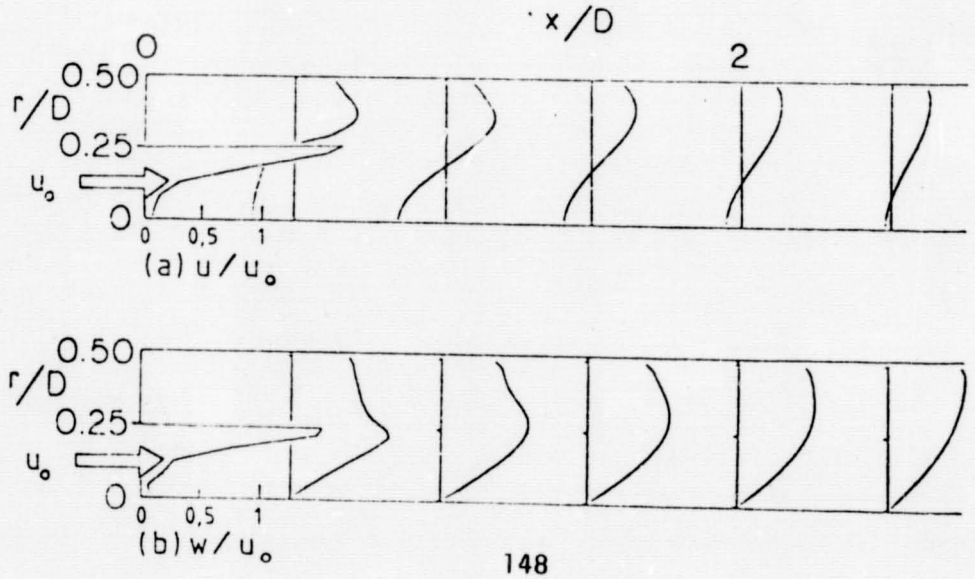

3.6 Predicted Profiles

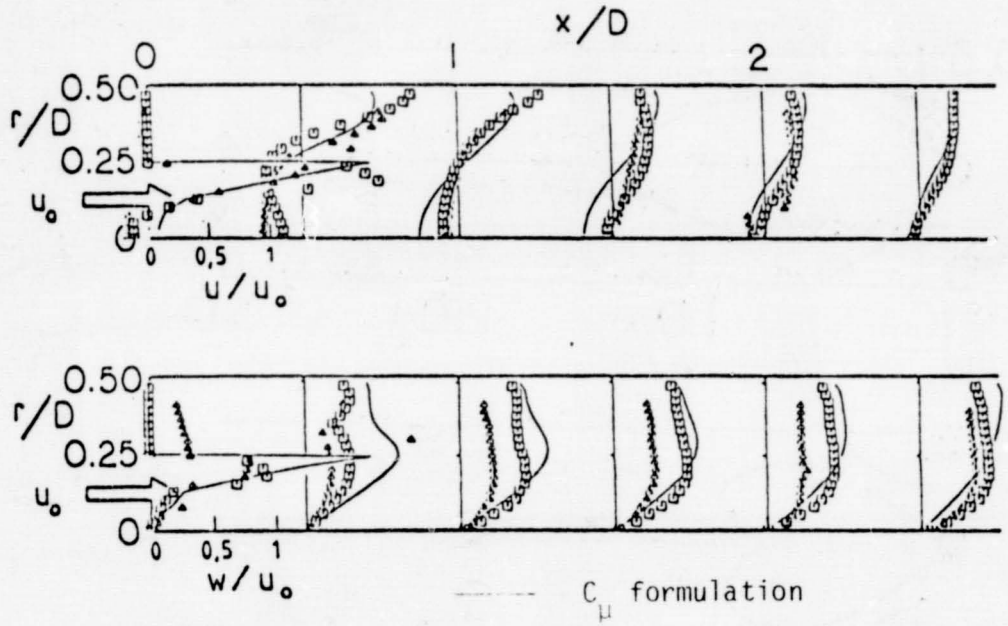

□ Ref. 6

△ Ref. 8

3.7 Central Recirculation Zone Envelope

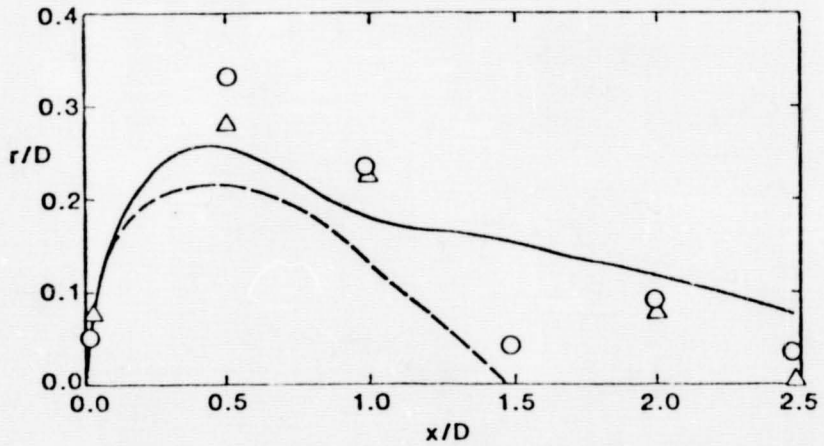

– – – k-ε constants

——— Optimum k-ε constants

o Ref. 6

△ Ref. 8

3.8 Experimental Streamlines - Nozzle Effect

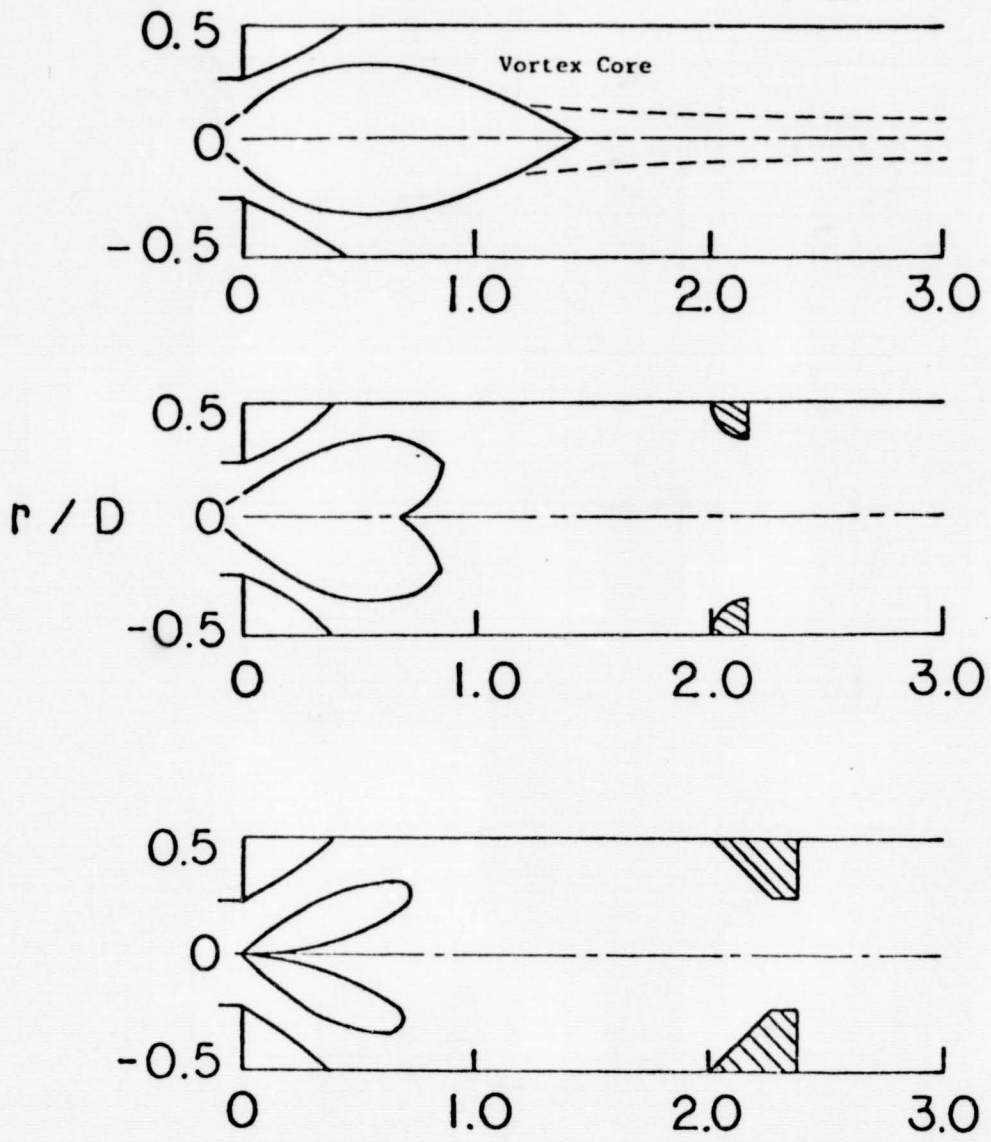

3.9 Experimental Streamlines - Confinement Effect

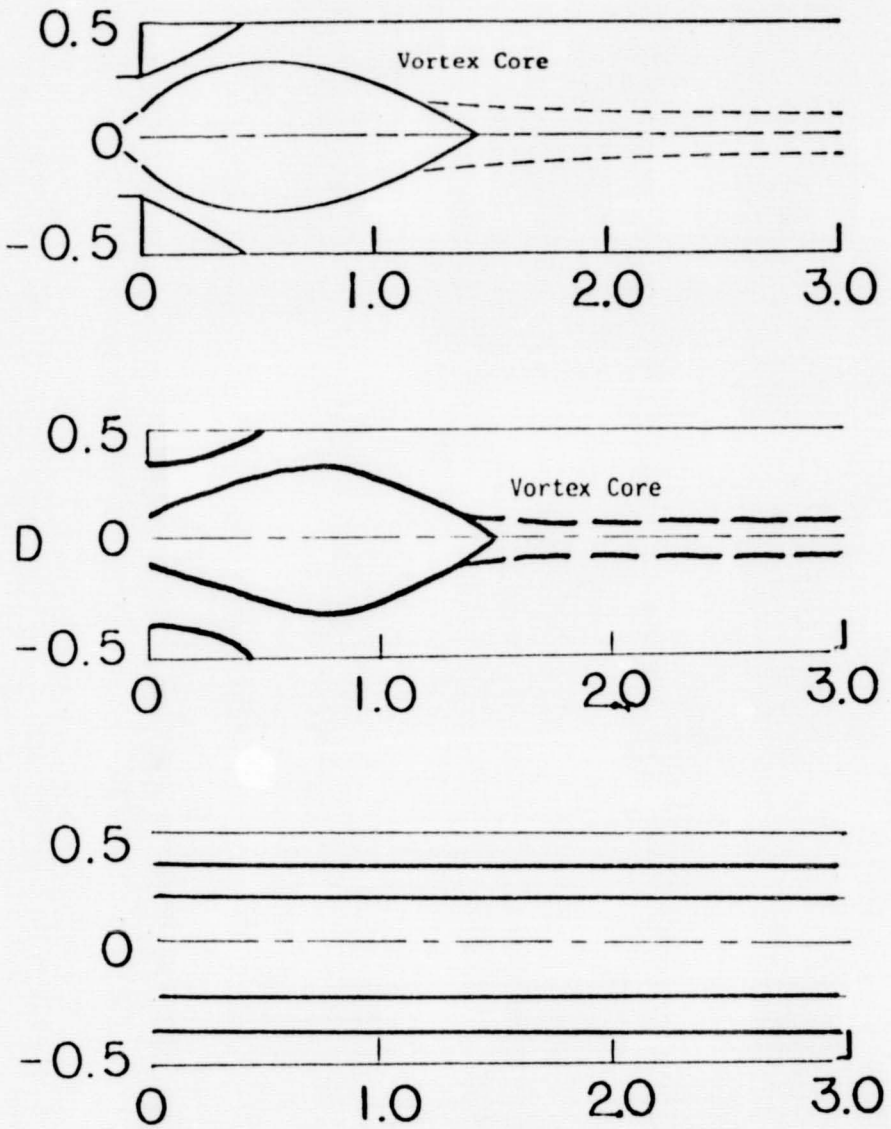

4. Closure

1. Measurements of effect of swirl, expansion angle and contraction blockage on flowfield patterns.
2. Computer prediction studies of associated phenomena.
3. Turbulence modeling developments for the simulation of swirling recirculating flow.

DILUTION JET EXPERIMENTS IN COMPACT COMBUSTOR CONFIGURATIONS

Isaac Greber

James Zizelman

Department of Mechanical and Aerospace Engineering
Case Western Reserve University

This project concerns the effects of cooling jets on the velocity and temperature fields in a compact reverse flow combustor. The work is motivated by the need to limit the temperatures of post-combustion gases in jet engines to values within the endurance capabilities of turbine blades. The application requires not only that the temperature be kept sufficiently low but also that a suitably tailored temperature profile be provided at the combustor exit, with higher temperatures generally permissible at the blade tip than at the blade root because of higher centrifugal loads at the root.

Flows in reverse flow combustor accelerate both longitudinally because of area changes and transversely because of flow turning. The current project started with flow visualization experiments in water, using aqueous solutions of zinc bromide to model the relatively higher density of cooling jets. These flow visualization experiments were conducted in simple two-dimensional configurations designed to examine separately the effects of longitudinal and transverse acceleration. The next phase of the work consisted of temperature measurements in a model reverse flow combustor, using

a rake of thermocouples which could be moved both longitudinally and transversely to provide transverse temperature profiles at a number of longitudinal stations. Single jets, and rows of cooling jets of different spacing, were injected at several locations with varying flow rates and temperatures to produce a useful range of momentum ratios and density ratios. In addition, a semi-empirical calculational model was developed to predict the behavior of a single cooling jet in the reverse flow combustor configuration.

Results of these experiments show that single jet temperature trajectories are swept toward the inner wall of the turn, whether injection is from the inner or outer wall. A widely spaced row of jets produces a trajectory similar to that of a single jet. As spacing is reduced, jet penetration is also reduced, and the cooling jets tend to remain close to the wall from which they are injected. These results suggest that suitable cooling and temperature distribution tailoring can be accomplished without injecting cooling jets upstream of the turn, and thus it appears that combustors can be made significantly smaller than current designs.

The current phase of this project is directed toward the acquisition of velocity measurements in the turn section of the combustor. To this end a combined pitot-static tube and thermocouple probe was constructed. Following successful tests of this probe, a five-probe rake using the same design was constructed. Velocity and temperature distributions are being obtained using this rake. Because of the large quantity of data required for adequate representation of the velocity and

temperature fields, the data is being directly computer acquired.

An attempt to develop a semi-empirical calculational model for a row of jets, similar to that for a single jet, was limited by the absence of fundamental mixing information for rows of jets. Consequently, experiments were performed to obtain entrainment rates for rows of jets. In these experiments volume flow rates were deduced by integrating velocity distributions obtained from hot wire anemometer transverses. A Master's thesis describing these results is in preparation. In a companion effort, vortex models of a jet in cross-flows have been developed in an attempt to understand the relative importance of viscous and inviscid phenomena in determining the jet trajectories.

Throughout this work we have been fortunate to have the support and advice of Steve Riddlebaugh of the NASA Lewis Research Center, and we are pleased here to thank him.

PUBLICATIONS

Lipshitz, A., "Dilution Jets in Accelerated Cross Flows", Ph.D. Dissertation, Case Western Reserve University, 1981.

Riddlebaugh, S., Lipshitz, A., and Greber, I., "Dilution Jet Behavior in the Turn Section of a Reverse Flow Combustor", AIAA paper 82-0192, 1982.

Lipshitz, A., and Greber, I., "Turbulent Jet Patterns in Accelerating Flows", AIAA paper 81-0348, 1982.

Karagozian, A., and Greber, I., "A Vortex Model for a Single Jet in a Cross Flow", Bulletin American Physical Society, November 1983.

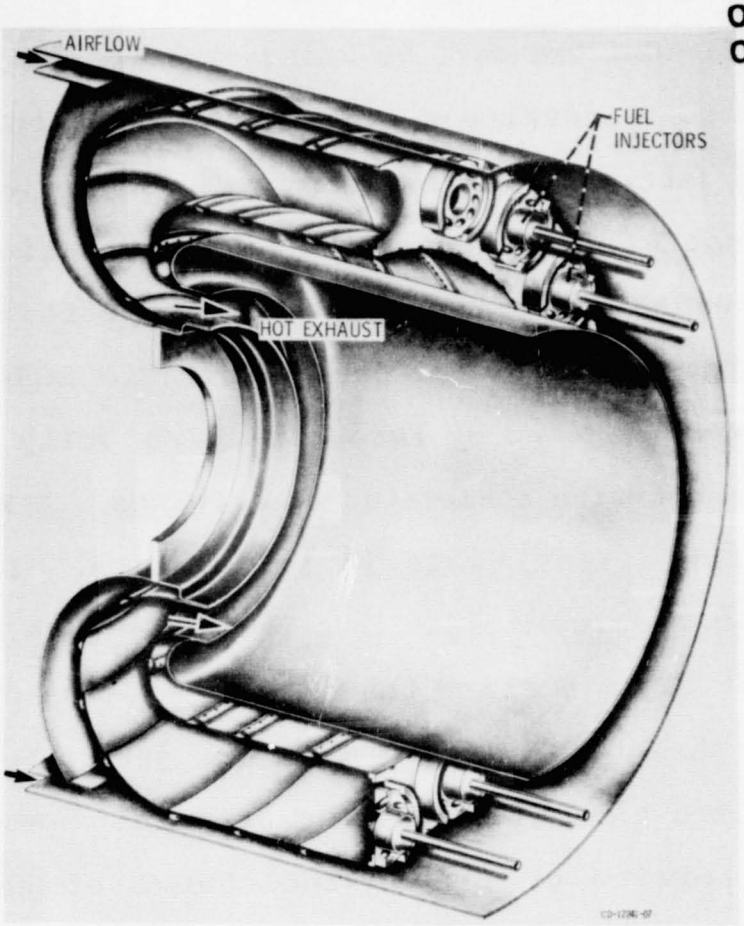

FIGURE 1. Reverse flow combustor.

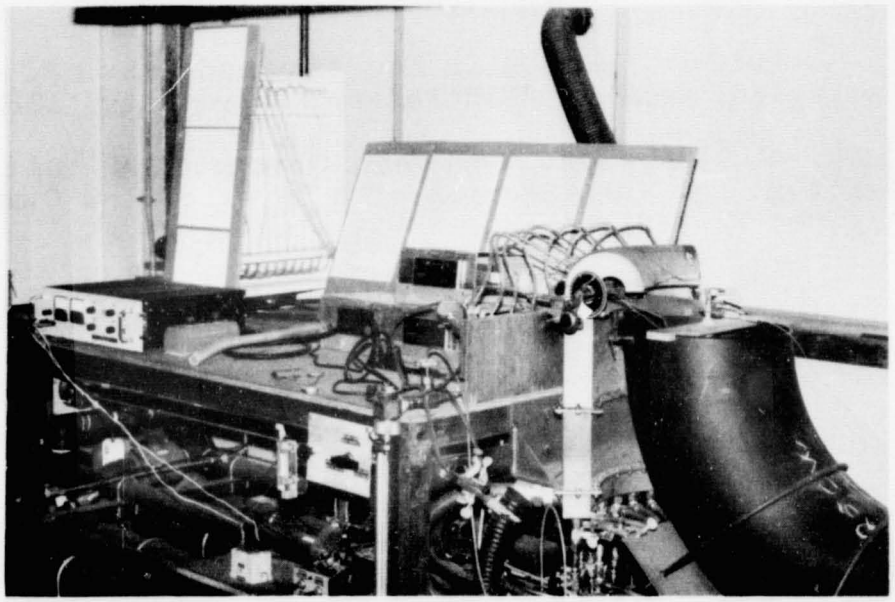

FIGURE 2. EXPERIMENTAL SETUP.

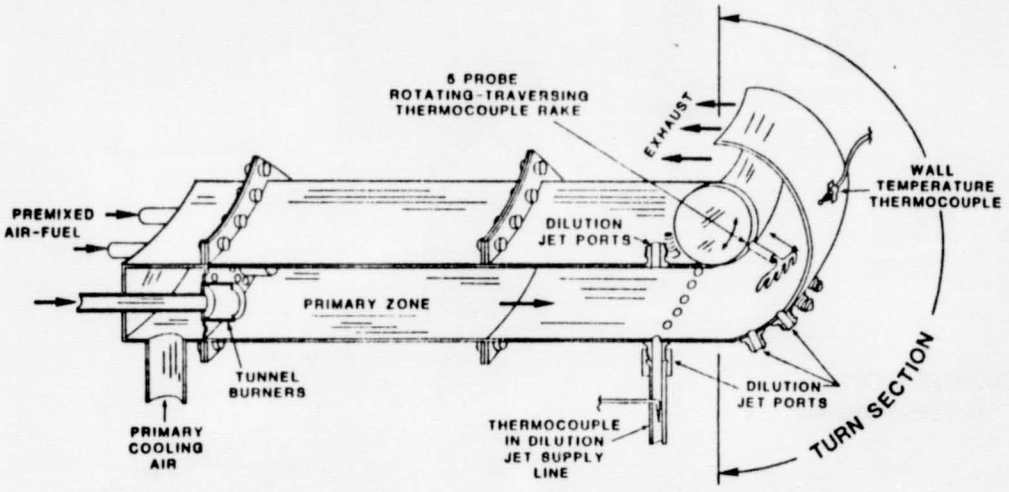

FIGURE 3. CUTAWAY SKETCH OF TEST COMBUSTOR

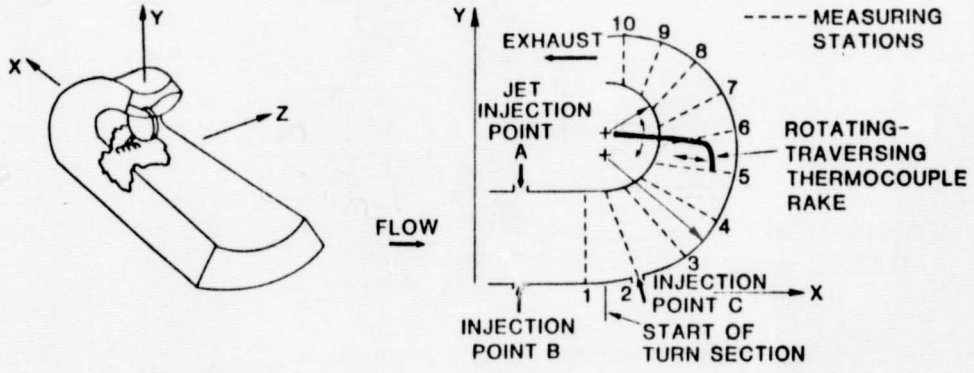

FIGURE 4. COMBUSTOR TURN SECTION GEOMETRY
AND TEMPERATURE MEASURING STATIONS

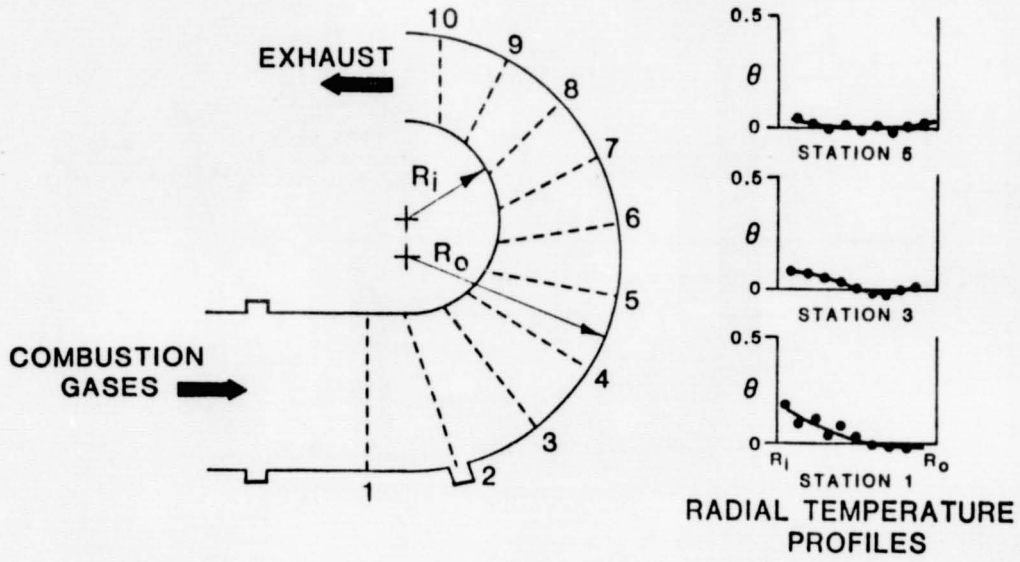

FIGURE 5. TEMPERATURE DISTRIBUTION IN THE COMBUSTOR TURN WITHOUT DILUTION JETS

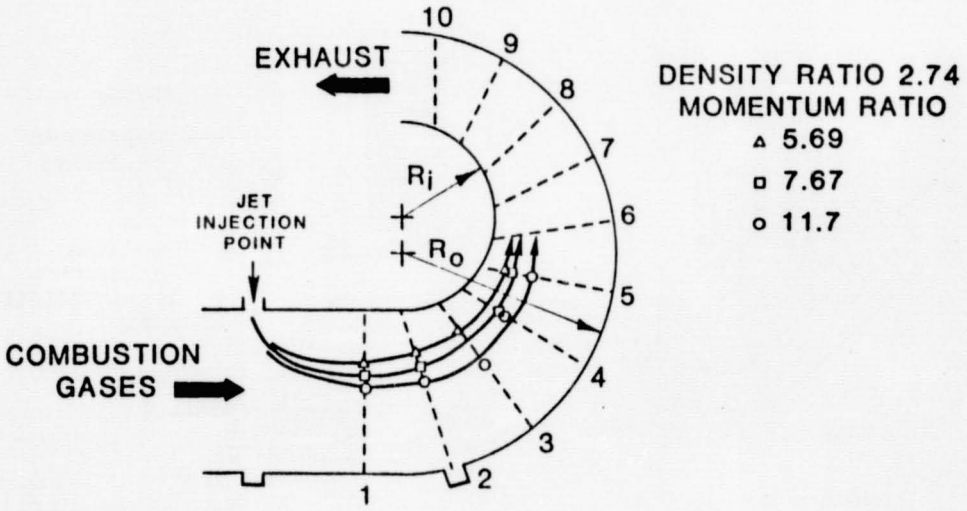

FIGURE 6. JET TRAJECTORIES SHOWING EFFECT OF MOMENTUM RATIO ON A JET INJECTED FROM THE INNER WALL

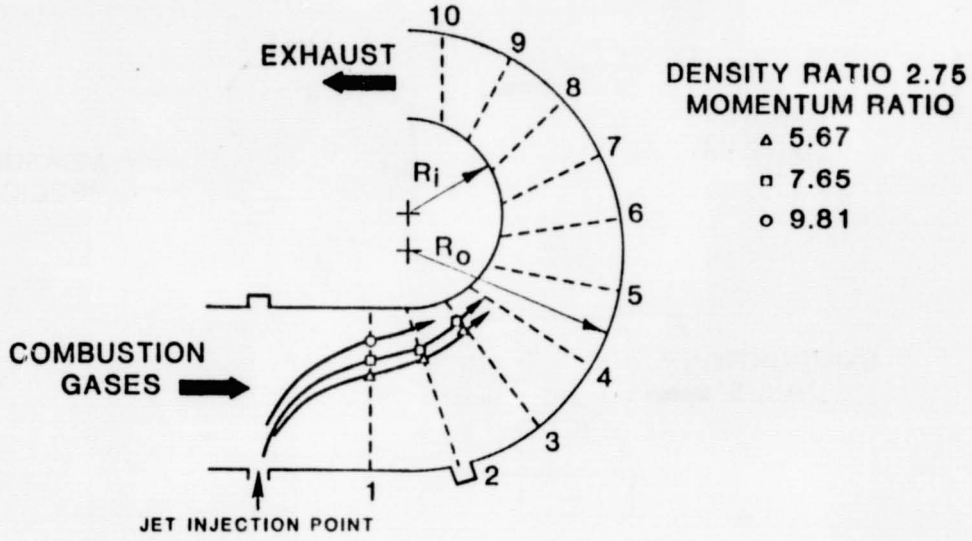

FIGURE 7. JET TRAJECTORIES SHOWING EFFECT OF MOMENTUM RATIO ON JET INJECTED FROM THE OUTER WALL

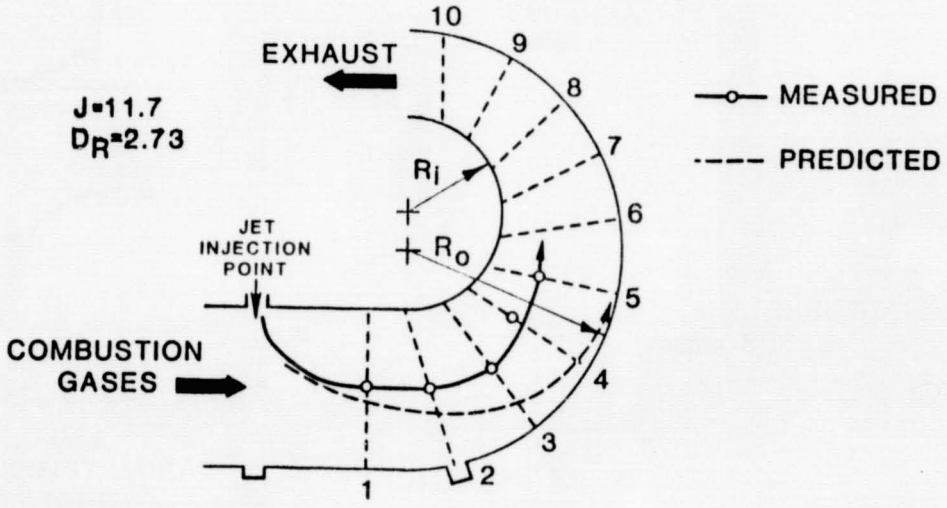

FIGURE 8. COMPARISON WITH MODEL FOR A SINGLE JET INJECTED FROM THE INNER WALL

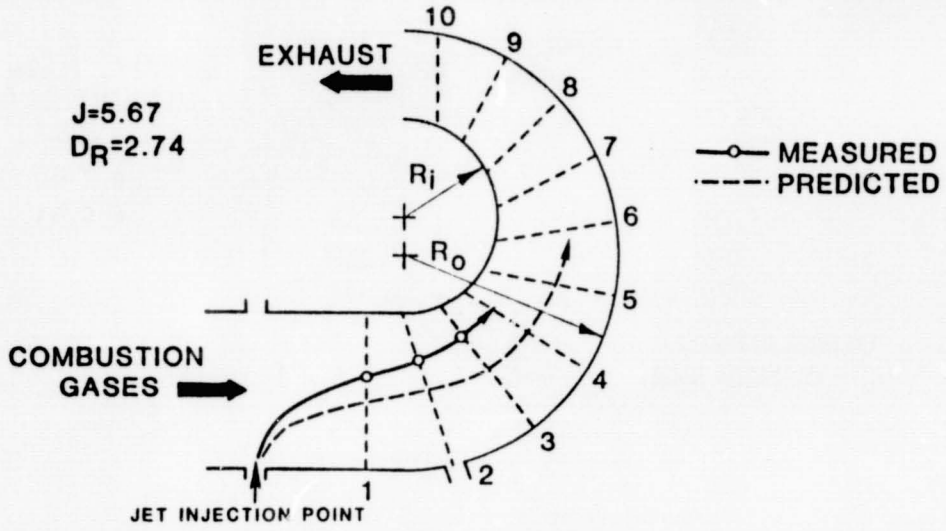

FIGURE 9. COMPARISON WITH MODEL FOR A SINGLE JET INJECTED FROM THE OUTER WALL

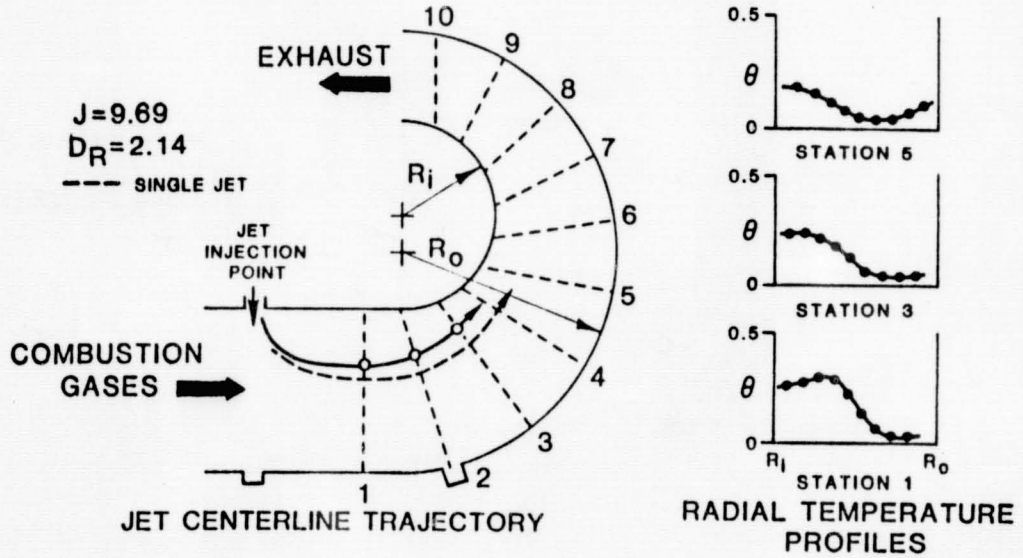

FIGURE 10. BEHAVIOR OF A WIDELY SPACED ROW OF JETS (SPACING RATIO OF 7.41) INJECTED FROM THE INSIDE WALL

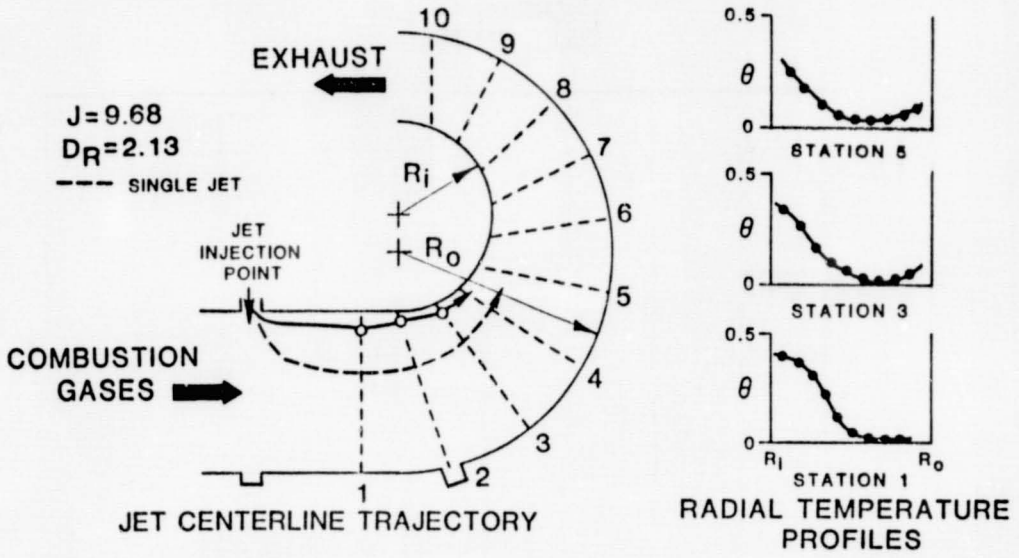

FIGURE 11. BEHAVIOR OF A CLOSELY SPACED ROW OF JETS (SPACING RATIO 2.47) INJECTED FROM THE INSIDE WALL

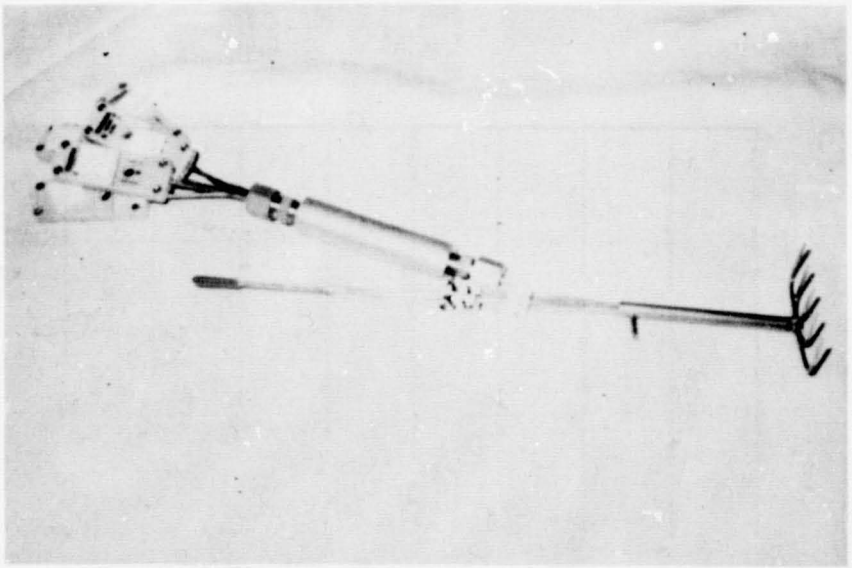

FIGURE 12. PITOT-STATIC/THERMOCOUPLE RAKE.

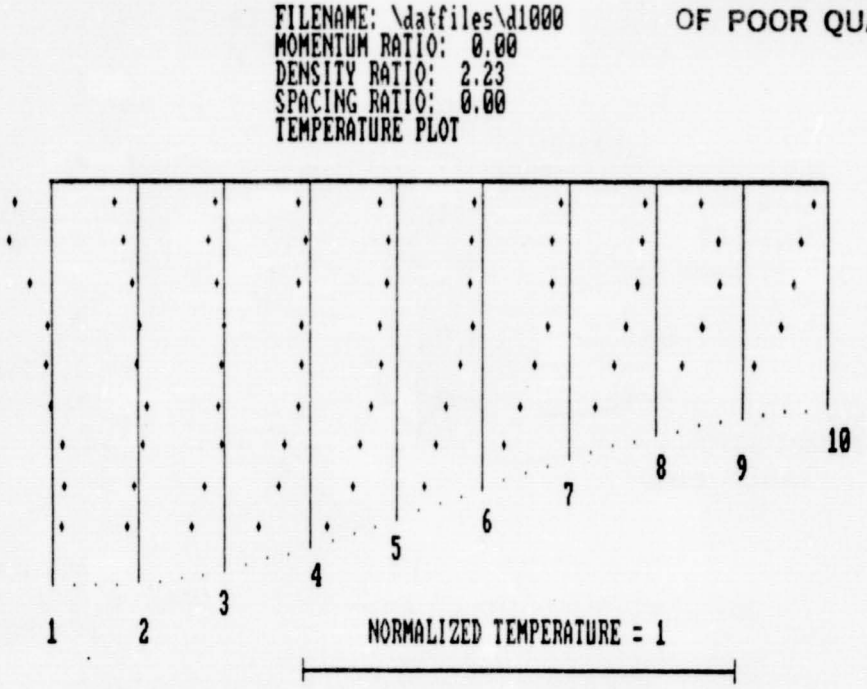

FIGURE 13. TEMPERATURE PROFILES WITH NO INJECTION.

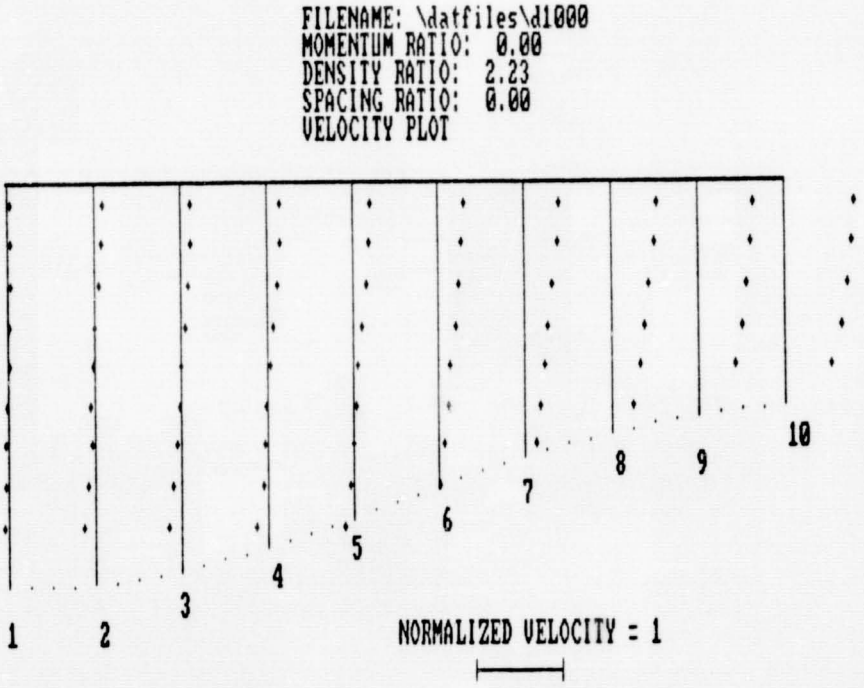

FIGURE 14. VELOCITY PROFILES WITH NO INJECTION.

N84 20546

D21

FREE STREAM TURBULENCE AND DENSITY RATIO EFFECTS ON THE INTERACTION REGION OF A JET IN A CROSS FLOW[1]

C.E. Wark[2] and J.F. Foss
Department of Mechanical Engineering
Michigan State University

Jets of low temperature air are introduced into the aft sections of gas turbine combustors for the purpose of cooling the high temperature gases and quenching the combustion reactions. Research studies, motivated by this complex flow field, have been executed by introducing a heated jet into the cross stream of a wind tunnel. The investigation by Kamotani and Greber[1] stands as a prime example of such investigations and it serves as the principal reference for the present study.

The low disturbance level of the cross stream, in their study and in similar research investigations, is compatible with an interest in identifying the basic features, of this flow field. The influence of the prototypes' strongly disturbed cross flow is not, however, made apparent in these prior investigations. The present study provides a direct comparison of the thermal field properties for a low ($\tilde{u}/U_\infty$ = 0.67%) and a high ($\tilde{u}/V_\infty$ ≃ 34%) disturbance level condition.

A novel technique was used for the data acquisition (Figure 1). Sixty-four fast response (λ ≃ 4msec) thermocouples were simultaneously sampled (and corrected for the time constant effect) at a downstream plane close to the jet exit (x/d=3-4). Various measures were used to characterize the thermal fields for the disturbed and undisturbed conditions, for two different momentum flux ratios ($J=\rho_j V_j^2/\rho_\infty V_\infty^2$=16,64), and for three overheat conditions (T_j=22.2, 47.1 and 61.1).

Two forms of data acquisition were used for this study. Stochastic values were obtained from triplet values: $T_K(t-\delta t)$, $T_k(t)$ and $T_k(t+\delta t)$, where K=1....64 is the thermocouple designation and the $\pm\delta t$ (δt=0.64msec) values were used to form the central difference time derivative from which the corrected temperature value: $\{T_k(t)\}_c$, was determined. These values were retained for t, t+Δt, t+2Δt....t+NΔt where N=5,000 for the undisturbed and 10,000 for the disturbed condition and $\Delta t \simeq 100$ms which ensured the statistical independence from its neighboring value. Instantaneous samples: Δt = 0.64ms and N=1,225 were stored for J=16, 64 and T_j = 61.1 °c.

---

1 Supported by NASA Grant NAG 3-245
2 M.S. 1984, presently at Illinois Institute of Technology

RESULTS

Histograms, formed from the independent samples, were sufficiently smooth to approximate a probability density function; examples are shown in Figure 2 for a thermocouple from the central region of the jet. A striking result, from all such histograms, is that the peak (non-dimensional) temperature did not exceed 0.25. Hence, even at the relatively close x/d locations of the present study, molecular diffusivity has played a dramatic role in the reduction of the temperature for the fluid elements of the jet.

The individual histograms, and the isothermal patterns that are fit to the mean values of the corrected temperatures, both reveal that the magnitude of the overheat exerts a significant dynamic effect on the jet in a cross flow problem; see Figures 3 and 4. It is pertinent to note that the increasing distance of the thermal center of gravity, from the source plate with increasing jet temperature, is opposite to that which would be expected from buoyancy and enhanced entrainment effects. The former agrees with the Kamotani and Greber results, the latter is in disagreement. The physical reasons for this unexpected behavior are not apparent; the consistency of the trend: an increased penetration of the thermal field with an increased jet temperature, is consistently observed and serves as a primary focus for further study. A further comparison with the results from Kamotani and Greber (see Figure 5) reveals a substantial difference between the jet penetration for the two studies. This difference is (at least in part) attributed to the present use of a sharp-edge nozzle and to the large ($\delta/d \simeq 1.3$) boundary layer for the present study.

One clearly apparent effect of the large disturbance condition is the migration of the centroid of the thermal field; see figure 6. Similar data for all of the instantaneous scans (6 disturbed, 3 undisturbed) are summarized in Table I; note: K_{st} is the normalized correlation coefficient between the vertical (s) and transverse (t) displacements of the thermal center of gravity.

TABLE I. Cross stream disturbance effect on centroid of temperature field

	J	$\sigma_{s_{c.g.}}$	$\sigma_{t_{c.g.}}$	K_{st}
undisturbed c.f.	16	.341	.253	.067
undisturbed c.f.	64	.233	.233	-0.13
disturbed c.f.	16	1.84	1.45	-0.33
disturbed c.f.	64	1.16	1.12	-0.45

The lower mean values, of the disturbed cross stream mean isotherms, are apparently caused by these large centerline migrations; figure 7 shows an instantaneous isotherm pattern that reveals maximum temperature values of the same order as those for the undisturbed case.

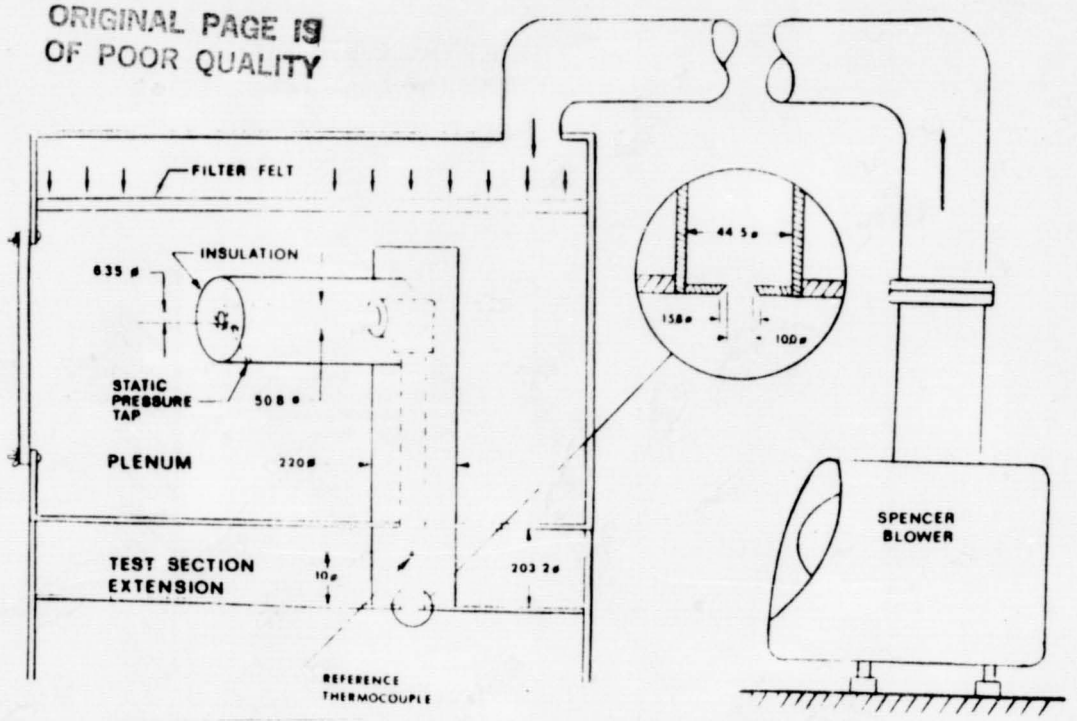

Figure 1a. Schematic of Jet Supply and Exit Conditions
Note: Lateral (i.e.,z) position of the jet corresponds to the undisturbed position. The jet exit was moved into the low speed portion of the shear layer: $\bar{u}/U_o$=0.25, for the disturbed flow condition.

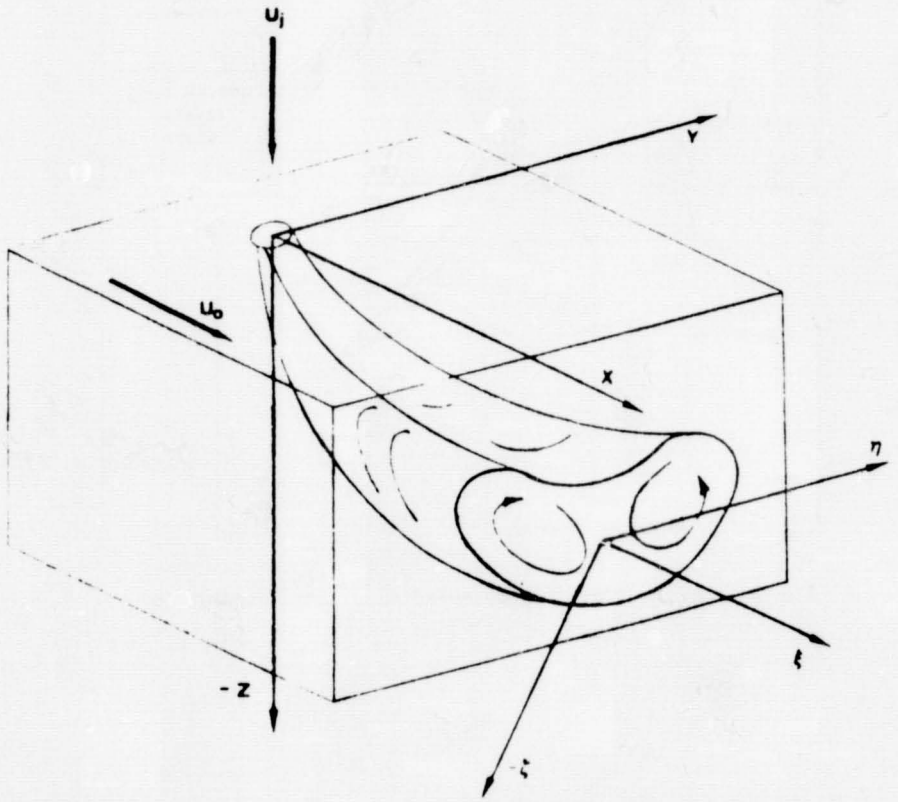

Figure 1b. Schematic Representation of Jet Trajectory, Showing Lab coordinates (x, y, z) and Jet Coordinates (ξ, η, ζ)
Note: Thermocouples were located in the y-z plane at x=3.5(for J=64) and 3.85 (J=16).

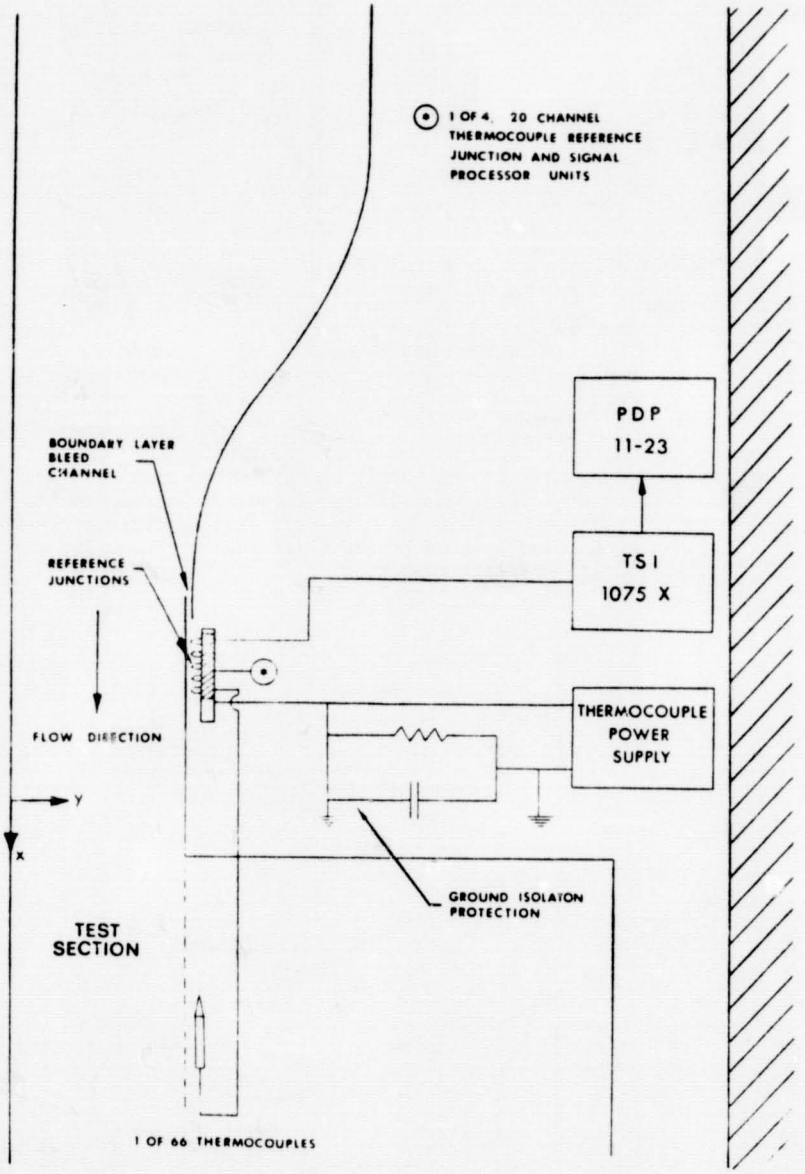

Figure 1c. Schematic Representation of the Temperature measurement system

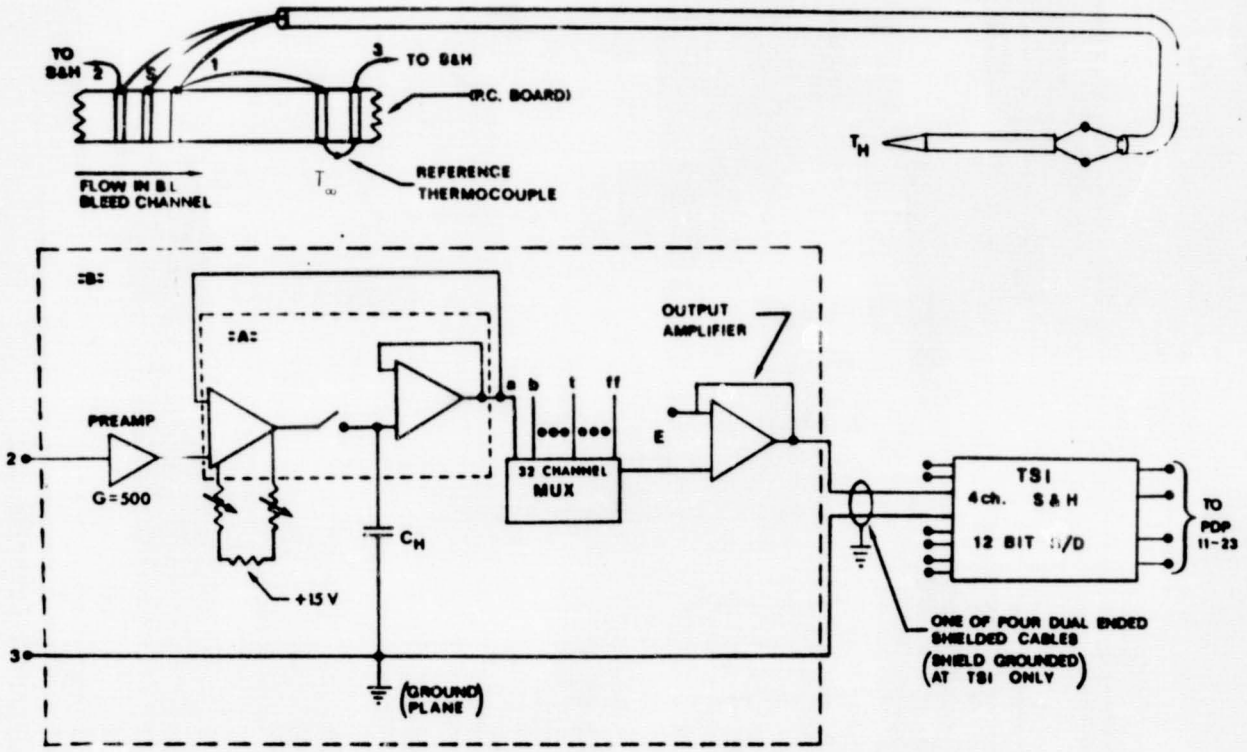

Figure 1d. Detail of a Sample and Hold Circuit.

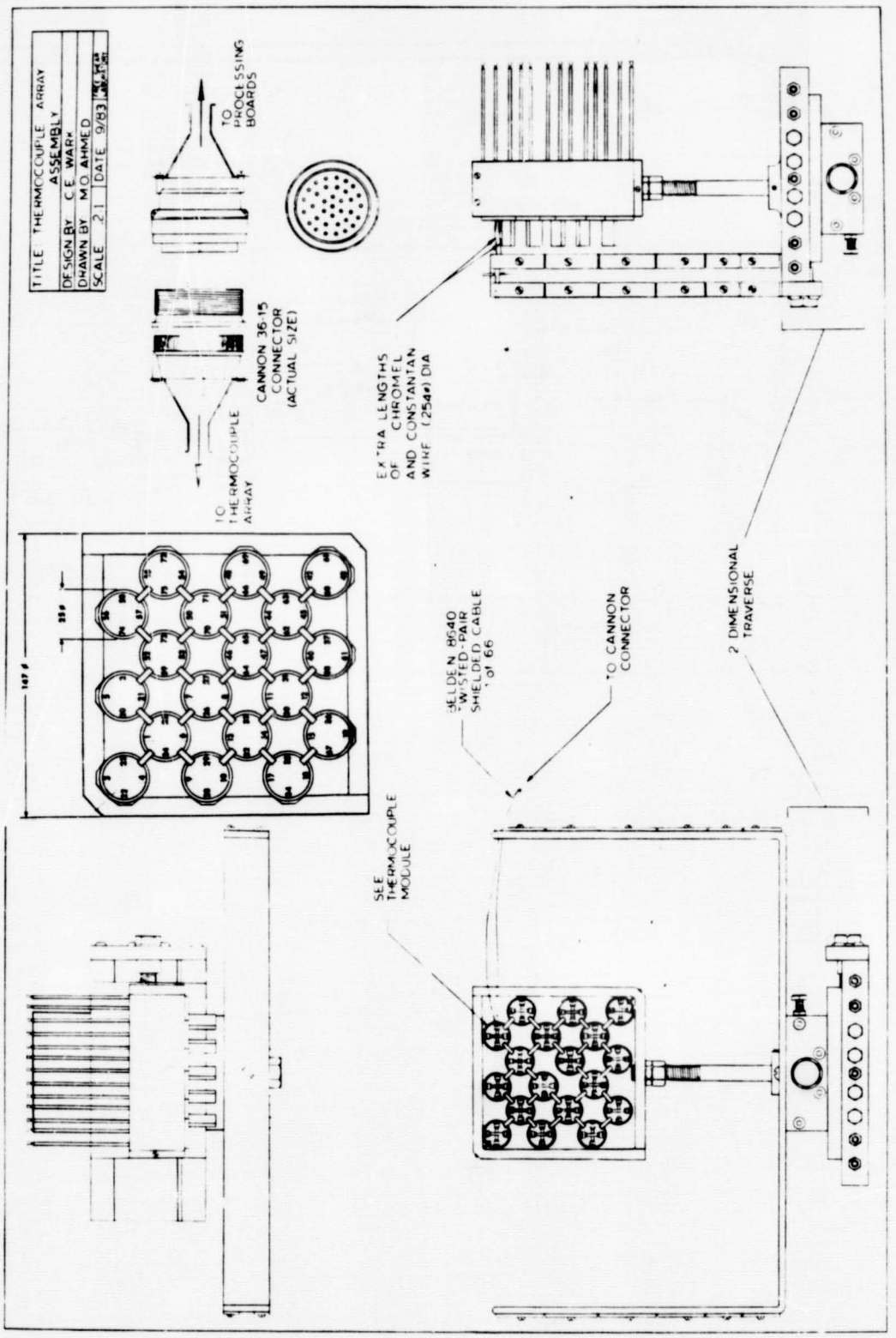

Figure 1e. Thermocouple Array Assembly

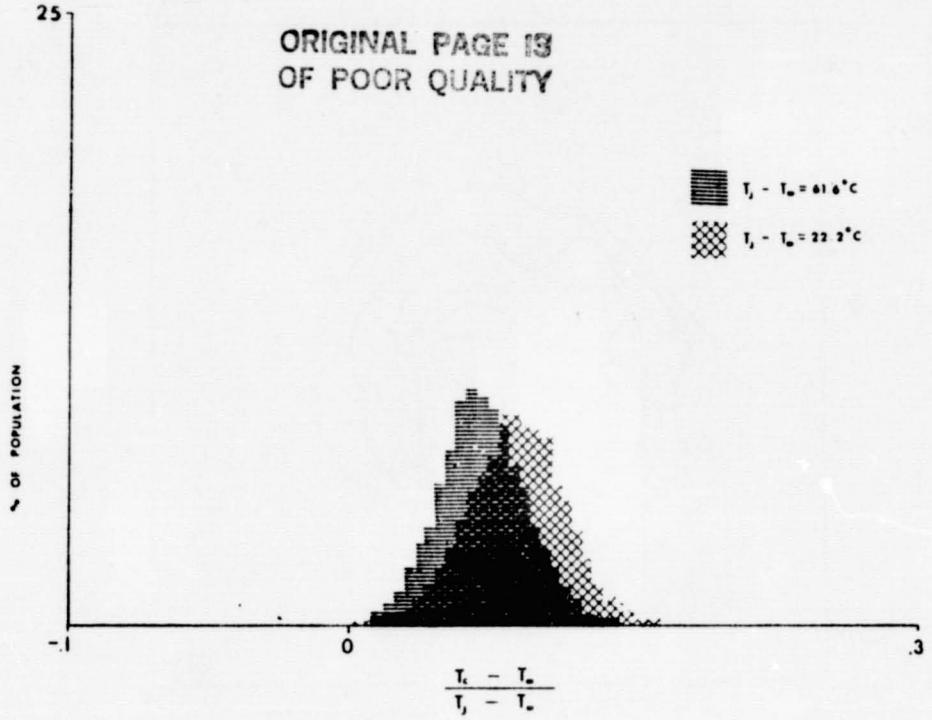

Figure 2a. Temperature Histogram for u.c.f.: J = 16, Thermocouple at s/d = 4.79, t/d = 4.73

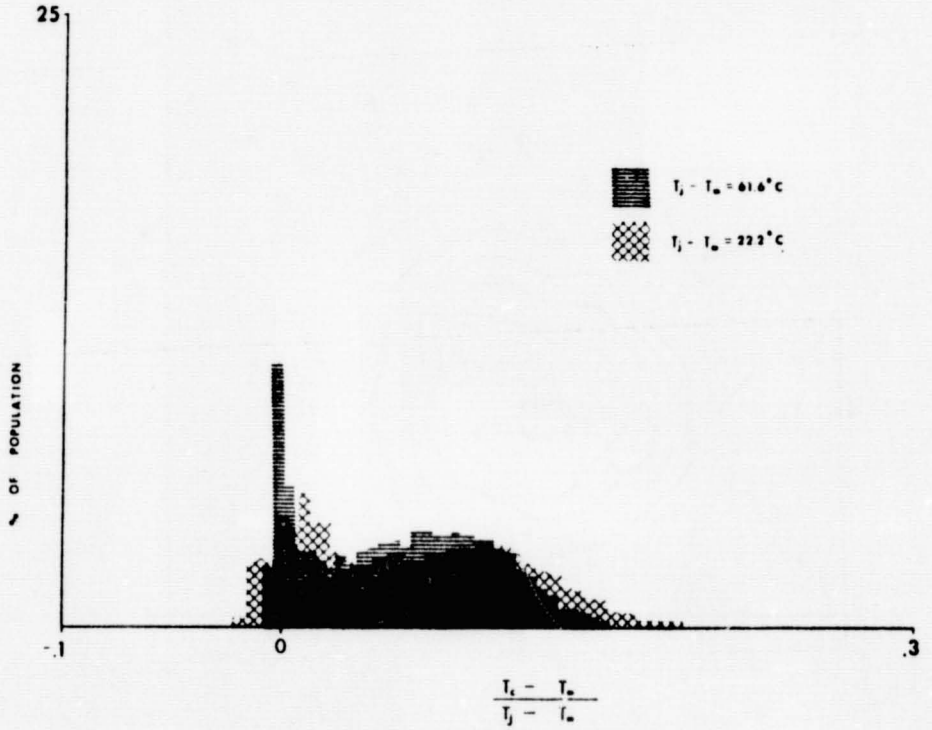

Figure 2b. Temperature Histogram for d.c.f.: J = 16, Thermocouple at s/d = 5.64, t/d = 3.64

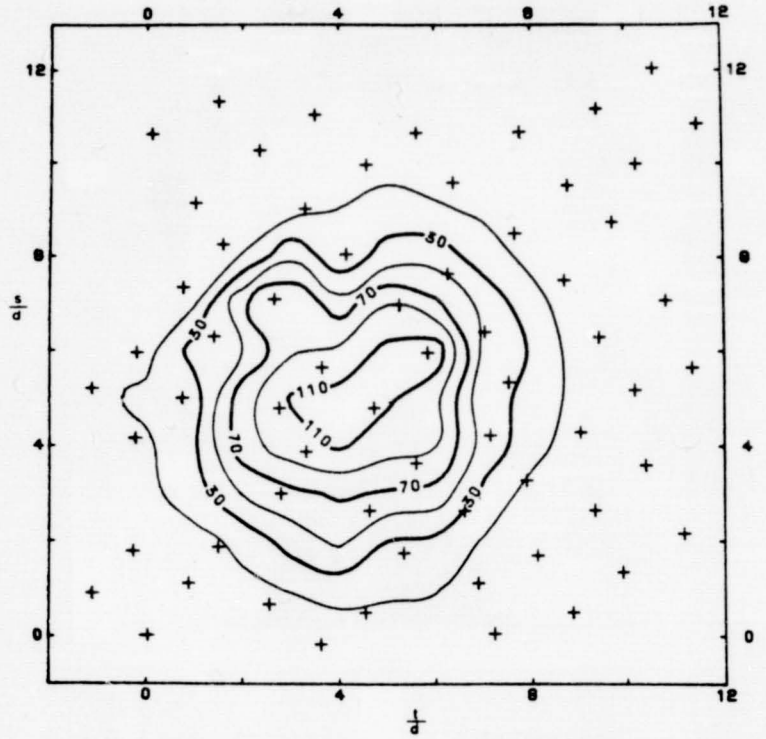

Figure 3a. Undisturbed Cross Flow (u.c.f.) Mean Temperature Isotherms: $J = 16$, $T_{jet} - T_\infty = 22.2°C$

NOTE: Contours shown are $\frac{T_c - T_\infty}{T_{jet} - T_\infty} \times 1000$ $s/d = 14.1\ (\pm .7) - z/d$, $t/d = 4.3(\pm .5) - y/d$

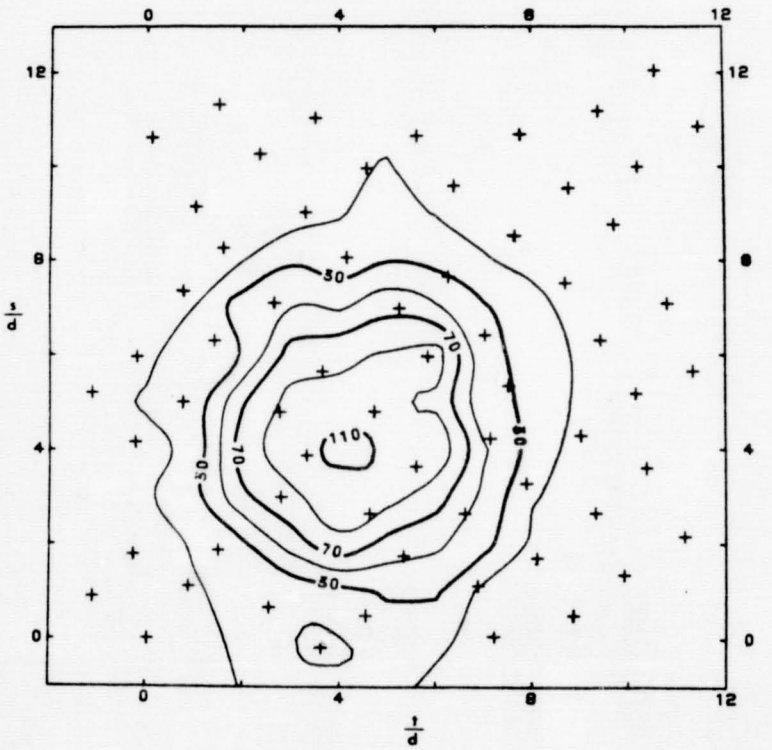

Figure 3b. u.c.f. Mean Temperature Isotherms: $J = 16$, $T_{jet} - T_\infty = 61.1°C$

NOTE: $s/d = 14.1(\pm .7) - z/d$, $t/d = 4.3(\pm .5) - y/d$

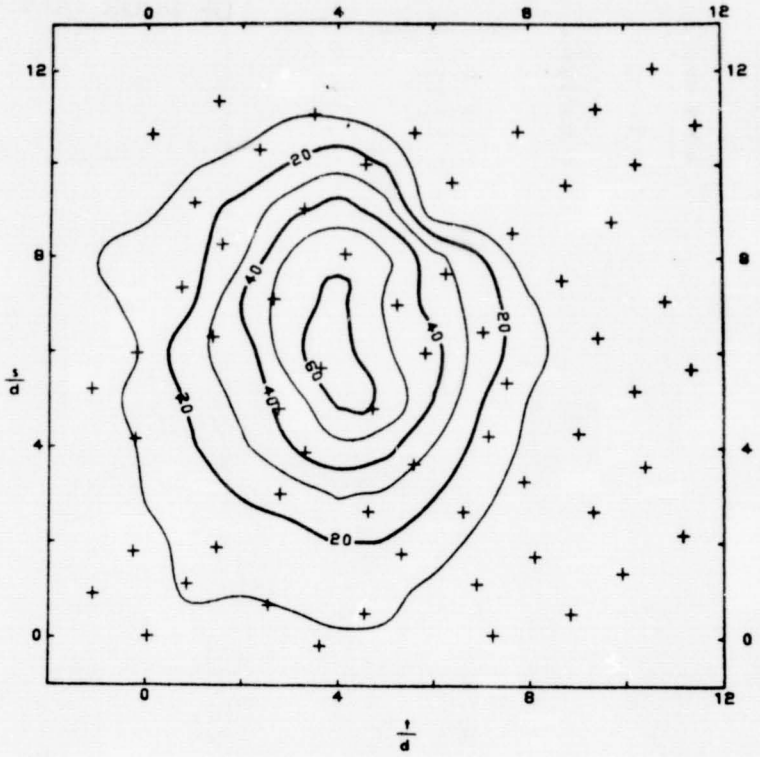

Figure 3c. Disturbed Cross Flow (d.c.f.) Mean Temperature Isotherms: J = 16, $T_{jet} - T_{\infty}$ = 22.2°C

NOTE: s/d = 14.1(± .7) - z/d, t/d = 4.2(± .5) - y/d

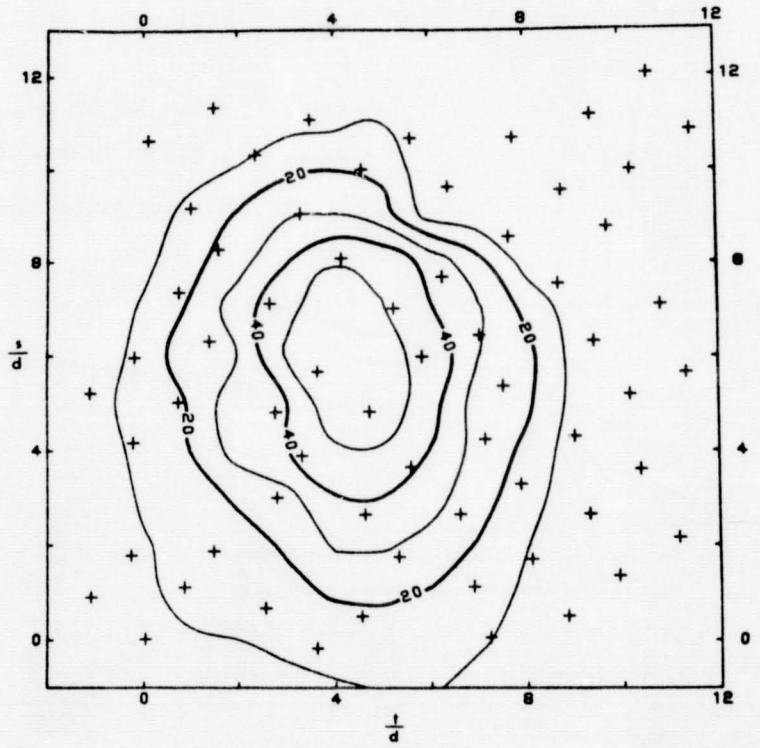

Figure 3d. d.c.f. Mean Temperature Isotherms: J = 16, $T_{jet} - T_{\infty}$ = 61.1°C

NOTE: s/d = 14.1(± .7) - z/d, t/d = 4.2(± .5) - y/d

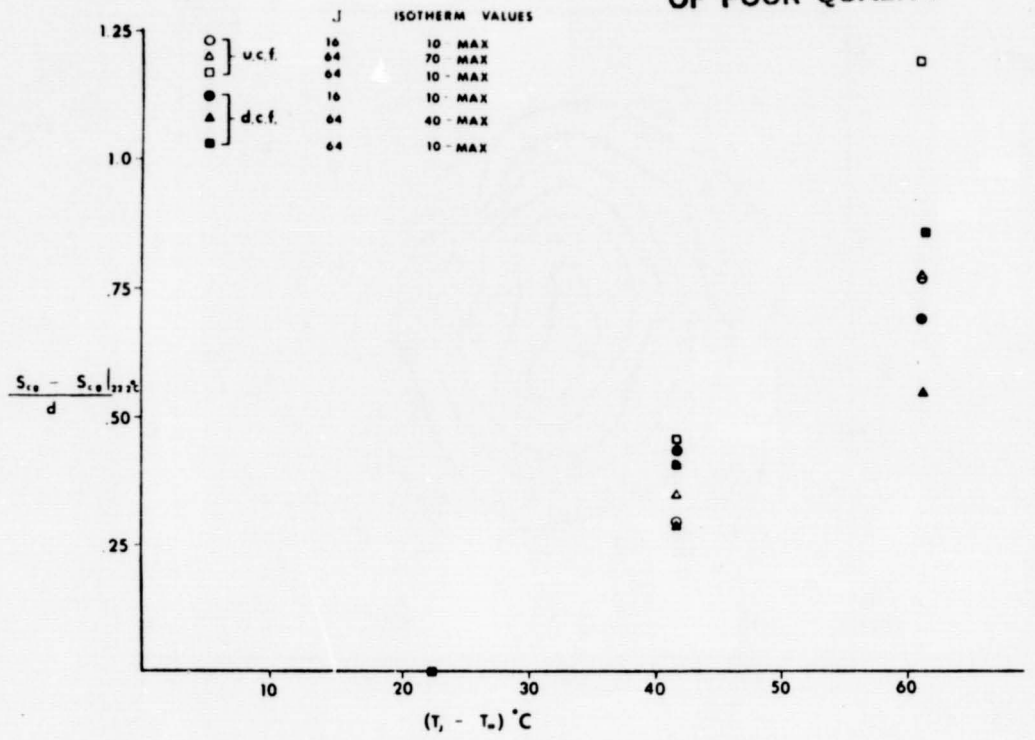

Figure 4. Overheat Influence on s Component Centroid
(calculated using isotherm contours)

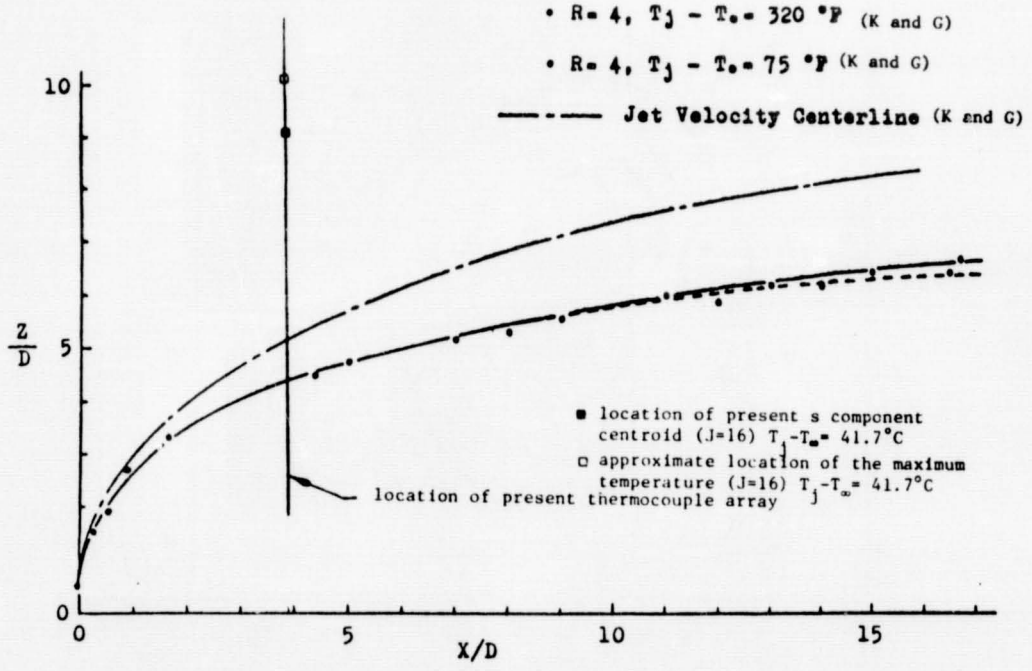

Figure 5a. Location of Temperature Centerline (R=4)
from Kamotani and Greber (1971)

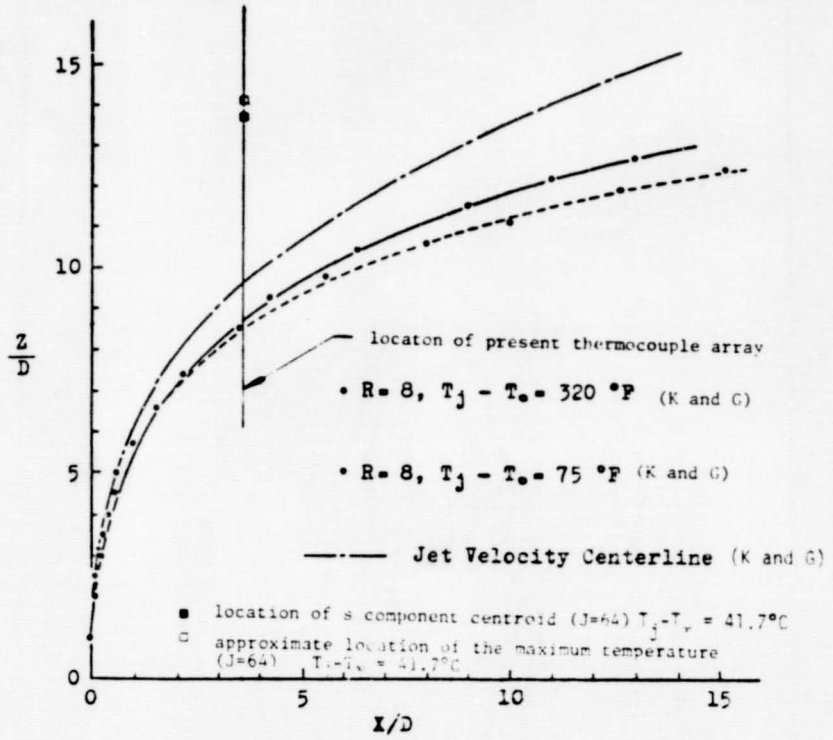

Figure 5b. Location of Temperature Centerline (R=8) from Kamotani and Greber (1971)

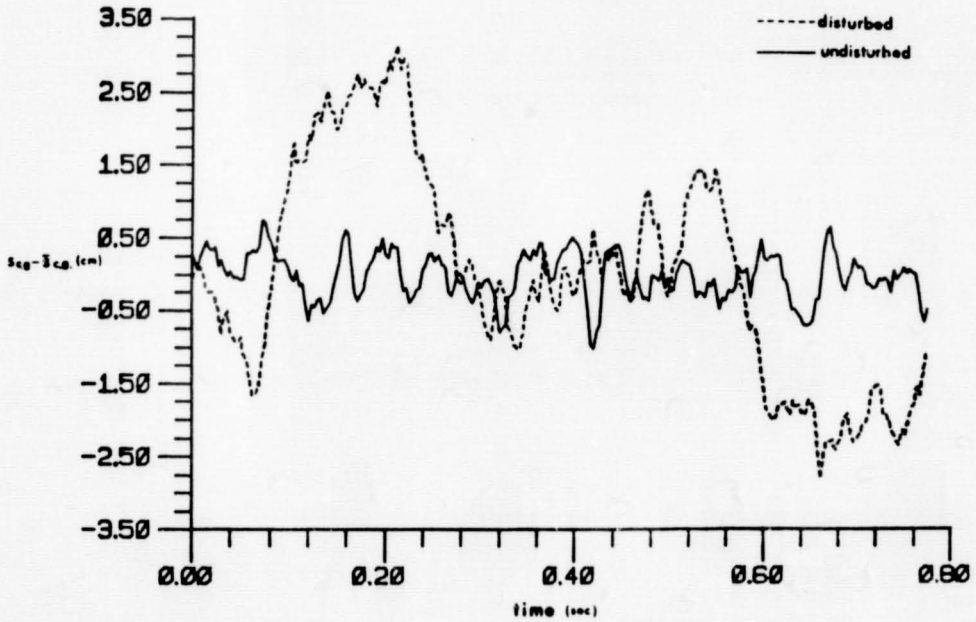

Figure 6. Variation of s Component of Centroid with Time
J = 16, $T_{jet} - T_\infty$ = 61.1°C

Note: $(t_{c.g.} - \bar{t}_{c.g.})$ distribution draws a similar fluctuation level.

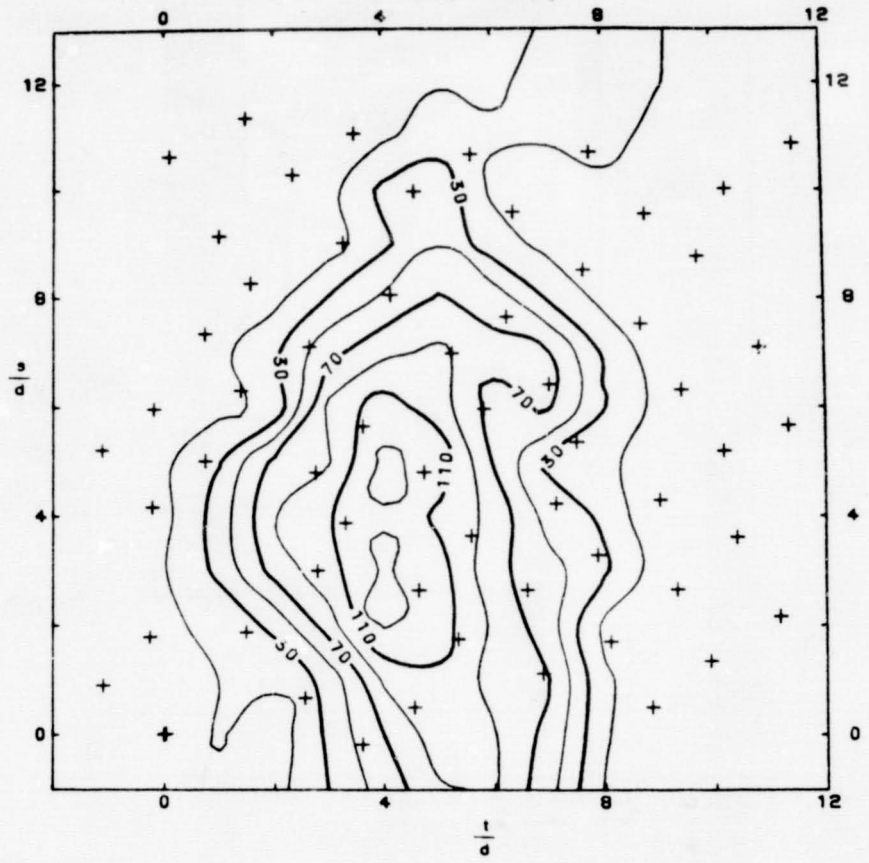

Figure 7. d.c.f. Instantaneous Temperature Isotherms
J = 16 , $T_{jet} - T_{\infty}$ = 61.1°C, Time = .65 sec

NOTE: Contours are $\frac{T_0 - T}{T_{jet} - T}$ X 1000, s/d and t/d as defined for the mean temperature isotherms

D22

MODELING OF DILUTION JET FLOWFIELDS

by J.D. Holdeman
NASA Lewis Research Center

and

R. Srinivasan
The Garrett Turbine Engine Company

Considerations of dilution zone mixing in gas turbine combustion chambers have motivated several studies of the mixing characteristics of a row of jets injected normally into a flow of a different temperature in a constant area duct.[1-4] Recently, experiments have been performed to extend these investigations to include geometric and flow variations characteristic of most gas turbine combustion chambers, namely a variable temperature mainstream, flow area convergence, and opposed rows of jets, either in-line or staggered;[5,6] see figures 1 & 2.

The present paper will compare temperature field measurements from selected cases in these investigations with distributions calculated with an empirical model based on assumed vertical profile similarity and superposition[6] and with a 3-D elliptic code using a standard K-E turbulence model.[7] The results will show the capability (or lack thereof) of the models to predict the effects of the principle flow and geometric variables.[2,4,6,7]

Variations with Orifice Size and Spacing. At constant orifice area, changes in orifice size and spacing can result in jets which vary from under-penetration to over-penetration. This is shown in figure 3a) and b), for jets from closely spaced small orifices and widely spaced larger orifices respectively. The empirical model reproduces the data very well in the small orifice case, since the data are consistent with the major assumption in the empirical model, that all vertical temperature distributions can be reduced to similar Gaussian profiles. The empirical model does not do as well in the larger orifice case however, as the jets have impinged on the opposite wall and the vertical profiles are not similar.

The analytical model calculations made with approximately 20,000 nodes, although in qualitative agreement with the data, under-predict the mixing. That is, the temperature gradients, especially in the transverse direction, are too steep. This result is typical of the analytical model calculations to be shown in this paper. For the small-orifice case a coarse-grid calculation using less than 6000 nodes was also performed. This solution illustrates the diffusive nature of the calculation

and the significant influence of grid selection on the solution obtained.

Coupled Spacing and Momentum Flux Ratio. Examination of the experimental data revealed that similar profiles can be obtained over a range of momentum flux ratios, independent of orifice diameter, if orifice spacing and momentum flux ratio are correctly coupled.[2,4,8,9] This is shown in figure 4a) to c).

In all of the combinations shown here, the empirical model results are in very good agreement with the data, as the data are consistent with the Gaussian profile assumption. The analytical model calculations using approximately 20,000 nodes for these cases agree qualititively with the data, as in the previous figure. In the medium momentum flux ratio case, a second calculation was performed with the same total number of grid points, but with the nodes slightly more concentrated in the vicinity of the jet exit. As can be seen in figure 4b), these two results are not substantially different.

Variable Temperature Mainstream. The influence of a non-isothermal mainstream flow on the profiles for medium momentum flux ratios with S/Ho=.5 and Ho/D=4 can be seen by comparing figures 5 & 6. The shape of the experimental profiles in figure 6 suggests modeling them as a superposition of the upstream profile and the corresponding jets-in-an-isothermal mainstream distribution.[9] This gives only a crude approximation however, as seen in the empirical model results, because of the cross-stream transport of mainstream fluid due to the blockage, which is not accounted for in superimposing the distributions.

In the variable temperature mainstream case the analytical model results agree well with the experimental data, especially on the jet centerplane, but the transverse mixing is underpredicted, as in the corresponding isothermal mainstream case in figure 5.

Opposed Rows of In-line Jets. For opposed rows of jets, with the orifice centerlines in-line, the optimum ratio of orifice spacing to duct height is one-half of the optimum value for single-side injection at the same momentum flux ratio.[9] As as example consider the single-side case with S/Ho=.5 and Ho/D=4 in figure 5 and the opposed row of in-line jets with S/Ho=.25 and Ho/D=8 in figure 7.

The empirical model predicts the opposed-jet case very well, verifying the primary assumption that the effect of a plane of symmetry is similar to that of an opposite wall.[8,9] Note that the experimental profiles on both sides of the plane of symmetry support the Gaussian profile assumption. The analytical model results show the steep transverse and lateral gradients seen in almost all of the previous calculations also,

but are in otherwise good agreement with the data.

Opposed Rows of Staggered Jets. For opposed rows of jets, with the orifice centerlines staggered, the optimum ratio of orifice spacing to duct height is double the optimum value for single-side injection at the same momentum flux ratio.[9] As an example consider the single-side case with S/Ho=.5 in figure 5, and the opposed row of staggered-jets with S/Ho=1 in figure 8.

The empirical model does not handle this complex case well, as the fluid dynamic interactions here are not amenable to a direct extension of the simple Gaussian profile and superposition type modeling appropriate for most of the single-side and opposed-jet cases of interest. The analytical model calculations give slightly better agreement with the data than does the empirical model, and would be expected to improve with overall improvements in the capability of the 3-D codes.

REFERENCES

1. Walker, R.E. and Kors, D.L.: Multiple Jet Study Final Report. NASA CR-121217, 1973.

2. Holdeman, J.D., Walker, R.E., and Kors, D.L.: Mixing of Multiple Dilution Jets with a Hot Primary Airstream for Gas Turbine Combustors. AIAA Paper 73-1249, 1973.

3. Walker, R.E. and Eberhard, R.G.: Multiple Jet Study Data Correlations. NASA CR-134796, 1975.

4. Holdeman, J.D. and Walker, R.E.: Mixing of a Row of Jets with a Confined Crossflow. AIAA Journal, vol.15, no.2, Feb.1977, pp243-249.

5. Srinivasan, R., Berenfeld, A., and Mongia, H.C.: Dilution Jet Mixing Program - Phase I Report. NASA CR-168031, 1982.

6. Srinivasan, R., Coleman, E., Johnson, K., and Mongia, H. C.: Dilution Jet Mixing Program - Phase II Report. NASA CR-174624, 1984.

7. Srinivasan, R., Reynolds, R., Ball, I., Berry, R., Johnson, K., and Mongia, H.: Aerothermal Modeling Program - Phase I Final Report. NASA CR-168243, 1983.

8. Holdeman, J.D.: Perspectives on the Mixing of a Row of Jets with a Confined Crossflow. AIAA-83-1200, 1983.

9. Holdeman, J.D., Srinivasan, R., and Berenfeld, A.: Experiments in Dilution Jet Mixing. AIAA-83-1201, 1983.

C-3

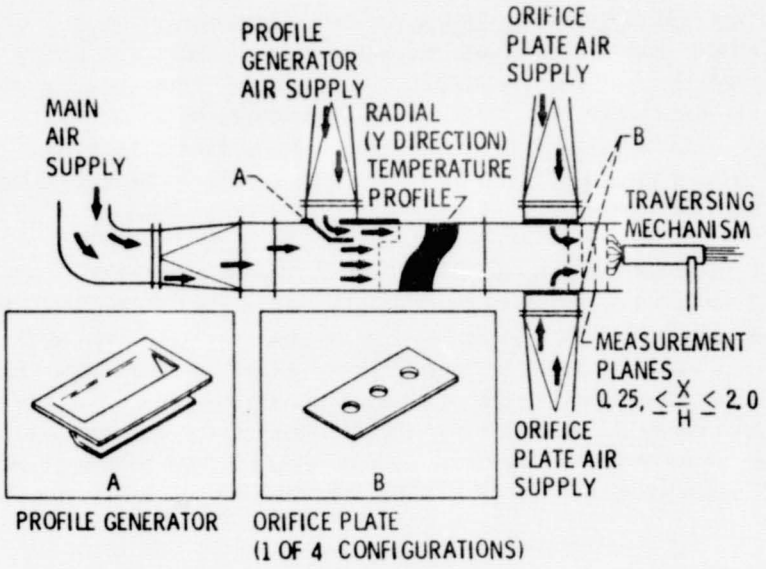

Figure 1. - Dilution Jet Mixing Flow Schematic.

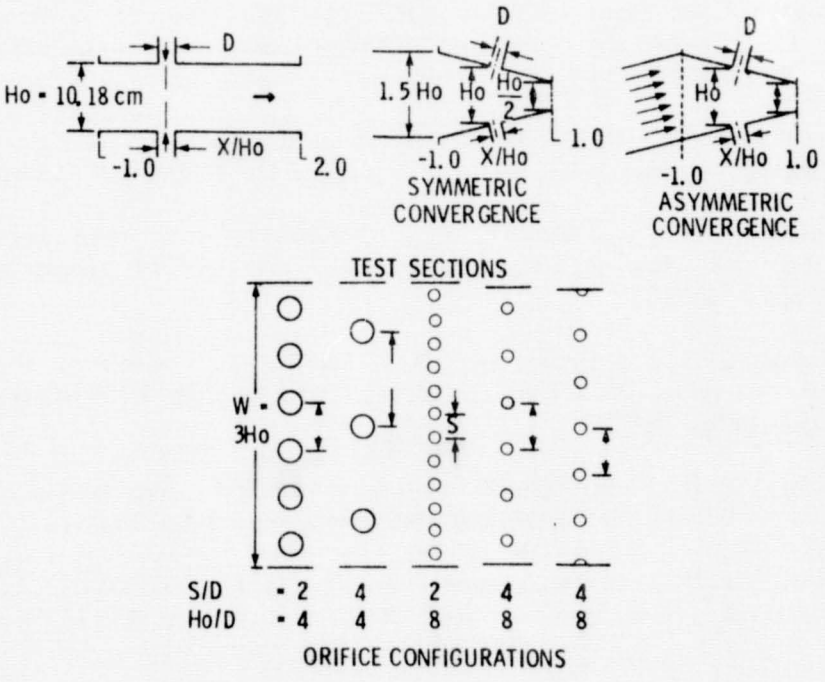

Figure 2. - Test Sections and Orifice Configurations.

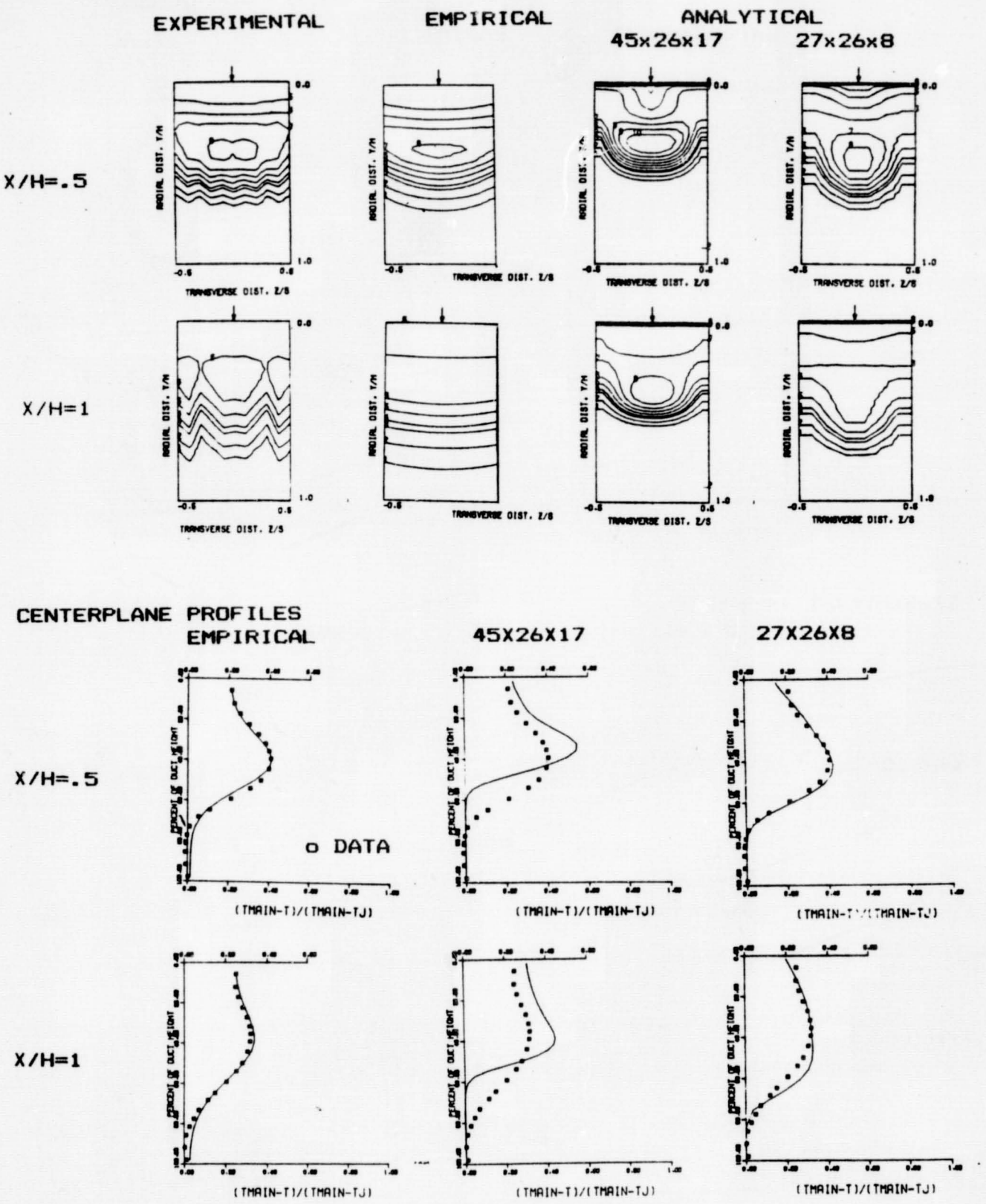

a) S/H_o=.25, H_o/D=8, A_j/A_m=.049, J=25.3, W_j/W_T=.169

Figure 3. Effect of Variations in Orifice Size and Spacing on Temperature Distributions

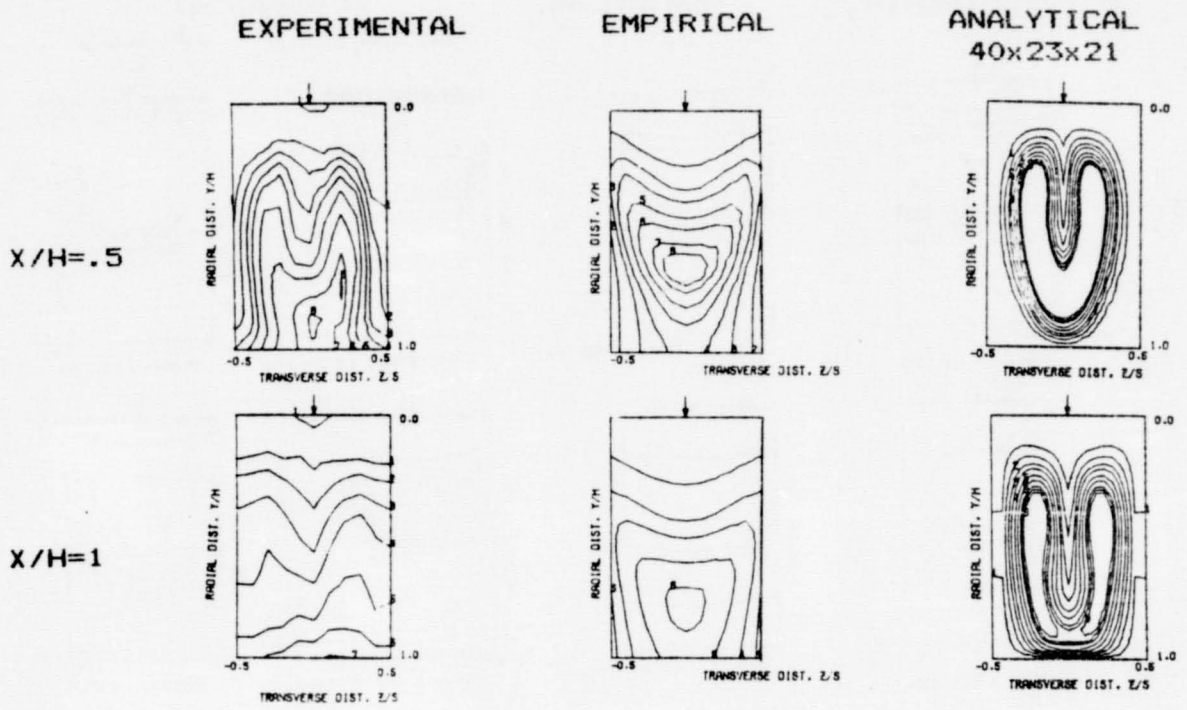

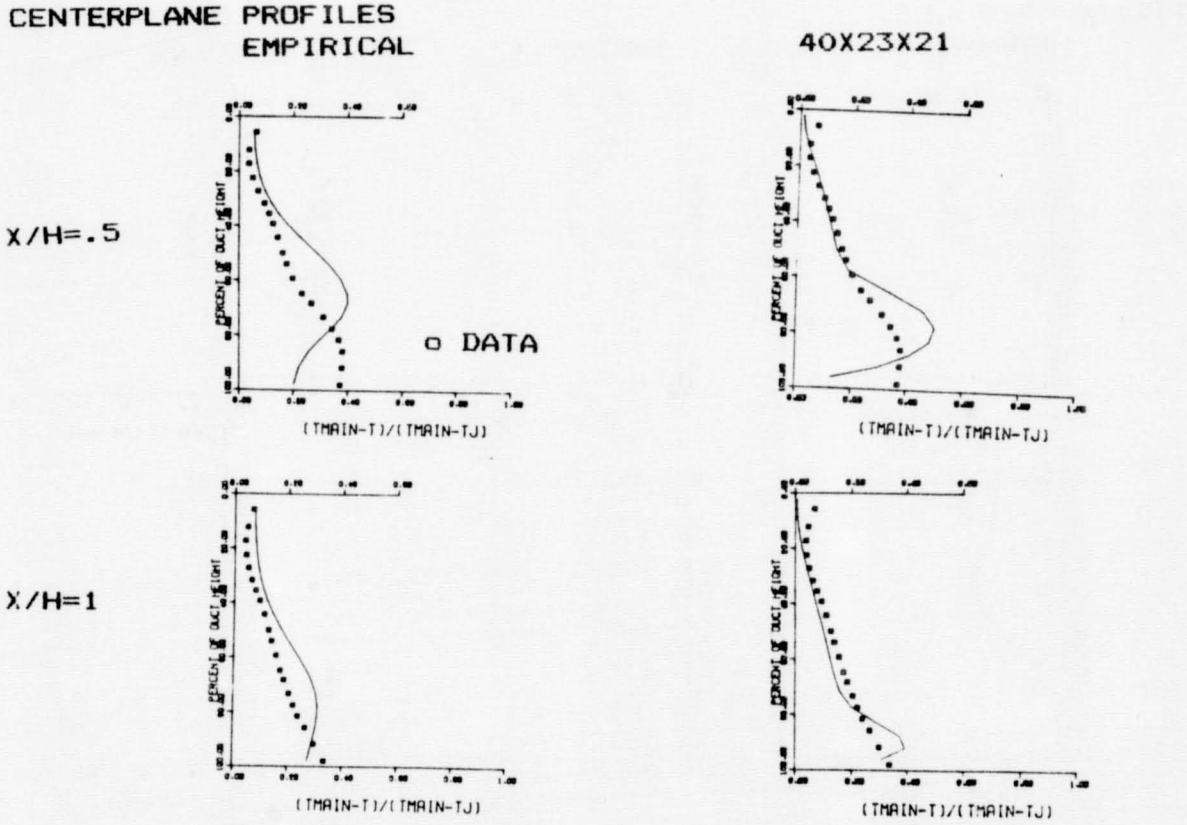

b) $S/H_o=1$, $H_o/D=4$, $A_j/A_m=.049$, $J=26.7$, $w_j/w_T=.192$

Figure 3. Effect of Variations in Orifice Size and Spacing on Temperature Distributions

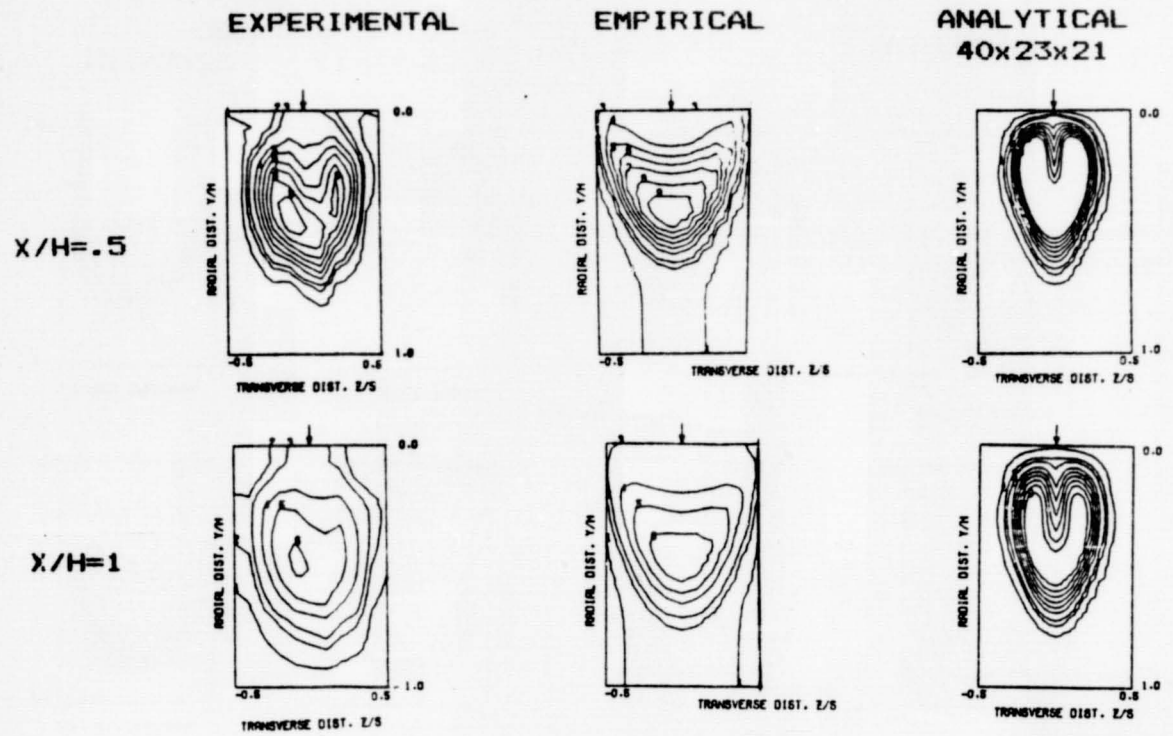

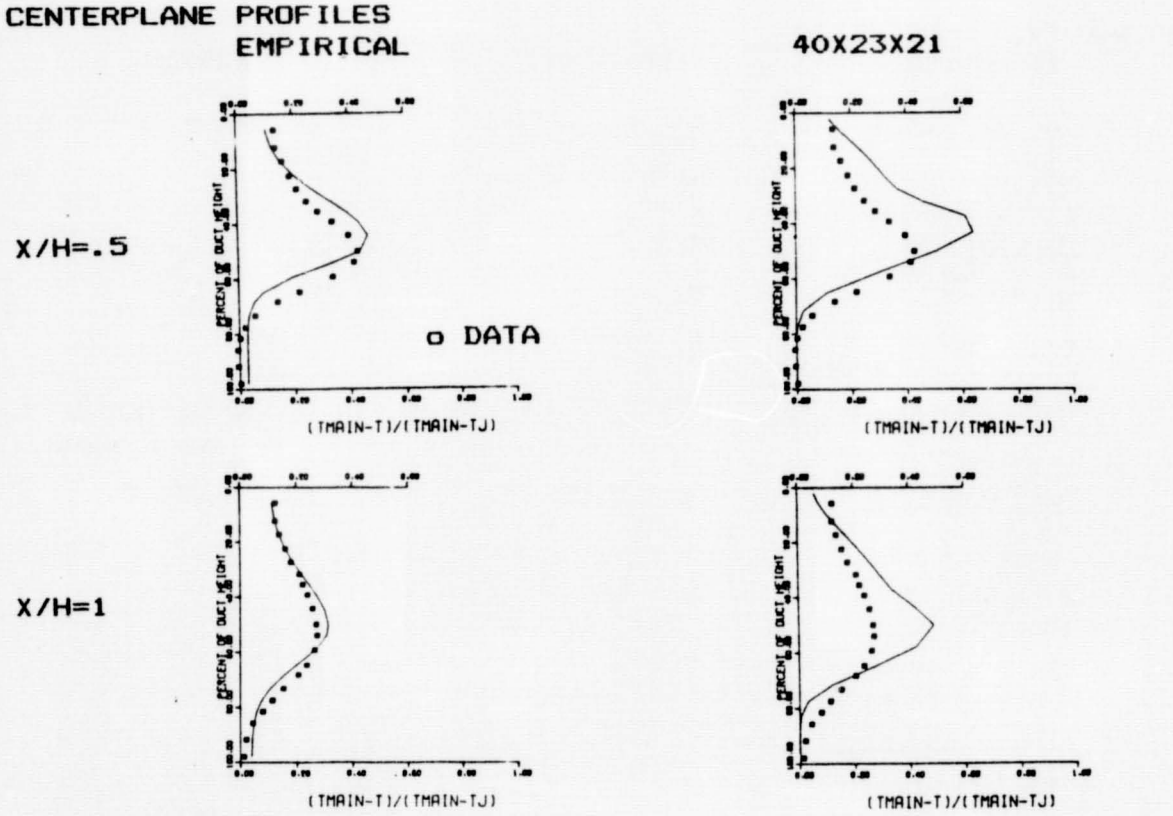

a) $S/H_o=1$, $H_o/D=4$, $A_j/A_m=.049$, $J=5.3$, $w_j/w_T=.107$

Figure 4. Temperature Distributions with Coupled Spacing and Momentum Flux Ratio.

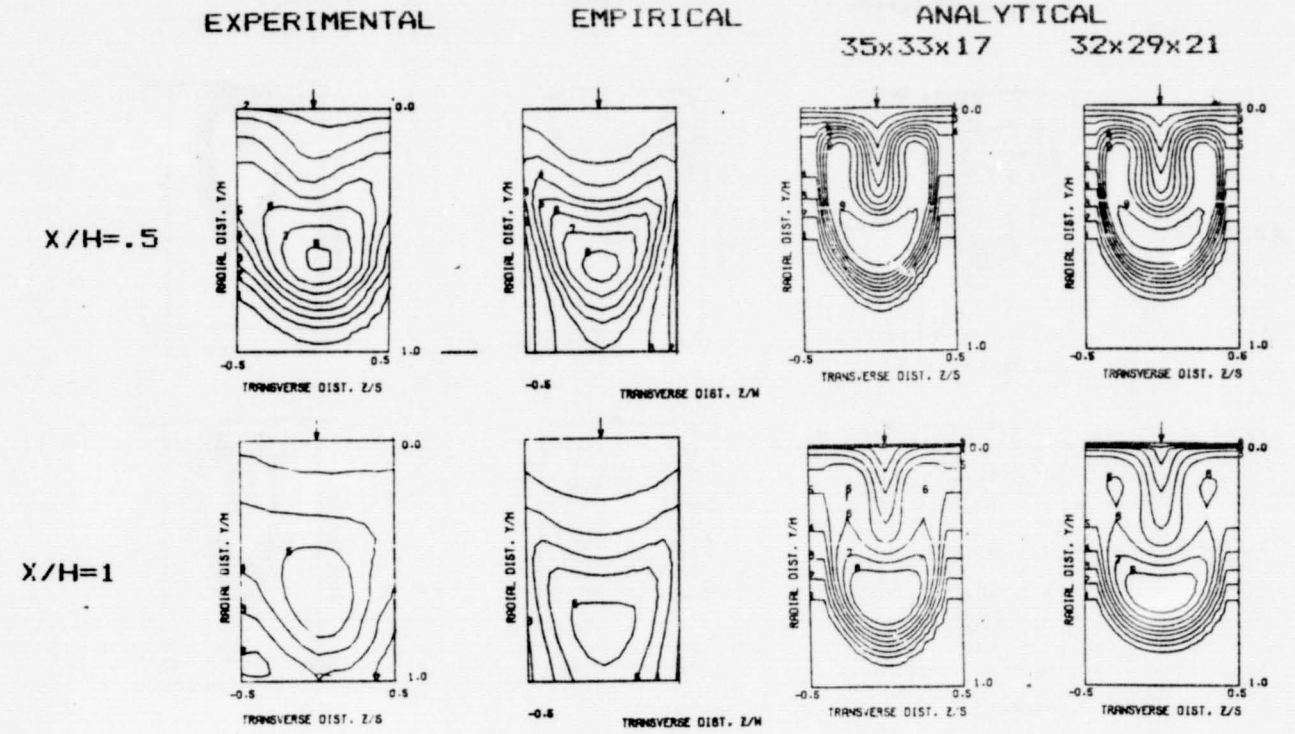

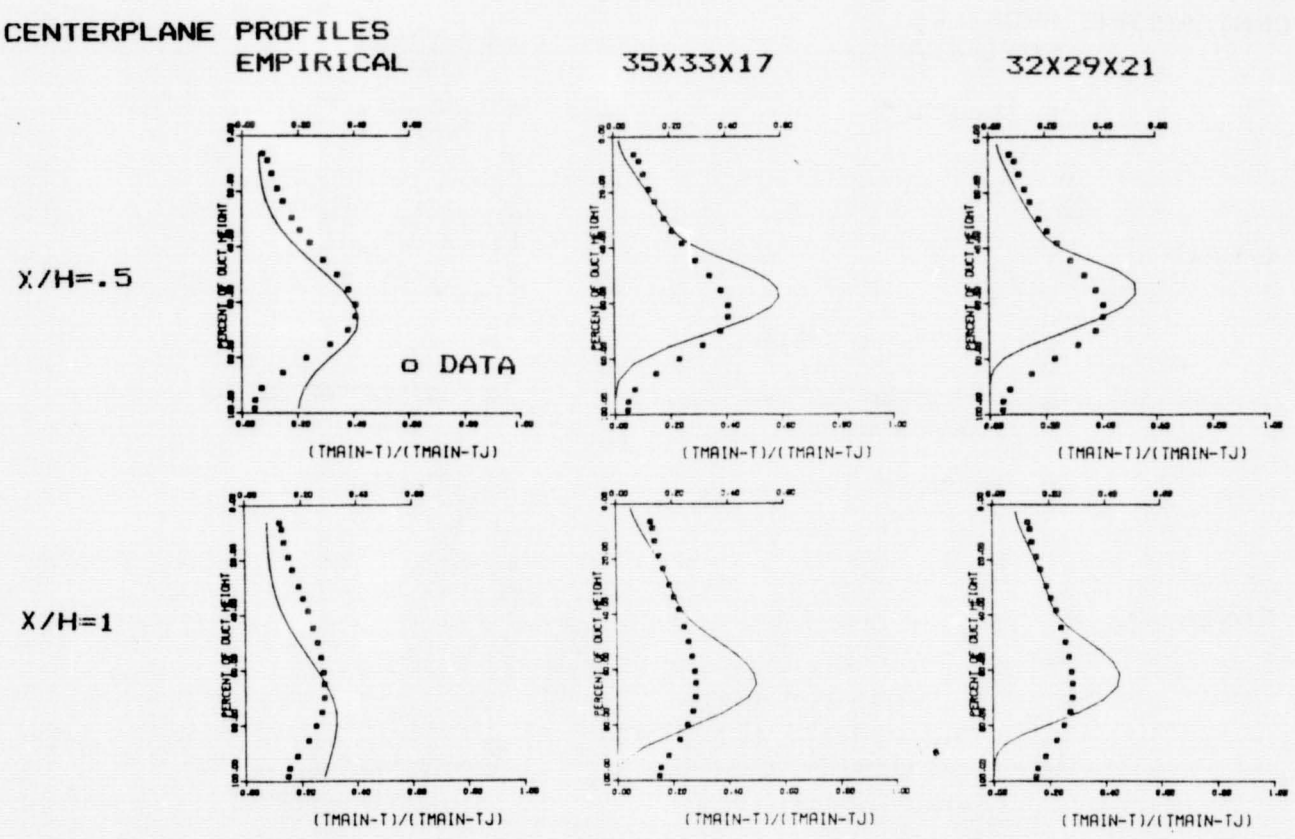

b) S/H_o=.5, H_o/D=5.66 A_j/A_m=.049, J=25.5, w_j/w_T=.205

Figure 4. Temperature Distributions with Coupled Spacing and Momentum Flux Ratio.

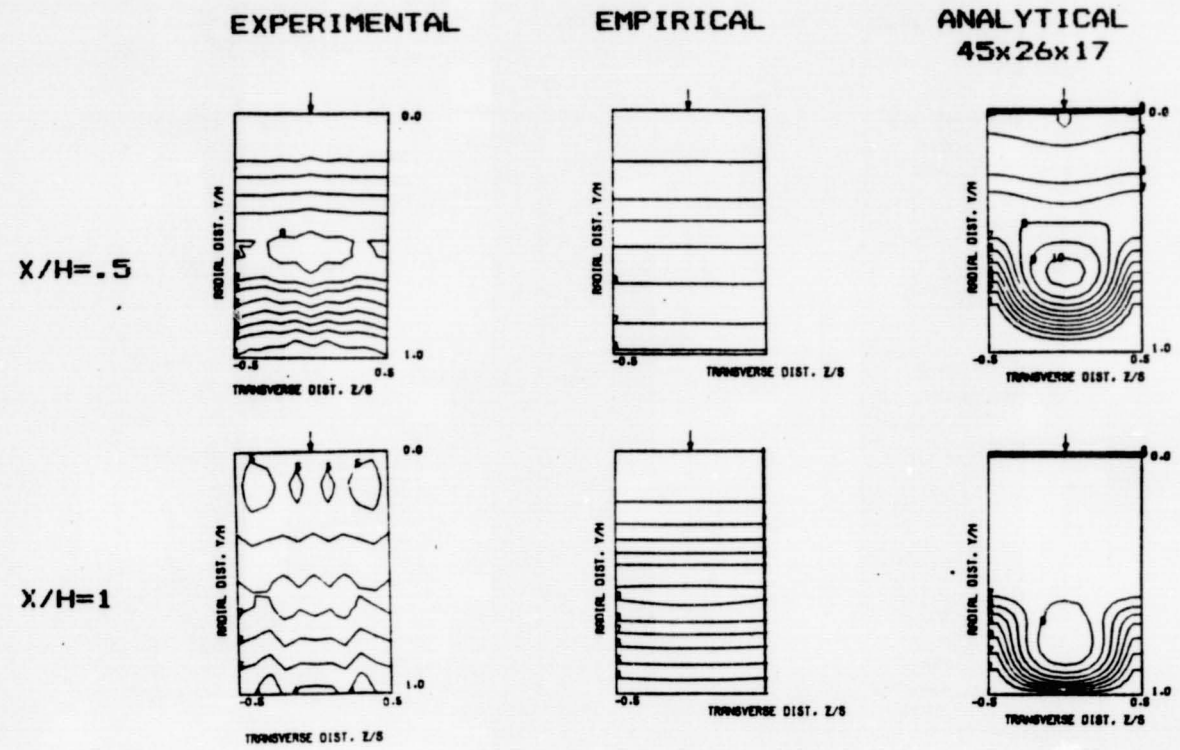

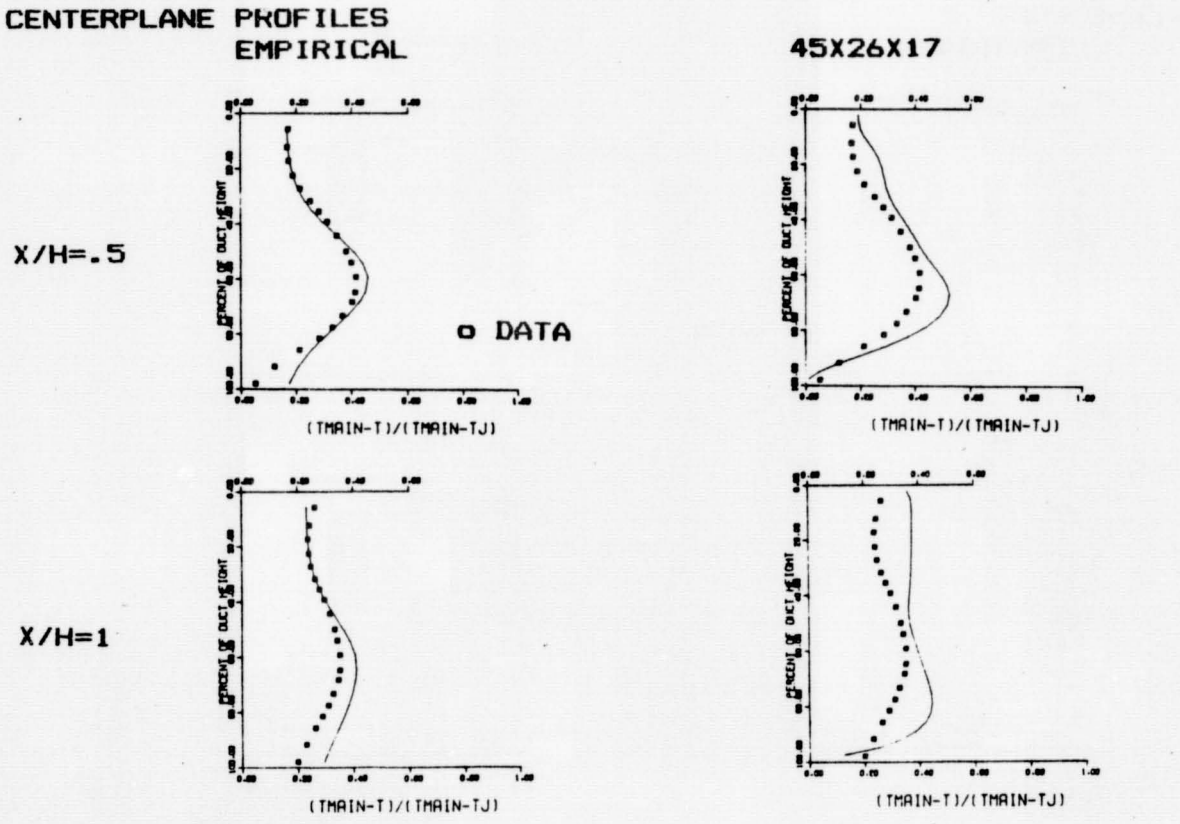

c) S/H_o=.25, H_o/D=8, A_j/A_m=.049, J=92.7, W_j/W_T=.302

Figure 4. Temperature Distributions with Coupled Spacing and Momentum Flux Ratio.

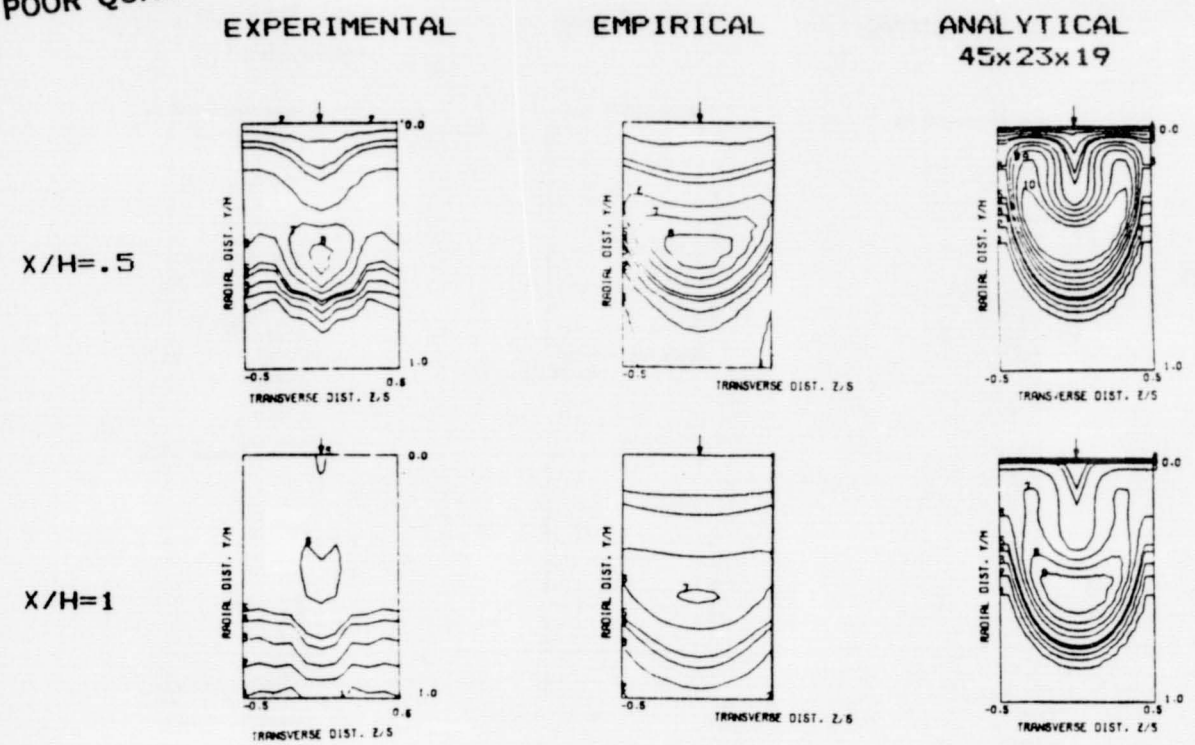

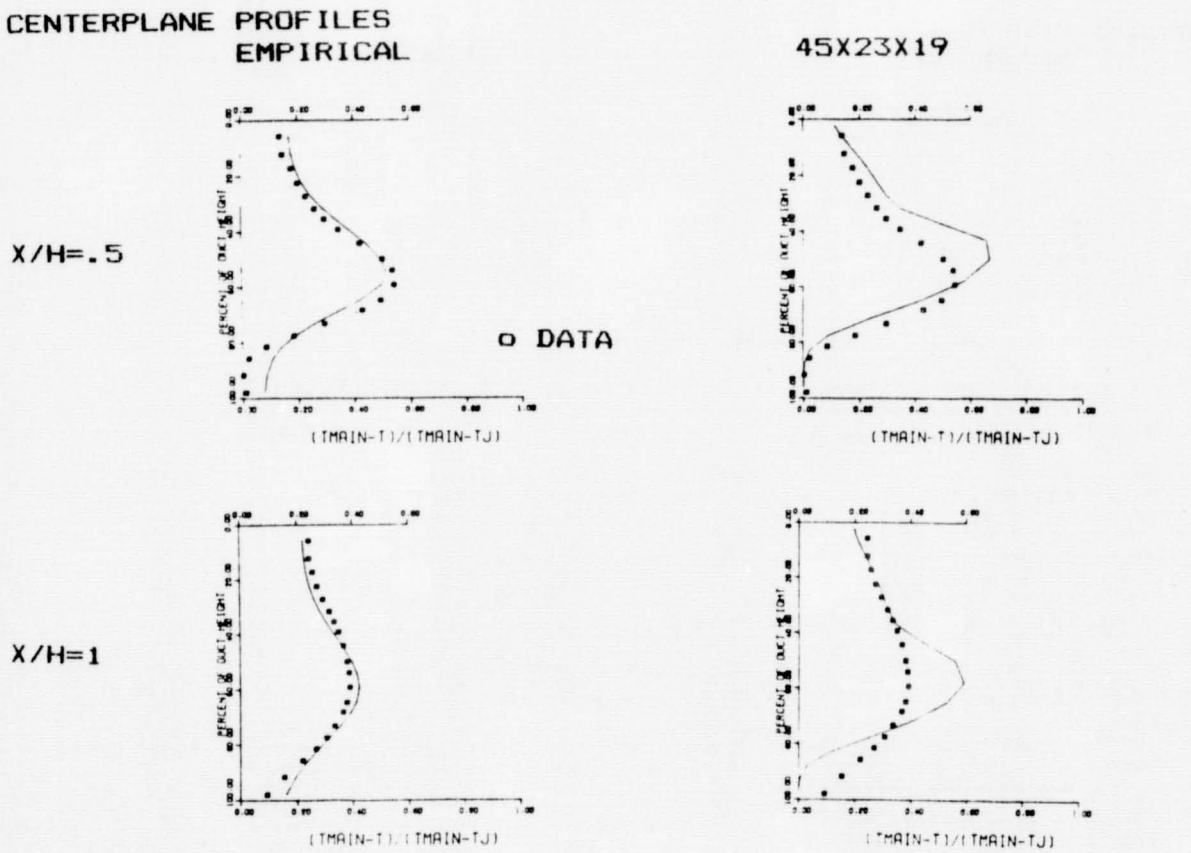

Figure 5. Temperature Distributions for Single-side (top) Injection into an Isothermal Mainstream (S/H_o=.5, H_o=4, A_j/A_m=.098, J=18.6, w_j/w_T=.271)

EXPERIMENTAL

EMPIRICAL

ANALYTICAL
45x23x19

X/H=.5

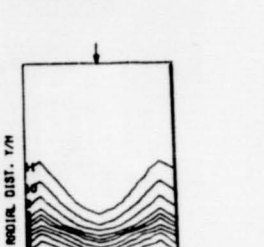

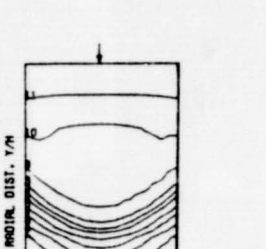

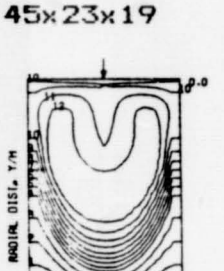

X/H=1

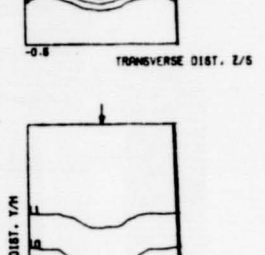

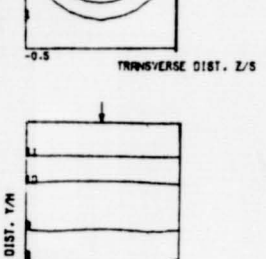

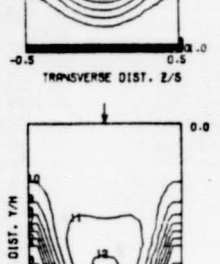

CENTERPLANE PROFILES
EMPIRICAL

45X23X19

X/H=.5

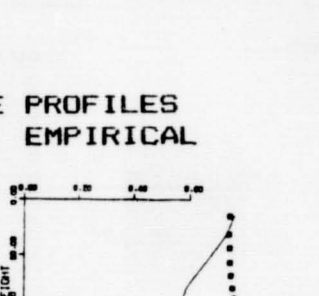

o DATA

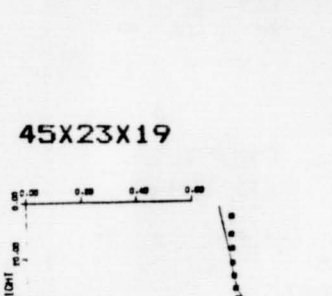

X/H=1

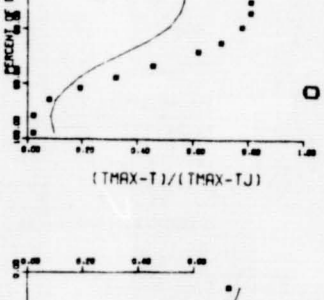

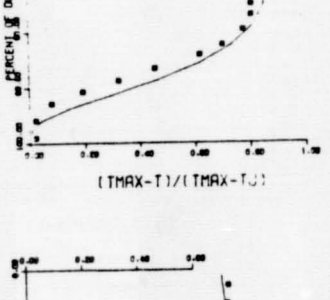

Figure 6. Temperature Distributions for Variable Temperature (Top Cold) Mainstream (S/H_o=.5, H_o/D=4, A_j/A_m=.098, J=31.3)

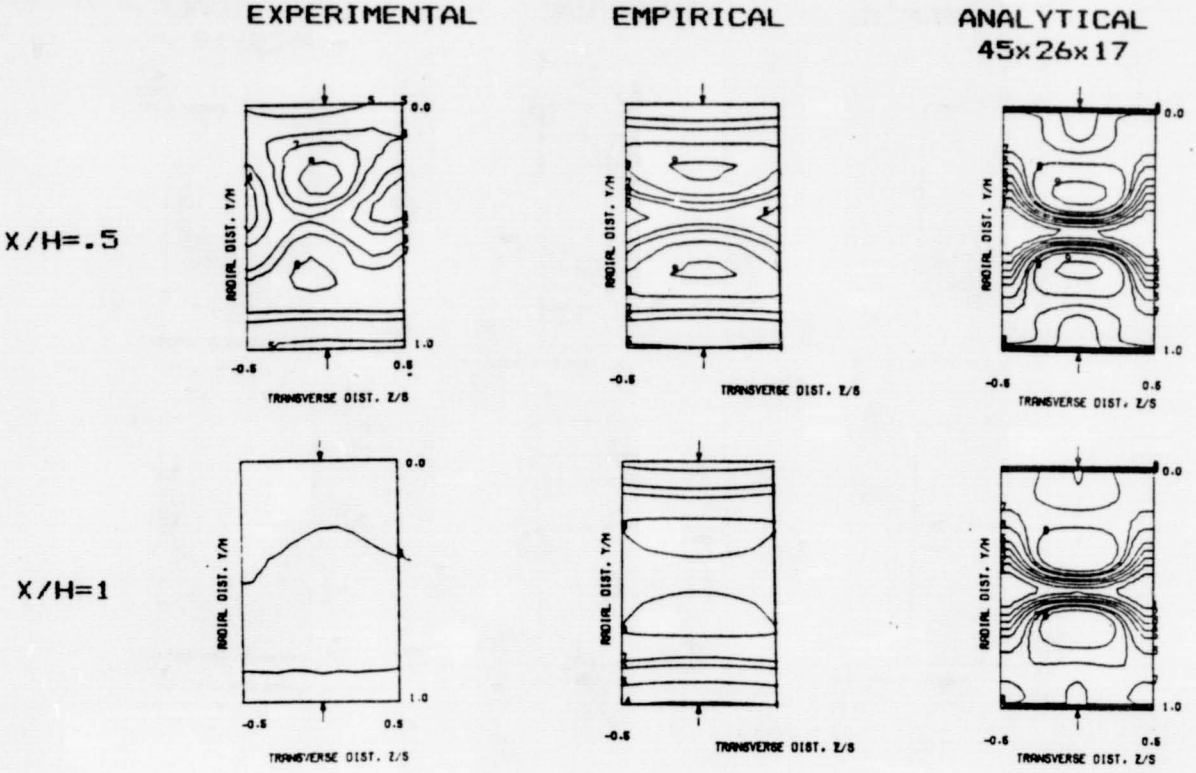

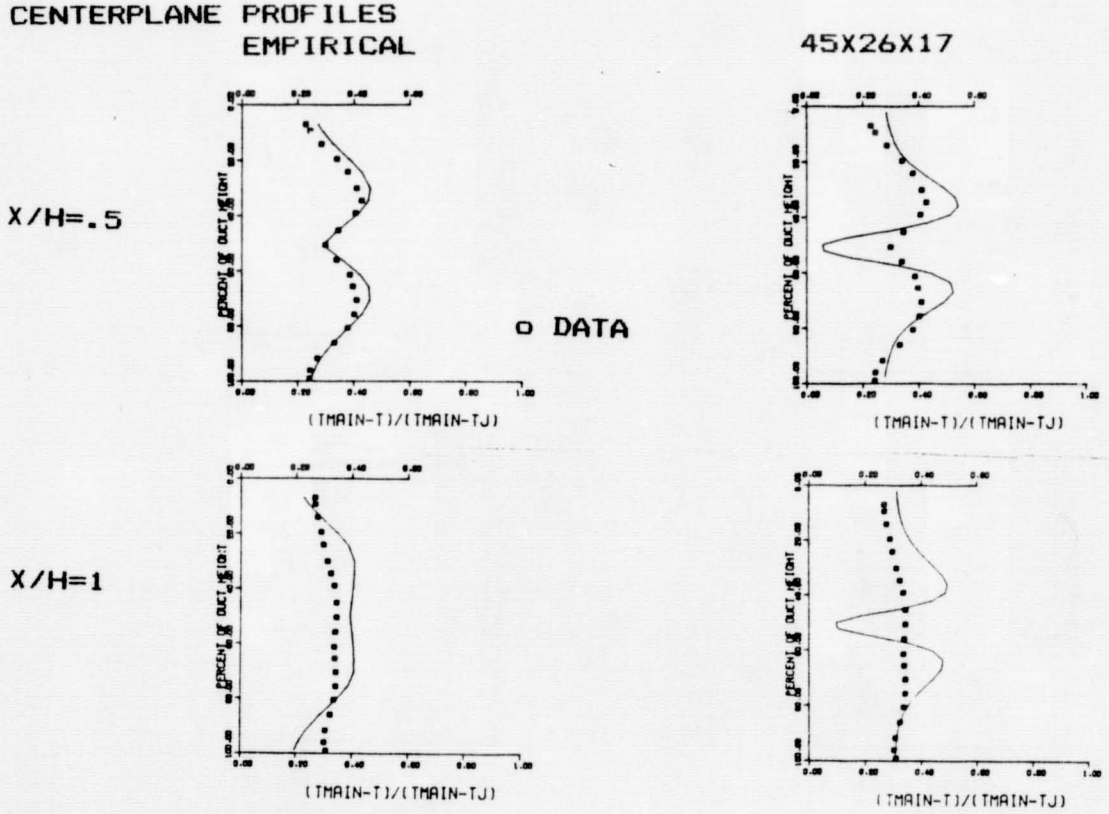

Figure 7. Temperature Distributions for Two-side (opposed) Injection
(S/H_o=.25, H_o/D=8, A_j/A_m=.098, J=25.0, W_j/W_T=.318)

EXPERIMENTAL

EMPIRICAL

ANALYTICAL
22x27x33

X/H=.5

X/H=1

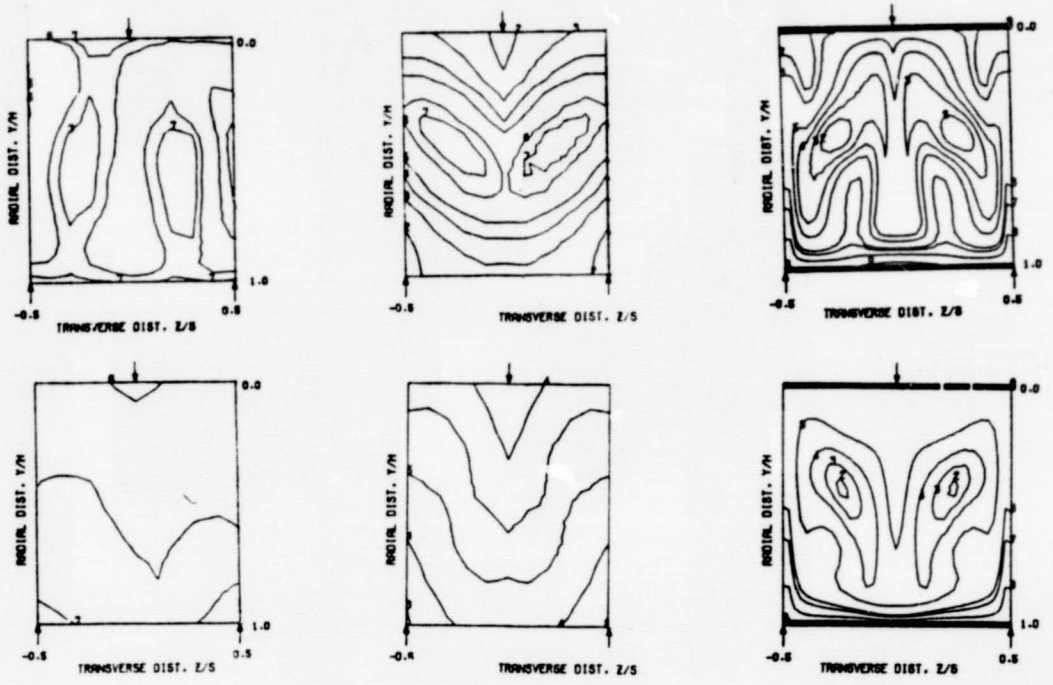

CENTERPLANE PROFILES

EMPIRICAL

22X27X33

X/H=.5

X/H=1

o DATA

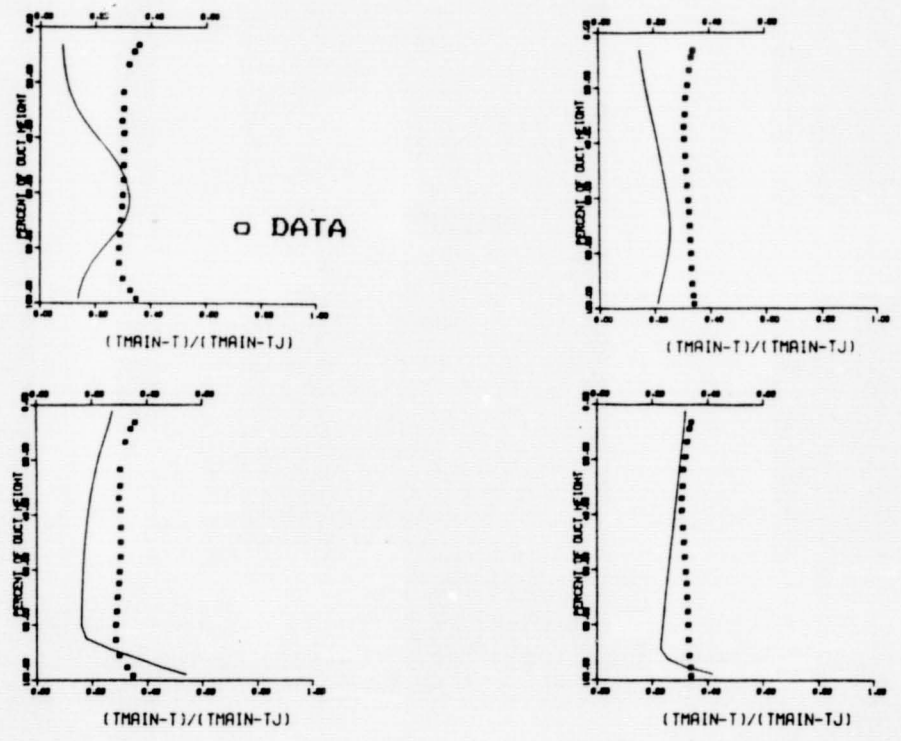

Figure 8. Temperature Distributions for Two-side (staggered) Injection
(S/H_o=1, H_o/D=4, A_j/A_m=.098, J=27.6, w_j/w_T=.327)

D23

TURBULENCE CHARACTERISTICS OF AN AXISYMMETRIC REACTING FLOW

Richard D. Gould, Warren H. Stevenson
and H. Doyle Thompson

Purdue University School of
Mechanical Engineering

Turbulent sudden expansion flows are of significant theoretical and practical importance. Such flows have been the subject of extensive analytical and experimental study for decades, but many issues are still unresolved. Detailed information on reacting sudden expansion flows is very limited, since suitable measurement techniques have only been available in recent years. The present study of reacting flow in an axisymmetric sudden expansion was initiated under NASA support in December 1983. It is an extension of a reacting flow program which has been carried out with Air Force support under contract F33615-81-K-2003. Since the present effort has just begun, results are not yet available. Therefore a brief overview of results from the Air Force program will be presented to indicate the basis for the work to be carried out. Details may be found in reference 1.

Laser velocimeter measurements of mean streamwise velocity and turbulence intensity were made in the highly turbulent flow field following a sudden pipe expansion. Both isothermal and reacting flows were studied. A fused quartz test section was used to permit laser velocimeter measurements throughout the flow field for x/H values from 0.33 to 15. A lean partially premixed propane-air mixture ($\phi = 0.28$) was used to keep the wall temperature low enough so that steady state operation was possible. The inlet flow condition was that of fully developed turbulent pipe flow with a centerline velocity of 22 m/s. The corresponding Reynold's number based on step height H and inlet centerline velocity U_1 was 5.5×10^4.

Three complete sets of LDV measurements were made. Two were in isothermal flow (biased and unbiased) and one was made in the reacting flow (biased). The biased and unbiased cold flow measurements were compared to determine the effects of velocity bias on the measurements. The hot and cold flow measurements were compared to determine the effect of combustion on the structure of the flow field. (Unbiased hot flow data could not be obtained because of particle seeder limitations.)

The scope of the investigation is outlined in figure 1. The experimental apparatus is shown in figures 2-4 and test parameters are presented in figure 5. Examples of some of the data obtained are given in figures 6-15 and conclusions which can be drawn are given in figure 16. A summary of the further research planned under the present NASA sponsored program is presented in figure 17.

REFERENCES

1. Stevenson, W. H., Thompson, H. D., and Gould, R. D.: Laser Velocimeter Measurements and Analysis in Turbulent Flows with Combustion - Part I, AFWAL-TR-82-2076 Part II, 1983.

2. Stevenson, W. H., Thompson, H. D., and Luchik, T. S.: Laser Velocimeter Measurements and Analysis in Turbulent Flows with Combustion - Part I, AFWAL-TR-82-2076 Part I, 1982.

3. Moon, L. F. and Rudinger, G.: Velocity Distribution in an Abruptly Expanding Circular Duct, ASME Journal of Fluids Engineering, vol. 99, March 1977, pp. 226-230.

4. Freeman, A. R.: Laser Anemometer Measurements in the Recirculating Region Downstream of a Sudden Pipe Expansion, Proceedings of the LDA Symposium, Copenhagen, 1975, pp. 704-709.

SCOPE OF THE STUDY*

1. Measured streamwise mean velocities and turbulence intensities.

2. 3 different measurements were made at each measurement location to form 3 complete data sets. They are identified as:

   + biased
   + unbiased } cold flow
   + biased — hot flow

3. Reattachment point was located.

4. Integrated mass flux at each measurement plane was calculated and was used as a continuity check.

5. Measured temperature at a plane located 17 step heights downstream of the sudden expansion.

6. Comparison of cold flow data with 2/E/FIX.

*AF Contract F33615-81-K-2003

Figure 1

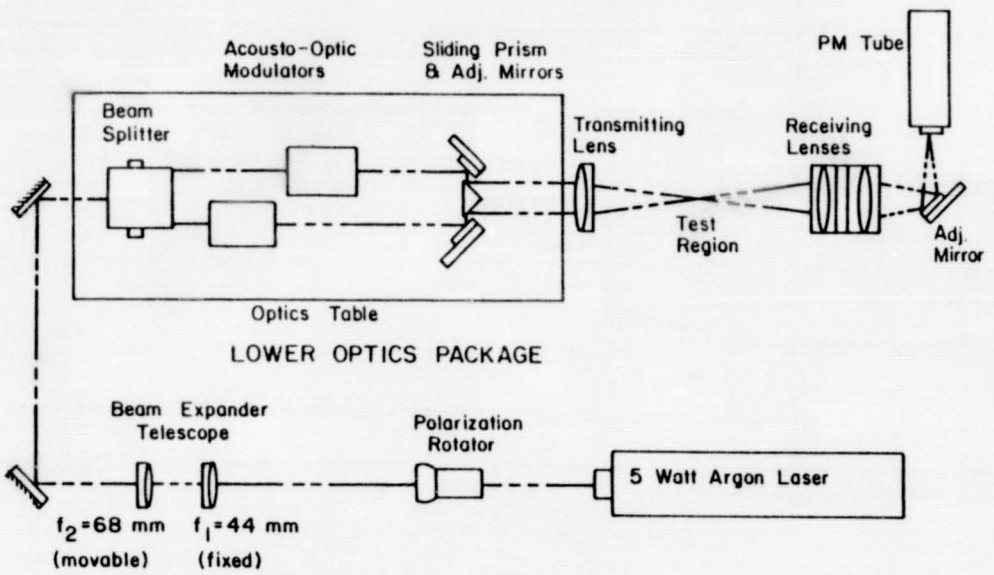

Figure 2. LDV Optics Package

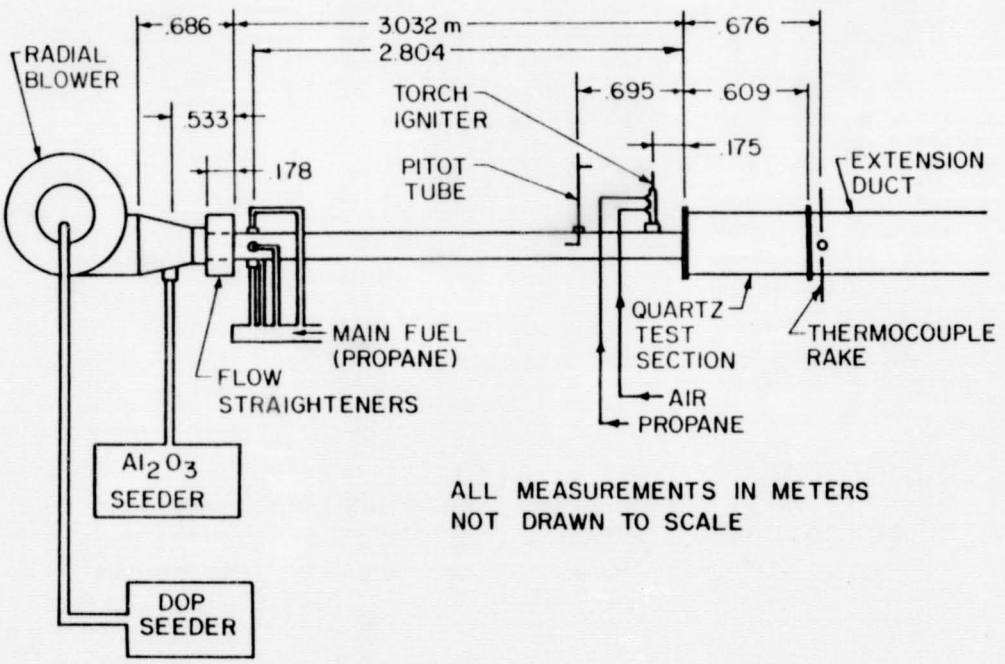

Figure 3. Flow System

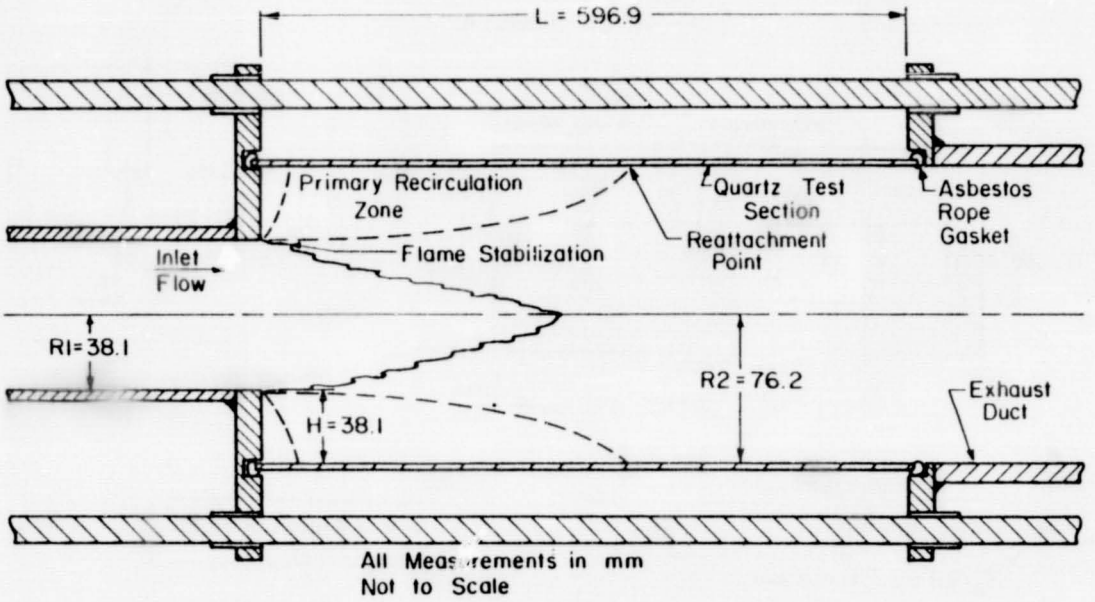

Figure 4. Geometry of Axisymmetric Test Section

TEST PARAMETERS

FLOW PARAMETERS

U_∞ = 22.07 m/s (PITOT TUBE MEASUREMENT)

$Re_D = 1.1 \times 10^5$

$Re_H = 5.5 \times 10^4$

OVERALL F/A = 0.0183 (GASEOUS PROPANE)

OVERALL EQUIVALENCE RATIO, $\phi = 0.28$

GEOMETRY

D_{IN} = 76.2 mm (3 in)

D_{OUT} = 152.4 mm (6 in)

AREA RATIO, $A_R = 4$

STEP HEIGHT, H = 38.1 mm (1.5 in)

DATA COLLECTION

	UNBIASED COLD	BIASED COLD	BIASED HOT
PARTICLE ARRIVAL RATE:	> 20,000	500-1500/sec	500-1500/sec
SAMPLE RATE:	50/sec	"FREE" (4700/sec)	"FREE" (4700/sec)
SEED:	DOP	Al_2O_3	Al_2O_3

Figure 5

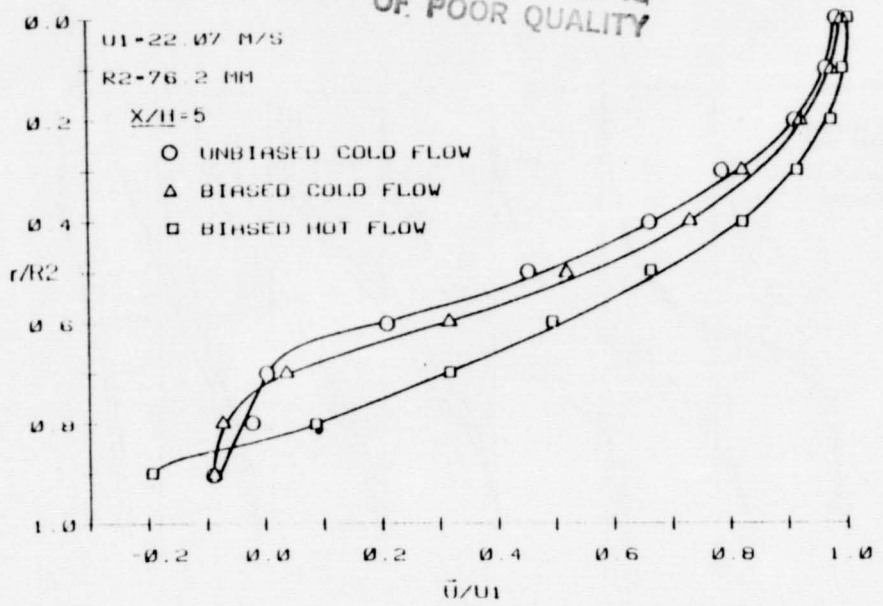

Figure 6. Measured Mean Streamwise Velocity Profiles at x/H = 5

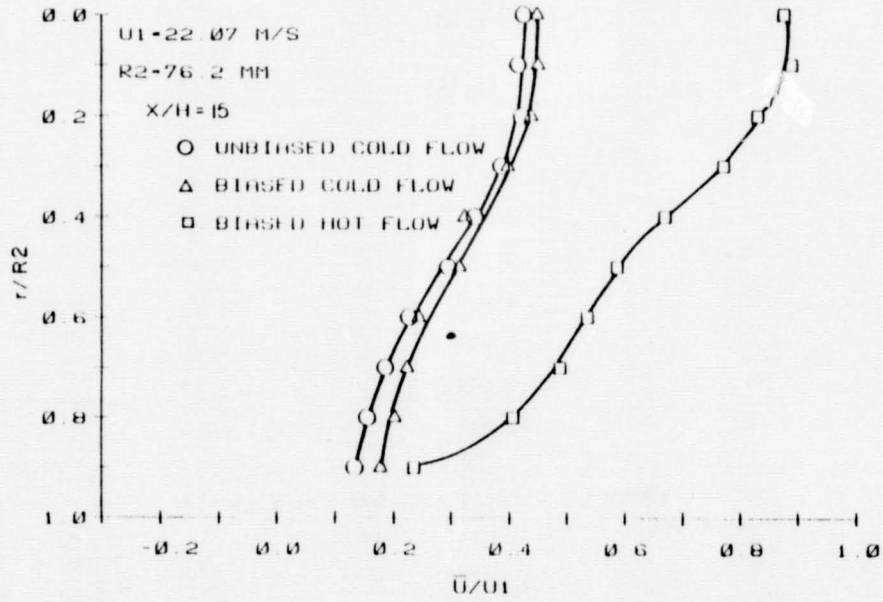

Figure 7. Measured Mean Streamwise Velocity Profiles at x/H = 15

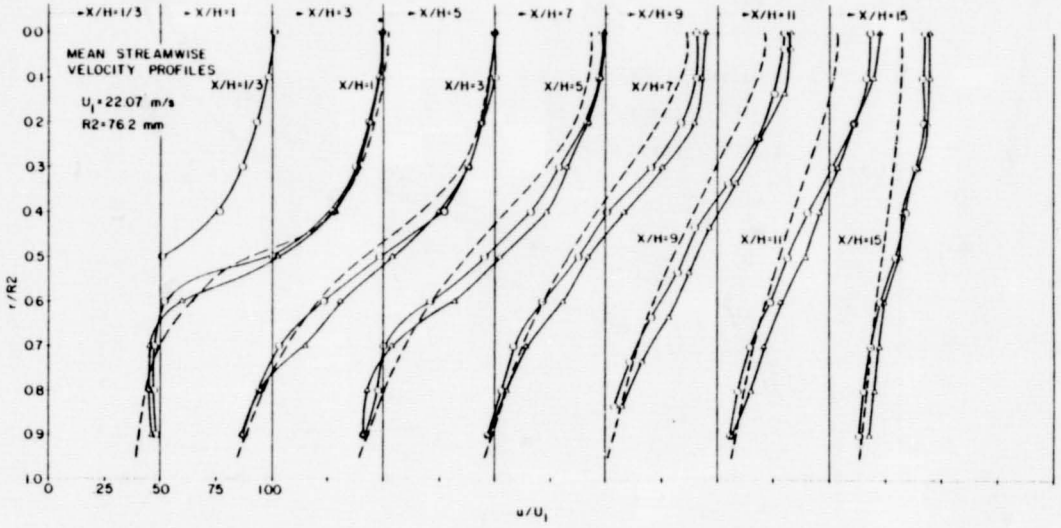

Figure 8. Measured Mean Streamwise Velocity Profiles in Cold Flow

(o - unbiased cold flow, Δ - biased cold flow, --- 2/E/FIX prediction)

NORMALIZED* INTEGRATED MASS FLUX
(COLD FLOW)

x/H	UNBIASED	BIASED
1/3	1.00	---
1	1.044	1.065
3	1.056	1.200
5	1.002	1.129
7	1.012	1.206
9	1.032	1.238
11	1.019	1.212
15	1.031	1.166

*VALUES NORMALIZE WITH ASSUMED 1/7 POWER LAW
INLET VELOCITY PROFILE

Figure 9

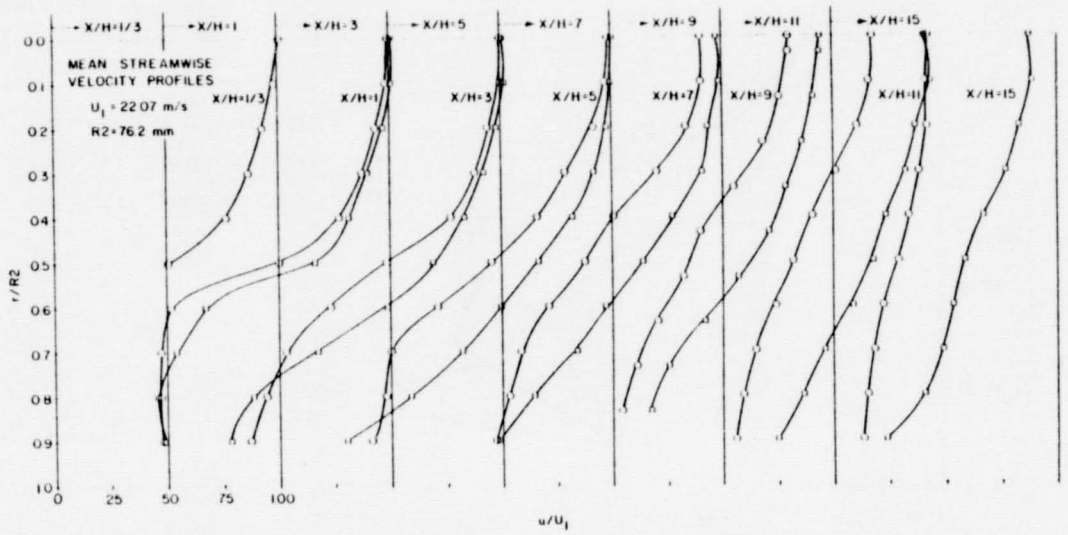

Figure 10. Measured Mean Streamwise Velocity Profiles in Cold Flow and in Reacting Flow

(o - unbiased cold flow, □- biased hot flow)

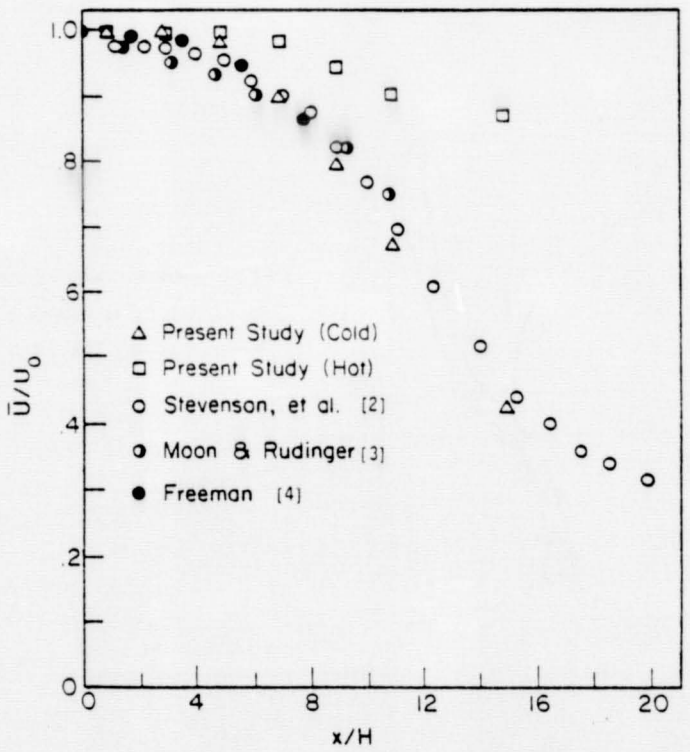

Figure 11. Measured Mean Centerline Velocity Decay

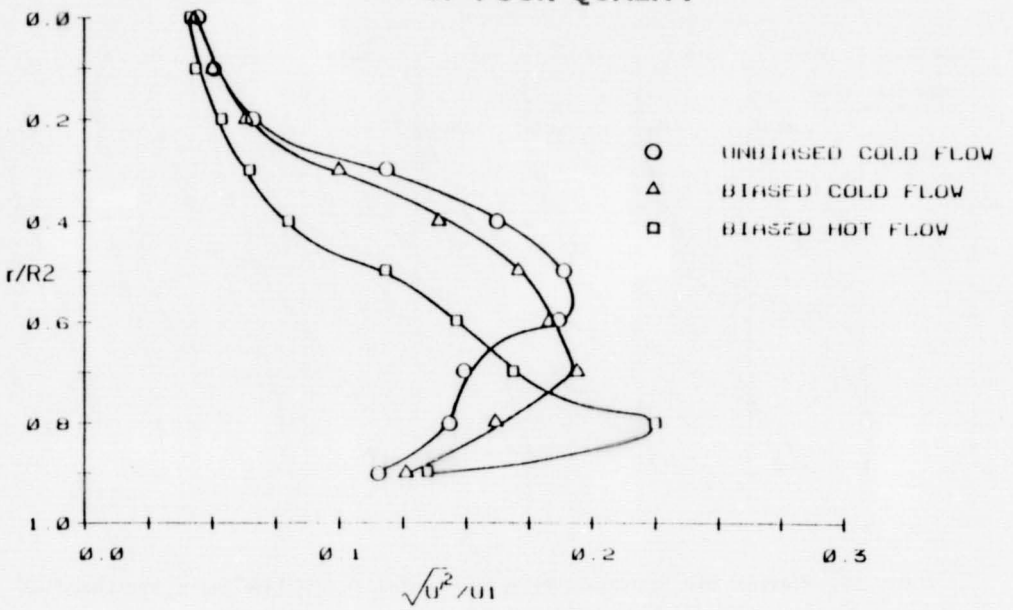

Figure 12. Measured Normalized Streamwise Turbulence Intensity Profiles at x/H = 5

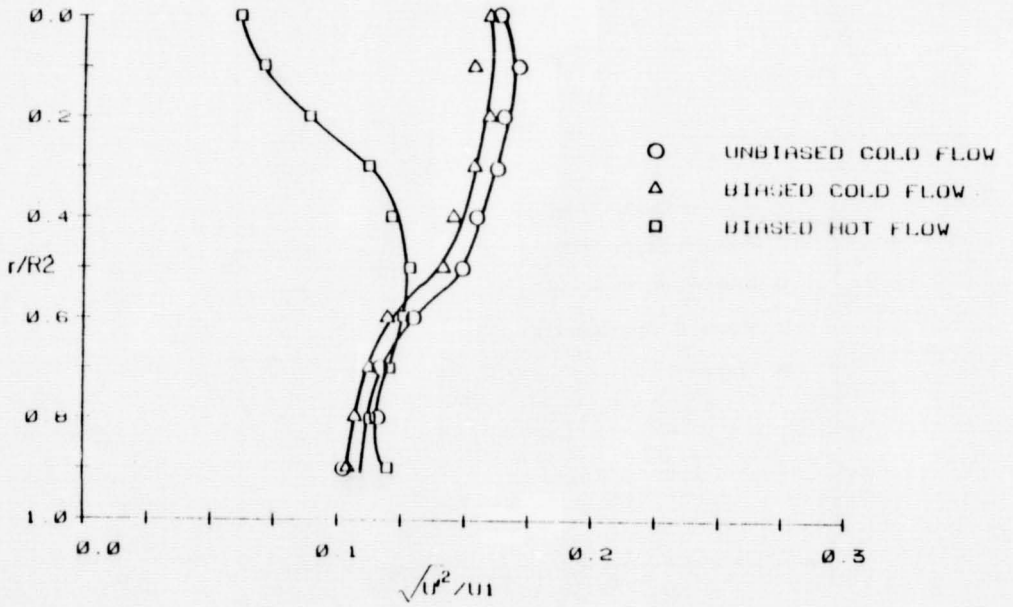

Figure 13. Measured Normalized Streamwise Turbulence Intensity Profiles at x/H = 15

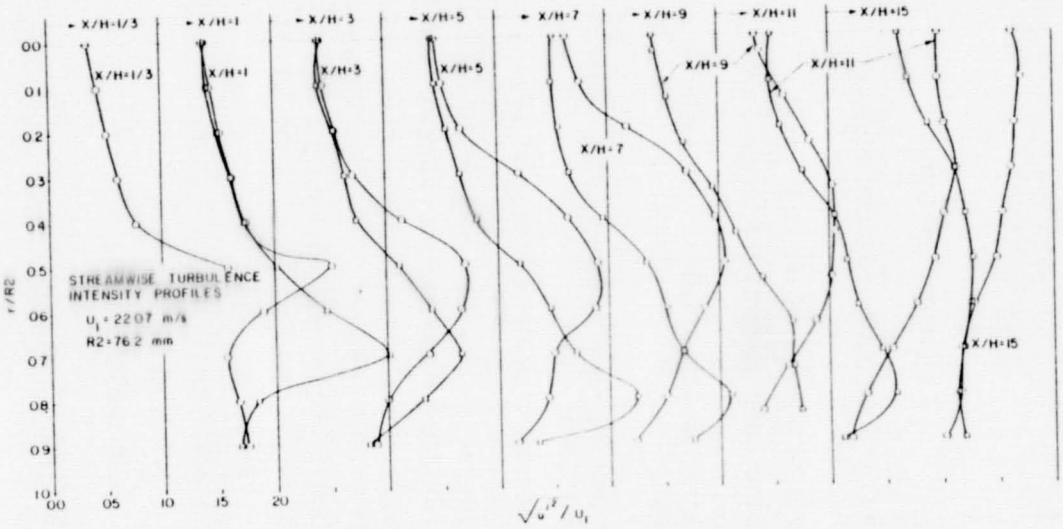

Figure 14. Measured Normalized Streamwise Turbulence Intensity Profiles

(o - unbiased cold flow, □- biased hot flow)

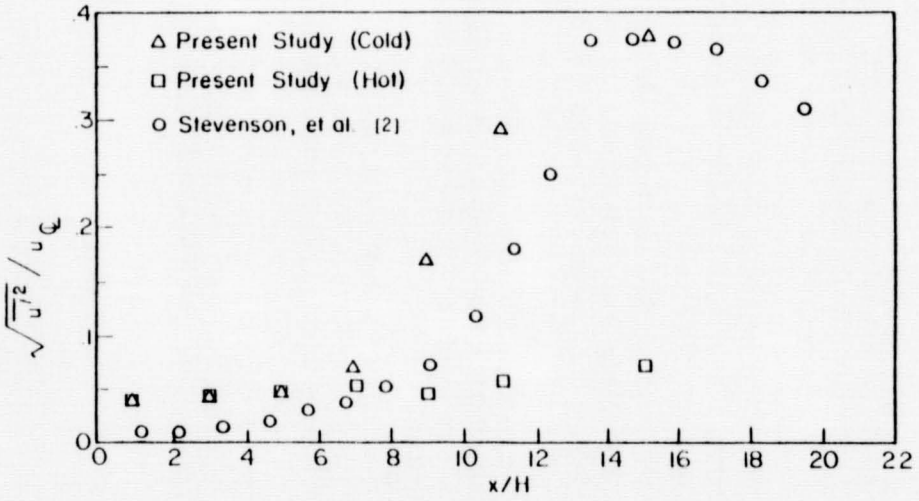

Figure 15. Measured Local Centerline Turbulence Intensity Profiles

CONCLUSIONS

1. Velocity measurements were made in a sudden expansion turbulent reacting flow at atmospheric pressure. Few difficulties were encountered in making these measurements.

2. The reacting flow exhibited several structural differences relative to the cold flow:

   a) The recirculation zone was smaller and more intense in the reacting flow. Reattachment occurred at X/H = 7.4 for the hot flow as compared to 8.6 for the cold flow.

   b) The position of peak turbulence intensity was different in the reacting flow, although the maximum normalized turbulence intensity was approximately the same in both cases.

   c) Local turbulence intensity was reduced by up to 60 percent in the reacting flow due to the higher local velocities resulting from the heat release.

3. Velocity bias had the expected effect on the mean velocity data. A significant shift in the normalized turbulence distribution in the shear layer was found to exist due to bias.

Figure 16

FUTURE WORK*

1. Develop 2 color - 2 component LDV system

   - Measure mean and fluctuating velocity simultaneously for two components
   - Measure Reynolds stress correlation
   - Obtain power spectrum and length scales.

2. Utilize correction lens system to make radial velocity measurements

   - Allows $\overline{uv}_R$ Reynolds stress correlation measurement
   - Important if studying effects of swirl

3. Utilize high frequency response thermocouple to make dynamic temperature measurements in reacting flow

   - Balance terms in the turbulent kinetic energy conservation equation in both hot and cold flow
   - Identify regions where the various turbulence mechanisms dominate in the hot and cold flow

     Production

     Advection

     Diffusion

     Dissipation

*NASA Grant NAG 3-502

Figure 17

D24

DIRECT NUMERICAL SIMULATION OF REACTING FLOWS

James J. Riley and Ralph W. Metcalfe
Flow Research Company

The objectives of this work are (i) to to extend the technique of direct numerical simulations to turbulent, chemically reacting flows, (ii) to test the validity of the method by comparing computational results with laboratory data, and (iii) to use the simulations to gain a better understanding of the effects of turbulence on chemical reactions. In particular, we address the effects of both the large-scale structure and the smaller-scale turbulence on the overall reaction rates, examine the relationship between infinite reaction rate and finite reaction rate chemistry, and compare some of the results of our calculations with existing theories and laboratory data. The direct numerical simulation method involves the numerical solution of the detailed evolution of the complex turbulent velocity and concentration fields. Using very efficient numerical methods (e.g., pseudospectral methods), the fully nonlinear (possibly low-pass filtered) equations of motion are solved and no closure assumptions or turbulence models are used. Statistical data are obtained by performing spatial, temporal, and/or ensemble averages over the computed flow fields.

The scope of work to do this involved the following. First, existing computer codes were modified to treat the present problem. Next, extensive numerical testing of the computer codes was performed. Finally, in order to examine the effects of the mixing layer turbulence, both the large-scale structure and the smaller-scale turbulence, on the overall reaction rates, a sequence of three problems was computed: (i) reactions on a unidirectional (one-dimensional) mixing layer, (ii) reactions on a mixing layer experiencing large-scale, two-dimensional vortex rollup, and (iii) reactions on a three-dimensional turbulent mixing layer. The simulations of the two-dimensional mixing layer with vortex rollup are intended to model the large-scale structure in the mixing layer, whereas the three-dimensional simulations contain both the large-scale structure and the smaller-scale turbulence.

The numerical testing involved the comparison of computed results with exact solutions for a number of different cases. Both rigid body rotation and vortex rollup flow fields were used. The work greatly extended the results of Orszag (ref. 1) for the advection of a passive scalar on a rigidly rotating flow field (the color problem) to include also diffusion, chemical reaction, and more complex flows. We have found that high accuracy of the spectral methods observed in the advection case is also obtained when these further complications are present. Our results indicate that spectral numerical methods may prove to be useful in the future both for solving the model equations for combustor processes as well as for future studies of chemically reacting turbulent flows employing direct numerical simulations.

The approach of direct numerical simulations allowed extensive examination and interpretation of the reaction process. From the one-dimensional simulations, we found that we could easily compute finite reaction rates near the fast reaction limit, that the results were fairly insensitive to the initial conditions (for the class of initial conditions computed), and that the results were in reasonable agreement with theoretical predictions.

For the two-dimensional simulations, we found that in all of the cases computed, the vorticity field and the product field approximately coincided. From the computation of volume averages, we observed the enhancement of the overall reaction rate due to the vortex rollup. It also appeared that the merging of vortex cores was a more significant mechanism in increasing the overall reaction rate than the straining of the reaction interface. Significant species segregation was apparent, so that, for example, the product of the average concentrations was approximately equal to and opposite the correlation between the fluctuating concentrations. Some of the higher order correlations were also examined.

In the three-dimensional simulations, the contour plots indicated that the vortex rollup takes longer to develop, and the vortices and braids are not as distinct as in the two-dimensional case. Also, the vortices that develop are not strongly correlated laterally. Both the contour plots and the statistical results indicated that the spatial segregation was also not as strong as in the two-dimensional case, probably due to the weaker vortex rollup as well as the effects of smaller-scale, three-dimensional turbulence.

Comparisons were made between the simulation results and results using similarity theory. Approximately linear growth rates of various computed length scales, including the mean velocity half-width, the mean vorticity thickness, and the mean product thickness, were obtained and were in agreement with the theory. Similarity scaling was found to collapse quite well the results for the average reactant concentrations, the rms fluctuating reactant concentrations, the concentration correlations, the average product concentrations, and the rms fluctuating product concentrations.

Some limited comparisons were made with laboratory data. Computed profiles that were qualitatively similar to corresponding laboratory profiles were obtained for the average reactant concentrations, the rms fluctuating reactant concentrations, the average product concentrations, the rms fluctuating product concentrations, and the concentration correlations.

We have made some comparisons with existing theories. Donaldson and Hilst have suggested, in addition to using the equations for the average concentrations, including the equations for the concentration fluctuations and correlation (ref. 2). These equations can be closed by neglecting certain triple moments when compared to certain lower order terms. However, our results indicate that the triple moment terms are as important as other terms in the equations, so that an assumption of this type will probably lead to poor predictions. Mason and Spaulding have proposed a model for the mean reaction term, suggesting that it will be proportional to the average concentration of the lean species divided by a turbulent time scale (ref. 3). We have found that such an assumption will only be moderately successful if applied to our case. Finally, Toor has suggested estimating the concentration correlation of the reacting species in terms of that for the nonreacting case, which is much easier to model (ref. 4). Although this was proposed mainly for statistically homogeneous flows, we find that it is a reasonable approximation for our reacting flow simulations.

REFERENCES

1. Orszag, S. A.: Numerical Simulation of Incompressible Flows within Simple Boundaries: Accuracy. J. Fluid Mech., vol. 49, 1971, pp. 75-112.

2. Donaldson, C. duP.; and Hilst, G. R.: Effect of Inhomogeneous Mixing on Atmospheric Photochemical Reactions. Env. Sci. Tech., vol. 6, 1972, pp. 812-816.

3. Mason, H. B.; and Spaulding, D. B.: Prediction of Reaction RAtes in Turbulent Premixed Boundary Layer Flows. Proc. First Symp. (European) on Comb., 1973, pp. 601-606, Academic Press.

4. Toor, H. L.: Turbulent Mixing of Two Species With and Without Chemical Reactions. Ind. Eng. Chem. Fundam., vol. 8, 1969, pp. 655-659.

OBJECTIVES

- Begin the Extension of Direct Numerical Simulations to Combustor Flows
  - Develop computational methodology
- Use Direct Numerical Simulations in Order to
  - Better understand the effects of turbulence on chemical reactions
  - Suggest model improvements
- Test Validity of the Method by Comparing Computational Results with Laboratory Data and Theoretical Models

PROBLEM CONSIDERED

- Temporally Growing, Three-Dimensional Mixing Layer
- Binary, Single-Step, Irreversible Chemical Reaction
  ($A + nB \rightarrow$ products) with negligible heat release
- Very Small Mach Number
- Initial Conditions – NonPremixed Species

PROBLEM CONSIDERED

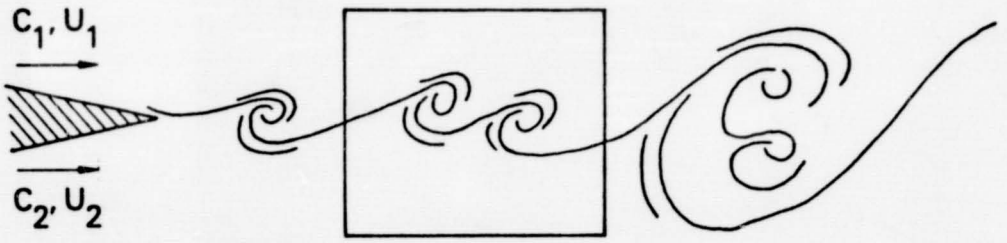

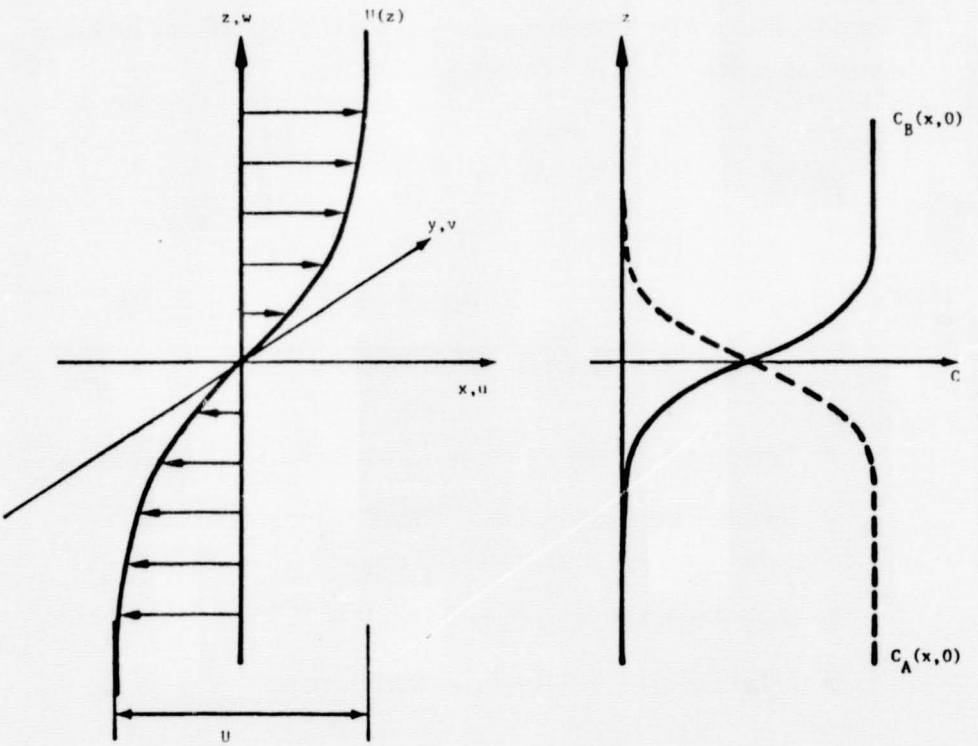

Problem Geometry - Initial Conditions

SCOPE OF WORK

- Modify Existing Computer Codes to Treat the Present Problem
- Perform Numerical Testing of the Computer Codes
- Compute the Following Sequence of Problems
  - Unidirectional (one-dimensional) flow
  - Large-scale, two-dimensional vortex rollup
  - Three-dimensional turbulent mixing layer

EQUATIONS OF MOTION

- Conservation of Momentum

$$\frac{\partial}{\partial t} u_i + u_j \frac{\partial}{\partial x_j} u_i = -\frac{1}{\rho} \frac{\partial}{\partial x_i} p + \nu \frac{\partial^2}{\partial x_j^2} u_i$$

- Conservation of Mass

$$\frac{\partial}{\partial x_i} u_i = 0$$

- Conservation of Species A and B

$$\frac{\partial}{\partial t} C_1 + u_j \frac{\partial}{\partial x_j} C_1 = -R_1 C_1 C_2 + D_1 \frac{\partial^2}{\partial x_j^2} C_1$$

$$\frac{\partial}{\partial t} C_2 + u_j \frac{\partial}{\partial x_j} C_2 = -R_2 C_1 C_2 + D_2 \frac{\partial^2}{\partial x_j^2} C_2$$

- Initial Boundary Conditions

DIRECT NUMERICAL SIMULATIONS

- Compute the Solution of the Navier-Stokes Equations Numerically
- Initial Conditions (or Upstream Conditions)

  Random, turbulent-like – so that the flow field starts out as turbulent-like – or

  Small amplitude perturbations -- compute the flow through transition to turbulence
- Compute the Time Development of the Detailed Structure of the Flow Field
- No Reynolds Averaging
- Statistical Results are Obtained by Performing Spatial, Temporal, or Ensemble Averages over the Computed Flow Field
- Analogous to Laboratory Experiments

NUMERICAL METHODS

- Pseudo-Spectral Methods
  - Expand the dependent variables in fast-converging series

    E. G.,

$$u(x) = \sum_{|k|<K} \hat{u}(k) e^{ikx}$$

- Resulting Equations

$$\frac{\partial}{\partial t}\hat{C}_1(\underset{\sim}{k},t) + i\underbrace{\sum_{\underset{\sim}{k}'} \hat{u}_j(\underset{\sim}{k}-\underset{\sim}{k}')k'_j \hat{C}_1(\underset{\sim}{k}')}_{\text{Convection}} = \underbrace{-R_1 \sum_{\underset{\sim}{k}'} \hat{C}_1(\underset{\sim}{k}-\underset{\sim}{k}')\hat{C}_2(\underset{\sim}{k}')}_{\text{Reaction}} \underbrace{-D_1 k^2 \hat{C}_1(\underset{\sim}{k})}_{\text{Diffusion}}$$

NUMERICAL TESTS

- Color Problem (Rigid Body Rotation of Passive Scalar)
  - Convection Alone (Orszag, Seinfeld et al.)
  - Convection Plus Reaction (Exact Solutions Available)
  - Convection Plus Diffusion (Exact Solutions Available)
- One-Dimensional, Diffusion-Reaction Problem
  - Test Against Exact Solutions
- Two-Dimensional Vortex Rollup
  - Convection, Diffusion, and Reaction
  - "Exact" Solution for $\theta = C_1 - C_2$ is Known from Previous Calculation

NUMERICAL TEST PROBLEMS

- Two Dimensional Rigid Rotation (Color Problem)
  - Initial condition: $C(x,z,0) = \exp\left(-\frac{x^2}{x_o^2} - \frac{z^2}{z_o^2}\right)$
- Analytical Solution for Identical Initial Concentration Fields (No Diffusion)

$$C(x',z',t) = \frac{C(x',z',C_i)}{1 + RtC(x',z',0)}$$

- Analytical Solution with Diffusion (No Reaction)

$$C(x',z',t) = \frac{1}{\sqrt{\left(1 + \frac{4Dt}{x_o^2}\right)\left(1 + \frac{4Dt}{z_o^2}\right)}} \exp\left[-\frac{x'^2/x_o^2}{\left(1 + \frac{4Dt}{x_o^2}\right)} - \frac{z'^2/z_o^2}{\left(1 + \frac{4Dt}{z_o^2}\right)}\right]$$

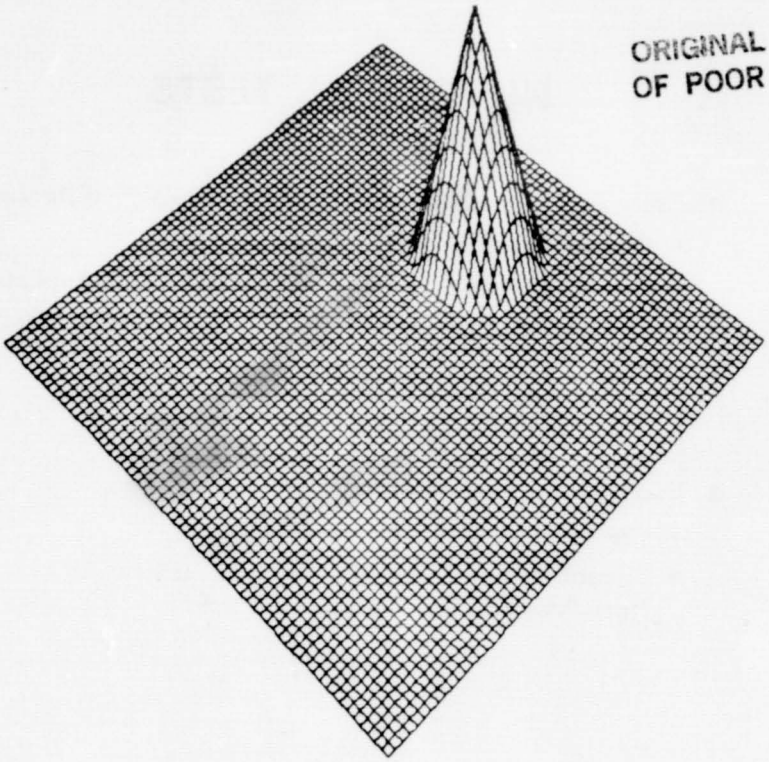

Initial Concentration Field for Color Problem Tests

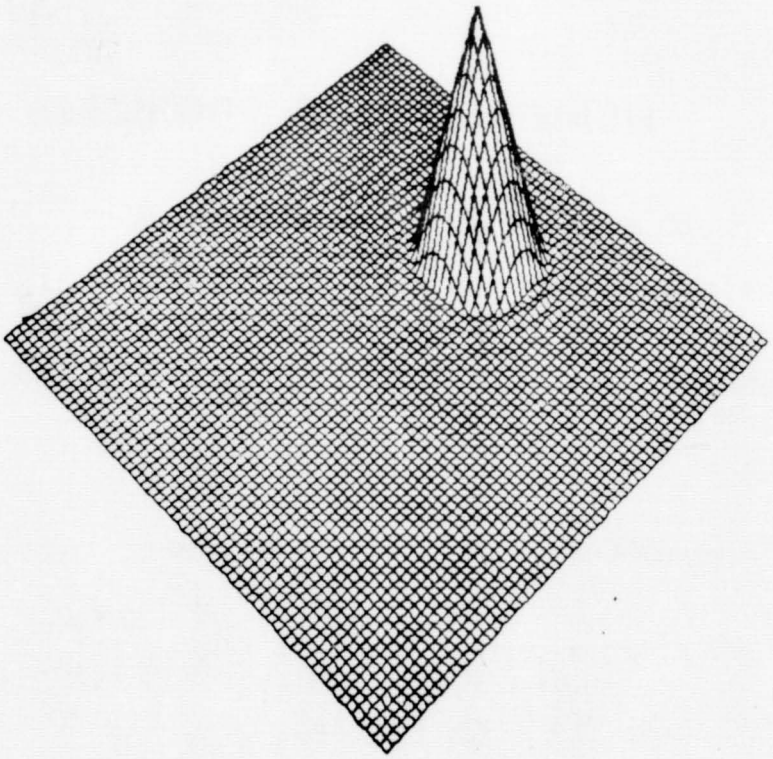

Computed Concentration Field After One Revolution - No Diffusion or Reaction

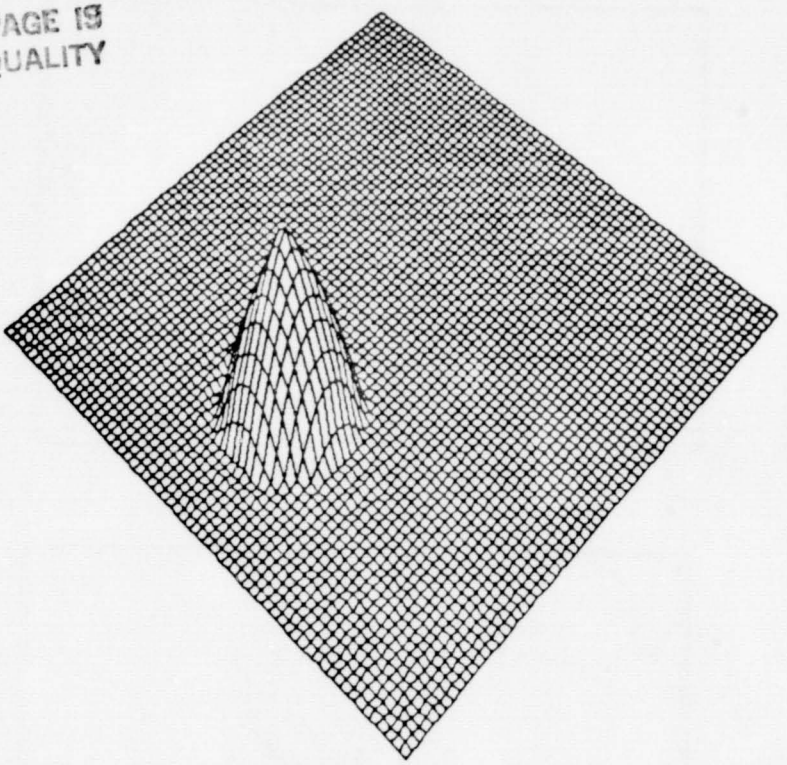

Computed Concentration Field After One-Half Revolution - No Diffusion, R = 1.0

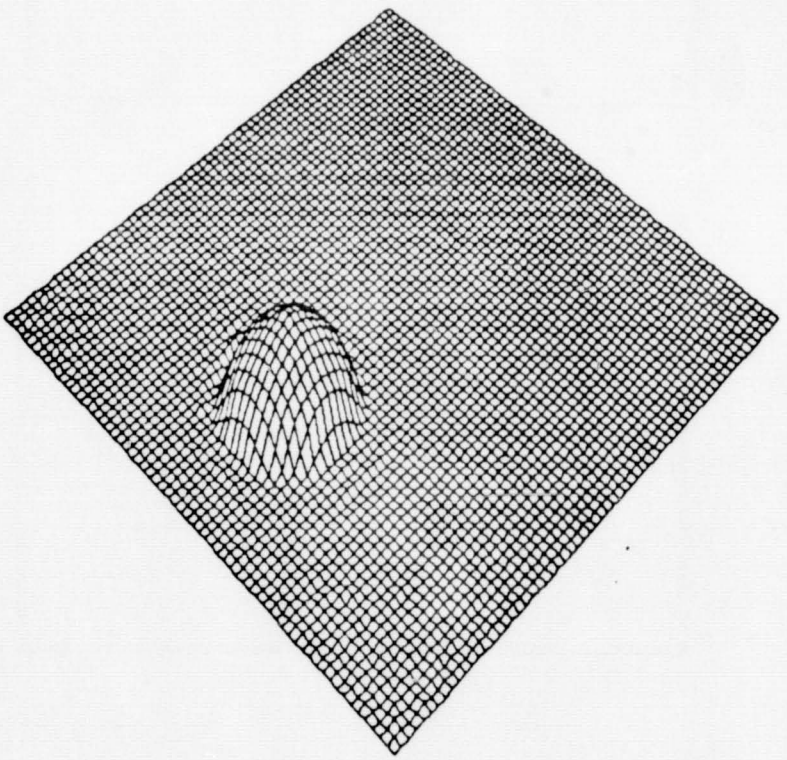

Computed Concentration Field After One-Half Revolution - No Diffusion, R = 4.0

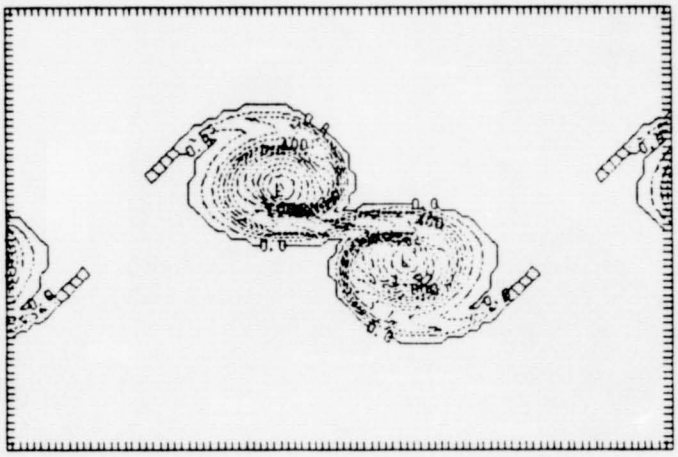

Figure 21a t = 12

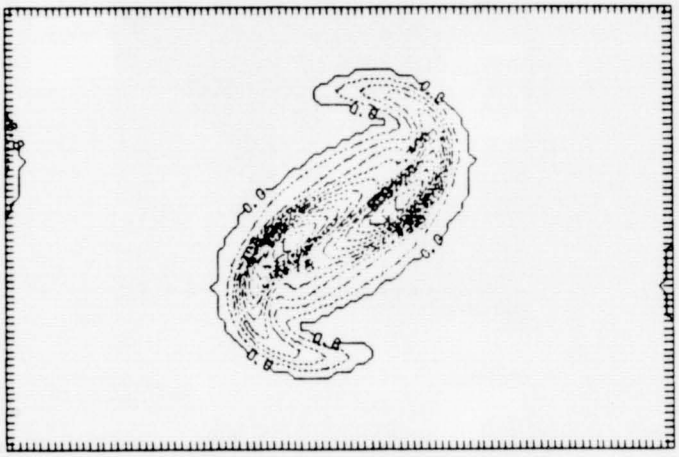

Figure 21b t = 24

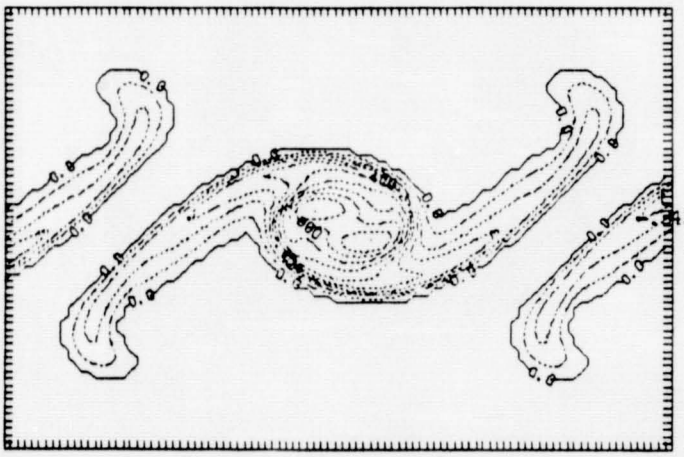

Figure 21c t = 36

Plots of Vorticity Contours for a Sequence of Times - Case 3
(Fundamental and Subharmonic Added Together Out-of-Phase)

TWO-DIMENSIONAL SIMULATIONS

- Case I: Most Unstable Mode Based Upon Linear Theory (Fundamental)
  - Results in a Single Rollup
- Case II: Subharmonic of the Most Unstable Mode
  - Results in a Single Rollup, of Approximately Twice the Size and Time Period
- Case III: Fundamental and Subharmonic 90° Out-of-Phase
  - Results in a Double Rollup

EQUATIONS (CONT.)

- Define Conserved Scalar $\theta = C_A - C_B$

  Then θ satisfies

  $$\boxed{1} \quad \frac{\partial \theta}{\partial t} + u \cdot \nabla \theta = D \frac{\partial^2}{\partial x_j^2} \theta \qquad \text{(No R dependence)}$$

  with initial conditions $\theta(t=0) = \theta(0) = C_A(0) - C_B(0)$

- Infinite Reaction Rate Limit

  $$C_1 = \begin{cases} \theta & \theta \geq 0 \\ 0 & \theta < 0 \end{cases} \qquad C_2 = \begin{cases} 0 & \theta \geq 0 \\ -\theta & \theta < 0 \end{cases}$$

  C_P can be obtained from conserved scalar

  $$\varnothing = C_P + C_A$$

  where $\varnothing$ also satisfies Equation [1]

  with initial conditions $\varnothing(t=0) = \varnothing(0) = C_A(0)$

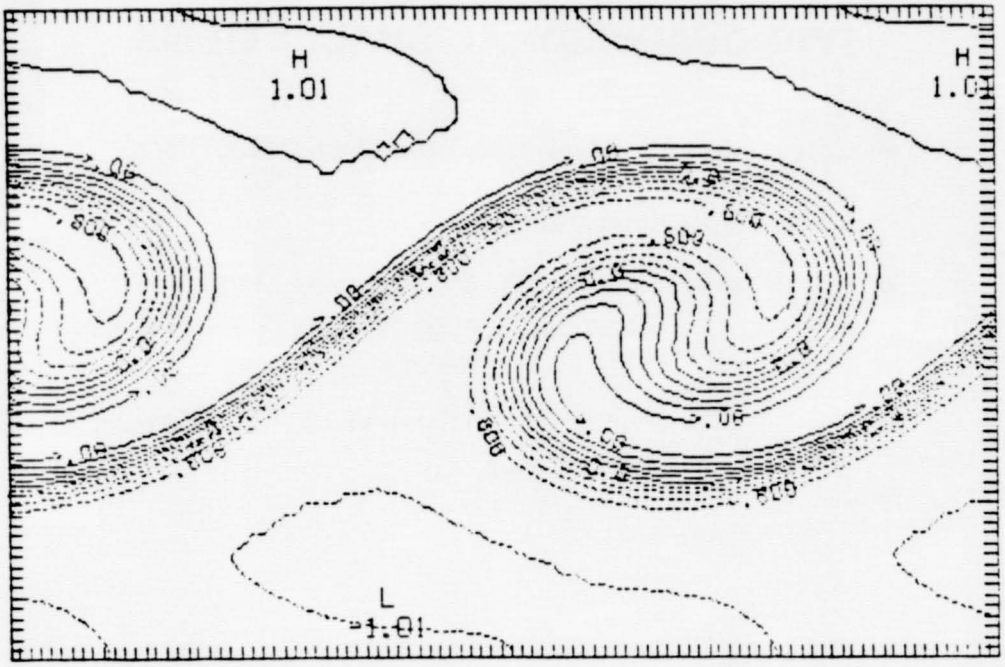

Constant Contour Plot of Conserved Scalar Computed Indirectly
from the Difference Between the Species Concentrations - t = 12

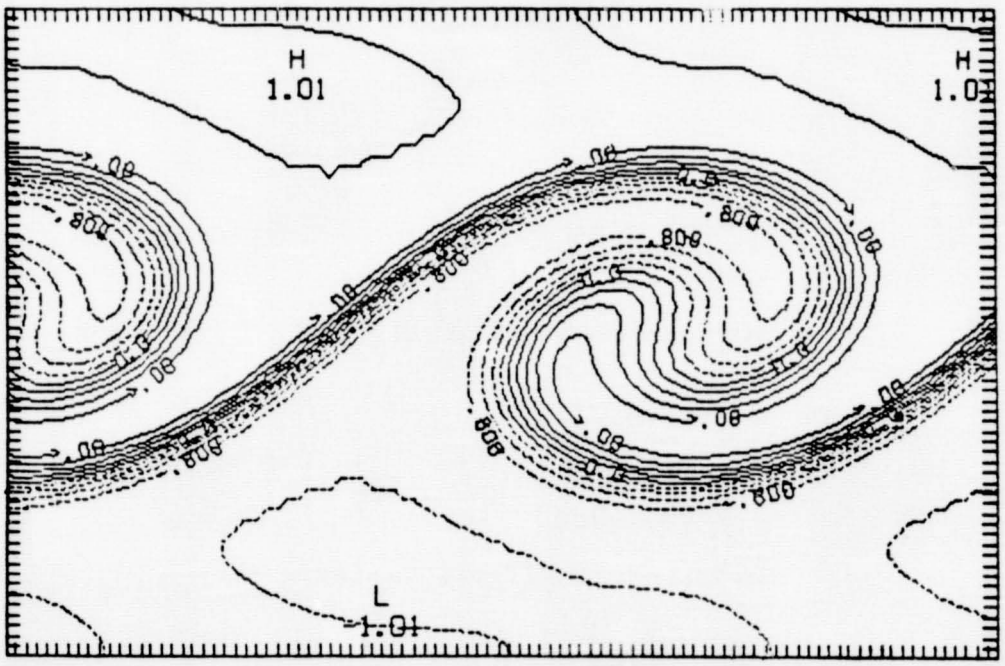

Constant Contour Plot of Conserved Scalar Computed Directly
from the Difference Between the Species Concentrations - t = 12

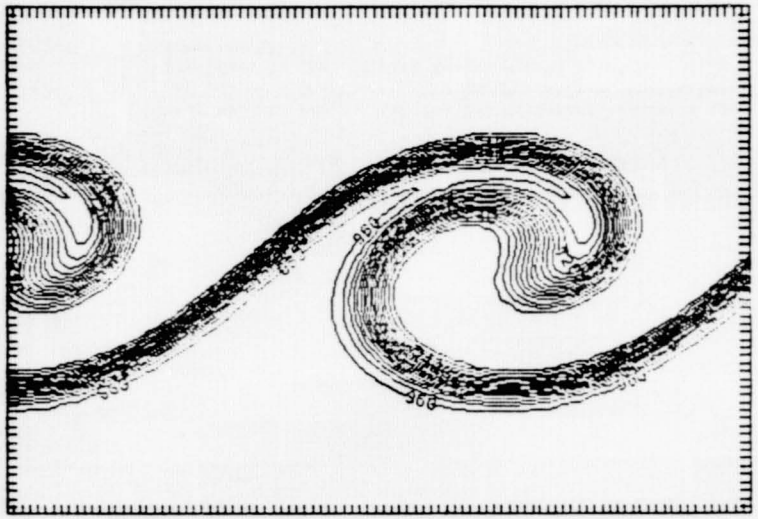

Figure 23a Species A

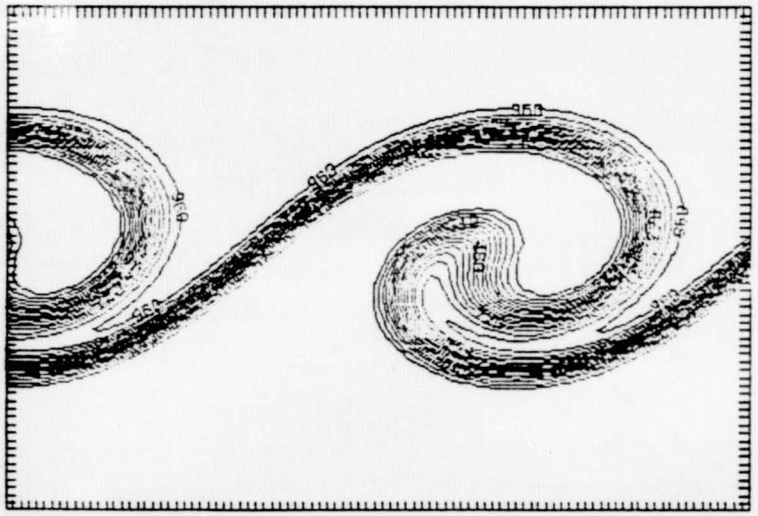

Figure 23b Species B

Plots of Concentration Contours for Species A and B at t = 12 for Case 1 (Fundamental Mode Alone) - Two-Dimensional Simulations

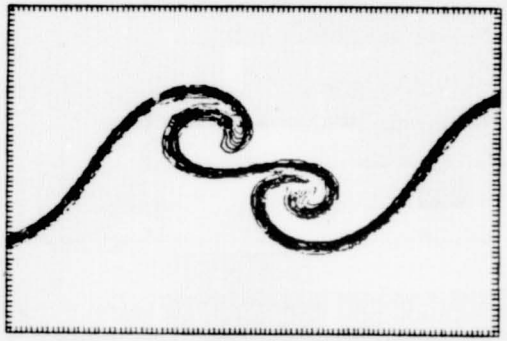

Figure 28a t = 12

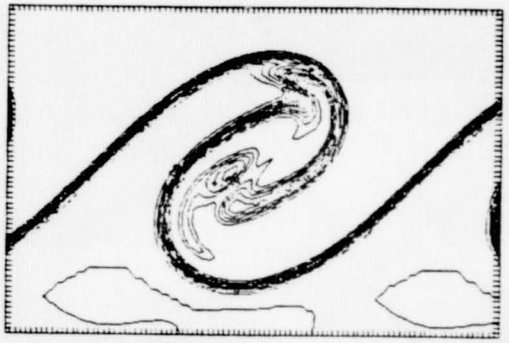

Figure 28b t = 24

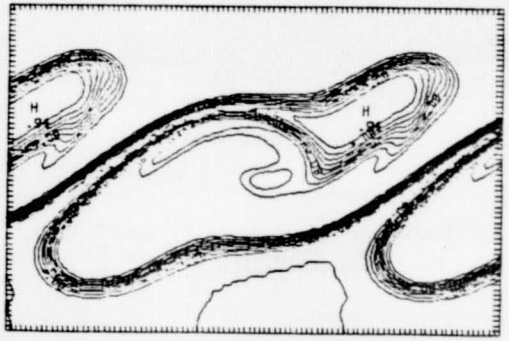

Figure 28c t = 36

Plots of Concentration Contours for Species A for a Sequence of Times for Case 3 (Fundamental and Subharmonic Added Together Out-of-Phase) - Two-Dimensional Simulations

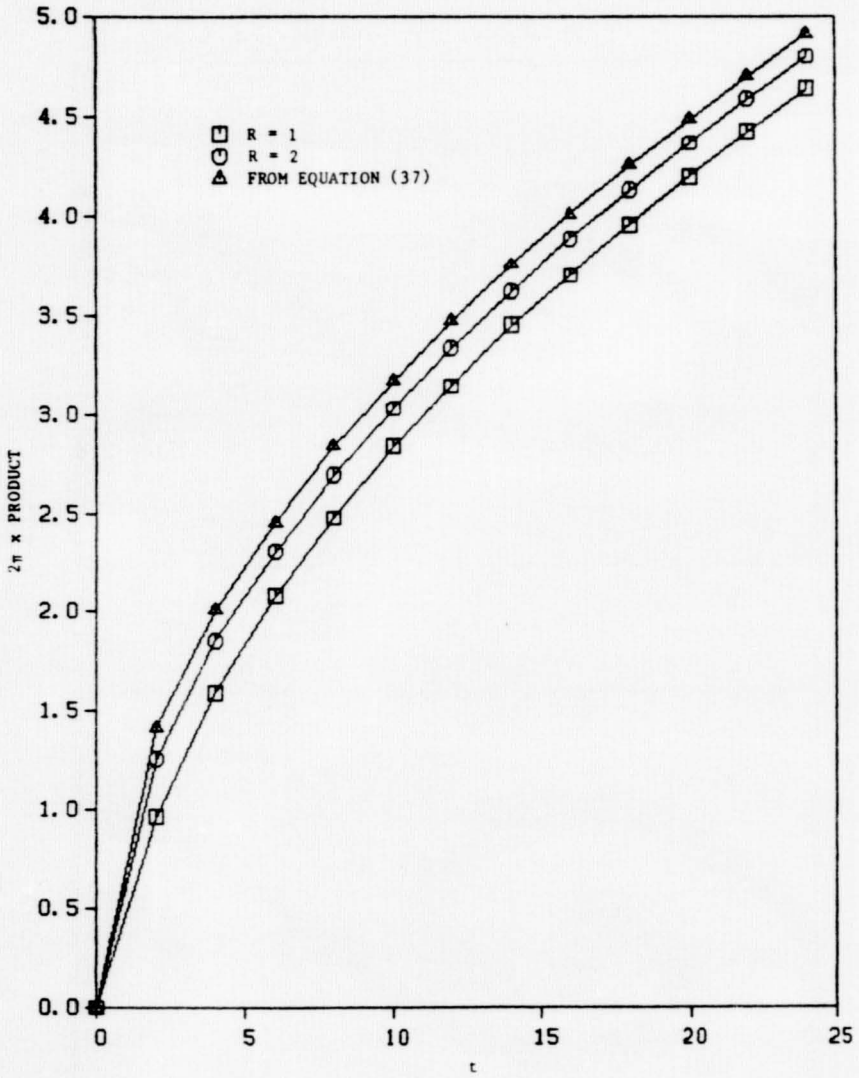

Total Product Versus Time for Two Different Values of the Reaction Rate Coefficient R - One-Dimensional Simulations. Also Shown Is the Infinite Reaction Rate Solution [Equation (37)]

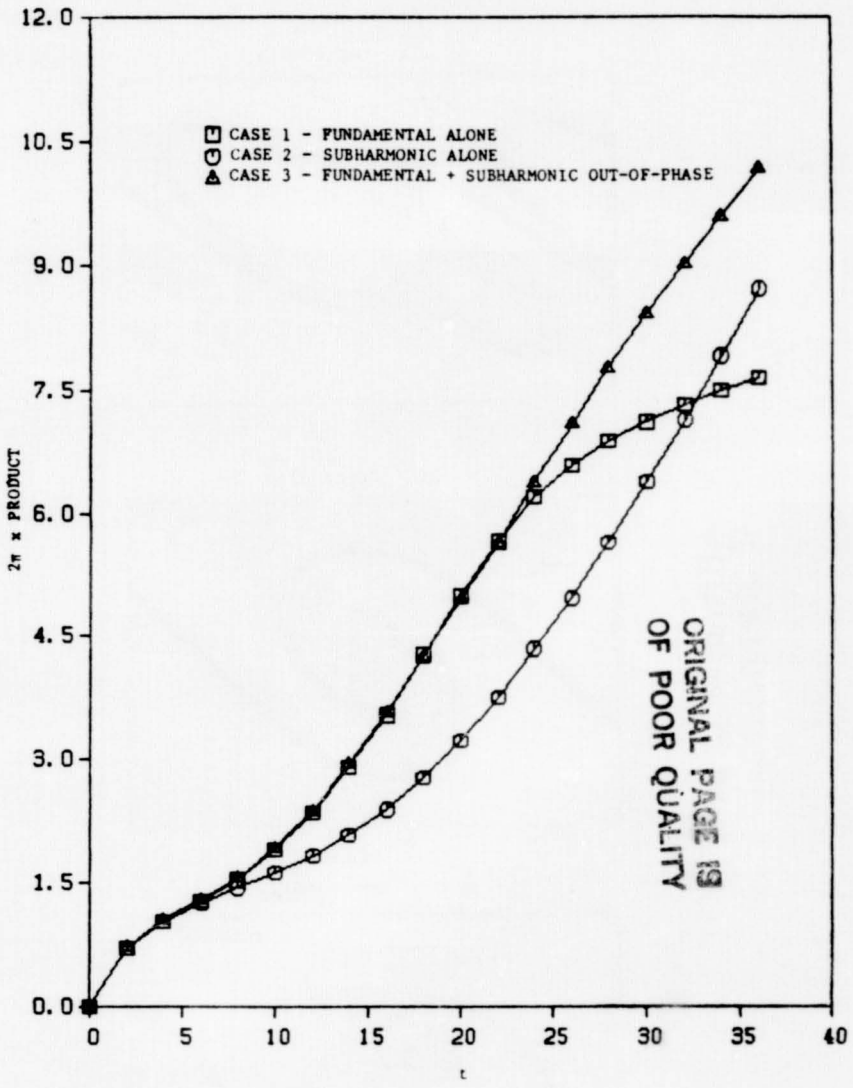

Total Product Versus Time - Two-Dimensional Simulations

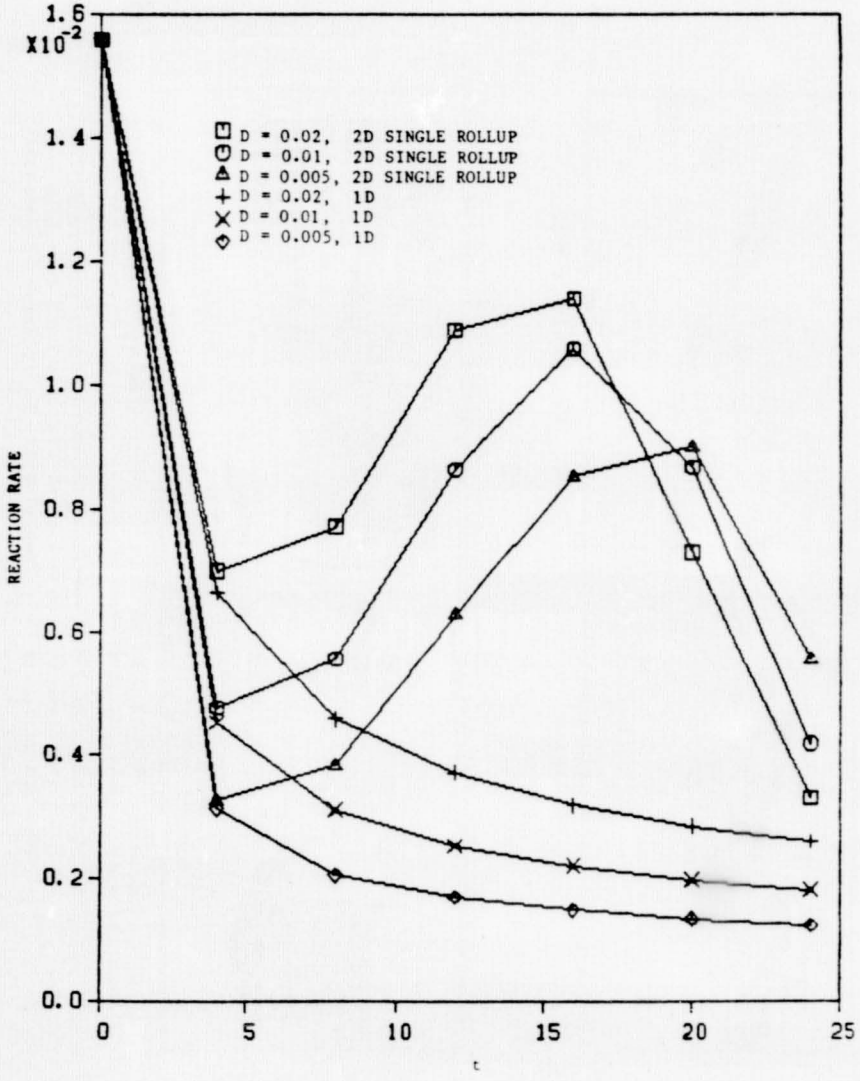

Total Reaction Rate Versus Time for Different Diffusivities - One- and Two-Dimensional Simulations

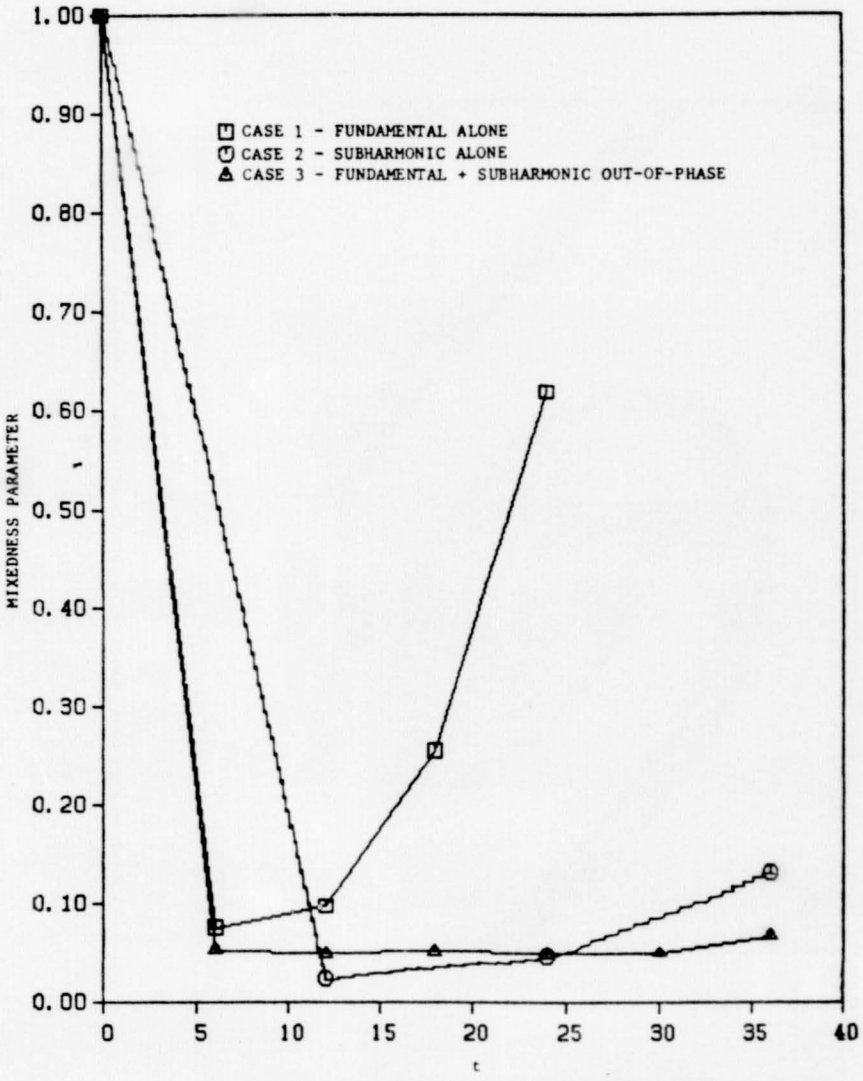

Mixedness Parameter Versus Time - Two-Dimensional Simulations

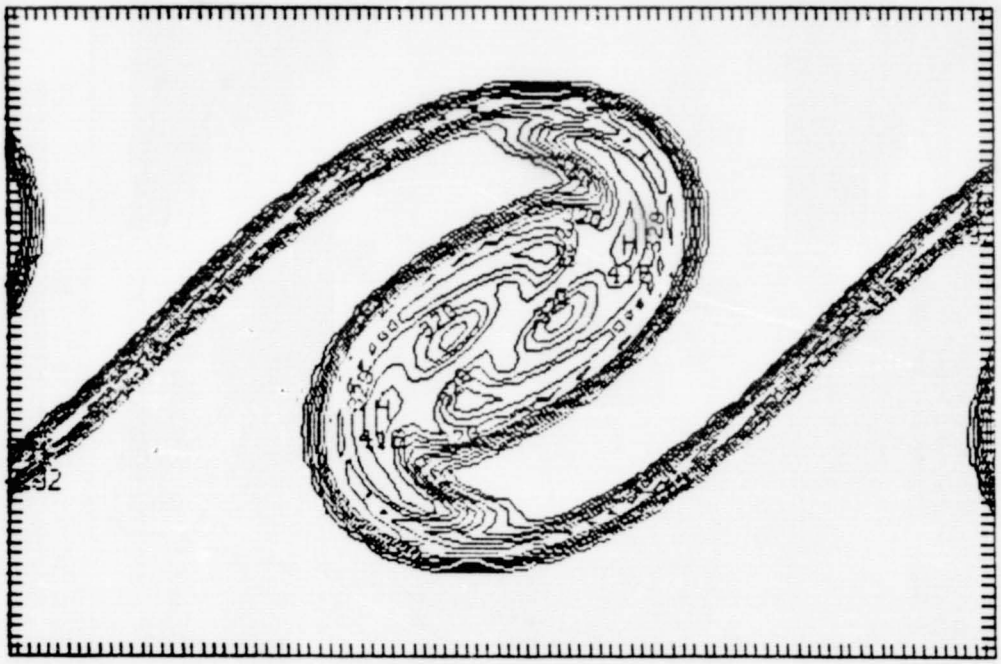

Plot of Product Concentration Contours at t = 24 for Case 3
(Fundamental and Subharmonic Added Together Out-of-Phase)
- Two-Dimensional Simulations

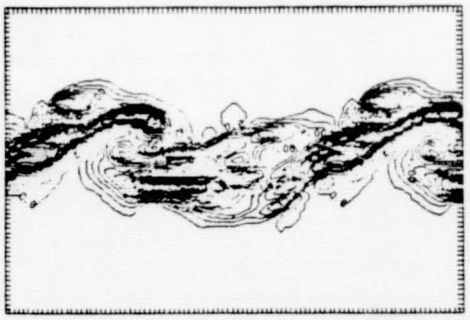

Figure 45a t = 6

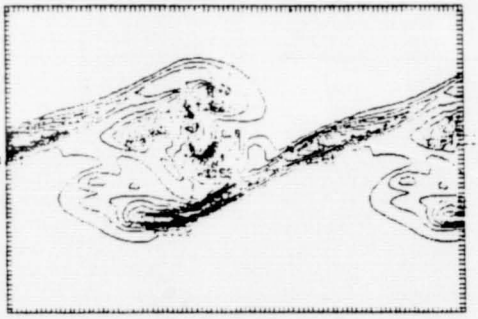

Figure 45b t = 12

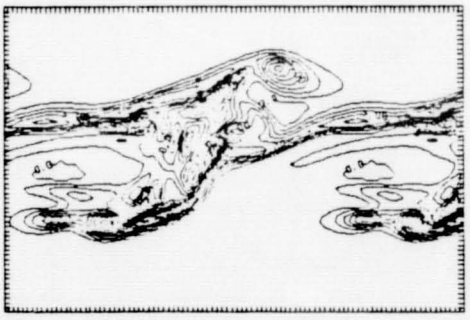

Figure 45c t = 18

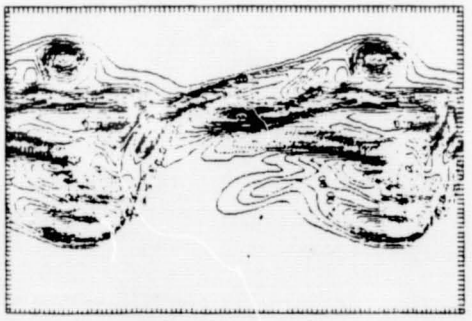

Figure 45d t = 24

Plots of Lateral (y) Vorticity Contours for a Sequence of Times in an x-z Plane Located a Lateral Distance $L_y/2$ from that Depicted in Figure 44 - Single Rollup Case, Three-Dimensional Simulations, Run JN20B

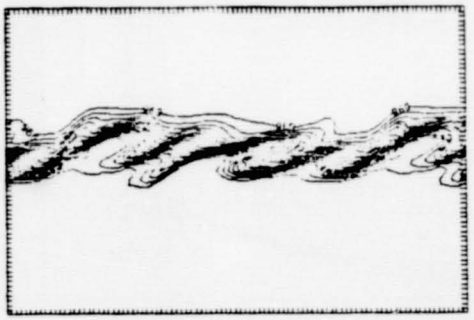

Figure 46a t = 6

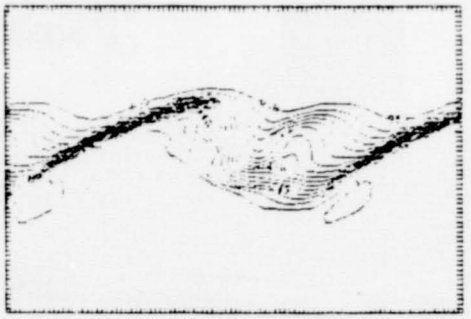

Figure 46b t = 12

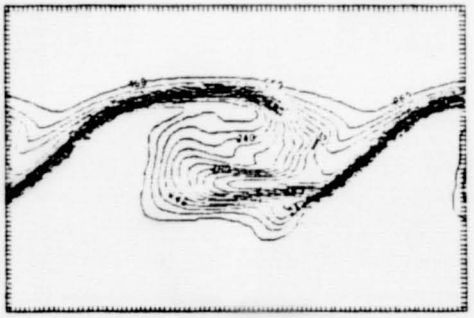

Figure 46c t = 18

Figure 46d t = 24

Plots of Concentration Contours for Species B for a Sequence of Times in the Same x-z Plane as for Figure 44 - Single Rollup Case, Three-Dimensional Simulations

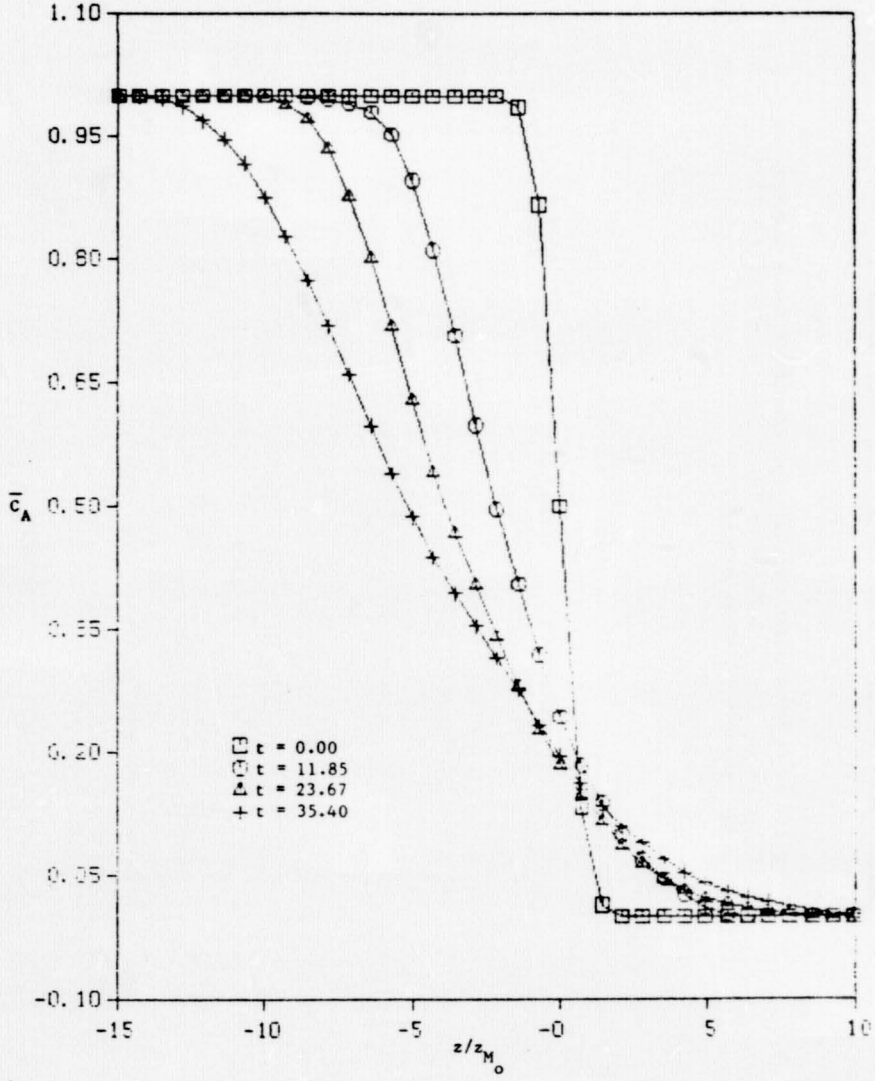

Average Concentration of Species A Versus z for a Sequence of Times - Realization II, Double Rollup Case, Three-Dimensional Simulations

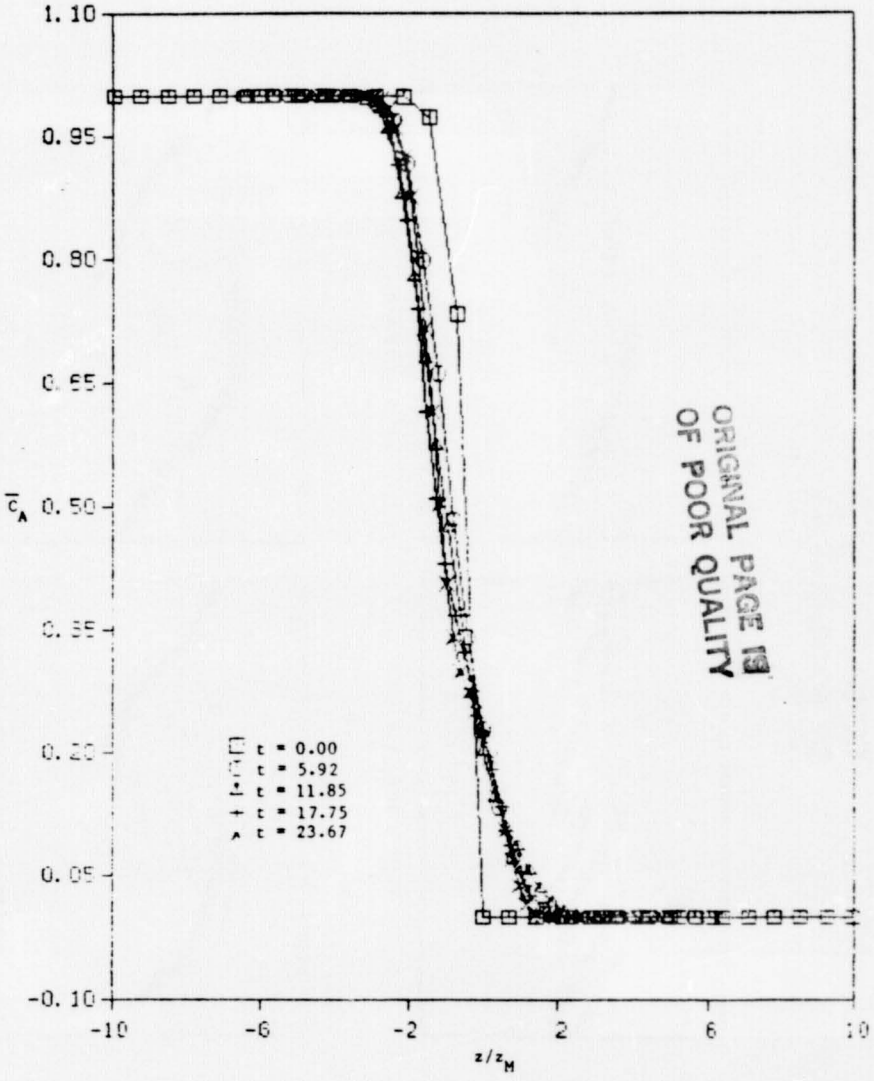

Similarity Plots of $\bar{C}_A/C_{A\infty}$ Versus z/z_M ($= z/z_{1/2}$) for Various Times - Single Rollup Case, Infinite Reaction Rate, Three-Dimensional Simulations

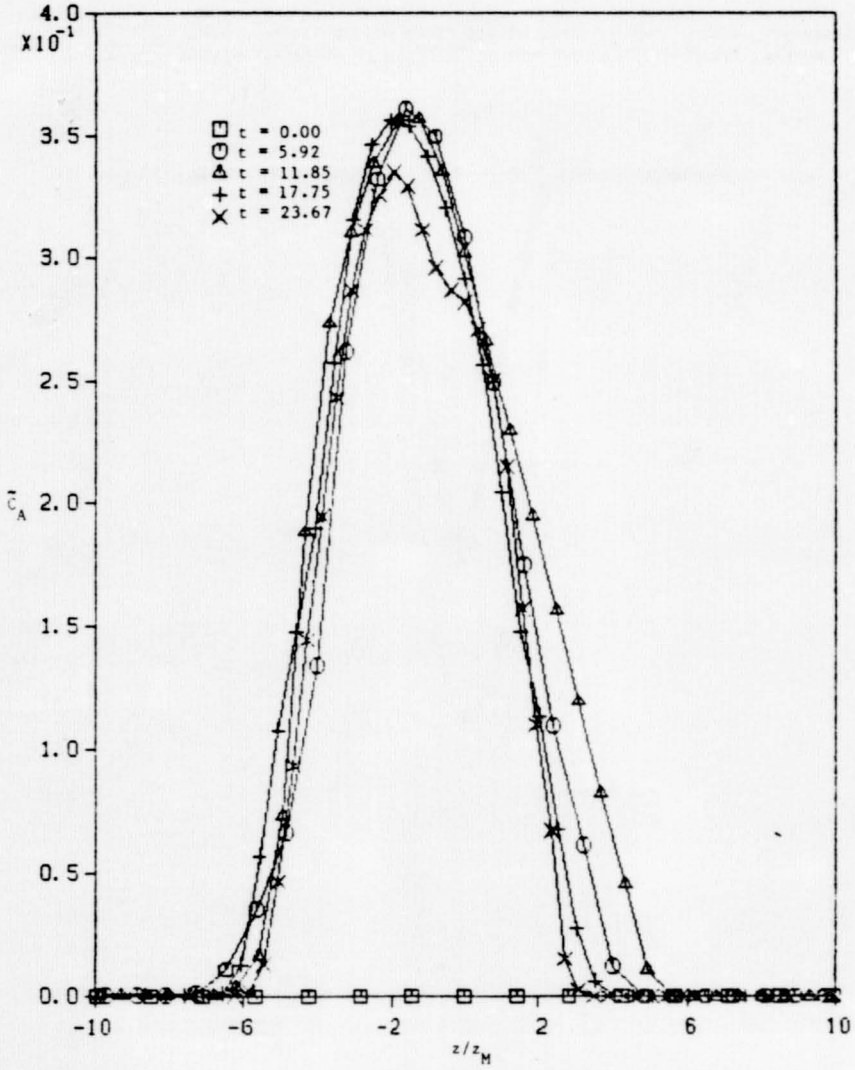

Similarity Plots of $\tilde{C}_A/C_{A\infty}$ Versus z/z_M (= $z/z_{1/2}$) for Various Times - Single Rollup Case, Infinite Reaction Rate, Three-Dimensional Simulations

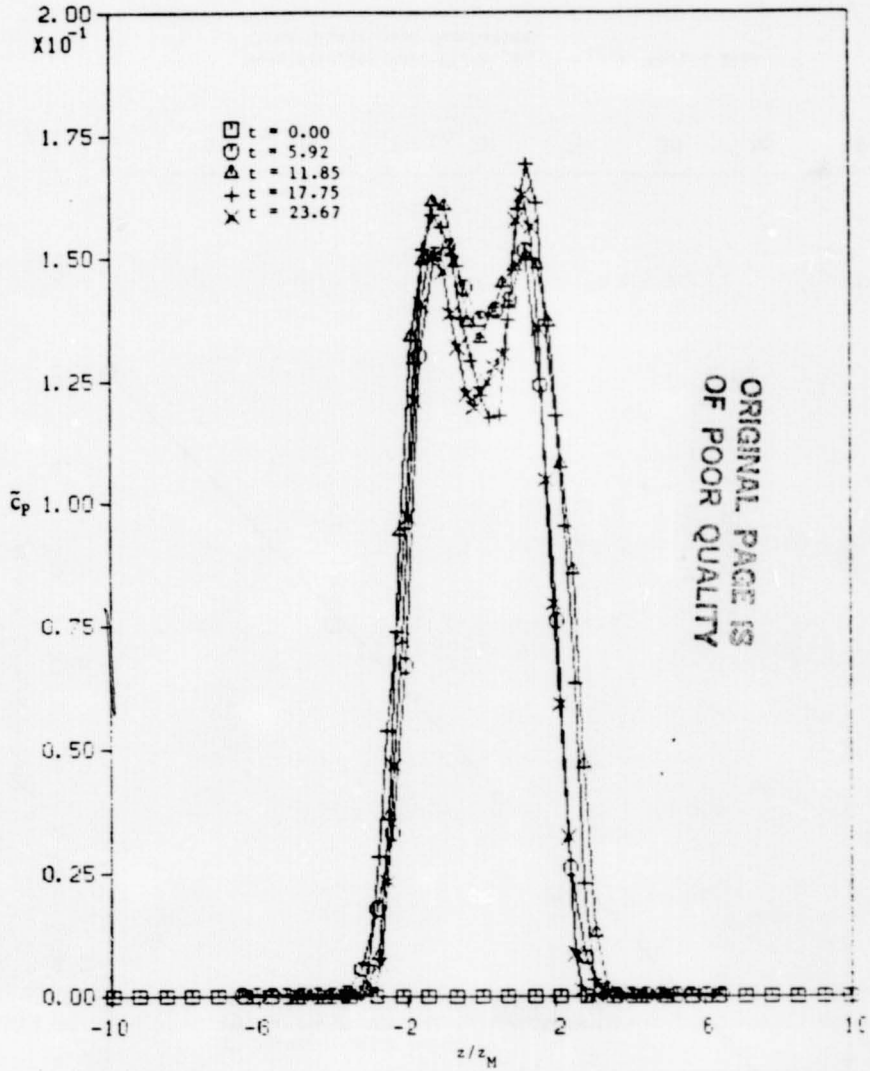

Similarity Plots of $\tilde{C}_P/C_{A\infty}$ Versus z/z_M (= $z/z_{1/2}$) for Various Times - Single Rollup Case, Infinite Reaction Rate, Three-Dimensional Simulations

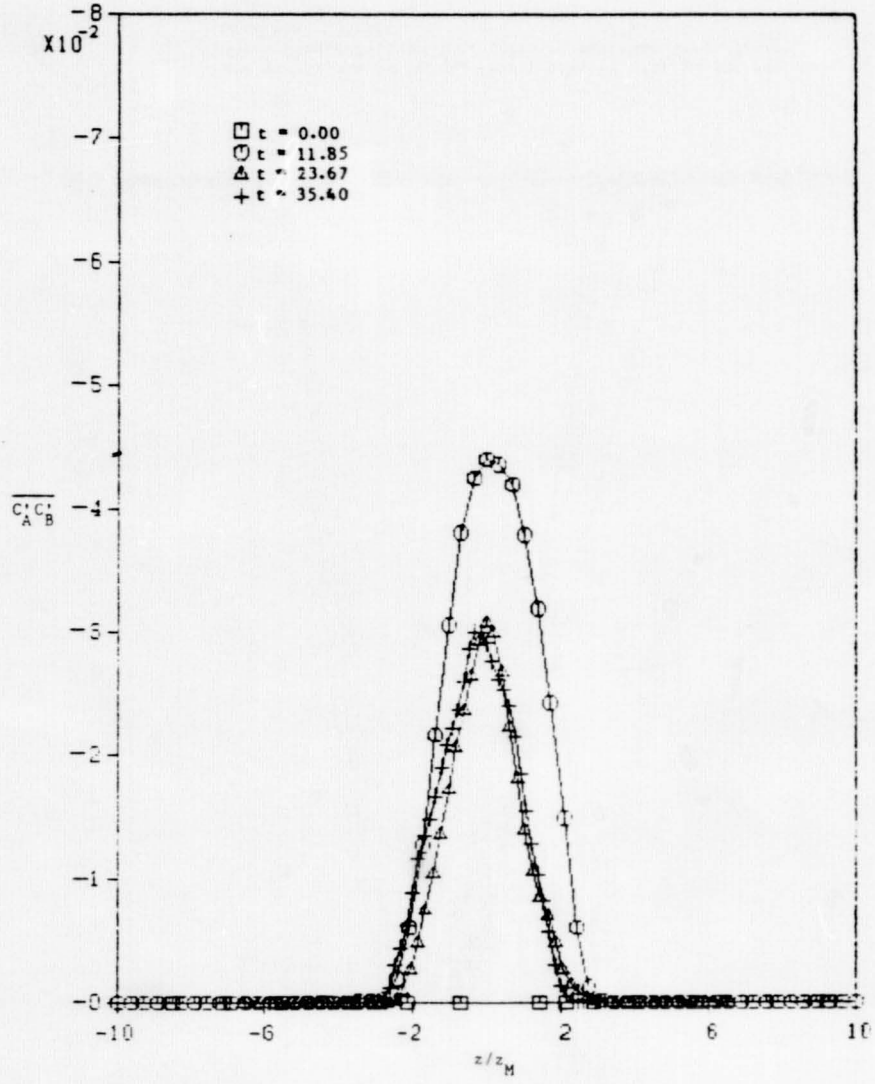

Similarity Plots of $\overline{C'_A C'_B}/C^2_{A_\infty}$ Versus z/z_M (= $z/z_{1/2}$) for Various Times - Double Rollup Case, Finite Reaction Rate, Three-Dimensional Simulations

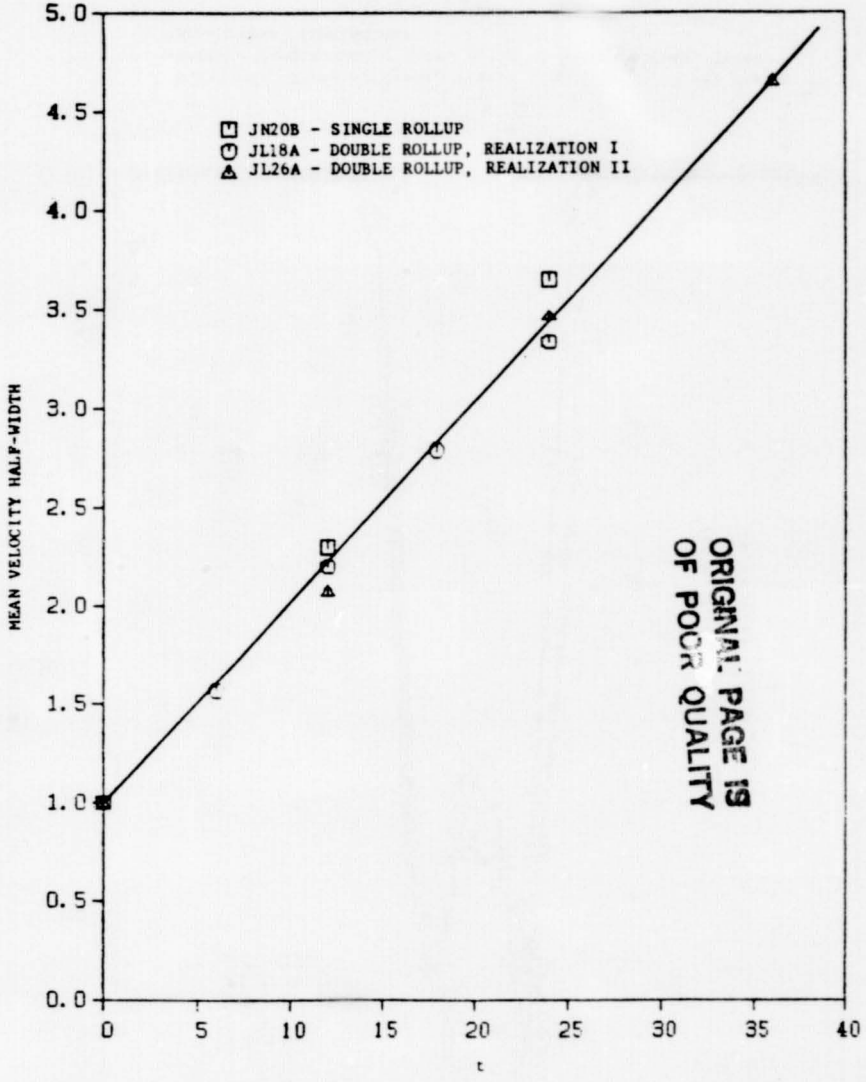

Mean Velocity Half-Width, z_M (= $z_{1/2}$), Versus Time - Three-Dimensional Simulations

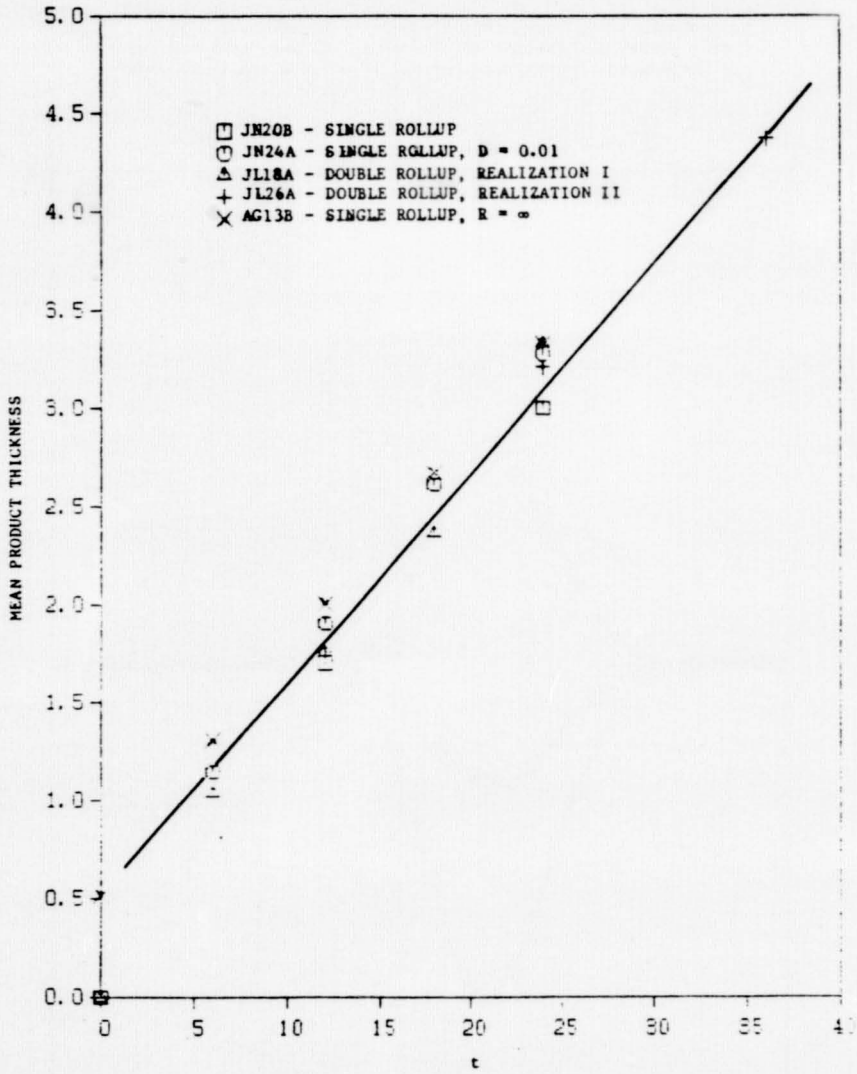

Mean Product Thickness, z_p, Versus Time - Three-Dimensional Simulations

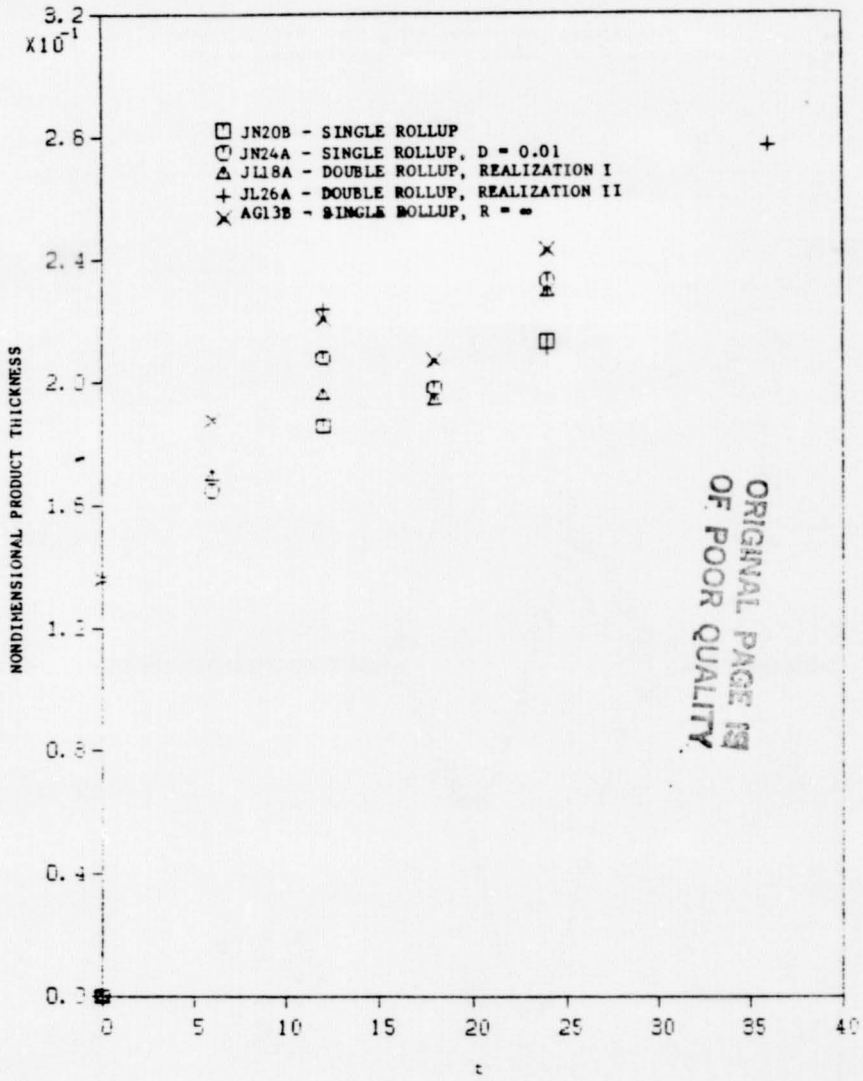

Nondimensional Product Thickness Versus Time - Three-Dimensional Simulations

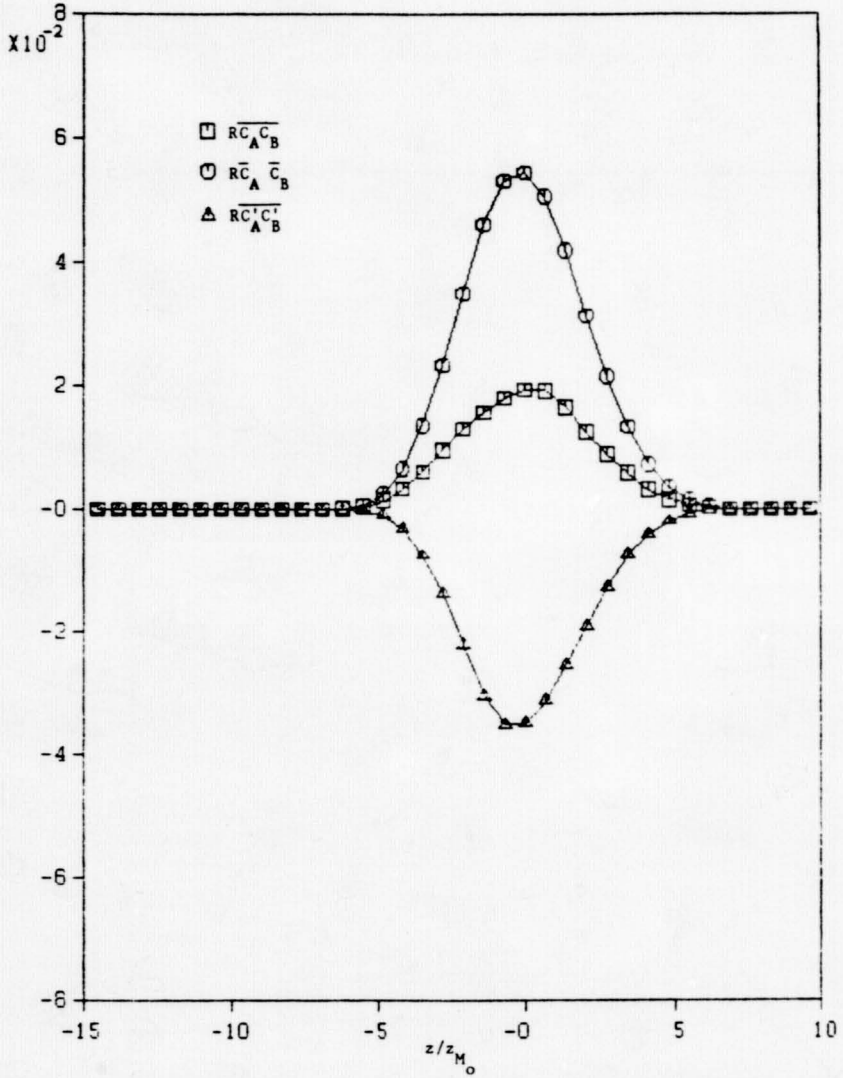

Average of the Product of the Concentrations, the Product of the Averages, and the Concentration Correlation Versus z at t = 12 - Realization I, Double Rollup Case, Three-Dimensional Simulations

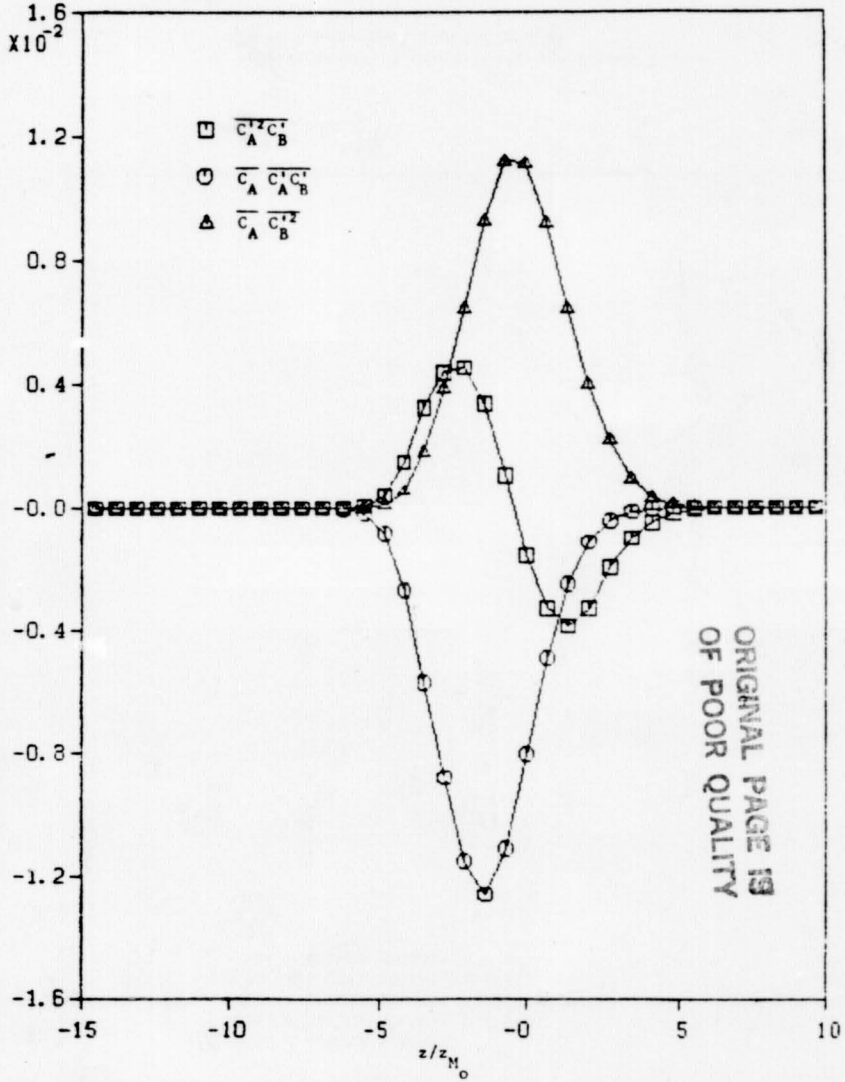

Various Concentration Moments Versus z at t = 12 - Realization I, Double Rollup Case, Three-Dimensional Simulations

CONCLUSIONS

- Color Problem Tests Showed That
  - Spectral methods produced high accuracy solutions in the presence of advection, reaction, and diffusion
  - Weak spatial filter insured numerical stability
- One Dimensional Simulations Showed That
  - Calculations close to the infinite reaction rate can be done
  - Results were fairly insensitive to initial conditions
  - Results were in reasonable agreement with theoretical predictions
- Two Dimensional Simulations Showed That
  - Reaction zone was significantly stretched by vortex rollup
  - Vorticity and product fields coincided
  - Significant species segregation and "flame shortening" effects were present

CONCLUSIONS (CONT.)

- Three Dimensional Simulations Showed That
  - Good agreement with self-similarity theory was obtained
  - Technique can treat entire range of reaction rates – from very slow to infinite
  - Computed profiles qualitatively similar to profiles from laboratory data
  - Quantitative comparisons will be made soon
  - Nondimensional product thickness was 0.22 – compared to values of 0.3 to 0.35 from laboratory data
  - No adjustable parameters are used
  - Some presently used estimates of correlation products can be significantly in error

D25

CHARACTERISTICS OF INHOMOGENEOUS JETS IN CONFINED SWIRLING AIR FLOWS

Ronald M. C. So and S. A. Ahmed
Arizona State University

Flow fields in the neighborhood of confined jets proved to be of great interest for gas turbine combustor designers. Although there have been numerous investigations on the characteristics of confined (1-4) jets, very little quantitative data exist for confined jets in a swirling flow. We have recently started an experimental program to study the characteristics of inhomogeneous jets in confined swirling flows to obtain detailed and accurate data for the evaluation and improvement of turbulent transport modeling for combustor flows. Our work was also motivated by the need to investigate and quantify the influence of confinement and swirl on the characteristics of inhomogeneous jets.

The flow facility at Arizona State University was constructed in a simple way which allows easy interchange of different swirlers and the freedom to vary the jet Reynolds number. The velocity measurements were taken with a one color, one component DISA Model 55L laser-Doppler anemometer employing the forward scatter mode. Standard statistical methods are used to evaluate the various moments of the signals to give the flow characteristics.

The current project started with the measurements of the velocity field. The second phase of the work will concentrate on the investigation of the scalar fluxes utilizing concentration probes. Finally, the two different sensors will be used simultaneously to determine the turbulent momentum and mass fluxes in the whole flow field.

The present work was directed at the understanding of the velocity field. Therefore, only velocity and turbulence data of the axial and circumferential

components are reported for inhomogeneous jets in confined swirling air flows. Results to date show that the jet centerline velocity decreases rapidly in a short distance for both Helium and air jets. However the similarity between Helium and air jets ends here. For air jets, the jet-like behaviour in the flow disappears at about 20 diameters downstream of the jet exit. This phenomenon is independent of the initial jet velocity. When this stage is reached for the mean flow, the turbulence field also decays to that of the background swirling flow. For Helium jets, the jet-like behaviour is noticed even at 40 diameters downstream of the jet exit. The turbulence field also reflects the same behaviour. Since the jets are fully turbulent (therefore, independent of jet Reynolds numbers) and the jet momentum fluxes for both air and Helium jets are the same, the cause of this difference in behaviour is attributed to the combined action of swirl and density difference. This behaviour could explain some of the common observations in gas turbine combustors.

The completion of the proposed work will make a substantial contribution to the understanding and predictive capability of complex turbulent swirling flows with inhomogeneous jets.

References

1. Janjua, S.I., McLaughlin, D.K., Jackson, T.W., and Lilley, D.G., turbulence Measurements in a Confined Jet Using a Six-Orientation Hot-Wire Probe Technique, AIAA Journal, Vol. 21, No. 12, pp. 1609-1610.

2. Habib, M.A., Whitelaw, J.H., Velocity Characteristics of a Confined Coaxial Jet, ASME Paper 79-WA/FE-9.

3. Habib, M.A., Whitelaw, J.H., Velocity Characteristics of Confined Coaxial Jets with and without Swirl, ASME Paper 79-WA/FE-21.

4. Johnson, B.V., Bennett, J.C., Mass and Momentum Turbulent Transport Experiments with Confined Coaxial Jets, NASA Report CR-165574.

OBJECTIVE

- MIXING IN COMBUSTOR
- ISOTHERMAL VARIABLE DENSITY MIXING
- SWIRL EFFECTS
- SCALE INFORMATION FOR COMBUSTOR DESIGN
- DATA FOR MODEL VERIFICATION

PROGRAM OF WORK

- EXPERIMENTAL STUDIES
  1 – AIR JETS
  2 – HELIUM JETS
  3 – CONCENTRATION AND FLUX MEASUREMENTS
  4 – EFFECTS OF VARYING SWIRL

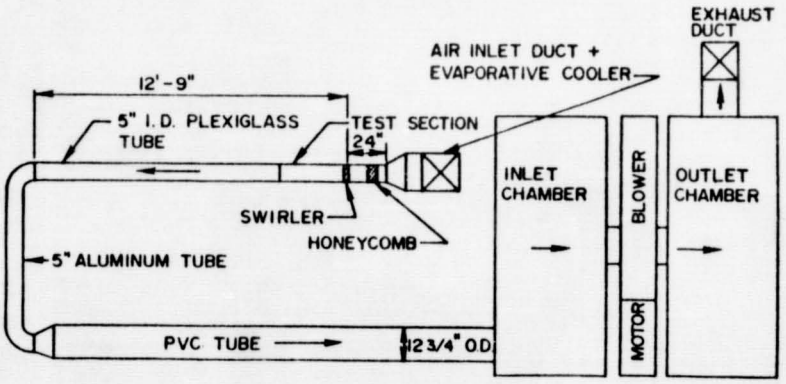

Schematic Diagram of the Flow System
(Note that the laser axis is perpendicular to the plane of the paper)

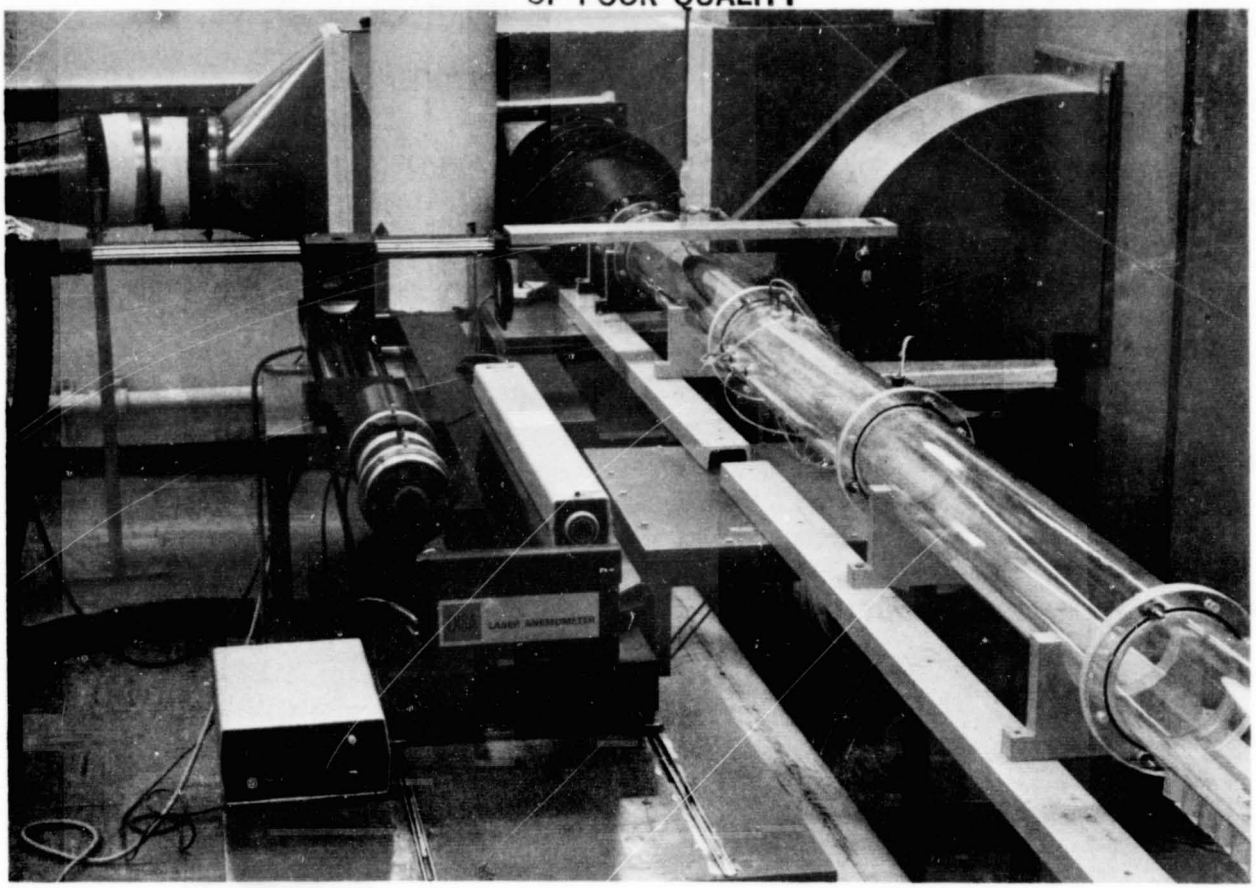

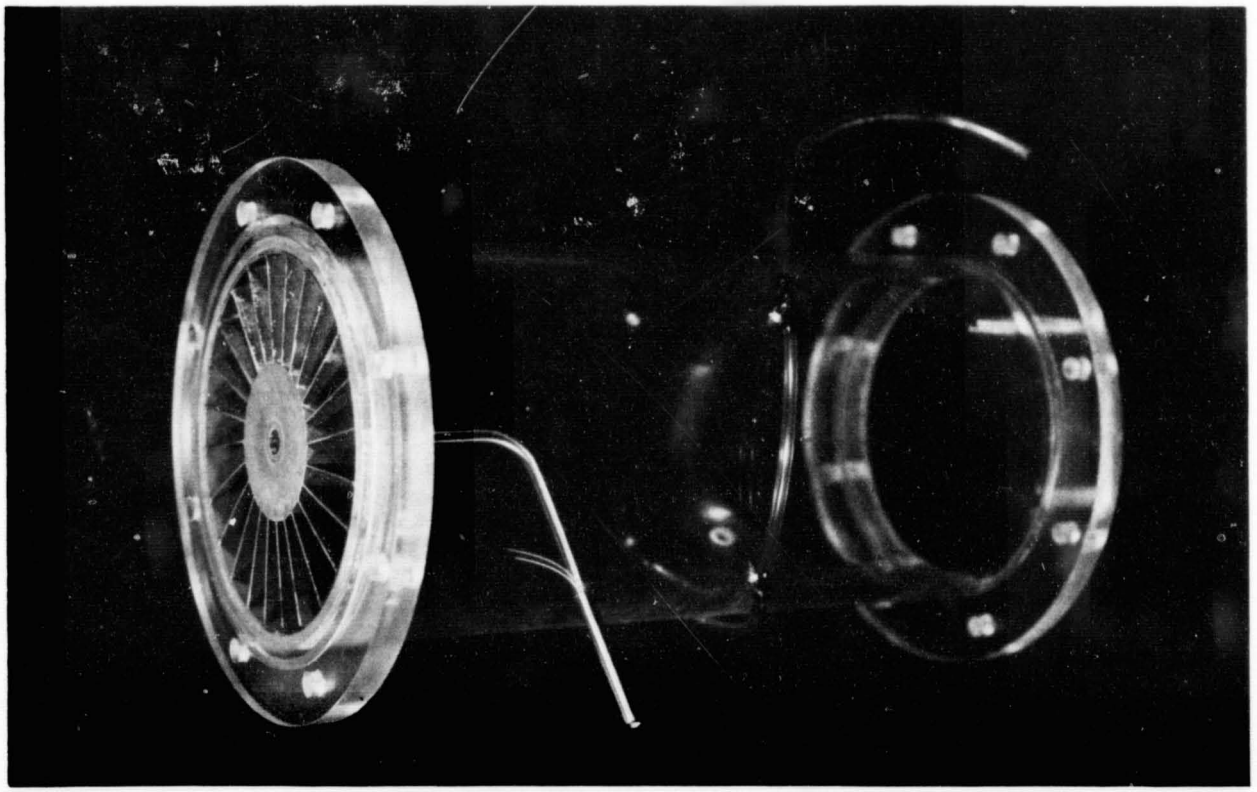

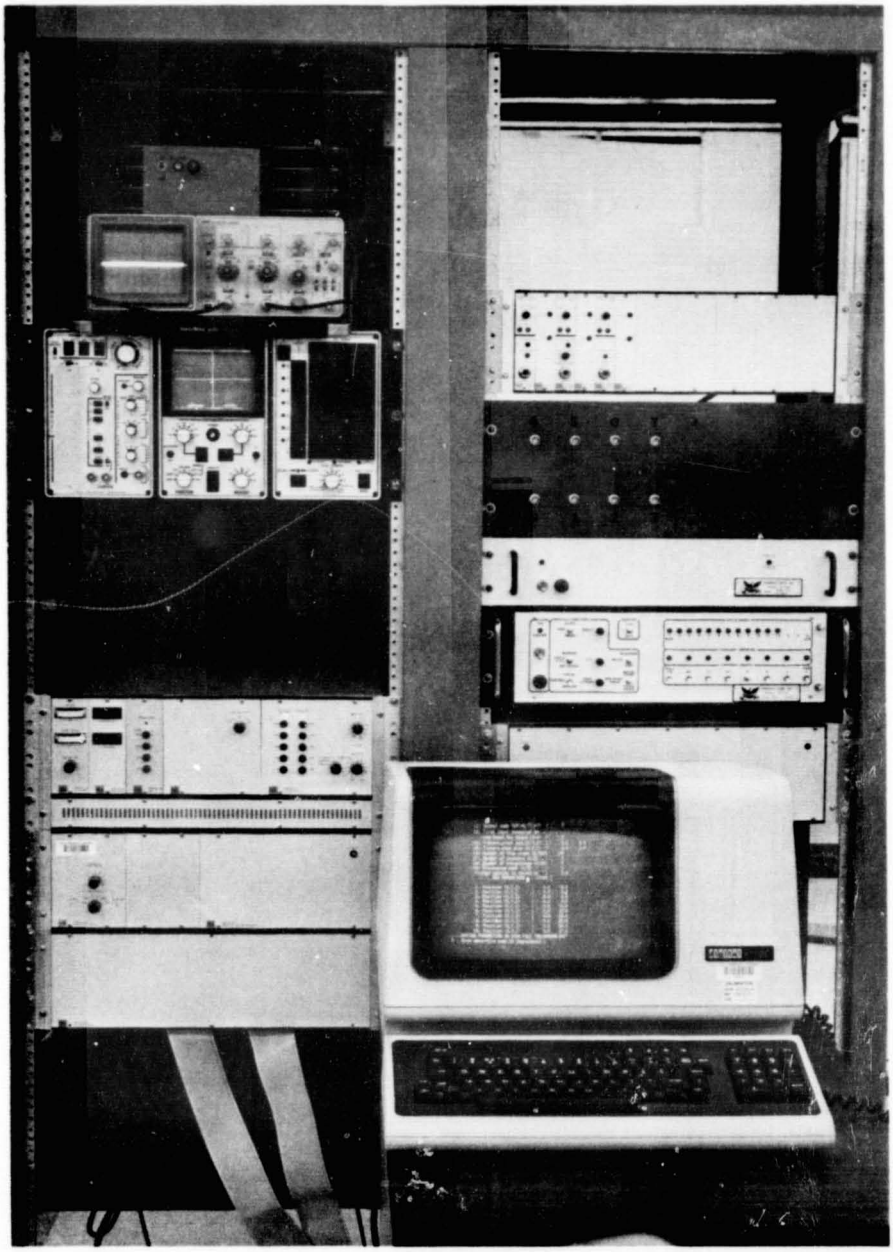

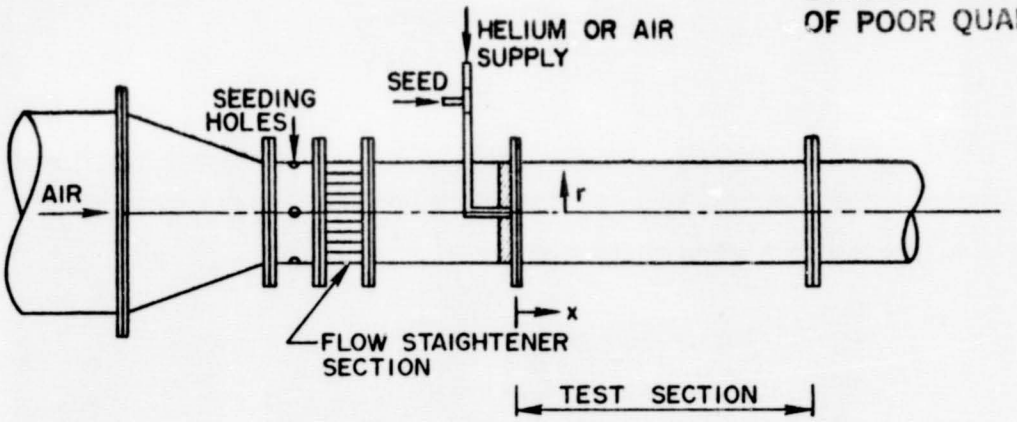

Schematic Diagram Showing the Test Section in Detail

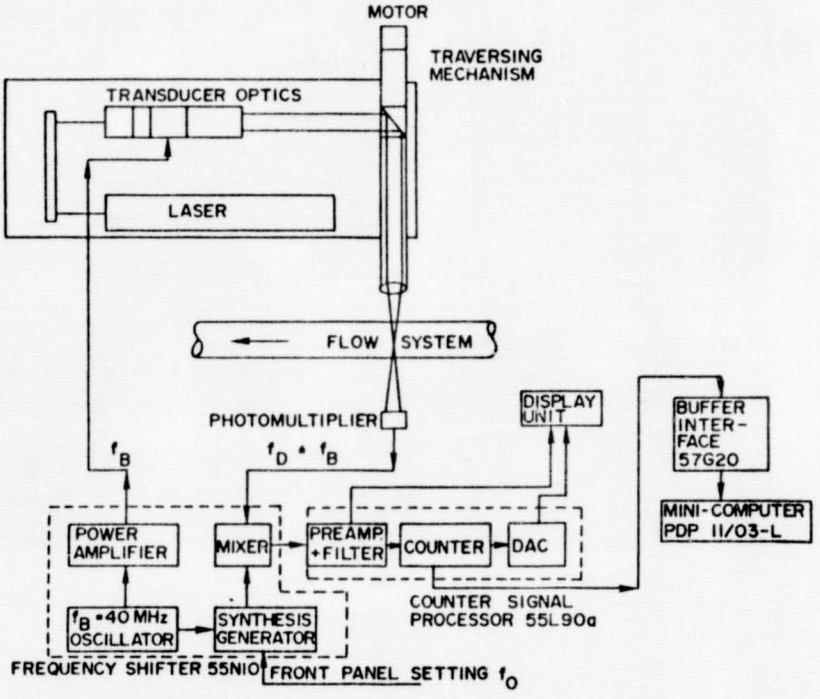

Block Diagram of the LDV and Data Acquisition System

FLOW CONDITIONS

$\bar{R}_e = 5.5 \times 10^4$

QUANTITY MEASURED	AIR JET		HELIUM JET	
U_j (mt/sec)	25.4	66.8	25.4	66.8
R_{e_j}	1.4×10^4	3.8×10^4	1.8×10^3	4.8×10^3
$M_j/\bar{M}$	0.071	0.491	0.010	0.068

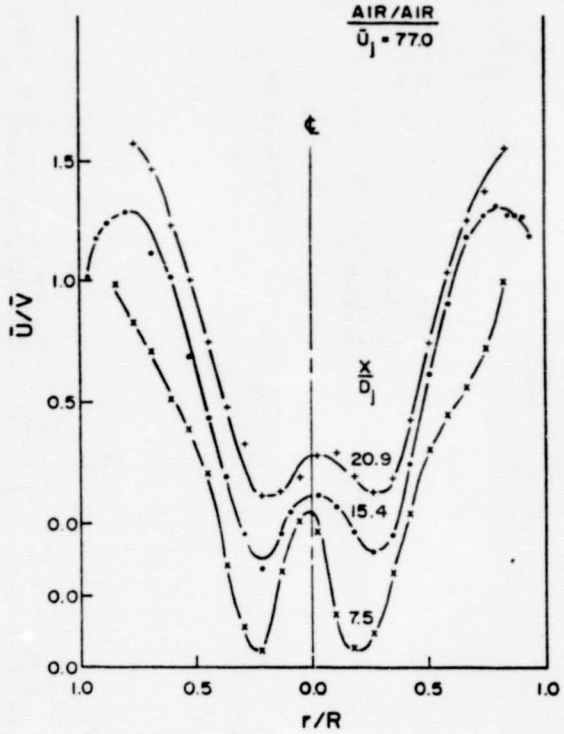

Check on the Flow Symmetry

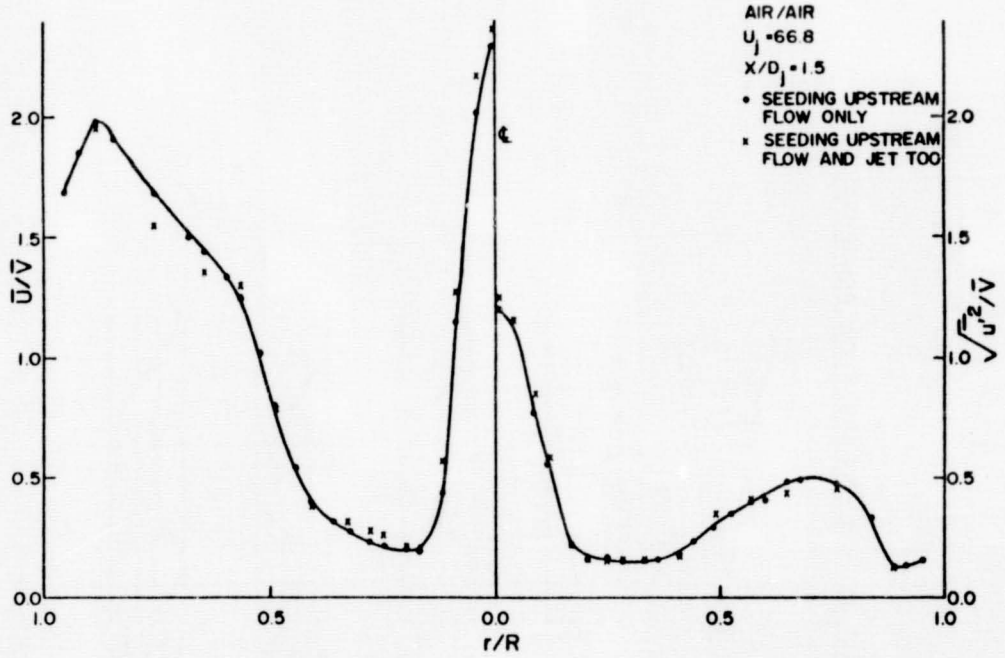

Check on the Seed Effects

AIR JET – SPECULATED FLOW BEHAVIOUR

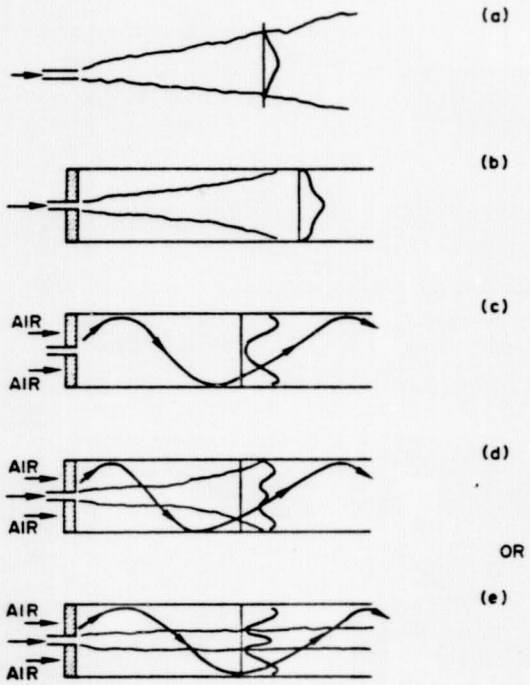

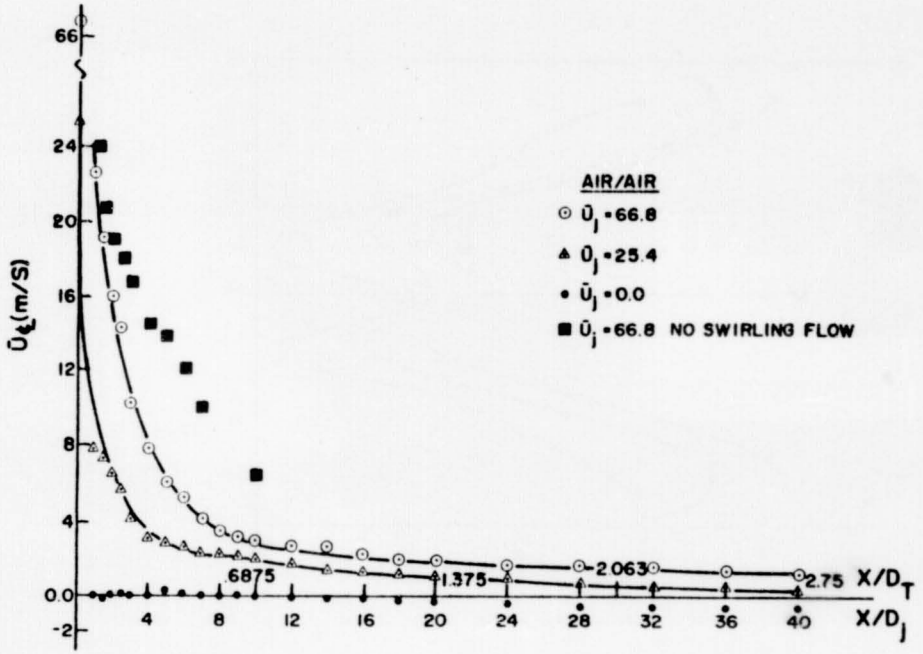

(a) Centerline Velocities at Different Flow Conditions

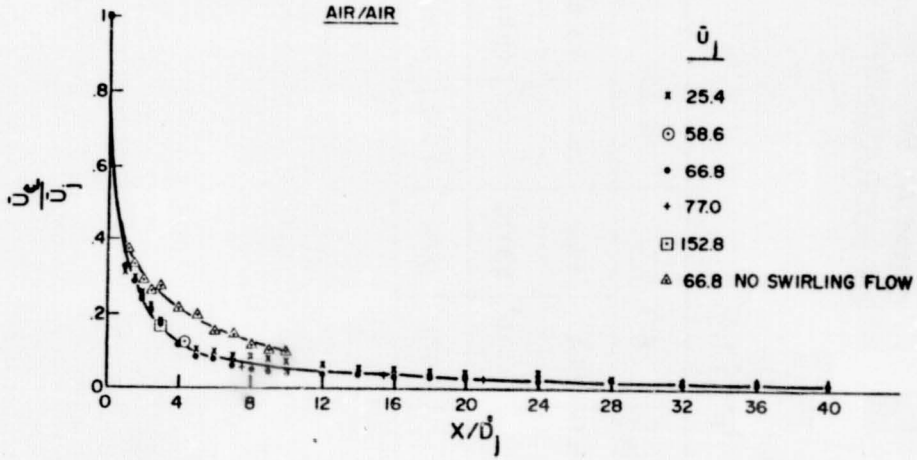

(b) Normalized Centerline Velocities at Different Conditions

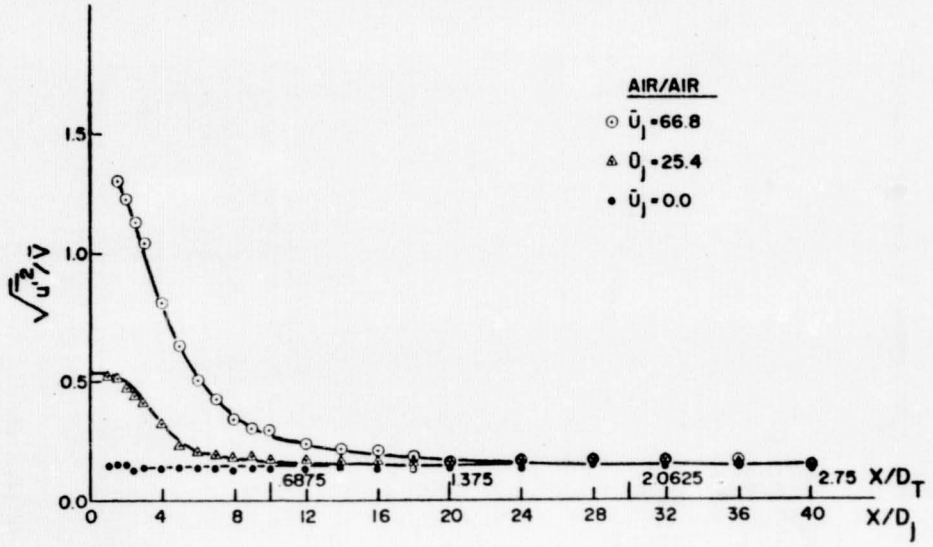

(c) Axial Distributions of $\sqrt{\overline{u'^2}}/\bar{V}$ at Different Flow Conditions

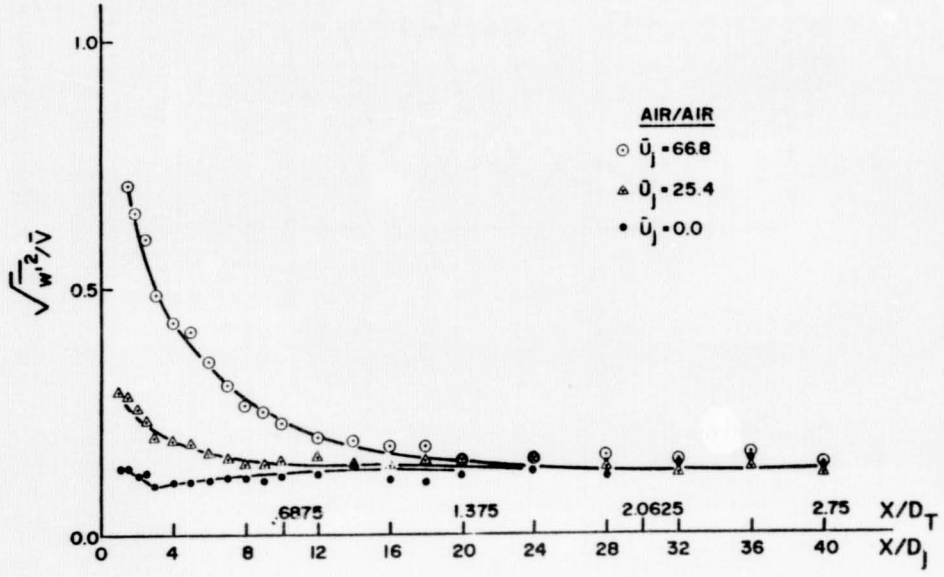

(d) Axial Distributions of $\sqrt{\overline{w'^2}}/\bar{V}$ at Different Flow Conditions

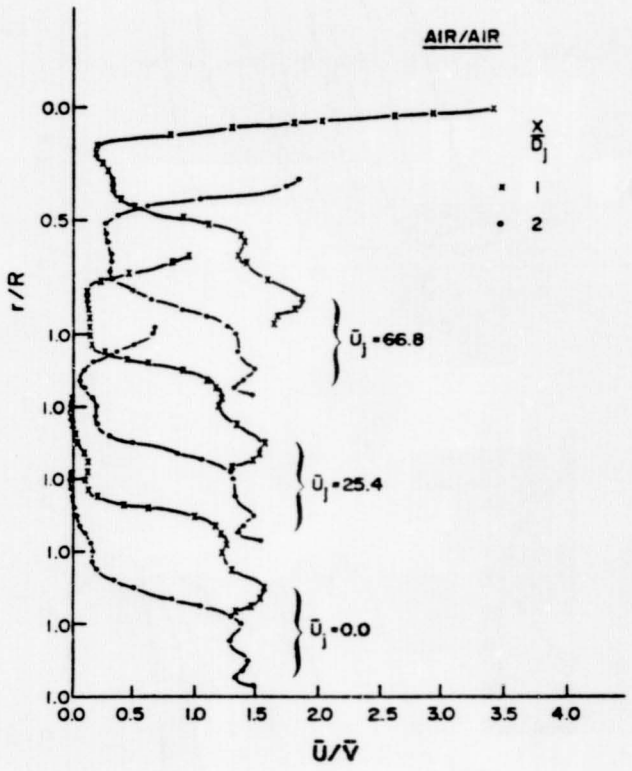

Flow Field Near the Jet at Different Flow Conditions

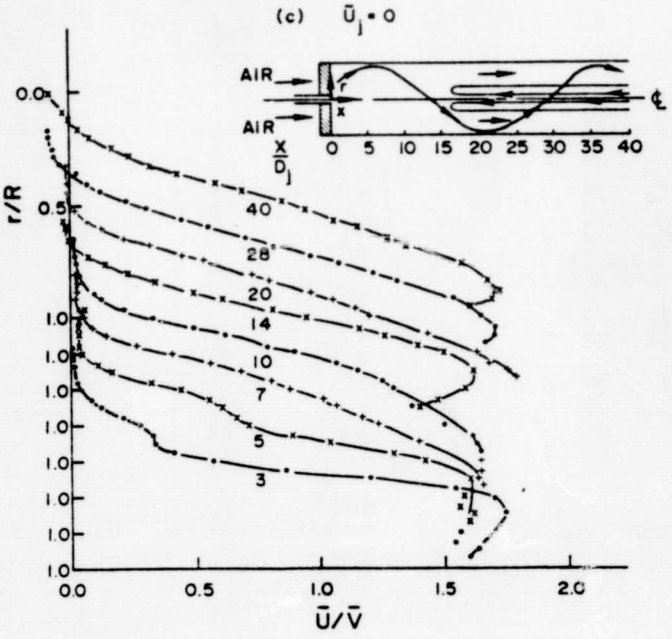

Axial Velocity Measurements at Different Locations

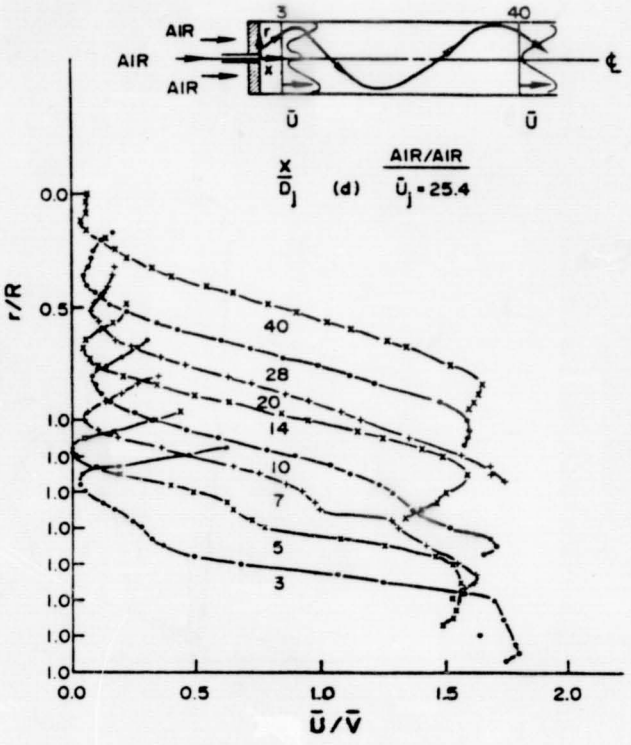

Axial Velocity Measurements at Different Locations

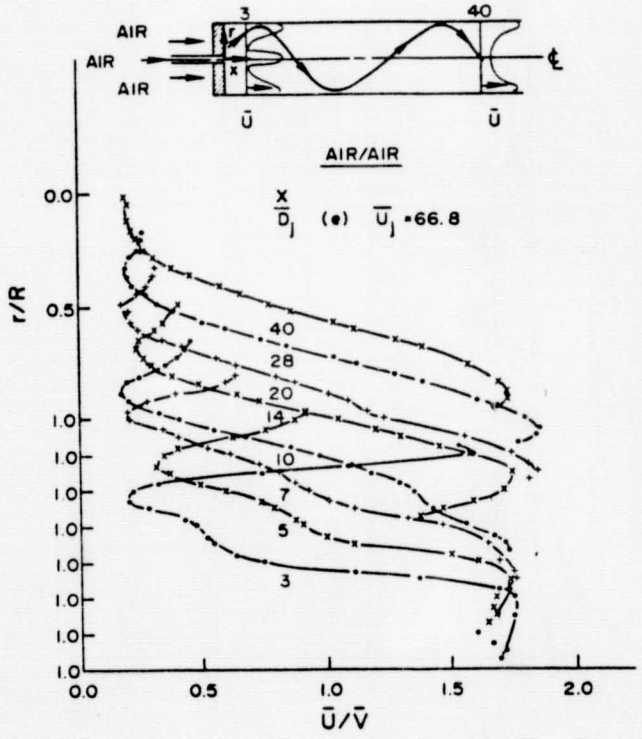

Axial Velocity Measurements at Different Locations

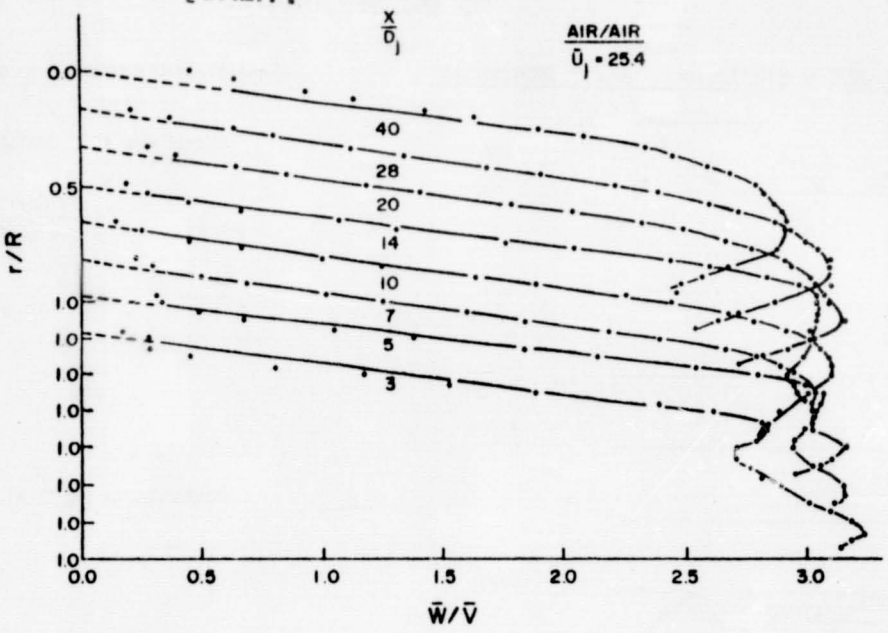

Circumferential Velocities at Different Axial Locations

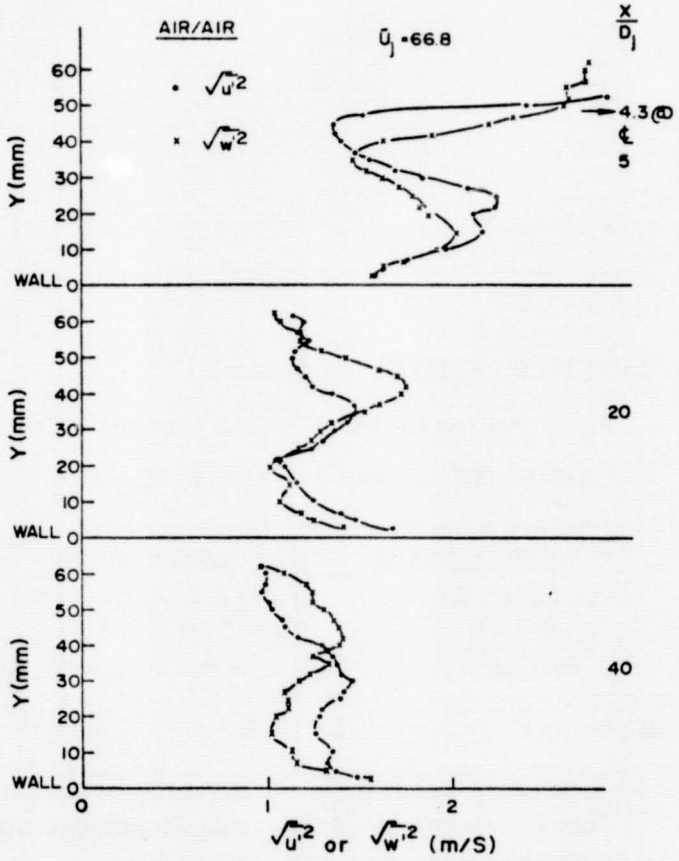

Disturbance Profiles at Different Axial Locations

HELIUM JET – SPECULATED FLOW BEHAVIOUR

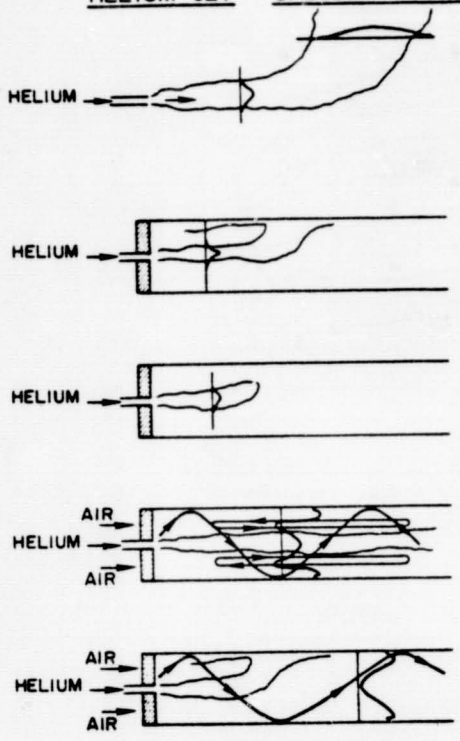

GRAVITATIONAL BUOYANCY = $g = 9.8\ m/s^2$

CENTRIFUGAL ACCELERATION = $\frac{\bar{w}^2}{R}$

$$= \frac{(19\ m/s)^2}{6.2 \times 10^{-2}\ m}$$

$$\simeq 6 \times 10^3\ m/s^2$$

RATIO = 600

DISTANCE FOR He TO RISE ONE R

$$x = \bar{U}_j\, t$$

SINCE $$\left(\rho_H + \frac{1}{2}\rho_A\right)\frac{d^2r}{dt^2} = g\left(\rho_A - \rho_H\right)$$

IF $$\rho_A = 7\rho_H$$

$$t \simeq \left(\frac{r}{.7g}\right)^{1/2}$$

$$\frac{x}{D_j} = \frac{\bar{U}_j\,(R/.7g)^{1/2}}{D_j}$$

$$= 800$$

EFFECTS OF ROTATION ON MIXING

FLUID PARTICLES ARE IN RADIAL EQUILIBRIUM DUE TO

RADIAL PRESS. GRAD. = CENTRIFUGAL FORCE

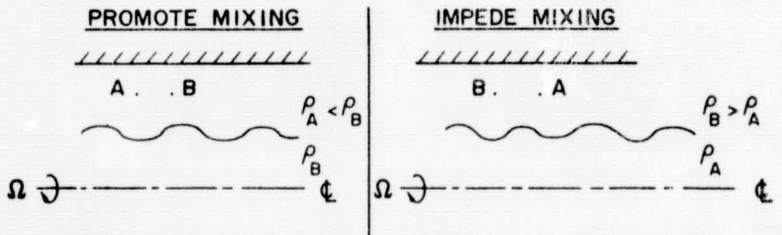

DISPLACED FLUID B CONTINUES TO MOVE TOWARDS FUEL SURFACE

DISPLACED FLUID A WILL BE FORCED BACK TOWARDS ℄

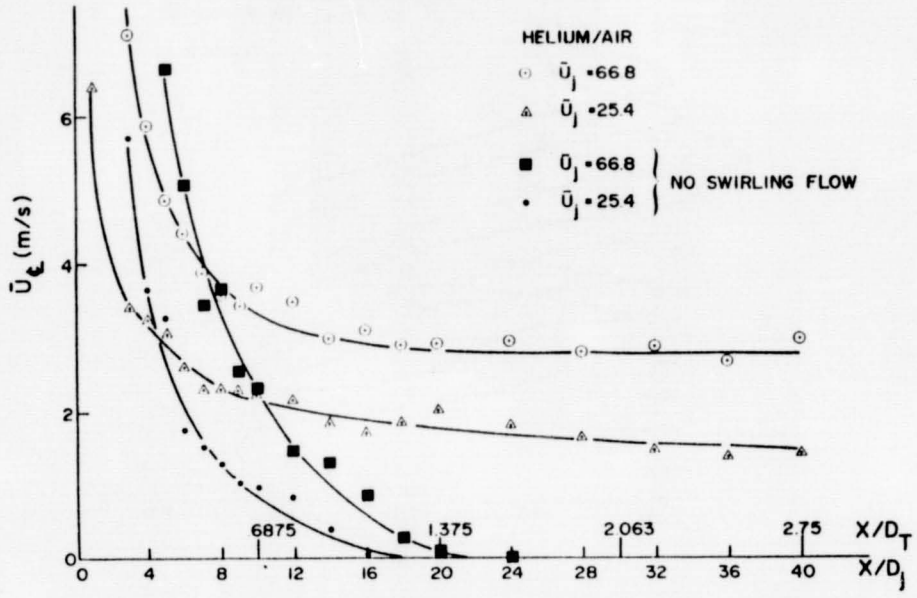

Centerline Velocities at Different Flow Conditions

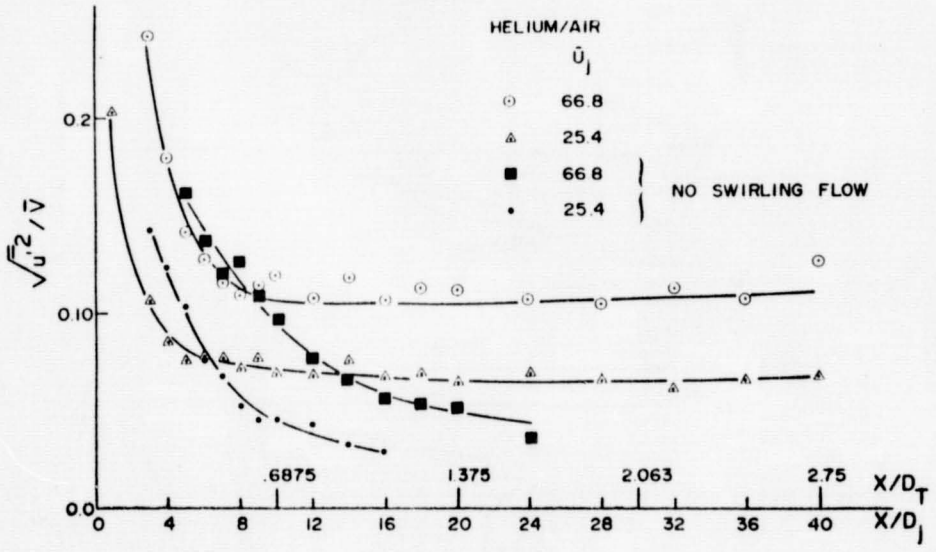

Axial Distributions of $\sqrt{\overline{u'^2}}/\bar{V}$ at Different Flow Conditions

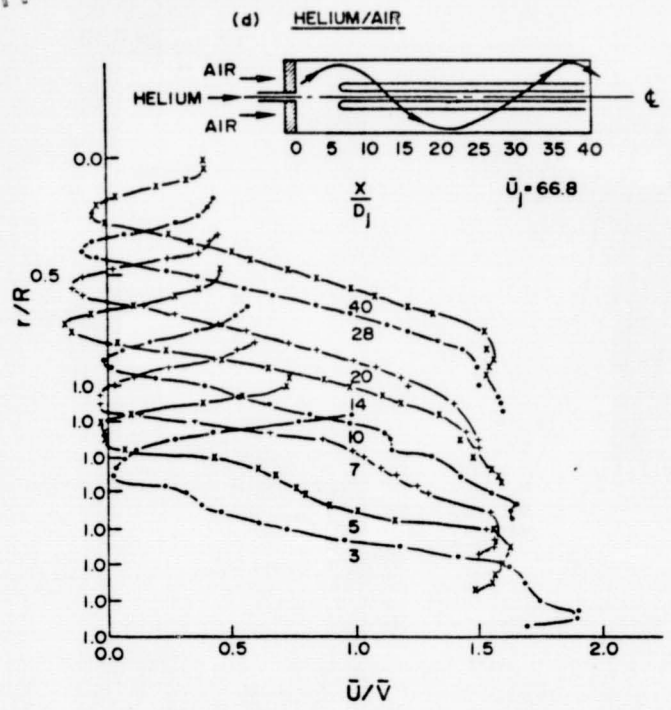

Axial Velocity Measurements at Different Locations

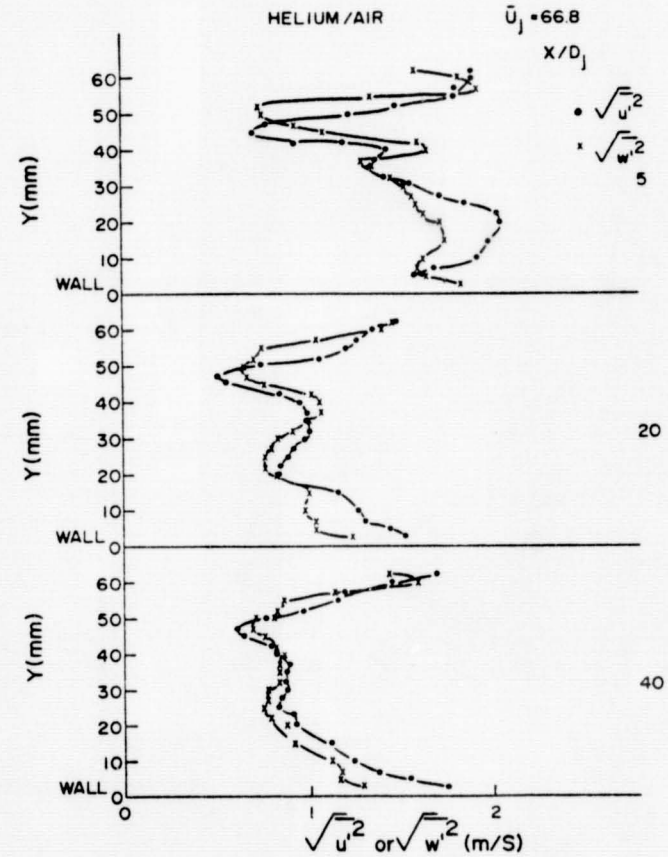

Disturbance Profiles at Different Axial Locations

SATURATED LASER FLUORESCENCE IN TURBULENT SOOTING FLAMES AT HIGH PRESSURE

Galen B. King
Campbell D. Carter
Normand M. Laurendeau

Flame Diagnostics Laboratory
School of Mechanical Engineering
Purdue University

The primary objective of this project is to develop a quantitative, single pulse, laser-saturated fluorescence (LSF) technique for measurement of radical species concentrations in practical flames. The species of immediate interest is the hydroxyl radical. Measurements will be made in both turbulent premixed and diffusion flames at pressures between 1 and 20 atm. Interferences from Mie scattering will be assessed by doping with particles or by controlling soot loading through variation of equivalence ratio and fuel type. The efficacy of the LSF method at high pressure will be addressed by comparing fluorescence and absorption measurements in a premixed, laminar flat flame at 1-20 atm.

Signal-averaging over many laser shots is sufficient to determine the local concentration of radical species in laminar flames. However, for turbulent flames, single pulse measurements are more appropriate since a statistically significant number of laser pulses is needed to determine the probability distribution function (PDF). PDFs can be analyzed to give true average properties and true local kinetics in turbulent, chemically reactive flows.

PROGRESS OF WORK

The construction phase of the high-pressure facility is nearing completion. This includes the fabrication of not only the high-pressure vessel, but also the optical table in which the pressure vessel is mounted and other support systems, including the high pressure burners and the gas flow control system.

The pressure vessel is constructed from a 109 cm long by 20 cm ID stainless steel tube, to which four 6.4 cm ID tubes are welded. Slip-on flanges are welded at the ends of these smaller tubes to hold the optical windows. Central to the design of the pressure vessel is the use of an internal burner-translation system rather than translation of the entire vessel to access the various points in the flame. This arrangement allows two dimensional movement of the burner within the pressure vessel. Maximum travel is greater than 11 cm in the vertical and 3.8 cm in the horizontal directions. The translation stage is driven by stepper motors which are in turn controlled by an Apple computer. The position of the burner is monitored with two linear transducers and a pressure transducer monitors the pressure within

the vessel. By counting the number of steps sent to the stepper motors, the position of the burner may be controlled to better than 3 μm in both travel directions.

Because of its size and mass, the pressure vessel will be located between two optical bread boards rather than on top of a single optical table. A framework to support the pressure vessel has been added to an existing table base and the optical bread boards have been mounted on the table framework. Additional modifications to the table are now underway, including (1) a cylindrical plexiglas shield to protect laboratory personnel in case of pressure failure and (2) steel plates which will surround the vessel to form a flat surface between the bread boards. A small winch is also being mounted in the ceiling of the laboratory to aid in movement of the pressure vessel during experiments.

Although initial plans for the high-pressure flame facility called for control of gases by mass flow transducers, a simpler gas flow control system will be used at this time. This strategy will allow greater variation in burner type during the exploratory stage of our research. The control system we have constructed uses ordinary regulators and rotometers. This system, while simple and easily varied, is limited to a useful pressure range of 10 atm. Therefore, we plan to eventually add mass flow controllers to the flame facility.

Two burners have been designed for initial testing of the high pressure flame facility. The first is a premixed water-cooled burner constructed with a Hasteloy, hexagonal-pattern, flame holder. The main body of this burner has been constructed and work is now in progress to shape the flame holder. A second flat flame burner is being built by McKenna Products. This burner is a scaled down version of their standard water-cooled sintered bronze, flate flame burner. The flame diameter for both burners is approximately 3 cm to avoid self-absorption problems at high pressure.

Significant advances have also been made in our ability to measure single-pulse OH radical concentrations in turbulent flames. Measurements of superequilibrium hydroxyl concentrations in nonpremixed flames at 1 atm using LSF have been made in a collaborative interaction between the Flame Diagnostics Laboratory at Purdue University and Corporate Research and Development at General Electric Company. The results of this study were presented at the 1983 Fall Meeting of the Western States Section of the Combustion Institute and a paper has been submitted to the Twentieth International Symposium on Combustion.

An improvement has also been made in our sampling technique as we can now discriminate against bad laser shots. With the use of a second sampling oscilloscope, the power level of the laser pulse is monitored and fed into a computer along with the fluorescence signal. We are currently using this technique for measurements of PAHs and will eventually incorporate it into our procedure for generating PDFs. In this method, the analogue-to-digital converter and both sampling oscilloscopes are triggered by the laser pulse and thus single pulse data for both the laser power and the fluorescence signal can be collected. Data points in which the laser pulse shape or energy level are not satisfactory are then eliminated from the data set.

BALANCED CROSS-RATE MODEL

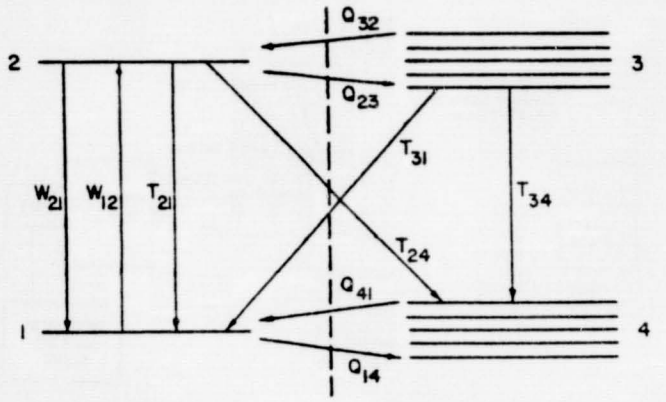

Laser-Coupled Rotational Levels

Rotational Levels Indirectly Affected by the Laser Pumping

System Rate and Conservation Equations

$$\dot{N}_1 = -N_1(W_{12}+Q_{14}) + N_2(W_{21}+T_{21}) + N_3T_{31} + N_4Q_{41}$$

$$\dot{N}_2 = N_1W_{12} - N_2(W_{21}+T_{21}+T_{24}+Q_{23}) + N_3Q_{32}$$

$$\dot{N}_3 = N_2Q_{23} - N_3(T_{31}+T_{34}+Q_{32})$$

$$N_T = N_1^0 + N_4^0 = N_1 + N_2 + N_3 + N_4$$

$$T_{ik} = Q_{ik} + A_{ik}$$

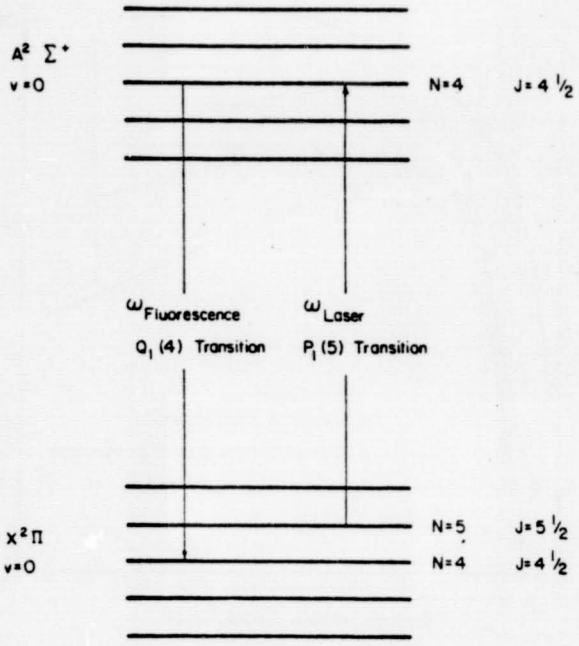

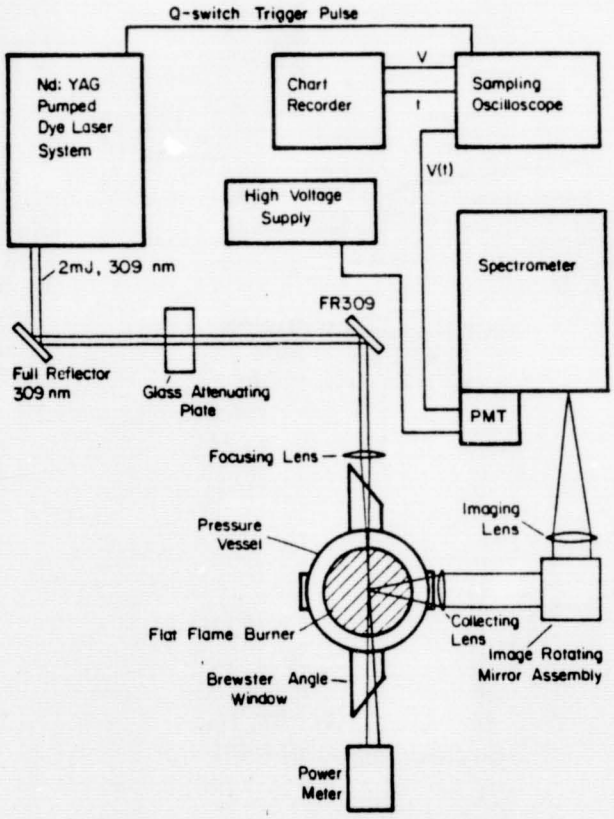

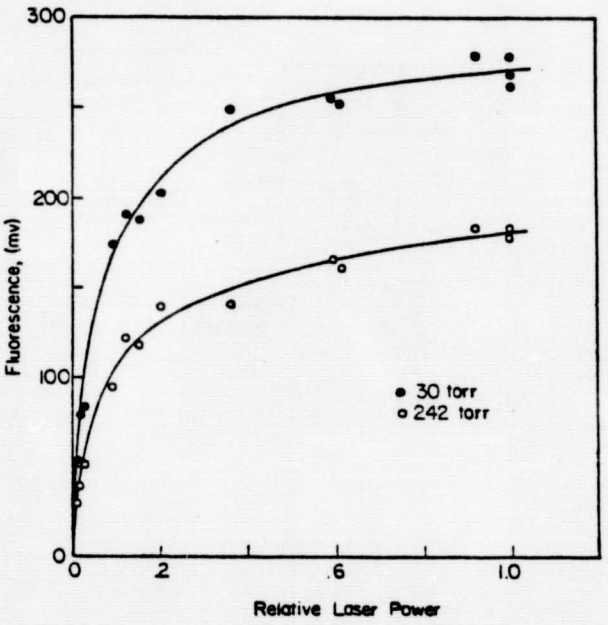

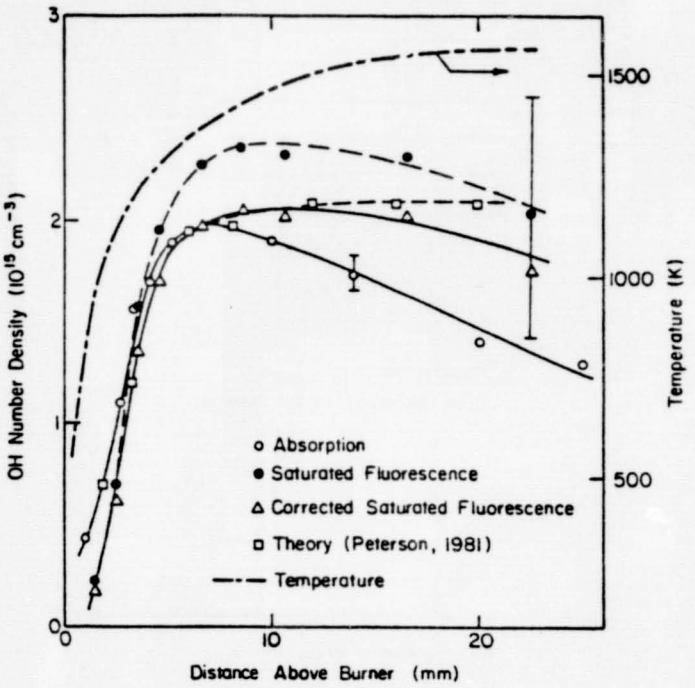

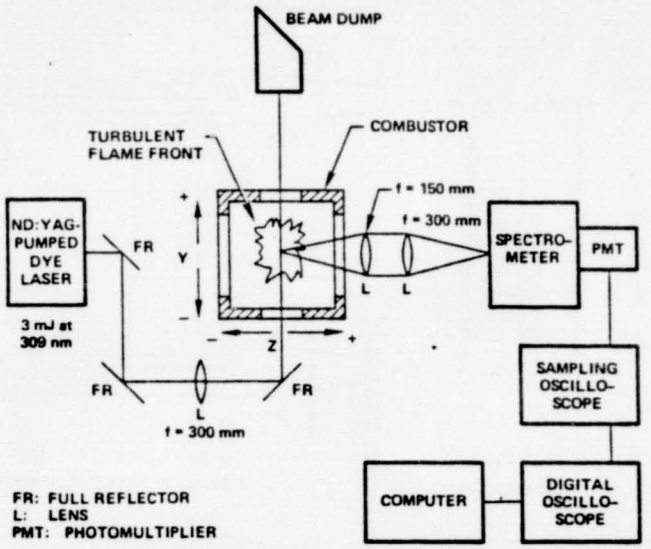

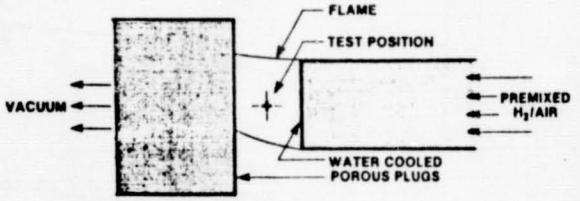

LAMINAR PREMIXED FLAME $\phi = 1$

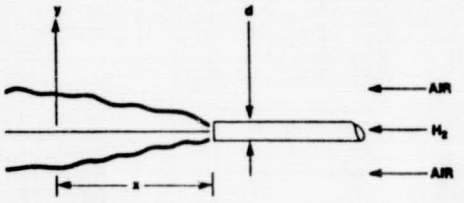

TURBULENT DIFFUSION FLAME Re = 8500
x/d = 25 y/d = 7.5

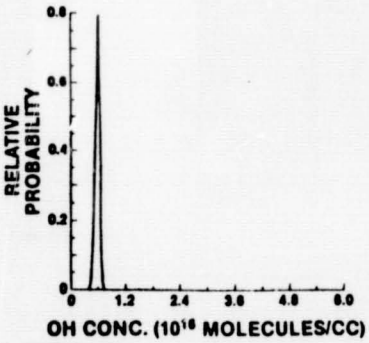

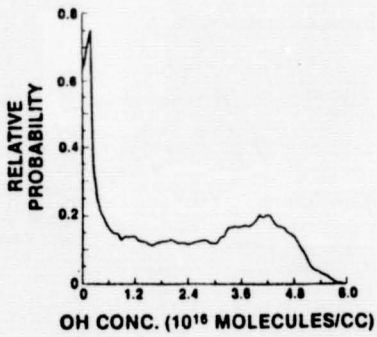

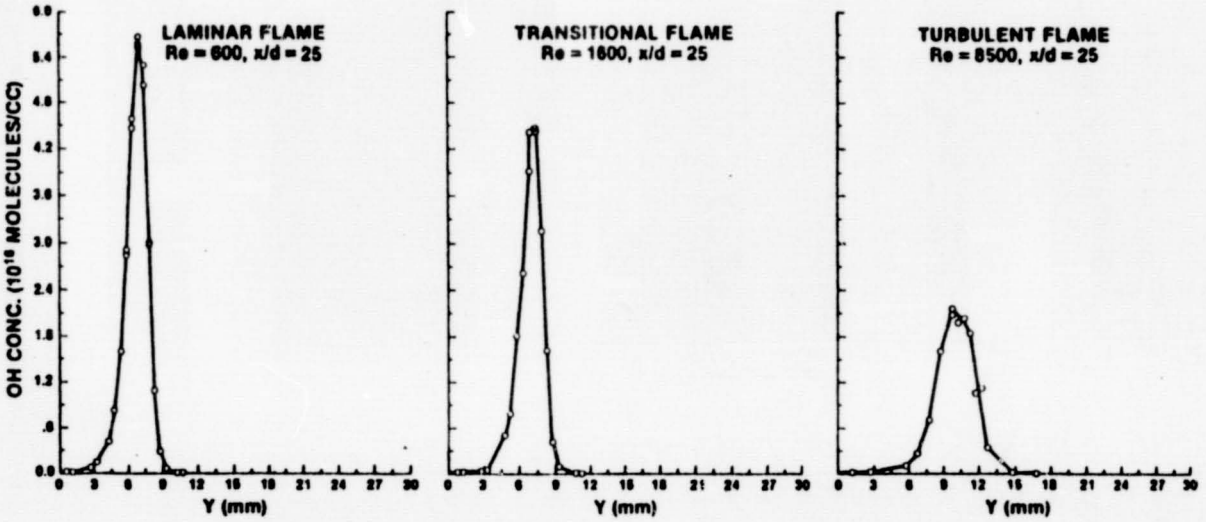

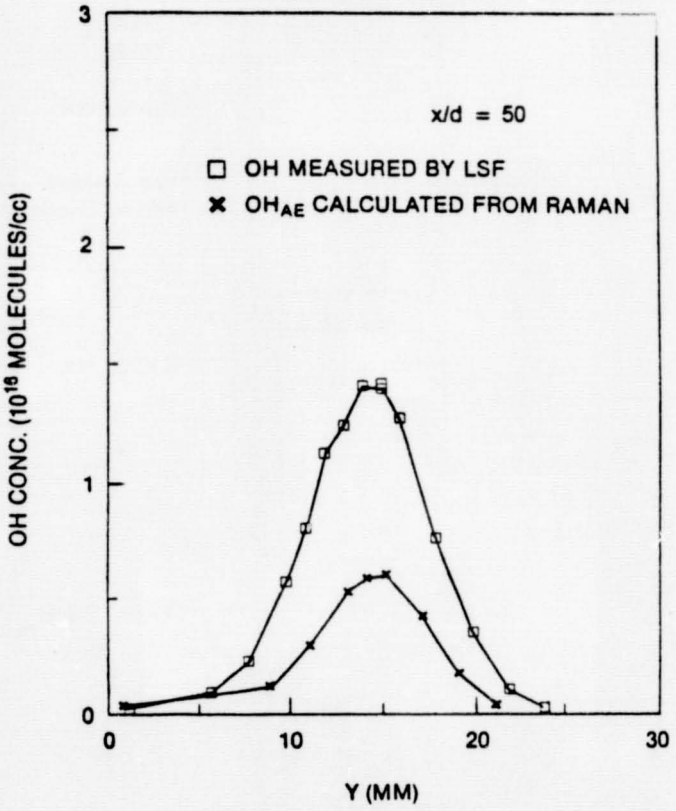

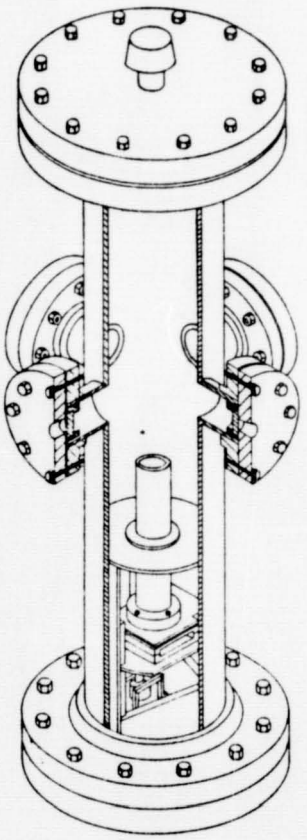

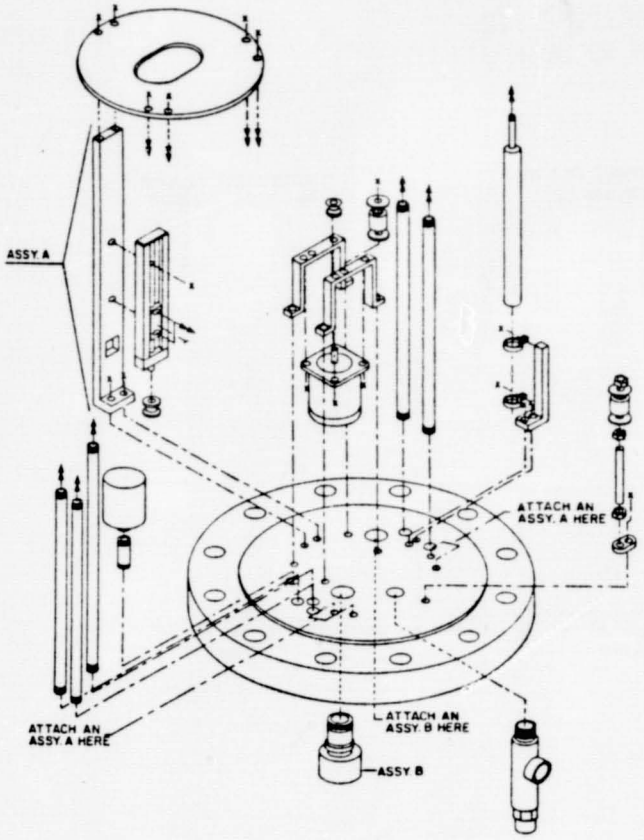

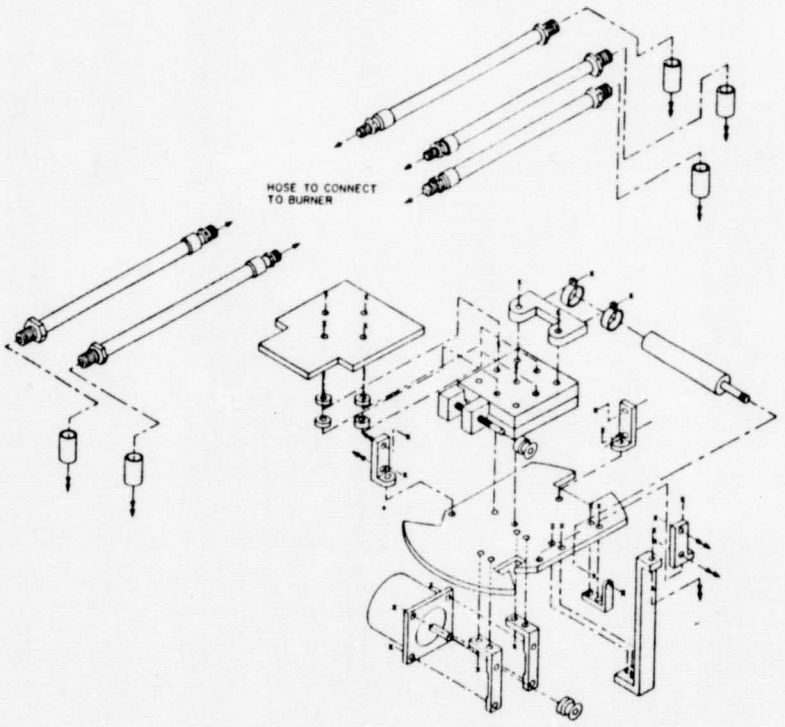

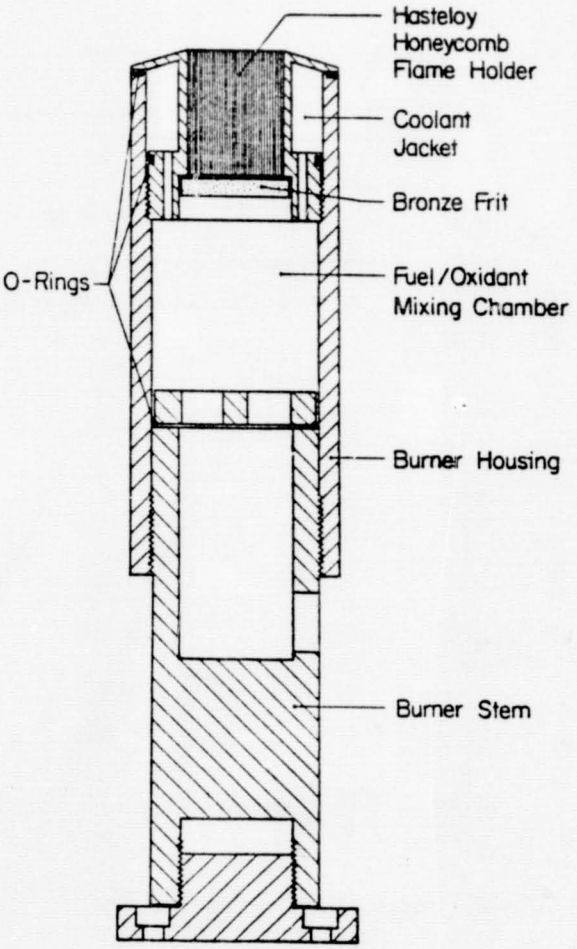

LEAN LIMIT PHENOMENA

C. K. Law
Northwestern University

Extensive theoretical and experimental research have been accomplished on the various aspects of the structure and extinction of premixed flames. The presentation will focus on only one specific topic of the lean/rich limit phenomena, namely the concept of flammability limits in the presence of flame interaction, and the existence of negative flame speeds. Attention is called to other topics reported in the publications listed; contributions from them are no less significant but will not be presented due to the lack of time.

To appreciate the importance of flame interaction, we first note that although predictions of complex flame phenomena are frequently based on understanding of isolated flames, it is clear that in most situations the combustion flow field is composed of an ensemble of flamelets, of different intensity and extent, which continuously interact with each other and thereby can cause significant modifications of the bulk combustion behavior.

In the present investigation downstream interaction between two counterflow premixed flames of different stoichiometries are experimentally studied. Various flame configurations are observed and quantified; these include the binary system of two lean or rich flames, the triplet system of a lean and a rich flame separated by a diffusion flame, and single diffusion flames with some degree of premixedness. Extinction limits are determined for methane/air and butane/air mixtures over the entire range of mixture concentrations.

The results show that the extent of flame interaction depends on the separation distance between the flames which are functions of the mixtures' concentrations, the stretch rate, and the effective Lewis numbers (Le). In particular, in a positively-stretched flow field Le<1 (>1) mixtures tend to interact strongly (weakly), while the converse holds for flames in a negatively-stretched flow.

An important consequence of flame interaction is the modification of the flammability limits of a mixture when it is stratified. If the mixture is only weakly stratified, then the conventional flammability limits for uniform mixtures may still apply. However, with more extensive stratification the stronger portion of the mixture may burn independent of the weaker portion, while the weaker portion can also burn by receiving support from the stronger flame. The mixture is made more flammable as a whole.

Our study has also established the existence of negative flames whose propagation velocity is in the same general direction as that of the bulk convective flow, being supported by diffusion alone. Their existence demonstrates the tendency of flames to resist extinction, and futher emphasizes the possibility of very lean or rich mixtures to undergo combustion.

Flame interaction is also of relevance to the modeling of turbulent flames. Within a turbulent flow field stratifications in temperature and reactant concentrations invariably exist, caused by mixing inhomogeneities or, more subtly, through the coupling between stretch and preferential diffusion even for an initially homogeneous mixture. Thus a flame kernel initiated within a turbulent eddy will manifest effects of downstream inteaction between flames of different intensities.

Publications

1. "Effects of Heat Loss, Preferential Diffusion, and Flame Stretch on Flame-Front Instability and Extinction of Propane/Air Mixtures," by S. Ishizuka, K. Miyasaka, and C. K. Law, Combustion and Flame, Vol. 45, pp. 293-308, (1982).

2. "On the Opening of Premixed Bunsen Flame Tips," by C. K. Law, S. Ishizuka, and P. Cho, Combustion Science and Technology, Vol. 28, pp. 89-96, (1982).

3. "On Stability of Premixed Flames in Stagnation-Point Flow," by G. I. Sivashinsky, C. K. Law, and G. Joulin, Combustion Science and Technology, Vol. 28, pp. 155-159, (1982).

4. "An Experimental Study of Extinction and Stability of Stretched Premixed Flames," by S. Ishizuka and C. K. Law, Nineteenth Symposium on Combustion, the Combustion Institute, Pittsburgh, Pa., pp. 327-335, (1983).

5. "Heat and Mass Transfer in Combustion: Fundamental Concepts and Analytical Techniques," Proc. of ASME-JSME Joint Thermal Engineering Conference, (Y. Mori and W. J. Yang, Ed.), Vol. 2. pp. 535-559, (1983). ** Plenary Paper**

6. "An Invariant Derivation of Flame Stretch," by S. H. Chung and C. K. Law, Combustion and flame, Vol. 55, pp. 123-125 (1984).

7. "Extinction of Premixed Flames by Stretch and Radiative Loss," by S. H. Sohrab and C. K. Law, to appear in International Journal of Heat and Mass Transfer.

8. " On the Determination of Laminar Flame Speeds from Stretched Flames," by C. K. Wu and C. K. Law, submitted.

9. "An Experimental Investigation on Flame Interaction and the Existence of Negative Flame Speeds," by S. H. Sohrab, Z. Y. Ye, and C. K. Law, submitted.

10. "Effects of Preferential Diffusion on the Burning Intensity of Curved Flames," by M. Mizomoto, Y. Asaka, S. Ikai, and C. K. Law, submitted.

1

OVERALL OBJECTIVES

- o TO UNDERSTAND THE FUNDAMENTAL MECHANISMS GOVERNING EXTINCTION OF PREMIXED FLAMES.
- o TO QUANTIFY FLAMMABILITY LIMITS OF MIXTURES AND IDENTIFY DOMINANT MECHANISMS IN OPERATION AT THESE LIMITS.
- o TO IDENTIFY POSSIBILITIES OF EXTENDING THESE EXTINCTION/ FLAMMABILITY LIMITS.

2

POTENTIAL EXTINCTION MECHANISMS

- o HEAT LOSS.
- o KINETIC TERMINATION.
- o FLAME STRETCH:
  - FLOW NONUNIFORMITY
  - FLAME CURVATURE
  - FLAME ACCELERATION

3

PREVIOUS CONTRIBUTIONS

- o FLAME STRETCH, COUPLED WITH PREFERENTIAL DIFFUSION (NON-UNITY LEWIS NUMBER) EFFECTS, WAS IDENTIFIED TO BE THE DOMINANT MECHANISM IN OPERATION AT THE FLAMMABILTY LIMITS.
- o FLAMMABILITY LIMITS, DETERMINED BY USING THE COUNTERFLOW FLAME, AGREE WELL WITH EXISTING DATA.

4

PRESENT ACCOMPLISHMENTS

- o IDENTIFIED AND QUANTIFIED THE IMPORTANCE OF FLAME INTERACTION.
- o INDENTIFIED THE EXISTENCE OF LAMINAR FLAMES WITH NEGATIVE FLAME SPEEDS.
- o STUDIED EFFECTS OF FLAME CURVATURE ON BURNING INTENSITY.
- o CRITICALLY RE-EXAMINED EXISTING METHODS IN LAMINAR FLAME SPEED DETERMINATION; PROPOSED NEW METHODOLOGY.
- o THEORETICAL STUDIES ASSOCIATED WITH THE ABOVE TOPICS.

5

IMPORTANCE OF FLAME INTERACTION

- o PRACTICAL COMBUSTION FLOW FIELDS CONSIST OF ENSEMBLES OF FLAMELETS.
- o INDIVIDUAL FLAMELETS BURN WITH DIFFERENT INTENSITY AND EXTENT.
- o INTERACTION BETWEEN THEM CAN EITHER CONTRACT OR WIDEN THE EXTINCTION LIMIT.
- o ESPECIALLY RELEVANT TO TURBULENT FLAME MODELING AND FLAME PROPAGATION IN FLOWS WITH CONCENTRATION STRATIFICATION OR POOR MIXING CHARACTERISTICS.

6

METHODOLOGY

- ESTABLISH TWO PREMIXED FLAMES OF UNEQUAL STRENGTH BY THE COUNTERFLOW OF TWO STREAMS WITH DIFFERENT MIXTURE CONCENTRATIONS.
- MAP THE FLAME CONFIGURATIONS AND EXTINCTION LIMITS AS FUNCTIONS OF STRETCH AND FUEL CONCENTRATIONS OF THE UPPER (Ω_U) AND LOWER (Ω_L) STREAMS.
- MEASURE THE TEMPERATURE PROFILE FOR THE INTERACTING FLAMES.

7

EXTINCTION LIMITS (METHANE-AIR MIXTURES)

- FOR $\Omega_L < 4\%$, $\Omega_U \approx 6\%$ AND IS INSENSITIVE TO Ω_L; WEAK INTERACTION; STRONG FLAME BURNS INDEPENDENTLY, WEAK FLAME PARASITIC.
- FOR $4\% < (\Omega_L, \Omega_U) < 6\%$, $(\Omega_L + \Omega_U)/2 \approx 5\%$; STRONG INTERACTION; SYMBIOTIC COMBUSTION.
- INTERACTION IS STRONG (WEAK) FOR LEAN (RICH) MIXTURES.
- THEORY SUBSTANTIATES THE ABOVE BEHAVIOR.

8

PRACTICAL CONCLUSIONS

- METHANE-AIR MIXTURES LEANER THAN 5% REMAINS NON-FLAMMABLE IF CONCENTRATION STRATIFICATION (OR MIXING INHOMOGENEITY) IS WITHIN 4-6%; A HIGHER STRATIFICATION WILL INDUCE BURNING.
- MIXTURES ABOVE 6% WILL ALWAYS BURN, HENCE AUGMENTED FLAMMABILITY LIMIT.
- INTERACTION IS STRONG (WEAK) FOR LEAN (RICH) MIXTURES.
- FLAMMABILTY LIMITS LESS (MORE) SUSCEPTIBLE TO CONCENTRATION STRATIFICATION FOR LEAN (RICH) MIXTURES.
- PROPANE-AIR AND BUTANE-AIR MIXTURES BEHAVE OPPOSITE TO METHANE-AIR MIXTURES.
- MIXING INHOMOGENEITY PROMOTES BURNING.
- EXISTENCE OF NEGATIVE FLAME SPEEDS DEMONSTRATES THE RESISTENCE OF FLAMES TO EXTINCTION.
- FLAME STRETCH AND PREFERENTIAL DIFFUSION ARE CRITICAL FACTORS IN DETERMINING FLAME CHARACTERISTICS, ESPECIALLY EXTINCTION.
- FRACTIONAL DEVIATION OF LEWIS NUMBER FROM UNITY CAN CAUSE SAME EXTENT OF DEVIATION OF FLAME TEMPERATURE.

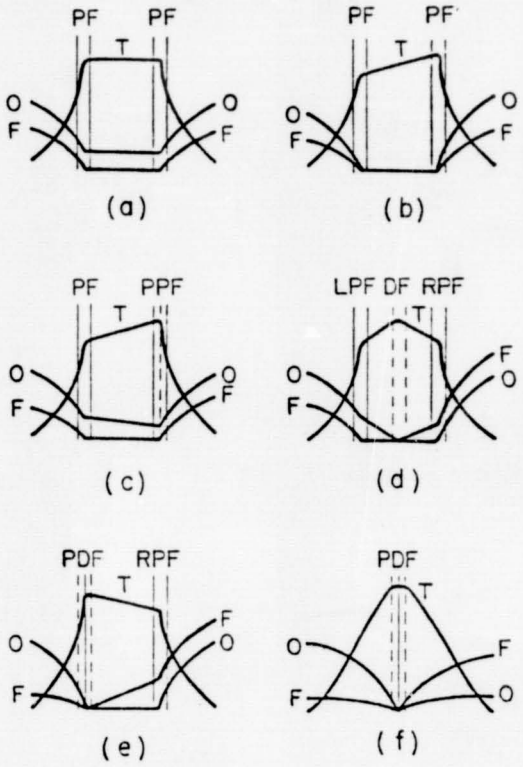

Figure 1. Possible modes of downstream interaction between two premixed flames. PF: Premixed Flame; DF: Diffusion Flame; LPF/RPF: Lean/Rich Premixed Flame; PPF: Partially Premixed Flame; PDF: Partial Diffusion Flame.

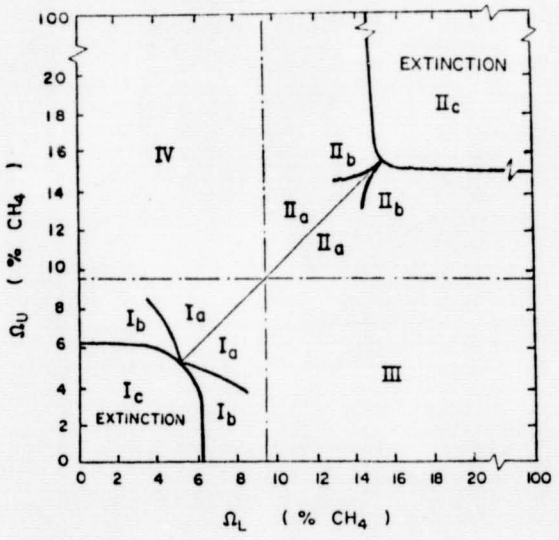

Figure 2. Mapping of the flame configurations and extinction boundaries for methane/air mixtures.

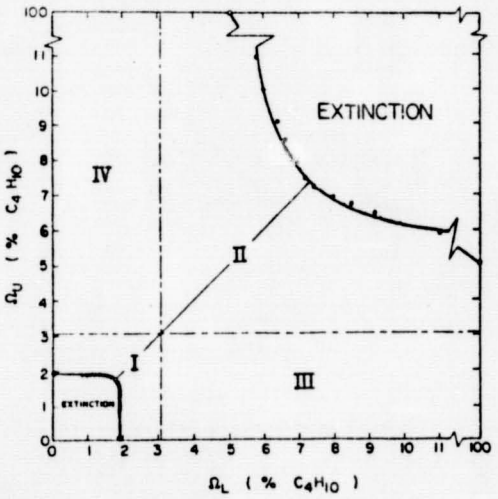

Figure 3. Mapping of the flame configurations and extinction boundaries for butane/air mixtures.

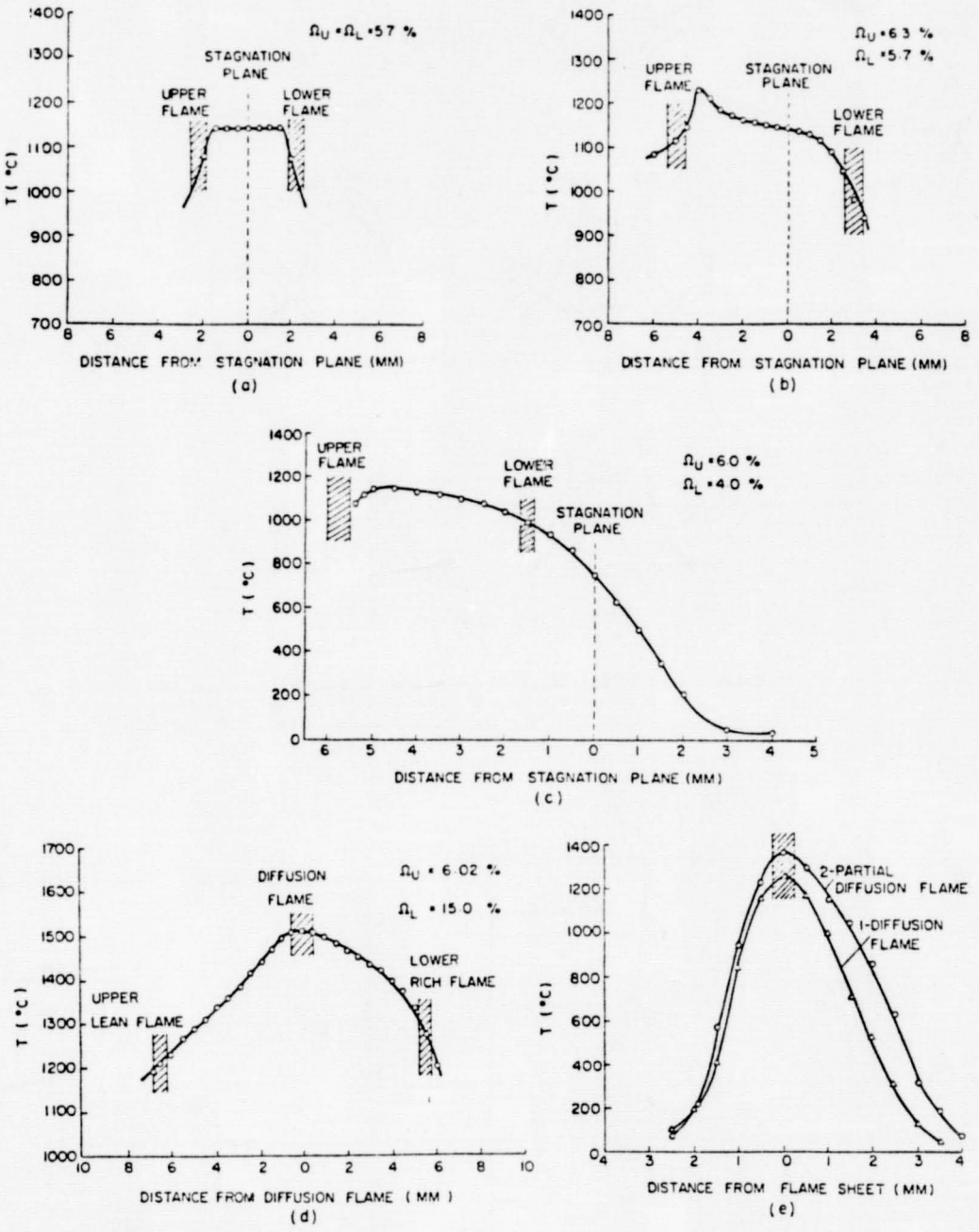

Figure 4. Temperature profiles of methane/air flames: (a) Symmetric flames; (b) Asymmetric flames; (c) Negative flame; (d) Triple flames; (e) 1. Diffusion flame; 2. Partial diffusion flame, concentrations are fuel + 10% stoich. O_2 in upper flow and air + 10% stoich. fuel in lower flow.

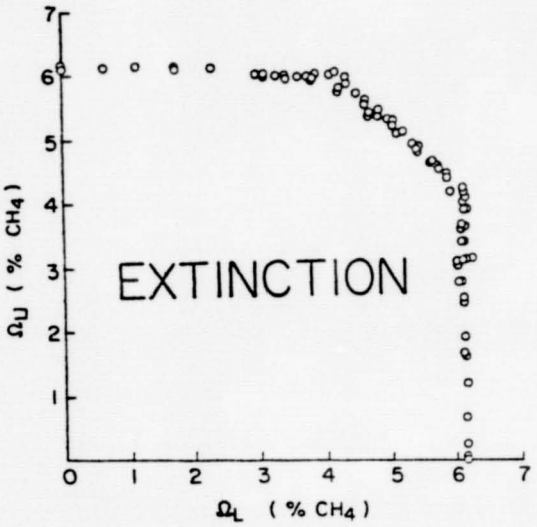

Figure 5. The extinction boundary for two lean premixed methane/air flames.

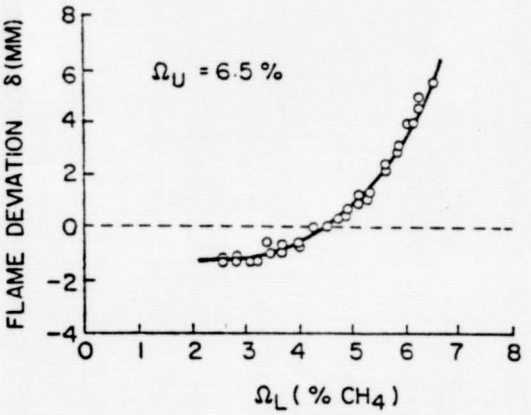

Figure 6. Distance between lower flame and stagnation surface, δ, as a function of Ω_L.

INTERACTIVE COMPUTER MODELING OF COMBUSTION CHEMISTRY
and
COALESCENCE-DISPERSION MODELING OF TURBULENT COMBUSTION

David T. Pratt
University of Washington

The goals of this research project are as follows:

1. Develop an interactive computer code for simulation of a high-intensity turbulent combustor as a "single point" inhomogeneous stirred reactor [1]. This will be developed from an existing batch processing computer code CDPSR [2].

2. Use the interactive CDPSR code as a guide for interpretation and direction of DOE-sponsored companion experiments utilizing Xenon tracer with optical laser diagnostic techniques to experimentally determine the appopriate mixing frequency, and for validation of CDPSR as a mixing-chemistry model for a laboratory jet-stirred reactor.

3. Incorporate the coalescence-dispersion model for finite rate mixing into an existing interactive code AVCO-MARK I, to enable simulation of a combustor as a modular array of stirred flow and plug flow elements, each having a prescribed finite mixing frequency, or axial distribution of mixing frequency, as appropriate.

4. Further increase the speed and reliability of the batch kinetics integrator code CREKID [3] by rewriting in vectorized form for execution on a vector or parallel processor, and by incorporating numerical techniques which enhance execution speed by permitting specification of a very low accuracy tolerance [4].

REFERENCES

1. Pratt, D. T.: Mixing and Chemical Reaction in Continuous Combustion, in Progress. Progress in Energy and Combustion Science, vol. 1, N. A. Chigier, Ed., Pergamon Press, 1976.

2. Pratt, D. T.: Coalescence/Dispersion Modeling of High Intensity Combustion, AIAA J. Energy, 3, 3, 177180, 1979.

3. Pratt, D. T.: CREK1D: A Computer Code for Transient, Gas-phase Combustion Kinetics, Paper No. WSCI 8321, Western States Section/The Combustion Institute, 1983.

4. Pratt, D. T.: Exponential-Fitted Methods for Integrating Stiff Systems of Ordinary Differential Equations: Applications to Homogeneous Gas-Phase Chemical Kinetics, paper presented at the 1984 JANNAF Propulsion Meeting, New Orleans, LA., February 1984.

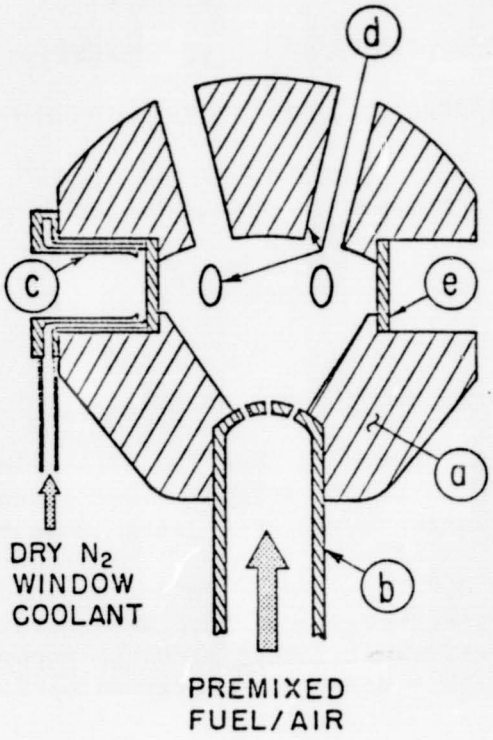

Figure 1. Jet-stirred reactor with optical access [2]. Details: (a) zirconia reactor wall; (b) reactant feed tube; (c) spring-loaded window holder; (d) exhaust ports; and (e) sapphire window

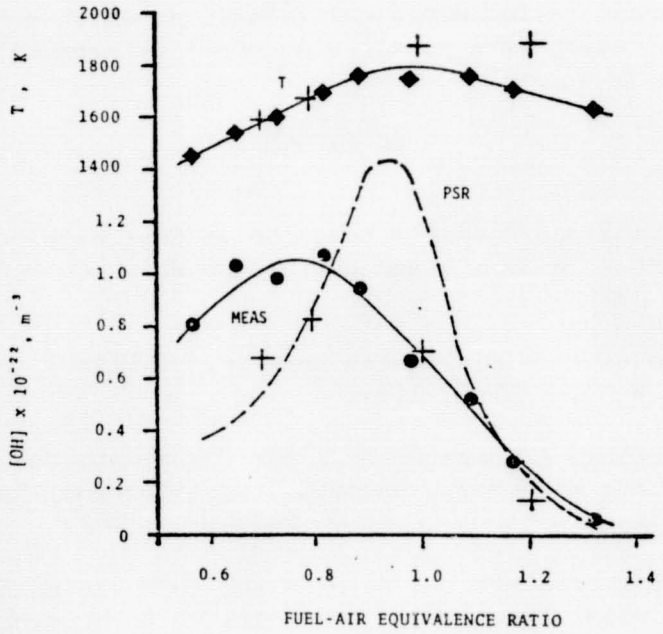

Figure 2. Measured and (homogeneous PSR) predicted [OH], and uncorrected thermocouple temperature for combustion of CH_4/air at $\dot{m}/V$ = 19 kg/cu m/sec. [2]
Crosses are values predicted from CDJSR code with NT = 20.

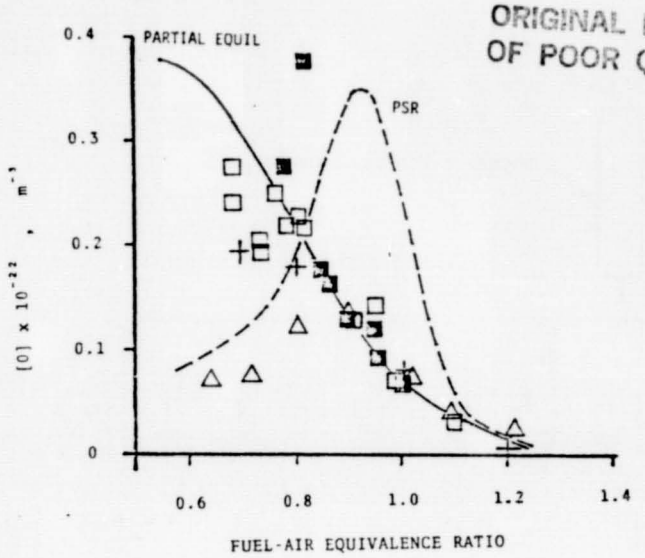

Figure 3. Measured [O] normalized by O-OH equilibrium, and (homogeneous PSR) predicted [O] for combustion of CH4/air at $\dot{m}/V$ = 19 kg/cu m/s. Crosses are predicted values from CDJSR code with NT = 20.

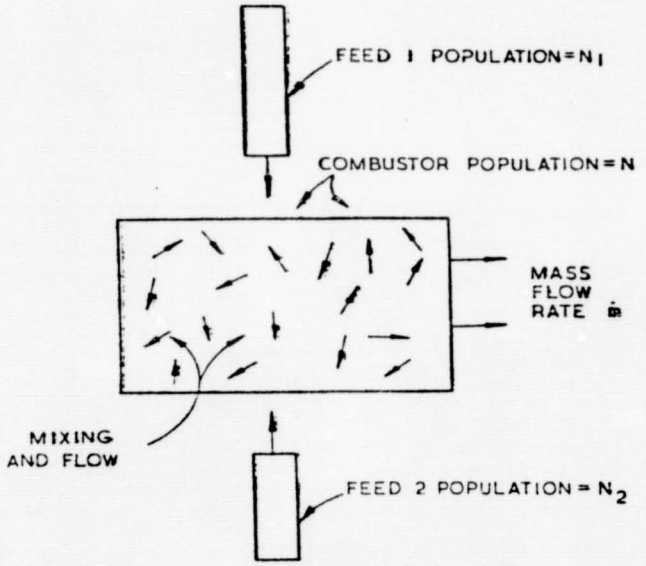

FIG. 4.1

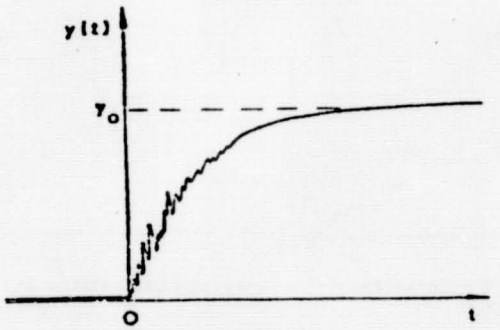

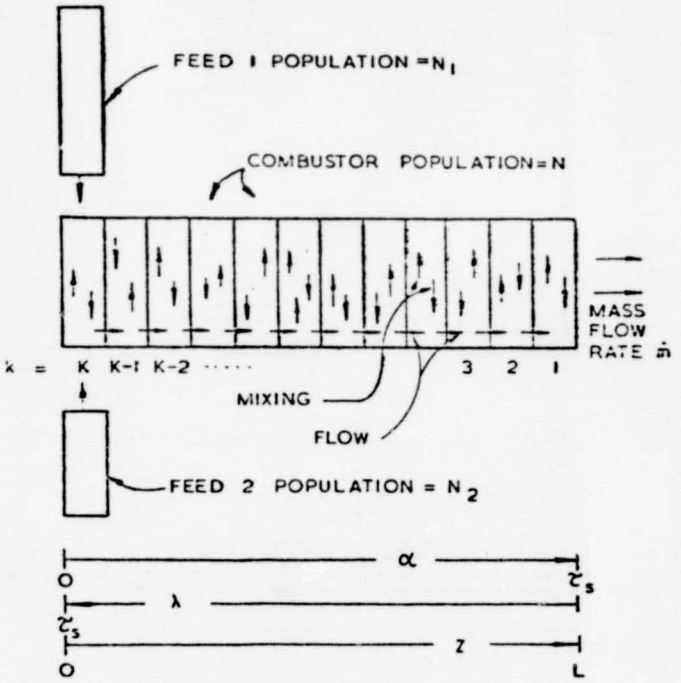

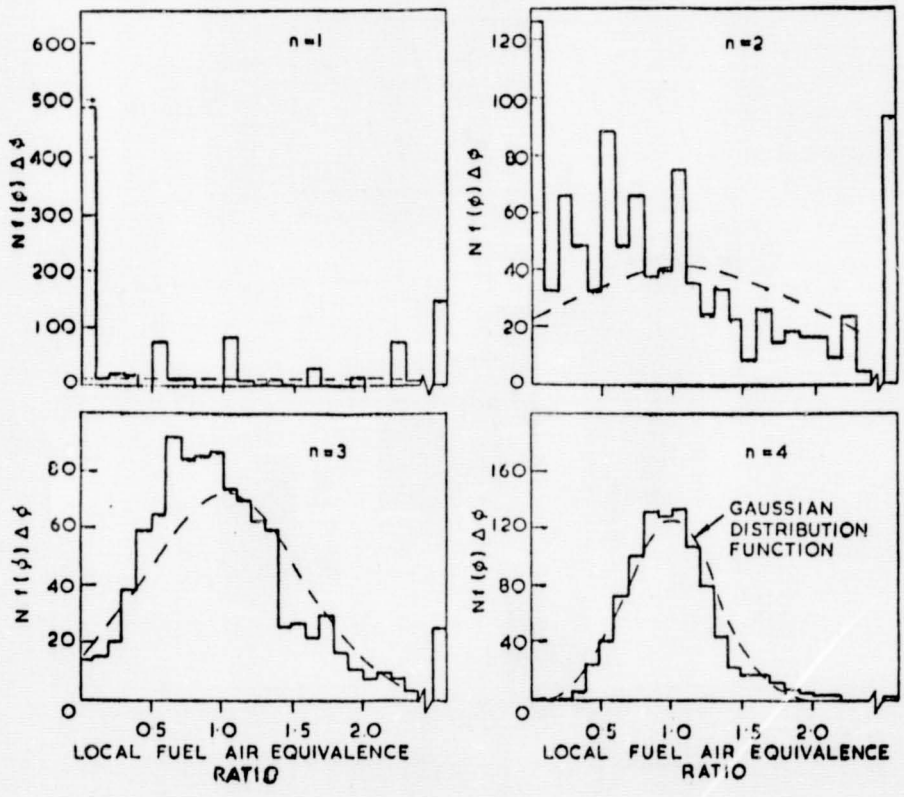

```
*** MARK2I ***
    'MARK2I' IS AN INTERACTIVE VERSION OF THE MARK-II COMBUSTOR MODEL.
THIS IS A PRELIMINARY DESIGN TOOL, A MEANS OF GAINING INTUITIVE INSIGHT
INTO EFFECTS OF CHANGES IN FUEL-AIR MIXING OR PARTITIONING ON TURN-DOWN
RATIO, COMBUSTION EFFICIENCY AND POLLUTANT FORMATION RATES.
AN INITIAL DATA SET IS TAKEN FROM DATA FILE 'MARK2.DAT' BUT CAN BE ALTERED
INTERACTIVELY, AND USED IN CONSECUTIVE RUNS.
    MARK-II REPRESENTS A SIMPLE BRAGG COMBUSTOR CONSISTING OF A
MAXIMUM OF 9 FLOW ELEMENTS WITH THE ADDITION OF A SINGLE RECYCLE
ELEMENT. FLOW ELEMENT TYPES MAY INCLUDE:
   1) NON-REACTING MIXERS ('MIX'), IN WHICH THE CHEMICAL REACTIONS ARE
ASSUMED TO HAVE STOPPED DURING THE MIXING PROCESS;
   2) PERFECTLY STIRRED REACTORS ('PSR'), WITHIN WHICH INTENSE SELF- OR
BACK-MIXING IS ASSUMED TO OCCUR, SO THAT THERE ARE NO AXIAL GRADIENTS;
   3) PLUG FLOW REACTORS ('PFR').
    THE USER MAY DEFINE THE MODEL AS HAVING UP TO 9 ELEMENTS IN
SERIES WITH AIR AND FUEL INLET JETS AT EACH ELEMENT. THE RECYCLE ELEMENT
MAY BE OF ANY OF THE THREE FLOW TYPES, AND MUST RECYCLE FROM A HIGHER
NUMBERED ELEMENT TO A LOWER. COOLING BOUNDARY LAYER EFFECTS AND CHEMICAL
REACTIONS WITHIN THE BOUNDARY LAYER ARE NOT CONSIDERED.

--- PLEASE WAIT A MOMENT WHILE INITIALIZATION IS COMPLETED.

--- INITIALIZED -- PRESS <RETURN> TO BEGIN --
```

```
*** INPUT DATA ***
   FLOW          AREA          LENGTH        FLOW        INLET AIR       INLET FUEL
 ELEMENT#      (SQ.IN)        (INCHES)       TYPE         (LBM/S)         (LBM/S)
    1        1.4600E+02     4.0000E-01       PSR      1.3450E+00      9.7200E-02
    2        1.4600E+02     1.0000E-01       MIX      6.9600E-01      0.0000E-01
    3        1.4600E+02     1.5000E+00       PSR      0.0000E-01      0.0000E-01
    4        1.4500E+00     2.0000E-01       MIX      7.9500E-01      0.0000E-01
RECYCLE      1.4600E+02     1.0000E+00       MIX       RECYCLE  20.00% OF # 3
                                                      OUTFLOW TO # 2 INFLOW

 AIR TEMP =  2.1000E+02 F        COMBUSTOR PRESSURE =  2.2100E+00 ATM
FUEL TEMP =  8.0000E+01 F      LOWER HEATING VALUE =  1.8500E+04 BTU/LBM

SELECT AN OPTION BY NUMBER:
-0- RUN WITH THIS DATA SET              -4- CHANGE NOMINAL COMBUSTOR PRESSURE
-1- CHANGE AIR TEMPERATURE              -5- CHANGE RECYCLE ELEMENT STATUS
-2- CHANGE FUEL TEMPERATURE             -6- CHANGE FLOW ELEMENTS STATUS
-3- CHANGE LOWER HEATING VALUE          -7- INSPECT SCHEMATIC MODEL LAYOUT
OPTION? (0-7) 7
```

MARK-II MODEL SCHEMATIC LAYOUT

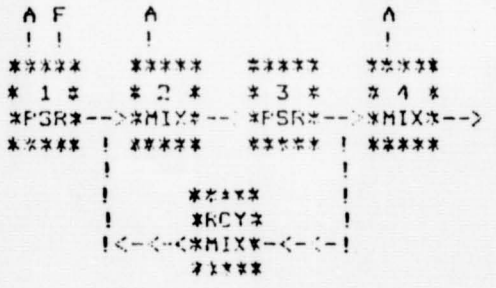

PRESS RETURN TO CONTINUE

FAST ALGORITHMS FOR COMBUSTION KINETICS CALCULATIONS: A COMPARISON*

Krishnan Radhakrishnan**
NASA Lewis Research Center

Many practical problems arising in chemically reacting flows require the simultaneous numerical integration of large sets of chemical kinetic rate equations of the type shown in figure 1. The initial value problem is that of finding the composition and temperature at the end of a prescribed time interval, given the initial mixture composition and temperature, the pressure, and the reaction mechanism. Multi-dimensional modeling of reactive flows requires the integration of the system of ordinary differential equations (ode's) given in figure 1 at several thousand grid points. To make such calculations practicable, it is necessary to have a very fast batch chemistry integrator.

To identify the fastest algorithm currently available for the numerical integration of chemical kinetic rate equations, several algorithms have been examined. In the present paper, we summarize our findings to date -- details are available in references (1) and (2). The algorithms examined in this work include two general-purpose codes EPISODE and LSODE (refs. 3 and 4), and three special-purpose (for chemical kinetic calculations) codes CHEMEQ (ref. 5), CREK1D (refs. 6 and 7), and GCKP84 (refs. 8 and 9). In addition, an explicit Runge-Kutta-Merson differential equation solver (ref. 10) (IMSL Routine DASCRU) is used to illustrate the problems associated with integrating chemical kinetic rate equations by a classical method. These methods are summarized in figure 3.

The algorithms summarized in figure 3 were applied to two test problems drawn from combustion kinetics. These problems, summarized in figure 4, included all three combustion regimes: induction, heat release and equilibration. Figures 5 and 6 present variations of the temperature and species mole fractions with time for test problems 1 and 2, respectively. Both test problems were integrated over a time interval of 1 ms in order to obtain near-equilibration of all species and temperature.

Of the codes examined in this study, only CREK1D and GCKP84 were written explicitly for integrating exothermic, non-isothermal combustion rate equations. These therefore have built-in procedures for calculating the temperature (T). For the other codes, two different methods, labeled as Methods A and B, were used to compute T. The following convention was adopted in naming these other codes: those using temperature method A were given the suffix-A (e.g. LSODE-A) and those using temperature method B were given the suffix-B (e.g. LSODE-B). In Method A, T was calculated from the mole numbers and the initial mixture enthalpy using an algebraic energy conservation equation (given in figure 7) and a Newton-Raphson iteration technique. In this method, the temperature is not an explicit independent variable, so the number of ode's is

* Work partially funded by NASA Grants NAG3-147 and NAG3-294.

** NRC-NASA Research Associate: on leave from The University of Michigan, Dept. of Mechanical Engineering and Applied Mechanics, Ann Arbor, MI 48109.

equal to the number, NS, of distinct chemical species in the mixture. The integrator therefore tracks only the solutions for the species mole numbers. In Method B, the temperature was treated as an additional independent variable and evaluated by integrating its time-derivative given in figure 7. In this method, the number of ode's is equal to NS+1, and the integrator tracks the solutions for both the temperature and the species mole numbers.

All codes were run on the NASA Lewis Research Center's IBM 370/3033 computer using single-precision accuracy, except GCKP84 which was in double-precision. A typical computational run consisted of initializing the species mole numbers, temperature, and CPU time. The integrator was then called with values for the necessary input parameters. On return from the integrator, the total CPU time required to solve the test problem was calculated. Other performance parameters were also recorded -- see reference (2) for details.

Figures 8 and 9 present the computational work (expressed as the CPU time in seconds) plotted against the local error tolerance, EPS, for test problems 1 and 2, respectively. For all codes except EPISODE, EPS is the local relative error tolerance. For EPISODE, EPS is a mixed error tolerance -- relative for species with initially nonzero mole numbers and for the temperature (method B) and absolute for species with initially zero mole numbers. Also shown on figures 8 and 9 are the CPU times required by the explicit Runge-Kutta method for one value of EPS. Note the excessive CPU times required by this technique. Its use would make multidimensional modeling of practical combustion devices prohibitively expensive.

For test problem 1, very small values for EPS had to be used for EPISODE (figure 8). For values of EPS $\geq 5 \times 10^{-6}$, EPISODE predicted little or no change in the composition and temperature after an elapsed time of 1 ms. Similar remarks apply to test problem 2 (figure 9), for which values of 10^{-4} and 10^{-3} had to be used for EPISODE-A and EPISODE-B, respectively. Although the runs with EPISODE-B and EPS $\geq 5 \times 10^{-4}$ were successfully completed, the solutions (especially for minor species) were significantly different from those given in figure 6. With GCKP84 and EPS = 10^{-2}, the solution for test problem 1 exhibited serious instability and so was terminated. A more detailed discussion of the accuracy of the codes tested in this study can be found in reference (2).

Examination of figure 8 shows that the difference in computational work required by methods A and B is small for test problem 1, with method B being more efficient. For test problem 2 (figure 9), the difference is small for large values of EPS. But for small values of EPS the difference is more marked, with method A being significanlty superior to method B.

Figures 8 and 9 show that LSODE and CREK1D are superior to the other codes. EPISODE is an attractive alternative, especially for test problem 2. However, in using EPISODE, a word of caution is in order. The computational work can be strongly dependent on the value for the initial steplength (H0) selected by the user. A poor guess for H0 can make EPISODE pronibitively expensive to use. Figure 10 illustrates this behavior for test problem 2. Note an order of magnitude increase in the CPU time for a change in H0 from 10^{-7} to 10^{-8} s. Although not shown here, a poor guess for H0 also resulted in inaccurate and unstable solutions. In addition, as discussed in reference (2), the error control performed by EPISODE is unsatisfactory for problems of the

type examined in this study.

A simple method for increasing the efficiency of the algorithms as applied to the present problem was explored. This involved updating the rate constants k_j and k_{-j} (which was calculated from k_j and the concentration equilibrium constant) only for temperature changes greater than an amount ΔT. To avoid a trial and error search for the optimum value of ΔT -- defined as that value which results in minimum computational work -- an approximation for it was derived and is presented in figure 11. Comparisons of figure 12 with figures 7 and 8 show the significant reductions in computational work realized by use of the above approximation for ΔT.

References

1) Radhakrishnan, K., "A Comparison of the Efficiency of Numerical Methods for Integrating Chemical Kinetic Rate Eqautions," NASA TM, 1984. Presented at the 1984 JANNAF Propulsion Conference, Specialists Session, New Orleans, LA, 7-9 February, 1984.

2) Radhakrishnan, K., "A Comparison of Numerical Techniques for the Integration of Stiff ODE's arising in Combustion Chemistry," NASA TP, 1984.

3) Hindmarsh, A.C. and Byrne, G.D., "EPISODE: An Effective Package for the Integration of Systems of Ordinary Differential Equations," Lawrence Livermore Laboratory Report UCID-30122, Rev. 1, 1977.

4) Hindmarsh, A.C., "ODEPACK, A Systematized Collection of ODE Solvers," Lawrence Livermore Laboratory Report UCRL-88007, 1982.

5) Young, T.R. and Boris, J.P., "A Numerical Technique for Solving Stiff Ordinary Differential Equations Associated with the Chemical Kinetics of Reactive-Flow Problems," J. Physical Chemistry, 81, 1977, pp. 2424-2427.

6) Pratt, D.T., "CREK-1D: A Computer Code for Transient, Gas-Phase Combustion Kinetics," Paper 83-21, Proceeding of the Spring Technical Meeting of the Western States Section of the Combustion Institute, April 1983.

7) Pratt, D.T. and Radhakrishnan, K., "CREK-1D: A Computer Code for Transient, Gas-Phase Combustion Kinetics," to appear as a NASA Contractor Report, 1984

8) Zeleznik, F.J. and McBride, B.J., "Modelling the Internal Combustion Engine," NASA RP1094, 1984.

9) Bittker, D.A. and Scullin, V.J., "GCKP84-General Chemical Kinetics Code for Gas-Phase Flow and Batch Processes Including Heat Transfer," NASA TP, 1984.

10) Fox, L. (ed.), "Numerical Solution of Ordinary and Partial Differential Equations," Addison-Wesley Publishing Co., Inc., Reading, MA, 1962.

11) Pratt, D.T., "New Computational Algorithms for Chemical Kinetics," National Bureau of Standards Special Publication 561, 1979, pp. 1265-1279.

Adiabatic, Constant-Pressure, Gas-Phase Chemical Reaction

$$\frac{dn_i}{dt} = f_i(n_k,T) \quad ; \quad i,k = 1,NS$$

$$f_i = -\rho^{-1} \sum_{j=1}^{JJ} (\nu_{ij}' - \nu_{ij}'')(R_j - R_{-j})$$

$$R_j = k_j \prod_{k=1}^{NS} (\rho n_k)^{\nu_{kj}'}$$

$$R_{-j} = k_{-j} \prod_{k=1}^{NS} (\rho n_k)^{\nu_{kj}''}$$

$$k_j = A_j T^{N_j} \exp(-E_j/RT)$$

$$k_{-j} = A_{-j} T^{N_{-j}} \exp(-E_{-j}/RT)$$

In the above equations,

f_i = molar rate of formation of species i per unit mass of mixture, kmol-i/kg-mixture s
k_j, k_{-j} = forward and reverse rate constants for reaction j
n_j^i = mole number of species i, kmol-i/kg-mixture
A_j, A_{-j} = pre-exponential constants in forward and reverse rate equations for reaction j
E_j, E_{-j} = activation energy in forward and reverse rate equations for reaction j, cal/mole
JJ = number of distinct elementary reactions in mechanism
NS = number of distinct species in gas mixture
R = universal gas constant, 1.987 cal/mol K
R_j, R_{-j} = forward and reverse molar reaction rates per unit volume for reaction j, kmol/m^3 s
T = temperature, K
ρ = mixture mass-density, kg/m^3
ν_{ij}' ν_{ij}'' = stoichiometric coefficients of species i in reaction j as a reactant, and as a product, respectively

Figure 1 Governing Ordinary Differential Equations

Given

Initial Mixture Composition and Temperature

Pressure

Reaction Mechanism

Find, at the End of a Prescribed Time Interval

Mixture Composition and Temperature

Figure 2 Problem Statement

Method	Description
CCKP84	Details not yet available.
CREK1D	Variable-step, predictor-corrector method based on an exponentially-fitted trapezoidal rule; includes filtering of ill-posed initial conditions and automatic selection of Jacobi-Newton iteration or Newton iteration.
LSODE EPISODE	Variable-step, variable-order backward-differentiation method with a generalized Newton iteration*.
CHEMEQ	Variable-step, second-order predictor-corrector method with an asymptotic integration formula for stiff equations.
DASCRU	Variable-step, fourth-order, explicit Runge-Kutta-Merson solver.

*Other options are included in these packages.

Figure 3 Summary of Methods Studied

Two Problems Describing Adiabatic, Constant Pressure Chemical Reactions

Test Problem 1:

Combustion of a Mixture of 33 % CO and 67 % H_2 with 100 % Theoretical Air
(taken from reference 11)

12 Reactions
11 Species + Temperature

Pressure = 10 atm.
Initial Temperature = 1000 K
Reaction Duration: 1 ms

Test Problem 2:

Combustion of a Stoichiometric Mixture of H_2 and Air
(taken from reference 9)

30 Reactions
15 Species + Temperature

Pressure = 2 atm.
Initial Mixture Temperature = 1500 K
Reaction Duration: 1 ms

Both Problems Include All Three Regimes of Combustion:
Induction, Heat Release and Equilibration.

Figure 4 Test Problems

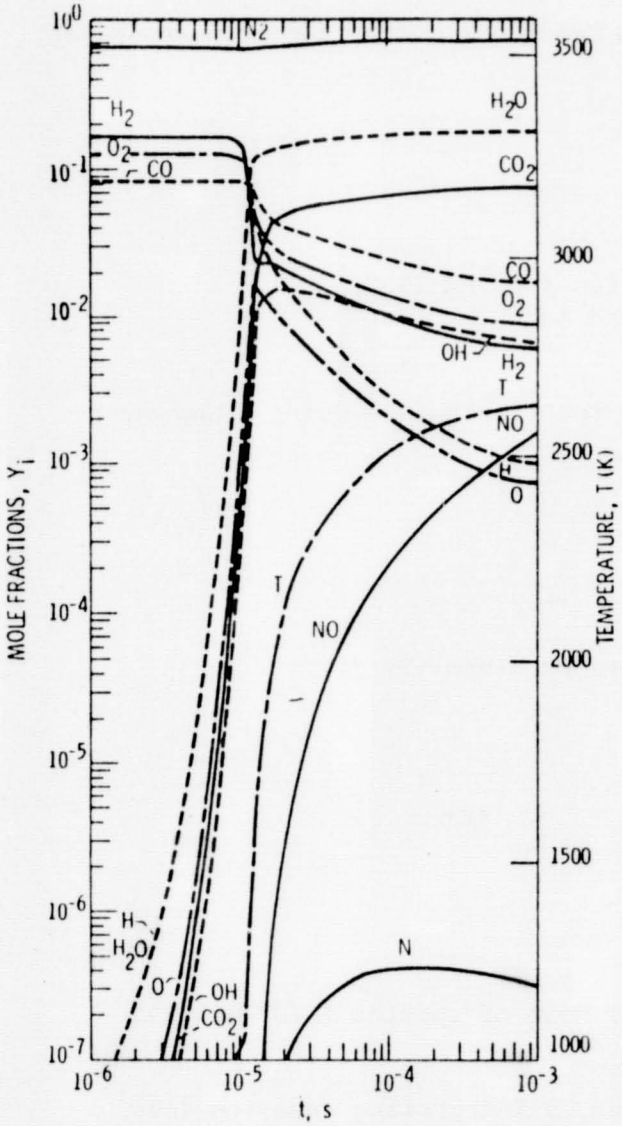

Figure 5 - Variation with time of temperature and species mole fractions for test problem 1. Solution generated with LSODE-B and EPS = 10^{-5}.

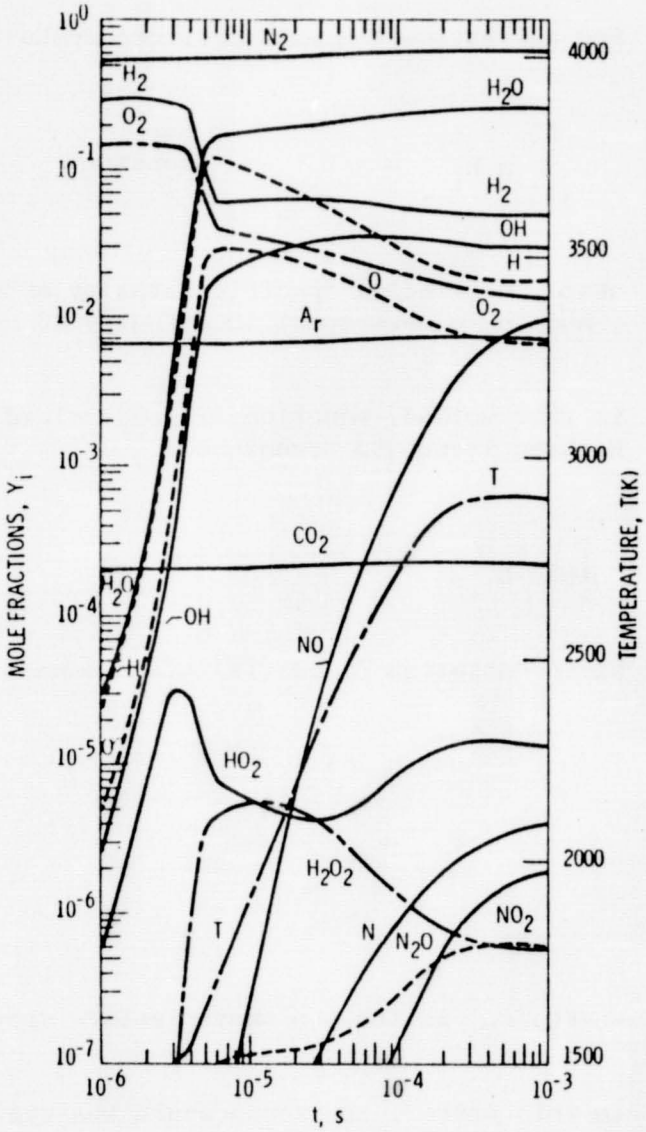

Figure 6 - Variation with time of temperature and species mole fractions for test problem 2. Solution generated with LSODE-B and EPS = 10^{-5}.

Method A

For adiabatic, constant-pressure combustion reaction, energy conservation gives

$$\sum_{i=1}^{NS} n_i h_i = h_0 = \text{constant} \qquad (1)$$

where, h_i = molal-specific enthalpy of species i (J/kmol)
and h_0 = mass-specific enthalpy of mixture (J/kg)

In this method, equation (1) was solved for the temperature using a Newton-Raphson iteration technique.

Method B

Differentiation of eq. (1) with respect to temperature (T) gives

$$\frac{dT}{dt} = - \frac{\sum_{i=1}^{NS} f_i h_i}{\sum_{i=1}^{NS} n_i c_{p_i}} \qquad (2)$$

where, c_{p_i} is the constant-pressure specific heat of species i (J/kmol K).

In this method, the temperature was evaluated by integrating equation (2).

Figure 7 Evaluation of Temperature
(for LSODE, EPISODE, and CHEMEQ)

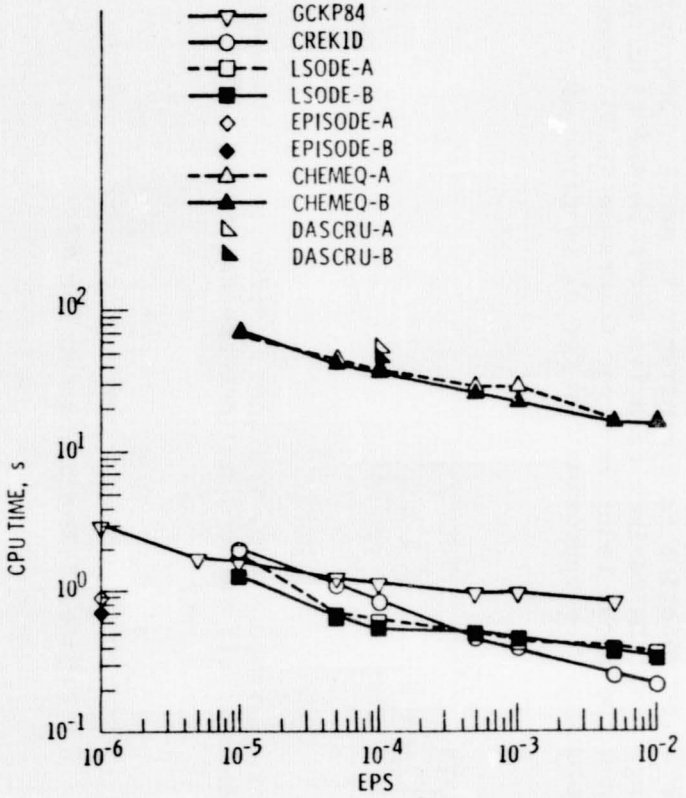

Figure 8 - Variation of the CPU time (s) with error tolerance, EPS, for test problem 1. All runs on IBM 370/3033.

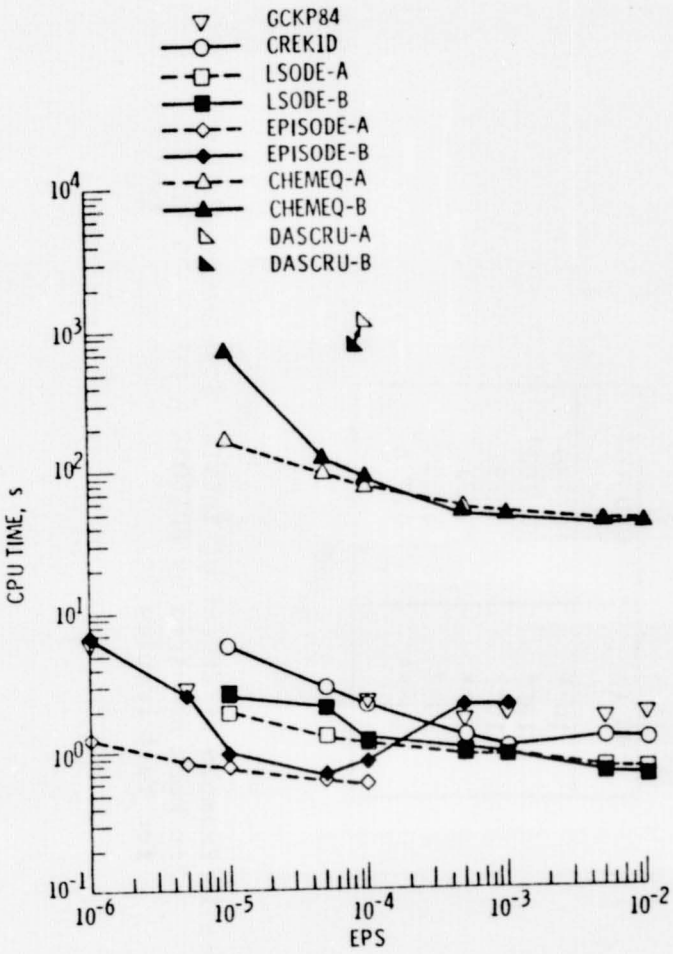

Figure 9 - Variation of the CPU time (s) with error tolerance, EPS, for test problem 2. All runs on IBM 370/3033.

H0 (s)	CPU (s)
10^{-5}	0.786
10^{-6}	0.783
10^{-7}	0.791
10^{-8}	7.91
10^{-9}	8.04
10^{-10}	0.772

Figure 10 Example of Effect of Initial Steplength (H0) on Work Required by EPISODE-A (EPS = 10^{-5}) for Test Problem 2

An approximate expression for ΔT -- the maximum allowable temperature change allowed before the reaction rate constants k_j and k_{-j} are updated -- was derived by requiring that the maximum relative error in the resultant reaction rates does not exceed the local relative error tolerance (EPS) required of the numerical solution. The approximation for ΔT is given by

$$\Delta T = \frac{EPS \cdot T}{\max_j \left| \frac{E_j}{RT} + N_j \; ; \; \frac{E_{-j}}{RT} + N_{-j} \right|} \qquad (3)$$

where, T is the current temperature, the bars $|\ \ |$ denote absolute value, and the maximum is taken over all forward and reverse reactions.

Figure 11 Approximation for ΔT

Method	Test Problem 1	2
GCKP84	0.85	1.73
CREK1D	0.23	1.04
LSODE-A	0.31*	0.52*
LSODE-B	0.29*	0.51*
EPISODE-A	0.75*	0.54*
EPISODE-B	0.70*	0.67
CHEMEQ-A	6.41*	13.6*
CHEMEQ-B	5.69*	12.3*

*method incorporated eq. (3)

Figure 12 Minimum CPU Time (in seconds on IBM 370/3033 computer) Required for the Test Problems

THE ROLE OF SURFACE GENERATED RADICALS IN CATALYTIC COMBUSTION*

D.A. Santavicca, Y. Stein and B.S.H. Royce
Princeton University

The role of surface generated OH radicals in determining the catalytic ignition characteristics for propane oxidation on platinum is under study. The experiments are being conducted in a stacked-plate, catalyst bed. Transient measurements, during catalytic ignition, of the catalyst's axial temperature profile have been made and the effect of equivalence ratio, inlet temperature and inlet velocity are being investigated. These measurements will provide insights which will be useful in planning and interpreting to OH measurements. Attempts to measure OH concentration in the catalyst bed using resonance absorption spectroscopy have been unsuccessful, indicating that OH concentrations are below 10^{16}/cc but still possibly above equilibrium values. Measurements are currently underway using forward scatter laser induced fluorescence which should extend the OH detection limits several orders of magnitude below the equilibrium concentrations.

INTRODUCTION

The advantages of catalytic combustion over conventional combustion are lower emissions, higher efficiency, increased operational stability, stable operation at lower equivalence ratios, improved pattern factors, and wider fuel specifications. The performance of a catalytic combustor is determined by the interaction of a number of physical and chemical processes, including convection and diffusion of species, heat and momentum; conduction and radiation heat transfer in the substrate; and gas phase and surface chemical reactions. An important, and as yet unresolved, question regarding the interaction of these fundamental physical and chemical processes is the effect of catalytic surface reactions on the gas phase chemistry. In particular, it is the effect of intermediate and radical species, generated by catalytic wall reactions, on the gas phase chemistry which has not been established. That radicals can be produced by catalytic surface reactions and that at sufficiently high surface temperatures the radicals are desorbed by the surface into the gas phase has been well documented in low pressure flow experiments [1-5]. However, the importance of this phenomenon in catalytic combustion and the role of these radicals in determining the performance characteristics of catalytic combustors has not been established.

EXPERIMENTS AND STATUS

A schematic drawing of the stacked-plate, catalytic combustor in which the propane-air catalytic ignition experiments are being conducted is shown in

* Sponsored by NASA-Lewis, Grant NAG 3-353 and AFOSR, Grant 6475.

Figure 1. The catalyst plates are 50 mm wide, 100 mm long and 1 mm thick. There are a total of nine plates in the catalyst bed with an inter-plate spacing of 6 mm. The catalyst plates are made from a steel alloy substrate, coated with aluminum oxide and then platinum. Six 0.75 mm diameter holes have been drilled into the side of the center plate at six axial locations. Thermocouples have been inserted into these holes for measurement of the plate's axial temperature profile during ignition. A water cooled gas sampling probe and a thermocouple are used to obtain gas composition and temperature measurements at the exit of the catalyst bed. Optical access is available through windows in the sides of the test section located at several axial positions. The window aperture is 10 mm, therefore the entire distance between two plates can be probed.

Based on a similar experiment by Cattolica and Schefer [6] it was anticipated that the OH concentrations would be large enough for detection by resonance absorption spectroscopy. Under the conditions of this experiment the OH detection limit using this technique is about 10^{16}/cc, as compared to equilibrium OH concentrations of about 10^{14}/cc (based on the overall equivalence ratio and the catalyst temperature - see Figure 2). Measurements were attempted in the stacked-plate combustor using resonance absorption and were unsuccessful, implying that the OH concentration is less than 10^{16}/cc but still possibly greater than the overall equilibrium concentration. In order to extend the OH detection limits it was decided to use laser induced fluorescence (LIF). Because of the limited optical access with the stacked-plate configuration, it has been necessary to use forward scatter collection. The spatial resolution with forward scatter collection is comparable to that of the absorption measurements, which is adequate for the 2-D flow field between the catalyst plates. The forward scatter LIF system is currently being evaluated in a flat flame burner by comparing it to simultaneous absorption measurements, after which it will be applied to the catalytic combustor.

Although there have been several [7-9] theoretical studies of catalytic ignition there have been no experimental studies reported to date. In order to better understand the characteristics of catalytic ignition, especially for the purpose of providing insights to guide the OH experiments, it was decided to investigate the effects of equivalence ratio, inlet temperature and inlet velocity on catalytic ignition. Experiments have been conducted where the inlet temperature and velocity are fixed, the fuel is turned on and the transient response of the catalyst axial temperature profile is measured. Preliminary results from the catalytic ignition experiments are shown in Figures 3-5.

REFERENCES

1. Tevault, D.E., Talley, L.D., and Lin, M.C.: Matrix Isolation and Laser Diagnostic Studies of Catalytic Oxidation of H_2 and D_2 on Platinum. J. Chem. Phys., Vol. 72, No. 5, 1980, pp. 3314-3319.

2. Talley, L.D. and Lin, M.C.: Energetics and Mechanism for Hydroxyl Radical Production from the Pt-Catalyzed Decomposition of Water. Chem. Phys., Vol. 61, 1981, p. 249-255.

3. Fujimoto, G.T., Selwyn, G.W., Keiser, J.T., and Lin, M.C.: Temperature Effect on the Removal of Hydroxyl Radicals by a Polycrystalline Platinum Surface. J. Phys. Chem., 1983, pp. 1906-1910.

4. Selwyn, G.S. and Lin, M.C.: Production of the NH RAdical from the Catalytic Decomposition of NH_3 on Polycrystalline Pt and Fe Surfaces at High Temperature. Chem. Phys., Vol. 67, 1982, pp. 213-220.

5. Selwyn, G.S., Fujimoto, G.T., and Lin, M.C.: Catalytic Removal of NH and NH_2 Free Radicals by Polycrystaline Pt and Fe Surfaces. J. Phys. Chem., 1982, pp. 760-765.

6a. Cattolica, R.J. and Schefer, R.W.: Laser Fluorescence Measurements of the OH Concentration in a Combustion Boundary Layer. Sandia Report SAND82-8649, 1982.

6b. Cattolica, R.J. and Schefer, R.W.: The Effect of Surface Chemistry on the Development of the (OH) in a Combustion Boundary Lyaer. Sandia Report SAND82-8617, 1982.

7. T'ien, J.S.: Transient Catalytic Combustor Model. Comb. Sci. and Tech., Vol. 26, 1981, pp. 65-75.

8. Prasad, R., Kennedy, L.A., and Ruckenstein, E.: A Model for the Transient Behavior of Catalytic Combustors. Comb. Sci. and Tech., Vol. 30, 1983, pp. 59-88.

9. Fakheri, A. and Buckius, R.O.: Transient Catalytic Combustion on Flat Plate. Comb. and Flame, Vol. 52, 1983, pp. 169-184.

C-4

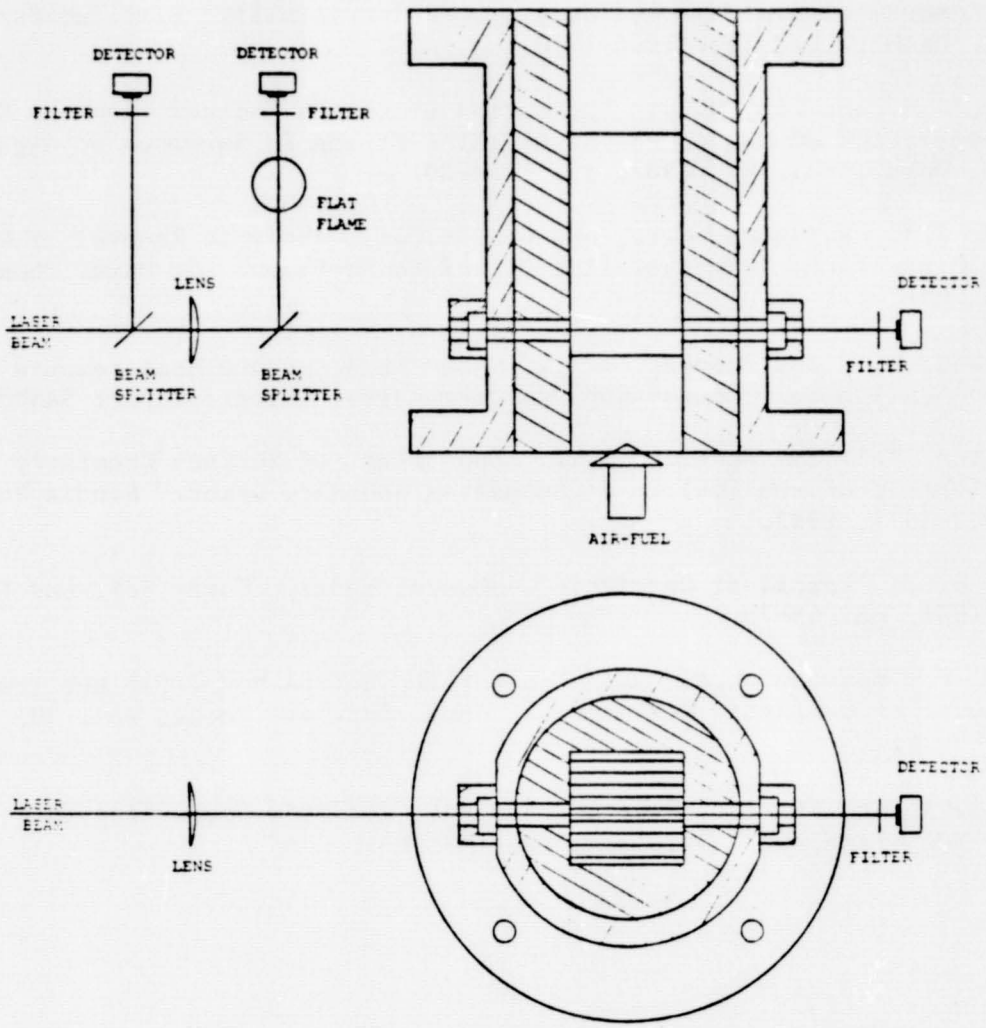

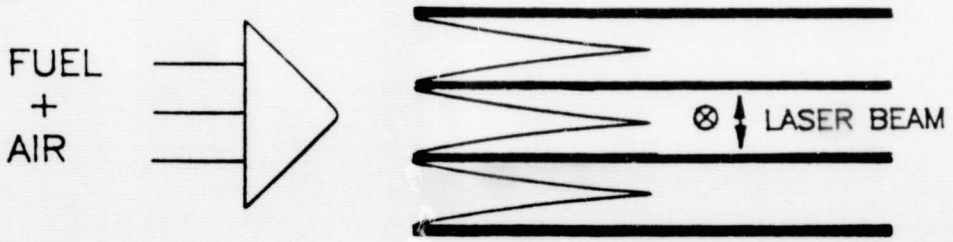

Figure 1 - Schematic drawing of stacked-plate catalytic combustor with OH absorption experiment.

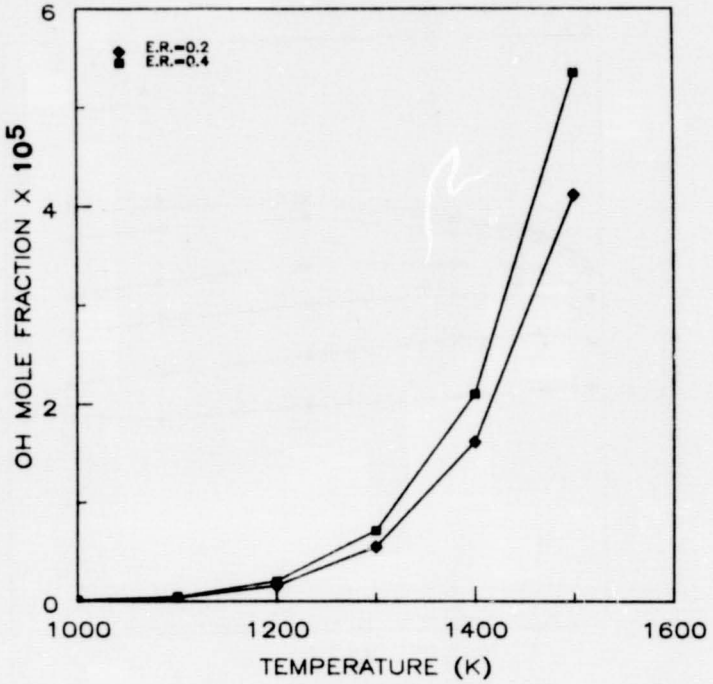

Figure 2 - OH equilibrium concentration versus temperature for initial equivalence ratios of 0.2 and 0.4. Calculated using NASA Equilibrium Code.

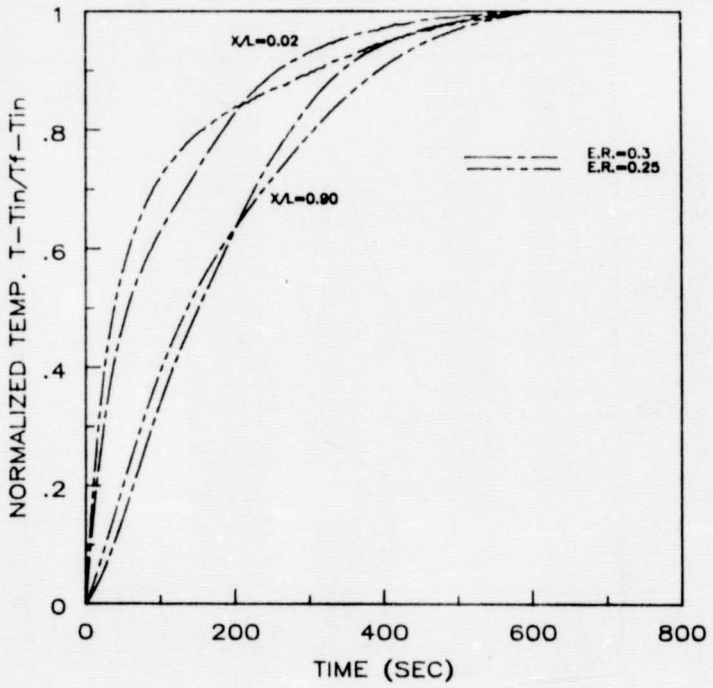

Figure 3 - Normalized temperature versus time at X/L = 0.02 and 0.90 for equivalence ratios of 0.25 and 0.30, 700°K inlet temperature and 6 m/sec reference velocity.

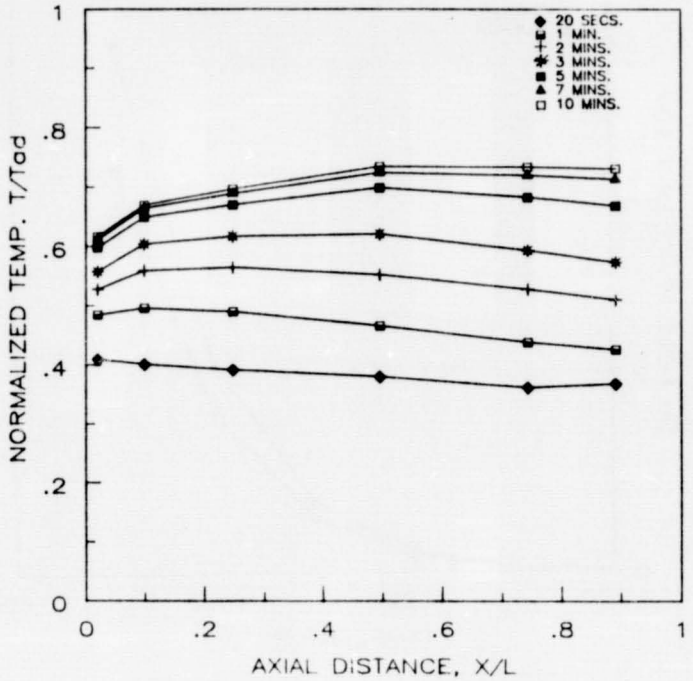

Figure 4 - Normalized temperature versus X/L at different times after ignition until steady state, for 700°K inlet temperature, 0.3 equivalence ratio and 6 m/sec reference velocity.

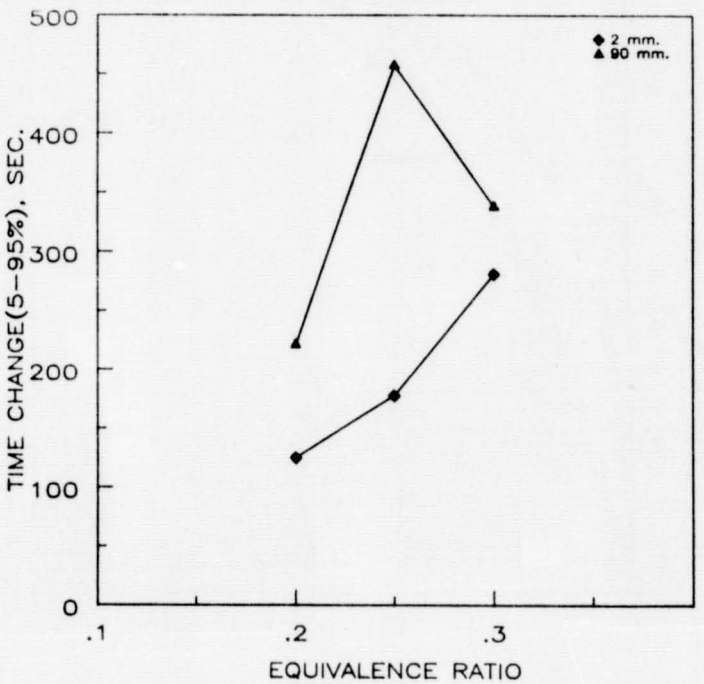

Figure 5 - Time required for $(T-T_{inlet})/T_{final}-T_{inlet})$ to go from 0.05 to 0.90 versus equivalence ratio at X/L = 0.02 and 0.90 for 700°K inlet temperature and 10 m/sec reference velocity.

D31

LINER ENVIRONMENT EFFECTS STUDY

K. S. Venkataramani and E. E. Ekstedt
General Electric Co.
Aircraft Engine Business Group

Estimation of the heat flux to the combustor liner is a key step in the design of aircraft engine combustion systems. This forms the basis for determining the amount of cooling air and the method of introducing it. Currently, this is largely an empirical effort. Future design constraints such as higher pressures and temperatures, shorter combustor lengths and tolerance to poorer quality fuels, however, accentuate the need for a firmer basis for the heat transfer calculations. In particular, it becomes necessary to account for the radiation contributions from the flame gases (in spectral bands) and soot particles (continuum) over a wide range of combustor operating conditions. Analytical efforts to model the liner heat transfer reflecting the above complexities are hampered by the lack of sufficient experimental data for model verification.

The Liner Environment Effects Study Program described here is designed to address this need. It is aimed at establishing a broad heat transfer data base under controlled experimental conditions by quantifying the effects of the combustion system conditions on the combustor liner thermal loading and on the flame radiation characteristics.

Five liner concepts spanning the spectrum of liner design technology from the very simple to the most advanced concepts will be investigated. These concepts comprise an uncooled liner, a conventional film cooled liner, an impingement/film cooled liner, a laser drilled liner approaching the concept of a porous wall and a siliconized silicon carbide ceramic liner. The liners will be accommodated in a simple test rig housing a three-inch diameter combustor.

Effect of fuel type will be covered by using fuels containing 11.8, 12.8, and 14% hydrogen. Tests at 100, 200, and 300 psia will provide a basis for evaluating the effect of pressure on the heat transfer. The effects of the atomization quality and spray characteristics will be examined by varying the fuel spray Sauter mean diameter and the spray angle. Additional parameters to be varied include reference velocity, a wide range of equivalence ratio, cooling flow rate, coolant temperature and the velocity of the coolant stream on the backside of the liner.

Both spectral and total radiation measurements will be made in addition to obtaining extensive liner metal and film temperature data.

Reference:

Claus, RW: Spectral Flame Radiance from a Tubular-Can Combustor, NASA TP-1722, 1981.

Liner Environment Effects Study Objectives

Establish Broad Data Base on the Effects of Combustion System Environment on Combustor Liner Temperatures and Flame Radiation Characteristics for a Variety of Liner Concepts and Fuel Properties.

Data Will Provide Basis for

- Detailed Combustor Modeling, and
- Combustor Design

Liner Cooling Designs

- Uncooled
- Film Cooled
- Impingement & Film Cooled
- Ceramic Liner
- Multi-Hole Liner

Uncooled & Convectively Cooled Liner

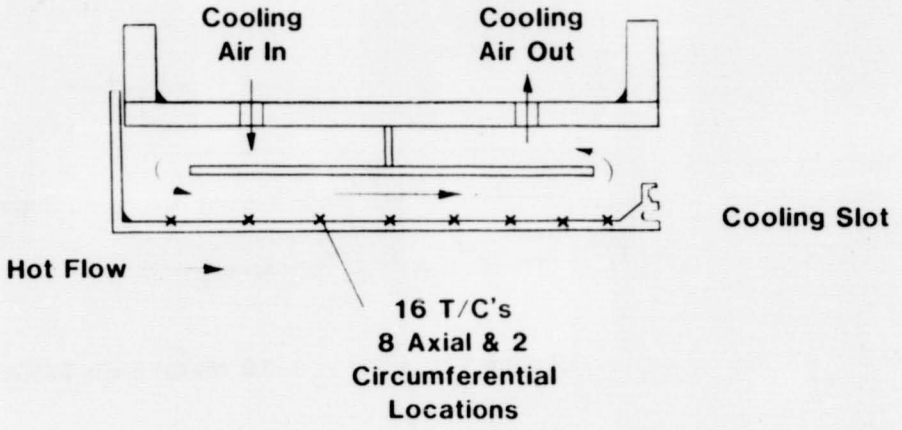

Film Cooled Liner

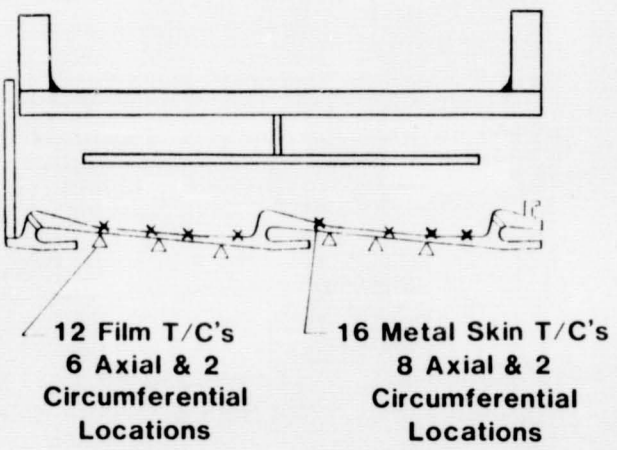

Impingement/Film Cooled Liner

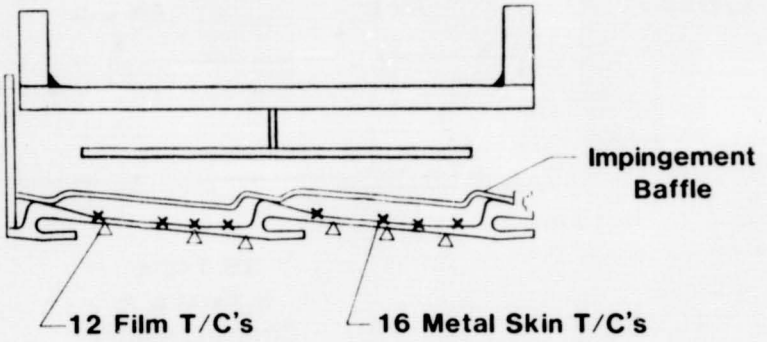

Ceramic Liner

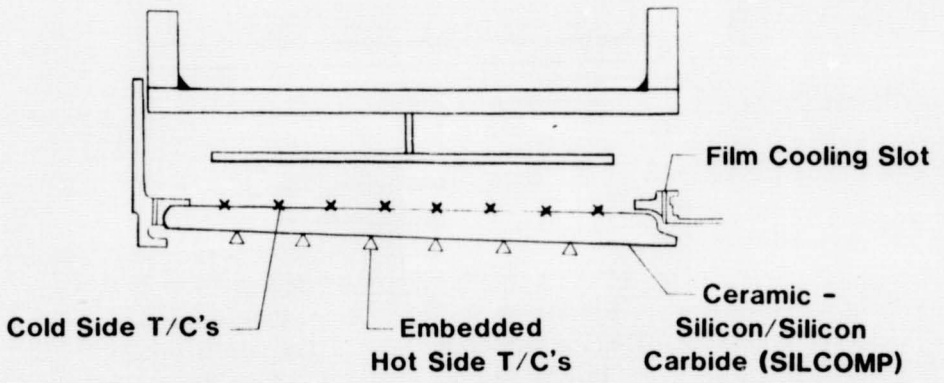

Multi-Hole Liner

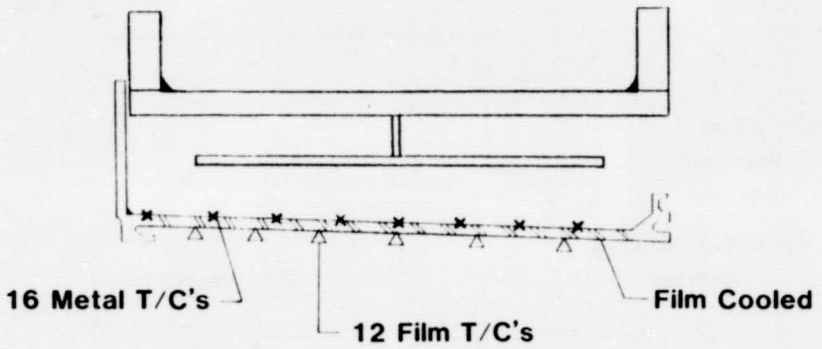

Test Rig Assembly

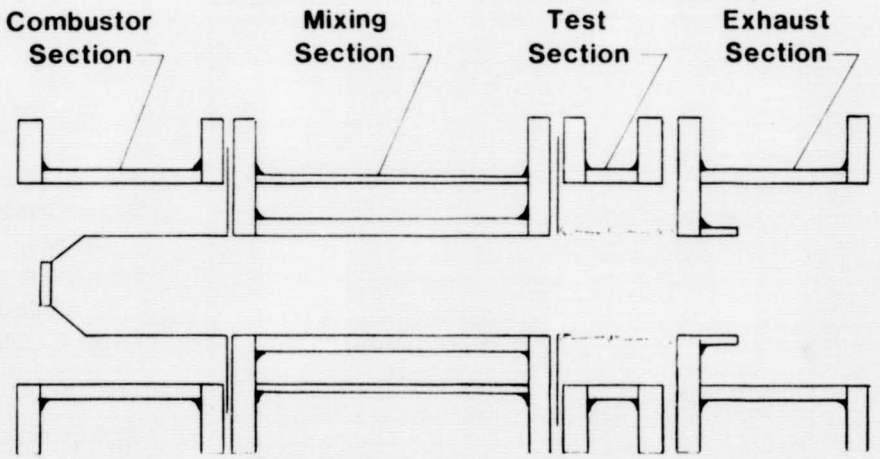

Combustor Section

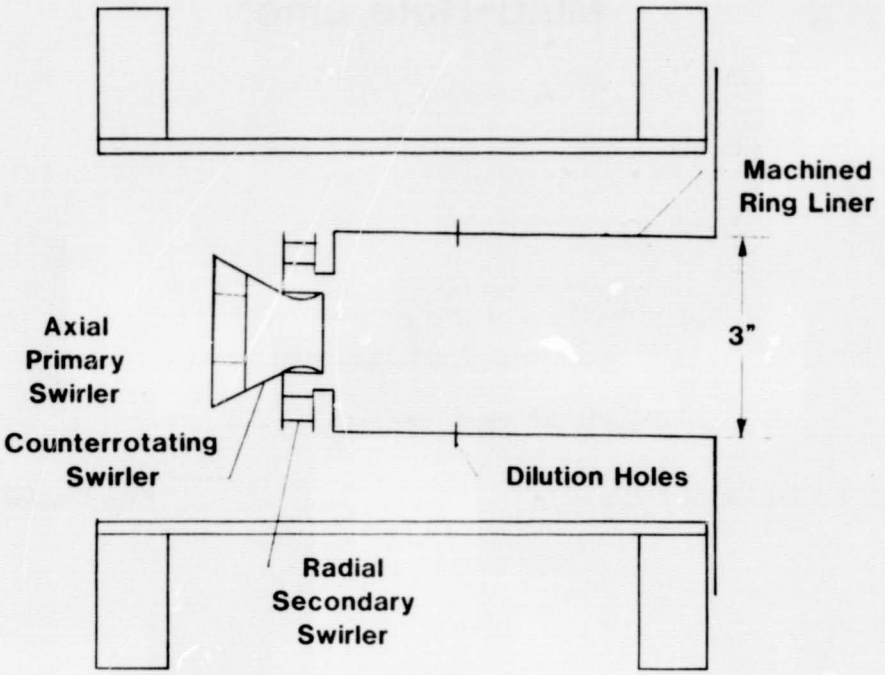

Mixing Section

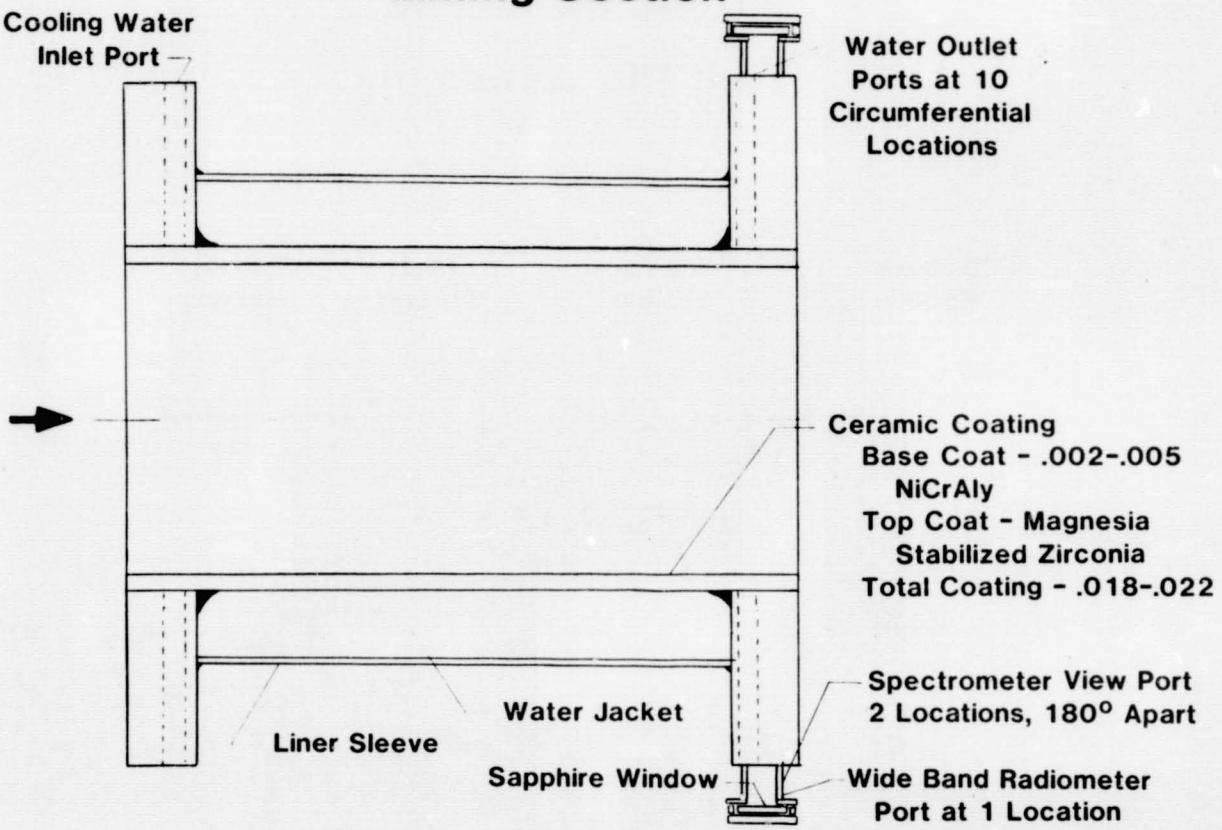

Test Section

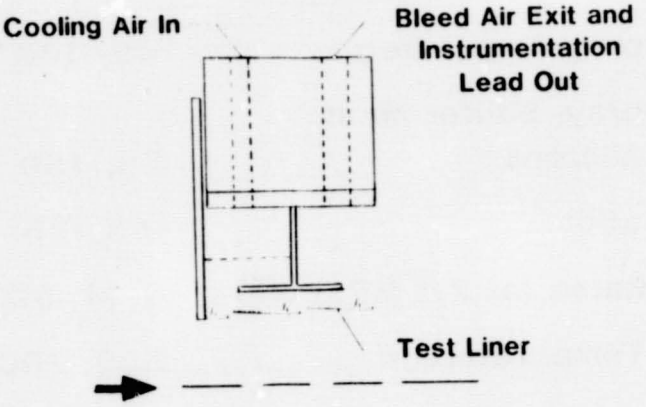

Exhaust Section

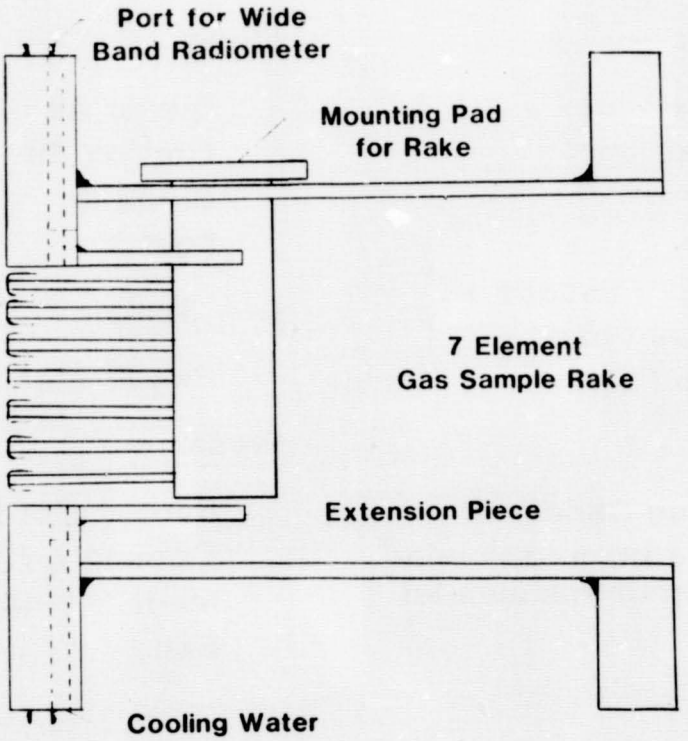

Test Variables

Parameters	Values
Liner	5 Concepts
Fuel Hydrogen , Wt. %	14.0, 12.8, 11.8
Fuel Nozzle Spray Angle, Deg	45, 100
Fuel Nozzle Spray, Sauter Mean Diameter, Microns	75, 150
Equivalence Ratio	0.3, 0.5, 0.8, 1.2, 1.3
Cooling Flow Rates (at 2.1 MPa), kg/s	0.14, 0.23, 0.32
Cooling Flow Temperature, K	589, 700, 811, 1000
Internal Reference Velocity, m/s	9.1, 18.3, 30.0, 41.0
Bleed Flow Rates(at 2.1 MPa), kg/s	0.18, 0.32, 0.45
Pressure, MPa	0.7, 1.4, 2.1

Test Instrumentation

Temperatures

- Burner Air Inlet
- Cooling Air Inlet
- Bleed Air
- Air Baffle
- Cooling Air Passage
- Liner Metal (16)
- Liner Film (12)

Radiation

- Total (Wide Band) - 2
- Spectral - Infrared Fourier Transform Radiometer

Humidity

- Inlet

Flows

- Burner Air
- Cooling Air
- Bleed Air
- Fuel

Gas Sample

- Exit (7 Element Probe)

Pressures

- Burner Inlet (Pt and P3)
- Cooling Air Passage
- Inner Impingement Plate
- Exit

Droplet Size Measurement

- Tests will be Conducted with the In-House Droplet Measurement Devices at 1 atm
- Air-Assist Fuel Nozzle with Several Combinations of Swirlers and Simplex Tips
- Establish Air Flow Requirements to Achieve Desired SMD's - Operational Considerations Likely to Require Compromise

Air-Assist Fuel Nozzle

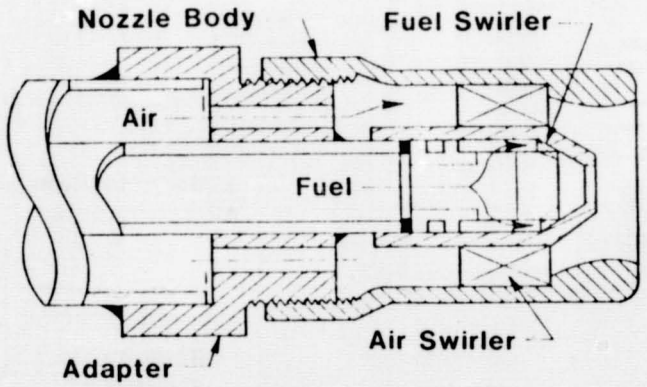

Spectral Radiation Measurement Scheme

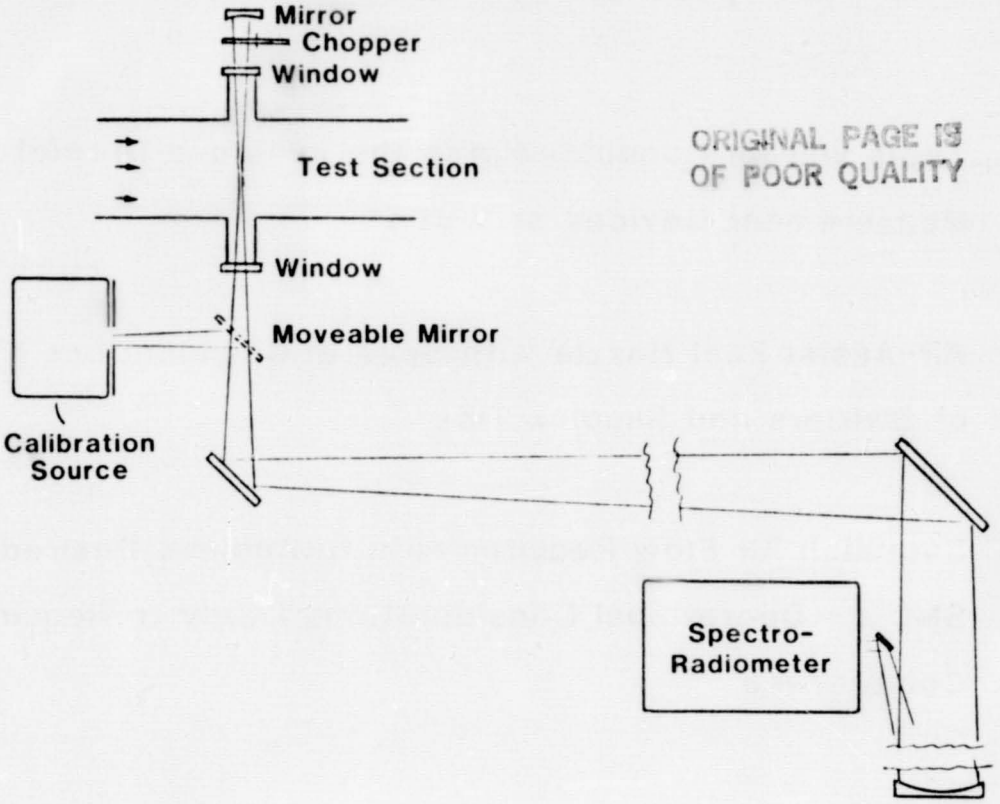

Control and Data Aquisition Spectral Radiation Measurements

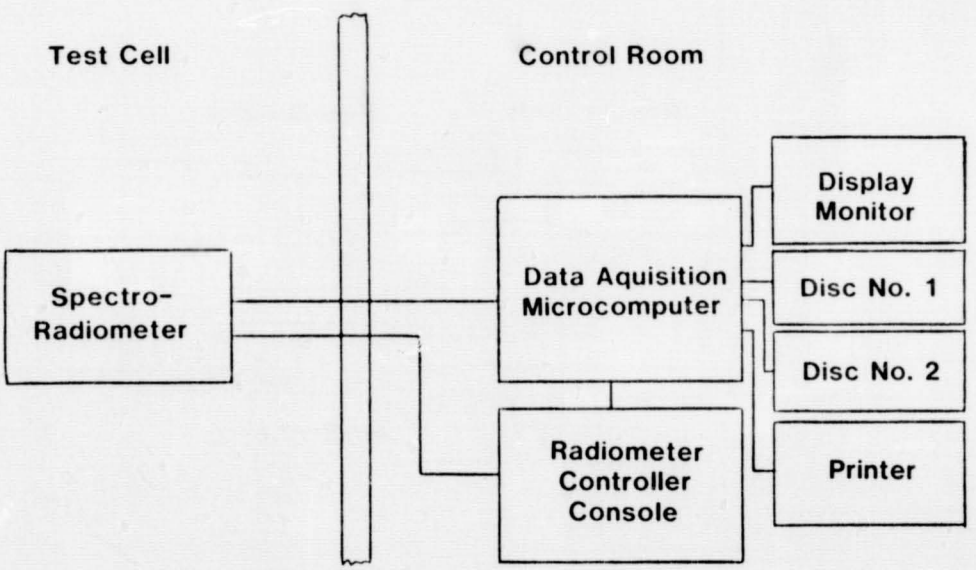

SPONTANEOUS IGNITION CHARACTERISTICS OF GASEOUS HYDROCARBON-AIR MIXTURES

G. Freeman and A. H. Lefebvre
Purdue University

Experiments are conducted to determine the spontaneous ignition delay times of gaseous propane, kerosine vapor, and n-heptane vapor in mixtures with air, and oxygen-enriched air, at atmospheric pressure. Over a range of equivalence ratios from 0.2 to 0.8 it is found that ignition delay times are sensibly independent of fuel concentration. However, the results indicate a strong dependence of delay times on oxygen concentration. The experimental data for kerosine and propane demonstrate very close agreement with the results obtained previously by Mullins and Lezberg respectively.

INTRODUCTION

Spontaneous ignition is a process whereby a combustible mixture undergoes chemical reaction leading to the rapid evolution of heat, in the absence of any concentrated source of ignition such as a flame or spark. In some practical combustion devices, such as the lean premix/prevaporize combustor which is now being actively developed for advanced aircraft gas turbine engines, spontaneous ignition must be avoided at all costs, since it could damage combustor components and produce unacceptably high levels of pollutant emissions (refs. 1 and 2). On the other hand spontaneous ignition is sometimes relied upon to provide the main source of ignition, as in the compression ignition-engine.

Spontaneous ignition delay may be defined as the time interval between the creation of a combustible mixture, say by injecting fuel into air at high temperature, and the onset of flame. In view of their practical importance, measurements of ignition delay times have been conducted for many fuels, over wide ranges of ambient conditions and in a variety of test vehicles, including constant volume bombs, rapid-compression machines, reciprocating engines, shock tubes, and continuous flow devices (refs. 3-14). The test methods employed and the results obtained are described in reviews by Mullins (ref. 3) and, more recently, by Spadaccini and Te Velde (ref. 5).

Although the subject of spontaneous ignition of liquid fuels has received considerable attention in the past, the role of fuel evaporation in the overall spontaneous ignition process is still unclear. It was decided, therefore, to conduct a series of experiments using only gaseous or vaporized fuels, sometimes with the injection of additional oxygen into the flowing air stream, in order to obtain more accurate data on chemical delay times under conditions where the effects of fuel evaporation are excluded. Having determined the role of chemical kinetics in the spontaneous ignition process, the second phase of the research would then comprise a number of carefully-designed experiments, using one or more liquid fuels, in which fuel evaporation time is varied systematically over a wide range while maintaining the chemical reaction time constant. This could be achieved, for

example, by conducting a series of measurements of ignition delay time, for several different values of mean fuel drop size (between 20 and 200 microns), while maintaining constant values of air flow rate, fuel flow rate, air pressure and air temperature. The results of these experiments, in conjunction with theoretical analyses, should then lead to expressions for the spontaneous ignition times of hydrocarbon fuel/air mixtures that take full account of all the physical and chemical properties of relevance to the gas turbine.

The main purpose of this paper is to present the results of some preliminary tests that have been carried out at atmospheric pressure using gaseous fuel-air mixtures.

EXPERIMENTAL

The apparatus employed in the measurement of spontaneous ignition delay time is shown schematically in Fig. 1. Air is supplied from a high pressure blower, the air flow rate being controlled by an electrically-activated pintle valve fitted into the blower inlet duct. Air flow rates are calculated from the dynamic pressure measured in the throat of a bell-mouth orifice through which inlet air enters the blower.

Two separate heaters are employed to raise the temperature of the incoming air. A preheat section contains two heaters which consist of coiled ni-chrome resistance wire would helically around four ceramic support tubes. Each of these preheaters operates at 3.5 kW, and can be turned on or off independently of the main heater. The main air heater consists of three hairpin-formed, incalloy-sheathed, "cal-rod" heating elements. These elements have a maximum sheath temperature of 1150 K and a maximum input power of 15 kW. Feedback proportional control is used on the main heater. Both heating sections are heavily insulated.

The fuel injector designed for the experiments on gaseous fuels and fuel vapors is illustrated in Fig. 2. For ease of manufacture and assembly, and to ensure structural integrity, a square tube matrix was constructed to provide the best distribution of holes as dictated by the round cross-section of the pipe. The location of each of the twenty-five fuel injection points was determined by dividing the cross-sectional area of the pipe into twenty-five sections of equal area and locating an injection point as close as possible to the center of each section. The objective was to achieve rapid mixing of fuel and air and to attain a uniform mixture strength in the fuel/air mixture entering the test section.

The fuel delivery system for vaporized fuels is illustrated in Fig. 3. Fuel is pumped from a reservoir to the fuel vaporizer/heater in the test cell. The liquid fuel-flow rate is monitored using a rotameter and is regulated by means of a throttle valve. A back pressure valve is installed at the vaporizer exit to eliminate the tendency of the vaporized fuel flow to surge due to small pressure fluctuations in the vaporizer. Since the vaporizer does not respond well to flow transients, the fuel cut-off valve (located just upstream of the injector) is equipped with an exhaust line to allow continuous fuel flow, as well as visual determination of complete vaporization.

The test section consists of a single length of drawn stainless steel tubing, having an internal diameter of 6.22 cm. Various lengths of tubing are available and can be joined together or interchanged to vary the length of the test section. Each segment is jacketed by a thick layer of insulating material to minimize the

axial temperature gradient in the flowing mixture. The test section is instrumented with four shielded, stagnation-type thermocouples, located along the axis of the tube. The axial locations of the four thermocouples are as follows: 1 - at the fuel injection plane, 2 - 18 cm downstream of the fuel injection plane, 3 - halfway down the test section, and 4 - at the end of the test section. Thermocouples 3 and 4 are withdrawn when ignition delay times are being measured.

Test Procedure

The experimental procedure developed to determine ignition delay times is as follows. Initially flow conditions are set at predetermined values of velocity, temperature, and equivalence ratio, and the mixture temperature is then slowly increased. The onset of spontaneous ignition is manifested as a clearly visible cool flame, accompanied by the odor of aldehydes in the exhaust gases. (Mullins reported this same phenomenon (ref. 3)). Spontaneous ignition first appears at a distance of thirty to fifty centimeters downstream of the exit of the test section as intermittent flashes of flame. As the mixture temperature continues to increase the flame becomes stable and its location moves slowly upstream. The flame assumes the shape of a cone with its apex pointing upstream, and has an attached flame brush extending downstream. The mixture temperature is allowed to increase until the tip of the flame is located near to the exit of the test section. At this point the inlet air temperature and the mixture temperature at one or more axial locations are recorded. Fuel flow is abruptly terminated, and temperature are again recorded at various axial locations in the test section. The delay time is then obtained as the length of the test section divided by the average velocity in the test section.

The initial mixture temperature, T_m cannot be measured directly because mixing takes a small, but finite length, so some other method of determining the initial temperature must be employed. The method that was chosen is to use a temperature measured at a distance downstream of the fuel-injection plane where the results of detailed temperature surveys showed that mixing is just complete. This temperature is then extrapolated back to obtain the true initial value of T_m, using as a baseline the axial temperature profile as measured at several stations along the test section with the fuel turned off. The procedure is illustrated in figure 4, which shows that the initial value of T_m is determined by lowering the baseline temperature profile until it passes through T_{ref}. T_{ref} is then taken as the temperature where the shifted profile intersects the temperature axis. If the test section were perfectly insulated this procedure would be superfluous because T_m would be equal to T_{ref}. However, as a finite heat loss occurs, despite the thick layer of external insulation, the above procedure is necessary and is considered satisfactory.

One drawback to this method is that the temperature profile of the reacting mixture is not exactly the same as that for air only. By plotting the actual mixture temperature profile and subtracting from it the air-only profile a graph is obtained depicting the temperature rise due to reaction, as shown in figure 5. To minimize errors due to this effect it is necessary to keep x_{ref} small, although it must be large enough to ensure that the temperature measurement carried out at x_f is downstream of the mixing region. It would be desirable to measure the axial temperature profile for each data point, but this is impractical due to the problems that would arise from insertion of the thermocouple into the flowing mixture. Insertion of a thermocouple at the upstream end of the working section would affect the fuel-air mixing process, while its presence further downstream could easily induce premature autoignition of the mixture.

In order to determine whether the presence of the flame front can influence ignition delay times by supplying heat or active species to the incoming fresh mixture, a nitrogen quench system was installed. This system includes a solenoid valve which can be opened and closed very rapidly to inject a transient flow of cold nitrogen gas into the test section. Injection of nitrogen causes the autoignition flame to vanish, but when the nitrogen flow is abruptly terminated the flame reappears instantly at its original location. This suggests that the presence of the flame has no discernible effect on ignition delay times, which is consistent with the observations of Spadaccini (ref. 9).

Although the flame position tends to remain fairly constant it occasionally leaps forward a few centimeters and then, almost instantaneously, returns to its original position. This phenomenon was also noticed by Mullins (ref. 3) who attributed it to inadequate mixing of fuel and air, resulting in pockets of rich mixture in the flow approaching the flame. This explanation is considered unsatisfactory, at least in its application to the present investigation, partly because the results of many detailed temperature surveys have shown that mixing is complete well upstream of the autoignition flame, and also because it is generally found that ignition delay times are fairly insensitive to variations in fuel/air ratio. No attempt has been made to study this phenomenon because it only occurs during the phase when the mixture temperature is being slowly raised in order to coax the autoignition flame toward the exit of the test section. Close to the test section the flame position usually remains quite steady so that measurements of ignition delay time can be made with good accuracy.

RESULTS

From global reaction rate considerations the chemical ignition delay time can be expressed as

$$\tau \propto \exp\left(E/RT_m\right) [\text{Fuel}]^m [\text{Oxygen}]^n \qquad (1)$$

where τ = ignition delay time, ms

T_m = initial mixture temperature, K

E = global activation energy, kcal/kg. mol.

R = universal gas constant, kcal/kg. mol -K

[Fuel] = fuel concentration

[Oxygen] = oxygen concentration

The form of equation (1) suggests that a plot of $\ln \tau$ versus $1/T_m$ should yield a straight line with a positive slope, and this is borne out by the results shown plotted in figure 6 for propane-air mixtures at a constant equivalence ratio of 0.5. The line displayed in this figure is drawn through three sets of data points corresponding to three different lengths of test section. The value of activation energy, E, calculated from the slope of this line is 38,200 kcal/kg. mol.

It is of interest to observe that all the data points lie in close proximity to the line drawn in figure 6. This is in marked contrast to the results of a previous investigation where it was found that ignition delay time was very dependent on the

length of the test section employed (ref. 15). This problem was attributed to excessive heat loss from the duct walls and was overcome effectively by increasing the internal diameter from 2.54 to 6.22 cm, and by applying a thick layer of insulating material to the outer pipe wall.

The results obtained using mixtures of vaporized kerosine with air are shown in Fig. 7. The straight line drawn through the data points in this figure corresponds to a value for E of 40,900 kcal/kg. mol.

Equivalence ratio was varied over a range from 0.2 to 0.8. For propane the results showed that equivalence ratio has an almost negligible effect on τ, although an increase in equivalence ratio tends to produce a 'stronger' tail flame. Equivalence ratios higher than 0.8 could not be used due to problems of flashback. It was found that as the auto-ignition flame located downstream of the test section was brought slowly upstream by gradually increasing the mixture temperature, it would suddenly flash upstream and stabilize on the fuel injector, thereby obscuring any results and incurring risk of damage to the injector.

Mixtures of vaporized n-heptane and air also exhibited only a slight dependence of ignition delay time on equivalence ratio. Analysis of the results showed that $\tau \propto [\text{fuel}]^{-0.23}$.

The results obtained for mixtures in air of propane, vaporized n-heptane, and vaporized Jet A, are shown in Fig. 8. The equivalence ratio is 0.5 in all cases. From inspection of this figure it is apparent that all three lines run roughly parallel to each other, thereby indicating that all three fuels have about the same value of activation energy. Moreover, it is also clear that ignition delay times for propane are appreciably longer than those for Jet A.

Figures 9 and 10 show for propane and vaporized kerosine respectively the effect of replacing some of the nitrogen in the air by oxygen, while maintaining the fuel concentration constant. Analysis of the results shows that for propane $\tau \propto [\text{oxygen}]^{-0.59}$, while for kerosine $\tau \propto [\text{oxygen}]^{-0.65}$.

In figure 11 the experimental data obtained in the present investigation for propane-air and Jet A-air mixtures are plotted, for the purpose of comparison, alongside the results of previous workers as compiled by Chiappetta and McVey (ref. 6). It is of interest to note that the results for Jet A (kerosine) show striking agreement with those of Mullins (ref. 3), who also conducted his experiments at normal atmospheric pressure. Equally noteworthy is the close consistency between the propane data obtained by Lezberg (ref. 14) and the results of the present experiments.

CONCLUSIONS

From the results of experiments conducted at atmospheric pressure on the influence of mixture temperature on the spontaneous ignition delay times of mixtures with air of propane, n-heptane vapor and kerosine vapor, the following conclusions are drawn.

1. Ignition delay times can be expressed in terms of mixture temperature, fuel concentration, and oxygen concentration, by the equation

$$\tau \propto \exp [E/RT_m] [\text{Fuel}]^m [\text{Oxygen}]^n$$

2. For the fuels employed in this study the value of E is fairly close to 40,000 kcal/kg mol. For example, for propane E = 38,200 kcal/kg mol., while for kerosine E = 40,900 kcal/kg mol.

3. The dependence of ignition delay time on fuel concentration is quite small, i.e. $m \simeq 0$. Of the fuels examined the strongest dependence on fuel concentration is exhibited by n-heptane, for which $m = -0.23$.

4. Ignition delay times are strongly dependent on oxygen concentration. For propane $n = -0.59$, while for kerosine $n = -0.65$.

5. The experimental data obtained in the present investigation for propane-air and kerosine-air mixtures are remarkably consistent with the results of previous studies by Lezberg and Mullins respectively.

REFERENCES

1. Lean, Premixed/Prevaporized Combustion, Workshop held at Lewis Research Center, NASA CP-2016, 1977.

2. Jones, R. E., L. A. Diehl, D. A. Petrash and J. Grobman, Results and Status of the NASA Aircraft Engine Emission Reduction Technology Programs, NASA TM 79009, 1978.

3. Mullins, B. P., Spontaneous Ignition of Liquid Fuels, AGARDograph No. 4, 1955.

4. Wentzel, W., Ignition Process in Diesel Engines, NACA TM 979, 1936.

5. Spadaccini, L. J. and J. A. Te Velde, Autoignition Characteristics of Aircraft Type Fuels, NASA CR-159886, 1980.

6. Chiappetta, L. M. and J. B. McVey, Literature Survey Conducted in Support of the Development of a Model for Autoignition, UTRC 81-64 Report, 1981.

7. Rao, K. V. L. and A. H. Lefebvre, Spontaneous Ignition Delay Times of Hydrocarbon Fuel/Air Mixtures, First Specialist Meeting (International) of the Combustion Institute, Bordeaux, France, July 1981.

8. Marek, C. J., L. C. Papathakos and P. W. Verbulecz, Preliminary Studies of Autoignition and Flashback in Premixing-Prevaporizing Flame Tube Using Jet-A Fuel at Lean Equivalence Ratios, NASA TM X-3526, May 1977.

9. Spadaccini, L. J., Autoignition Characteristics of Hydrocarbon Fuels at Elevated Temperatures and Pressures, Journal of Engineering for Power, Trans. ASME, Vol. 99, Series A, January 1977.

10. Stringer, F. W., A. E. Clarke and J. S. Clarke, The Spontaneous Ignition of Hydrocarbon Fuels in a Flowing System, Proc. Auto, Div., Institution of Mechanical Engineers, 1970.

11. Taback, E, D., The Autoignition Characteristics of JP-4 at High Temperature and Pressure, P&WA TDM-2284, 1971.

12. Mestre, A. and F. Ducourneau, Recent Studies of the Spontaneous Ignition of Rich Kerosine-Air Mixtures, Combustion Institute European Symposium, 1973.

13. Spadaccini, L. J. and J. A. Te Velde, Autoignition Characteristics of No. 2 Diesel Fuel DOE/NASA/0066-2 NASA CR-165315.

14. Lezberg, E. A., Preliminary Investigation of Propane Combustion in a 3-Inch Diameter Duct at Inlet-Air Temperatures of 1400° to 1600°F, NACA TN 4028, 1957.

15. Freeman, G. and A. H. Lefebvre, Spontaneous Ignition Characteristics of Gaseous Hydrocarbon-Air Mixtures. Paper presented at Central States Combustion Meeting, Lexington, March 1983.

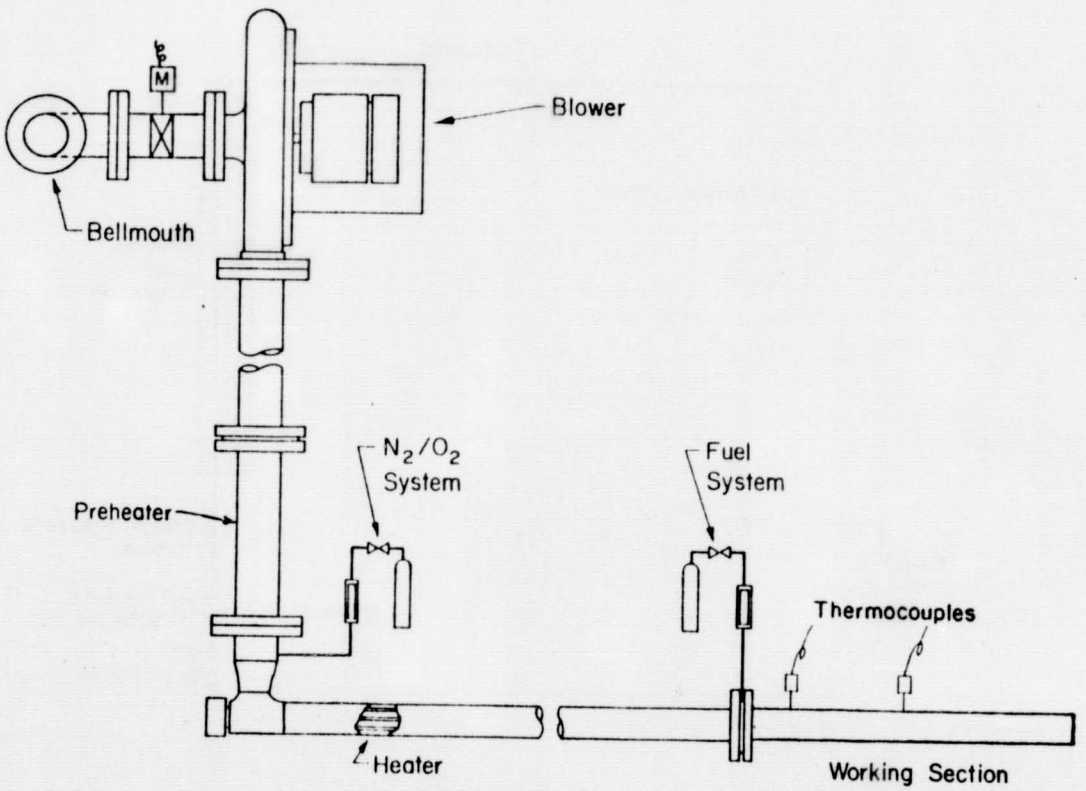

Fig. 1. Schematic diagram of test rig.

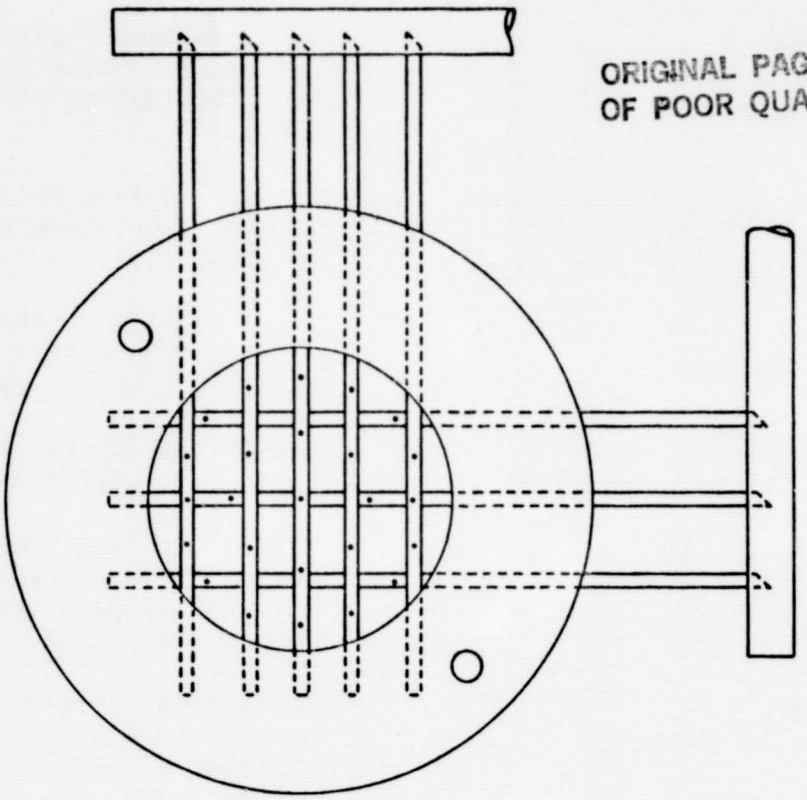

Fig. 2. Fuel injector

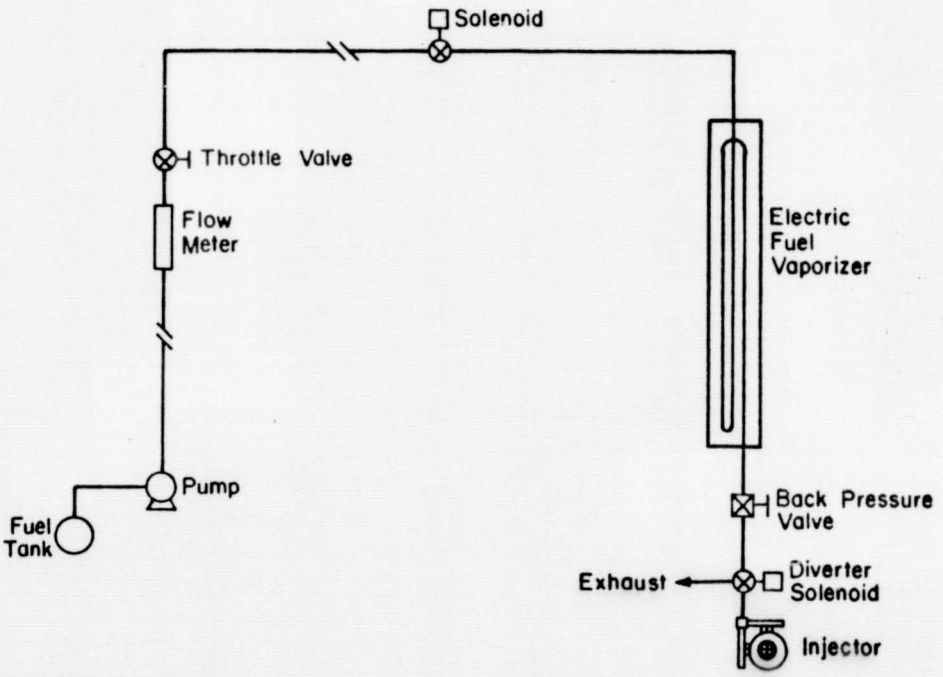

Fig. 3. Fuel delivery system for liquid fuels.

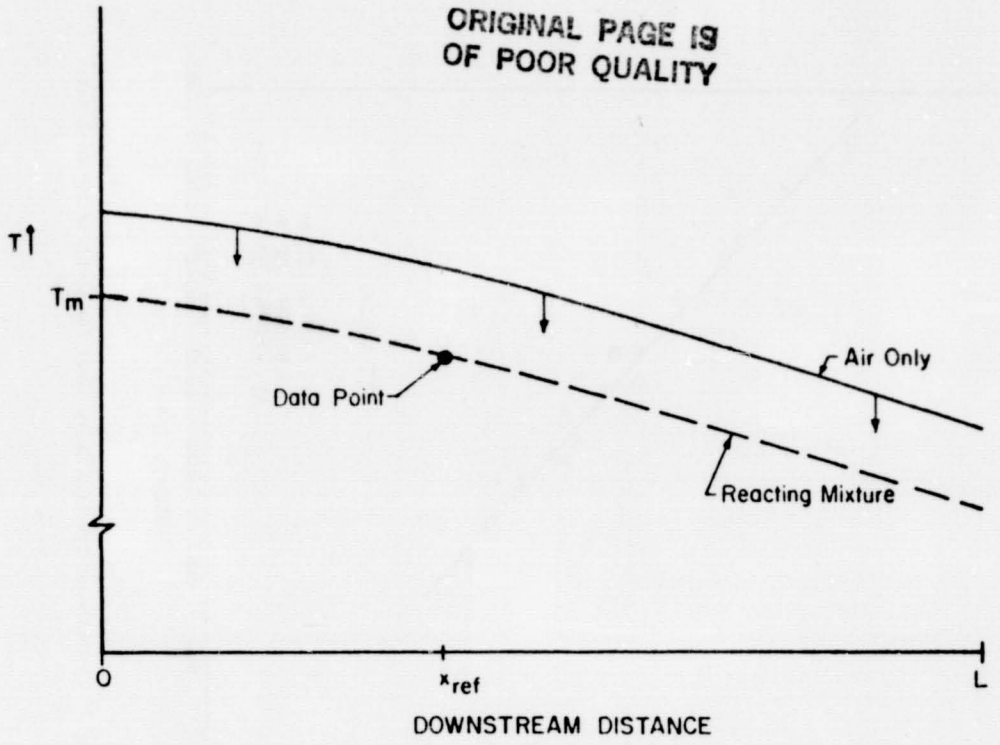

Fig. 4. Graphs illustrating method of determining initial mixture temperature.

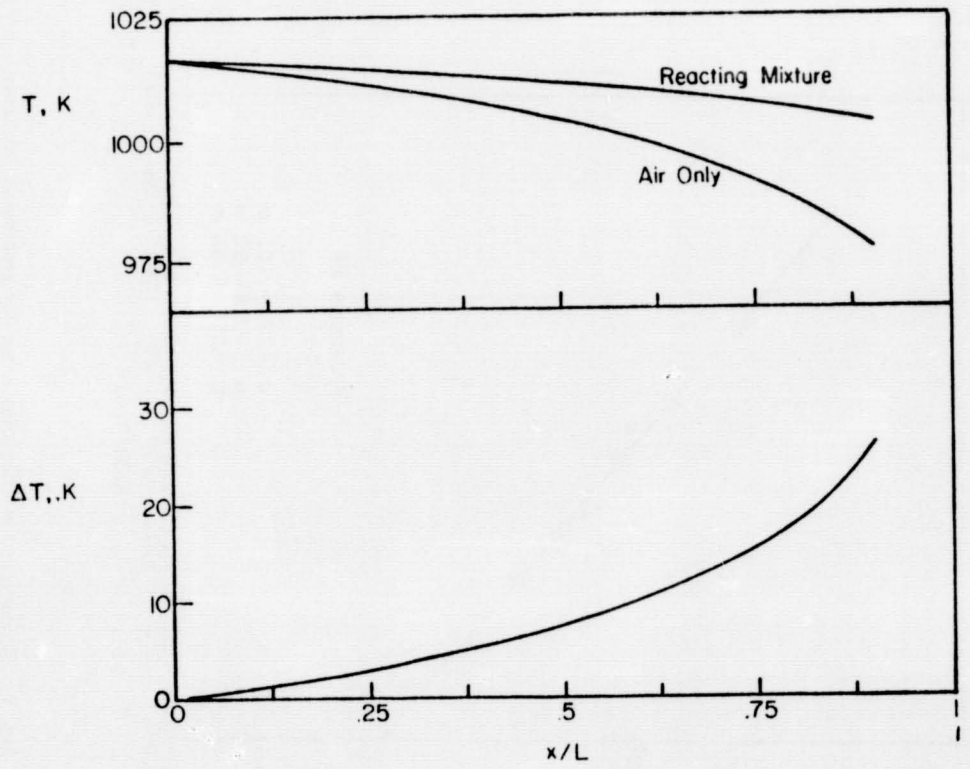

Fig. 5. Graphs illustrating preflame temperature rise as a function of axial distance.

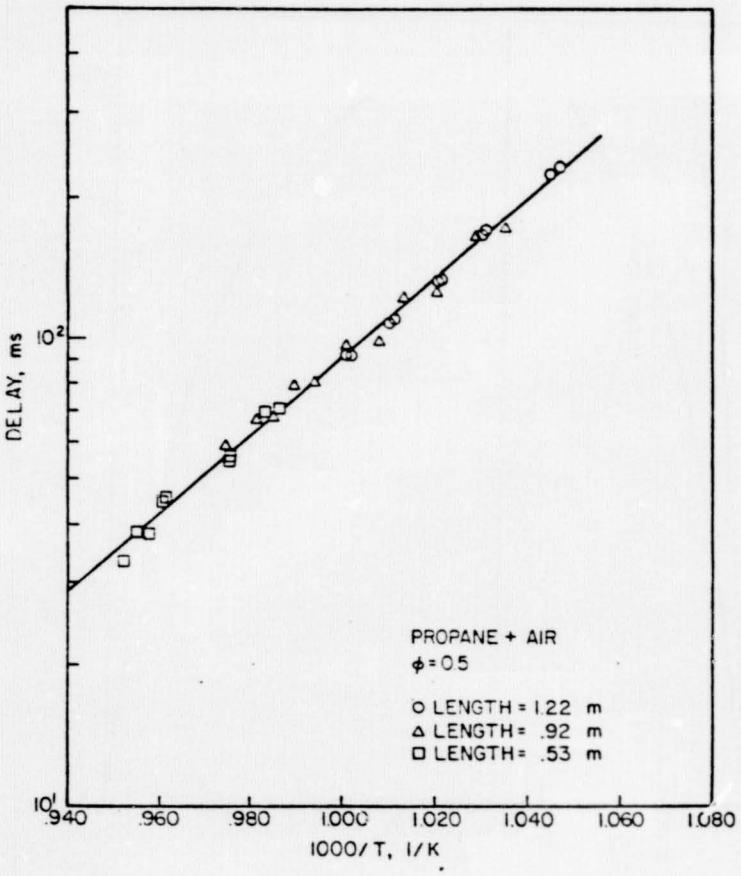

Fig. 6. Spontaneous ignition delay times for propane-air mixtures.

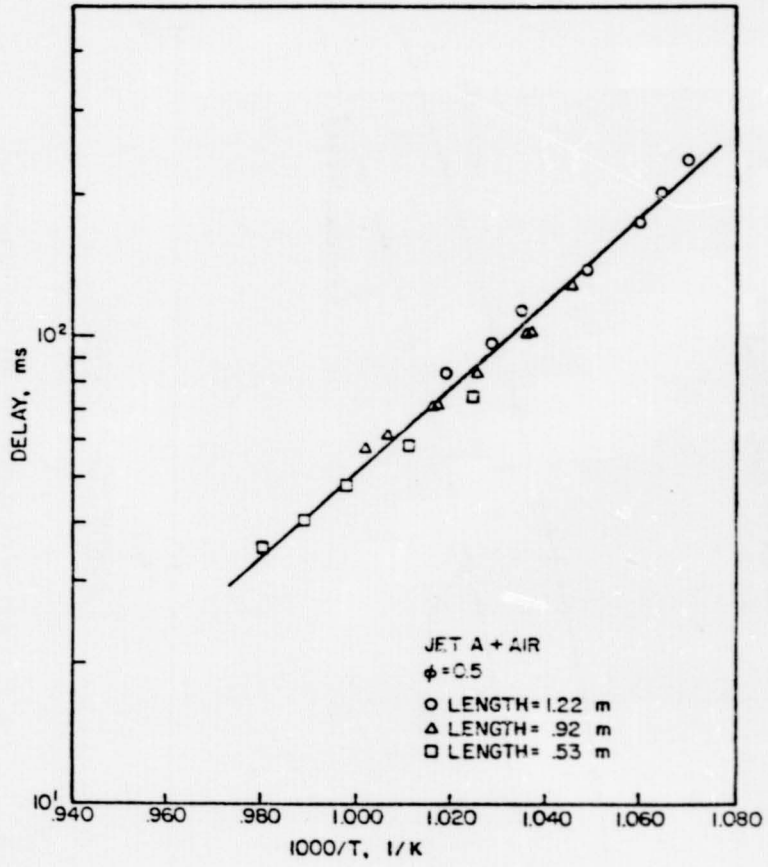

Fig. 7. Spontaneous ignition delay times for kerosine air mixtures.

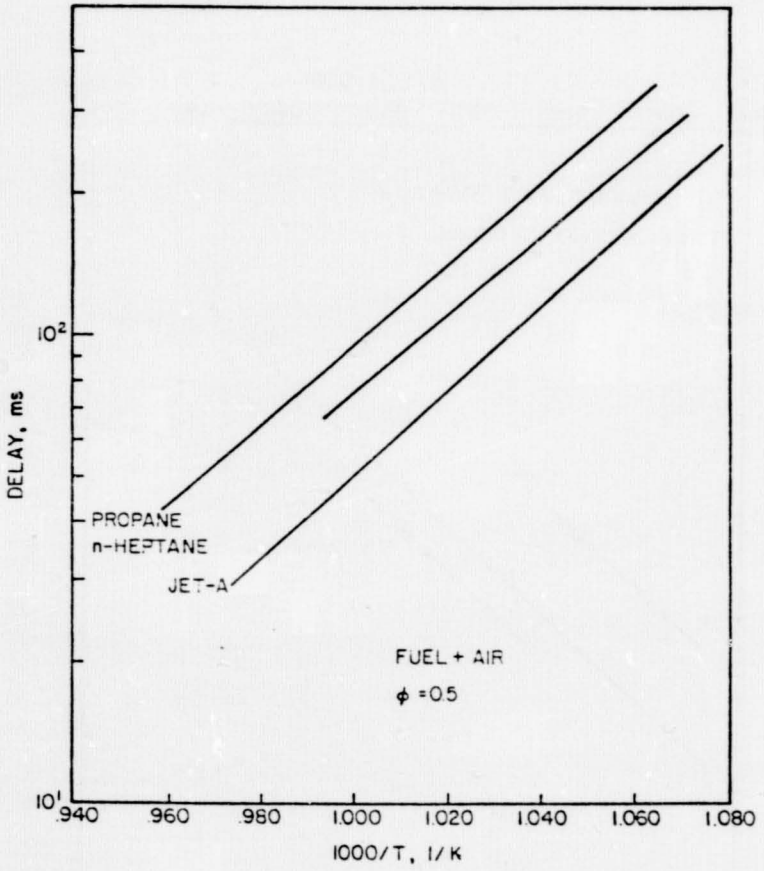

Fig. 8. Comparison of ignition delay times for various fuel-air mixtures.

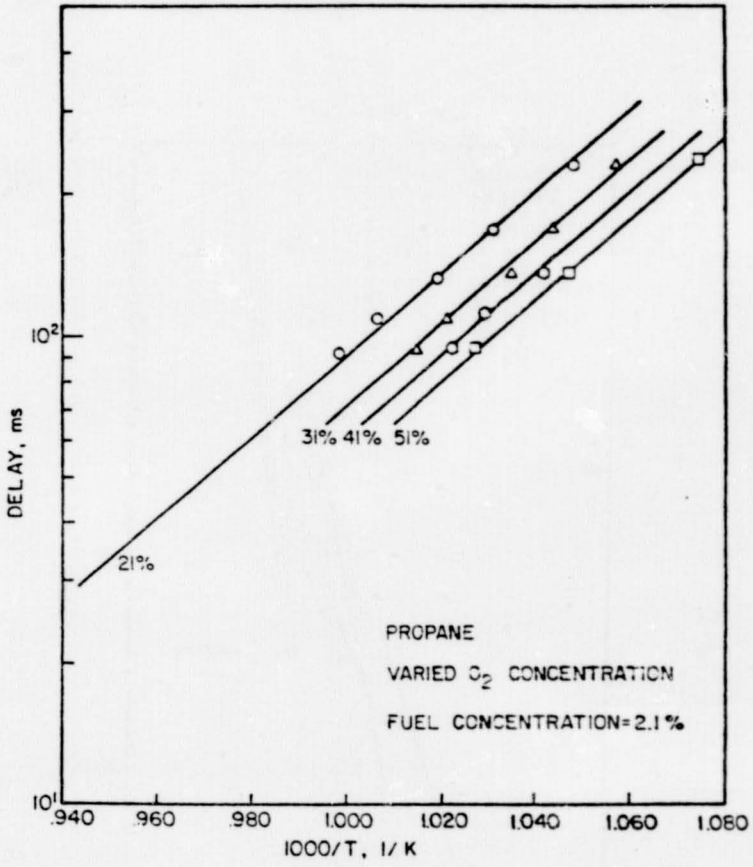

Fig. 9. Graphs illustrating influence of oxygen concentration on ignition delay times.

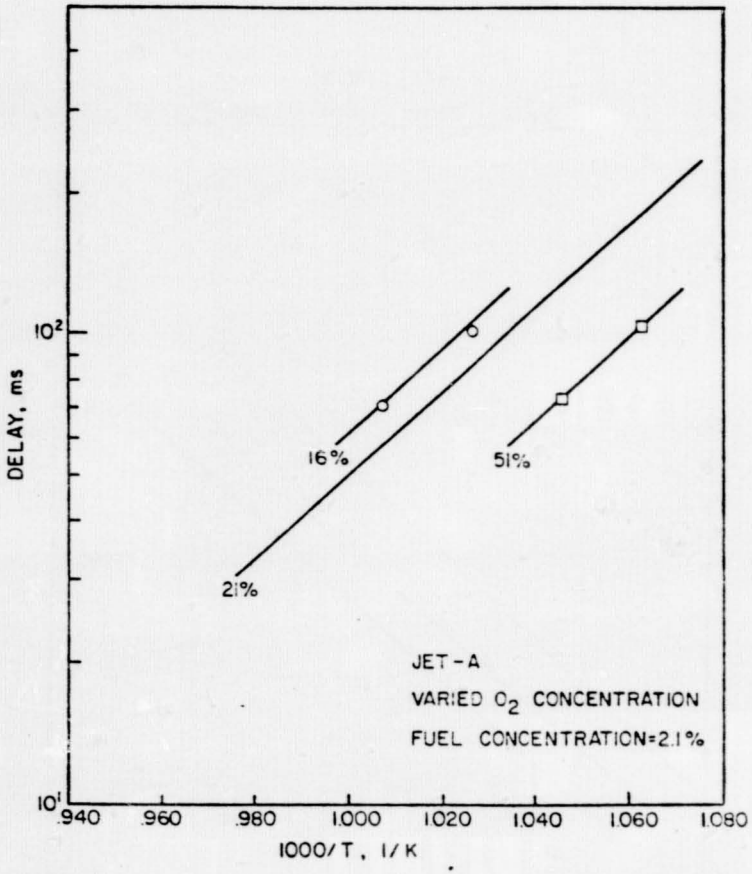

Fig. 10. Graphs illustrating influence of oxygen concentration on ignition delay times.

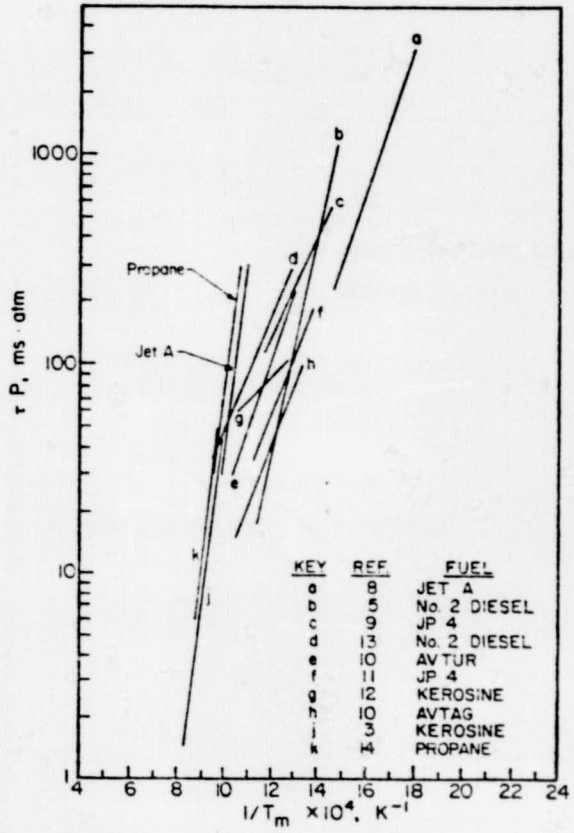

Fig. 11. Comparison of present data with results of previous workers as compiled by Chiappetta and McVey [6].

RANDOM VORTEX METHOD FOR COMBUSTING FLOWS

C. J. Marek
NASA Lewis Research Center

The random vortex method RVM of Chorin has been developed by the University of California - Berkeley to compute turbulent, reacting, recirculating flows,ref. 1. The RVM method models turbulence from first principles, tracking the vorticity and obtaining the interaction of vorticity with the bulk flow field. A computer program has been produced called MIMOC, Modeling the Interface Motion of Combustion, which can be used to calculate the reacting flow field behind a rearward facing step, ref. 2

Several comparisons between experimental data and calculations have been made, refs. 3-4. The RVM method computes qualitatively good results, but the quantitative agreement as yet is not completely satisfactory. Much of the difficulty may be caused by the treatment of boundary conditions and the techniques used for obtaining statistical averages of velocities and turbulence quantities. For the rearward facing step the computed reattachment length equals the experimental value as shown in figure 1. However the reverse velocity in the recirculation zone is over predicted by 300 percent, figure 2. In the calculations, a uniform entrance velocity was assumed with no boundary layer at the step lip. This high velocity may be overdriving the reverse flow region. The profile shown in figure 2 is the worst agreement obtained. Figure 3 shows that the time steps used to obtain the statistical average also is important. As the calculation continues, stationary values should be obtained for the mean values, but the averages must be taken over the time of several large scale vortex sheddings.

In house calculations are being conducted to look at the comparison between the turbulence quantities and the experimental values.

Recent calculations by Hsiao, ref. 4, show much better agreement between computations of the mean velocities and experimental data, figure 4. Hsiao has included the inlet passage within the calculation domain. The statistical quantities are not in good agreement, figure 5, but the averages were computed over only 20 time steps.

The results from the RVM method have been very encouraging and much can be learned through continued study of the calculation method.

References

1. Ghoniem, A.F.; Chorin, A.J.; and Oppenheim, A.K.: Numerical Modeling of Turbulent Flow in a Combustion Tunnel. Phil. Tran. R. Soc. London Ser. A, vol. 304, 1982, pp. 303-325.

2. Ghoniem, Ahmed F.; Marek, Cecil J.; and Oppenheim, Antoni K.: Modeling Interface Motion of Combustion (MIMOC). NASA TP 2132, August 1983.

3. Dai, Y.-W.; Ghoniem, A.F.; Sherman, F.S.; and Oppenheim, A.K.: Numerical modeling of Turbulent Flow in a Channel. NASA CR-168278, March 1983.

4. Hsiao, C.C.; Ghoniem, A.F.; Chorin, A.J.; and Oppenheim, A.K.: Numerical Simulation of a Turbulent Flame Stabilized Behind a Readward-Facing Step; submitted to the Twentieth Symposium (International) of Combustion, Aug. 12-17, 1984.

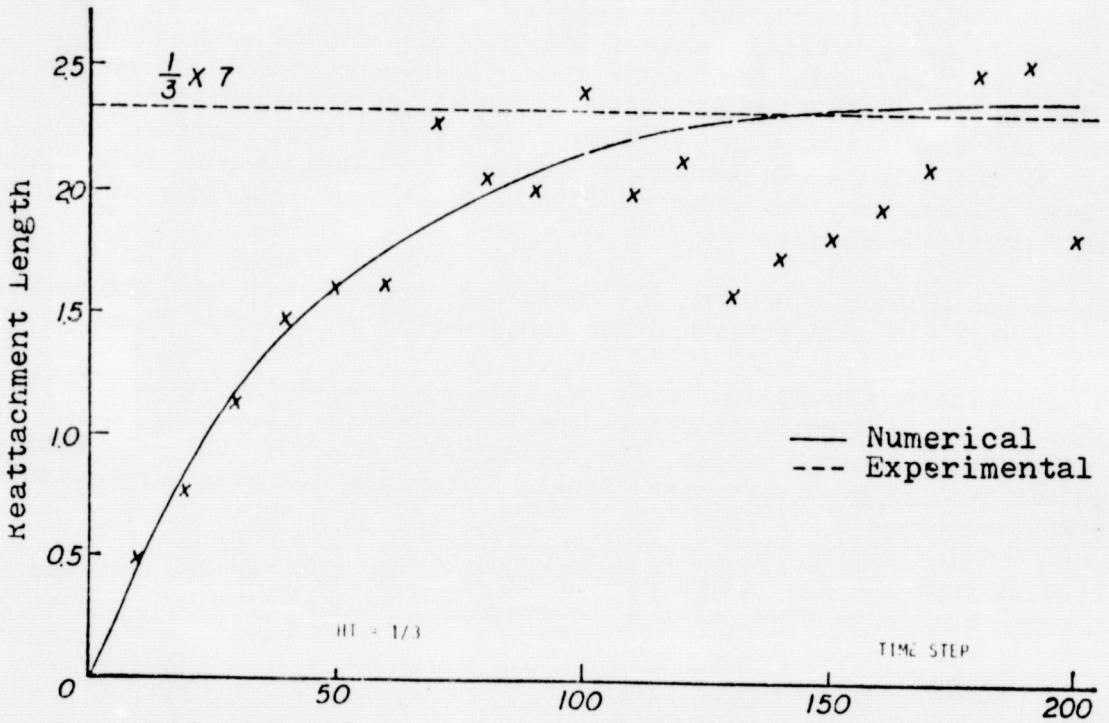

Figure 1. Comparison of reattachment length, from ref. 3.

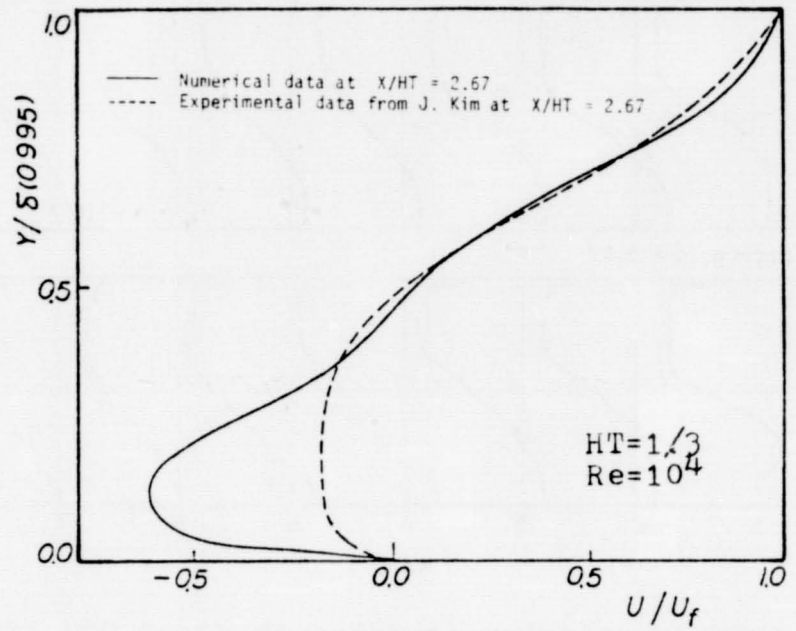

Figure 2. Comparison of mean velocity profile, between time steps 158 to 200, from ref. 3.

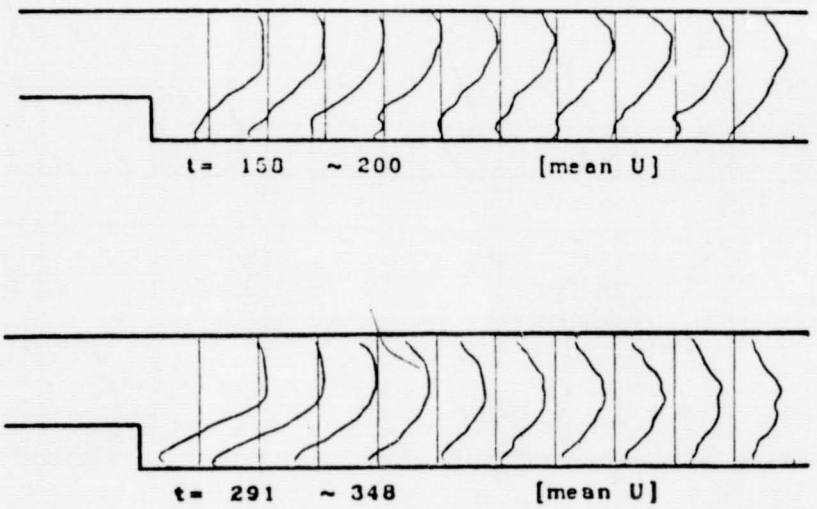

Figure 3 Comparison of mean velocity profile at HT = 1/3 and Re = 10^4 with different averaging time period., from ref. 3.

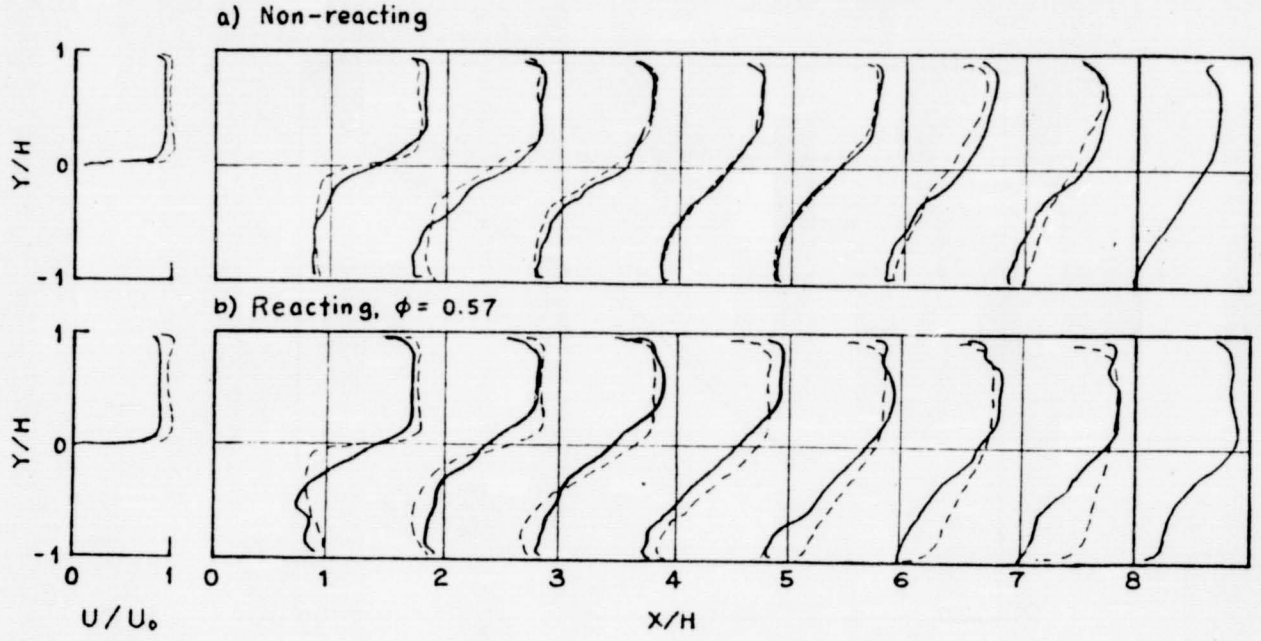

Figure 4. Average velocity profiles at Re=22,000, from ref. 4. Solid-Numerical: Dashed-Experimental.

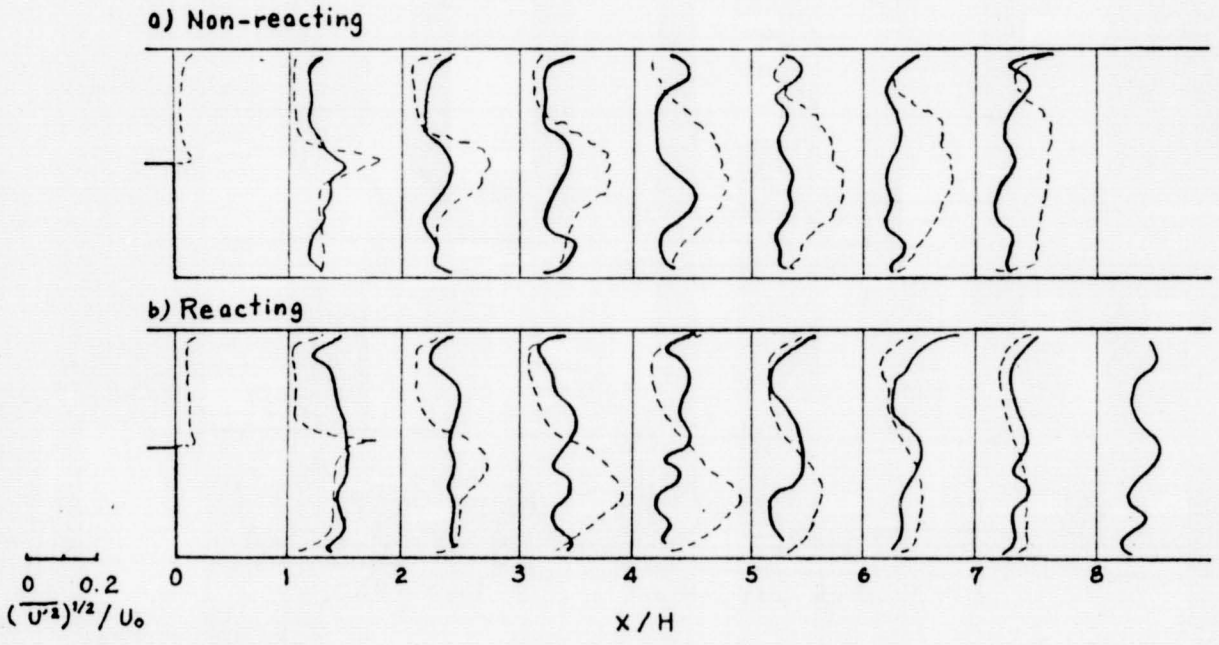

Figure 5. Streamwise turbulence intensity profiles, from ref. 4. Re=22,000; Solid-Numerical: Dashed-Experimental

AERODYNAMIC FEATURES OF FLAMES IN PREMIXED GASES

A.K. Oppenheim
University of California, Berkeley

A variety of experimentally established flame phenomena in premixed gases are interpreted by relating them to basic aerodynamic properties of the flow field. On this basis the essential mechanism of some well known characteristic features of flames stabilized in the wake of a bluff-body or propagating in ducts are revealed. Elementary components of the flame propagation process are shown to be: (1) rotary motion, (2) self-advancement, and (3) expansion.

Their consequences are analyzed under a most strict set of idealizations that permit the flow field to be treated as potential in character while the flame is modelled as a Stefan-like interface capable of exerting a feed-back effect upon the flow field. The results provide an insight into the fundamental fluid-mechanical reasons for the experimentally observed distortions of the flame front, rationalizing in particular its ability to sustain relatively high flow velocities at amazingly low normal burning speeds.

Schwarz-Christoffel Transformation:

(i) channel with open ends:

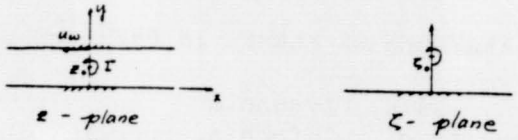

$$F(\zeta) = \frac{d\zeta}{dz} = \pi\zeta$$

$$\zeta = e^{\pi z}$$

location of vortex center in the physical plane $z_0 = \frac{1}{2}i$,
in the transformed plane $\zeta_0 = e^{\pi z_0} = i$

Complex velocity in the transformed plane:

$$w(\zeta) = -i\Gamma\left(\frac{1}{\zeta-\zeta_0} - \frac{1}{\zeta+\zeta_0}\right) = \frac{2\Gamma}{\zeta^2+1}$$

Complex velocity in the physical plane

$$w(z) = u - iv = w(\zeta)F(\zeta)$$

$$= \frac{2\Gamma}{\zeta^2+1}\cdot\pi\zeta$$

$$= \frac{2\pi\Gamma}{\zeta+\zeta^{-1}} = \frac{2\pi\Gamma}{e^{\pi z}+e^{-\pi z}}$$

at $z_w = i$ (i.e. $x=0$, $y=1$)

if $\Gamma = 1/\pi \Rightarrow w(z_w) = -1 = u_w$

$|u_w| = 1$ is thus taken as the reference velocity.

(ii) channel with one closed end

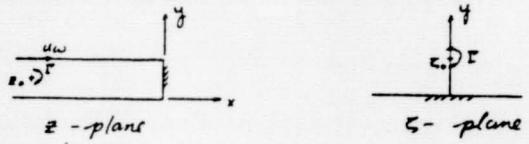

$$F(\zeta) = \frac{d\zeta}{dz} = -\pi\sqrt{\zeta^2-1}$$

$$\zeta = \cosh[\pi(i-z)]$$

location of vortex center in the physical plane: $z_0 = -x + \frac{1}{2}i$,

in the transformed plane: $\zeta_0 = \cosh[\pi(i-z_0)]$

$$= \cosh[\pi(x+\tfrac{1}{2}i)]$$

$$= i\sinh x\pi$$

Complex velocity in the transformed plane:

$$w(\zeta) = -i\Gamma\left(\frac{1}{\zeta-\zeta_0} - \frac{1}{\zeta+\zeta_0}\right) = -i\Gamma\frac{2\zeta_0}{\zeta^2-\zeta_0^2}$$

Complex velocity in the physical plane:

$$w(z) = w(\zeta)F(\zeta)$$

$$= -\frac{i2\Gamma\zeta_0}{\zeta^2-\zeta_0^2}\cdot -\pi\sqrt{\zeta^2-1}$$

$$= \mp\frac{2\pi\Gamma\sinh x\pi\sinh\pi z}{(\cosh\pi z)^2+(\sinh x\pi)^2}$$

If $\Gamma = -1/\pi$ and $x = 3$

at $z_w = -3+i$, $\quad w(z_w) = 1 = u_w$

Case 1 Deformation of flame fronts due to effects of three elementary components of flame propagation mechanism

* initial interface - straight line
* vortex is located at the center of the interface with circulation $\Gamma = 1/\pi$ and core radius $r_0 = 0.05$
* flame propagation speed $S_u = 0.4$
* density ratio $\beta = 3.0$
* time step $\delta t = 1.7857 \times 10^{-3}$

Fig. 1. Deformed flame fronts and velocity field in the physical plane at 80th time step.

Fig. 2. Deformed flame fronts and velocity field in the transformed plane at 80th time step

Fig. 3. Enlargement of inner portion of Fig 2

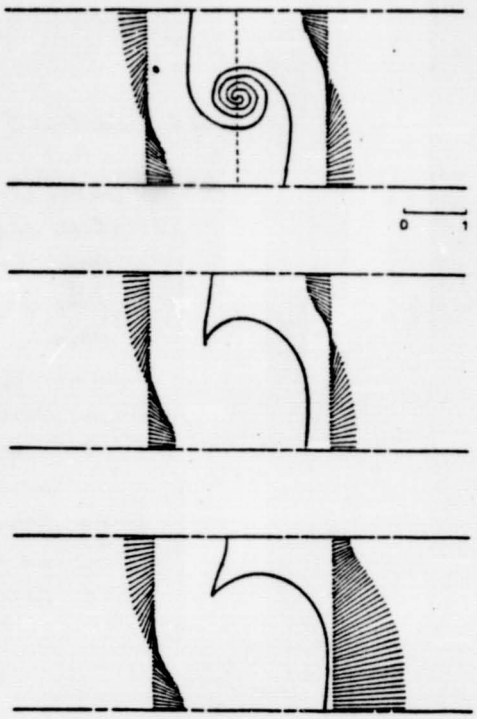

Fig 1

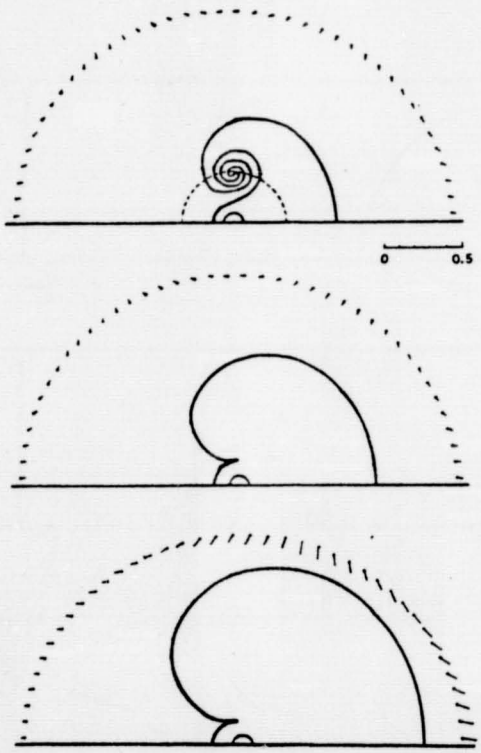

Fig 2

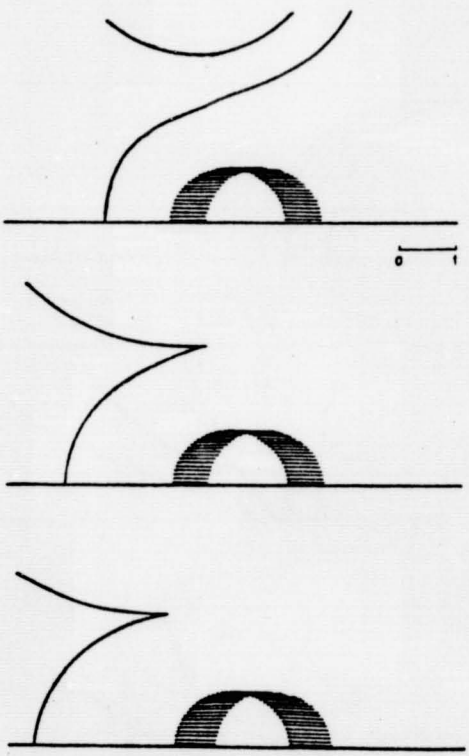

Fig 3

Case 2: Turbulent Flame propagation in a channel

* initial interface: straight line
* vortex with circulation $\Gamma = 1/\pi$ is located at the center of the channel and 0.5 to the left of the interface — stays stationary.
* flame propagation speed $S_u = S_u(r_f)$ with $S_{umax} = 0.4$
* density ratio $\beta = 3.0$
* time step $\Delta t = 1.7857 \times 10^{-2}$

Fig. 4 Deforming flame fronts at every 40 time steps.

Fig. 5 Flame fronts and velocity field in the physical plane at 120th time step.

Fig. 6 Flame fronts and velocity field in the transformed plane at 120th time step.

Fig. 7 Enlargement of the inner portion of Fig 6.

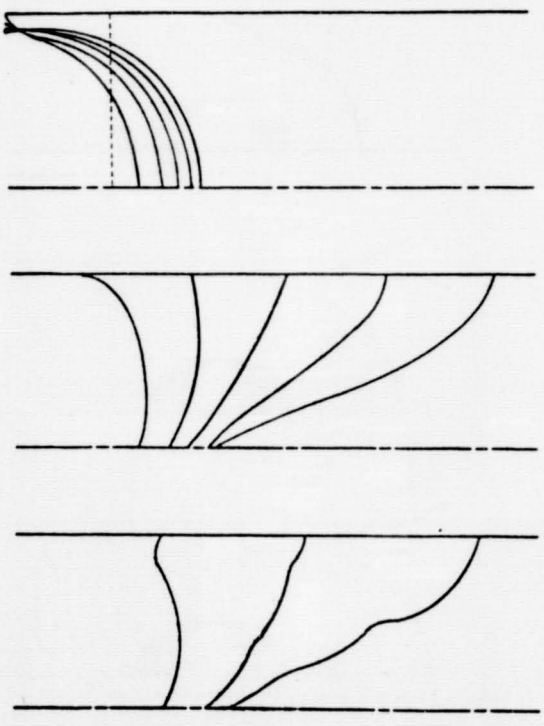

Fig 4

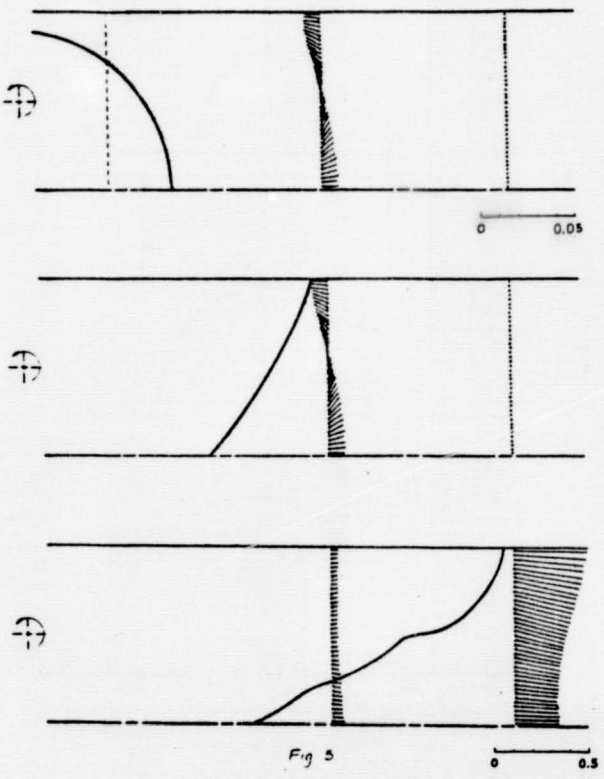

Fig 5

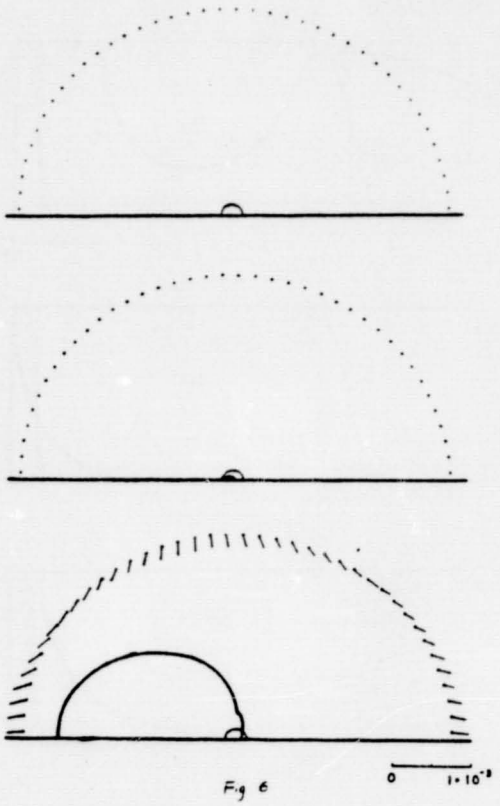

Fig 6

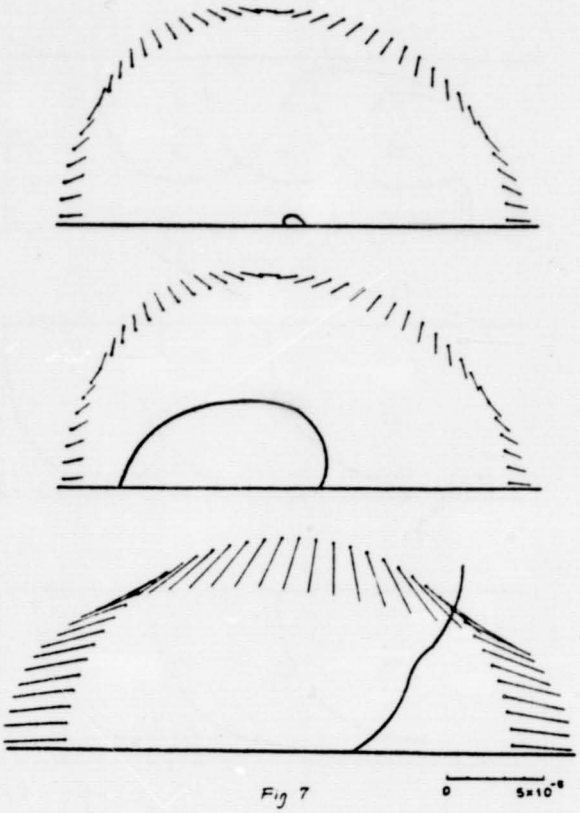

Fig 7

Case 3. Laminar flame propagation in a channel

* initial interface: straight line
* vortex is also located 0.5 to the left of the interface with circulation $\Gamma = -1/\pi$ and moving to the right at constant speed 0.0075
* flame propagation speed $S_u = 0.4$
* density ratio $\beta = 3.0$
* time step $\Delta t = 1.7857 \times 10^{-2}$

Fig. 8. Flame fronts and locations of vortices at 40th, 120th and 200th time step

Fig. 9. Flame fronts and velocity fields in the physical plane at 200th time step.

Fig. 10. Flame fronts and velocity field at different location in the physical plane.

Fig. 11. Flame fronts and velocity field in the transformed plane at 200th time step.

Fig. 12. Enlargement of inner portion of Fig. 11.

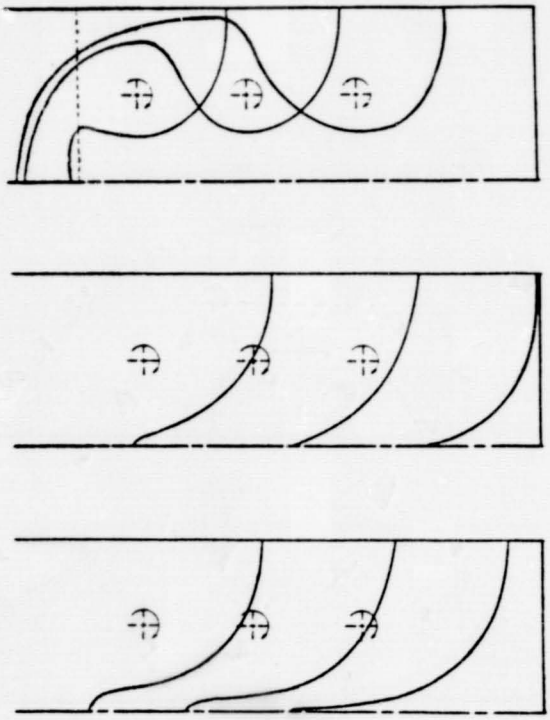

Fig 8

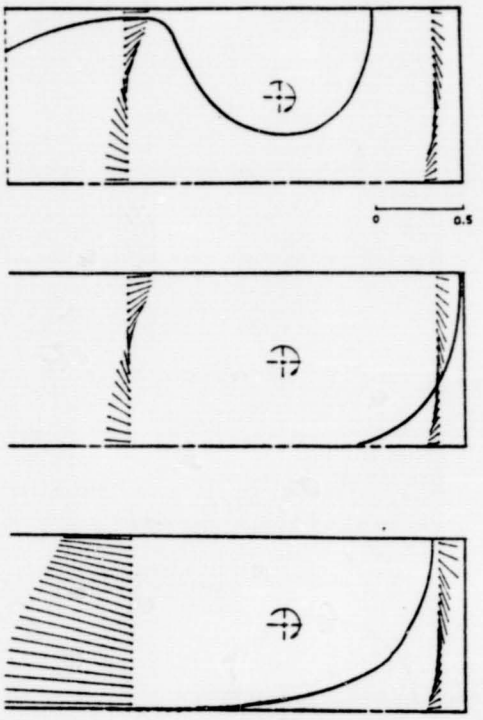

Fig 9

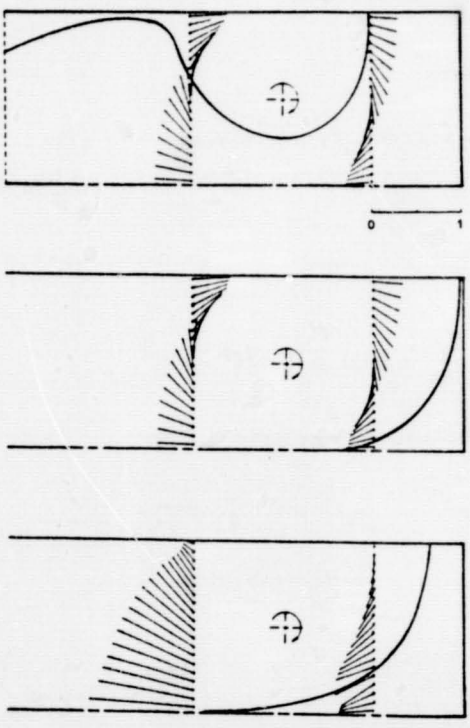

Fig 10

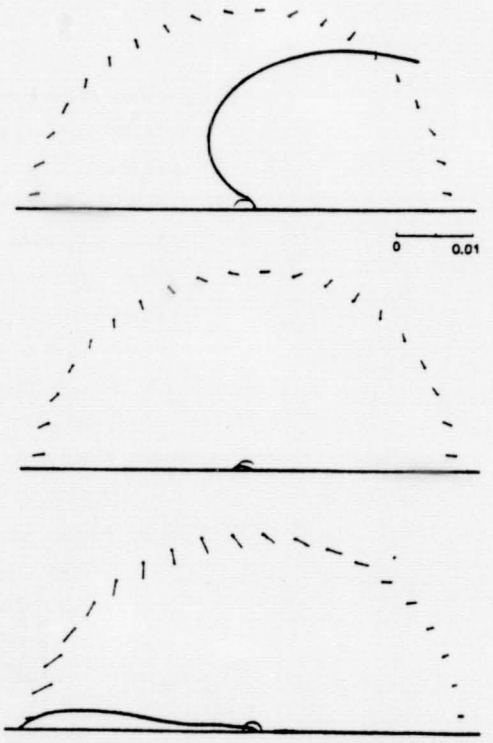

Fig 11

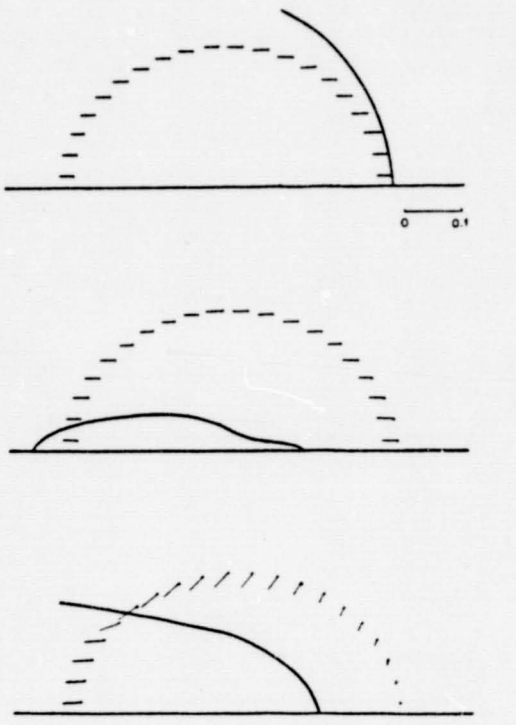

Fig 12

D35

TRANSIENT FLOW COMBUSTION

Robert R. Tacina
NASA Lewis Research Center

Non-steady combustion problems can result from engine sources such as accelerations, decelerations, nozzle adjustments, augmentor ignition, and air perturbations into and out of the compressor. Also non-steady combustion can be generated internally from combustion instability or self-induced oscillations. A premixed-prevaporized combustor would be particularly sensitive to flow transients because of its susceptability to flashback-autoignition and blowout. An experimental program, the "Transient Flow Combustion Study" is in progress to study the effects of air and fuel flow transients on a premixed-prevaporized combustor.

This experiment is to be performed at LeRC CE5b, test stand 3. The transient capability is provided by high response hydraulic valves (full traverse in 100 ms) that are installed upstream and downstream of the test section to control airflow and pressure and in the fuel line to control fuel flow. Figure 1 shows the salient features of the test rig and the hardware. Nonvitiated preheated air flows through the upstream control valve to a diffuser section with straightening vanes to provide a uniform velocity profile to the test section. The inlet velocity profile is measured with a traversing total pressure probe. Test hardware for lean premixed-prevaporized combustor tests is shown. The airflow splits at the test section inlet. Half the air goes through the center zone for premixing- prevaporizing with the fuel and downstream burning. The other half enters an outer annulus and is used for film cooling in the downstream burning section. In the center zone, fuel is distributed uniformly by a concentric multi-point fuel injector. The fuel injector can be located either 15 cm or 38 cm upstream of the flameholder. The fuel-air distribution is measured in a plane 4 cm upstream of the flameholder with a traversing probe. High response pressure transducers, thermocouples and a photodetector are installed in the premixing-prevaporizing section to monitor transient response, in particular to detect if autoignition or flashback should occur. Downstream of the premixing-prevaporizing section there is a perforated plate flameholder and a combustion section. The walls of the flame tube are film cooled. The exit conditions will be measured with a traversing total pressure, temperature and emissions probe. Emission measurements will only be taken at steady state conditions. The back pressure valve is a specially designed water cooled valve. This eliminates the need to cool the combustor exhaust products with water spray upstream of the back pressure valve. Water spray upstream of the valve can introduce flow transients if there is two-phase flow.

Preliminary tests have been performed at an inlet air temperature of 600 K, a reference velocity of 30 m/s, and a pressure of 700 kPa. Ramping the airflow down (at constant fuel-air ratio) indicated that this combustor is less sensitive to flashback than anticipated. The airflow was reduced to 1/3 of its orginal value in a 40 ms ramp before flashback occurred. Ramping the airflow up has shown that blowout is more sensitive than flashback to flow transients. Blowout occurred with a 25 percent increase in airflow (at a constant fuel-air ratio) in a 20 ms ramp. Combustion resonance has been found at some conditions and may be important in determining the effects of flow transients.

TRANSIENT-FLOW STUDY COMBUSTOR RIG

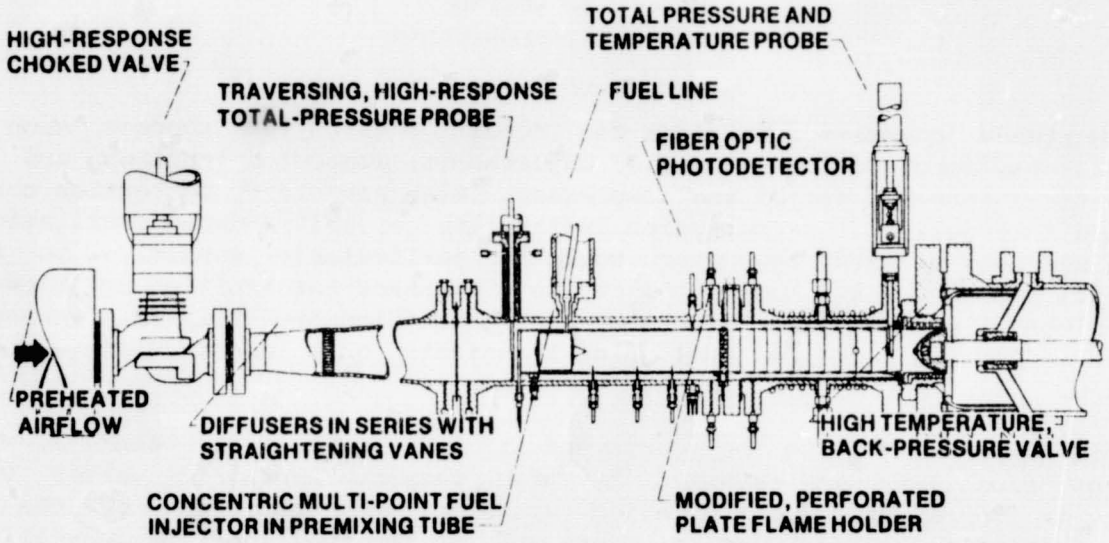

D36

N84 20561

COMBUSTOR FLAME FLASHBACK

Margaret P. Proctor
Case Western Reserve University

David N. Anderson
NASA Lewis Research Center

and

James S. T'ien
Case Western Reserve University

Flashback, a problem that occurs in premixed-prevaporized combustors, is the upstream propagation of the flame from the combustor into the premixing tube. Not only does flashback change the combustion process from premixed burning to diffusion burning, thus creating more pollutants, but it also inflicts considerable damage to the fuel injector, premixing tube and other equipment upstream. This study attempts to define the conditions at which flashback occurs in steady burning and the mechanism that causes flashback in both steady and transient flow.

Part of the experimental setup is shown in the attached figure. The stainless steel test section is a two-dimensional (rectangular cross-section) center dump combustor. The 4" x 1" premixing tube, 6"-long, dumps into the 4"x4" combustor, 10"-long. The combustor empties into the exhaust plenum through a 2"-diameter hole that may be partially blocked by a conical plunger. Movement of the plunger, powered by two solenoids, creates a pressure pulse for transient data. The fuel injector stationed 1½" upstream of the premixer in the transition section supplies gaseous propane to the test section. One or both sides of the test section may be fitted with ½"-thick quartz windows to view the entire combustion process.

The equivalence ratio at which flashback occurs is being measured for inlet temperatures of 600-950 K, premixer wall temperatures of 450-1050 K and premixer velocities of 40-80 ft/s. These data will be presented. It is hoped that by the time of the conference high speed film will be available to show the mechanism of flashback. Future work involves the buildup of a slightly modified Hastelloy test section that will withstand inlet temperatures of 1100 K. Transient data will also be collected.

FLASHBACK STUDY

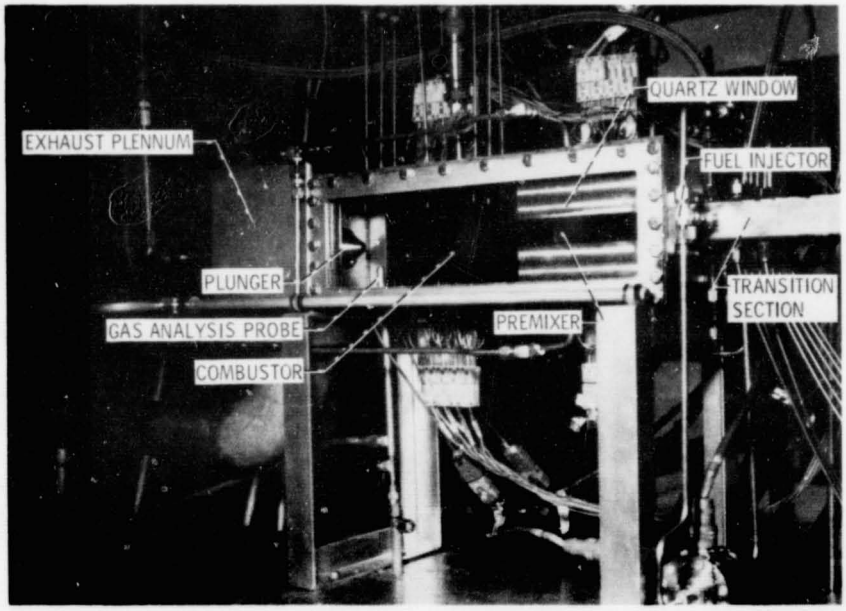

V-1962